

Marine Molecular Biotechnology

Subseries of Progress in Molecular and Subcellular Biology

Series Editor Werner E. G. Müller

Progress in Molecular and Subcellular Biology

Series Editors W. E. G. Müller (Managing Editor)

Ph. Jeanteur, Y. Kuchino, M. Reis Custódio,

R.E. Rhoads, D. Ugarkovic

47

Volumes Published in the Series

Progress in Molecular
and Subcellular Biology

Subseries:
Marine Molecular Biotechnology

Volume 33

Silicon Biomineralization

W.E.G. Müller (Ed.)

Volume 34

**Invertebrate Cytokines
and the Phylogeny of Immunity**

A. Beschin and W.E.G. Müller (Eds.)

Volume 35

**RNA Trafficking and Nuclear Structure
Dynamics**

Ph. Jeanteur (Ed.)

Volume 36

Viruses and Apoptosis

C. Alonso (Ed.)

Volume 38

Epigenetics and Chromatin

Ph. Jeanteur (Ed.)

Volume 40

**Developmental Biology of Neoplastic
Growth**

A. Macieira-Coelho (Ed.)

Volume 41

Molecular Basis of Symbiosis

J. Overmann (Ed.)

Volume 44

Alternative Splicing and Disease

Ph. Jeanlevr (Ed.)

Volume 45

Asymmetric Cell Division

A. Macieira Coelho (Ed.)

Volume 37

Sponges (Porifera)

W.E.G. Müller (Ed.)

Volume 39

Echinodermata

V. Matranga (Ed.)

Volume 42

Antifouling Compounds

N. Fusetani and A.S. Clare (Eds.)

Volume 43

Molluscs

G. Cimino and M. Gavagnin (Eds.)

Volume 46

Marine Toxins as Research Tools

N. Fusetani and W. Kem (Eds.)

Volume 47

**Biosilica in Evolution, Morphogenesis,
and Nanobiotechnology**

W.E.G. Müller and M.A. Grachev (Eds.)

Werner E.G. Müller • Mikhael A. Grachev
Editors

Biosilica in Evolution, Morphogenesis, and Nanobiotechnology

Case Study Lake Baikal

 Springer

Editors

Prof. Dr. Werner E. G. Müller
Universität Mainz
Inst. Physiologische Chemie
Abt. Angewandte
Molekularbiologie
Duesbergweg 6
55099 Mainz
Germany
wmueller@uni-mainz.de

Dr. Mikhael A. Grachev
Russian Academy of Sciences
Siberian Branch
Limnological Institute
Ulan-Batorskaya st. 3
Irkutsk
Russia 664033

ISSN 1611-6119

ISBN 978-3-540-88551-1

e-ISBN 978-3-540-88552-8

DOI 10.1007/978-3-540-88552-8

Library of Congress Catalog Number: 2008938188

© 2009 Springer-Verlag Berlin Heidelberg

This work is subject to copyright. All rights reserved, whether the whole or part of the material is concerned, specifically the rights of translation, reprinting, reuse of illustrations, recitation, broadcasting, reproduction on microfilm or in any other way, and storage in data banks. Duplication of this publication or parts thereof is permitted only under the provisions of the German Copyright Law of September, 9, 1965, in its current version, and permission for use must always be obtained from Springer-Verlag. Violations are liable for prosecution under the German Copyright Law.

The use of general descriptive names, registered names, trademarks, etc. in this publication does not imply, even in the absence of a specific statement, that such names are exempt from the relevant protective laws and regulations and therefore free for general use.

Product liability: The publisher cannot guarantee the accuracy of any information about dosage and application contained in this book. In every individual case the user must check such information by consulting the relevant literature.

Cover design: WMXDesign, Heidelberg, Germany

Printed on acid-free paper

9 8 7 6 5 4 3 2 1

springer.com

Foreword

Lake Baikal, the oldest (>24 million years), deepest (1,637 m) and most voluminous lake on Earth, comprising one-fifth of the world's unfrozen freshwater, harbors the highest number of known endemic animals in a freshwater lake. Until recently, it remained enigmatic why such a high diversity evolved in this closed and isolated lake. Focusing on sponges (phylum Porifera) as examples, some answers have produced a deeper understanding of the evolutionary forces that have driven this process. The most likely scenarios are outlined in this volume, explaining the high rate of evolution/diversification of Baikalian sponge species, especially focusing on their method of reproduction and their specific habitat with its extreme temperature and particular chemical composition. A further trigger of evolution of the endemic sponges in Lake Baikal may be their sophisticated symbiotic relationship with unicellular autotrophic eukaryotes. As a basis for understanding the exceptional habitat, the geological history of the lake and its surrounding basins is described in greater detail. Another exciting finding is that (almost) all sponge species in Lake Baikal harbor mobile genetic elements (retrotransposons) which have been implicated in the endemic progress during evolution.

It is likewise remarkable that the Baikalian sponges are characterized by a distinct and elaborate body plan which characterizes them as the most subtle freshwater sponges on Earth. The basic characteristics of the body plan construction are given with the main emphasis on the organization, construction, and association of the needle-like skeletal elements, the spicules. It is further highlighted that the basis for the exceptional morphogenetic organization of the sponges in Lake Baikal must be seen in the expression of those genes which result in the synthesis of proteins governing the synthesis of spicules and their associated proteins. In particular, by comparing sponge species in lakes adjacent, but not connected, to Lake Baikal, it became apparent what a high degree of morphological construction their sponges have reached.

The inorganic material from which spicules are made is silica, a material which has recently gained increasing attention. Here, the siliceous sponges in general and the Lake Baikal (siliceous) sponges in particular, are featured for their property to synthesize polymeric silica enzymatically. The key enzyme involved in this process is silicatein which exists in the endemic sponges of Lake Baikal as a family of more than five different members. No other sponge taxon comprises such a high poly-

morphism, thus qualifying the Lake Baikal species as exceptional with respect to their genetic toolkit for silica formation. In order to successfully approach the exploitation of this unique property in a sustainable way, and by applying modern molecular biology and cell biology techniques, the sponge silicateins have been prepared in a recombinant way in bacteria.

Based on these findings, it is now the challenge to apply the process of enzymatic silica formation for the fabrication of biosilica-based materials used, e.g., in biomedicine. A major breakthrough came recently with experiments which showed that silicatein can be immobilized on inorganic matrices as well as on organic polymer layers through a linker molecule, comprising a nitrilotriacetic acid group which binds via nickel ions to histidine-tagged silicatein. The immobilized enzyme catalyzes not only the condensation of biosilica but also, importantly, the formation of structured titania and zirconia nanoparticles from soluble precursors. This finding will surely have a considerable impact for the construction of three-dimensional semiconductors if nanowires can be decorated with such biocatalytically-formed titania and/or zirconia nanoparticles.

The stability of spicules' biosilica is highly impressive. Besides this property, it is now being investigated whether biosilica has additional properties which are important for biomedical applications: (1) to be biocompatible and (2) to be biodegradable. In this volume, the first approaches to reaching sufficient biocompatibility of biosilica are conceptualized. In order to meet the demands for novel bioactive supports in surgery, orthopedics, and tissue engineering, recombinant silicatein has been applied for the synthesis of silica-containing bioactive surfaces under ambient conditions that do not damage biomolecules such as proteins. In nature, an anabolic reaction is counterbalanced by a catabolic one. This also holds true for enzymic processes. Driven by this experience, silicatein has been screened for a biosilica-degrading enzyme, which was discovered with silicase. Both silicase and, to a much lesser extent also carbonic anhydrase, allow the decomposition of biosilica, again under ambient conditions.

This volume focuses on state-of-the-art issues of biosilica biochemistry, cell biology, and biotechnology, which allow an estimation of the inherent high economical value that can be attributed to this material. However, the treasures of Lake Baikal are larger; it is a unique place at which (1) evolution in action can be studied, (2) a unique and conserved climate situation exists, which may provide us with early warning markers of the present day global warming process, and (3) solid methane is found, a powerful greenhouse gas that is also a valuable fuel for mechanical and electrical energy generation.

Professor Dr. W.E.G. Müller
Dr. Mikhail A. Grachev (Academician)

Preface to the Series

Recent developments in the applied field of natural products are impressive, and the speed of progress appears to be almost self-accelerating. The results emerging make it obvious that nature provides chemicals, secondary metabolites, of astonishing complexity. It is generally accepted that these natural products offer new potential for human therapy and biopolymer science. The major disciplines which have contributed, and increasingly contribute, to progress in the successful exploitation of this natural richness include molecular biology and cell biology, flanked by chemistry. The organisms of choice, useful for such exploitation, live in the marine environment. They have the longest evolutionary history during which they could develop strategies to fight successfully against invading organisms and to form large multicellular plants and animals in aqueous medium. The first multicellular organisms, the plants, appeared already 1,000 million years ago (Ma), then the fungi emerged and, finally, animals developed (800 Ma).

Focusing on marine animals, the evolutionary oldest phyla, the Porifera, the Cnidaria and the Bryozoa, as sessile filter feeders, are exposed not only to a huge variety of commensal, but also toxic microorganisms, bacteria and fungi. In order to overcome these threats, they developed a panel of defense systems, for example, their immune system, which is closely related to those existing in higher metazoans, the Protostomia and Deuterostomia. In addition, due to this characteristic, they became outstandingly successful during evolution: they developed a chemical defense system which enabled them to fight in a specific manner against invaders. These chemicals are of low molecular weight and of non-proteinaceous nature. Due to the chemical complexity and the presence of asymmetrical atom centers in these compounds, a high diversity of compounds became theoretically possible. In a natural selective process, during evolution, only those compounds were maintained which caused the most potent bioactivity and provided the most powerful protection for the host in which they were synthesized. This means that during evolution nature continuously modified the basic structures and their derivatives for optimal function. In principle, the approach used in combinatorial chemistry is the same, but turned out to be painful and only in few cases successful. In consequence, it is advisable to copy and exploit nature for these strategies to select for bioactive drugs. Besides the mentioned metazoan phyla, other animal phyla, such as the higher evolved animals, the mollusks or tunicates, or certain algal groups, also

produce compounds for their chemical defense which are of interest scientifically and for potential application.

There is, however, one drawback. Usually, the amount of starting material used as a source for the extraction of most bioactive compounds found in marine organisms is minute and, hence, not sufficient for their further application in biomedicine. Furthermore, the constraints of the conventions for the protection of nature limit the commercial exploitation of novel compounds, since only a small number of organisms can be collected from the biotope. Consequently, exploitation must be sustainable, i.e., it should not endanger the equilibrium of the biota in a given ecosystem. However, the protection of biodiversity in nature, in general, and of organisms living in the marine environment, in particular, holds an inherent opportunity if this activity is based on genetic approaches. From the research on molecular biodiversity, benefits for human society emerge which are of obvious commercial value; the transfer of basic scientific achievements to applicable products is the task and the subject of *Marine Molecular Biotechnology*. This discipline uses modern molecular and cell biological techniques for the sustainable production of bioactive compounds and for the improvement of fermentation technologies in bioreactors.

Hence, marine molecular biotechnology is the discipline which strives to define and solve the problems regarding the sustainable exploitation of nature for human health and welfare, through the cooperation between scientists working in marine biology/molecular biology/microbiology and chemistry. Such collaboration is now going on successfully in several laboratories.

It is the aim of this new subset of thematically connected volumes within our series *Progress in Molecular and Subcellular Biology* to provide an actual forum for the exchange of ideas and expertise between colleagues working in this exciting field of *Marine Molecular Biotechnology*. It also aims to disseminate the results to those researchers who are interested in the recent achievements in this area or are just curious to learn how science can help to exploit nature in a sustainable manner for human prosperity.

Werner E.G. Müller

Preface

By tradition, both Russia and Germany place a high value on education, research and science. Now more than ever before, education and research are the keys to the economic and social future of all countries. Well-qualified experts enable new insights into the fields of science and research. They have the power to safeguard and strengthen prosperity across the world. If we want to achieve long-term economic growth, we need to give young people the opportunity to acquire valid qualifications.

Scientific cooperation between Russia and Germany is characterized by excellent, long-standing relations. An agreement on scientific and technological cooperation was originally concluded 20 years ago. It was exceptionally successful and opened up numerous opportunities for scientific cooperation. In 2005, the heads of government of the two countries signed a joint declaration on a “Strategic Partnership in Education, Research and Innovation”, thus reiterating their willingness to work together. The aim of the declaration is to give the many existing ties a more strategic orientation. At the same time, it initiates long-term relations between their research institutions and universities.

As part of this strategic partnership, the German-Russian “Joint Lab Baikal” was established in 2005, with the support of the Federal Ministry of Education and Research. It specializes in molecular biology and the sustainable use of endemic sponges in Lake Baikal. The scientific coordinator of the project is Prof. Werner E.G. Müller, head of the Department of Applied Molecular Biology at the University of Mainz’s Institute for Physiological Chemistry. On the Russian side, the project is headed by Prof. Michael A. Grachev, Member of the Russian Academy of Sciences and Director of the Limnology Institute of the Russian Academy of Sciences (Siberian Branch) in Irkutsk.

I am delighted that the latest results of this productive collaboration are being presented in this study – “Biosilica in Evolution, Morphogenesis and Nanobiotechnology. Case Study Lake Baikal“. This is an excellent reflection of the vitality of German-Russian cooperation in the field of research.

Thomas Rachel
Parliamentary State Secretary of the
German Federal Ministry of Education and Research
Deutscher Bundestag
Platz der Republik 1
11011 Berlin
Deutschland



Preface

Biom mineralization, in particular biosilicification, has become an exciting source of inspiration for novel bionic approaches. This book describes the exploitation of biom mineralization principles which have been perfected by nature all the way through the course of evolution. Harnessing the unique capability of sponges to form silica under ambient conditions enables the industrial production of biosilica in a sustainable way, which opens opportunities for a range of innovative applications and processes including lithography, microelectronics and biomedicine. The strategies described in this book support the objectives of the European Commission's „Nanosciences, Nanotechnologies, Materials and new Production Technologies – NMP“ program by delivering tools to improve the competitiveness, innovation potential and sustainability of European industry. The nanobiotechnology concept promoted by the NMP Thematic priority of the Seventh Framework Program is targeted by using nature as model for new nanotechnology-based processes, and these technologies can contribute to the transformation of European industry from resource-intensive to knowledge-intensive. Some of the most promising perspectives for new technologies stem from the converging interfaces of different disciplines. The novel techniques based on the principles of biom mineralization/ biosilicification are thus expected to bring about long-term innovation in the rapidly growing field of nanobiotechnology. The international collaboration presented by the European and Russian organizations is a perfect means of establishing lasting cooperation and signifies the partnership activity of the European Research Area on a global scale.

Herbert von Bose
Director

Directorate G: Industrial Technologies
Directorate-General for Research

[The views expressed are purely those of the writer and may not in any circumstances be regarded as stating an official position of the European Commission]

Preface

On 11 April 2005, a Joint Declaration on a “Strategic Partnership in Education, Research and Innovation“ was signed by Russian President Vladimir Putin and German Chancellor Gerhard Schröder. The establishment of the Russian - German “Joint Lab Baikal” is an example of the successful implementation of the aims expressed in this document. This joint lab is headed by Dr. Michael A. Grachev, Member of the Russian Academy of Sciences and Director of the Limnology Institute of the Siberian Branch of the Russian Academy of Sciences in Irkutsk and Prof. Dr. Werner E.G. Müller, head of the Department of Applied Molecular Biology at the Institute for Physiological Chemistry of the University of Mainz in Germany.

Lake Baikal is the greatest, deepest and most ancient lake in the world. The endemic sponges inhabiting this lake are important not only for basic science but also for the innovative discipline of nanobiotechnology, as highlighted in this book. This monograph underlines the excellent development in the relations between both countries in the field of science and technology.

Wladimir N. Fridlyanov
Deputy Minister of Education and Science
pl. Miusskaja 3
125993 Moscow
The Russian Federation



Contents

Part I Geology – Paleontology – Paleoclimate

Overview of Geology and Tectonic Evolution of the Baikal-Tuva Area	3
Dmitry Gladkochub and Tatiana Donskaya	
Tectonics of the Baikal Rift Deduced from Volcanism and Sedimentation: A Review Oriented to the Baikal and Hovsgol Lake Systems	27
Alexei V. Ivanov and Elena I. Demonterova	
Paleoclimate and Evolution: Emergence of Sponges During the Neoproterozoic	55
Werner E.G. Müller, Xiaohong Wang, and Heinz C. Schröder	

Part II Organisms: Sponges

Studies on the Taxonomy and Distribution of Freshwater Sponges in Lake Baikal	81
Yoshiki Masuda	
Towards a Molecular Systematics of the Lake Baikal/Lake Tuva Sponges	111
Matthias Wiens, Petra Wrede, Vladislav A. Grebenjuk, Oxana V. Kaluzhnaya, Sergey I. Belikov, Heinz C. Schröder, and Werner E.G. Müller	
Symbiotic Interaction Between Dinoflagellates and the Demosponge <i>Lubomirskia baicalensis</i>: Aquaporin-Mediated Glycerol Transport	145
Werner E.G. Müller, Sergey I. Belikov, Oxana V. Kaluzhnaya, L. Chernogor, Anatoli Krasko, and Heinz C. Schröder	

Part III Evolution

Silicon in Life: Whither Biological Silicification?	173
Christopher Exley	

Fossil Sponge Fauna in Lake Baikal Region	185
Elena Veynberg	

Identification and Isolation of a Retrotransposon from the Freshwater Sponge <i>Lubomirskia baicalensis</i>: Implication in Rapid Evolution of Endemic Sponges	207
Matthias Wiens, Vladislav A. Grebenjuk, Heinz C. Schröder, Isabel M. Müller, and Werner E.G. Müller	

Part IV Role of Biosilica in Morphogenesis

Modelling the Skeletal Architecture in a Sponge with Radiate Accretive Growth	237
Jaap A. Kaandorp	

Part V Biosilica Formation

Silicatein: Nanobiotechnological and Biomedical Applications	251
Heinz C. Schröder, Ute Schloßmacher, Alexandra Boreiko, Filipe Natalio, Malgorzata Baranowska, David Brandt, Xiaohong Wang, Wolfgang Tremel, Matthias Wiens, and Werner E.G. Müller	

Part VI Role of Biosilica in Materials Science

Role of Biosilica in Materials Science: Lessons from Siliceous	277
George Mayer	

An Overview of Silica in Biology: Its Chemistry and Recent Technological Advances	295
Carole C. Perry	

Optical and Nonlinear Optical Properties of Sea Glass Sponge Spicules	315
Yu. N. Kulchin, A.V. Bezverbny, O.A. Bukin, S.S. Voznesensky, A.N. Galkina, A.L. Drozdov, and I.G. Nagorny	

Nanobiotechnology: Soft Lithography	341
Elisa Mele and Dario Pisignano	

The Application of Silicon and Silicates in Dentistry: A Review	359
A.-K. Lührs and Werner Geurtsen	

Part VII Role of Biosilica in Nanobiotechnology

Sustainable Exploitation and Conservation of the Endemic Lake Baikal Sponge (<i>Lubomirskia baicalensis</i>) for Application in Nanobiotechnology	383
Werner E.G. Müller, Heinz C. Schröder, and Sergey I. Belikov	

Index	417
--------------------	------------

Contributors

Malgorzata Baranowska

Institut für Physiologische Chemie, Abteilung Angewandte Molekularbiologie,
Universität, Duesbergweg 6, D-55099 Mainz, Germany

Sergey I. Belikov

Limnological Institute of the Siberian Branch of Russian Academy of Sciences,
Ulan-Batorskaya 3, RUS-664033 Irkutsk, Russia

A.V. Bezverbny

Institute for Automation and Control Processes of Far Eastern Branch of RAS,
Radio St. 5, 690041 Vladivostok, Russia

Alexandra Boreiko

Institut für Physiologische Chemie, Abteilung Angewandte Molekularbiologie,
Universität, Duesbergweg 6, D-55099 Mainz, Germany

David Brandt

Institut für Physiologische Chemie, Abteilung Angewandte Molekularbiologie,
Universität, Duesbergweg 6, D-55099 Mainz, Germany

O.A. Bukin

Institute for Automation and Control Processes of Far Eastern Branch of RAS,
Radio St. 5, 690041 Vladivostok, Russia

L. Chernogor

Limnological Institute of the Siberian Branch of Russian Academy of Sciences,
Ulan-Batorskaya 3, RUS-664033 Irkutsk, Russia

Elena I. Demonterova

Institute of the Earth's Crust, Siberian Branch, Russian Academy of Sciences,
Lermontov street 128, RUS-664033 Irkutsk, Russia

Tatiana Donskaya

Institute of Earth's crust, the Siberian Branch of Russian Academy of Sciences,
Lermontov St., 128, RUS-664033 Irkutsk, Russia

A.L. Drozdov

Institute of Marine Biology of Far Eastern Branch of RAS, Palchevsky St. 17,
690041 Vladivostok, Russia

Christopher Exley

Birchall Centre for Inorganic Chemistry and Materials Science, Lennard-Jones
Laboratories, Keele University, Staffordshire, UK

A.N. Galkina

Institute for Automation and Control Processes of Far Eastern Branch of RAS,
Radio St. 5, 690041 Vladivostok, Russia

W. Geurtsen

Department of Conservative Dentistry, Periodontology & Preventive Dentistry,
Medical University Hannover, Hannover, Germany

Dmitry Gladkochub

Institute of Earth's crust, the Siberian Branch of Russian Academy of Sciences,
Lermontov St., 128, RUS-664033 Irkutsk, Russia

Vladislav A. Grebenjuk

Institut für Physiologische Chemie, Abteilung Angewandte Molekularbiologie,
Universität, Duesbergweg 6, D-55099 Mainz, German

Alexei V. Ivanov

Institute of the Earth's Crust, Siberian Branch, Russian Academy of Sciences,
Lermontov St., 128, RUS-664033 Irkutsk, Russia

Jaap A. Kaandorp

Section Computational Science, Faculty of Science, University of Amsterdam,
Kruislaan 403, 1098 SJ Amsterdam, The Netherlands

Oxana V. Kaluzhnaya

Limnological Institute of the Siberian Branch of Russian Academy of Sciences,
Ulan-Batorskaya 3, RUS-664033 Irkutsk, Russia

A. Krasko

Institut für Physiologische Chemie, Abteilung Angewandte Molekularbiologie,
Universität, Duesbergweg 6, D-55099 Mainz, German

Yu. N. Kulchin

Institute for Automation and Control Processes of Far Eastern Branch of RAS,
Radio St. 5, 690041 Vladivostok, Russia

A.-K. Lühns

Department of Conservative Dentistry, Periodontology & Preventive Dentistry,
Medical University Hannover, Hannover, Germany

Yoshiki Masuda

Department of Biology, Kawasaki Medical School, Matsushima, Kurashiki-shi,
Okayama, 701-01, Japan

George Mayer

Department of Materials Science and Engineering, University of Washington,
Seattle, WA 98195–2120, USA

Elisa Mele

National Nanotechnology Laboratory of Istituto Nazionale di Fisica della
Materia-Consiglio Nazionale delle Ricerche, Distretto Tecnologico ISUFI,
Università degli Studi di Lecce, via Arnesano, I-73100 Lecce, Italy

Isabel M. Müller

Institut für Physiologische Chemie, Abteilung Angewandte Molekularbiologie,
Universität, Duesbergweg 6, D-55099 Mainz, Germany

Werner E.G. Müller

Institut für Physiologische Chemie, Abteilung Angewandte Molekularbiologie,
Universität, Duesbergweg 6, 55099 Mainz, Germany

I.G. Nagorny

Institute for Automation and Control Processes of Far Eastern Branch of RAS,
Radio St. 5, 690041 Vladivostok, Russia

Filipe Natalio

Institut für Physiologische Chemie, Abteilung Angewandte Molekularbiologie,
Universität, Duesbergweg 6, D-55099 Mainz, Germany

Carole C. Perry

School of Science and Technology, Nottingham Trent University, Clifton Lane,
Nottingham NG11 8NS

Dario Pisignano

National Nanotechnology Laboratory of Istituto Nazionale di Fisica della
Materia-Consiglio Nazionale delle Ricerche, Distretto Tecnologico ISUFI,
Università degli Studi di Lecce, via Arnesano, I-73100 Lecce, Italy

Ute Schloßmacher

Institut für Physiologische Chemie, Abteilung Angewandte Molekularbiologie,
Universität, Duesbergweg 6, D-55099 Mainz, Germany

Heinz C. Schröder

Institut für Physiologische Chemie, Abteilung Angewandte Molekularbiologie,
Universität, Duesbergweg 6, 55099 Mainz, Germany

Wolfgang Tremel

Institut für Anorganische Chemie und Analytische Chemie, Universität,
Duesbergweg 10–14, D-55099 Mainz, Germany

Elena Veynberg

Limnological Institute, Siberian Branch of the Russian Academy of Sciences,
Ulanbartorskaya 3, RUS-664033 Irkutsk, Russia

S.S. Voznesensky

Institute for Automation and Control Processes of Far Eastern Branch of RAS,
Radio St. 5, 690041 Vladivostok, Russia

Xiaohong Wang

National Research Center for Geoanalysis, 26 Baiwanzhuang Dajie, CHN-100037
Beijing, PR China

Matthias Wiens

Institut für Physiologische Chemie, Abteilung Angewandte Molekularbiologie,
Universität, Duesbergweg 6, D-55099 Mainz, Germany

Petra Wrede

Institut für Physiologische Chemie, Abteilung Angewandte Molekularbiologie,
Universität, Duesbergweg 6, D-55099 Mainz, German

Overview of Geology and Tectonic Evolution of the Baikal-Tuva Area

Dmitry Gladkochub and Tatiana Donskaya

1	Introduction	4
2	Major Geological Structures of the Baikal-Tuva Region	5
2.1	The Siberian Craton	5
2.2	Central Asian Orogenic Belt	5
3	Main Tectonic Units of the Baikal-Tuva Region and Studied Lakes Basins Development	7
3.1	Geology, Tectonics, and Cenozoic Activity of the Baikal Unit	7
3.2	Geology, Tectonics, and Cenozoic Activity of the Khubsugul Unit	14
3.3	The Geology and Tectonics of the Tuva Unit	20
4	Conclusions	22
	References	23

Abstract This chapter provides the results of geological investigations of the main tectonic units of the Baikal-Tuva region (southwestern part of Siberia) during the last decades: the ancient Siberian craton and adjacent areas of the Central Asian Orogenic belt. In the framework of these main units we describe small-scale blocks (terranes) with focus on details of their inner structure and evolution through time. As well as describing the geology and tectonics of the area studied, we give an overview of underwater sediments, neotectonics, and some phenomena of history and development of the Baikal, Khubsugul, Charygtai, and Tore-Chol Lakes basins of the Baikal–Tuva region. It is suggested that these lakes’ evolution was controlled by neotectonic processes, modern seismic activity, and global climate changes.

D. Gladkochub (✉)

Institute of Earth’s crust, the Siberian Branch of Russian Academy of Sciences,
Lermontov St., 128, Irkutsk, Russia
e-mail: gladkochub@mail.ru

1 Introduction

The Baikal-Tuva region is a territory in the south of eastern Siberia located between Lake Baikal to the northeast and the Russian–Mongolian border to the southwest. As an administrative unit, this area belongs to Irkutsk region, Buriatia and Tuva Republics (all of the Russian Federation), and northern Mongolia.

In terms of geology, the Baikal-Tuva region corresponds to two main geological structures of northern Eurasia – the Siberian craton and the Central Asian Orogenic belt. A short overview is given below in terms of “Terrane analyses.” A terrane is a crustal block or fragment that preserves a distinctive geologic history that is different from the surrounding areas and that is usually bounded by faults (Gary et al. 1972; Parfenov et al. 1993). Superterraneans are defined as composite terranes grouping individual terranes and other assemblages sharing a distinctive tectonic history. The International Stratigraphic Chart (Gradstein et al. 2004) which provides the explanation of the geological time (eon, era, period, age) used in this chapter is presented in Table 1.

Table 1 The International Stratigraphic Chart (Simplified after Gradstein et al. 2004)

	Eon	Era	Period	Epoch	Age, Ma			
P h a n e r o z o i c	C e n o z o i c	Cenozoic	Quaternary		Holocene	0-2		
					Pleistocene			
			Tertiary	Neogene		Pliocene	2-5	
						Miocene	5-23	
						Oligocene	23-34	
				Paleogene		Eocene	34-65	
						Paleocene	56-65	
			Mesozoic	Cretaceous				65-145
				Jurassic				145-200
	Triassic				200-251			
	Permian				251-299			
	Paleozoic	Carboniferous	Pennsylvanian		299-318			
			Mississippian		318-359			
		Devonian				359-416		
		Silurian				416-444		
		Ordovician				444-488		
Cambrian				488-542				
Proterozoic	Neoproterozoic				542-1000			
	Mesoproterozoic				1000-1600			
	Paleoproterozoic				1600-2500			
Archean	Neoarchean				2500-2800			
	Mesoarchean				2800-3200			
	Paleoarchean				3200-3600			
	Eoarchean				3600-4600			

2 Major Geological Structures of the Baikal-Tuva Region

2.1 *The Siberian Craton*

The Siberian craton contains a few of the oldest fragments of the continental crust present on the Earth's surface. Most of the Siberian craton building blocks are by age Archean (Rosen 2003). The oldest zircons discovered in the Siberian craton basement complexes show an age of about 3.4 giga annum (Ga) (Poller et al. 2005; Bibikova et al. 2006) and even 3.6 Ga (Smelov et al. 2001). Major tectonic and metamorphic events caused by the assembling of the Siberian craton occurred at ~2.1–1.8 Ga (Rosen 2003; Poller et al. 2004). These Paleoproterozoic metamorphic and tectonic processes broadly coincide with important orogenic events on nearly every continent (Zhao et al. 2002), and are possibly related to an assembly of the older putative Paleoproterozoic supercontinent (Condie 2002; Zhao et al. 2002).

Some minor extensional events in Siberian craton occurred in Mesoproterozoic (~1.6–1.0 Ga) causing the appearance of intra-continental basins (Gladkochub et al. 2002, 2008). No traces of the Grenville-age (~1.2–1.0 Ga) orogeny were found in the Siberian craton, implying that this craton was on the periphery of the Rodinia supercontinent (Gladkochub et al. 2001, 2006a, b). Southern parts of the eastern and western cratonic boundaries probably faced the ocean since the Early Mesoproterozoic (~1.3 Ga). Evidence for Mesoproterozoic passive margins in the northern part of Siberia is less convincing. Passive margins developed along the southwestern Siberian boundary later, in the Neoproterozoic (~0.8 Ga) (Gladkochub et al. 2006b). This might have been caused by the break-up of Rodinia and the opening of the Paleoasian Ocean.

The main igneous events in the Phanerozoic [since 540 mega annum (Ma) until now] stage of the Siberian craton evolution were widespread intrusions of basaltic rocks (trapps) (~250 Ma). By the Cenozoic (~25 Ma), the Baikal rift system was formed along the Siberian craton's southern flank. This rift system is characterized by distinct morphological features, intensive basaltic volcanism, considerable geophysical anomalies, and high seismic activity (Logachev 1984). The development of the Baikal rift system still proceeds now and is accompanied by numerous and rather strong earthquakes.

2.2 *Central Asian Orogenic Belt*

The Central Asian Orogenic belt (Hu et al. 2000; Jahn et al. 2000) or Central Asian mobile belt (according to Zonenshain et al. 1990) traces along the southern margin of the Siberian craton. The Orogenic belt in the area studied is separated from the craton by the Main-Sayan and Primorsky Faults (Fig. 1). Like most accretionary orogens that are as wide as they are long, the Central Asian Orogenic belt extends

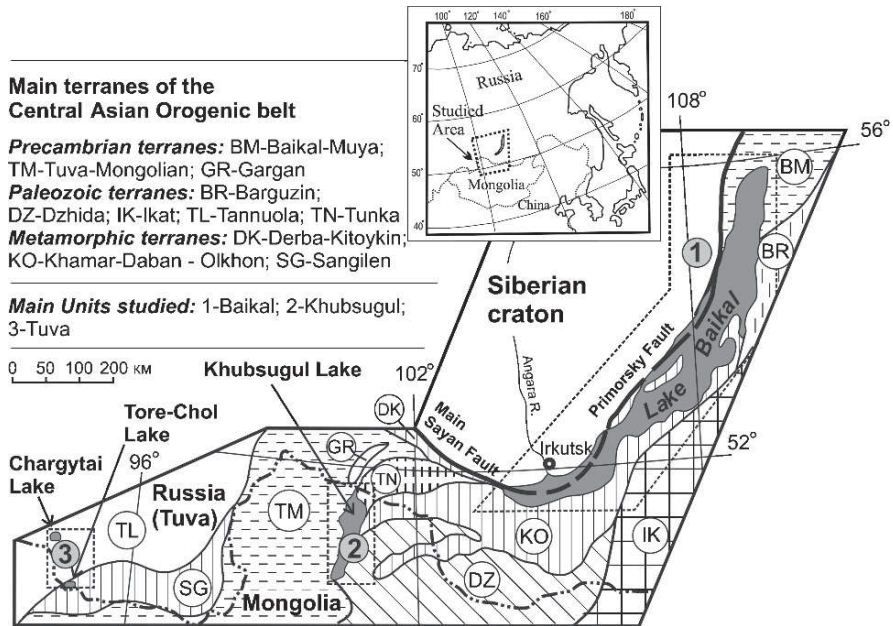


Fig. 1 Tectonic (terrace) scheme of the Baikal-Tuva region (Compiled after Sklyarov et al. 2001)

from the Urals to the Pacific Ocean and from the Siberian and East European (Baltica) cratons to the North China (Sino-Korean) and Tarim cratons. It began its growth at ca. 1.0 Ga (Khain et al. 2003) and continued to ca. 250 Ma.

Early (Vendian–Ordovician) accretion events in the Central Asian Orogenic belt took place when East European (Baltica) and Siberian cratons were separated by a wide ocean. Island-arcs and Precambrian microcontinents accreted to the margins of ancient crustal blocks (the Siberian, North China and Tarim cratons) or were amalgamated in an oceanic setting (as in the Kazakhstan block) by roll-back and collision, forming a huge accretionary collage (Windley et al. 2006). Closure of the Paleasian and Mongol-Okhotsk oceans might be considered as the main tectonic processes responsible for the Central Asian Orogenic belt generation.

The structure of the Central Asian Orogenic belt close to the Siberian craton is determined by the interaction of the Siberian craton margins and numerous terranes accreted to them during an Early Paleozoic collision event. These collisions were of the terrane-continent type along the southern margin of the Siberian craton and of various versions of the terrane – terrane, island-arc–terrane, and island-arc–island-arc types inside the collision system itself (Fedorovsky et al. 1995). The features of the tectonics, magmatism, and metamorphism of the most widespread island-arc–terrane collision variant are considered by using the Baikal-Tuva region as an example. Such zones are characterized by the obduction of island-arc complexes over terrane margins (with continental-type crust), the formation of fold systems, and the realizing of several metamorphic events.

The Baikal-Tuva area could be subdivided into three main Units according to their territory position: Baikal Unit, Khubsugul Unit, and Tuva Unit. These main Units composed of smaller-scale blocks are called terranes and superterranes.

A terrane is a crustal block that contains a distinctive set of geological complexes (rocks associations) and preserves its own geologic history. A terrane differs from the surrounding areas and is usually bounded by faults.

3 Main Tectonic Units of the Baikal-Tuva Region and Studied Lakes Basins Development

3.1 Geology, Tectonics, and Cenozoic Activity of the Baikal Unit

The Baikal Unit is a mountain area (uplift). The Baikal Lake basin is surrounded by ridges which reach a maximum of about 3,000 m.

The water level of Lake Baikal is 453 m a.s.l., the lake length is 636 km, and the width varies from 26 to 79 km. Baikal depression (basin) is the largest unit in the chain of depressions related to development of the Baikal rift zone (BRZ). Other depressions (Khubsugul, Tunka, etc.) vary in size, depth, and landscape, but have a lot of structural features in common and are of the same origin.

Baikal is a unique geological object on the Earth. One of its remarkable features is the distance between the top of the ridges surrounding the lake (~2,840 m), the maximal depth (1,637 m) and the ediments thickness of the Baikal basin (8,500 m). The sum of these values is 12,977 m; this value is about 2 km deeper than the deepest point of the Earth (Mariana Trench). Such a deep rift valley is currently not known anywhere else on the Earth.

The major feature of the Baikal Unit geological structure is that just here lies the boundary between the main tectonic units of northern Eurasia: the Siberian craton (platform) in the west and the Central Asian Orogenic belt in the east. The western shore of Lake Baikal belongs mainly to the Siberian craton but the eastern coastline (shore) is part of the Central Asian Orogenic belt. According to this feature, the geological complexes of the Baikal Unit could be subdivided into two main groups: mainly Precambrian exposed within its western shore and predominantly Paleozoic outcropped along its eastern shore.

Along the western shore of Lake Baikal there are several well-exposed salients of the Precambrian basement of the Siberian craton such as the Sharizhalgai, Goloustnaja, Primorsk, and Baikal blocks (Fig. 2). The dominant crystalline rocks are gneisses, schists, amphibolites, granulites, migmatites, and granitoids. The majority of these rocks are rich in silica.

The metamorphic complexes of the Sharizhalgai salient (Fig. 2) include gneisses, schists, amphibolites, and granulites (mainly acid and rare mafic in composition). Among these occur beds of marbles and sillimanite-rich rocks. On the basis of

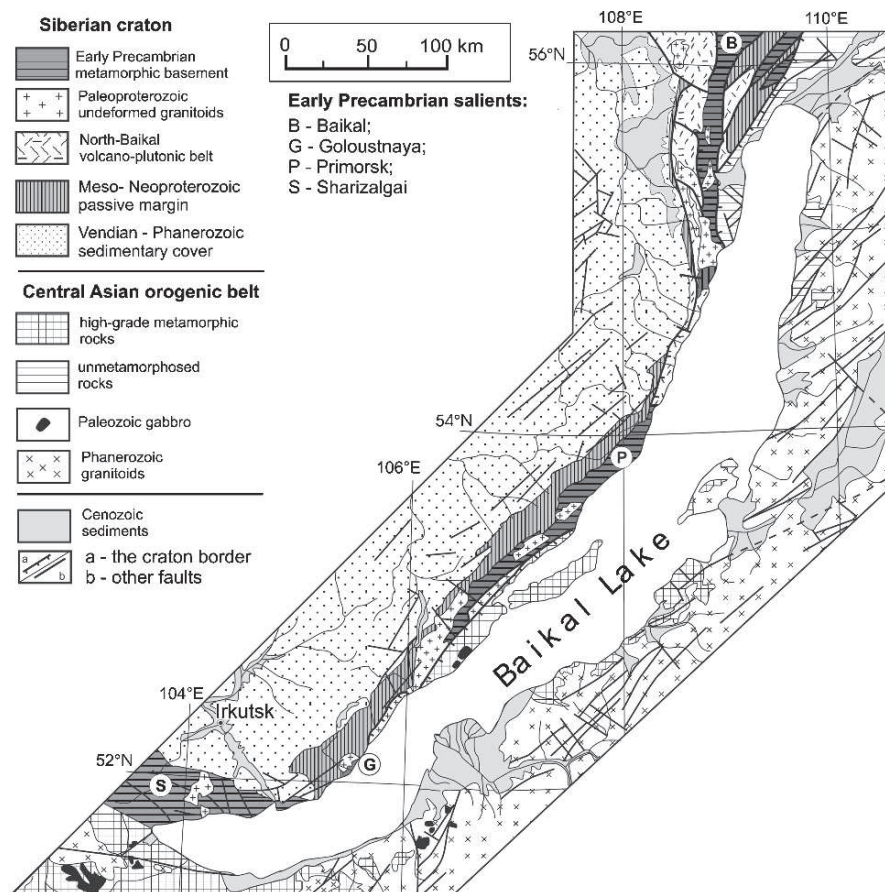


Fig. 2 The geological map of the Baikal area (Baikal Unit)

geochronological data reported by Aftalion et al. (1991) and Poller et al. (2005) for the igneous and metamorphic rocks of the Sharizhalgai salient two age groups were distinguished: Archean and Paleoproterozoic. The Paleoproterozoic are common for voluminous granite complexes intruding the Archean rocks.

The Goloustnaja salient is exposed on the western coastline (shore) of Lake Baikal (Fig. 2). The salient consists of migmatite, gneiss, and amphibolite. This metamorphic basement complex is intruded by the 2.0 and 1.86 Ga-old granites (Donskaya et al. 2003; Poller et al. 2005).

The Primorsk salient (Fig. 2) is composed of the Paleoproterozoic schists, gneisses, amphibolite, and rare granulite. The metamorphic section of the salient is intruded by 1.86 Ga rapakivi-like granite.

The basement of the Baikal salient (North-Baikal Ridge) (Fig. 2) is built by Archean (2.9 Ga) foliated tonalite (alkaline-poor granite) and Paleoproterozoic metamorphic rocks including metamorphosed sediments and volcanics. All these rocks

regarded as basement complex are covered by volcanic and volcanic-sedimentary sequence of the Akitkan series (1.87–1.85 Ga) (Larin et al. 2003) and intruded by Paleoproterozoic granites. Volcanic, volcanic-sedimentary rocks, and granite are usually considered as the North-Baikal volcanic plutonic belt (Fig. 2).

Recent geological and geochronological studies give evidence for a multistage evolution of the basement salient of the Siberian craton exposed along the western shore of Lake Baikal. It starts with an Archean precursor (~3.4 Ga) and includes Archean (~2.6 Ga) and Paleoproterozoic (~1.9 Ga) granulite (high-grade metamorphism) formations. Additionally, a Proterozoic migmatization (~2.0 Ga) event and two stages of granite emplacement (~1.88 and 1.85 Ga) along the margin of the craton have been documented as happening in the Paleoproterozoic (Poller et al. 2005).

Neoproterozoic sedimentary rocks regarded as passive-margin sediments are exposed within the western shore of Lake Baikal (Fig. 2). They are represented (from the bottom to the top) by the Baikal Formation (Goloustnaya, Uluntui, Kachergat suites), and the Ushakovka and Kurtun suites. Passive margin sediments are overlaid by Late Neoproterozoic–Early Cambrian deposits of the Siberian craton sedimentary cover (Usol'e suite).

Basal beds of Baikal Formation (Goloustnaya suite) in the area studied are represented by dolomites or arkosic-graywacke conglobreccias overlying ~1.86 Ga granites (Donskaya et al. 2005). Feldspar-quartz, quartz sandstones, and dolomites are typical for the lower part of the Baikal Formation. There are dark carbon-bearing limestones and silt-pelite schists in the upper parts of the Goloustnaya suite. The middle part of the Baikal Formation (Uluntuy suite) begins with siltstones and sandstones. The upper part of this suite is represented by stromatolite and oncolite bearing limestones and lime-dolomites. The basal beds of upper part of the Baikal Formation (Kachergat suite) are composed of aleurolite-sandstones, siltstones, and claystones with feldspar-quartz sandstone bands. Snuff-color and dark carbon-bearing silt-claystones are typical of the uppermost parts of the suite.

The Neoproterozoic sedimentary sequences of the Siberian craton are completed by conglomerates of the Ushakovka and Kurtun suites. Composition of the clastogenic part of their sediments is polymictic, arkosic-graywacke up to feldspar-quartz in the upper layers (Stanevich et al. 2001). The beginning of the Ushakovska period is determined by maximum sea transgression on the craton.

Phanerozoic sedimentary cover of the Siberian craton is represented within it, and the nearby Western Baikal coastline is represented mainly by Early Paleozoic (Cambrian) and Mesozoic (Jurassic) Formations. Cambrian sections contain mainly dolomite and limestones with salt-bearing beds. These carbonatic rocks are locally silicified. Jurassic sediments are represented by conglomerate, sandstone, and aleurolite. Some parts of this sequence contain coal beds.

In the northern part of the Central Asian Orogenic belt, in the framework of the Baikal Unit, the Baikal-Muya, Barguzin, Ikat, and Khamar-Daban-Olkhon terranes (Fig. 1) are located.

The Baikal-Muya terrane (Fig. 1) extends from northern Baikal in the west to the Vitim River in the east. In the lower parts of the terrane section occur relicts of Precambrian continental crust (Muya massif), ophiolite sequences, and island-arc

complexes. Ophiolite sequences (fragments of ancient oceanic crust) include metabasalts, hemipelagic sediments, slices of metagabbro, and ultramafic rocks. The Neoproterozoic island-arc complexes consist of basalt-andesite-plagioryholite volcanic series and gabbro-plagiogranite intrusive massifs. Ophiolite and island-arc rock associations are metamorphosed under greenschist facies pressure–temperature (P–T) conditions. The upper part of the Baikal-Muya terrane is composed of non-metamorphosed Late Neoproterozoic–Early Cambrian terrigenous-carbonate series. Paleozoic granites intrude metamorphosed as well as non-metamorphosed complexes of the Baikal-Muya terrane (Fig. 2).

The Barguzin terrane (Fig. 1) is composed of predominantly Paleozoic (~300 Ma) granites (Fig. 2). The majority of these granites are regarded as huge-scale Angara-Vitim batholith. Rare relicts of earlier volcanic-sedimentary sequences locally spread within the Barguzin terrane, however, have abundant Paleozoic granites making it difficult to recognize the nature and age of these rocks (Sklyarov et al. 2001).

The Ikat terrane consists mostly of Vendian-Cambrian terrigenous, terrigenous-carbonate, carbonate, and volcanic-sedimentary sequences. The carbonate sequence includes fossil-bearing limestones and dolomites. The terrigenous sequence belongs to the flysch formation. Sedimentary and volcanic-sedimentary rocks are composed of relatively small blocks remaining after intrusion into the sequence of Early and Late Paleozoic granitoids. Among sediments and granites occur rare slices of serpentinized dunite and peridotite.

The Khamar-Daban–Olkhon metamorphic terrane extends from Lake Khubsugul in the southwest to the northeastern shore of Lake Baikal. Pressure–temperature (P–T) conditions of metamorphic alterations of rock complexes of the terrane vary from amphibolite to granulite facies. For a long time, the age of the metamorphic series was believed to be Paleoproterozoic and even Archean. Recent data allow us to recognize the Early Paleozoic age of high-grade (granulite) metamorphism corresponding to the range of 500–480 Ma (Bibikova et al. 1990; Salnikova et al. 1998; Fedorovsky et al. 2005; Gladkochub et al. 2008). The terrane is composed of carbonate-terrigenous and terrigenous series. The age of the protholith is supposed to be Early Paleozoic up to Archean, on the basis of the Nd model (Fedorovsky et al. 2005; Mishina et al. 2005) and ages of detrital zircon cores (Gladkochub et al. 2008). The Khamar-Daban–Olkhon terrane is considered as a fragment of combination of passive margin (Reznitsky et al. 2004) and relicts of island-arc systems accreted to the Siberian craton in the Early Paleozoic (Fedorovsky et al. 1995; Gladkochub et al. 2008).

3.1.1 Cenozoic Sediments of Baikal Unit and Baikal Depressions Formation

Cenozoic sediments are most spectacularly represented in depressions of Baikal rift system (Baikal, Tunka, Khubsugul, etc.). Lower parts of the Cenozoic section (Paleocene–Eocene) are composed of red-colored clay sediments corresponding

to kaolinitic, hydromica-koalinitic, and allitic clays in mineral composition. Some clay sections contain layers of bauxite, phosphorite, and coal.

Deposition of these sediments was related to continental crust weathering processes and pre-rifting surface erosion. The thickness of the Paleocene–Eocene sediments in the Baikal rift system reaches 450 m.

Middle part of Cenozoic section (Oligocene–Upper Pliocene) consists of green-colored polymineral (often monomineral–montmorillonitic) clay, aleurolite, coal, rare sands, and limestones (Logachev 1984). Numerous basalt intrusions occur in the Oligocene–Miocene sequence located near the southern extremity of Lake Baikal (Tunka depression).

Upper Pliocene alluvial-proluvial boulder-pebble deposits occur in the south of Lake Baikal and in the Tunka depressions. These sediments contain mammalian remains and malacofauna.

The thickness of the middle part of Cenozoic sediments is a few hundreds of meters. The maximum depth of the Eocene sediments distribution is reported for the Selenga River delta region. Here, Eocene age sediments were found at the level of 2,900 m in a drill hole.

The upper part of the Cenozoic section (Pliocene–Holocene) begins with sub-aerial sediments (loess and soil) and sands. Sometimes, glacial and lacustrine facies occur in the sandy sequence. Upper levels of these sections are mainly composed of coarse-grained sediments sometimes with glacial deposits (Logachev 1984).

Lake Baikal's original slopes and its bottom were investigated in 1990–1991 within the framework of the International Program “Global Changes in Inner Asia on the Basis of Complex Studies of Lake Baikal.” The results of deepwater investigations were obtained by using manned submersibles “Pisces” (Bukharov and Fialkov 1996). Further, during 1989–1999, under the joint Russian–American–Japanese “Baikal Drilling Program,” five sets of boreholes were drilled in various sites of the lake. The main results of this Program were presented in detail in Kuz'min et al. (2001). The investigations of the Baikal slope and bottom sequences mentioned above were focused on studying the main depressions divided within the lake basin. Within Lake Baikal, three main depressions are found: Southern, Central, and Northern (Kuz'min et al. 2001 and references therein). The Southern and Central depressions are frequently considered together as the Central depression (Fig. 3) (Bukharov and Fialkov 1996).

The results of the deepwater investigations and drill cores analyses in combination with earlier reported data (Goldyrev 1982; Logachev 1984), and investigations of sedimentary sequence of the Baikal depressions by methods of seismic profiling, provided additional details of the sedimentary sequences of the inner structure and gave a background for the reconstruction of the main events in the depressions' evolution. The simplified scenario of Baikal basin evolution is presented in Fig. 4.

On the basis of combined stratigraphic and seismic data, the Baikal bottom sedimentary sequences were subdivided into four main groups (complexes) (Bukharov and Fialkov 1996).

The lowest (fourth from the top) complex of Baikal bottom sediments (Fig. 4a) is composed of sand, aleurolite, and argillite. The age of this complex is suggested

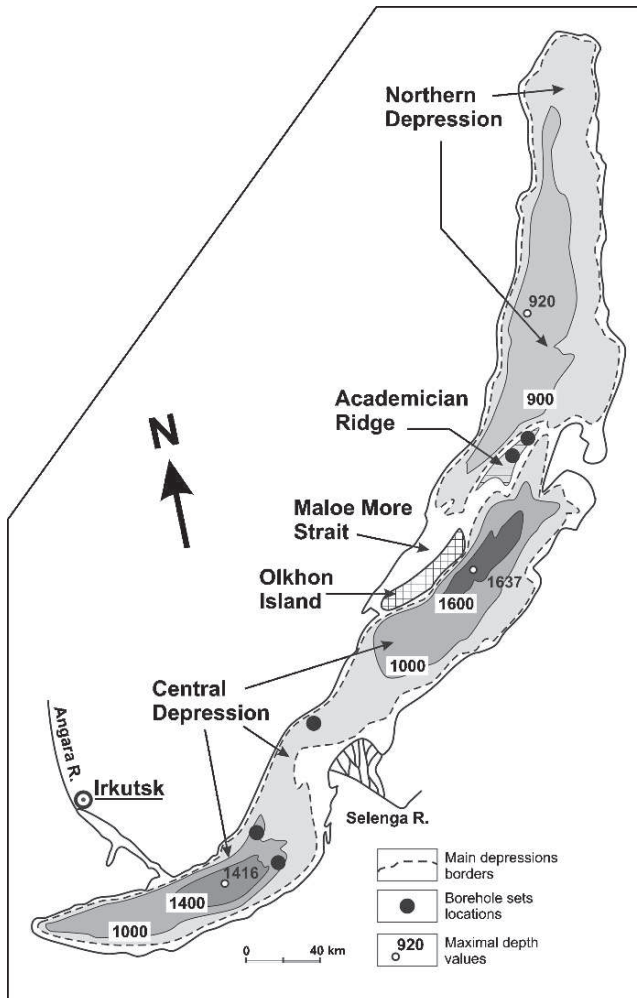


Fig. 3 Simplified scheme of the Baikal basin with the locations of the main depressions (Bukharov and Fialkov 1996)

to be Miocene–Early Pliocene. These sediments are considered as evidence of the earliest stage of the Central Baikal depression formation (Fig. 4a). The maximal thickness of “fourth” complex sediments (up to 2 km) is reported for the southern extremity of the Central Baikal depression. In the Northern depression of Lake Baikal, the same kind of sediments are almost absent. Similar sediments have a local distribution in the northern part of this depression only where they are interpreted as the deposits of small lakes.

According to seismic observations done by Nikolaev et al. (1985), 50- to 60-m-thick relicts of terrigenous sediments regarded as “fourth complex” occur on the

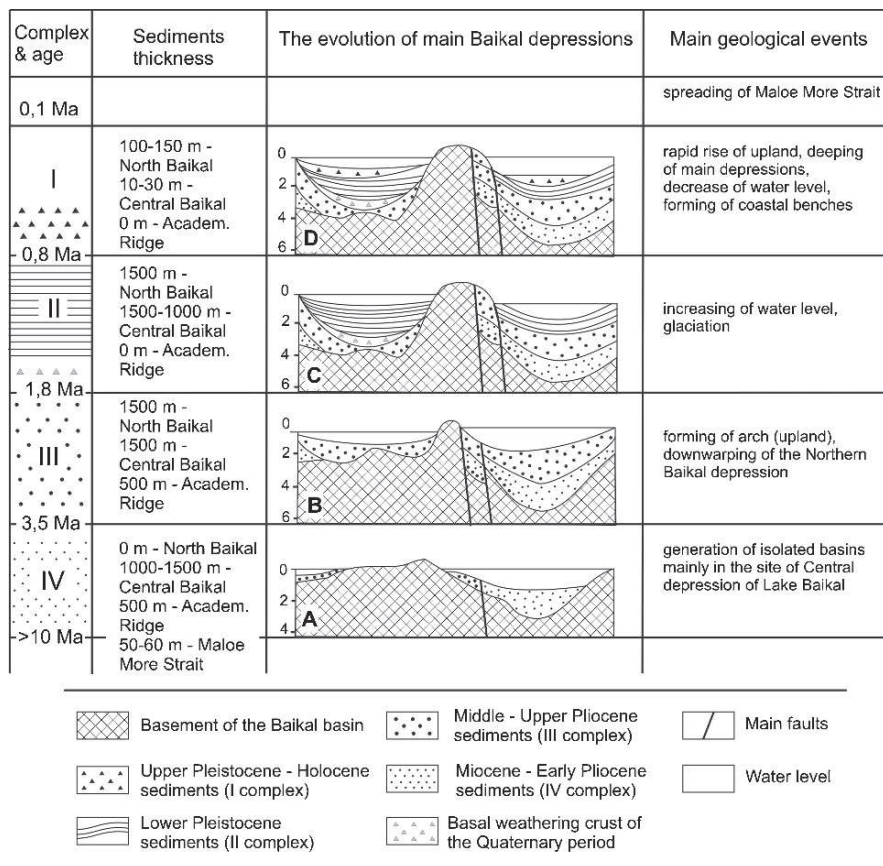


Fig. 4 Main stages of Lake Baikal basin evolution (Modified after Bukharov and Fialkov 1996)

southern slope of the Northern depression (Maloe More Strait area). Such distribution of the earliest sediments of Lake Baikal allows to consideration of the existence of mountain ridges which separated the Central and Northern depressions in the Early Neogene (Miocene up to Early Pliocene) period (Fig. 4a).

The third sedimentary complex is composed of sand and clay. According to stratigraphic correlation, the age of this complex is suggested to be Middle–Upper Pliocene. The thickness of these sediments is about 1.5 km in the Central depression and about 0.5 km on the ridge located between the Central and Northern depressions (Academician Ridge) (Fig. 4b). In the basin between Olkhon Island and the lake’s western coast (Maloe More Strait), Middle–Upper Pliocene (“third complex”) sediments have never been observed. During this period, the Academician Ridge represented a highland on which there was an accumulation of red-colored subaerial clay and loess. In the Upper Pliocene, there began a downwarping of the northern part of Baikal territory that has resulted in the formation of the Northern depression.

The second sedimentary complex is represented by bedding of clays and sands. In southern Baikal and in the Central depression, the thickness of these sediments is usually about 1.0–0.5 km or even less than hundreds of meters (Fig. 4c). The maximal thickness of the “Second sedimentary complex” (~1.5 km) is reported from the Northern depression. These sediments are absent on the Academician Ridge and only locally distributed in the bottom section of Maloe More Strait. Disconformity in the basis of the Second sedimentary complex is very important for understanding the sedimentation processes in Lake Baikal as reflected by the boundary between the Pliocene and Quaternary systems. In terrestrial areas of the Baikal region, this boundary is marked by an Early Quaternary weathering crust consisting of thick residual deposits (gruses) with traces of glacial erosion.

The upper part of the Baikal bottom sedimentary sequence (“First complex,” Fig. 4d) consists of pelite, clay, and mud. The thickness of such sediments varies from 20–30 m in the Central depression up to 100–150 m in the Northern depression (Fig. 4c). On the Academician Ridge, these sediments are unknown. The age of the “First sedimentary complex” is considered as Middle–Upper Pleistocene.

3.2 Geology, Tectonics, and Cenozoic Activity of the Khubsugul Unit

The Khubsugul Unit is located within the Central Asian Orogenic belt. The formation of the Trans-Khubsugulian step-arch uplift can be suggested as the main event in the Unit structures development (Marinov 1967; Zolotarev et al. 1989). The Khubsugul depression has been formed in the axial part in the Cenozoic. The depression is a normal graben produced by long-living downwarping processes, accompanied by faulting. This graben-forming stage is not yet finished for the Khubsugul Unit (Zolotarev et al. 1981, Krivonogov et al. 2004). As the result of these movements, the Trans-Khubsugulian step-arch uplift was divided into the West-Khubsugul dome-blocky uplift and the East-Khubsugul arch-like structure during the neotectonic stage. The border between these two structures is the Khubsugul rift basin (Zolotarev et al. 1989).

The major part of the Khubsugul Unit is engaged in the Tuva–Mongolian microcontinent (terrane) (Fig. 1). The northeastern part of the Unit consists of Khamar-Daban-Olkhon and Tunka terranes. At the southern part of the Khubsugul Unit, the Dzida terrane rock associations are well exposed.

Granite complexes and basalt fields are widespread along the northern and eastern coasts of Lake Khubsugul. In the central part of the Unit is located the Khubsugul depression. This depression belongs to the Baikal rift system.

The oldest rocks of the Khubsugul Unit are outcropped in the Tuva–Mongolian terrane.

The Tuva–Mongolia terrane is one of several Precambrian microcontinents (or superterranes) incorporated into the Central Asian Orogenic belt (Fig. 5). The base-ment of the Tuva–Mongolian terrane could be regarded as a collage of Meso- and

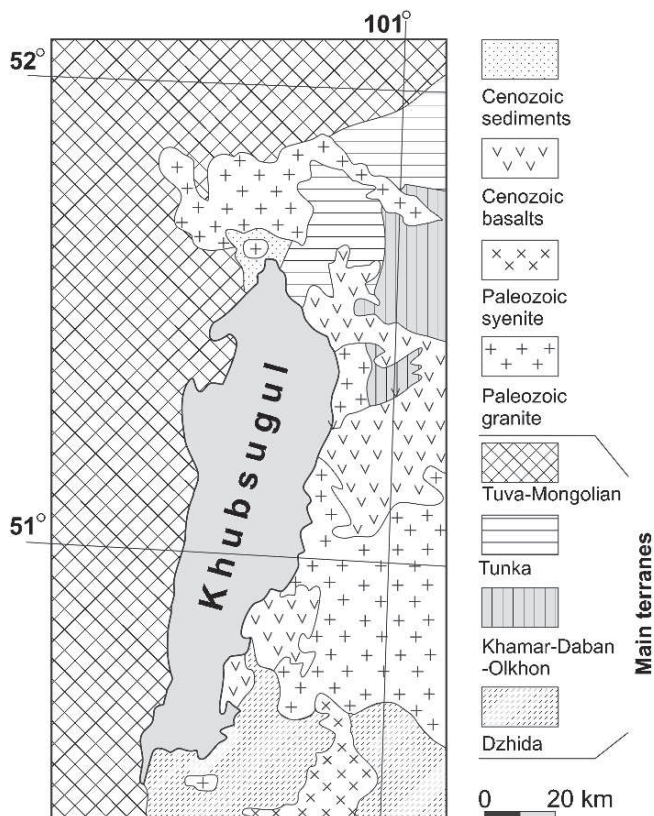


Fig. 5 Tectonic scheme of the Khubsugul Unit (Modified after Belichenko et al. 2005)

Neoproterozoic fragments of oceanic crust (ophiolites), island-arcs, and relicts of Early Precambrian (even Archean; see Fig. 1) rock associations. The basement complex of the Tuva–Mongolian terrane concludes the Gargan sub-terrane (Fig. 1). This sub-terrane composed of amphibolites, tonalite, and granite-gneisses with relicts of mineral paragenesis reflecting high-grade metamorphic alteration (granulite metamorphism). The oldest tonalite of the Gargan sub-terrane has an age of 2.7 Ga (Kovach et al. 2004). The Neoproterozoic sedimentary cover of the Tuva–Mongolian terrane is represented mainly by carbonate rocks including dolomites and limestones with layers of bauxites and phosphorites which were deposited under a sub-platform geodynamic setting. The Late Neoproterozoic (Ediacaran)–Early Cambrian sediments overlie the Precambrian basement and Neoproterozoic deposits of the Tuva–Mongolian terrane. The terrigenous (sandstones, aleurolite) and carbonate sediments of the terrane cover were accumulated under a stable tectonic regime in continental shelf (slope) setting. In the early Ordovician, the Tuva–Mongolia terrane collided with the surrounding terranes and was attached to the southern part of the Siberian craton.

The Derba–Kitoykin metamorphic terrane (Fig. 1) was formed as result of the collision of the Tuva–Mongolian terrane with the Siberian craton's southern margin. This collision event was accompanied by strong deformation, metamorphism, and abundant granite intrusion into the transition zone between the Tuva–Mongolia terrane and the Siberian craton. The width of zone of granulite facies metamorphic rocks reaches up to 5–6 km. This terrane can be traced along the margin of craton for a distance more than 200 km. This terrane is composed of high-grade metamorphic series (originally carbonate-terrigenous sequence, regarded as fragments of Mesozoic and Neoproterozoic passive margin). The age of the metamorphic event was reported by Donskaya et al. (2000) as 473 Ma. This age corresponds strongly to the beginning of the Central Asian Orogenic belt building.

The Dzhida terrane (Fig. 5) unites three different types of complexes: relicts of island-arc, seamounts (or oceanic uplands), and flysch of marginal paleo-basins. All these complexes were brought together during the Late Paleozoic collision.

The essential part of the island-arc relicts of the Dzhida terrane consists of igneous rocks (plagiogranite-tonalite-diorite). Volcanic rocks are less well distributed and include basalt (with the bodies of ultramafic rocks), andesite, and rhyolite. The island-arc-type sedimentary sequence is composed mainly of limestones and red conglomerates. The Dzhida seamount represents large-scale allochthon. The lower part of the Dzhida seamount includes large tectonic blocks of ancient oceanic crust (mafic and ultramafic rocks). The top of the section is represented by subalkaline basalts, limestones, silicilitic sediments, and dolomites. Limestones are often represented by oolitic varieties. They are pure, with a carbonate content of 96–98%. The admixture is mainly represented by autigenic quartz. Silicites form separate layers and interlayers in the limestones, but rarely among the volcanites. They consist of 80–98% of silicic minerals. The admixture is represented mainly by opaque minerals or carbonaceous material and clay mineral (up to 15% wt.). In the silicites, the key role belongs to material of biogenic or hydrothermal genesis. The dolomites sequence consists of dolomites with subordinate limestones, micro-quartzites, rare volcanoclastite, aleuropelites, argillites, and clayish dolomite layers. According to the features of the dolomite sequence (association of the dolomites with red aleuropelites, presence of barite, typomorphism of silica minerals in concretions, absence of terrigenous material, etc.), their deposition setting may be interpreted as a basin with limited water exchange and high evaporation (Gordienko and Filimonov 2005).

The upper part of the Dzhida terrane sequence (flysch) is divided into four main rock associations: psephytic (including conglomerates and rhythmic sandstones of different grain size), terrigenous (sandstones), carbonate-terrigenous (fine-grained carbonate psammites and sandstones), and olistostrome (carbonate sandstones, limestones, siliceous rocks) sediments.

The geodynamic environment of the flysch sequence deposition can be suggested as a paleo-basin connected with island-arcs (Gordienko and Filimonov 2005). The age of this basin is Silurian–Devonian, according to microfossil findings (miospore, acritarchs, chitinzoa).

The Khamar-Daban–Olkhon metamorphic terrane in the Khubsugul Unit (Fig. 5) is only locally represented in its northern part. The main part of this terrane in the area studied is composed of metamorphosed terrigenous and carbonate-terrigenous sediments of the Late Neoproterozoic (Ediacaran)–Early Paleozoic. As against the Baikal Unit, the degree of metamorphic alteration of the Khubsugul Unit complexes does not reach high-pressure and high-temperature conditions and is usually limited by P–T values of amphibolite (not granulite) facies. The metamorphosed sedimentary sequence of the Khamar-Daban–Olkhon terrane in frame of the Khubsugul Unit has a rhythmic structure mainly composed of sediments of passive-continental margin. A chaotic complex related to the Late Paleozoic continental collision includes large tectonic blocks of the Early Paleozoic shelf and continental slope sediments as well as littoral and continental sediments of small paleo-basins of the Late Devonian–Carboniferous age (Gordienko and Filimonov 2005). Mafic-ultramafic complexes associated with the chaotic complex of the Khamar-Daban–Olkhon terrane have a local distribution within the Khubsugul Unit.

The Tunka terrane (Fig. 5) is composed of metamorphosed sedimentary and volcanic-sedimentary complexes. Two main sequences building the terrane may be distinguished: predominantly sedimentary (including carbonate and terrigenous rocks), and volcanic (volcanic-sedimentary). The sedimentary sequence is represented by metamorphosed limestone, dolomite, and metasandstones. The volcanic and volcanic-sedimentary sequence includes basalts and tuffs of mafic/intermediate composition. The age of the Tunka terrane protholith is supposed to be Lower Paleozoic according to the microfossil findings. The geodynamic setting is responsible for the Tunka terrane sediments and volcanic generation is considered as back-arc basin on the basis of sequence stratigraphy analyses and the chemical characteristics of the basalt investigated.

The granite complexes are widespread in the Khubsugul Unit and comprise about a quarter of its territory, surrounding the Khubsugul depression (Fig. 5) mainly along its eastern part. The granite massifs are concentrated along contacts of the Tuva–Mongolian, Tunka, Khamar-Daban–Olkhon, and Dzhida terranes. The age of the granite intrusions varies from 470 to 490 Ma and reflects the time of accretion (uniting) these terranes into one common structure within the Central Asian Orogenic belt.

Cenozoic basalt covers represent a volcanic formation, and this is broadly developed in the Khubsugul Unit (Fig. 5). Eastward from the lake, the covers occupy extensive watershed areas. The significant part of the basalts was destroyed by denudation and washed down to Lake Khubsugul. In general, the basalt covers of the Khubsugul area could be regarded as fragments of a great volcanic plateau. The thickness of the covers is up to 100–150 m. Covers are laminated and consist of 6–10 separate flows. Near the Khubsugul coast, the basalt plateau is usually step-like. In some places, up to 3–4 terrace-like steps, divided by scarps with heights from 5–8 to 30–40 m, are observed (Shuvalov, Nikolaeva 1989). Devyatkin (1982) proposed the existence of centers of volcanism in the place of current Lake Khubsugul, based on regularities of the basalt and pyroclastic

material distribution (Krivonogov et al. 2004). According to available dates, volcanic activity in the Khubsugul Unit occurred during the Late Oligocene–Early Pliocene, mainly in the Miocene (Yarmoluk et al. 2003). Any evidence of later volcanic activity in the area has not been found (Ivanenko et al. 1989; Shuvalov, Nikolaeva 1989).

3.2.1 The Lake Khubsugul Sediments

Gravimetric survey results provided the data on the crystalline basement surface of the Khubsugul depression and the thickness of the sediment cover. According to geophysical data for the basement surface, three main depressions (basins) could be considered. Two of them: the northern and southern ones are more than 700 m deep (Zorin et al. 1989). The maximum thickness of the sediments (about 550 m) is detected in the northern part of Lake Khubsugul. In the southern part of the lake, the thickness of sediments rarely exceeds 350 m (Fig. 6).

On the basis of the stratigraphic correlations of Lake Kubsugul sediments with the Tunka depression, the age of the Khubsugul sediments was reported as the Pliocene and Pleistocene (Zorin et al. 1989). The Oligocene and Middle Miocene sediments are probably absent in the sedimentary section of the lake.

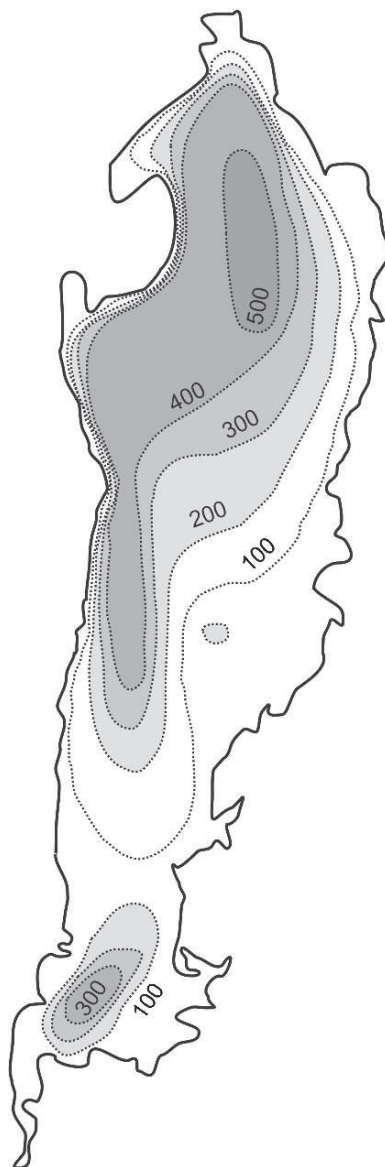
The Lake Khubsugul bottom sediments available for study (upper part of the sedimentary section) are composed of deepwater pelagic silt. Among these sediments, the following variations in composition were recognized (from top to bottom): oxidation area up to 10 cm thick, gray or grayish-green silt, and gray or grayish-blue clay. The oxidized zone is thicker (20–25 cm) on the underwater slopes.

The bottom sediments in the central parts of large bays are similar to those in the deepwater. In general, such sediments are full of sand, mollusk shells, and terrestrial plants. Abundance of carbonates is a distinctive feature of the Lake Khubsugul sediments (Altunbaev, Samarina 1977a). Deepwater silt usually contains 4–6% of carbonate, and sometimes up to 38% (sample with oolite carbonates).

Some detailed information about Lake Khubsugul sediments was obtained during the geothermal study (Golubev 1992). Special probes provided information on properties of the upper 2 m of the bottom sediments. According to this investigation, the upper layer of sediments is described as dark-gray and shine-gray silt (Kazansky et al. 2005; Fedotov et al. 2006). The under-stratum is represented by dense viscous clay with an admixture of sand and rougher material. Clay is colored in yellowish-brown, reddish-brown, and bluish-gray tones.

Sediments of the Pleistocene located on the Khubsugul Lake bottom have been compared to those of the Holocene section. Transition from the Upper Pleistocene to the Holocene resulted in an increase of organic matter from <1 to >6% and of BiSi from 1 to 20% (Grachev et al. 2003). A 220-cm-long core was taken in the northern part of Lake Khubsugul (Hatgal bay). The core consists of peat and clayey gyttja layers. For the basal and middle parts of the sequence, two radiocarbon dates ($5,800 \pm 100$ and $3,910 \pm 60$ years, respectively) were reported. Both these values correspond to the Holocene (Dorofeyuk, Tarasov 1998). The sediment

Fig. 6 Simplified scheme of the Lake Khubsugul basin with thickness of Cenozoic sediments (Zorin et al. 1989)



accumulation rate in the Holocene was estimated as about 4 cm/ky (Grachev et al. 2003). The detailed description of lithology, ground moisture, organic silica, diatom, palynologic, and ostracods analyses of Northern Khubsugul sediments is reported by Fedotov et al. (2001, 2006) and Krivonogov (2000) on web site www.Giscenter.ru/Carpos/Digital_publ/Khubsugul_review2000.

3.2.2 Main Late Cenozoic Events in the Khubsugul Unit

The Khubsugul Unit was a part of a relatively stable territory during the Lower Cretaceous–Paleogene (Ufland et al. 1969) before the beginning of the rifting processes. The crystalline basement of this region felt uplift in the Oligocene–Miocene. This process was continued by basalt explosions. Lava flows formed the basalt plateau during the Late Oligocene–Early Pliocene (Ivanenko et al. 1989; Shuvalov, Nikolaeva 1989). The following stage of the area's evolution is characterized by vertical movements of rather small-scale blocks. This stage started in the Pliocene (Eopleistocene) and continues to the present (Zolotarev et al. 1989). Such orogenic movements caused the formation of the Khubsugul depression, and they are still not completely finished (Zolotarev et al. 1981). The age of the earliest sediments of the Khubsugul Lake is expected to be not older than Pliocene (Zorin et al. 1989).

The maximal glaciation in the Unit took place in the Middle Pleistocene. Ice covered the high mountains in the northern and western parts of the Khubsugul area. A sizeable reduction of the Khubsugul level was probably connected with this glaciation. The Late Pleistocene glaciation was of mountain-and-valley type; its scale was less than that of the Middle Pleistocene one (Krivonogov 2004).

3.3 The Geology and Tectonics of the Tuva Unit

The Tuva Unit is located in western part of the Baikal-Tuva region. Geographically, the Unit covers the area near the border of the Tuva Republic of the Russian Federation and Mongolia (Fig. 7). The area studied has been divided into two main geological complexes, generally northeast trending (Fig. 7), based on lithological and structural observations as well as on geochronological data. According to the tectonic structure of the area, these complexes correspond to the Sangilen metamorphic and Tannuola island-arc terranes (Fig. 1). In the central part of the area studied, metamorphic rocks (schist and gneisses after terrigenous sediments) occur which are considered to be a basement of the Sangilen terrane (or microcontinent) (Fig. 7).

The Sangilen metamorphic terrane basement complex has been reworked by metamorphism and gneiss-dome tectogenesis during the microcontinent collision with the Tannuola island-arc terrane (Fig. 7) (Vladimirov et al. 2000). The crystalline basement of the Sangilen terrane is overlapped by carbonate-terrigenous cover which belongs to the Late Neoproterozoic–Early Paleozoic.

The Agardak back-arc basin complex (Fig. 7), which represents ~10% of the Tuva Unit, consists of an assemblage of metamorphosed mafic and ultramafic rocks (serpentinite), terrigenous sediments (cherts and turbidites), and pillow-lavas. The back-arc complex traces the boundary between the Sangilen metamorphic terrane (microcontinent) and the Tannuola island-arc terrane. The U-Pb zircon age of mafic rock from this assemblage was estimated as about 570 Ma (Vladimirov et al. 2005). Numerous mafic intrusions cut the back-arc basin assemblage.

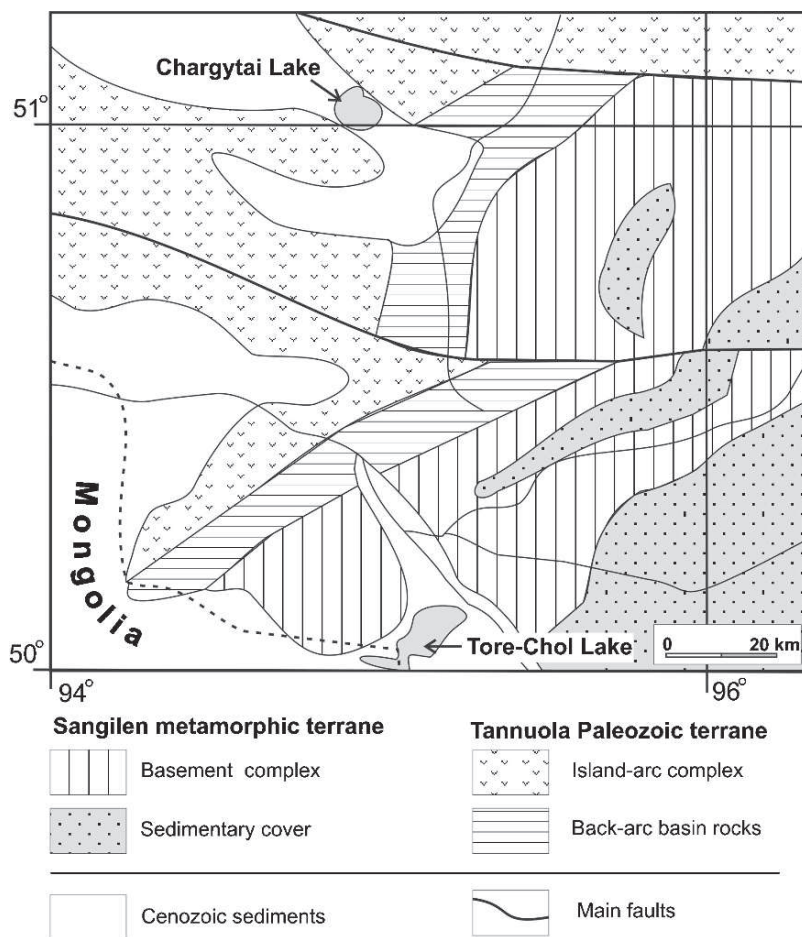


Fig. 7 The tectonic scheme of the Tuva Unit (Modified after Vladimirov et al. 2000)

The Tannuolaterrene in the area studied is represented mainly by Late Neoproterozoic (Ediacaran)–Early Paleozoic island-arc volcanic and sedimentary sequences which are located in the northwestern part of the Unit (Fig. 7). These sequences belong to the Tannuola island-arc. Its volcanic sections are composed of basalts, andesites, and rhyolites. The main part of the sedimentary sequence is composed of carbonate rich in organic material.

The granites are widespread in the Tuva Unit. They intrude the Sangilen terrane basement and its cover assemblages (not shown on Fig. 7 as numerous small granite veins and massifs are less than the scale of the map permits). Moreover, granite cuts the Agardak back-arc and the Tannuola island-arc sequences. The oldest granite massifs were dated at ~470–480 Ma and the youngest granite group represented by rocks yielded a U-Pb zircon age ~440 Ma. Both granite group intrusions were controlled by strike-slip faulting and general extension of the Tuva Unit.

Two main phases of deformation and metamorphism affected the Tuva Unit. The oldest one, Precambrian regional metamorphism of the kyanite type, is restricted to the Sangilen terrane basement schists and gneisses. The second phase (Early Paleozoic), corresponding to amphibolite up to granulite facies, affects all basement, sedimentary cover, back-arc basin assemblage and island-arc complex. Shallow-depth granulites were formed in the Cambrian–Ordovician (540–490 Ma) period. This interval is considered to be the beginning of the Tuva Unit forming by the collision of the Precambrian Sangilen microcontinent (Sangilen metamorphic terrane) and the Tannuola island-arc including the Agardak back-arc basin (Tannuola Paleozoic terrane). The final (post-collisional) stage of the Tuva Unit building is fixed by voluminous intrusion of ~440 Ma granites.

The Mesozoic complexes are not represented in the area studied and therefore Cenozoic sediments lie directly on the Precambrian basement and Paleozoic rocks. The earliest Cenozoic sediments (Miocene) have a local distribution in the area. Such sediments were found in the shaft being explored located to northeastward of Shargytai Lake. Pliocene deposits in the area studied are composed of red-colored clays and adobes. Pliocene sedimentary sequence consists of sands, loamy sands, and adobes. Their thickness reaches 200 m.

3.3.1 Chargytai and Tore-Chol Lakes Sediments

The Chargytai and Tore-Chol are the largest fresh-water lakes in the area studied. The lakes are located in highland depressions. The altitude of their water-level surface is 1,010 and 1,150 m a.s.l., respectively. The average depth of the lakes is about 3–4 m. The maximal depth (17 m) is reported for Chargytai Lake. Both lakes are surrounded mainly by Cenozoic sediments including sands, gravels, and boulder beds.

The bottom sequence of the lakes is composed of Pleistocene clay, adobe, which is covered by gravel and loamy sand. Thickness of lower sediments in the lakes depressions reaches 10 m. Holocene sediments are represented by clay which are locally distributed in the upper part of the lake bottom sequences.

Recently, the reduction in size of both lakes has been observed, probably caused by the influence of modern seismic activity and also by global climate changes.

4 Conclusions

The Baikal-Tuva region has been studied for several decades. As a result, a great deal of data on geology, geophysics, and tectonics of this area have been obtained. However, even at the present time there is not enough information about the underwater geology and evolution of numerous lakes of the Baikal-Tuva region or also of Lake Baikal.

The study of stratigraphy, lithology, and geochemistry of sedimentary strata, hydrothermal activity, and processes of ore formation in lakes of this region remains an real task. All this requires coordination of different fields of research and carrying out them as an indivisible complex.

References

- Aftalion M, Bibikova EV, Bowes DR, Hopwood AM, Perchuk LL (1991) Timing of Early Proterozoic collisional and extensional events in the granulite-gneiss-charnokite-granite complex, lake Baikal, USSR: A U-Pb, Rb-Sr and Sm-Nd isotopic study. *The Journal of Geology* 99:851–861
- Altunbaev VKh, Samarina AV (1977) Characteristics of the Khubsugul Lake bottom sediments. Natural conditions and resources of Trans-Khubsugulia. *Transactions of the Soviet-Mongolian Complex Khubsugulian Expedition* 5:80–90 (in Russian)
- Belichenko VG, Reznitsky LZ, Makrigina VA, Barash IG (2006) Terranes of the Baikal-Khubsugul fragment of the Central-Asian mobile belt: an overview of the problem. In: Sklyarov EV (ed) *Geodynamic Evolution of Lithosphere of the Central-Asian Mobile Belt*, vol 2. IG Press, Irkutsk, pp 37–41 (in Russian)
- Bibikova EV, Karpenko SF, Sumin LV, Bogdanovskii OG, Kirnozova TI, Lyalikov AV, Makarov VA, Arakelyanz MM, Korikovskii SP, Fedorovskii VS, Petrova ZI, Levizkii VI (1990) U-Pb, Sm-Nd, Pb-Pb and K-Ar age of metamorphic and magmatic rocks of the Olkhon area (Western Baikal). In: Shemyakin VM (ed) *Precambrian Geology and Geochronology of the Siberian Platform and Its Periphery*. Nauka, Leningrad, pp 170–183 (in Russian)
- Bibikova EV, Turkina OM, Kirnozova TI, Fugzan MM (2006) Ancient Plagiogneisses of the Onot Block of the Sharyzhalgai Metamorphic Massif: Isotopic Geochronology. *Geochemistry International* 44(3):310–321
- Bukharov AA, Fialkov VA (1996) Geological structure of the bottom of Lake Baikal. Nauka, Novosibirsk (in Russian)
- Condie KC (2002) Breakup of a Paleoproterozoic supercontinent. *Gondwana Research* 5(1): 41–43
- Devyatkin EV (1982) Neogene-Antropogene (stage of neotectonic activation). *Geomorphology of Mongolian Peoples Republic*. *Transactions of Joint Soviet-Mongolian Research Expedition* 28:230–245
- Donskaya TV, Sklyarov EV, Gladkochub DP, Mazukabzov AM, Salnikova EB, Kovach VP, Yakovleva SZ, Berezhnaya NG (2000) The Baikal collisional metamorphic belt. *Doklady Earth Sciences* 374(4):1075–1079
- Donskaya TV, Bibikova EV, Mazukabzov AM, Gladkochub DP, Kozakov IK, Kirnozova TI, Plotkina JV, Reznitskiy LZ (2003) Granitoids of the Primorsky complex of the Western Baikal area: geochronology and geodynamic typification. *Russian Geology and Geophysics* 44(10):968–980
- Donskaya TV, Gladkochub DP, Kovach VP, Mazukabzov AM (2005) Petrogenesis of Early Proterozoic postcollisional granitoids in the Southern Siberian craton. *Petrology* 13:229–252
- Dorofeyuk NI, Tarasov PE (1998) Vegetation and levels of the lakes in the north of Mongolia during the last 12500 years, by the data of palynologic and diatom analyses. *Stratigraphy. Geological Correlation* 6(1):73–87
- Fedorovskiy VS, Vladimirov AG, Khain EV, Kargopolov SA, Gibsher AS, Izokh AE (1995) Tectonics, metamorphism, and magmatism of collisional zones of the Central Asian Caledonides. *Geotectonics* 29:193–212
- Fedorovskiy VS, Donskaya TV, Gladkochub DP, Khromykh SV, Mazukabzov AM, Mekhonoshin AS, Sklyarov EV, Sukhorukov VP, Vladimirov AG, Volkova NI, Yudin DS (2001)

- The Ol'khon collision system (Baikal region). In: Sklyarov EV (ed) *Structural and Tectonic Correlation Across the Central Asia Orogenic Collage: North-Eastern Segment* (Guidebook and abstract volume of the Siberian Workshop IGCP-480). IEC SB RAS, Irkutsk, pp 5–77
- Fedotov AP, Bezrukova EV, Vorob'eva SS, Khlystov OM, Levina OV, Mizandronev IB, Mazepova GF, Semenov AR, Zheleznyakova TO, Krapivina SM, Chebykin EP, Grachev MA (2001) Sediments of Lake Hovsgol as a record of paleoclimates of the Holocene and Late Pleistocene. *Russian Geology and Geophysics* 42(1–2):384–390
- Fedotov AP, Batist MDe, Pouls T (2006) Tectonic evolution of the southwestern wall of the Baikal Rift Zone. *Doklady Earth Sciences* 410(4):503–505
- Gary M, Bates RL, Jackson JA (1972) *Glossary of geology*. American Geological Institute, Washington
- Grachev MA, Fedotov AP, Phedorin MA, Tomurtogoo O, Batist MDe (2003) A long record of paleoclimates from north Mongolia: sediments of Lake Khubsugul. XVI INQUA Congress Abs, Reno, p 168
- Gladkochub DP, Sklyarov EV, Donskaya TV, Mazukabzov AM, Menshagin YuV, Panteeva SV (2001) Petrology of gabbro-dolerites from Neoproterozoic dike swarms in the Sharyzhalgai Block with reference to the problem of breakup of the Rodinia supercontinent. *Petrology* 9(6):560–577
- Gladkochub DP, Donskaya TV, Mazukabzov AM, Sklyarov EV, Ponomarchuk VA, Stanevich AM (2002) The Urik-Iya graben of the Sayan inlier of the Siberian craton: new geochronological data and geodynamic implications. *Doklady Earth Sciences* 386(7):74–78
- Gladkochub DP, Pisarevsky SA, Donskaya TV, Natapov LM, Mazukabzov AM, Stanevich AM, Sklyarov EV (2006a) Siberian Craton and its evolution in terms of Rodinia hypothesis. *Episodes* 29(3):169–174
- Gladkochub DP, Wingate MTD, Pisarevsky SA, Donskaya TV, Mazukabzov AM, Ponomarchuk VA, Stanevich AM (2006b) Mafic intrusions in southwestern Siberia and implications for a Neoproterozoic connection with Laurentia. *Precambrian Research* 147(3–4):260–278
- Gladkochub DP, Donskaya TV, Mazukabzov AM, Stanevich AM, Sklyarov EV, Ponomarchuk VA (2007) Signature of extension events in the southern Siberian craton. *Russian Geology and Geophysics* 48(1):17–41
- Gladkochub DP, Donskaya TV, Wingate MTD, Poller U, Kröner A, Fedorovsky VS, Mazukabzov AM, Todt W, Pisarevsky SA (2008) Petrology, geochronology, and tectonic implications of c. 500 mya metamorphic and igneous rocks along the northern margin of the Central-Asian Orogen (Olkhon terrane, Lake Baikal, Siberia). *Journal of the Geological Society of London* 165(1): 235–246
- Goldirev GS (1982) *Sedimentation and Quaternary history of Baikal basin*. Nauka, Novosibirsk (in Russian)
- Golubev VA (1992) Dense clay in the upper layer of the bottom sediments of the Khubsugul Lake (MPR). *Reports of the Russian Academy of Sciences* 324(5):1091–1095
- Gordienko IV, Filimonov AV (2005) The Dzhida zone of the Paleo-Asian Ocean: main stages of geodynamic evolution (Vendian–Early Paleozoic oceanic, island-arc and back-arc basin complexes). In: Sklyarov EV (ed) *Structural and Tectonic Correlation Across the Central Asia Orogenic Collage: North-Eastern Segment* (Guidebook and abstract volume of the Siberian Workshop IGCP-480), IEC SB RAS, Irkutsk, pp 98–165
- Gradstein FM, Ogg JG, Smith AG, Bleeker W, Lourens L (2004) A new Geologic Time Scale, with special reference to Precambrian and Neogene. *Episodes* 27(2):83–100
- Hu AQ, Jahn BM, Zhang GX, Chen YB, Zhang QF (2000) Crustal evolution and Phanerozoic crustal growth in northern Xinjiang: Nd isotopic evidence: Part I. Isotopic characterization of basement rocks. *Tectonophysics* 328:15–51
- Ivanenko VV, Karpenko MI, Jashina RM, Andreeva ED, Ashikhmina NA (1989) New data about potassium-argon age of the basalts of the west board of the Khubsugul rift (MPR). *Reports of the USSR Academy of Sciences* 309(4):915–930 (in Russian)

- Jahn BM, Wu FY, Chen B (2000) Granitoids of the Central Asian Orogenic Belt and continental growth in the Phanerozoic. *Transactions of Royal Society of Edinburgh: Earth Sciences* 91:181–193
- Kazansky AYu, Fedotov AP, Matasova GG, Ziborova GA, Zheleznyakova TO, Vologina EG, Oyuntcimeg T, Narantsetseg T, Tomurkhoo D. (2005) First paleomagnetic results from the bottom sediments of Lake Hövsgöl based on drilling data. *Russian Geology and Geophysics* 46(4):448–451
- Khain EV, Bibikova EV, Salnikova EB, Kröner A, Gibsher AS, Didenko AN, Degtyarev KE, Fedotova AA (2003) The Palaeo-Asian ocean in the Neoproterozoic and early Palaeozoic. New geochronologic data and palaeotectonic reconstructions. *Precambrian Research* 122:329–358
- Kovach VP, Matukov DI, Berezhnaya NG, Kotov AB, Levitsky VI, Barash IG, Kozakov IK, Levsky LK, Sergeev SA (2004) SHRIMP zircon age of the Gargan block tonalites – find Early Precambrian basement of the Tuvino-Mongolian microcontinent, Central Asia mobile belt. 32nd International Geological Congress Abstracts (vol 2), p 1263
- Krivonogov SK, Takahara H, Kuzmin YV, Jull AJT, Orlova LA, Nakamura T, Miyoshi N, Kawamuro K, Bezrukova EV (2004) Radiocarbon chronology of the Late Pleistocene–Holocene paleogeographic events in Lake Baikal region (Siberia). *Radiocarbon* 46:745–754
- Kuz'min MI, Karabanov EV, Kawai T., Williams D, Bychinskii VA, Kerber EV, Kravchinskii VA, Bezrukova EV, Prokopenko AA, Geletii VF, Kalmichkov GV, Goreglyad AV, Antipin VS, Khomutova MYu, Soshina NM, Ivanov EV, Khursevich GK, Tkachenko LL, Solotchina EP, Ioshida N, Gvozdkov AN (2001) Deep drilling on Baikal: Main Results. *Russian Geology and Geophysics* 42(1–2):8–34
- Larin AM, Sal'nikova EB, Kotov AB, Kovalenko VI, Rytsk EYu, Yakovleva SZ, Berezhnaya NG., Kovach VP, Buldygerov VV, Sryvtsev NA (2003) The North Baikal Volcanoplutonic Belt: age, formation duration, and tectonic Setting. *Doklady Earth Sciences* 392(7):963–967
- Logachev NA (1984) South of East Siberia. Nauka, Moscow
- Marinov NA (1967) The Khubsugul (Kosogol) Lake depression in the North Mongolia. In: Logachev NA (ed) *Materials of the Commission on the Study of the Underground Water of Siberia and Far East*, vol 3. USSR Academy of Sciences. Publishing house, Moscow, pp 186–196 (in Russian)
- Mishina EI, Kostitsin YuA, Fedorovsky VS (2005) Archean age of the protolith of the Paleozoic granite-gneiss of Olkhon region (Baikal area): Sm-Nd and Rb-Sr isotope data. In: Sklyarov EV (ed) *Geodynamic Evolution of Lithosphere of the Central-Asian Orogenic Belt*, vol 3. IG SB RAS, Irkutsk, pp 56–59 (in Russian)
- Nikolaev VG, Vanyakin LA, Kalinin VV, Milanovsky VE (1985) Structure of sedimentary cover of Baikal Lake. *Bulletin of the Moscow Society of Naturalists, Geological Series* 60(2):48–58 (in Russian)
- Parfenov LM, Natapov LM, Sokolov SD, Tsukanov NV (1993) Terrane analysis and accretion in northeast Asia. *The Island Arc* 2:35–54
- Poller U, Gladkochub DP, Donskaya TV, Mazukabzov AM, Sklyarov EV, Todt W (2004) Timing of Early Proterozoic magmatism along the Southern margin of the Siberian craton. *Transactions of the Royal Society of Edinburgh: Earth Sciences* 95:215–225
- Poller U, Gladkochub DP, Donskaya TV, Mazukabzov AM, Sklyarov EV, Todt W (2005) Multistage magmatic and metamorphic evolution in the Southern Siberian craton: Archean and Paleoproterozoic zircon ages revealed by SHRIMP and TIMS. *Precambrian Research* 136: 353–368
- Reznitsky LZ, Shkol'nik SI, Levitsky VI (2004) Geochemistry of Calcareous–Silicate Rocks of the Kharagol Formation, Southern Baikal Region. *Lithology and Mineral Resources* 39 (3):230–242
- Rosen OM (2003) Siberian craton: tectonic zonation and evolution stages. *Geotectonics* 37(3): 175–192
- Salnikova EB, Sergeev SA, Kotov AB, Yakovleva SZ, Reznitskii LZ, Vasil'ev EP (1998) U-Pb zircon dating of granulite metamorphism in the Slyudyanskiy complex, Eastern Siberia. *Gondwana Research* 1:195–205

- Shuvalov VF, Nikolaeva TV (1989) On the age and geomorphologic position of the Cenozoic plate-basalts in the Central, North and Southeast Mongolia. *Bulletin of the Leningrad State University* 3:102–106 (in Russian)
- Smelov AP, Zengenizov AN, Timofeev VF (2001) The basement of the Siberian craton. In: Parfenov LM (ed) *Tectonics, Geodynamics and Metallogeny of the Sakha Republic (Yakutia)*. MAIK Nauka/Inetperiodica, Moscow, pp 81–113
- Sklyarov EV, Belichenko VG, Mazukabzov AM, Gladkochub DP (2001) General geology of the southern margin of the Siberian craton and NE segment of the Central-Asian foldbelt. In: Sklyarov EV (ed) *Assembly and Breakup of Rodinia Supercontinent: Evidence from South Siberia*. IEC SB RAS, Irkutsk, pp 7–16
- Stanevich AM, Mazukabzov AM, Bragina AA (2001) Neoproterozoic sedimentary series of continental shelf of the southern margin of the Siberian craton. In: Sklyarov EV (ed) *Assembly and Breakup of Rodinia Supercontinent: Evidence from South Siberia*. IEC SB RAS, Irkutsk, pp 52–71
- Ufland AK, Iljin AV, Spirkin AI (1969) The Baikal-type depressions of the North Mongolia. *Bulletin of the Moscow Society of Naturalists, Geological Series* 44(6):5–22 (in Russian)
- Vladimirov AG, Kruk NN, Vladimirov VG, Gibsher AS, Rudnev SN (2001) Synkinematic granites and collision-shear deformations in Western Sangilen (Southeastern Tuva). *Russian Geology and Geophysics* 41(3):398–411
- Vladimirov VG, Vladimirov AG, Gibsher AS, Travin AV, Rudnev SN, Shemelina IV, Barabash NV, Savinykh YaV (2005) Model of the Tectonometamorphic Evolution for the Sangilen Block (Southeastern Tuva, Central Asia) as a Reflection of the Early Caledonian Accretion–Collision Tectogenesis. *Transactions of the Russian Academy of Sciences/Earth Science Section* 405(8):1156–1160
- Windley BF, Alexeiev D, Xiao W, Kroener A, Badarch G (2006) Tectonic models for accretion of the Central Asian Orogenic Belt. *Journal of the Geological Society, London* 164:31–47
- Yarmolyuk VV, Ivanov VG, Kovalenko VI, Pokrovskii BG (2003) Magmatism and Geodynamics of the Southern Baikal Volcanic Region (Mantle Hot Spot): Results of Geochronological, Geochemical, and Isotopic (Sr, Nd, and O) Investigations. *Petrology* 11(1):1–30
- Zhao G, Cawood PA, Wilde SA, Sun M (2002) Review of global 2.1–1.8 Ga orogens: implications for a pre-Rodinia supercontinent. *Earth-Science Reviews* 59:125–162
- Zolotarev AG, Suldin VA, Kulakov VS (1981) Structure and present movements of the Khubsugul depression in the North Mongolia. In: Logachev NA (ed) *Natural conditions and resources of Trans-Khubsugulia (Transactions of the Soviet-Mongolian complex Khubsugulian expedition)*, IEC, Irkutsk, pp 20–30
- Zolotarev AG, Khilko SD, Kulakov VS (1989) Neotectonics. *Atlas of the Khubsugul Lake (MPR)*. GUGK, Moscow (in Russian)
- Zorin Yu A, Tumtanov E Kh, Arvisbaatar N (1989) Structure of Cenozoic basins of the Prekhubsugul region from gravity data. *Russian Geology and Geophysics* 29(10):130–136

Tectonics of the Baikal Rift Deduced from Volcanism and Sedimentation: A Review Oriented to the Baikal and Hovsgol Lake Systems

Alexei V. Ivanov and Elena I. Demonterova

1	Introduction.....	28
2	Basic Information About the Lake Systems	30
3	Evidence from Sedimentary Records on Tectonic and Environmental Changes.....	31
3.1	Lake Baikal.....	31
3.2	Lake Hovsgol.....	36
4	Volcanism as a Marker of Tectonic Processes	40
4.1	Dating of Volcanism	41
4.2	Evidence from Volcanism on Tectonics.....	43
5	Discussion.....	48
6	Conclusions.....	50
	References.....	51

Abstract As known from inland sedimentary records, boreholes, and geophysical data, the initiation of the Baikal rift basins began as early as the Eocene. Dating of volcanic rocks on the rift shoulders indicates that volcanism started later, in the Early Miocene or probably in the Late Oligocene. Prominent tectonic uplift took place at about 20Ma, but information (from both sediments and volcanics) on the initial stage of the rifting is scarce and incomplete. A comprehensive record of sedimentation derived from two stacked boreholes drilled at the submerged Akademichesky ridge indicates that the deep freshwater Lake Baikal existed for at least 8.4Ma, while the exact formation of the lake in its roughly present-day shape and volume is unknown. Four important events of tectonic/environmental changes at about ~7, ~5, ~2.5, and ~0.1 Ma are seen in that record. The first event probably corresponds to a stage of rift propagation from the historical center towards the wings of the rift system. Rifting in the Hovsgol area was initiated at about this time. The event of ~5Ma is a likely candidate for the boundary between slow and

A.V. Ivanov (✉) and E.I. Demonterova
Institute of the Earth's Crust, Siberian Branch, Russian Academy of Sciences,
Lermontov street 128, 664033 Irkutsk, Russia
e-mail: aivanov@crust.trk.ru

fast stages of rifting. It is reflected in a drastic change of sedimentation rate due to isolation of the Akademichesky ridge from the central and northern Lake Baikal basins. The youngest event of 0.1 Ma is reflected by the $^{87}\text{Sr}/^{86}\text{Sr}$ ratio increase in Lake Baikal waters and probably related to an increasing rate of mountain growth (and hence erosion) resulting from glacial rebounding. The latter is responsible for the reorganization of the outflow pattern with the termination of the paleo-Manzurka outlet and the formation of the Angara outlet. The event of ~ 2.5 Ma is reflected in the decrease of the $^{87}\text{Sr}/^{86}\text{Sr}$ and Na/Al ratios in Lake Baikal waters. We suggest that it is associated with a decrease of the dust load due to a reorganization of the atmospheric circulations in Mainland Asia. All these tectonic and climatic events could (and actually did) influence the biota of Lake Baikal. The Hovsgol rift basin was shaped to its recent form between 5.5 and 0.4 Ma. However, freshwater Lake Hovsgol appeared only in the latest pre-Holocene time as a result of meltwater inflow and increase of atmospheric precipitations during the Bølling-Allerød warming. Prior to this, a significantly smaller, saline outflow-free precursor of Lake Hovsgol existed. It explains why two, now connected, lakes of similar water chemistry within similar climatic and tectonic conditions differ so much in their biodiversity.

1 Introduction

Lake Baikal is the deepest lake in the world and the largest freshwater reservoir. It is unique not only for its size and volume (e.g., Galaziy 1993), its drinkable water with low trace element composition (e.g., Suturin et al. 2003), but also for the enormous amount of endemic fauna and flora (e.g., Timoshkin 2004). Molecular dating and geological records show that evolution of biota in Lake Baikal took place on a scale of 10^4 – 10^6 years (e.g., Mashiko et al. 1997; Sherbakov 1999; Koskinen et al. 2002; Hidding et al. 2003; Müller et al. 2006; Froufe et al. 2008), thanks to the long geological history of the lake and the complex history of environmental changes. Radioisotopic dating of sediments in the submerged Akademichesky ridge places the upper limit on the age of the (freshwater) Lake Baikal to as much as 8.4 million years ago (Ma; Mega annum) (Horiuchi et al. 2003, 2004), whereas rift basins, which host Lake Baikal and its precursory lakes, are tracked back to the Middle Eocene (~ 45 – 50 Ma; Logatchev and Florensov 1978; Mats 1993) or even the Late Cretaceous (~ 75 Ma; Logachev 2003).

In Mainland Asia, the second largest freshwater reservoir is Lake Hovsgol (also written in English literature as Khubsugul, Chovsgul, or similar, and often referred to in Russian popular literature as a little brother of Lake Baikal due to the visual similarity of their environment). It is located within the same rift system (Fig. 1) with similarly severe climate conditions of long cold winters and short hot summers (Bogoyavlensky 1989; Galaziy 1993). The lakes are connected through the Egin-Gol and Selenga Rivers (Fig. 1). However, Lake Hovsgol is barren in biota compared to Lake Baikal (see Table 1). A remarkable example is the absence of sponges in Lake Hovsgol, which cannot be attributed either to present-day

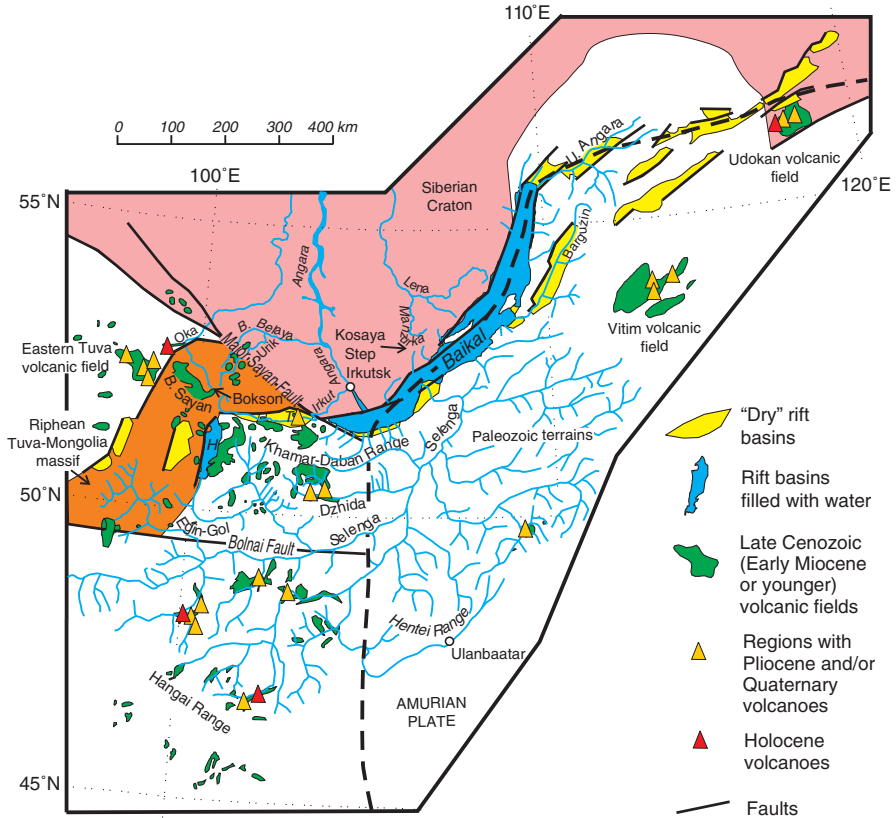


Fig. 1 Baikal rift system and surrounding regions. Rift system partially occupies a weakness zone between an ancient Siberian craton and the Pre-Cambrian Tuva-Mongolia massif with Paleozoic accreted terranes. It is limited in the south by the Bolnai Fault. The boundary of newly formed stable Amurian plate is shown by a **bold dotted line**. Its anticlockwise rotation is thought to be responsible for the opening of the Baikal basins (Zonenshain and Savostin 1981). The inflowing river pattern to Lake Baikal is shown in detail. A few rivers mentioned in the text, not connected with Lake Baikal, namely Lena, Manzurka, Irkut, Oka, Urik, Bolshaya Belaya, are also shown. *T* Tunka basin, *H* Lake Hovsgol, *B. Belaya* Bolshaya (Big) Belaya, *U. Angara* Upper Angara, *B. Sayan* Bolshoi (Big) Sayan

geographic conditions or water mineralization (Table 1) since sponges are known in much smaller Siberian lakes at high altitudes with higher water mineralization (e.g., Lake Chagytai; Müller et al. 2006). Some species of fauna are common to both lakes, but the fauna of Lake Baikal is more diverse (e.g., Slugina 2006).

Biota is sensitive to environmental changes, which in the past were controlled by both the climate and tectonics. The primary purpose of this chapter is to review the available information on tectonic changes in the watershed area of Lake Baikal, which includes the watershed area of Lake Hovsgol, and some adjacent regions (Fig. 1). The timing of the tectonic changes is inferred from analyses of sediments

Table 1 Comparison of Lake Baikal and Hovsgol systems

	Lake Baikal	Lake Hovsgol
Size (10 ³ km ²)	31.5 ^a	2.76 ^j
Volume (10 ³ km ³)	23 ^a	0.38 ^j
Average outflow (km ³ /year)	57.45 ^b	0.57 ^k
Watershed area (10 ³ km ²)	570 ^a	5.13 ^j
Ratio of watershed area to the lake size	18 ^a	1.8 ^j
Elevation (m a.s.l.)	~455 ^a	~1,645 ^j
Maximal depth (m)	Southern basin – 1,423 ^a Central basin – 1,637 ^a Northern basin – 890 ^a	262 ^j
Maximal thickness of sediments (m)	Southern and central basins – 7,500–8,000; Northern basin – 4,000–4,400 ^c	350–450 ^l
Initiation of rift basin formations (Ma)	~45–50 ^d , 70–75 ^e	>8 ^m
Beginning of shaping the rift basins (Ma)	~5 ^{e,g}	~5.5 ⁿ
Existence of fresh-water lake (Ma)	>8.4 ^b	~0.015 ^o
Level of water mineralization (mg/l)	~150 ^a	~200 ^{i,p}
Number of animal (sub)species	>2,500 ⁱ	<300 ⁱⁱ
Endemic animal (sub)species (%)	60 ⁱ	~5 ⁱⁱ

Reported values have been used, or calculated from data from the following sources:

^aGalaziy (1993)

^bKimstach et al. (1998)

^cHutchinson et al. (1992)

^dLogatchev and Florensov (1978)

^eLogachev (2003)

^fLogachev and Zorin (1987)

^gIvanov (2004)

^hHoriuchi et al. (2003, 2004)

ⁱTimoshkin (2004)

^jBogoyavlensky (1989)

^kPisarskiy et al. (1978)

^lZorin (1971)

^mRasskazov et al. (2003)

ⁿFedotov et al. (2006)

^oFedotov et al. (2002, 2004)

^pThis study

within rift basins and positions of volcanic rocks on rift shoulders. In addition, some information on paleoclimate and water chemistry is also given.

2 Basic Information About the Lake Systems

Basic information about the Baikal and Hovsgol lake systems is summarized in Table 1. In general, Lake Baikal is ten times larger and has a watershed area about ten times wider. The latter is due to the significantly lower elevation of Lake Baikal

compared to Lake Hovsgol. Lake Baikal is very deep and its bottom line is below sea level. Lake Hovsgol is shallower, but also deep compared to numerous other lakes in Mainland Asia.

In their classical paper, Logatchev and Florensov (1978) suggested that development of the Baikal rift basin started in the Middle Eocene with the formation of the Southern Baikal basin. Then the rift spread in two directions, western and northeastern. The initiation of the Hovsgol rift basin was placed by Logatchev and Florensov (1978) to the Pliocene–Quaternary, but more recent studies suggest that development of the Hovsgol basin started earlier, at least in the Late Miocene (Fedotov et al. 2006; see more information below on this topic). As a consequence of the early initiation of the Baikal rift basins the sedimentary infill there is much thicker compared to the Hovsgol rift basin (Table 1).

Water mineralization of Lake Baikal and Lake Hovsgol is very low; about 150 and 200 mg/l, respectively (Table 1). Elemental and strontium isotope compositions are similar except for Pb and to a lesser extent for Ba, Cu, Al, and Sr (Table 2). Baikal waters are more pristine. Probably, minor differences in water chemistry, especially in Pb, are controlled in some way by biochemical processes (see, for example, Paradina et al. 2004 for study of sponge chemistry).

3 Evidence from Sedimentary Records on Tectonic and Environmental Changes

Deepening of rift basins and growth of their shoulders (mountings), as well as climatic variations, are reflected in the rates of sedimentation and composition of the sediments associated with variations of suspended sediment and dissolved element influx by rivers and ground waters, and by variations of atmospheric precipitations. Growing mountains can also control atmospheric circulations and glaciations.

3.1 *Lake Baikal*

Based on analyses of sedimentary records within the Lake Baikal and Tunka basin, it was considered that rifting in the Baikal rift system had two major stages: first (pre-rift) stage of slow rifting and second stage of fast rifting (Logatchev and Florensov 1978; Logatchev and Zorin 1987). Later studies conventionally accept this subdivision into two stages for the whole rift system, but the timing for their boundary and argumentation differ. Logatchev and Zorin (1987) placed the boundary between the slow and fast rifting to ~3–4 Ma. Mats (1993) described the second stage as the stage of rifting starting from the Oligocene (~25 Ma), but he further subdivided this stage into several substages separated by pulses of increased tectonic activity, which correspond to about 3.5, 0.7–0.8, and 0.1 Ma. A substage starting from 3.5 Ma was named the Neobaikalian stage (Mats 1993). Yarmolyuk

Table 2 Minor elements, trace elements, and strontium isotope data for Lake Hovsgol, its outlet and tributary rivers sampled in anomalously dry summer of 2002 in comparison with Lake Baikal and its major tributary, the Selenga River

	MN-02-01 Hovsgol center	MN-02-06 Hovsgol north	MN-02-04 Egin-Gol	MN-02-03 Uliin-Gol	MN-02-02 Alag-Tsar-Gol	MN 02-05 Ih- Dalbain-Gol	Lake Baikal ^a	Selenga ^b
Na (mg/l)	2.9	3.1	2.4	1.2	4.8	6.7	3.3	7.1
Mg	10.9	7.3	9.1	6.1	3.7	1.2	2.6	5.5
K	0.8	1	0.8	0.4	0.6	0.8	1.02	1.4
Ca	36.1	38.1	34.1	42.1	58.1	20.0	15.7	24.3
HCO ₃	151.3	151.3	146.4	161.1	207.5	90.3	N.R.	N.R.
Cl	1.1	1.1	1.8	1.1	1.1	1.1	N.R.	2.1
F	0.3	0.3	0.3	0.1	0.3	0.3	N.R.	N.R.
SO ₄	2	2	4	4	4	2	N.R.	N.R.
H ₄ SiO ₄	4	2	5	4	16	22	N.R.	N.R.
Li (µg/l)	2.9	2.8	2.8	2.0	3.9	3.8	2.1	3.4
Al	8.9	17.1	18.9	22.5	29.2	31.6	3.1	6.5
V	0.6	0.7	0.6	0.5	0.8	1.1	0.6	1.9
Mn	0.6	0.7	0.5	0.6	0.6	2.7	0.4	N.R.
Co	0.09	0.06	0.07	0.09	0.11	0.06	0.11	N.R.
Cu	2.8	6.7	2.0	2.5	3.4	2.6	0.9	1.0
Rb	0.63	0.87	0.55	0.25	0.64	0.38	0.84	N.R.
Sr	127	125	119	215	161	109	105	168
Mo	1.54	1.53	1.66	0.99	0.90	2.84	1.54	N.R.
Ba	29	29	27	39	34	22	11	14.4
Pb	2.1	6.2	1.1	1.4	1.5	1.0	0.064	N.R.
U	0.40	0.40	0.42	0.18	0.95	0.34	0.56	1.6
⁸⁷ Sr/ ⁸⁶ Sr	0.70869	0.70873	0.70874	0.70778	0.70953	0.70758	0.7088	0.7079

Minor elements were determined by classical “wet chemistry” at the analytical center of the Institute of the Earth’s crust SB RAS. Trace elements (Li to U) were determined by inductively coupled plasma mass spectrometry using the same PlasmaQuad 2+ instrument and a similar protocol as in Suturin et al. (2003). Strontium isotopes were measured at the Institute of the Earth’s crust SB RAS by thermal ionization mass spectrometry using Finnigan MAT 262 instrument. Details of analytical conditions can be found elsewhere (Ivanov et al. 2008).

N.R. – not reported

^aData from Suturin et al. (2003)

^bData from Falkner et al. (1997)

and Kuzmin (2004) used the same terminology, but placed the beginning of the Neobaikalian stage to 7 Ma. This stage was subdivided into earlier and modern sub-stages with a boundary at about 2.8 Ma. Parfeevets and Sankov (2006) recognized a stage of compression at the end of the Miocene—beginning of the Pliocene (~5 Ma), which could be naturally placed as a boundary between the two extension (rifting) stages of Logatchev and Zorin (1987). Ivanov (2004), using data of Horiuchi et al. (2003, 2004), noted that the major change of sedimentation on the submerged Akademicheskyy ridge occurred at about the same time (see later). Below, we consider borehole data for the Akademicheskyy ridge, because it provides the most comprehensive information on the environmental changes within Lake Baikal, and we discuss data on reorganization of the outlet-river pattern.

3.1.1 Sedimentary Record of Submerged Akademicheskyy Ridge

Due to international efforts, a number of deep sub-bottom boreholes were drilled as part of the Baikal Drilling Project (BDP) in winter seasons 1993–2003. The longest sedimentary record was obtained by two cores of the BDP-96-1 and BDP-98-2 boreholes drilled at the submerged Akademicheskyy ridge (Fig. 2). There was some

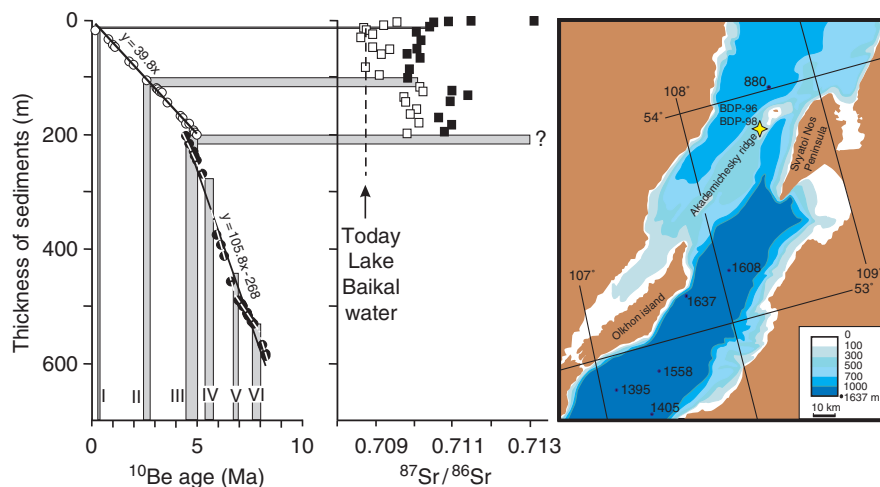


Fig. 2 Age of sediments calculated by ^{10}Be abundance in sediments versus sedimentary thickness (*left*; after Horiuchi et al. 2003, 2004), $^{87}\text{Sr}/^{86}\text{Sr}$ variations in terrigenous and diatom sediments (*center*; after Kuzmin et al. 2007) and bathymetry in vicinity of the submerged Akademicheskyy ridge (*right*). *Open* and *solid circles* are, respectively, for boreholes BDP-96-1 and BDP-98-2 taken from the submerged Akademicheskyy ridge. *Open* and *solid squares* are, respectively, for diatom and terrigenous sediments from the BDP-96-1 borehole. *Shadowed* areas numbered I–VI mark environmental changes seen from the data (see text). *Solid lines* are linear regressions for BDP-96-1 and BDP-98-2 samples. *Dotted white lines* are eye-fitted lines through subsets of the BDP-98-2 samples. *Yellow star* is the location of the BDP-96-1 and BDP-98-2 borehole sites

debate about the correct stacking of the two cores and the dating of the BDP-98-2 core, which was resolved by the ^{10}Be dating method (Horiuchi et al. 2003, 2004). The sedimentation rate of ~ 0.04 mm/year within the upper 200 m of the sediments (which account for about 5 Ma) is very constant. However, starting from environmental change No III, deeper (older) sediments are characterized by a more variable rate of sedimentation with an average of ~ 0.11 mm/year. This can be explained by the rapid isolation of the Akademicheskyy ridge from the Central and Northern Baikal basins. Prior to 5 Ma, terrigenous sediments from major rivers (e.g., Selenga, Barguzin, Upper Angara) deposited on the precursor of the Akademicheskyy ridge had a relatively high rate of sedimentation. After the building of the Akademicheskyy ridge, the influx of terrigenous sediments dropped and the rate of sedimentation also dropped (Fig. 3). Changes in the sedimentation rate also took place at about 5.5 Ma (IV in Fig. 2, left), 7 Ma (V in Fig. 2, left) and 8 Ma (VI in Fig. 2, left). Considering these environmental changes and our hypothesis of the absence of the Akademicheskyy ridge prior to 5 Ma, an increase of the sedimentation rate would mean an increasing rate of denudation in the watershed area, which can be related to rapid tectonic growth of mountains. The rate of sedimentation increased at environmental change No V (7 Ma), which probably marks the beginning of the Neobaikalian stage in terms of Yarmolyuk and Kuzmin (2004).

BDP-96-1 core is represented by laminated layers of terrigenous and diatom-rich sediments. The former layers are characterized by a higher $^{87}\text{Sr}/^{86}\text{Sr}$ ratio compared to diatom-rich sediments, because diatoms gain strontium from the water, which is generally less radiogenic than dominant ancient (Paleozoic and Pre-Cambrian) rocks sampled by incoming rivers (Kuzmin et al. 2007). $^{87}\text{Sr}/^{86}\text{Sr}$ ratios in the most recent sediments are higher compared to present-day Lake Baikal water (Fig. 2) because terrigenous sediments are admixed with diatoms at variable proportions.

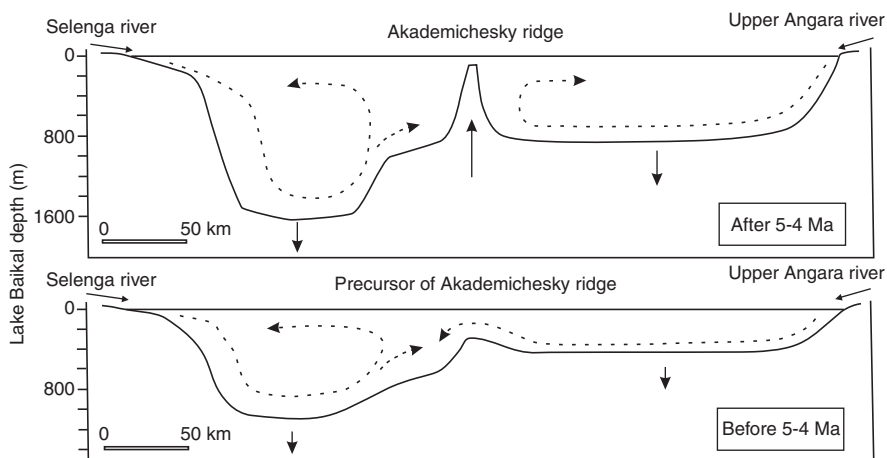


Fig. 3 Schematic representation of formation of the submerged Akademicheskyy ridge (after Ivanov 2004)

About 2.5–2.8 Ma (II in Fig. 2, left), $^{87}\text{Sr}/^{86}\text{Sr}$ ratios in both the terrigenous and diatom-rich sediments dropped significantly and then increased again to higher values in more recent times (I in Fig. 2, left). At environmental change No II, the Al/Na ratio of sediments also changed ($\text{Al}_2\text{O}_3/\text{Na}_2\text{O}$ increased from about 0.1 to 0.15 at a depth of about 100 m) (Yarmolyuk and Kuzmin 2004). Strontium isotope (and other chemical indices) variations at 2.5–2.8 Ma are not reflected in the sedimentation rate. Hence, they are not due to any tectonic changes in the watershed area, but rather to climatic changes (in addition to this argumentation, a tectonic uplift within the Lake Baikal watershed area and resulting increase of erosion-related influx of terrigenous sediments would increase the $^{87}\text{Sr}/^{86}\text{Sr}$ ratio in BDP samples, while the opposite is observed). As noted by the Stratigraphy Commission of the Geological Society of London, the Gauss-Matuyama magnetic chron boundary (~2.6 Ma) is the natural beginning of the Quaternary, instead of the Pliocene–Quaternary boundary at 1.8 Ma (see Gibbard et al., 2005). Here, we suggest that the decrease of the $^{87}\text{Sr}/^{86}\text{Sr}$ ratio at about 2.5–2.8 Ma reflects the change of atmospheric circulations in mainland Asia. A study of the Chinese Loess Plateau for the last 7 Ma revealed a drop of $^{87}\text{Sr}/^{86}\text{Sr}$ ratio in acid-insoluble residue of sediments from 0.7230 to 0.7223, which occurred at about 2.5 Ma, and a further decrease of this ratio to the present-day ratio of 0.7182 (Wang et al. 2007). This has been attributed to sorting of dust particles by the East Asian winter monsoon (of intracontinental origin), whose intensity increased at about 2.5 Ma (Wang et al. 2007). The latter can be related with the growth of the Tibetan Plateau that occurred at about the same time, which prevented penetration of Indian monsoons into Mainland Asia (Wan et al. 2007).

The recent increase of $^{87}\text{Sr}/^{86}\text{Sr}$ ratio in both terrigenous and diatom-rich sediments of the Akademicheskyy ridge was assumed to be due to a catastrophic earthquake like those which formed Proval Bay in 1861 (Kuzmin et al., 2007). However, as we argue in a section below, this could also reflect a rapid growth of mountains as the result of postglacial rebounding.

3.1.2 Paleo-Outlets of Lake Baikal

The present-day outlet of Lake Baikal, which is the uppermost branch of the Angara River (Fig. 1), was formed fairly recently in the Late Pleistocene (e.g., Kononov and Mats 1986). The time of formation of the Angara source was estimated by molecular dating on gammarid populations as ca. 60 Ka (Mashiko et al. 1997), *Thymallus* (Grayling) as ca. 225–325 Ka (or 100–500 Ka if overall error is included; see Koskinen et al. 2002), and *Brachymystax lenok* as ca. 50–400 Ka (Froufe et al. 2008). Prior to this time, the outlet was by the so-called paleo-Manzurka River, which connected Lake Baikal with the Lena River (e.g., Logachev et al. 1974) (Fig. 1). Timing for this paleo-outlet system was estimated through palinological analysis of alluvial deposits of the paleo-Manzurka River combined with thermoluminescence (TL) dating (Trofimov et al. 1995). In earlier studies, the time of termination of the paleo-Manzurka River outlet was estimated as the Middle Pleistocene, some 200 Ka (e.g., Logachev et al. 1974; Mats 1993).

On the basis of palinology combined with thermoluminescence dating, Trofimov et al. (1995) have extended the paleo-Manzurka River outlet up to the Late Pleistocene (TL dates of 78 ± 20 Ka and 133 ± 30 Ka). All studies agree that initiation of the paleo-Manzurka River outlet took place in the Early Pliocene (before ca. 4Ma as estimated by correlations of palinocomplexes of the paleo-Manzurka and volcanic regions of northern Mongolia). It should be noted that the results of Trofimov et al. (1995) withdraw a suggestion about a transitory Middle Pleistocene paleo-outlet with a candidate locality between southern Baikal and the Irkut River (Kononov and Mats 1986, and later works of these authors) (Fig. 1).

The question is why the paleo-Manzurka River terminated? Romashkin and Williams (1997) (following Mats 1993 and his earlier works on Lake Baikal terraces) suggested water level fluctuations due to climatic changes with a drop in water level by 300m and a rise by 150m over the present-day level during the last 600Ka. According to them, water level decrease started at ca. 400Ka and reached its minimum at ca. 300Ka. This was postulated as a reason for paleo-Manzurka termination (in addition, formation of the Angara outlet requires rapid tectonic subsidence in the uppermost Angara current). Colman (1998) pointed out that such estimations of water level fluctuations are unrealistic. He considered that terraces were formed mainly due to tectonic uplifting of the region while climatic changes were responsible for water fluctuations in the order of no more than a few meters. If we look at the site of the paleo-Manzurka alluvial deposit dated by TL as 133 ± 30 Ka in the vicinity of the Kosaya Step village near the present-day watershed boundary (Trofimov et al. 1995) (Fig. 1) and consider its present-day elevation of 700m, the rate of tectonic uplifting will be about 2 mm/year. Such a rate is trivial for the modern mountain framing of Lake Baikal resulting from combined effects of active tectonics and glacial rebounding (Levi et al. 2002). Thus, we concur with Colman (1998) that 100m scale of water fluctuations with much higher water levels than today are not reasonable. Moreover, recent estimations for climate-related water level fluctuations suggest up to about a 35 m drop (not rise!) of water level from about 100 Ka to about 70 Ka (at the transition from interglacial period MIS5–MIS4) (Urabi et al. 2004). Thus, high terraces along the Lake Baikal shores are due to a tectonic uplift. Increase of $^{87}\text{Sr}/^{86}\text{Sr}$ in recent diatom and terrigenous sediments (Fig. 2, center) can be related with glacial rebounding, which increased the rate of mountain growth and erosion, and is at the origin of the high terraces.

3.2 *Lake Hovsgol*

3.2.1 Sedimentation Records

Major information on sedimentation in Lake Hovsgol came from sub-bottom borehole KDP-01 (Fig. 4) which penetrated 53 m of sediments, from a number of a few meters long gravity cores, and from seismic profiling (e.g., Fedotov et al. 2002, 2004, 2008; Kazansky et al. 2005). Paleomagnetic dating suggests that the 53 m of KDP-01 drill-core account for 1,070 Ka. If this rate of sedimentation remained

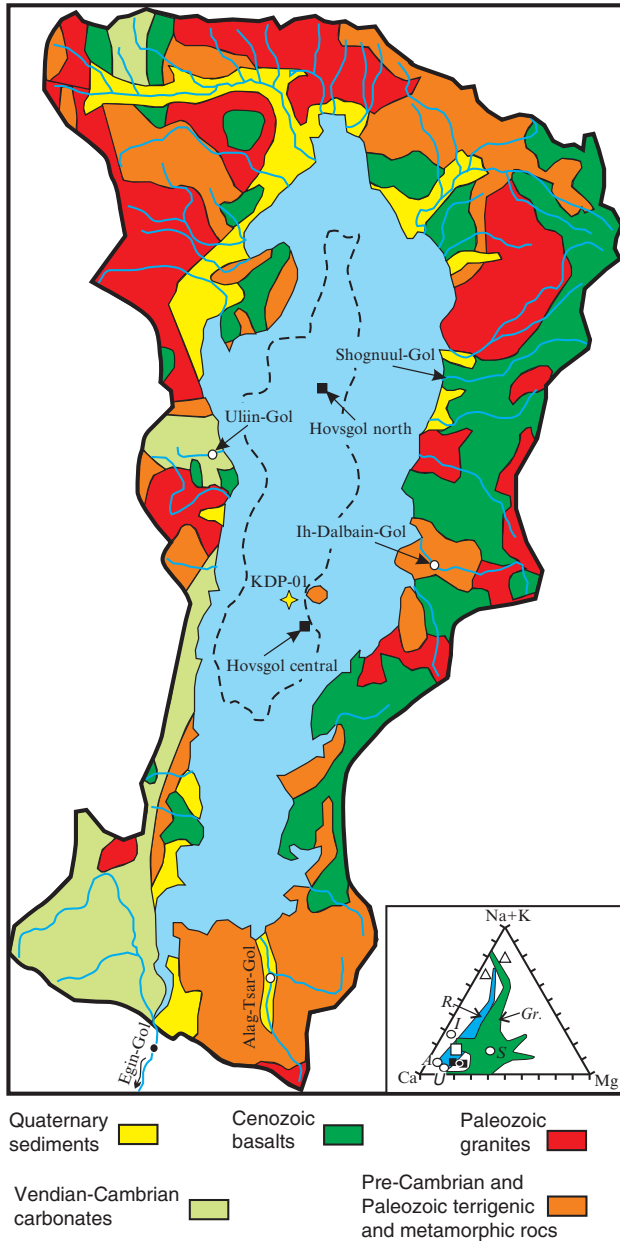


Fig. 4 Geology of the watershed area of Lake Hovsgol. *Yellow star* marks position of sub-bottom borehole KDP-01. *White circles, black circle and black squares* represent sampling sites of tributary rivers, outlet river, and Lake Hovsgol, respectively (see Table 2). *Dashed contour* in the middle of the lake marks the Late Pleistocene paleo-lake level, which was 170m below the present-day lake level (Fedotov et al. 2004). *Insert* shows classification of river and lake waters: *white circles* are tributary rivers (A Alag-Tsar-Gol, U Uliin-Gol, I Ih-Dalbain-Gol, S Shognuul-Gol), *black circle* is an outlet river (E Egin-Gol), *black squares* are for Lake Hovsgol water, *white triangles* are for rain water sampled in 1969 and 1971 (Sodnom and Losev 1976), *white square* is for Lake Baikal water (Suturin et al. 2003). *Green and blue areas* show range of compositions measured in 1969 and 1971 for ground water (Gr.) and river water (R.), respectively (Sodnom and Losev 1976)

constant on average during the basin formation, then 350–450 m of sediments in the Hovsgol basin (Table 1) reflect that the deepest sediments are about 7–9 Ma. As will be shown in Section 4.1 this crude estimation is close to data on the beginning of rifting based on volcanism dating.

From analyses of seismic images, confirmed by gravity core data, it has been suggested that Lake Hovsgol in the latest Pleistocene was 170 m shallower compared to the present-day level (Fedotov et al. 2002, 2004) (Fig. 4). This precursory lake therefore had no outlet and was salty (Fedotov et al. 2004). The lake volume rose to the present-day volume in connection with glaciers melting and increased precipitation during the Bølling-Allerød warming (about 15–12 Ka). Analysis of the upper half of the KDP-01 core has shown that water level fluctuated several times in the lake's history (Fedotov et al. 2008). Fedotov et al. (2004) calculated an index of tectonic activity looking at seismic images of sediments, which are derived from the angle of sediment unit deepening and number of singenetic faults in each unit. This revealed a highly active tectonic phase from 5.5 to 0.4 Ma with peaks of activity at about 3 and 1 Ma.

3.2.2 Strontium Balance in Water

Strontium isotope composition of water in Lakes Baikal and Hovsgol represent a mixture of strontium derived from atmospheric precipitations and terrigenous sources in the watershed area. Terrigenous sources are highly heterogeneous and depend on rock age and composition, as well as on the degree of chemical leaching of strontium from the rocks by natural waters. Climatic conditions (and hence degree of leaching) are similar for both lakes. Composition of the atmospheric precipitations is also expected to be similar, thus only composition and age of the rocks are major variable parameters. As seen from Fig. 1, rivers that flow into Lake Baikal drain mainly rocks of Paleozoic terrains, which are composed of granites, carbonate, and terrigenous rocks. Contribution from ancient granites of the Siberian craton with highly elevated $^{87}\text{Sr}/^{86}\text{Sr}$ (>0.720) and young basalts with low (~ 0.705) $^{87}\text{Sr}/^{86}\text{Sr}$ is small. Modeling of strontium balance for Lake Baikal was done by Falkner et al. (1997) and is not considered here. We only note that $^{87}\text{Sr}/^{86}\text{Sr}$ ratios in Lakes Baikal and Hovsgol waters are similar (Table 2).

The geology of the watershed area of Lake Hovsgol is shown in Fig. 4. Both, granites and basalts are abundant and are important sources of strontium for river waters. An additional important component is carbonate rocks of the Riphean Tuva-Mongolia massif. The insert to Fig. 4 shows that Lake Hovsgol waters are mixtures of rivers and ground waters with atmospheric precipitations. We sampled Lake Hovsgol (and the Egin-Gol River 1.5 km below its source, which is expectedly close to Lake Hovsgol in composition), Uliin-Gol, Alag-Tsar-Gol, and Ih-Dalbain-Gol Rivers in the anomalously dry summer of 2002 in a period from July 24 to August 1. We were not able to sample Shognuul-Gol, which is the only river close to ground water compositions by major compounds (insert to Fig. 4).

The contribution of different sources was modeled using the $^{87}\text{Sr}/^{86}\text{Sr}$ ratio and Sr concentrations (Faure 1986; Capo et al. 1998). First, we modeled the contribution of strontium derived from different rocks for the rivers Uliin-Gol, Alag-Tsar-Gol, and Ih-Dalbain-Gol. We discovered that Uliin-Gol waters receive 85.7%, 4%, and 10.3% of strontium from carbonates, basalts, and rain (and melted snow, which exists in high mountains in the catchment area of the Uliin-Gol through the summer), respectively. Alag-Tsar-Gol receives 41.5% and 58.5% of strontium from metamorphic rocks and rain, respectively. Ih-Dalbain-Gol receives 9%, 10%, and 81% of strontium from granites, basalts, and rain, respectively (see captions to Fig. 5

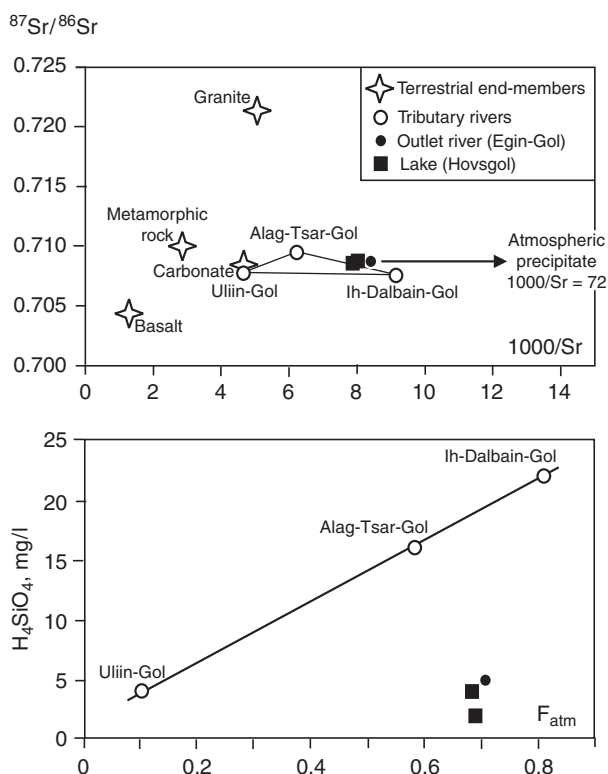


Fig. 5 $^{87}\text{Sr}/^{86}\text{Sr}$ versus $1,000/\text{Sr}$ (top) and H_4SiO_4 versus model fraction of atmospheric precipitations (bottom) in Lake Hovsgol, tributary, and outlet rivers. Mixing curves $^{87}\text{Sr}/^{86}\text{Sr} - 1,000/\text{Sr}$ diagram are represented by straight lines (Faure 1986). Average compositions for local terrestrial sources are shown: granites (Reznitskii et al. 2001; $^{87}\text{Sr}/^{86}\text{Sr} = 0.7214$ and $\text{Sr} = 200$ ppm), basalts (unpublished authors' data; $^{87}\text{Sr}/^{86}\text{Sr} = 0.7044$ and $\text{Sr} = 790$ ppm), carbonates (Gorokhov et al. 1995; $^{87}\text{Sr}/^{86}\text{Sr} = 0.7085$ and $\text{Sr} = 215$ ppm). For metamorphic rocks, we arbitrarily set $^{87}\text{Sr}/^{86}\text{Sr} = 0.71$ and $\text{Sr} = 350$ ppm. Atmospheric water composition ($^{87}\text{Sr}/^{86}\text{Sr} = 0.70896$ and $\text{Sr} = 14 \mu\text{g}/\text{l}$) is after Sandimirov et al. (2002). The bottom figure shows excellent correlation between the amount of dissolved silica and the modeled fraction of atmospheric precipitations for tributary rivers. Lake and outlet-river samples do not fall on this trend due to consumption of dissolved silica in the lake by diatoms

for composition of the basalts, carbonates, granites, and metamorphic rocks, and rain waters). The ratio of the modeled contribution from different rock types is close to their ratio in the catchment area, though in the case of Uliin-Gol carbonate rocks provide even more strontium than basalts because the former are more easily leached compared to the latter. Second, we modeled the contribution of atmospheric precipitations to the total amount of strontium in Lake Hovsgol water. We found that Uliin-Gol, Alag-Tsar-Gol, and Ih-Dalbain-Gol type of waters contribute 12%, 9%, and 10% of strontium, respectively. The major source of strontium (71%) is from atmospheric precipitations. This can also be seen from the $^{87}\text{Sr}/^{86}\text{Sr}$ versus $1/\text{Sr}$ diagram; Lake Hovsgol waters together with Egin-Gol waters are shifted far to the right on the diagram from rivers' composition (Fig. 5, top). Calculations performed in 1969–1971 have shown that direct atmospheric precipitations to Lake Hovsgol are 48% of the total input (Sodnom and Losev 1976). This value is about 20% lower than that obtained from our modeling based on strontium data. Whether this mismatch could result from incomplete sampling or is a real feature cannot be answered at present. To decrease the amount of atmospheric precipitation in our modeling we need to assume that the contribution of strontium from rivers of the Uliin-Gol type is higher than 1/3 (as in our modeling); this, however, is unlikely. An interesting and at the moment speculative idea is that Lake Hovsgol still contains ancient ice-melted waters. Considering the average outflow rate of $0.57\text{ km}^3/\text{year}$, the entire volume of Lake Hovsgol should have been completely overturned in 670 years if no evaporation was considered, and thus no ancient meltwaters from Bølling-Allerød warming could be preserved (note: Lake Baikal overturn is twice as high; Table 1). However, the present-day lake volume was not formed instantaneously at the Bølling-Allerød warming by meltwaters; it depended on variations of humidity/aridity of the climate. As pointed out by Fedotov et al. (2004), at about 5.5 Ka there was aridification of the climate, which could have decreased the Lake Hovsgol volume (thus reducing or even stopping the Egin-Gol outflow). Assuming a lower outflow rate, it seems probable that some ancient waters might exist in Lake Hovsgol. But this question requires additional studies.

Interestingly, concentrations of dissolved silica in inlet-river samples correlate with the modeled fraction of atmospheric precipitations (Fig. 5, bottom). Lake and outlet-river samples are characterized by depletion in dissolved silica; if this is not an artifact of limited sampling, it shows that silica is consumed in Lake Hovsgol by diatoms.

4 Volcanism as a Marker of Tectonic Processes

Basaltic volcanism is surface expression of melting at mantle depth (e.g., the source of melting beneath the Hovsgol region was estimated to be ~50–85 km deep; Demonterova et al. 2007). Melting is thought to be induced by upwelling from the transition zone of the mantle (410–660 km depth) of hotter and also fertile (with lower melting point) material compared to ambient mantle (Zorin et al. 2006).

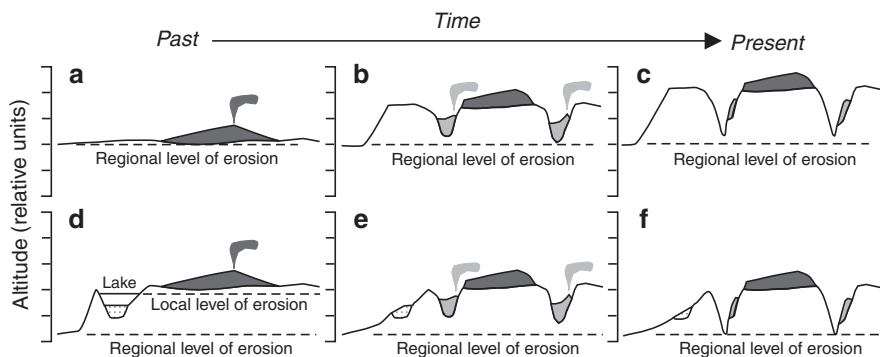


Fig. 6 A schematic model for formation of “summit” and “valley” lava remnants due to tectonic uplift at constant basal level of erosion (a–c) and due to sudden lowering of the regional level of erosion, in this case, as a result of a lake drainage (d–f). In both cases, the final effect will be the same: older lavas situated at higher elevations, usually on top of the mountains, and younger lavas occupying river terraces. Dark and light gray colors are for older and younger lavas, respectively. Dotted area is for lacustrine sediments

According to gravity data, several upwellings, referred to as upper mantle plumes, were the origin of high mountains; namely Hangai, Hentei, and Sayan ranges and uplands close to the Udokan and Vitim volcanic fields (Fig. 1) (Zorin et al., 2003). Thus, one may expect that rapid mountain growth should be followed by volcanic events. Schematically, this principle is shown in Fig. 6. Mountain uplift leads to fast erosion and formation of river valleys, which are filled by later lavas. It is worth mentioning that rapid river valley formation can result from the decrease of local level of erosion without any uplift, as for example in the case of paleolake drainage (Fig. 6). Such paleolakes existed in the Baikal rift system; for instance, Miocene lacustrine deposits are buried beneath lavas of the Vitim volcanic field (Rasskazov et al. 2000). Having this in mind, we focus only on those examples, where erosion could only result from tectonic uplift.

Similar argumentation was used by Rasskazov et al. (1998) in reconstruction of tectonic uplifts. Based on analysis of dated lava in relief Rasskazov et al. (1997), defined four episodes of tectonic uplifts: at about 20, 16, 8–5, and 0.7 Ma.

4.1 Dating of Volcanism

4.1.1 A Comment on Dating Methods

Volcanic rocks are dated by K-Ar and $^{40}\text{Ar}/^{39}\text{Ar}$ methods, which explore the ^{40}K - ^{40}Ar radioactive chain. Discussion of principles of these methods and their limitations are beyond the scope of the present review; it can be found elsewhere (e.g., McDougall and Harrison 1988; Ivanov et al. 2003; Chernyshev et al. 2006).

It should be mentioned that some laboratories (especially in earlier years; e.g., Bagdasar'yan et al. 1981) produced for Baikal rift volcanics erroneous K-Ar ages due to their laboratory procedures, and many of these erroneous ages were included in popular reviews (e.g., Whitford-Stark 1987), which are still in use in western literature. Besides this, K-Ar and $^{40}\text{Ar}/^{39}\text{Ar}$ methods can produce erroneous (beyond stated errors) ages because of some natural phenomena; K-Ar (and to some extent) $^{40}\text{Ar}/^{39}\text{Ar}$ ages for young volcanic rocks can be too old due to so-called excess argon (the closer to recent times, the more critical this problem becomes), whereas the true age of old volcanic rocks can be underestimated due to loss of radiogenic ^{40}Ar . In part, the $^{40}\text{Ar}/^{39}\text{Ar}$ method allows the controlling of these two problems and thus $^{40}\text{Ar}/^{39}\text{Ar}$ ages are generally considered as more reliable compared to K-Ar ages.

4.1.2 Brief Consideration of Timing of Volcanism in the Baikal Rift System

Published ages of volcanics erupting within and in the vicinity of the Baikal rift system were reviewed recently by Rasskazov et al. (2000). According to this review with reference to the original publication (Rasskazov 1993), the oldest (with Oligocene K-Ar ages) volcanic rocks are located in the area between the Bolshaya Belaya and Urik Rivers. We resampled and dated volcanic rocks from this area because no description of the analytical technique was provided in Rasskazov (1993). The results, which show that all volcanic rocks in this region fall into the Early Miocene, are discussed in Section 4.2.2. Lavas of probably Oligocene age have been dated in the western Hovsgol area (Ivanenko et al. 1988), but this was questioned by Rasskazov et al. (2003) (see Section 4.2.1). The Early Miocene volcanic rocks have also been dated by $^{40}\text{Ar}/^{39}\text{Ar}$ and K-Ar methods in Dzhida (22–17.5 Ma), Southern Baikal (~18 Ma), Hovsgol (22–16.5 Ma), East Sayan (20–16.5 Ma), and Eastern Tuva (~18–16 Ma) regions (Rasskazov et al. 2000; 2003), showing that volcanism occurred over a vast territory of the southwestern Baikal rift at that time (Fig. 1). In different regions, different numbers of volcanic events occurred at different times. There were volcanic events in the Middle and Late Miocene period and from the Pliocene to the Quaternary. Hovsgol and East Sayan examples for the Early and Late Miocene are considered in Sections 4.2.1 and 4.2.2, respectively. Pliocene to Quaternary volcanism of Dzhida and Eastern Tuva regions are considered in Section 4.2.3.

In the northwestern Baikal rift, volcanism started later in the Middle Miocene and pulsated up to the Quaternary and Holocene in the Vitim and Udokan volcanic fields, respectively (Fig. 1). In the Udokan, volcanic episodes of ~14, 7–9, 2.5–4, ~1.7–1.8, and 0.7 Ma to Holocene were recorded (Rasskazov et al. 2000; Stupak et al. 2008). In the Vitim, volcanic episodes of 13–14, 9–12, 3–4, and 0.6–1.1 Ma were recorded (Rasskazov et al. 2000). Since we have no additional information on these two fields compared to that of Rasskazov et al. (2000) and Stupak et al. (2008), and because these regions are outside the watershed area of Lake Baikal (Fig. 1) we remove them from further consideration.

4.2 Evidence from Volcanism on Tectonics

4.2.1 Example from Hovsgol

Figure 7 represents a natural example of the concept schematically shown in Fig. 6. Late Oligocene–Early Miocene “summit” lavas in the western Hovsgol area occupy a level of 2,700 m, whereas Late Miocene “valley” lavas are located within the paleo-river valley at a lower level of 2,100 m. This means that about 600 m of uplift and erosion have happened between 21–24 and 7.8 Ma. There is no strong constraint to assume that either the uplift was continuous (or in a number of rapid, but small magnitude uplifts) with an average rate of about 0.04 mm/year (~ 600 m/13–16 Ma), which is very small (see, for example, Section 3.1.2 for comparison), or that it took place rapidly between these two events of volcanic eruptions. Paleo-river terraces with Early and Middle Miocene alluvial deposits are not observed in the area. Thus, we conclude that the 600-m uplift took place rapidly just before the volcanic event dated at 7.8 Ma (Rasskazov et al. 2003). Importantly, the “valley” lava unit is displaced by the major rift-controlling fault. Two lava piles with exactly the same $^{40}\text{Ar}/^{39}\text{Ar}$ ages are displaced by the fault with an amplitude of about 400 m. There are no additional

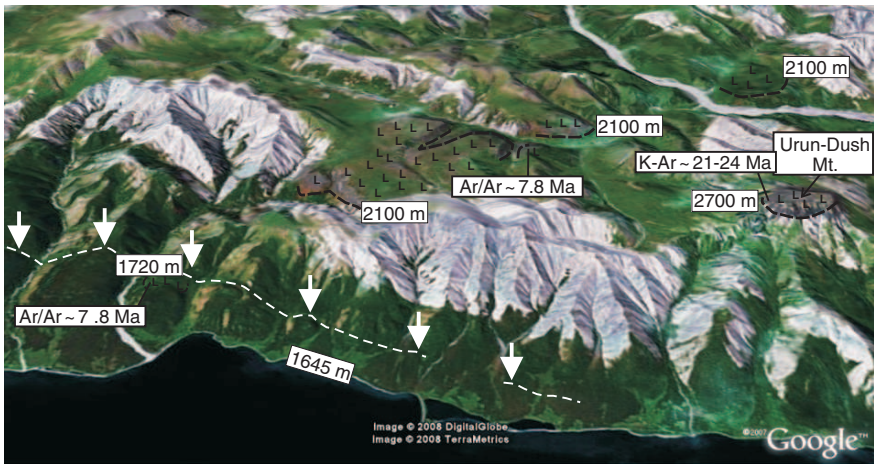


Fig. 7 A 3-D east to west view of the location of Miocene basalts (marked by “L” symbols) in relief of the western Hovsgol rift shoulder. *Bold dashed lines* mark the basal level of basaltic lavas, whose elevation is shown in m a. s. l. *Tips of white arrows* point to a rift fault, whose surface expression is traced by the *white dashed line*. $^{40}\text{Ar}/^{39}\text{Ar}$ ages (7.76 ± 0.12 and 7.84 ± 0.06 Ma for 2,100-m and 1,700-m-level lavas, respectively) have been obtained at Vrije Universiteit Brussel (Belgium) (Rasskazov et al. 2003). For a description of the analytical details see Ivanov et al. (2003). These ages are in agreement with earlier K-Ar ages for the 2,100-m-level lava unit (Ivanenko et al. 1988). However, there is some disagreement on the K-Ar dating of the 2,700-m-level lavas. Ivanenko et al. (1988) and Rasskazov et al. (2003) reported ages of 24.3 ± 0.4 (as the mean of two ages) and 21.4 ± 0.8 Ma, respectively. The correct age is an important subject for a future check-up study, because this is a likely candidate for the earliest eruption in the Baikal rift system

constraints when exactly the displacement took place (this could have happened any time between 7.8 Ma and the present day). However, it is logical to assume that rifting in the Hovsgol area initiated about 7–8 Ma, close in time to the Late Miocene volcanic event. There is no evidence for uplift and erosion prior to 21–24 Ma.

4.2.2 Examples from East Sayan

Rasskazov (1993) reported K-Ar ages of 23.7 ± 1.1 Ma and 15.8 ± 0.9 Ma, respectively, for the base and top of the continuous “summit” lava unit at Ermoshyn-Sardyk mounting (Urik–Bolshaya Belaya drainage area) (Fig. 1). The former age is one of the oldest among those published for the Baikal rift system and needs to be verified. It is also important to know whether these ages are correct, because, if yes, they suggest no uplift and erosion between 24 and 16 Ma, which would be in disagreement with nearby regions (Rasskazov et al. 1998). A few other K-Ar ages between 21 and 11 Ma were also reported for different hypsometric levels of the Urik–Bolshaya Belaya drainage area (Rasskazov 1993).

Figure 8 (bottom) shows the position of lavas in the modern relief in this area. It may be seen that different lava units occupy levels between 2,200 and 1,500 m a.s.l. (Urik and Bolshaya Belaya Rivers are 880 and 1,030 m, respectively, at their crossing the Major Sayan Fault). However, all newly dated samples (seven in total) from five different lava units yielded K-Ar ages practically within their analytical errors at about 15–17 Ma (Table 3). Neither Oligocene nor Late Miocene lavas were found, and thus we disregard the earlier K-Ar data.

Figure 8 (top) provides evidence that the Early Miocene lava filled a ~100-m-deep paleo-river valley and that the lava flows accumulated rapidly. The remnants of this valley are now at the summit elevations in the region, suggesting differentiated tectonic movements of small blocks at the boundary of two large distinct lithospheric structures; namely the Tuva-Mongolia massif and the Siberian craton. It means, first, that there was tectonic-related erosion prior to the volcanic event of 15–17 Ma and, second, that much of the uplift (about 1 km) was formed after this volcanic event due to contraction at the boundary of the Tuva-Mongolia massif and the Siberian craton. Another representative example in East Sayan is a location at the Bokson River mouth, where Bokson joins the Oka River (Rasskazov 1993; Rasskazov et al. 1998, 2000) (Fig. 1). Figure 9 shows that there were two episodes of uplift and erosion; first, before the volcanic event at about 20 Ma with up to 600–1,000 m of uplift and erosion, and second, before the volcanic event at about 5 Ma with about 150 m of uplift and erosion.

4.2.3 Example from Khamar-Daban

Volcanism in the drainage area of the Dzhida River and at the southern end of Lake Baikal in the Khamar-Daban range started in the Early Miocene. Rasskazov et al. (2003) provided evidence that initial lava with a $^{40}\text{Ar}/^{39}\text{Ar}$ age of 21.9 ± 0.2 Ma

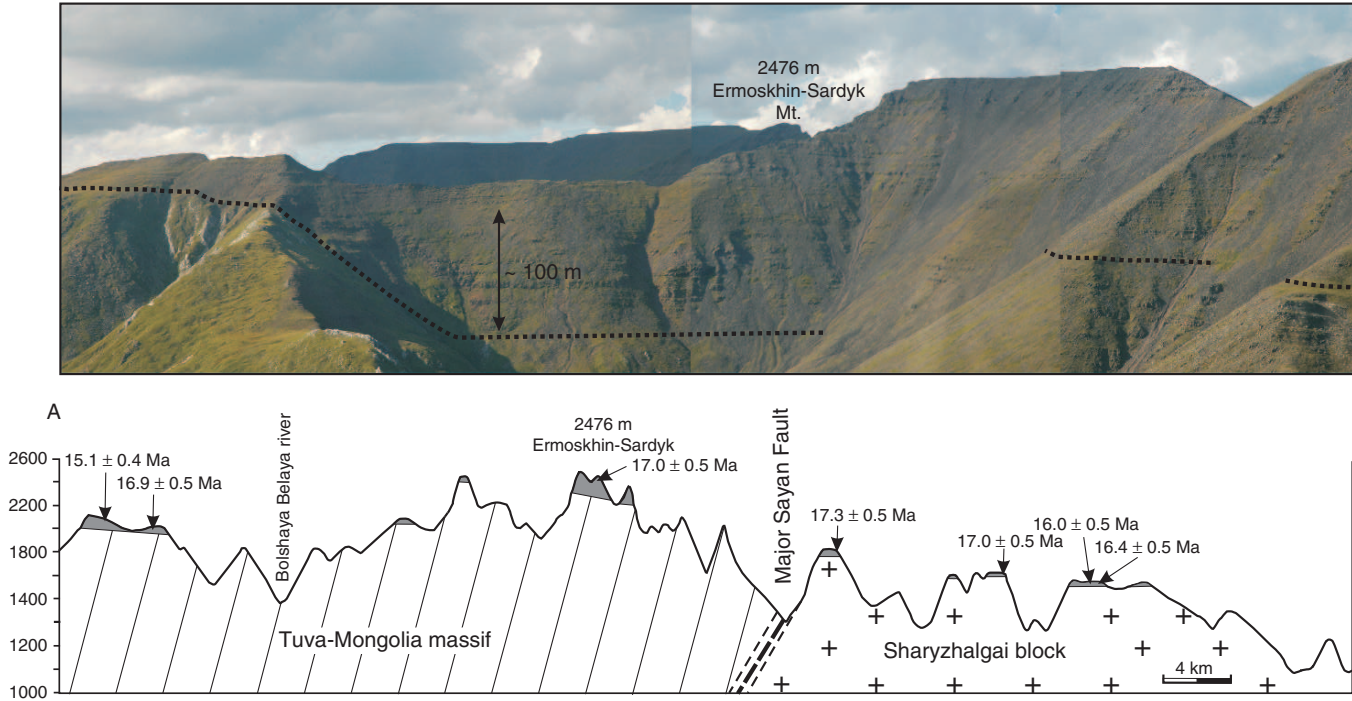


Fig. 8 A profile (*bottom*) across the Major Sayan Fault showing the position of remnants of the Early Miocene lava flows in the area between Urik and Bolshaya Belaya Rivers. Lava units are shown in *gray*. Locations of K-Ar dated samples (Table 3) are marked. A photo (*top*) gives a view on the Ermoskhin-Sardyk lava unit. *Dotted line* traces the bottom of the lava unit, showing that Early Miocene lavas buried a river valley of about 100 m deep. There is no visual discontinuity in the lava unit, providing evidence for rapid accumulation of the lava within the Early Miocene volcanic episode.

Table 3 New K-Ar ages for basaltic lavas from Urik and Bolshaya Belaya watershed area, East Sayan

Sample	Location	K (%) $\pm \sigma$	$^{40}\text{Ar}_{\text{rad}}$ (ng/g) $\pm \sigma$	$^{40}\text{Ar}_{\text{atm}}$ (%)	Age (Ma) $\pm 2\sigma$
UB-07-4	52°43'52" 101°26'05"	1.23 \pm 0.02	1.407 \pm 0.006	10.2	16.4 \pm 0.5
UB-07-3	52°43'52" 101°26'05"	1.44 \pm 0.02	1.603 \pm 0.008	10.6	16.0 \pm 0.5
UB-07-9	52°42'10" 101°23'30"	0.97 \pm 0.015	1.143 \pm 0.005	8.2	17.0 \pm 0.5
UB-07-16	52°39'14" 101°16'03"	1.62 \pm 0.02	1.954 \pm 0.008	8.8	17.3 \pm 0.5
UB-07-27	52°33'18" 100°47'31"	1.33 \pm 0.02	1.568 \pm 0.007	9.4	16.9 \pm 0.5
UB-07-34	52°34'34" 101°08'28"	1.55 \pm 0.02	1.835 \pm 0.009	11.1	17.0 \pm 0.5
UB-07-40	52°34'13" 100°45'02"	1.61 \pm 0.02	1.689 \pm 0.008	10.7	15.1 \pm 0.4

Measurements of argon isotopes were performed at Institute of Geology of Ore Deposits, Petrography, Mineralogy, and Geochemistry, Russian Academy of Sciences (Moscow) using MI-1201 IG mass-spectrometer with ^{38}Ar spike. K concentrations were determined by flame photometry at the same Institute. Analytical description can be found in Chernyshov et al. (2006). For the age calculations, conventional constants were used (Staiger and Jäger 1978).

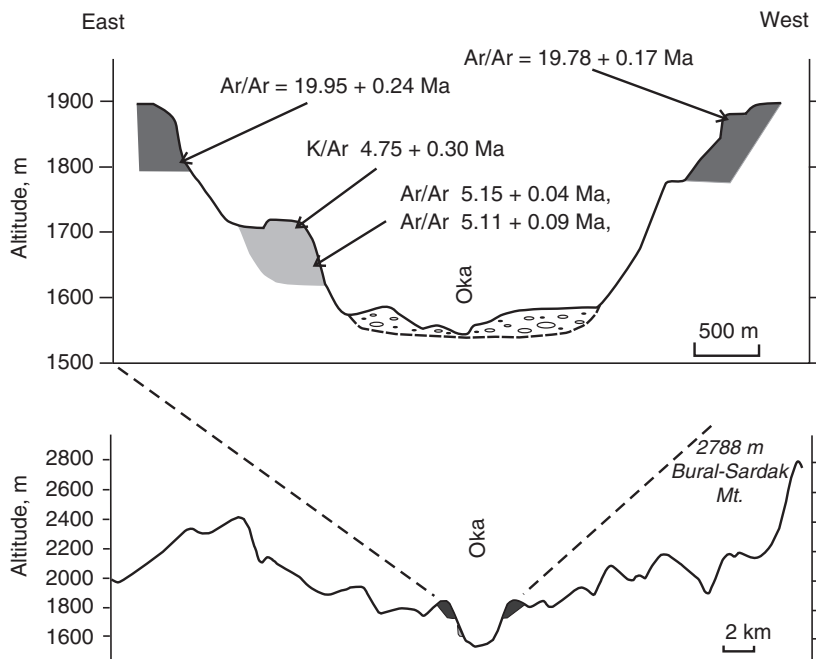


Fig. 9 A profile showing the position of the Early Miocene and Early Pliocene lava units at the site where Bokson River joins the Oka River. Lava units of different ages are shown in grays of different intensity. The *top* figure is reproduced after Rasskazov et al. (2000). The *bottom* figure gives an extended view to show that the Early Miocene lava erupted in an up to 600–1,000 m deep river valley

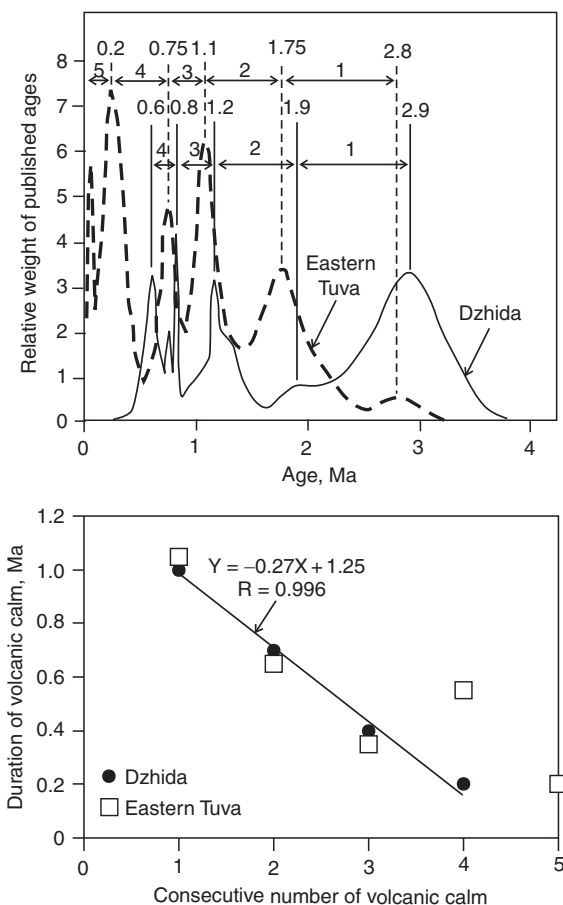
erupted on a flat surface, whereas lava with $^{40}\text{Ar}/^{39}\text{Ar}$ ages between 19 and 17.5 Ma filled river valleys on both sides of the Khamar-Daban range. This places the timing of the uplift to about 20 Ma.

4.2.4 Tectonically Triggered Pulses of the Pliocene and Quaternary Volcanism

The Pliocene and Quaternary volcanism occurred over the Baikal rift system and adjacent regions of Mongolia (Fig. 1); however, most of the magma volume (~87%) erupted within the Eastern Tuva volcanic field (Demonteirova 2002). The reasons for this are not understood. The Pliocene–Quaternary episode of volcanism in the Eastern Tuva was preceded by two episodes of less intensive volcanism in the Early and Middle Miocene (Rasskazov et al. 2000). Here, we compare the latest pulse of volcanism in the Eastern Tuva with that in the Dzhida area, because these two regions were most thoroughly dated by K-Ar and $^{40}\text{Ar}/^{39}\text{Ar}$ methods. The Pliocene–Quaternary volcanism in the Dzhida area was also preceded by the Early Miocene volcanic event.

Published ages for the Eastern Tuva and Dzhida volcanic fields are summarized in Fig. 10 (top). A number of brief volcanic pulses are seen. Some peaks are small compared to others, reflecting different degrees of sampling of different units. With some uncertainty, we separate pulses of about 2.9, 1.9, 1.2, 0.8 (or duplicated peaks at 0.8 and 0.75 Ma), and 0.6 Ma for the Dzhida volcanic field and those of about 2.8, 1.75, 1.1, 0.75, 0.2 Ma, and in the Latest Pleistocene–Holocene for the Eastern Tuva volcanic field (Fig. 10, top). It seems that volcanic pulses in the Eastern Tuva concordantly followed that in Dzhida with a delay of about 0.1 Ma starting from the Pliocene until the Middle Pleistocene. The duration of the volcanic calms (between peaks of volcanism) in both regions shows the same correlation with the consecutive number of volcanic calms (Fig. 10, bottom). However, in the Middle Pleistocene (0.8–0.6 Ma), volcanism stopped in the Dzhida area, while in the Eastern Tuva it attained another periodicity. There is no simple explanation for that. Probably, volcanic eruptions were triggered by movement of the lithospheric blocks (plates and microplates). For example, movement of the Amurian plate is thought to be at the origin of opening of the Baikal rift basins (Zonenshain and Savostin 1981) (Fig. 1). A number of other, smaller plates were also defined by GPS data (e.g., Lukhev et al. 2003). For example, ancient structures, like the Tuva-Mongolia massif, played a role in controlling extension and volcanism in the southwestern Baikal rift system (Vasil'ev et al. 1997; Demonteirova et al. 2007). Movement of one plate should create additional forces on boundaries of other plates and, in such a way, tectonic stress propagates. Here, we assume that deformations at the Amurian plate western boundary controlled periodicity of volcanism in the Dzhida volcanic field. These deformations propagated with delay to the western boundary of the Tuva-Mongolia massif and controlled volcanism in the Eastern Tuva volcanic field. This tectonic regime was a characteristic from the Pliocene until the Middle Pleistocene. At 0.8–0.6 Ma, some tectonic reorganization took place, which resulted in termination of volcanism in the Dzhida area and another periodicity of volcanism in the Eastern Tuva.

Fig. 10 Relative probability distribution of K-Ar and $^{40}\text{Ar}/^{39}\text{Ar}$ ages for the Pliocene–Quaternary volcanism in Dzhida and Eastern Tuva volcanic fields (*top*) and relation between duration of volcanic calms in respect the consecutive number of the calms (*bottom*). Age data are after Kononova et al. (1988), Rasskazov et al. (1996, 2000) and Yarmolyuk et al. (1999, 2003) (25 and 39 ages for the Dzhida and Eastern Tuva, respectively). In the *top* figure, peaks of volcanic activity are shown in millions of years (Ma) and intervolcanic calms are separately numbered for each volcanic field. Height of peaks reflects a relative number of published ages and does not necessarily correspond to the amount of erupted magma.



5 Discussion

The beginning of the initial stage of rifting can be placed to the Eocene or an earlier time (Logatchev and Florensov 1978; Mats 1993; Logachev 2003). However, the record of this stage is incomplete due to the rarity of outcrops with sediments of this age on the shore of Lake Baikal. The complete history of the initial stage is stored in the lowermost sediments of the Southern and Central Baikal basin, which cannot be achieved currently due to great thickness of the sediments (Table 1).

Volcanism started in the Early Miocene or probably in the Late Oligocene. The Early Miocene pulse of volcanism was widespread throughout the southwestern Baikal rift system and was preceded by tectonic uplift, which happened at about 20 Ma. At this time, the East Sayan range was created and, probably, the drainage pattern in the region was completely reorganized.

The precise time when Lake Baikal came to its present-day shape is not known, but it is obvious that the lake is among the oldest on Earth. ^{10}Be dating of drill-core

sediments recovered at the BDP-98-2 borehole provides evidence for at least 8.4 Ma of its history (Horiuchi et al. 2003, 2004). Analysis of the rate of sedimentation suggests that there was a major change at about 5 Ma when the rate decreased by about 2.5 times (Fig. 2, left). The only reasonable explanation for this is tectonic isolation of the submerged Akademichesky ridge from sedimentary input of tributary rivers. The Akademichesky ridge built up and the Central and Northern Baikal basins deepened (Fig. 3). The East Sayan range experienced an additional uplift as seen from eruption of lava into deepened river valleys at about this time (Fig. 9).

In the Late Miocene (5–8.4 Ma), a few changes of the sedimentation rate are also visible in the sedimentary record of Lake Baikal. Because at this time there was no isolated Akademichesky ridge, the increasing rate of sedimentation means an increasing rate of erosion in the watershed area, which in its turn is directly related to an increasing rate of mountain growth. Such an event is seen in the sedimentary record at about 7 Ma (Fig. 2, left). It is known that the Baikal rift system originated at the Southern and Central Baikal basins and propagated towards its southwestern and northeastern wings (e.g., Logachev 2003). The event of 7 Ma is a likely candidate for the timing of such propagation. Data for the Hovsgol basin are in general agreement with this.

The latest tectonic event, which reorganized the outlet pattern of Lake Baikal, probably took place at about 0.1 Ma. It is recorded by a rapid increase of the $^{87}\text{Sr}/^{86}\text{Sr}$ ratio in sediments which reflects an efficient proxy of terrigenous input. This event was probably, at least in part, due to glacial rebounding of the region.

Plausibly, the four tectonic events discussed here are far from complete, but these four are more pronounced and this could influence biota evolution through such mechanisms as reorganization of drainage patterns, which can control migration of animal species. For instance it has been documented that the fish species *Thymallus* (Grayling) and *Brachymystax lenok* migrated from Lena to Baikal and then to Angara and Lake Hovsgol (Koskinen et al. 2002; Froufe et al. 2008). The tectonic uplift was also at the origin of increasing rates of erosion and thus led to increased flux of terrigenous material into Lake Baikal. This could affect transparency of water and its chemical composition, and thus affect the environment. Beyond tectonics, the paleoclimate controlled biota evolution and in some cases paleoclimate could also control tectonic and volcanism patterns. For example, cessation of volcanism in the Dzhida and Vitim volcanic fields happened at about 0.6 Ma and reorganization of periodicity of volcanism in Eastern Tuva took place at about 0.8 Ma. Previously, we have shown that the outlet pattern of Lake Baikal reorganized at about 0.1 Ma. Study of diatoms in sedimentary cores of the BDP-96-1 and BDP-96-2 has shown that *Cyclotella minuta* and *Aulacoseira baicalensis* became important in Lake Baikal starting from 760 and 120 Ka, respectively, because of interglacial episodes of global warming (Grachev et al. 1998). Is that merely a coincidence? The answer could be that climate controlled the diatom evolution, and climate controlled volcanism and tectonics at these landmarks of time.

Siberia was covered nearly completely by glaciers several times (Grosvald 1965), though the number of such glaciations and their extents are debated (e.g., Karabanov et al. 2001). Warming at the interglacial period of MIS5, known in

Siberia as the Kazantsevsky interglacial, started at about 130 Ka. It not only made the climate comfortable for diatoms such as *A. baicalensis* but also led to rapid degradation of glaciers and increasing rates of mounting growth. The latter was responsible for termination of the paleo-Manzurka outlet as argued above.

Quaternary volcanoes of the Eastern Tuva erupted under thick ice sheets several times forming specific volcanic edifices, referred to as tuya, during glacial times and forming normal lava flows and cinder cones at interglacials (Grosvald 1965; Yarmolyuk et al. 1999; Rasskazov et al. 2000; Komatsu et al. 2004; Yarmolyuk and Kuz'min 2004). It seems that one important interglacial period in this region happened at about 0.7–0.6 Ma (because K-Ar ages of 0.82–0.72 and ~0.6 Ma have been obtained for tuya volcanic edifices; Yarmoyuk et al. 1999; Rasskazov et al. 2000; Demonterova 2002). Glaciers at 0.8–0.7 Ma covered almost the entire Eastern Tuva volcanic field. Having in mind uncertainties of K-Ar ages for such a young period of time, the dated interglacial of 0.7–0.6 Ma in Eastern Tuva cannot be distinguished from the interglacial derived from more accurately dated BDP cores (starting from about ~760 Ka; Grachev et al. 1998). Warming at this time created comfort conditions for *C. minuta* in Lake Baikal and stipulated the postglacial uplift in Eastern Tuva. Disappearance of the thick ice sheet led to glacial isostasy of the whole lithospheric section and probably resulted in an increase of partial melting due to decompression. It could explain why volcanism terminated in the Dzhida area, which did not experience total glaciations in the Pleistocene, and is still continuing in Eastern Tuva.

Lake Hovsgol underwent a completely different history compared to Lake Baikal. It was a small saline lake until fairly recently. In the Pre-Holocene, melt-water income and increase of atmospheric precipitations at the Bølling-Allerød warming raised water level of Lake Hovsgol to the present-day level and connected with Lake Baikal through the Egin-Gol and Selenga Rivers. This allowed new, Baikalian-like species to evolve in new ecological niches.

6 Conclusions

To summarize, we suggest that tectonic events at 20, 7, 5, and 0.1 Ma could have influenced biota evolution in Lake Baikal and the surrounding regions through reorganization of drainage patterns and increasing influx of sediments into the lake. Sudden extinctions and appearances of animal and plant species as well as their degradations and flourishing recorded at other periods of time were likely associated with climatic changes and not related to tectonic activity in the Baikal rift system.

Acknowledgements We thank Professor W.E.G. Müller for his kind invitation and editorial handling. V.A. Lebedev performed K-Ar age determinations and O.A. Skyarova analyzed water samples for trace elements. The work was financially supported by the President of Russian Federation (grant MK-1228.2008.5 for E.I.D.) and Russian Foundation for Basic Research (grant 08-05-98100 for E.I.D. and A.V.I.). E.I.D. also thanks Russian Scientific Support Foundation.

References

- Bagdasar'yan GP, Gerasimovskii VI, Polyakov AI, Gukasian RH (1981) New data on age and chemical composition of the volcanic rocks from Baikal rift system. *Geochimiya* 3:342–350.
- Bogoyavlensky BA (Ed-in-Chief) (1989) Atlas of Lake Hovsgol. Irkutsk State University, Mongolian National University, Institute of Geography SB USSR. Moscow
- Capo RC, Stewart BW, Chadwick OA (1998) Strontium isotopes as tracers of ecosystem processes: theory and methods. *Geoderma* 82:197–225.
- Chernyshev IV, Lebedev VA, Arakelyants MM (2006) K-Ar dating of Quaternary volcanics: methodology and interpretation of results. *Petrology* 14:62–80.
- Colman MS (1998) Water-level changes in Lake Baikal, Siberia: tectonism versus climate. *Geology* 26:531–534.
- Demonterova E.I. (2002) Late Cenozoic magmatism of the Eastern Tuva [Pozdnekainozoiskii magmatizm Vostochnoi Tuvy]. Candidate science (Ph.D. equivalent) thesis. Irkutsk, Institute of the Earth's Crust (in Russian).
- Demonterova EI, Ivanov AV, Rasskazov SV, Markova ME, Yasnygina TA, Malykh YuM (2007) Lithospheric control on Late Cenozoic magmatism at the boundary of the Tuva-Mongolian massif, Khubsugul area, Northern Mongolia. *Petrology* 15:90–107.
- Falkner KK, Church M, Measures CI, LeBaron G, Thouron D, Jeandel C, Stordal MC, Gill GA, Mortlock R, Froelich P, Chan L-H (1997) Minor and trace element chemistry of Lake Baikal, its tributaries, and surrounding hot springs. *Limnol Oceanogr* 42:329–345.
- Faure G (1986) Principles of isotopic geology. New York: Wiley.
- Fedotov A, San'kov V, De Batist M, Kazansky A, Parfeevets A, Miroshnitchenko A, Pouls T (2006) Chronology of the Baikal rift system. *Eos* 87:246–250.
- Fedotov AP, Chebykin EP, Semenov MYu, Vorobyova SS, Osipov EYu, Goobokova LP, Pogodaeva TV, Zheleznyakova TO, Grachev MA, Tomurhuu D, Oyunchimeg Ts, Narantsetseg Ts, Tomurtogoo O, Dolgikh PT, Arsenyuk MI, De Batist M (2004) Changes in the volume and salinity of Lake Khubsugul (Mongolia) in response to global climate changes in the upper Pleistocene and the Holocene. *Palaeogeogr Palaeoclimat Palaeoecol* 209:245–257.
- Fedotov AP, Phedorin MA, De Batist M, Ziborova GA, Kazansky AY, Semenov MY, Matasova GG, Khabuev AV, Kugakolov SA, Rodyakin SV, Krapivina SM, Pouls T. (2008) A 450-ka long record of glaciation in Northern Mongolia based on studies at Lake Khubsugul: high-resolution reflection seismic data and grain-size variations in cored sediments. *J Paleolimnology* 39:335–348.
- Fedotov FP, De Batist V, Shapron T, De Ryker R, Pauls N (2002) Seismic profiling of the sediments of Lake Khubsugul. *Doklady Earth Sci* 382:75–77.
- Froufe E, Alekseyev S, Alexandrino P, Weiss S (2008) The evolutionary history of sharp- and blunt-snouted lenok (*Brachymystax lenok* (Pallas, 1773)) and its implications for the paleohydrological history of Siberia. *BMC Evol Biol* 8: doi:10.1186/1471-2148-8-40
- Galaziy GI (Ed-in-Chief) (1993) The Baikal, atlas. Russian Academy of Sciences, Siberian Branch, Interdepartmental scientific committee for the program "Siberia", Federal service on geodesy and mapping of Russia. Moscow.
- Gibbard PL, Smith AG, Zalasiewicz JA, Barry TL, Cantrill D, Coe AL, Cope JCW, Gale AS, Gregory FJ, Powell JH, Rawson PF, Stone P, Waters CN (2005) What status for the Quaternary? *Boreas* 34:1–6.
- Gorokhov IM, Semikhatov MA, Baskakov AV, Kutyavin EP, Melnikov NN, Sochava AV, Turchenko TL (1995) Sr isotopic composition in the Riphean, Vendian and Lower Cambrian carbonates from Siberia. *Stratigr Geol Corr* 3:1–28.
- Grachev MA, Vorobyova SS, Likhoshway YV, Goldverg EL, Ziborova GA, Levina OV, Khlystov OM (1998) A high-resolution diatom record of the paleoclimates of East Siberia for the last 2.5 My from Lake Baikal. *Quat Sci Rev* 17:1101–1106.
- Grosvald MG (1965) Development of relief in the Sayan-Tuva highland [Razvitie rel'efa Sayano-Tuvinskogo nagor'ya] Moscow: Nauka.

- Hidding B, Michel E, Natyaganov AV, Sherbakov DYu (2003) Molecular evidence reveals a polyphyletic origin and chromosomal speciation of Lake Baikal's endemic asellid isopods. *Mol Ecol* 12:1509–1514.
- Horiuchi K, Matsuzaki H, Kobayashi K, Gol'dberg EL, Shibata Y (2003) Be-10 record and magnetostratigraphy of a Miocene section from Lake Baikal: re-examination of the age model and its implication for climatic changes in continental Asia. *Geophys Res Lett* 30:1602.
- Horiuchi K, Gol'dberg EL, Matsuzaki H, Kobayashi K, Shibata Y (2004) Verification of magnetostratigraphic scales of Miocene core section from Lake Baikal. *Geologiya i Geofizika* 45:408–412.
- Hutchinson DR, Golmshtok AJ, Zonenshain LP, Moore TC, Scholz CA, Klitgord KD (1992) Depositional and tectonic framework of the rift basins of Lake Baikal from multichannel seismic data. *Geology* 20:589–592.
- Ivanenko VV, Karpenko MI, Yashina RM, Andreeva ED, Ashihmina NA (1988) New data on potassium-argon ages of basalts in the western slope of the Khubsugul rift (Mongolia) [Novye dannye o kali-argonovom vozraste basaltov zapadnogo borta Khubsugul'skogo rifta (MNR)]. *Doklady Akademii Nauk SSSR* 300:925–929.
- Ivanov A (2004) One rift – two models. *Sci First Hand* 1:50–61.
- Ivanov AV, Boven AA, Brandt SB, Brandt IS, Rasskazov SV (2003) Achievements and limitations of the K-Ar and ⁴⁰Ar/³⁹Ar methods: what's in it for dating the Quaternary sedimentary deposits? *Berliner Paläobiolog Abh* 4:65–75.
- Ivanov AV, Demonterova EI, Rasskazov SV, Yasnygina TA (2008) Low-Ti melts from the Southeastern Siberian Traps Large Igneous Province: evidence for a water-rich mantle source? *J Earth Syst Sci* 117:1–21.
- Karabanov EB, Prokopenko AA, Kuz'min MI, Williams DF, Gvozdkov AN, Kerber EV (2001) Glacial and interglacial periods of Siberia: paleoclimate record of Lake Baikal and correlation with West Siberian stratigraphic scheme (the Bruhnes Cron). *Geologiya i Geofizika* 42:48–63.
- Kazansky AYu, Fedotov AP, Matasova GG, Yuldashev AA, Ziborova GA, Zheleznyakova TO, Vologina EG, Oyunchimeg Ts, Narantssetseg Ts, Tomurhuu D (2005) First paleomagnetic results from the bottom sediments of Lake Hovsgol based on drilling data. *Russ Geol Geophys* 46:446–449.
- Kimstach V, Meybeck M, Barovdy E. (1998) A water quality assessment of the Former Soviet Union. Taylor & Francis, London.
- Komatsu G, Arzhannikov SG, Arzhannikova AV, Ershov K (2004) Geomorphology of subglacial volcanoes in the Azas Plateau, the Tuva Republic, Russia. *Geomorphology* 88:312–328.
- Kononov EE, Mats VD (1986) History of the Baikal water runoff [Istoriya formirovaniya stoka vod Baikala]. *Izv Vyssh Uchebn Zaved Geol Razved* 6:91–98 (in Russian).
- Kononova VA, Karpenko MI, Akakeliants MM, Andreeva ED, Pervov VA (1988) New K-Ar data on Cenozoic continental basalts from the Baikal rift system [Novye dannye o K-Ar vozraste kainozoiskih kontinental'nykh basal'tov Baikal'skoi riftovoi sistemy]. *Doklady Akademii Nauk USSR* 303:454–457 (in Russian).
- Koskinen MT, Knizhin I, Primmer CR, Schlötterer C, Weiss S (2002) Mitochondrial and nuclear DNA phylogeography of *Thymallus* spp. (grayling) provides evidence of ice-age mediated environmental perturbations in the world's oldest body of fresh water, Lake Baikal. *Mol Ecol* 11:2599–2611.
- Kuzmin MI, Drill SI, Sandimirov IV, Sandimirova GP, Geletii VF, Chukanov VS, Kalmychikov GV, Bychinskii VA (2007) Strontium isotope variations in the sedimentary sequence of Lake Baikal. *Doklady Earth Sci* 412:131–135.
- Levi KG, Zadonina NV, Berdnikov NE, Voronin VI, Glyzin AV, Kusner YuS (2002) Modern geodynamics and heliodynamics [Sovremennaya geodinamika I geleodinamika]. Irkutsk, IrGTU Publisher (in Russian).
- Logachev NA (2003) History and geodynamics of the Baikal rift. *Geologiya i Geofizika* 44:391–406.
- Logatchev NA, Florensov NA (1978) Baikal system of rift valleys. *Tectonophysics* 45:1–13.
- Logachev NA, Zorin YuA (1987) Evidence and causes of the 2-stage development of the Baikal rift. *Tectonophysics* 143:225–234.
- Logachev NA, Antoshenko-Olenev NA, Bazarov DB, Galkin VI, Goldyrev GS, Endrichinskii AS, Zolotarev GG, Sizikov AI, Fufimtsev GF (1974). Highlands of the Near-Baikal and Trans-Baikal areas [Nagor'ya Pribaikal'ya i Zabaikal'ya]. Moscow: Nauka (in Russian).

- Lukhev AV, San'kov VA, Miroshnichenko AI, Levi KG, Bashkuev YB, Dembelov MG, Zalutskii VT, Calais E, Deverchere J, Vernol M, Bekhtur B, Amarzhargal S (2003) New data on recent tectonic deformations in the South mountain framing of the Siberian Platform. *Dokady Earth Sci* 389:263–266.
- Mashiko K, Kamaltynov RM, Sherbakov DYu, Morino H (1997) Genetic differentiation among gammarid (*Eulimnogammarus cyaneus*) populations by localized topographic changes in ancient Lake Baikal. *Archive fur Hydrobiologie* 139:379–387.
- Mats VP (1993) The structure and development of the Baikal Rift Depression. *Earth Sci Rev* 34:81–118.
- McDougall I, Harrison MT (1988) *Geochronology and thermochronology by $^{40}\text{Ar}/^{39}\text{Ar}$ method*. New York/Oxford: Oxford University Press/Clarendon
- Müller WEG, Schröder HC, Wrede P, Kaluzhnaya OV, Belikov SI (2006) Speciation of sponges in Baikal-Tuva region: an outline. *J Zool Syst Evol Res* 44:105–117.
- Paradina LP, Kulikova NN, Sutin AN, Saibatalova YV (2004) Sampling, sample preparation and ICP-MS chemical analysis of Lake Baikal sponges. *Geostand Geoanal Res* 28:225–232.
- Parfeevets AV, Sankov VA (2006) Stress-field conditions of the Earth's crust and geodynamics of the south-western Baikal rift system [Napryazhennoe sostoyanie zemnoi kory i geodinamika yugo-zapadnoi chasti Baikal'skoi riftovoi sistemy]. Novosibirsk: "Geo" Publisher.
- Pisarkiy BI, Shpeizer GM, Badrakh D, Mineyeva LA (1978) Formation of naleds in basin of Khubsugul Lake (Mongolian People's Republic). In: Sanger FJ (ed) *Permafrost: Second International Conference*, National Academy of Sciences, Washington, DC, pp. 396–400.
- Rasskazov SV (1993). Magmatism of the Baikal rift system [Magmatizm Baikal'skoi riftovoi sistemy]. Novosibirsk: Nauka (in Russian).
- Rasskazov SV, Kunk MJ, Luhr JF, Bowring SA, Brandt IS, Brandt SB, Ivanov AV (1996) Episodes of eruptions and compositional variations of the Quaternary lavas in the Baikal rift system (Ar-Ar and K-Ar dating of volcanism in the Dzhida River area). *Rus Geol Geophys* 37:1–12.
- Rasskazov SV, Logatchev NA, Ivanov AV (1998) Correlation of tectonic and magmatic events between the Baikal rift system and the Southeastern Eurasian plate. *Geotectonics* 32:272–285.
- Rasskazov SV, Logachev NA, Brandt IS, Brandt SB, Ivanov AV (2000) Geochronology and geodynamics in the Late Cenozoic: (South Siberia–South and East Asia) [Geokhronologiya i geodinamika pozdnego kainozoya (yuzhnaya Sibir' – yuzhnaya i vostochnaya Aziya)]. Novosibirsk: Nauka
- Rasskazov SV, Luhr JF, Bowring SA, Ivanov AV, Brandt IS, Brandt SB, Demonterova EI, Boven AA, Kunk M, Housh T, Dungan MA (2003) Late Cenozoic volcanism in the Baikal rift system: evidence for formation of the Baikal and Khubsugul basins due to thermal impacts on the lithosphere and collision-derived tectonic. *Berliner Paläobiologie Abh* 4:33–48.
- Reznitskii LZ, Belichenko VG, Sandimirova GP, Barash IG, Nekrasova EA, Pakhol'chenko YuA (2001) First occurrence of rapakivi-like granites in Eastern Khubsugul area and its significance for paleotectonic reconstructions [Pervaya nahodka rapakivividnykh granitov d Vostochnom Prikhubsugul'e I ih znachenie dlya paleotektonicheskikh rekonstruktsiy]. In: Sizykh AI (ed) *Geodynamic regimes of the Central Asia fold belt formig*. Intermet Engineering, Moscow, pp. 165–177.
- Romashkin PA, Williams DF (1997) Sedimentation history of the Selenga Delta, Lake Baikal: simulation and interpretation. *J Paleolimnol* 18:181–188.
- Sandimirov IV, Bashina VS, Sandimirova GP, Pakhol'chenko YuA (2002) Strontium isotopic composition of water system and bottom sediments of Lake Baikal [Izotopnyi sostav strontsiya v vodnoi sisteme i donnykh osadkakh oz. Baikal]. *Proceedings of Conference on Geology, Geochemistry and Geophysics at XX and XXI Centuries*. RFBR in Asian region. Irkutsk, pp. 408–410.
- Sherbakov DYu (1999) Molecular phylogenetic studies of the origin of biodiversity in Lake Baikal. *Trends Ecol Evol* 14:92–95.
- Slugina ZV (2006) Endemic bivalvia in ancient lakes. *Hydrobiologia* 568(S):213–216.
- Sodnom N, Losev NF (eds) (1976) *Natural conditions and resources of Mongolian People's Republic*. [Prirodnye usloviya i resursy MNR] Moscow: Nedra (in Russian).
- Steiger RH, Jäger E (1977) Subcommission on geochronology: convention on the use of decay constants in geo- and cosmochronology. *Earth Planet Sci Lett* 36:359–362.

- Stupak FM, Lebedev VA, Kudryashova EA (2008) The stages and distribution areas of the late Cenozoic volcanism in the Udokan Range in Transbaikalia based on geochronologic studies. *J Volcan Seism* 2:30–39.
- Suturin AN, Paradina LF, Epov EN, Semenov AR, Lozhkin VI, Petrov LL (2003) Preparation and assessment of a candidate reference sample of Lake Baikal deep water. *Spectrochim Acta B* 58:277–288.
- Timoshkin O (2004) Siberian “Freshwater Australia”. *Sci First Hand* 1:62–75.
- Trofimov AG, Malaeva EM, Kulikov OA, Popova SM, Kulagina NV, Shibanova IV, Ufimtsev GF (1995) Manzurka alluvium (data for geology and paleogeography) [Manzurskii allyuvii (dannye po geologii i paleogeografii)]. Preprint of the Institute of the Earth’s Crust SB RAS, Irkutsk.
- Urabi A, Tateishi M, Inouchi Y, Matsuoka H, Inoue T, Dmitriev A, Khlystov OM (2004) Lake-level changes during the past 100,000 years at Lake Baikal, southern Siberia. *Quater Res* 62:214–222.
- Vasil’ev EP, Belichenko VG, Reznitskii LZ (1997) Relationship between Ancient and Cenozoic Structures at the Southwestern Flank of the Baikal Rift Zone. *Doklady Earth Sci* 353:381–384.
- Wan S, Li A, Clift PD, Stuu J-BW (2007) Development of the East Asian monsoon: mineralogical and sedimentologic records in the northern South China Sea since 20 mya. *Palaeogeogr Palaeoclim Palaeoecol* 254:561–582.
- Wang Y-X, Yang J-D, Chen J, Zhang K-J, Rao W-B (2007) The Sr and Nd isotopic variations of the Chinese Loess Plateau during the past 7 mya: implications for the East Asian winter monsoon and source areas of loess. *Palaeogeogr Palaeoclim Palaeoecol* 247:351–361.
- Whitford-Stark JL (1987) A survey of Cenozoic volcanism on mainland Asia. *Geol Soc Am Special Paper* 213. pp. 1–74.
- Yarmolyuk VV, Kuz’min MI (2004) Interaction of endogenic and exogenic factors in the recent geological history of the southwestern Baikal rift zone. *Geotectonics* 38:203–223.
- Yarmolyuk VV, Lebedev VI, Arakelyants MM, Lebedev VA, Prudnikov SG, Sugorakova AM, Kovalenko VI (1999) The recent volcanism of Tuva: chronology of the volcanic events according to K-Ar data. *Doklady Earth Sci* 368:244–249.
- Yarmolyuk VV, Arakelyants MM, Lebedev VA, Ivanov VG, Kozlovskii AM, Lebedev VI, Nikiforov AV, Sugorakova AM, Baikin DN, Kovalenko VI (2003) Chronology of valley eruptions in the South Baikal volcanic region: evidence from K-Ar dating. *Doklady Earth Sci* 391:636–640.
- Zonenshain LP, Savostin LA (1981) Geodynamics of the Baikal rift zone and plate tectonics of Asia. *Tectonophysics* 76:1–45.
- Zorin YuA (1971) Recent structure and isostasy of the Baikal rift zone and adjacent areas [Noveishaya struktura i izostaziya Baikal’skoi riftovoi zony i sopredel’nykh territorii]. Moscow: Nauka (in Russian)
- Zorin YuA, Turutanov EK, Mordvinova VV, Kozhevnikov VM, Yanovskaya TB, Treusov AV (2003) The Baikal rift zone: the effect of mantle plumes on older structure. *Tectonophysics* 371:153–173.
- Zorin YuA, Turutanov EK, Kozhevnikov VM, Rasskazov SV, Ivanov AV (2006) The nature of Cenozoic upper mantle plumes in East Siberia (Russia) and Central Mongolia. *Rus Geol Geophys* 47:1046–1059.

Paleoclimate and Evolution: Emergence of Sponges During the Neoproterozoic

Werner E.G. Müller, Xiaohong Wang, and Heinz C. Schröder

1	Introduction.....	56
2	Habitat Prior to the Varanger-Marinoan Ice Age.....	59
3	Monophyletic Origin of Present-Day Multicellular Animals.....	59
4	Sponges: Fossil Records.....	63
5	Sponges Are Provided with Survivor Strategies.....	64
6	Basis of Metazoan Pattern Formation During the Neoproterozoic: Stem Cells in Sponges.....	66
7	Skeleton of the Earliest Metazoans.....	68
8	Origin of Metazoan Pattern Formation in the Proterozoic Sponges.....	71
9	Concluding Remarks.....	74
	References.....	74

Abstract In the last 15 years, we had to cope with many technological and conceptual obstacles. The major hindrance was the view that sponges are primitive and exist separated from the other metazoan organisms. After answering these problems, the painful scientific process to position the most enigmatic metazoan phylum, the Porifera, into the correct phylogenetic place among the eukaryotes in general and the multicellular animals in particular came to an end. The well-studied taxon Porifera (sponges) was first grouped to the animal-plants or plant-animals, then to the Zoophyta or Mesozoa, and finally to the Parazoa. Only by the application of molecular biological techniques was it possible to place the Porifera monophyletically with the other metazoan phyla, justifying a unification of all multicellular animals to only one kingdom, the Metazoa. The first strong support came from the discovery that cell–cell and cell–matrix adhesion molecules, that

W.E.G. Müller (✉) and H.C. Schröder

Institut für Physiologische Chemie, Abteilung Angewandte Molekularbiologie, Universität, Duesbergweg 6, 55099 Mainz; Germany; tel.: +49-6131-392-5910; fax: +49-6131-392-5243; e-mails: wmueller@uni-mainz.de (<http://www.biotechmarin.de>); hschroed@uni-mainz.de

X. Wang

National Research Center for Geoanalysis, 26 Baiwanzhuang Dajie, CHN-100037 Beijing, China; tel./fax: +86 10 68999591; e-mail: wxh0408@hotmail.com

were cloned from sponges (mainly the demosponges *Suberites domuncula* and *Geodia cydonium*) and that were subsequently expressed, share high DNA sequence and protein function similarity with the corresponding molecules of other metazoans. Together with the molecular biological studies and with the use of the cell culture technologies (primmorphs), which allowed an insight into the stem cell system of these simple organisms, it was possible to stethoscope back in the paleontological history of animals. These studies confirmed the view that the sponges evolved between two epochal ice times, 710–680 Ma (Sturtian glaciation) and 605–585 Ma (Varanger-Marinoan ice age), a period which allowed evolution to proceed but resulted also in a mass extinction of most animal taxa, with the exception of the Porifera. These animals could develop in the aqueous milieu which was rich in silica, due also to their ability to live in a symbiosis with unicellular organisms (prokaryotic and also eukaryotic). Those organisms provided the sponges with the nutrition to survive and to overcome the food deprivation in cold water and even in an environment under the ice. Based on the diverse genetic toolkit, the sponges could also resist the adverse temperature and sunlight climatic influences. It is fortunate that the sponges survived the last 800 million years with their basic body plan. This fact might qualify the sponges to become model organisms not only in biology and molecular biology but also to be used – as living fossils – as reference organisms to deduce important and new insights in the understanding of fossil records explored from the Neoproterozoic. Taken together, these data caused a paradigmatic change; the Porifera are complex and simple, but by far not primitive, and they contribute to the understanding of the deep evolution of animals in molecular biological and paleontological views.

1 Introduction

The first metazoans that evolved during the Neoproterozoic, the period between 1,000 and 630 million years ago (Ma), have been the sponges (phylum Porifera). This information is taken from “molecular clock” analyses with, e.g., the receptor tyrosine kinase (RTK) from a demosponge (*Geodia cydonium*) (Schäcke et al. 1994). Those calculations indicated the appearance of these animals between 665 and 650 Ma. Equally old, or a little younger, are the famous Ediacaran eukaryotes, which appeared 630–530 Ma (see Butterfield 2007). The conspicuously ornamented acritarchs found there (Ediacaran eukaryotes) are small organic structures, which are non-acid-soluble structures of non-carbonate or non-siliceous origin (Knoll 1994). It is highly interesting that the sponges are the only metazoans existing prior to the Ediacaran–Cambrian boundary (542 Ma) that are characterized by a hard skeleton; it is composed of bio-silica (see Knoll and Carroll 1999; Müller et al. 2007a). This must be especially mentioned since the sponges evolved between two major “snowball earth events,” the Sturtian glaciation (710–680 Ma) and the Varanger-Marinoan ice age (605–585 Ma); the earth was then covered by an almost continuous ice layer (Hoffman et al. 1998). It has been proposed that as a conse-

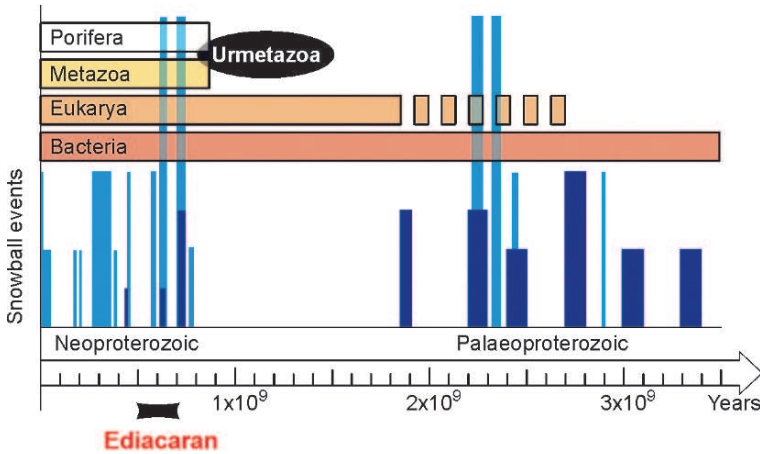


Fig. 1 Frequency of occurrence of major glacial periods (*blue*). The appearance of the different organismic groups (Bacteria, Eukarya, Metazoa, and Porifera) are indicated. The Urmetazoa evolved during the inter-ice period between 600Ma and approximately 800Ma (Modified after Hoffmann and Schrag 2002)

quence of these ice ages most organisms, perhaps more than 85%, went extinct (Mayr 2001) (Fig. 1).

Near the Ediacaran–Cambrian boundary, a rapid appearance of different animal types occurred, an event that was called the “Cambrian Explosion.” The development and divergence of the major animal clades were certainly driven by the genetic tool kits available at that time. The major, or very likely even the only, phylum existing at the border from Late Neoproterozoic to Cambrian which did not become extinct are the sponges. Consequently, sponges were also termed “living fossils” (Müller 1998a, b); they represent the evolutionary oldest, still extant, taxon, which testifies to the developmental level of the animals that lived in the Neoproterozoic eon (1,000–520 Ma) (Fig. 2). The origin of the first ancestor of all metazoan phyla remained mysterious and enigmatic until the first sequences coding for informative proteins from a sponge (phylum Porifera) had been identified by application of molecular biological techniques (Pfeifer et al. 1993). Before that, it was speculated that the sponges were metazoans composed of individually reacting and acting cells (see Pechenik 2000). With the identification of the first sponge protein sequence, a galectin, it became apparent that these animals have the genetic toolkit to allow their cells to differentiate from omnipotent via pluripotent to, finally, determined somatic cells (reviewed in Pilcher 2005; Müller 2006); most of the functional analyses were performed with the sponges *Suberites domuncula* and *Geodia cydonium* (see Müller et al. 2004) (Fig. 2). With the identification of a first cell–matrix adhesion molecule, an integrin (Pancer et al. 1997), it could be substantiated that the sponges represent organisms that are composed of cells expressing cell-surface molecules allowing their cross talks and in turn also divisions/restrictions of their physiological functions (Müller and

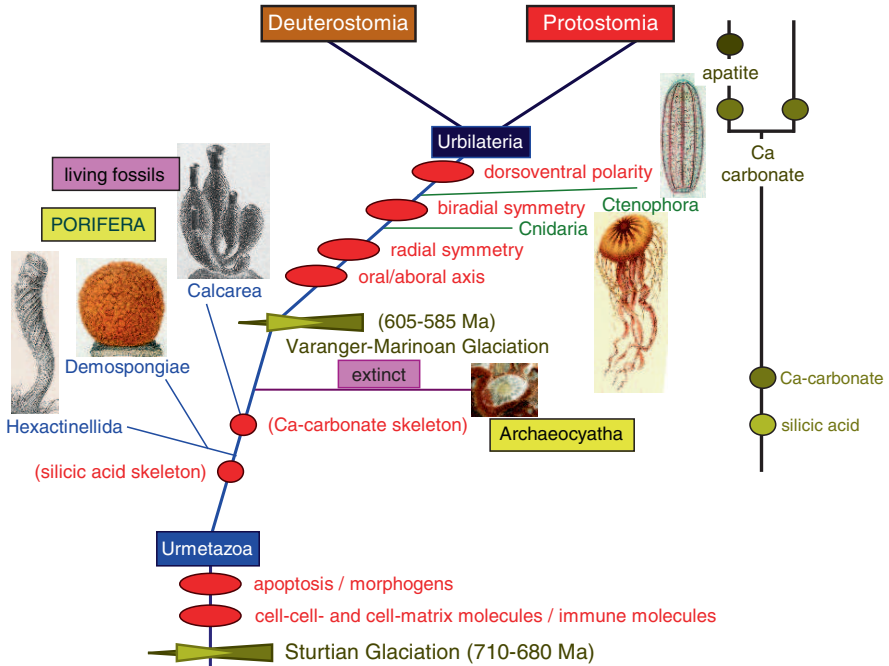


Fig. 2 Phylogenetic position of the Porifera between the Urmetazoa and the Urbilateria. The major evolutionary novelties which have to be attributed to the Urmetazoa are those molecules which mediate apoptosis and control morphogenesis, the immune molecules and primarily the cell adhesion molecules. The siliceous sponges with the two classes Hexactinellida and Demospongiae emerged first and finally the Calcarea, which possess a calcareous skeleton, appeared. These three classes of Porifera are living fossils that provide a reservoir for molecular biological studies. The Archaeocyatha, sponge-related animals with a calcareous skeleton, became extinct. The Calcarea are very likely a sister group of the Cnidaria. From the latter phylum, the Ctenophora evolved which comprise not only an oral/aboral polarity but also a biradial symmetry. Finally, the Urbilateria emerged from which the Protostomia and the Deuterostomia originated. Very likely, the Urmetazoa emerged between the two major “snowball earth events,” the Sturtian glaciation (710–680Ma) and the Varanger-Marinoan ice ages (605–585Ma). In two poriferan classes, Hexactinellida and Demospongiae, the skeleton is composed of amorphous and hydrated silica, while the spicules of Calcarea are composed of calcium carbonate. The latter biomineral is also prevalent in Protostomia and Deuterostomia. In vertebrates, the bones are composed of calcium phosphate (apatite)

Müller 2003). The individuality of a sponge specimen and the morphogenetic arrangement of its cells according to a defined body plan was underscored by the discovery of apoptotic as well as organizer-specific axis-forming molecules in *S. domuncula* (reviewed in Wiens et al. 2004; Müller 2005; Wiens and Müller 2006). The next challenge was to identify those factors that allowed the evolution of the phylogenetically oldest animals, the sponges; one of those key elements was silicon, which comprises both morphogenetic and also structural properties (see Müller et al. 2007a).

2 Habitat Prior to the Varanger-Marinoan Ice Age

The Varanger-Marinoan ice age (605–585 Ma) was the most widespread and most easily recognizable of the snowball events (Rice et al. 2003). It appears that the major victims of this ecological catastrophe were the acritarchs which were completely exterminated (Corsetti et al. 2006). The tropical oceans froze over due to an ice albedo runaway; sea ice reached approximately the latitude of about 30°. Due to the increased albedo, heat reflected back to space resulting in a freezing of the earth with a mean annual surface temperature of -40°C . It has been suggested that no free water existed in the superficial environments at that time (reviewed in Corsetti et al. 2006). The thick sea ice meant a great challenge for life, not only because of the severe temperatures but also because photosynthesis by organisms was prevented, resulting in a reduced oxygen pressure. The major oxygenic photosynthetic organisms that probably lived during the Neoproterozoic and also today are the cyanobacteria; they form oxygen-rich microbiotopes and contribute to the conversion of the atmosphere of the Earth from anoxic to oxic. Under anoxic conditions, ferrous iron (Fe^{2+}), present in silicate minerals, dissolves like magnesium according to the following reaction; $\text{Fe}_2\text{SiO}_4 + 4\text{H}^{2+} \rightarrow 2\text{Fe}^{2+} + \text{H}_4\text{SiO}_4$. This reaction is pH-dependent (Lasaga 1998). When Fe^{2+} (ferrous iron) is oxidized to Fe^{3+} (ferric iron), it becomes very insoluble and precipitates as (hydr)oxides: $\text{Fe}^{2+} + 1/4\text{O}_2 + 5/2\text{H}_2\text{O} \rightarrow \text{Fe}(\text{OH})_3 + 2\text{H}^+$. The dissolution/precipitation cycle of iron ions results in iron formation, especially in the form characteristic for banded iron formation, and is characteristic for the early Precambrian stratigraphic records. Hence, the Precambrian oceans were supposedly very iron-rich (reviewed in Lindsay and Brasier 2004), especially during or in consequence of the ice-covered seas.

The primordial earth surface initially comprised insoluble silicates and carbonates as well as, to a small extent, phosphates. During the silicate weathering–carbonate precipitation cycle, prior or simultaneously with the glaciations, a dissolution of these surface rocks composed of insoluble silicates (CaSiO_3) resulted in formation of soluble calcium carbonate (CaCO_3) and soluble silica (SiO_2), under consumption of atmospheric CO_2 (Walker 2003). The resulting soluble minerals leached into the waters of the rivers, lakes, and oceans. Silicate weathering also caused an increase in ocean alkalinity. There, they were again re-precipitated into new composites, as part of the sedimentary rocks. In turn, oceans became rich both in iron ions and in silicate, as seen today in the deep sea.

3 Monophyletic Origin of Present-Day Multicellular Animals

Our group has analyzed genes of sponges in order to obtain an insight into their genomic organization as well as the roles of gene coding for functional proteins. In detail, genes from Demospongiae, *S. domuncula* and *G. cydonium*, from

Calcarea, *Sycon raphanus*, as well as from Hexactinellida, *Aphrocallistes vastus* and *Rhabdocalyptus dawsoni*, were analyzed and the results used to describe the hypothetical ancestral Metazoa, the Urmetazoa.

Hexactinellidan sponges are syncytial rather than cellular. Approximately 75% of the tissue forms a multinucleate syncytium; the remaining tissue consists of uninucleate “cells” which are connected to the syncytium by perforated (aqueous) plugged junctions (Mackie and Singla 1983). In two early approaches to resolve the phylogenetic relationships of the three poriferan classes (Schulze 1887; Lendenfeld 1889), the Calcarea were considered to form the basis of the sponge taxon. While Schulze (1887) suggested that together with the Calcarea the Hexactinellida represent the earliest classes (Fig. 3), Lendenfeld (1889) proposed that the Demospongiae group together with the Calcarea and the Hexactinellida appeared later in evolution. With respect to their phylogenetic relationships, two contrary views have been presented. One considers cellular sponges, the Calcarea and the Demospongiae, as the sister groups of the syncytial sponges, the Hexactinellida (Mehl and

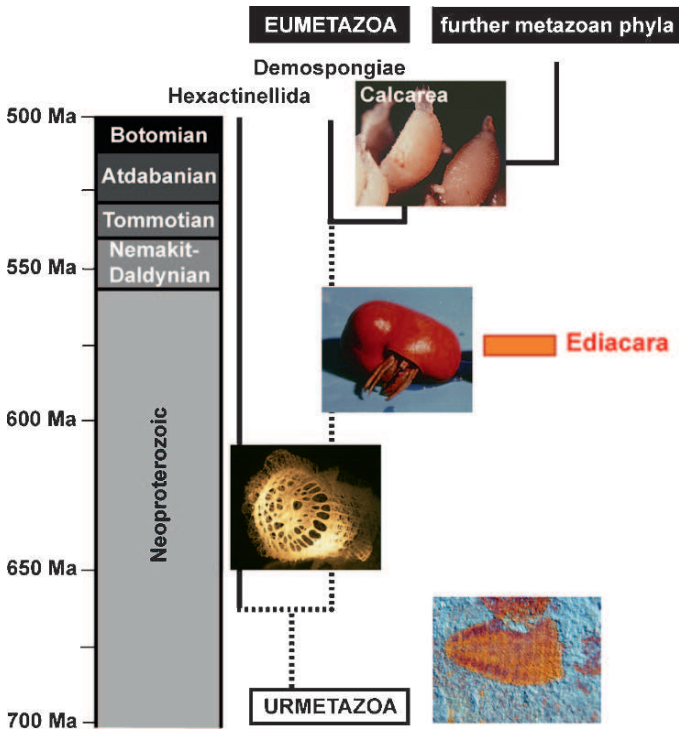


Fig. 3 Sponge phylogeny, fossil records, and minimal inferred gaps. Sponges [classes: Hexactinellida (phylogenetically oldest taxon); living species *Euplectella aspergillum*; Demospongiae; *Suberites domuncula*; and Calcarea (youngest taxon); *Sycon raphanus*] are a monophyletic group; the other metazoan phyla evolved from a common ancestor with the Calcarea. The Urmetazoa appeared around 1Ma; the fossil *Diagoniella robisoni* (Middle Cambrian from Utah) shows the basal characters of a hexactinellid

Reiswig 1991), while in the opposite view, the siliceous sponges, Hexactinellida and Demospongiae, form the sister group to the calcareous sponges, the Calcarea (Böger 1988). Here, the sequencing data from rRNA were not conclusive enough to solve this question (Medina et al. 2001). The study of several sequences of informative molecules, such as housekeeping proteins, e.g., heat shock protein (Kozioł et al. 1997) or β -tubulin (Schütze et al. 1999), and proteins involved in signal transduction, e.g., Ser/Thr kinase (Kruse et al. 1997, 1998) or calmodulin (Schütze et al. 1999), from the three poriferan classes, revealed that the Hexactinellida is the phylogenetically oldest taxon, while Calcarea is the class most closely related to higher metazoan phyla.

Based on calculations described earlier (Schütze et al. 1999), it has been outlined that the transition to multicellularity took place about 800–1,000 Ma. Later in evolution, 700 Ma, the green algae evolved. The first sponge fossils have been dated back to at least 580 Ma. Hence, sponges lived more than 30–50 million years before the Cambrian Explosion, the time of the main divergence of metazoan phyla. This conclusion is supported by calculations based on the extent of amino acid (aa) substitutions of two galectins from *G. cydonium*, indicating that these molecules diverged from the galectin isolated from the nematode *C. elegans*, approximately 800 Ma (Hirabayashi and Kasai 1993; Pfeifer et al. 1993). Furthermore, data especially from studies with series of Ser/Thr kinases suggested that the Calcarea might be a sister group to higher metazoan phyla (see Kruse et al. 1998) (Fig. 3).

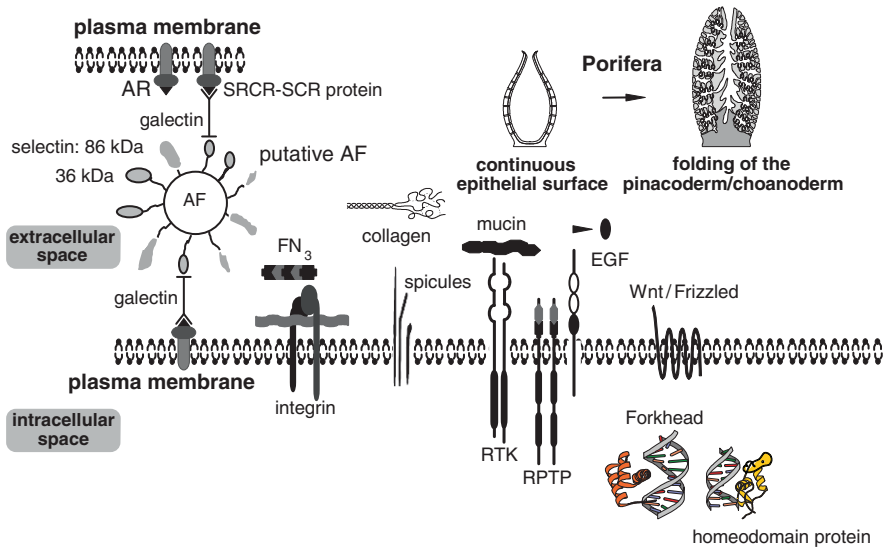
The sponges comprise all structural features of a metazoan body plan, as worked out in our group in the last 10 years (reviewed in Müller et al. 2004). A survey of the functions of these molecules is given in Fig. 4. They comprise:

MOLECULES INVOLVED IN CELL–CELL INTERACTION. With the isolation of a galectin sequence as the first cell–cell adhesion molecule, and with integrin sequence as the first cell–matrix adhesion receptor in the demosponge *G. cydonium*, it became apparent that sponges contain highly related molecules also known to promote adhesion in Protostomia and Deuterostomia. Sequence analyses of the galectin cloned from *G. cydonium* revealed that those aa residues which are involved in binding of galectins from mammals to galactose are also conserved in the sponge sequence. The putative aggregation receptor was cloned from *G. cydonium* and found to comprise 14 scavenger receptor cysteine-rich domains, six short consensus repeats, a C-terminal transmembrane domain, and a cytoplasmic tail.

MOLECULES INVOLVED IN CELL–SUBSTRATE INTERACTION: The dominant molecule present in the extracellular matrix of sponges which functions as a cell–matrix adhesion molecule is collagen. The corresponding gene was cloned both from the freshwater sponge *Ephydatia muelleri* as well as from the demosponge *S. domuncula*. Cell surface-spanning receptors, in particular the single-pass as well as the seven-pass transmembrane receptor proteins, serve as receivers for extracellular signaling molecules.

MOLECULES INVOLVED IN MORPHOGENESIS: Two classes of proteins are addressed here, the morphogens and the transcription factors. Morphogens have been identified in the extracellular space of sponges, e.g., the endothelial-monocyte-activating polypeptide or myotrophin. Both are very likely involved in the organization/differentiation of cells within the sponge body.

TRANSCRIPTION FACTORS: During development of animals, a set of genes, most of them transcription factors that are responsible for cell fate and pattern determination, is expressed. Among them, T-box, forkhead, and homeobox gene families have been found to be extremely conserved, at sequence and functional level.



outside-in signaling: SELECTIVE GENE EXPRESSION

cell-cell adhesion: CELL ASSOCIATION

cell-matrix adhesion: TISSUE/SKELETON FORMATION

cell proliferation and differentiation: GROWTH

solute factors: MORPHOGENS

secreted molecules: AXIS FORMATION

transcription factors: AXIS FORMATION

Fig. 4 Different phases required for the initiation of pattern formation (schematic model based on studies with the demosponges *Geodia cydonium* and *Suberites domuncula*). First, cell–cell- and second cell–matrix adhesion molecules allow the mechanical interaction between adjacent cells or cells and extracellular matrix molecules. Aggregation factors (AF) in the extracellular space interact with aggregation receptors (AR) and mediate the first mechanical contact. The AF and the AR are complexes which are held together by protein–protein or protein–glycoprotein interactions. The AF-mediated cell–cell recognition is species-specific and very likely controlled by the complex SRCR/SCR-AR, that is embedded in the plasma membrane. Third, after this primary AF-AR-AF contact, intracellular signal transduction pathways are activated, resulting in a selective gene expression. New insertion of adhesion receptors into the plasma membrane follows; e.g., integrin and other receptors, involved in tissue and skeleton formation. Also, like those, the receptor tyrosine kinases (RTK) and the receptor protein–tyrosine phosphatases (RPTP) are uniquely found in Metazoa. Together with these receptors their ligands are synthesized, e.g., collagen, molecules containing the fibronectin FN₃ modules, or mucin-like molecules, which establish the cell–matrix adhesion system. During this phase, growth factors are synthesized, e.g., the precursor and the mature epidermal growth factor (EGF), which interact with the newly synthesized receptors. Fourth, solute molecules are released which initiate axis formation. Fifth, after completion of these phases pattern formation can start, a process which is controlled by “morphogenetic” cell-surface receptors, like Frizzled, and by transcription factors, e.g., forkhead. Also, LIM-class homeodomain transcription factors are activated. It is suggested that in parallel with the expression of these gene cascades, the complexity of the sponge body plan, as an example, increases (*upper right*)

MOLECULES PRESENT IN TIGHT JUNCTIONS: Our screening for a gene encoding a tight junction scaffold protein from a sponge, here *S. domuncula*, was successful; the scaffold protein membrane-associated guanylate kinase with inverted arrangement (MAGI) was identified (Adell et al. 2003). In addition, the existence of one tetraspan receptor, tetraspanin, in *S. domuncula* has been reported. The tetraspanins belong to a group of hydrophobic proteins, comprising four transmembrane domains with a series of conserved aa residues in the extracellular loops.

4 Sponges: Fossil Records

The oldest sponge fossils (Hexactinellida) have been described from Australia, China, and Mongolia (from more than 540 Ma) (Gehling and Rigby 1996; Brasier et al. 1997; Li et al. 1998). Hence, the Hexactinellida are the oldest group of sponges exemplarily found in fossil records of the Sansha section in Hunan (Early Cambrian; China; [Steiner et al. 1993]). There, in both lower and upper levels of the Niutitang Formation, more or less completely preserved sponge fossils, e.g., *Solactiniella plumata* (Fig. 5A-a–a-c), have been discovered (Steiner et al. 1993). The occurrence

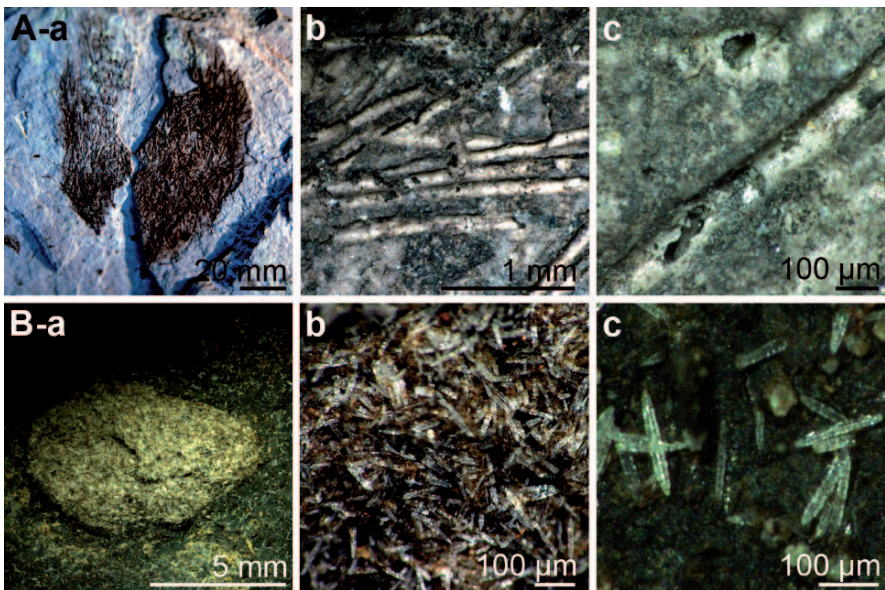


Fig. 5 Fossil marine and freshwater sponges. **(A)** One of the oldest fossil marine sponges in body preservation is from the Lowermost Cambrian Sansha section (Hunan, China); *Solactiniella plumata* (Hexactinellida) **(A-a)**. This fossil is composed of highly intact spicules **(A-b)**. **(A-c)** Some spicules are broken and expose the internal axial canals. **(B)** One of the oldest fossil freshwater sponges; *Spongilla gutenbergiana* from the Middle Eocene (Lutetian) near Messel (Darmstadt, Germany). **(B-a)** Spicule assembly, reminiscent of a complete animal. **(B-b)** Oxeas in these nests. **(B-c)** Oxeas with the flashing centers, representing the axial canals. Size bars are given

of almost intact sponge fossils also in the basal part of this formation is real (Rigby and Guang 1996) and is stratigraphically equivalent to the Chengjiang assemblage in Yunnan (China). Except for one questionable demosponge, all sponges described from this section can be attributed to the Hexactinellida.

Very likely, the oldest isolated spicules were also found in China, observed in thin sectioned material from the Dengying Formation, “Shibantan” Member, Hubei Province (Steiner et al. 1993). These spicules are mainly monaxial spicules, but some are also rather definite “crosses,” the evidence of triaxones from hexactinellids. The “Shibantan” Member in Hubei is of Late Proterozoic age and stratigraphically equivalent with the Ediacara (South Australia), which is famous because of its exceptionally preserved Vendian fossils. The Ediacara fauna has been considered to have begun about 600 Ma, although new stratigraphic data place the base of the Ediacara fauna at ≈ 565 Ma, and suggest that it ranged up to the Precambrian/Cambrian boundary (Grotzinger et al. 1996). Still, the Ediacara-type Vendian fossils are the oldest megafossils, which may, at least partly, be interpreted as metazoans, although this interpretation is still controversial (Seilacker 1989; Morris 1993, 1994; Retallack 1994). It is thus justified to call the Porifera the oldest organismic group in the Earth history, which can now be proven as definitely belonging to the animal kingdom, and which furthermore has survived successfully until present times. Compared with the marine Hexactinellida and Demospongiae, the freshwater demosponges are much younger; one of the first fossil freshwater sponges, *Spongilla gutenbergiana*, has been described from the Middle Eocene (Lutetian); (Müller et al. 1982; Fig. 5B-a–b-c).

The earliest evidence of the Demospongiae and the Calcarea is the presence of isolated spicules in thin sections of rocks from Early Cambrian (Atdabatian) Archaeocyath mounds of the Flinders Ranges (South Australia). The Calcarea documented from these Archaeocyath mounds are both isolated spicules and also more or less complete rigid skeletons of small calcarean sponges sitting on Archaeocyaths. The spicules are of the triaene, equal-angular type characteristic of the modern Calcarea, but quite different from those typical of the Paleozoic Heteractinellida. Very similar, perhaps identical, spicules from the Early Cambrian of Sardinia were described as *Sardospongia triradiata* and attributed to the Heteractinellida (Mostler 1985). The complete calcarean sponge *Gravestockia pharetronensis* (Reitner 1992) from the Flinders Ranges possessed a rigid calcitic skeleton with affinity to the modern Pharetronida. As one of the earliest families of the Demosponges, the Geodiidae have been described on the basis of their ster-rasters (Reitner and Mehl 1995).

5 Sponges Are Provided with Survivor Strategies

The question arises why sponges were so successful during evolution and could cope with the adverse climatic and nutritional conditions. It had been assumed, and in the last 10 years also experimentally proven, that sponges, as sessile animals,

are provided with a sophisticated genetic toolkit to live in an efficient symbiotic relationship with both unicellular eukaryotes and bacteria. The taxon Porifera that survived the “snowball earth” episodes is provided with the genetic repertoire to cope with the most adverse conditions, meaning it possesses: (1) proteins to protect against adverse temperature, (2) the possibility to survive food restriction, and also (3) – not to be forgotten – the protection machinery against ultraviolet radiation. During the pre-Sturtian period, atmospheric CO₂ had been consumed and removed from the atmosphere resulting in extreme temperature amplitudes.

Sponges comprise *cryoprotective proteins*, e.g., galactose-specific lectins (Pfeifer et al. 1993, Wiens et al. 2003) which display cryoprotective protein-membrane activity, or, interestingly, also $\beta\gamma$ -crystallins, proteins which contain only low amounts of water and hence are resistant to adverse protein folding (Krasko et al. 1997).

Food restriction/symbiosis was probably compensated by the establishment of a symbiotic relationship with microorganisms (Breter et al. 2004), such as Gram-positive (Thakur et al. 2005) and Gram-negative bacteria (Wiens et al. 2005) as well as fungi (Perovic-Ottstadt et al. 2004). This eukaryotic–prokaryotic “labor-division” allowed the sponges a flexible and rapid adaptation to the changing environment. Already in 1993, Arillo et al. (1993) predicted a metabolic integration between symbiotic cyanobacteria and sponges.

It is furthermore amazing that sponges have an unexpected variety of protection systems against *mutagens*, also including ultraviolet *radiation*. Several protection systems against radiation have been described; e.g., the (6-4) photolyase system (Krasko et al. 2003) or the SOS-response-like mechanism (Krasko et al. 1998), and the literature on protection systems against environmental stress is large (e.g., Efremova et al. 2002).

Perhaps the greatest fortune for the sponges was their ability to utilize silicic acid as substrate for their skeleton. When sponges emerged, the insoluble silicate minerals were converted to monomeric, soluble silica providing the sponges with an advantageous basis for survival and diversification, with respect to the number of the species and their abundance. Early assumptions postulated that those taxa which survived mass extinction, e.g., the Foraminifera, became ecologically and morphologically generalized species (Cifelli 1969). Furthermore, the number of species, the diversity of the biota, increased rapidly after each period of extinction (Futuyama 1986). Hence, the sponges (survivor taxon) became the beneficiaries of the glaciation crises and received the chance to colonize those habitats which had been depopulated.

As mentioned above, the urmetazoans/sponges already had the basic genetic toolkit for all deriving metazoans which emerged during the “Cambrian Explosion” (Figs. 2 and 3). This statement implies that the genetic repertoire of the sponges, which survived the glaciations, gives the frame potentials/potentialities but also the limits of the body plan construction, seen in higher “crown” groups and which exist in the present-day animal phyla. The “crown” taxa utilized the pre-existing molecules and pathways for their diversification of patterning and for an increase in the genetic network complexity. It can be postulated that during the progress of evolution the degree of entropy decreased at the expense of an increase of complexity. This progressive “perfection” might be detrimental to the stability and survival of most of the species which are evolutionarily younger.

6 Basis of Metazoan Pattern Formation During the Neoproterozoic: Stem Cells in Sponges

Multicellular animals are characterized by the existence of a series of differentiated somatic cells, in addition to the totipotent germ cells. During evolution from the lowest metazoans, the sponges, to the crown taxa the number of distinct cell types increased steadily. The different somatic cell types derive from the zygote through the respective stem cell stage; the differentiation processes proceed in niches which form a microenvironment in which defined expression patterns of signaling molecules and local environmental factors direct the fate of the cells. These niches modify their regulatory properties in response to a changing environment to ensure that stem cell activities meet the needs of an organism for a given differentiated cell type. Two major types of stem cells derive from the zygote, the germline stem cells and the somatic stem cells. While the germline stem cells retain their total differentiation capacity, this property is restricted in the somatic stem cells which gradually lose their stem cell propensity. However, recent studies indicate that this traditional view of an irreversible loss of the stem cell ability during maturation of somatic cells might not completely reflect the physiological situation. It appears that such fixed “points of no return” do not always exist but that, at all levels of differentiation from the pluripotent progenitor cells to the committed progenitors to the lineage progenitors and finally the terminally differentiated cells, the propensity to act as a stem cell is retained, even though with a decreasing potential. In consequence, the differentiation lineages of somatic cells are dynamic and plastic and the strong distinction between embryonic stem cells and adult stem cells should be reconsidered. The data which allowed the establishment of the stem cell concept in sponges has been recently summarized (Müller 2006).

It is generally agreed that the archaeocytes are the toti/pluripotent cells in sponges from which the other cells originate; recently, evidence was presented indicating a localization of archaeocytes not only within the mesohyl, but also in the endopinacoderm layer. Archaeocytes give rise to the major classes of differentiated somatic cells: (1) the epithelial cells, pinacocytes, and choanocytes, (2) the cells forming the skeleton, collencytes, and sclerocytes, and (3) the contractile cells, myocytes (Fig. 6). It appears that in Porifera the archaeocytes gave rise not only to the different somatic cells (epithelial-, skeletal-, and contractile cells) but also to the germ cells from which the embryos originate. Another line of differentiation of the archaeocytes is to the thesocytes, the totipotent cells of gemmules which are asexual propagative dissemination bodies. Pinacocytes, collencytes/sclerocytes, and myocytes are cells with a low stem cell propensity, implying that these somatic cells are “terminally” differentiated.

In order to underline the view that the metazoan stem cell concept can also be applied for Porifera, characteristic marker genes have been cloned from *S. domuncula*. The first cDNAs identified whose deduced proteins share sequence similarity to mammalian stem cell markers were the mesenchymal stem cell-like protein (MSCP) and noggin. MSCP is present in mesenchymal human stem cells;

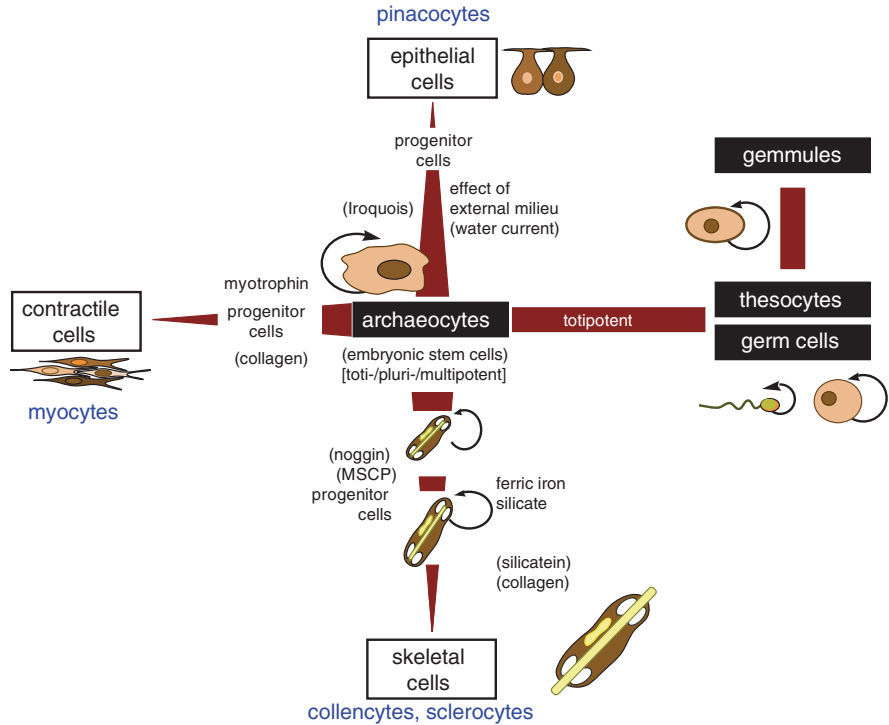


Fig. 6 Sponge stem cell system. Schematic outline of the relationship of the totipotent sponge embryonic stem cells, the archaeocytes, with the germ cells on one side and the three major differentiated cell types, the epithelial cells, the contractile cells, and the skeletal cells. It is proposed that the archaeocytes are expressing both sponge-specific receptor tyrosine kinase (RTKvs) and EED2. During progression of the totipotent archaeocytes to cells forming gemmules, the putative stem cell marker gene EED2, is expressed, while during their progression to germ cells the gene RTKvs remains expressed. No data are available to indicate that the stem cell propensity decreases from the primordial archaeocytes to the gemmules or the germ cells. The stem cell propensity decreases during proliferation of the archaeocytes to the main somatic cell lineages, the skeletal cells, the contractile cells, and the epithelial cells. The triangles indicate schematically the decrease in stem cell propensity during the differentiation process. It is highlighted that factors, e.g., noggin and the mesenchymal stem cell-like protein (MSCP) on the path to the skeletal cells, trigger this differentiation. Data suggest that the silicate/Fe(+++) stimulus initiates the differentiation of this lineage. During the transition to the contractile cell lineage and the epithelial cell lineage, myotrophin, and Iroquois are expressed, respectively

experimental evidence exists that *MSCP* is expressed in osteogenic mesenchymal stem cells. The functional studies revealed that in sponges the expression of this gene is under positive control of the morphogenetic inorganic elements, silicon and ferric iron. In addition, two further potential genes involved in the differentiation of stem cells in sponges were isolated; *noggin* and the *glia maturation factor*. *Noggin* is a glycoprotein that binds bone morphogenetic proteins selectively and antagonizes their effects. It was initially isolated from *Xenopus* and found to be expressed

in the Spemann's organizer. In vertebrate development, noggin is involved in the formation of dorsal mesoderm derivatives, e.g., the skeletal muscles.

In the initial phase of formation, the *in vitro* 3-D-cell primmorph system contains predominantly the toti/pluripotent archaeocytes which can be stimulated to differentiate into four main tissue-specific directions. If they are induced by the inorganic factors silicate or ferric iron, the archaeocytes give rise to the skeletal cells through an increased expression of genes encoding the structural proteins silicatein and collagen; a process which is mediated by noggin and MSCP (Fig. 6). Second, if archaeocytes are exposed to a morphogen (myotrophin) they are directed towards the contractile cell lineage. A third lineage, which gives rise to the aquiferous canal system, is induced by a physical factor; there, *Iroquois* gene expression is induced as a result of an increased water current which is paralleled with the formation of canal-like pores in the primmorphs. In higher metazoans, the expression of the *Iroquois* genes is thought to confer identity to a particular region, and hence it can be classified to the homeotic selector genes. The sponge *S. domuncula* not only contains in its genome an *Iroquois* gene, which comprises a remarkable sequence similarity to those sequences described from triploblastic animals, but also expresses it during the formation of one major morphogenetic remodeling process, the construction of the aquiferous canal system (Fig. 6).

7 Skeleton of the Earliest Metazoans

In living organisms, four major groups of biominerals exist: (1) iron compounds, which are restricted primarily to Prokaryota, (2) calcium phosphates, found in Metazoa, (3) calcium carbonates, used by Prokaryota, Protozoa, Plantae, Fungi, and Metazoa, and (4) silica (opal) present in sponges and diatoms. It is surprising that the occurrence of silica as a major skeletal element is restricted to some unicellular organisms and to sponges (Demospongiae and Hexactinellida). At present, it is not known why sponges have used silica as a biomineral to form one major innovation during the evolution from Protozoa to Metazoa. Since the transition from Protozoa to Metazoa dates back 600–1,000 Ma it has been proposed that oxygen level, temperature, and seawater chemistry played a major role in the evolution from Protozoa to Metazoa. In particular, it was assumed that during the period of appearance of sponges the ocean was richer in sodium carbonate than in sodium chloride; such a “soda ocean” probably had a pH of above 9. Under such conditions, the concentration of silica, the dioxide form of silicon, was presumably higher in seawater than today.

The formation of the skeleton is a multifaceted process and will be explained in an exemplary way for Porifera. Even though these animals comprise the most simple body plan, their biomineral structure formation is already highly complex and certainly not completely understood. As also in triploblasts, the diploblastic Porifera skeleton formation has a pronounced effect on morphogenesis. As an example, if the animals are growing under unfavorable conditions, which do not

allow formation of the inorganic deposits (silica or calcium biominerals), the growth of the specimens is greatly suppressed.

Silica is the major constituent of sponge spicules in the classes Demospongiae and Hexactinellida. The spicules of these sponges are composed of hydrated, amorphous, noncrystalline silica. The secretion of spicules occurs in Demospongiae in specialized cells, the sclerocytes; there, silica is deposited around an organic filament. If the formation of siliceous spicules is inhibited, the sponge body collapses. The synthesis of spicules is a rapid process; 100- μm -long megascleres are formed within 40 h (see Weissenfels 1989).

Inhibition studies revealed that skeletogenesis of siliceous spicules is enzyme-mediated, more particularly by an Fe^{++} -dependent enzyme. The dominant enzyme which catalyzes the formation of monomeric to polymeric silica was termed silicatein; it belongs to the cathepsin subfamily (see Müller et al. 2007b).

The formation of siliceous spicules in sponges is genetically controlled; this process initiates the morphogenesis phase. Data demonstrated that, at suitable concentrations, silicate induces genes, e.g., those encoding collagen, silicatein, and myotrophin. A major step forward to elucidate the formation of the siliceous spicules on molecular level was the finding that the “axial organic filament” of siliceous spicules is in reality an enzyme, silicatein, which mediates the apposition of amorphous silica and hence the formation of spicules (reviewed in Müller et al. 2006).

The skeletal framework of the sponges is highly ordered. In two examples, the demosponge *Lubomirskia baicalensis* (Fig. 7a) and the hexactinellid *Euplectella aspergillum* (Fig. 7b), it can strikingly be seen that the growth of the sponges proceeds in a radiate accretive manner, meaning that growth zones which are highly ordered are delimited by growth lines. These growth centers are constructed by an ordered arrangement of the spicules within the body. Most siliceous sponges are composed of larger megascleres $>10\ \mu\text{m}$ long, and smaller microscleres ($<10\ \mu\text{m}$). Some microscleres have a bizarre shape (Fig. 7c), while the megascleres have usually a long central rod with ends that in some cases are decorated with spines. Interestingly, the spicules (Fig. 7d) have, both in the central hole and also around the outer concentric silica layers, the enzyme silicatein. The central core rod of the spicule is synthesized first by the silicatein fiber which exists in the central hole around which a 1- to 3- μm -thick siliceous hollow fiber is formed. This layer becomes surrounded by an organic silicatein layer which synthesizes the second siliceous layer and so on. This process of growth is very reminiscent of bone formation (reviewed in Müller et al. 2007c).

Applying the *in vivo* cell culture technique of sponges, the primmorphs, the (Fig. 7e) the dynamics and cell biology of spicule formation could be studied. These experiments revealed that the spicules are formed extracellularly in close association with fibrils (Fig. 7f, g). Cross sections through a young spicule within cells from primmorphs show that the amorphous silica of the spicule is initially not very compact (Fig. 7h).

At present, no experimental data are available which could explain the species-specific form and shape of the spicules; it has been suggested that their polarity is the result of homeobox genes.

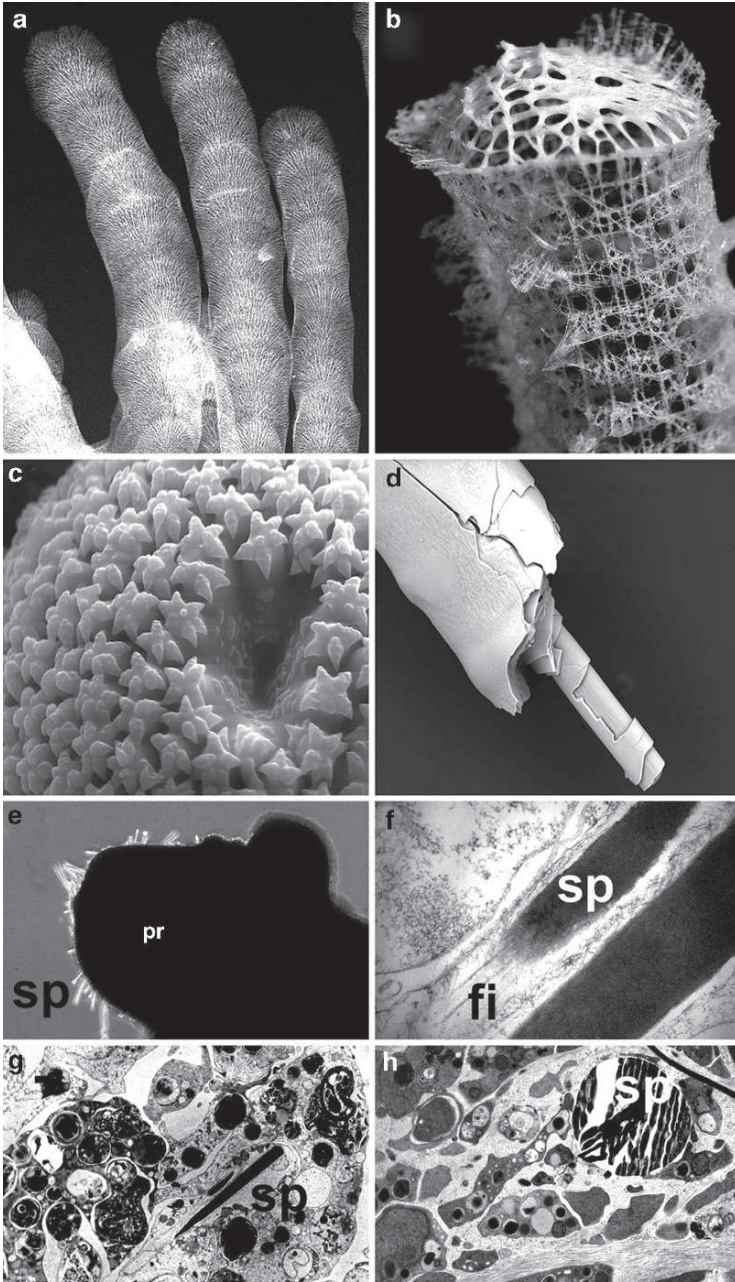


Fig. 7 The skeletal framework of the sponges is highly ordered. Radiate accretive growth pattern seen in the skeletal arrangement of the spicules from the freshwater demosponge *Lubomirskia bai-calensis* (a) [$\times 1$] and the marine hexactinellid *Euplectella aspergillum* [$\times 1.0$] (b); the zones which are uniformly constructed are dissected by growth lines. (c) A microsclele from *Geodia cydonium*; $\times 10,000$. (d) Scanning electron microscopic analysis of basal spicules from *Hyalonema sieboldi*

8 Origin of Metazoan Pattern Formation in the Proterozoic Sponges

The major difference in the genetic control of the body plan patterning between diploblasts (Porifera and Coelenterata) and triploblasts (Protostomia and Deuterostomia) must be seen in the fact that only the triploblasts comprise clusters of homeotic genes (see Wolpert 1998). In diploblasts, those clusters are missing and non-clustered paired-class (*Pax-2/5/8*)-genes and *LIM/homeodomain* genes control pattern formation (see Galliot and Miller 2000). In triploblasts as well as in diploblasts, body plan formation starts by polarization of the embryo, and the subsequent development is followed in diploblasts only to the stage of serial module patterning, while in triploblasts the development to the adults includes both compartmental and the subsequent segmental patterning (Fig. 8). More comprehensive reviews have been given recently (Nüsslein-Volhard and Wieschaus 1980; Dewel 2000; Grunz 2004; Maldonado 2004; Müller 2005).

Focusing on Porifera, after fertilization the zygote increases in size and develops flagellae. Depending on the taxa, morphologically slightly different types of larvae (amphiblastulae, parenchymellae, or coeloblastulae) are formed and released from the maternal body. During this phase, the embryo polarizes, a process which is morphologically primarily obvious in the localization of the cilia and the formation of the body cavity (Fig. 8). Then gastrulation takes place driven by an asymmetric and tangentially arranged cleavage. The epithelia within the body cavity invaginate under formation of the choanocyte chambers. The embryos become sessile and the young sponge forms an oscule, through which the body cavity opens to the external milieu; with this process, the young sponge forms an oscular/apical–basal axis.

The oscule region can be considered as an organizer, since there the characteristic vertebrate organizer genes are expressed. In addition, this region is provided with a regeneration capacity which is distinguished from the rest of the animal. There are especially the organizer-specific genes, *LIM-homeodomain*, *Brachyury*, *Frizzled receptor*, *noggin*, and *Iroquois*, which are expressed along the aquiferous system and the oscule. This water canal system is the combined route for feeding, secretion, and gas exchange. Strong evidence has been collected in the last 2 years which indicate that these “organizer” genes are not only expressed around the canals and the oscule but also display morphogenetic activity.

Already, morphological inspection shows that sponge species grow with defined patterns, resulting in the construction of a distinct body plan. X-ray analysis of the

Fig. 7 (continued) showing the concentric layers of silica by which they are built. The center of the spicule is composed of an organic filament which comprises of the silica-forming enzyme silicatein forms the and first hollow fiber. Around the first fiber structure silicatein is deposited again and forms the second concentric layer; $\times 10$. **(e)** A primmorph (*pr*), the cell culture spheroid from *Suberites domuncula*, has the capacity to synthesize spicules (*sp*); $\times 20$. Formation of spicules in primmorphs: **(f)** The newly formed spicule (*sp*) is closely associated with fibrils (*fi*); $\times 5,000$. **(g)** Synthesis of a spicule in a sclerocyte within a primmorph; $\times 1,000$. **(h)** Section through a primmorph, showing a sectioned young spicule; the amorphous silica of the spicule is not very compact

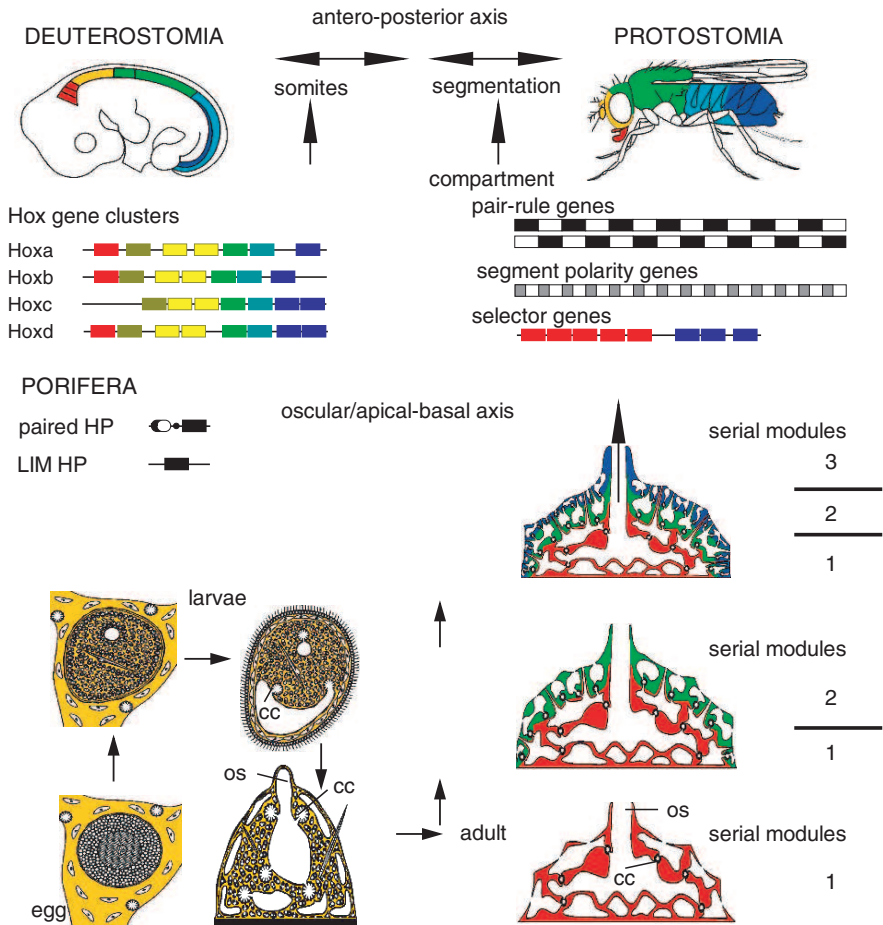


Fig. 8 Schematized view of the pattern formation in Metazoa. In the triploblasts both the Deuterostomia, the mouse as a model system, and the Protostomia, with the *Drosophila melanogaster* model, pattern formation is spatially and temporally controlled by homeobox gene clusters. In the mouse, several different clusters exist; their genes are positionally and combinatorially expressed along the antero-posterior axis. Colinearity exists between the order of Hox genes on the chromosome and the order by which the individual genes are expressed along this axis. In the insect, *Drosophila*, regular segmentation along the antero-posterior axis takes place. Prior to segment formation, parasegments develop. Sets of gene clusters (pair-rule genes) control parasegment formation; both genes defining odd-numbered parasegments and even-numbered parasegments are in action. Parasegment polarity is accomplished by the “segment polarity” genes. Subsequently segments are formed from one anterior and one posterior region of a parasegment. Homeotic selector genes that confer to the particular identity of a region are present in a cluster and are grouped into an Antennapedia and a bithorax complex. In contrast to these triploblasts, the sessile diploblastic Porifera comprise an axis which is defined by the location of the oscule (*os*). During embryogenesis the fertilized egg develop to a larva which comprises a cavity. During and after the settlement of the larvae first choanocyte chambers (*cc*) are formed and the body cavity opens to the external milieu through an oscule. The growth of the adult proceeds along the oscule axis, apical/oscular–basal axis in a compartmental manner. It is proposed that the growth of sponges, occurring by serial modules, along the body axis; these processes are controlled by paired-class and LIM-class homeoproteins (*HP*), which are not arranged in a cluster on the chromosome

skeleton of the Lake Baikal sponge *L. baicalensis* reveals that the architecture of the specimens comprises a highly ordered arrangement of the spicules within the body (Fig. 7a). *L. baicalensis* follows an organized growing pattern, reflecting a radiate accretive growth process. This pattern is maintained throughout the body of the animals and can be seen both in the growing parts of the specimens, the tips, and in the base. During growth, new layers/rings of new longitudinal spicule bundles are added at the tips of the branches. A similar highly regular arrangement of the spicule formation can also be seen in the hexactinellid *E. aspergillum* (Fig. 7b). The latter species shows a regular arrangement of the spicules which form the lateral stabilization network which leaves holes for the water canal system. Also, the apical end of the specimens which harbors the oscule(s) shows a considerably ordered arrangement.

There is no doubt that this highly ordered growth process of the Porifera is genetically controlled. With the discovery that organizer-specific genes are present at the tips of the branches, around the oscules, and together with the fact that growth along the oscular/apical–basal axis proceeds by a radiate accretive pattern, it is suggested that at the “growth lines,” which are readily seen between the preceding and the succeeding growth layers, genes are expressed which form SERIAL MODULES along the oscular/apical axis (Fig. 8). The serial modules should not be termed segments because this would imply that they are built by a more complex genetic network, like a system seen in insects.

The genetic programs that control development and body plan formation of multicellular organism, plants, and animals have been shaped during evolution. In consequence, such gene networks that control development also provide information about the evolution of these organisms. During development, distinct cell types are generated in distinct spatial and morphological domains which establish organized structures and a functional organism. After fertilization of an egg a genetic program controls cleavage divisions, resulting in a rapid increase of cells during the different stages of embryogenesis, a phase which is usually not characterized by an increase in cell mass. In these phases, pattern formation starts a process which organizes the cells of different affinities and activities in a spatial and temporal pattern/way.

Pattern formation in diploblasts and triploblasts is also strikingly initiated by homeobox genes, e.g., *Paired-class* and *LIM-class* genes. Also, these genes have been isolated and (partially) functionally analyzed from Porifera to triploblasts (see Wiens et al. 2003; Müller 2005). However, with respect to these genes, a characteristic difference exists between the arrangement of the sponge and the Cnidaria/*Hydra* genes on the chromosome and those in triploblasts. Both in insects and in vertebrates the morphogenetic homeobox genes are arranged in clusters. In insects, the pair-rule genes and the homeotic selector genes are clustered on the chromosomes, and likewise in vertebrates, the four Hox gene complexes are arranged and expressed in a colinear way. Since the body plan/axis formation in diploblasts is established in the absence of homeobox gene clustering, it has been suggested that clustering of the homeobox genes is not a prerequisite for axis

formation. As one consequence of the absence of homeobox gene clusters, the body axis in diploblasts is established in a compartmental construction (which form SERIAL MODULES, along the oscular/apical axis), while in triploblasts compartmental arrangement of the tissue stripes is the basis for a segmental/somital construction of the body plan.

9 Concluding Remarks

Some evolutionary novelties gave the sponges the power/capacity to survive as fossils and also as living animal lines the adverse climatic situation during the Neoproterozoic. At first, they invented the genetic toolkit for the construction of the skeleton, which is already very elaborated. The siliceous skeleton allowed fossilization of these animals. More importantly, the inorganic support of the large multicellular animals provided the platform for the development of larger organisms, some of those can reach over 2 m. The sponges are also witnesses for the rapid and diverse evolution of the animals in the Pre-Neoproterozoic. It appears obvious that they were not only the sponges in the Pre-Neoproterozoic which lived in this period; it must be assumed that they evolved together with other taxa which went extinct.

From the sponges, as the only living fossils from the Pre-Neoproterozoic area, we can learn the characteristic basic metazoan genetic circuits and basic body plans and can deduce and also predict from this information the basic genetic and morphological structure of other multicellular animals with only soft bodies. Sponges are a rich source for study by biologists (seeking to understand the integrative construction of a multicellular organism with “monophyletic” strategies of the cells to develop and interact, with a basic and general body plan, with common strategies to resist and adopt to a changing environment), geneticists (looking for genetic circuits as the basis for development and morphogenesis) and also for material scientists working in the field of one of the most promising biomaterials, bio-silica.

Acknowledgments This work was supported by grants from the European Commission, the Deutsche Forschungsgemeinschaft, the Bundesministerium für Bildung und Forschung Germany (project: Center of Excellence *BIOTEC*marin), the National Natural Science Foundation of China (No. 50402023) and the International Human Frontier Science Program.

References

- Adell T, Nefkens I, Müller WEG (2003) Polarity factor “Frizzled” in the demosponge *Suberites domuncula*: identification, expression and localization of the receptor in the epithelium/pinacoderm. *FEBS Lett* 554:363–368
- Arillo A, Bavestrello G, Burlando B, Sara M (1993) Metabolic integration between symbiotic cyanobacteria and sponges: a possible mechanism. *Marine Biol* 117:159–162

- Böger H (1988) Versuch über das phylogenetische System der Porifera. *Meyniana* 40:67–90
- Brasier M, Green O, Shields G (1997) Ediacarian sponge spicule clusters from southwest Mongolia and the origins of the Cambrian fauna. *Geology* 25:303–306
- Breter HJ, Grebenjuk VA, Thakur NL, Müller IM, Müller WEG (2004) Oxygen-controlled bacterial growth in the sponge *Suberites domuncula*: towards a molecular approach to understand the symbiotic relationship sponge-bacteria. *Appl Environ Microbiol* 70:2332–2341
- Butterfield NJ (2007) Macroevolution and macroecology through deep time. *Palaeontology* 50:41–55
- Corsetti FA, Olcott AN, Bakermans C (2006) The biotic response to Neoproterozoic snowball earth. *Palaeogeogr, Palaeoclimatol, Palaeoecol* 232:114–130
- Dewel RA (2000) Colonial origin of Eumetazoa: major morphological transitions and the origin of bilaterian complexity. *J Morphol* 243:35–74
- Efremova SM, Margulis BA, Guzhova IV, Itskovich VB, Lauenroth S, Müller WEG, Schröder HC (2002) Heat shock protein Hsp70 expression and DNA damage in Bakalian sponges exposed to model pollutants and wastewater from Baikalsk Pulp and paper plant. *Aquat Toxicol* 57:267–280
- Futuyma DJ (1986) *Evolutionary biology*. Sinauer, Sunderland, MA
- Galliot B, Miller D (2000) Origin of anterior patterning – how old is our head? *Trends Genet* 16:1–5
- Gehling JG, Rigby JK (1996) Long expected sponges from the Neoproterozoic Ediacara Fauna of South Australia. *J Paleontol* 70:185–195
- Grotzinger JP, Bowring SA, Saylor B, Kauffmann AJ (1995) New biostratigraphic and geochronologic constraints on early animal evolution. *Science* 270:598–604
- Grunz H (2004) *The vertebrate organizer*. Springer-Verlag, Berlin/Heidelberg/New York
- Hirabayashi J, Kasai K (1993) The family of metazoan metal-independent β -galactoside-binding lectins: structure, function and molecular evolution. *Glycobiology* 3:297–304
- Hoffmann PA, Schrag DP (2002) The snowball Earth hypothesis: testing the limits of global change. *Terra Nova* 129–155
- Hoffman PF, Kaufman AJ, Halverson GP, Schrag DP (1998) A Neoproterozoic snowball earth. *Science* 281:1342–1346
- Knoll AH (1994) Proterozoic and Early Cambrian protists: evidence for accelerated evolutionary tempo. *Proc Natl Acad Sci USA* 91:6743–6750
- Knoll AH, Carroll SB (1999) Early animal evolution: emerging views from comparative biology and geology. *Science* 284:2129–2137
- Kozioł C, Leys SP, Müller IM, Müller WEG (1997) Cloning of Hsp70 genes from the marine sponges *Sycon raphanus* (Calcarea) and *Rhabdocalypus dawsoni* (Hexactinellida). An approach to solve the phylogeny of sponges. *Biol J Linn Soc* 62:581–592
- Krasko A, Müller IM, Müller WEG (1997) Evolutionary relationships of the metazoan β -crystallins, including the one from the marine sponge *Geodia cydonium*. *Proc Roy Soc Lond B* 264:1077–1084
- Krasko A, Schröder HC, Hassanein HMA, Batel R, Müller IM, Müller WEG (1998) Identification and expression of the SOS-response, *aidB*-like, gene in the marine sponge *Geodia cydonium*: implication for the phylogenetic relationships of metazoan Acyl-CoA dehydrogenases and Acyl-CoA oxidases. *J Mol Evol* 47:343–352
- Krasko A, Gundacker D, Leys SP, Schröder, HC, Müller IM, Müller WEG (2003) Molecular and functional analysis of the (6–4) photolyase from the hexactinellid *Aphrocallistes vastus*. *Biochim Biophys Acta* 1651:41–49
- Kruse M, Müller IM, Müller WEG (1997) Early evolution of Metazoan serine/threonine- and tyrosine kinases: identification of selected kinases in marine sponges. *Mol Biol Evol* 14:1326–1334
- Kruse M, Leys SP, Müller IM, Müller WEG (1998) Phylogenetic position of the Hexactinellida within the phylum Porifera based on amino acid sequence of the protein kinase C from *Rhabdocalypus dawsoni*. *J Mol Evol* 46:721–728
- Lasaga AC (1998) *Kinetic theory in the earth sciences*. Princeton University Press, Princeton, NJ
- Lendenfeld R V (1889) *A monograph of the horny sponges*. Royal Society, London

- Li CW, Chen JY, Hua TE (1998) Precambrian sponges with cellular structures. *Science* 279:879–882
- Lindsay JF, Brasier MD (2004) The evolution of the Precambrian atmosphere: carbon isotopic evidence from the Australian continent. In: Eriksson PG, Altermann W, Nelson DR, Mueller WU, Catuneanu O (eds) *The precambrian earth: tempo and events*. Elsevier, Amsterdam, pp 388–421
- Mackie GO, Singla CL (1983) Studies on hexactinellid sponges. I. Histology of *Rhabdocalyptus dawsoni* (Lambe, 1873). *Phil Trans Roy Soc Lond B* 301:365–400
- Maldonado M (2004) Choanoflagellates, choanocytes, and animal multicellularity. *Invertebr Biol* 123:1–22
- Mayr E (2001) *What evolution is*. Basic Books, New York
- Medina M, Collins AG, Silberman JD, Sogin ML (2001) Evaluating hypothesis of basal animal phylogeny using complete sequences of large and small subunit rRNA. *Proc Natl Acad Sci USA* 98:9707–9712
- Mehl D, Reiswig HM (1991) The presence of flagellar vanes in choanomers of Porifera and their possible phylogenetic implications. *Z Zool Syst Evolut-Forsch* 29, 312–319
- Morris CS (1993) The fossil record and the early evolution of the Metazoa. *Nature* 361:219–225
- Morris CS (1994) Why molecular biology needs palaeontology. *Development, Suppl*:1–13
- Mostler H (1985) Neue heteractinide Spongien (Calcispongiae) aus dem Unter- und Mittelkambrium Südwestsardiniens. *Ber Nat Med Ver Innsbruck* 72:7–32
- Müller WEG (1995) Molecular phylogeny of Metazoa (animals): monophyletic origin. *Naturwiss* 82:321–329
- Müller WEG (1998a) Origin of Metazoa: sponges as living fossils. *Naturwiss* 85:11–25
- Müller WEG (ed) (1998b) *Molecular evolution: Evidence for monophyly of Metazoa* *Progr Molec Subcell Biol* 19. Springer-Verlag, Berlin/Heidelberg/New York
- Müller WEG (2001) How was metazoan threshold crossed: the hypothetical Urmetazoa. *Comp Biochem Physiol [A]* 129:433–460
- Müller WEG (2005) Spatial and temporal expression patterns in animals. In: Meyers RA (ed) *Encyclopedia of molecular cell biology and molecular medicine*, vol 13. Wiley-VCH, Weinheim, pp 269–309
- Müller WEG (2006) The stem cell concept in sponges (Porifera): metazoan traits. *Semin Cell Dev Biol* 17:481–491
- Müller WEG, Müller IM (2003) Origin of the metazoan immune system: identification of the molecules and their functions in sponges. *Integr Comp Biol* 43:281–292
- Müller WEG, Zahn RK, Maidhof A (1982) *Spongilla gutenbergiana* n.sp., ein Süßwasserschwamm aus dem Mittel-Eozän von Messel. *Senckenbergiana lethaea* 63:465–472
- Müller WEG, Wiens M, Adell T, Gamulin V, Schröder HC, Müller IM (2004) The Bauplan of the Urmetazoa: The basis of the genetic complexity of Metazoa using the siliceous sponges [Porifera] as living fossils. *Int Rev Cytol* 235:53–92
- Müller WEG, Belikov SI, Tremel W, Perry CC, Gieskes WWC, Boreiko A, Schröder HC (2006) Siliceous spicules in marine demosponges (example *Suberites domuncula*). *Micron* 37:107–120
- Müller WEG, Li J, Schröder HC, Qiao L, Wang XH (2007a) The unique skeleton of siliceous sponges (Porifera; Hexactinellida and Demospongiae) that evolved first from the Urmetazoa during the Proterozoic: a review. *Biogeosciences* 4:219–232
- Müller WEG, Boreiko A, Wang XH, Belikov SI, Wiens M, Grebenjuk VA, Boreiko A, Schloßmacher U, Schröder HC (2007b) Silicateins, the major biosilica forming enzymes present in demosponges: protein analysis and phylogenetic relationship. *Gene* 395:62–71
- Müller WEG, Wang XH, Belikov SI, Tremel W, Schloßmacher U, Natoli A, Brandt D, Boreiko A, Tahir MN, Müller IM and Schröder HC (2007c) Formation of siliceous spicules in demosponges: example *Suberites domuncula*. In: Bäuerlein E (ed) *Handbook of biomineralization*, vol 1. Biological aspects and biology of biominerals structure formation. Wiley-VCH, Weinheim, pp 59–82
- Nüsslein-Volhard C, Wieschaus E (1980) Mutations affecting segment number and polarity in *Drosophila*. *Nature* 287:795–801

- Pancer Z, Kruse M, Müller I, Müller WEG (1997) On the origin of adhesion receptors of metazoa: cloning of the integrin α subunit cDNA from the sponge *Geodia cydonium*. *Mol Biol Evol* 14:391–398
- Perović-Ottstadt S, Četković H, Gamulin V, Schröder HC, Kropf K, Moss C, Korzhev M, Diehl-Seifert B, Müller IM, Müller WEG (2004) Molecular markers for germ cell differentiation in the demosponge *Suberites domuncula*. *Int J Dev Biol* 48:293–305
- Pfeifer K, Haasemann M, Gamulin V, Bretting H, Fahrenholz F, Müller WEG (1993) S-type lectins occur also in invertebrates: high conservation of the carbohydrate recognition domain in the lectin genes from the marine sponge *Geodia cydonium*. *Glycobiol* 3:179–184
- Pilcher H (2005) Back to our roots. *Nature* 435:1022–1023
- Reitner J (1992) Coralline Spongien. Der Versuch einer phylogenetisch-taxonomischen Analyse. *Berliner Geowiss Abh (E)* 1:1–352
- Reitner J, Mehl D (1995) Early Paleozoic diversification of sponges: new data and evidences. *Geol Paläont Mitt Innsbruck* 20:335–347
- Retallack GJ (1994) Were the Ediacaran fossils lichens? *Paleobiology* 20:523–544
- Rice HN, Halverson GP, Hoffmann PF (2003) Three for the Neoproterozoic: Sturtian, Marinoan and Varanger glaciations. EGS-AGU-EUG Joint Assembly, Nice, France, April 2003
- Rigby JK, Hou X-G (1995) Lower Cambrian demosponges and hexactinellid sponges from Yunnan, China. *J Paleontol* 69:1009–1019
- Schäcke H, Müller IM, Müller WEG (1994) Tyrosine kinase from the marine sponge *Geodia cydonium*: the oldest member belonging to the receptor tyrosine kinase class II family. In: Müller WEG (ed) Use of aquatic invertebrates as tools for monitoring of environmental hazards. Gustav Fischer Verlag, New York/Stuttgart, pp 201–211
- Schulze FE (1887) Zur Stammesgeschichte der Hexactinelliden. Akademie der Wissenschaften, Berlin
- Schütze J, Reis Custodio M, Efremova SM, Müller IM, Müller WEG (1999) Evolutionary relationship of Metazoa within the eukaryotes based on molecular data from Porifera. *Proc Roy Soc Lond B* 266:63–73
- Seilacker A (1989) Vendozoa: Organismic construction in the proterozoic biosphere. *Lethaia* 22:229–239
- Steiner M, Mehl D, Reitner J, Erdtmann BD (1993) Oldest entirely preserved sponges and other fossils from the Lowermost Cambrian and a new facies reconstruction of the Yangtze Platform (China). *Berliner Geowiss Abh (E)* 9:293–329
- Thakur NL, Perović-Ottstadt S, Batel R, Korzhev M, Diehl-Seifert B, Müller IM, Müller WEG (2005) Innate immune defense of the sponge *Suberites domuncula* against gram-positive bacteria: induction of lysozyme and AdaPTin. *Marine Biol* 146:271–282
- Walker G (2003) Snowball earth: the story of the great global catastrophe that spawned life as we know it. Crown Publishers, New York
- Weissenfels (1989) Biologie und Mikroskopische Anatomie der Süßwasserschwämme (Spongillidae). Gustav Fischer Verlag, Stuttgart
- Wiens M, Müller WEG (2006) Cell death in Porifera: molecular players in the game of apoptotic cell death in living fossils. *Can J Zool/Rev Can Zool* 84:307–321
- Wiens M, Mangoni A, D'Esposito M, Fattorusso E, Korchagina N, Schröder HC, Grebenjuk VA, Krasko A, Batel R, Müller IM, Müller WEG (2003) The molecular basis for the evolution of the metazoan bodyplan: extracellular matrix-mediated morphogenesis in marine demosponges. *J Mol Evol* 57:1–16
- Wiens M, Perović-Ottstadt S, Müller IM, Müller WEG (2004) Allograft rejection in the mixed cell reaction system of the demosponge *Suberites domuncula* is controlled by differential expression of apoptotic genes. *Immunogenetics* 56:597–610
- Wiens M, Korzhev M, Krasko A, Thakur NL, Perović-Ottstadt S, Breter HJ, Ushijima H, Diehl-Seifert B, Müller IM, Müller WEG (2005) Innate immune defense of the sponge *Suberites domuncula* against bacteria involves a MyD88-dependent signaling pathway: induction of a perforin-like molecule. *J Biol Chem* 280:27949–27959
- Wolpert L (1998) Principles of development. Oxford University Press, Oxford

Studies on the Taxonomy and Distribution of Freshwater Sponges in Lake Baikal

Yoshiki Masuda

1	Freshwater Sponges Collected on Our Expeditions to Lake Baikal (1993–2001)	85
2	Horizontal and Vertical Distribution of Freshwater Sponges in Lake Baikal.....	102
2.1	Discussion.....	103
	References.....	109

Abstract During the summers of 1993–2001, we carried out expeditions in order to collect sponges and to review their taxonomy and distribution in Lake Baikal. A total of 1,539 specimens were collected in our expeditions. Most specimens were classified into 2 families 7 genera, and 14 species, though some remained unclassified because of taxonomic confusion. Most sponges belonged to the family of Lubomirskiidae which were distributed widely in Lake Baikal. A few sponges with gemmules, which were confined to the “Little sea” near Olkhon Island and to an estuary in the North Basin, belonged to the Spongillidae. In qualitative survey of vertical distribution, *B. intermedia* showed the highest frequency among all species and found more often in shallow zones. *L. baicalensis* was second with regard to frequency and also found more often in shallow zones. Though *S. papyracea* had been believed to inhabit only deeper zones, it occurred in shallow zones as well. In this survey, the biomass of sponges at 10 m depth showed maximum value and showed the second largest at 20m depth.

Lake Baikal is the oldest and largest lake in the world and eminent for its incomparable biodiversity. The lake hosts numerous freshwater sponges. Skeletons of all freshwater sponges consist of bundles of spicules which are composed of hydrated silica. The Baikalian sponges are classified into two families. One is a small group of Spongillidae, which is a cosmopolitan species and distributed only in restricted

Y. Masuda (✉)
Department of Biology, Kawasaki Medical School, Matsushima,
Kurashiki-shi, Okayama, 701-01, Japan
e-mails: masuda@med.kawasaki-m.ac.jp; shokoi@med.kawasaki-m.ac.jp

areas of the lake. The other is the Lubomirskiidae, which is an endemic family and distributed widely and abundantly within the lake.

The Baikalian sponges have been studied by Dybowski (1882), Swartschewski (1902), Annandale (1913, 1914), Rezvoj (1936), and Kozov (1963). Despite the intense scientific efforts of these spongologists, the taxonomy of some sponges still remains under debate. One of the reasons is that Lubomirskiidae do not produce gemmules, which are asexual reproductive bodies. A gemmule is protectively covered by spicules called gemmoscleres which constitute the most important taxonomic character in freshwater sponges. Another reason is that the shapes and arrangements of spicules called megascleres which form the skeleton may show morphological varieties even within one species and sometimes also have strong resemblances between two species. On the basis of these characteristics, Efremova studied many collections of her own and other scientists and established a new genus and five new species of sponges of the family Lubomirskiidae (Efremova 2001). Although she described *Trochospongilla* sp., which does not produce any gemmules in open Baikal, we do not refer to them as Spongillidae in this paper because their taxonomy is still under active research.

There have been only a few reports on the recent distribution of Baikalian sponges. Therefore, during the summers of 1993–2001 we carried out expeditions to collect sponges and to review their taxonomy and distribution in Lake Baikal

Table 1 List of freshwater sponges collected in our survey in Lake Baikal (1993–2001)

Family Lubomirskiidae Rezvoj, 1936
Genus Lubomirskia, Dybowski, 1880
1) <i>Lubomirskia baicalensis</i> (Pallas, 1771)
1') <i>L. baicalensis littoralis</i> Rezvoj, 1936
2) <i>Lubomirskia fusifera</i> Soukatschhoff, 1895
3) <i>Lubomirskia abietina</i> (Swartschewski, 1902)
4) <i>Lubomirskia incrustans</i> Efremova, 2001
Genus Baikalospongia Annandale, 1914
5) <i>Baikalospongia bacillifera</i> (Dybowski, 1880)
6) <i>Baikalospongia fungiformis</i> (Makuschok, 1927)
7) <i>Baikalospongia recta</i> Efremova, 2001
8) <i>Baikalospongia martinsoni</i> Efremova, 2001
9) <i>Baikalospongia intermedia</i> (Dybowski, 1880)
9') <i>B. intermedia profundalis</i> (Rezvoj, 1936)
Genus Swartschewskia Makuschok, 1927
10) <i>Swartschewskia papyracea</i> (Dybowski, 1880)
Genus Rezinkovia Efremova, 2001
11) <i>Rezinkovia echinata</i> Efremova, 2001
Family Spongillidae Gray, 1867
Genus <i>Ephydatia</i> Lamouroux, 1816
12) <i>Ephydatia muelleri</i> (Lieberkühn, 1855)
Genus <i>Spongilla</i> Lamarck, 1816
13) <i>Spongilla lacustris</i> (Linnaeus, 1758)
Genus <i>Eunapius</i> Gray, 1867
14) <i>Eunapius</i> sp.

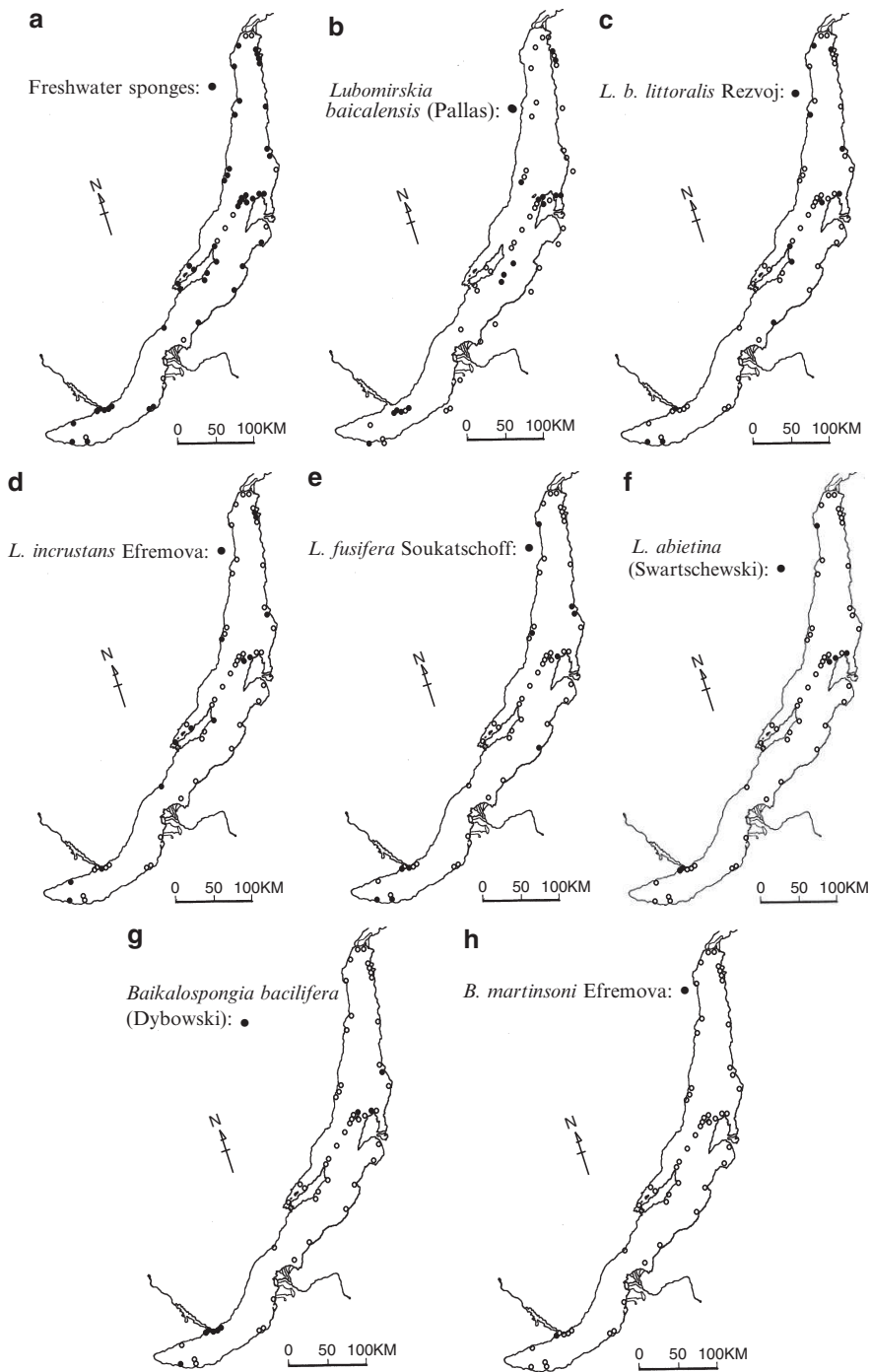


Fig. 1 Maps showing the sampling sites (○) and collection sites (●) in Lake Baikal (1993–1996) **a** Freshwater sponges; **b** *Lubomirskia baicalensis* (Pallas); **c** *L. b. littoralis* Rezvoj; **d** *L. incrustans* Efremova; **e** *L. fusifera* Soukatschoff; **f** *L. abietina* (Swartschewski); **g** *Baikalospongia bacilifera* (Dybowski); **h** *B. martinsoni* Efremova;

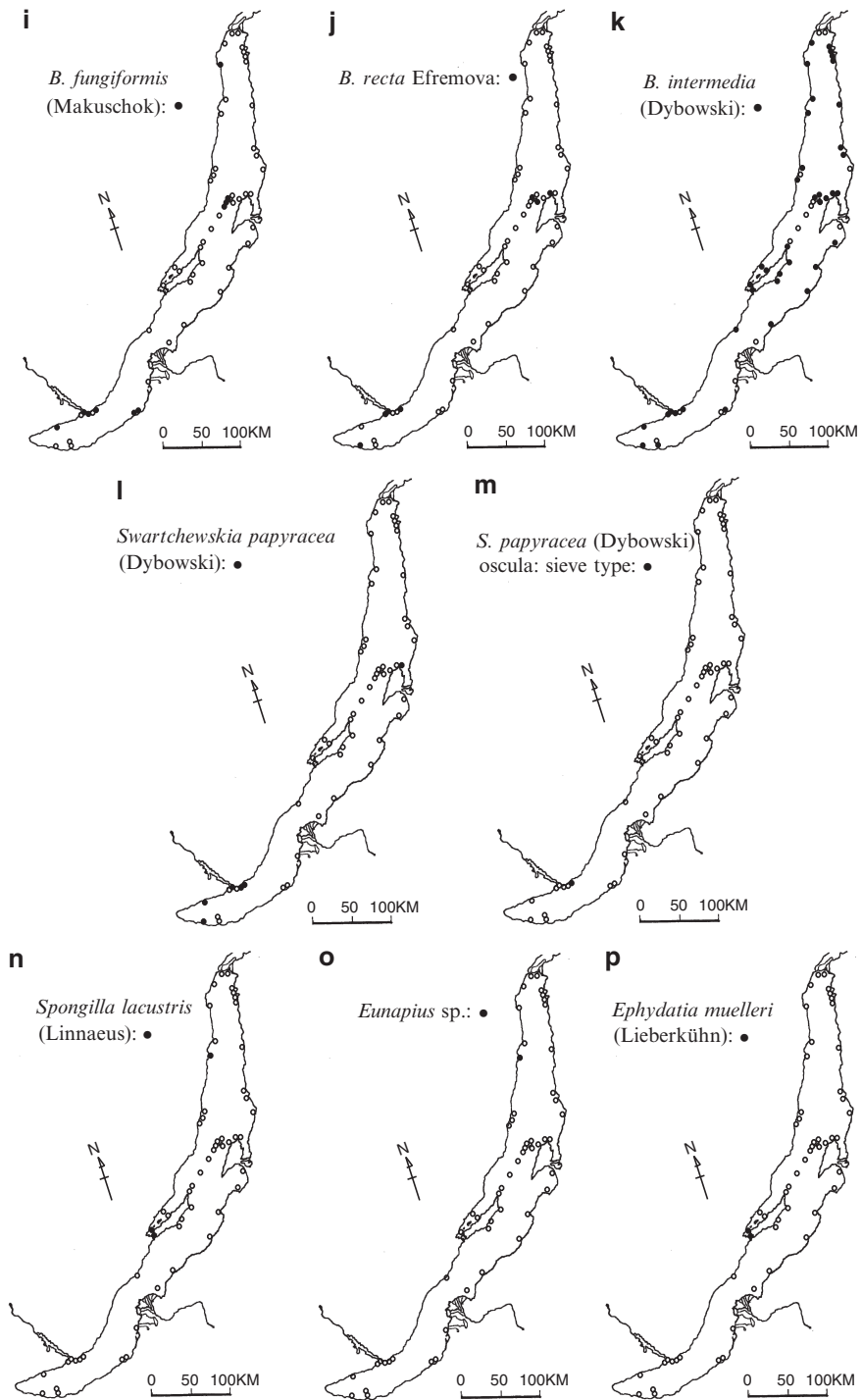


Fig. 1 (continued) **i** *B. fungiformis* (Makuschok); **j** *B. recta* Efremova; **k** *B. intermedia* (Dybowski); **l** *Swartschewskia papyracea* (Dybowski); **m** *S. papyracea*, oscula: sieve type; **n** *Spongilla lacustris* (Linnaeus); **o** *Eunapius* sp.; **p** *Ephydatia muelleri* (Lieberkühn)

(Masuda et al. 1999, and unpublished data). During the summers of 1997 and 1998, we also surveyed the vertical distribution of sponges in the littoral zone (0–45 m depth) at 24 stations by shore inspections and by diving expeditions. In the summers of 2000 and 2001, we conducted expeditions for a quantitative survey on the vertical distribution of sponges in the littoral zone (0–40 m depth) at five stations by diving (Masuda et al., unpublished data).

In our expeditions during the summers from 1993 to 2001, a total of 1,539 specimens were collected; most of them were classified into 2 families, 7 genera, and 14 species (Table 1), while some specimens remained unclassified because of taxonomic confusion. As expected, most sponges belonged to the family of Lubomirskiidae and were widely distributed in Lake Baikal. A few sponges with gemmules, which were confined to the “Little Sea” near Olkhon Island and to an estuary in the North Basin, belonged to the Spongillidae.

1 Freshwater Sponges Collected on Our Expeditions to Lake Baikal (1993–2001)

Family Lubomirskiidae Rezvoj 1936

(a) Genus *Lubomirskia* Dybowski 1880

1. *Lubomirskia baicalensis* (Pallas) (Fig. 2a–c)

Description – The almost invariably mature sponges had long cylindrical erect branches arising from the crustal base. The cylindrical processes fused with neighboring ones when they were contiguous. The skeleton was differentiated into main and cross bundles. Spicules in the bundles were located regularly and parallel to the bundle length. The main bundles ended in spicules forming brushes on the sponge surface (Fig. 2b). The consistency of live sponges was elastic and not fragile. When alive, the color was bright green due to the presence of a great number of zoochlorellae. The spicules were slightly curved amphioxea, fusiform, and covered with many spines along the whole length (Fig. 2c); length 152.9–212.5 μm (mean 187.2 μm , SD 11.6), width 8.4–15.3 μm (mean 11.9 μm , SD 1.2).

Distribution – This species was collected from 16 stations distributed in the North, the Central, and the South Basins (Fig. 1b). The substrata in the habitats of this species were rocky, not sand, pebbles, or cobbles.

1. *L. b. littoralis* Rezvoj (Fig. 3a–c)

Description – Sponges had crustal forms with no cylindrical branches. The thickness of the crust varied in the range of 1 cm. The skeleton resembled that of *L. baicalensis* typica (Fig. 3b). The consistency and the color of live sponges was like that of *L. baicalensis* typica. Spicules were slightly curved amphioxea,

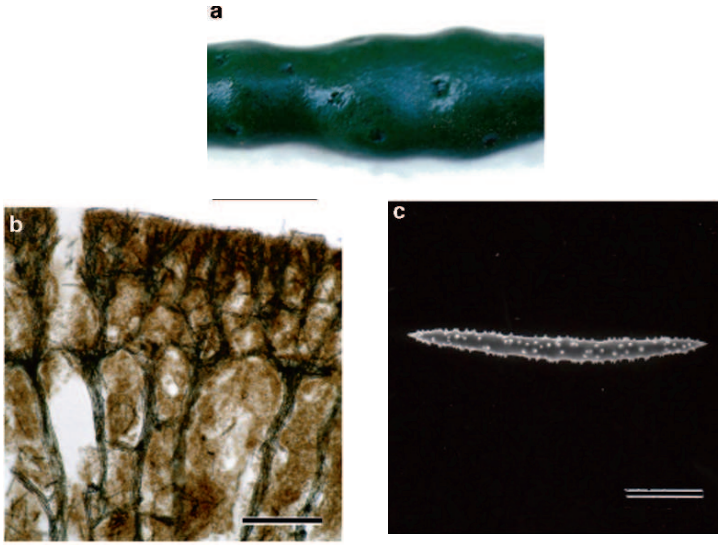


Fig. 2 *Lubomirskia baicalensis* (Pallas). **a** Part of the cylindrical body. *Scale bar* = 1 cm. **b** Skeleton (arrangement of spicules). *Scale bar* = 500 μ m. **c** A spicule. *Scale bar* = 50 μ m

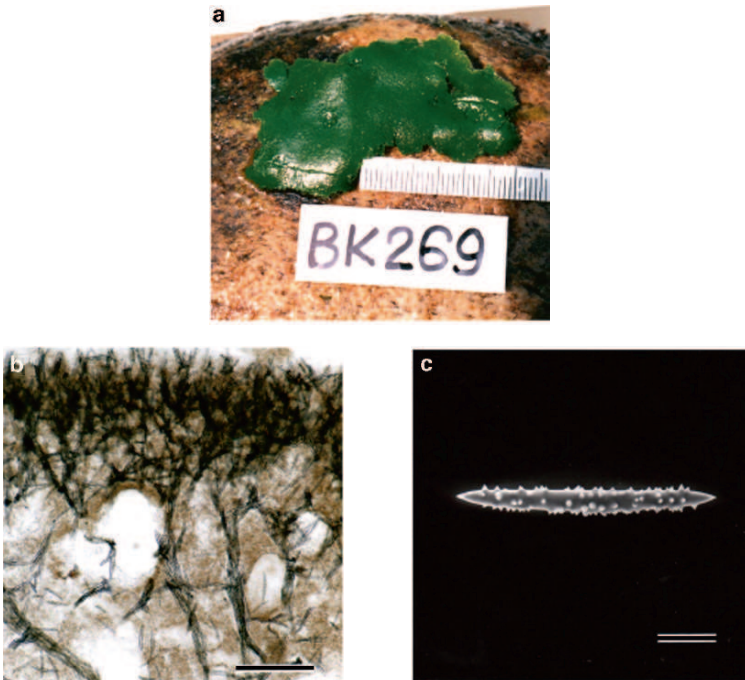


Fig. 3 *L. b. littoralis* Rezvoj. **a** Part of the crustal body. Each division of the *scale* = 1 mm. **b** Skeleton (arrangement of spicules). *Scale bar* = 500 μ m. **c** A spicule. *Scale bar* = 50 μ m

fusiform, and covered with many spines along the whole length except at their tips (Fig. 3c); length 153.0–225.2 μm (mean 197.8 μm , SD 15.4), width 13.6–22.1 μm (mean 17.8 μm , SD 1.7).

Distribution – This subspecies was collected from 12 stations in the North, Central, and South Basins (Fig. 1c). Though this subspecies was collected at fewer stations than *L. b. typica*, it was distributed more widely with regard to the distance.

2. *Lubomirskia incrustans* Efremova (Fig. 4a–c)

Description – Sponges had thin crustal forms. The thickness of the crust varied in the range of 0.5 mm. The consistency of live sponges and their color was that of *L. baicalensis*. Though the skeleton resembled that of *L. baicalensis*, the main and cross bundles were thinner (Figs. 4b, 17a). The skeleton displayed vertical ramified major bundles that were bound with single or doubled spicules. Forming brushes, fan-shaped ends of spicule bundles protruded over the surface. Spicules were slightly curved amphioxea, fusiform, and covered with many small spines except at the distal ends (Figs. 4c, 18a). The spicules were longer than those of

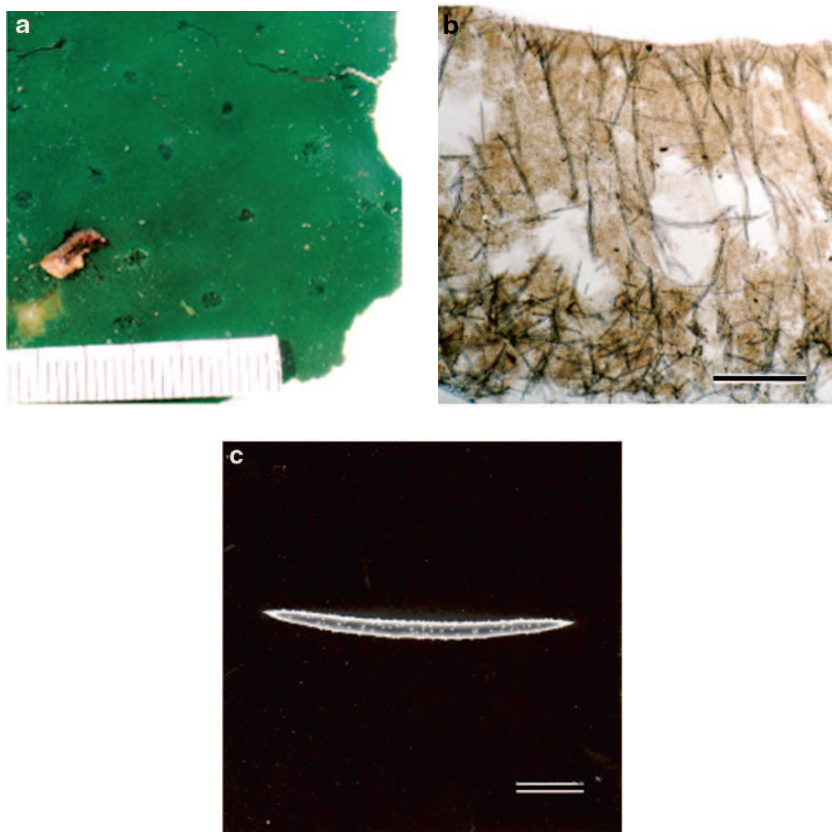


Fig. 4 *L. incrustans* Efremova. **a** Part of crustal body. Each division of the scale = 1 mm. **b** Skeleton (arrangement of spicules). Scale bar = 500 μm . **c** A spicule. Scale bar = 50 μm

L. baicalensis; length 224.2–293.2 μm (mean 257.7 μm , SD 16.2), width 8.5–15.9 μm (mean 12.8 μm , SD 1.3).

Distribution – This species was collected from 14 stations distributed in the North, Central, and South Basins (Fig. 1d). This species was also collected from stations in the Little Sea near Olkhon Island and from stations where *L. baicalensis* was not found.

3. *Lubomirskia fusifera* Soukatschoff (Fig. 5a–c)

Description – Sponges had crustal forms with no cylindrical branches. The thickness of the crust varied from 1 to 2 cm. The skeleton resembled that of *L. baicalensis* (Fig. 5b). The live sponges were elastic and not fragile and of green color due to the great number of zoochlorellae. Spicules were slightly curved amphioxea, typically fusiform and covered with spines especially near their tips (Fig. 5c); length 176.3–226.8 μm (mean 206.5 μm , SD 10.3), width 14.4–22.2 μm (mean 17.6 μm , SD 1.6).

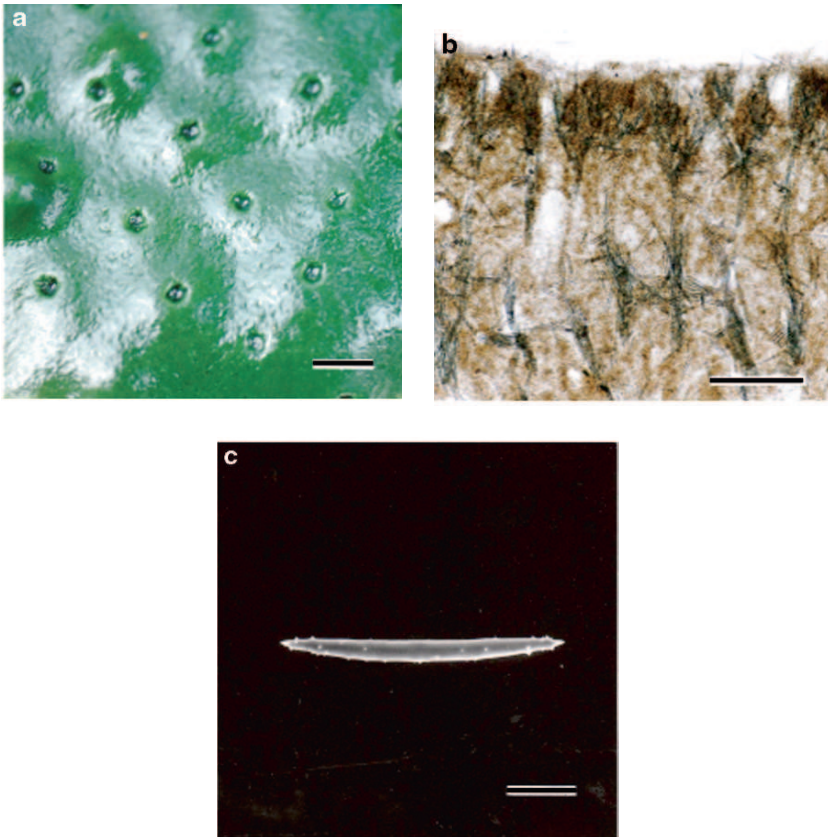


Fig. 5 *L. fusifera* Soukatschoff. **a** A part of the crustal body. Scale bar = 1 cm. **b** Skeleton (arrangement of spicules). Scale bar = 500 μm . **c** A spicule. Scale bar = 50 μm

Distribution – This species was collected from ten stations in the North, Central, and South Basins (Fig. 1e).

4. *Lubomirskia abietina* (Swartschewski) (Fig. 6a–c)

Description – Sponges had crustal forms with no cylindrical branches. The thickness of the crust varied from 0.5 to 1 cm. The outer surface of these sponges had a characteristic pattern of a net of small furrows (Fig. 6a). The skeleton consisted of the main bundles of unique structures. The spicules in the main bundles deviated slightly from the bundle axis to their distal ends. The main bundles gradually became wider towards the upper surface and ended in brushes of spicules; these main bundles were connected by cross bundles of one or a couple of spicules (Fig. 6b). Also, these live sponges were elastic and not fragile in consistency with bright green color due to the presence of a great number of zoochlorellae. Spicules

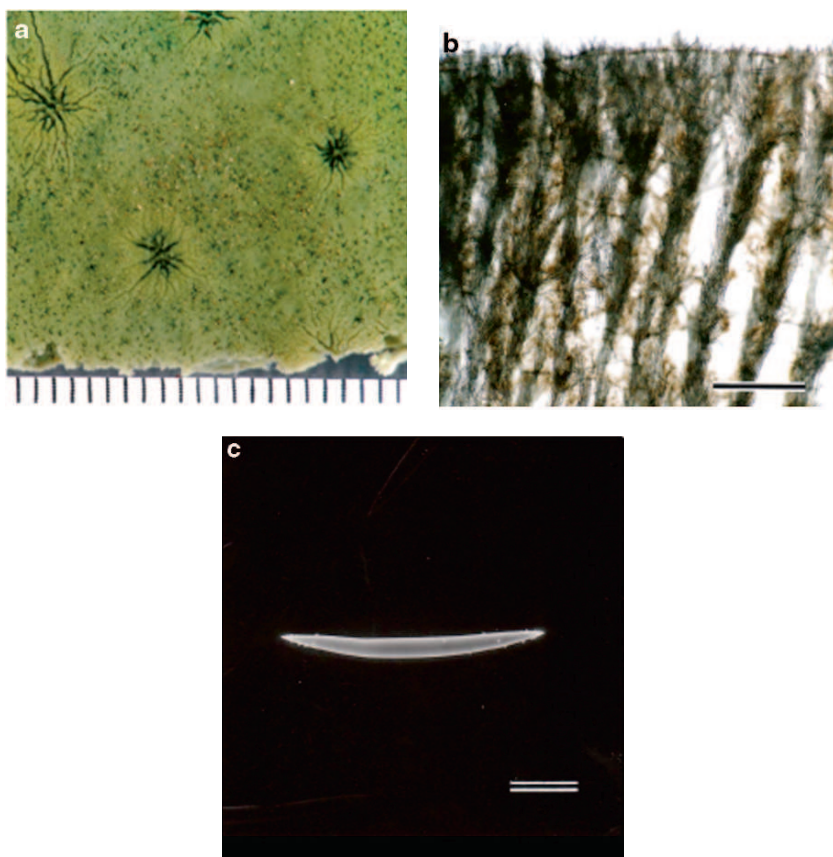


Fig. 6 *L. abietina* (Swartschewski). **a** Part of the crustal body. Each division of scale = 1 mm. **b** Skeleton (arrangement of spicules). Scale bar = 500 μ m. **c** A spicule Scale bar = 50 μ m

were slightly curved amphioxea, typically fusiform and covered with spines only near their tips (Fig. 6c); only rarely, the spicules had spines in the middle part; length 168.4–218.5 μm (mean 192.3 μm , SD 11.9), width 12.9–19.0 μm (mean 15.8 μm , SD 1.4).

Distribution – This species was collected from only six stations. Though this species was distributed in the North, Central, and South Basins, its dispersion was uneven in each Basin (Fig. 1f).

(b) Genus *Baikalospongia* Annandale 1914

1. *Baikalospongia bacillifera* (Dybowski) (Fig. 7a–c)

Description – Sponges had massive bodies in the shape of balls or ellipsoids (Fig. 7a). The skeleton consisted of thick main bundles with numerous spicules and thin cross bundles. Individual sponges had various colors, such as light green, green, and brown. The spicules in the main bundles deviated from the bundle axis

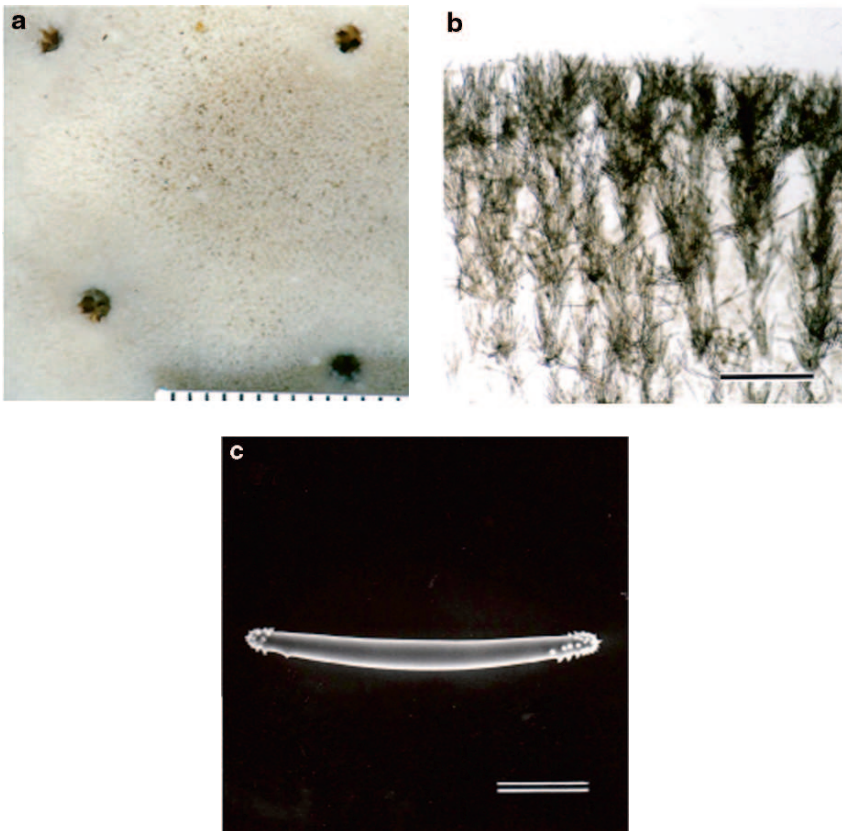


Fig. 7 *Baikalospongia bacillifera* (Dybowski). The faded color of this sample was due to dehydration by ethanol for fixation. **a** A part of the massive body. Each division of the scale = 1 mm. **b** Skeleton (arrangement of spicules). Scale bar = 500 μm . **c** A spicule. Scale bar = 50 μm

to their distal ends (Fig. 7b). The main bundles were connected by cross bundles of several spicules. In contrast to the sponges described above, the consistency of live sponges was rigid and fragile. Spicules were slightly curved amphistrongyla that were covered with spines near their ends (Fig. 7c); length 172.5–217.1 μm (mean 200.0 μm , SD 9.1), width 12.4–19.6 μm (mean 16.7 μm , SD 1.5).

Distribution – This species was collected from nine stations in the North and South Basins. It was distributed unevenly in both Basins (Fig. 1g).

2. *Baikalospongia martinsoni* Efremova (Fig. 8a–c)

Description – Sponges had crustal forms with no branches (Fig. 8a) and their color was dark green. The skeleton which consisted of thick main bundles with numerous spicules had continuous dichotomy. Forming brushes close to surface, the spicules in the main bundles deviated from the bundle axis to their distal ends and were arranged into a fan shape. Transverse spicules were frequently single

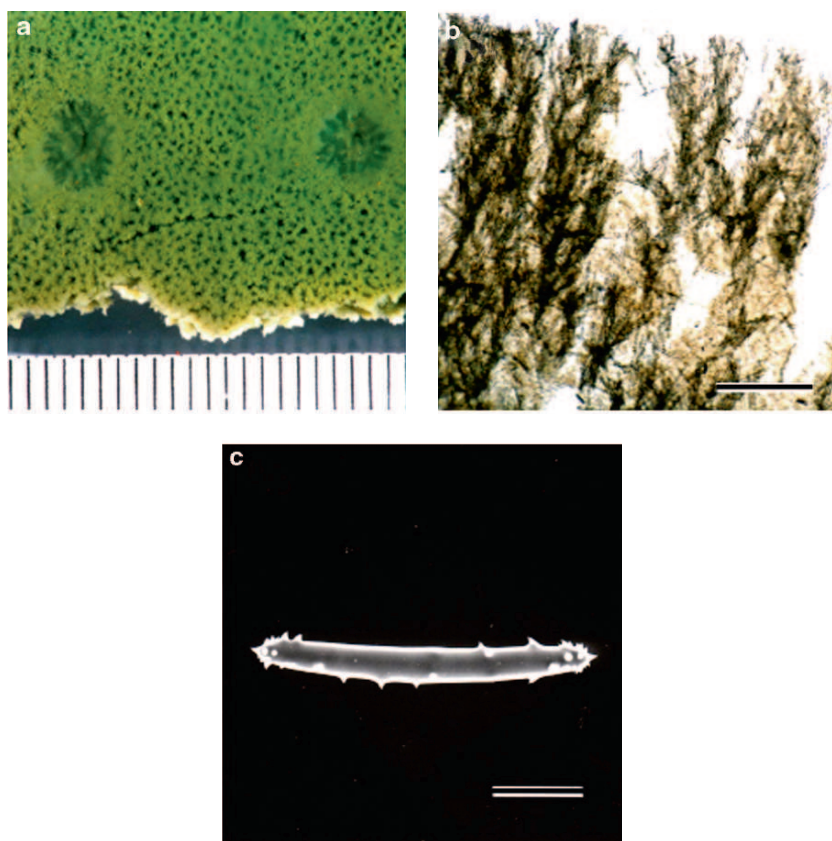


Fig. 8 *B. martinsoni* Efremova. **a** Part of the crustal body. Each division of the scale = 1 mm. **b** Skeleton (arrangement of spicules). Scale bar = 500 μm . **c** A spicule. Scale bar = 50 μm

and were not joined into main bundles (Figs. 8b, 17b). The consistency of live sponges was rigid and fragile. Spicules were slightly curved amphistrongyla and had a few spines along the whole length and also at the tips (Figs. 8c, 18b). The spines near the tips were frequently curved downward to the middle of the spicule; length 160.7–211.1 μm (mean 190.7 μm , SD 10.1), width 13.7–21.5 μm (mean 17.9 μm , SD 1.7).

Distribution – This species was collected from only one station (Listvinichnyi) in the South Basin (Fig. 1h).

3. *Baikalospongia fungiformis* (Makuschok) (Figs. 9, 10)

Description – This species was classified into two groups by their forms. One group had massive forms in the shape of ovoidal balls or fungi (Fig. 9a). The other had a crustal form (Fig. 10a). Each sponge has individual colors, such as green, dark green, and light brown. The skeleton consisted of thick main bundles with numerous spicules and thick cross bundles. The spicules in the main and

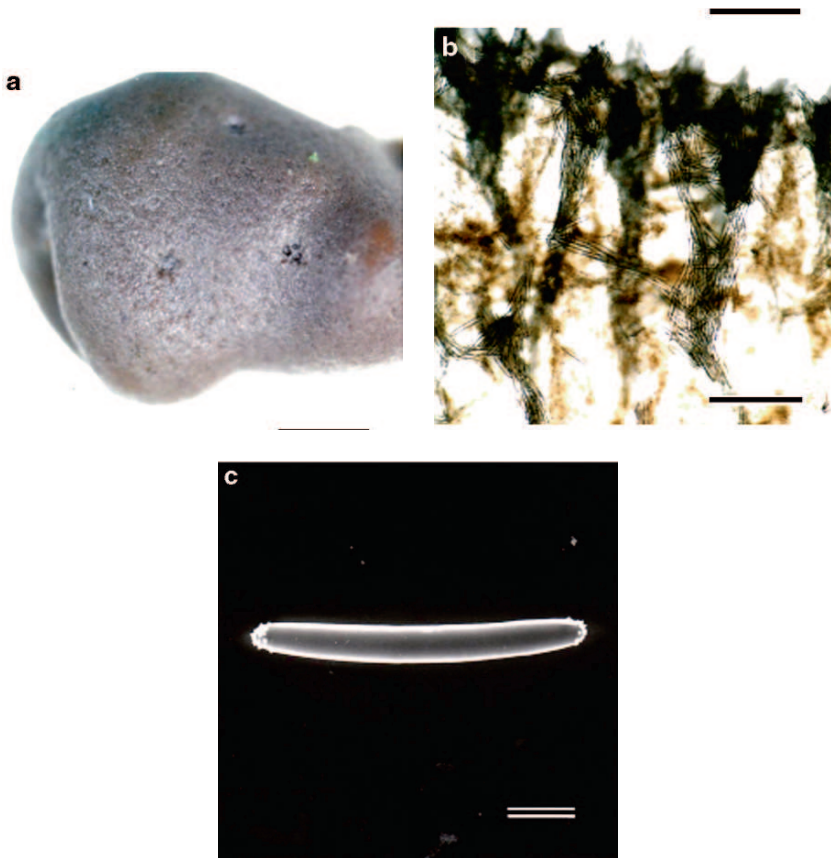


Fig. 9 *B. fungiformis* (Makuschok). **a** Part of the massive body. Scale bar = 1 cm. **b** Skeleton (arrangement of spicules). Scale bar = 500 μm . **c** A spicule. Scale bar = 50 μm

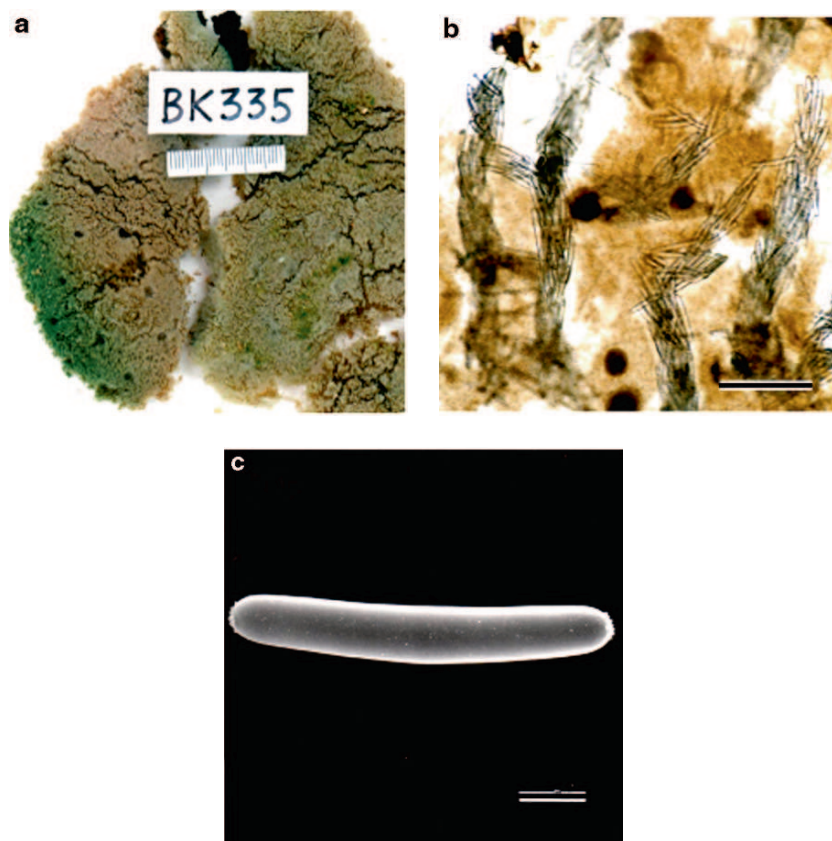


Fig. 10 *B. fungiformis* (Makuschok). **a** Part of the crustal body. Each division of the scale = 1 mm. **b** Skeleton (arrangement of spicules). Scale bar = 500 μm . **c** A spicule. Scale bar = 50 μm

cross bundles were arranged regularly, almost parallel to the bundle length. The main bundles ended on the sponge surface in conical tips (Figs. 9b, 10b, 17c). The consistency of live sponges was rigid and fragile. Spicules were slightly curved thick amphistrongyla and covered with spines only at the ends (Figs. 9c, 10c, 18c); Spicules of massive form: length 223.8–274.7 μm (mean 250.1 μm , SD 10.4), width 20.3–31.8 μm (mean 26.3 μm , SD 2.1). Spicules of crustal form: length 261.8–316.4 μm (mean 291.3 μm , SD 11.4), width 28.8–45.3 μm (mean 36.4 μm , SD 3.6).

Distribution – This species was collected from ten stations in the North and South Basins (Fig. 1i).

4. *Baikalospongia recta* Efremova (Fig. 11)

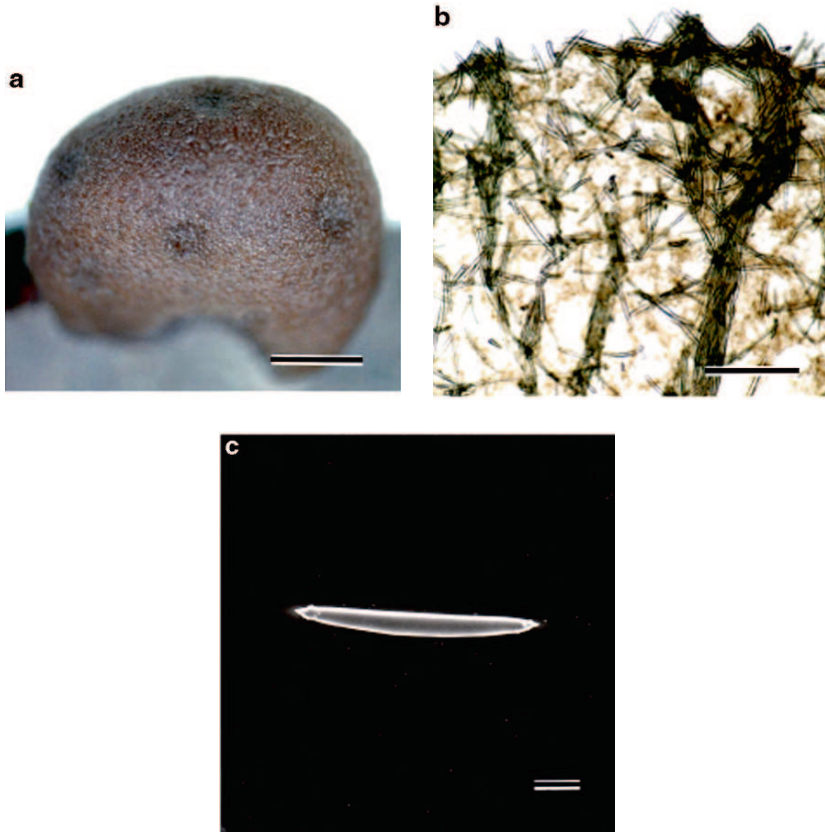


Fig. 11 *B. recta* Efremova. **a** Part of the massive body. *Scale bar* = 1 cm. **b** Skeleton (arrangement of spicules). *Scale bar* = 500 μ m. **c** A spicule. *Scale bar* = 50 μ m

Description – Sponges had massive forms in the shape of balls or ellipsoids (Fig. 11a). The color was green due to symbiotic zoochlorellae or dark brown. The skeleton consisted of thick main bundles with numerous spicules and thin cross bundles. Main bundles were almost straight. Ramification was not so distinct. The spicules in the main bundles ran almost parallel from the bundle axis to their distal ends. The main bundles ended on the sponge surface in conical tips. The cross bundles consisted of only a few spicules (Figs. 11b, 17d). The consistency of live sponge was rigid and fragile. Spicules were slightly curved amphioxea and covered with a few spines at their ends (Figs. 11c, 18d); length 244.2–346.0 μ m (mean 294.0 μ m, SD 16.6), width 18.3–27.9 μ m (mean 22.6 μ m, SD 2.3).

Distribution – This species was collected from seven stations in the North and South Basins. It was distributed unevenly in both Basins (Fig. 1j).

5. *Baikalospongia intermedia* (Dybowski) (Figs. 12, 13)

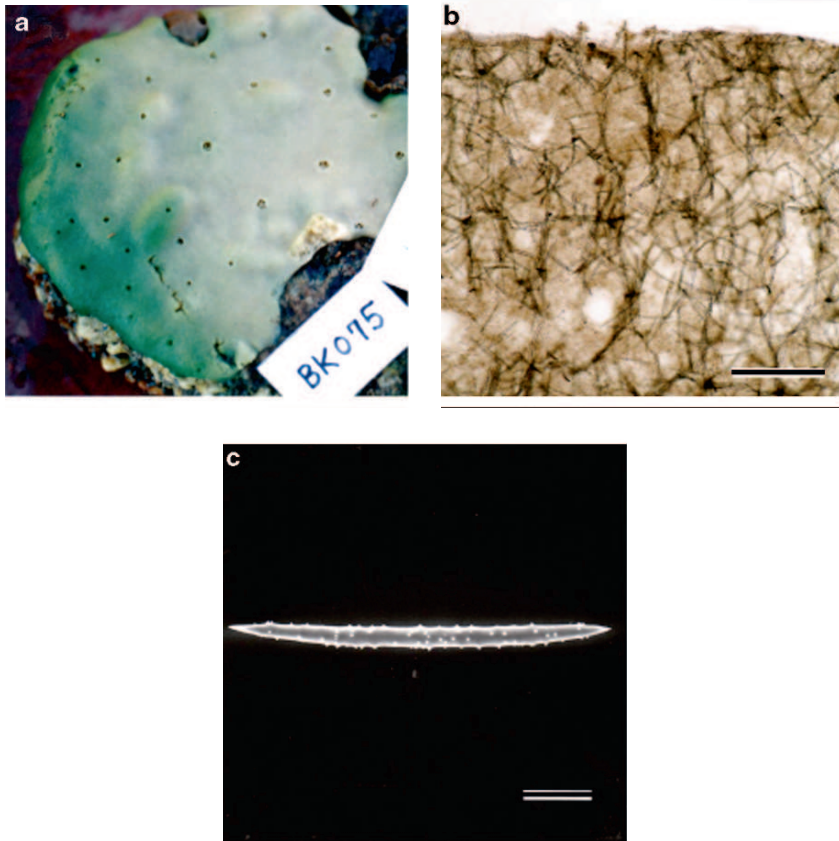


Fig. 12 *B. intermedia* (Dybowski). **a** Part of the crustal body. Each division of the *scale* = 1 mm. **b** Skeleton (arrangement of spicules). *Scale bar* = 500 μm . **c** A spicule. *Scale bar* = 50 μm

Description – This sponge was classified into two groups by their forms. One had a crustal form (Fig. 12a) and some specimens had several protuberances on their crustal forms. The thickness of the crust varied from 0.5 to 1 cm. The other had massive forms in the shape of ovoidal balls (Fig. 13a, c). This group was named by Rezvoj *B. intermedia profundalis*. The skeleton of both types was irregular and weak in spite of main and cross bundles (Figs. 12b, 13b, 17e). The skeleton was less developed than that of *B. bacillifera*, and the developmental levels of individuals varied significantly. The consistency of live sponges was soft and fragile. *B. intermedia profundalis* was especially soft. When alive, color was pale or dark green depending on the quantity of zoochlorellae. *B. intermedia* typica had amphioxea (Fig. 12c) or sometimes amphistrongyla. *B. intermedia profundalis* had only amphistrongyla (Figs. 13c, 18e). Both spicule types were covered with spines along the whole length (Fig. 13c). Amphioxea spicules: length 228.8–273.6 μm (mean 251.8 μm , SD 10.1), width 10.8–18.8 μm (mean 15.2 μm ,

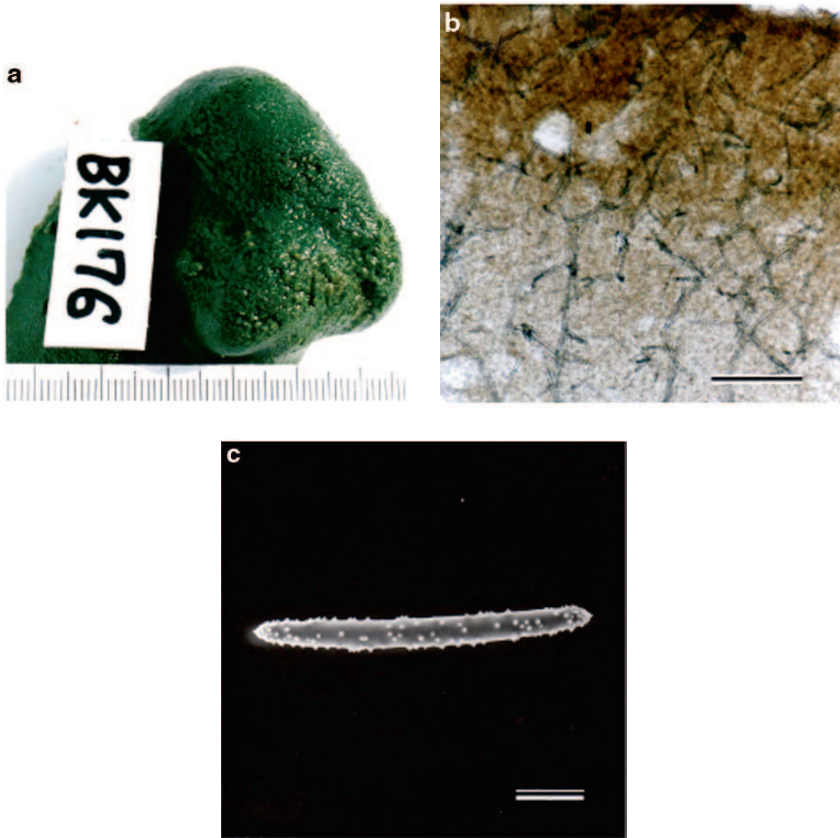


Fig. 13 *B. intermedia profundalis* (Rezvoj). **a** A part of the massive body. Each division of the scale = 1 mm. **b** Skeleton (arrangement of spicules). Scale bar = 500 μm . **c** A spicule. Scale bar = 50 μm

SD 1.8). Amphistrongyla spicules: length 181.6–249.8 μm (mean 226.2 μm , SD 13.6), width 14.0–22.7 μm (mean 18.6 μm , SD 1.7).

Distribution – This species was collected from 40 stations and distributed in the whole littoral zones except some stations where the substratum was sand, mud, and pebbles (Fig. 1k).

(c) Genus *Swartschewskia* Makuschok 1927

1. *Swartschewskia papyracea* (Dybowski) (Figs. 14, 15)

Description – This species was classified into two groups based on the form of sponges. One group had a domed form (Fig. 14a), the other group had a crustal form (Fig. 14b). The former had one or two oscula at the top of the dome. The

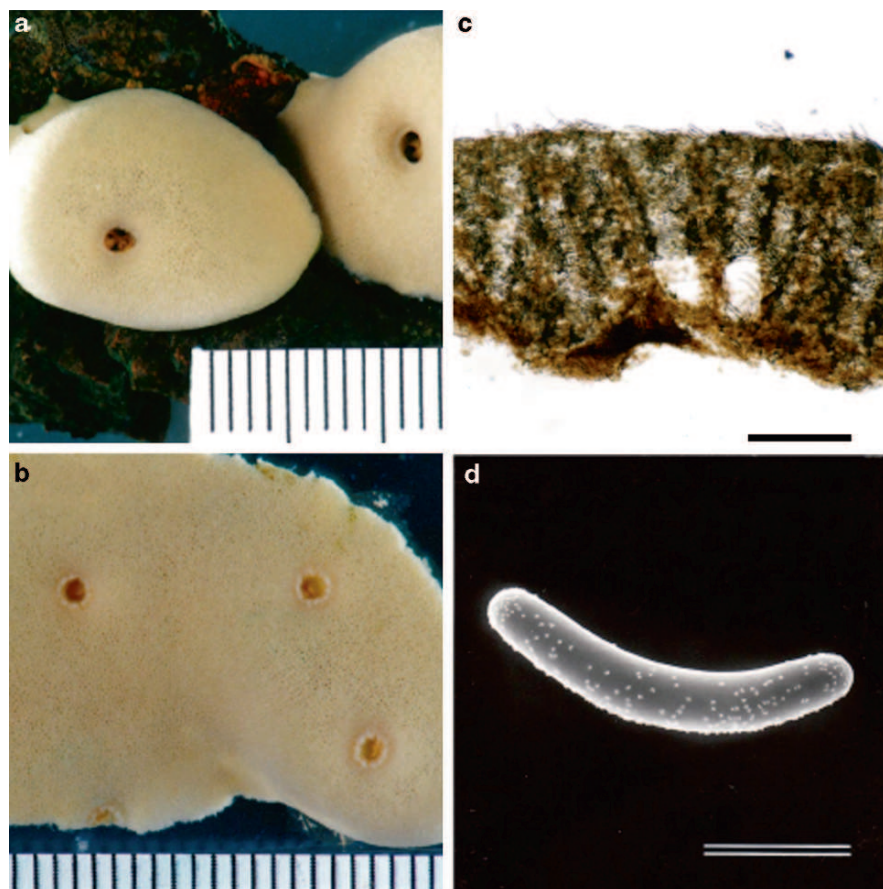


Fig. 14 *Swartschewskia papyracea* (Dybowski). **a** Two domed bodies. Each division of the *scale* = 1 mm. **b** Part of the flattened body. Each division of the *scale* = 1 mm. **c** Skeleton (arrangement of spicules). *Scale bar* = 500 μm . **d** A spicule. *Scale bar* = 50 μm

oscula of domed sponges usually had a deep hollow (Fig. 14a) and were sometimes like a sieve (Fig. 15). When alive, color was yellowish. The skeleton of both groups was not differentiated into main or cross bundles. The polygonal net of bundles was evident in the dermal layer which consisted of thick tangentially arranged spicules (Fig. 14c). The consistency of the outer crust was rigid and fragile. The inner tissue was soft and loose. Spicules were slightly curved short amphistrongyla and covered with spines along the whole length (Figs. 14d, 15b): length 87.9–144.3 μm (mean 111.7 μm , SD 9.5), width 14.6–24.4 μm (mean 18.6 μm , SD 1.8).

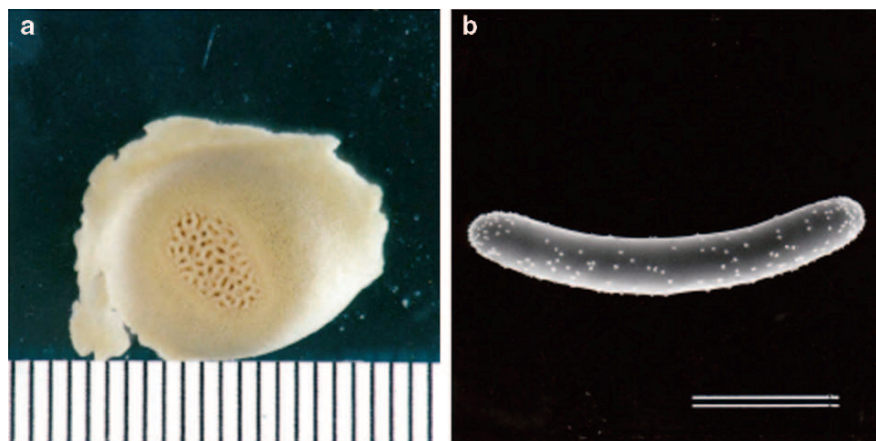


Fig. 15 *S. papyracea* (Dybowski). **a** The domed body. The oscula are like a sieve. Each division of the *scale* = 1 mm. **b** A spicule. *Scale bar* = 50 μ m

Distribution – This species was collected from only six stations in the North and South Basins. It was distributed unevenly in both Basins (Fig. 11)

(d) Genus *Rezinkovia* Efremova 2001

1. *Rezinkovia echinata* Efremova (Figs. 16a–c, 17f, 18f)

Description – The sponges were irregular shaped massive forms with many small projections of main bundles on their surface (Fig. 16a). When alive, color was light brown. The skeleton consisted of thick main bundles with numerous spicules and thin cross bundles. The spicules in the main bundles ran almost parallel from the bundle axis to their distal ends. The main bundles ended on the sponge surface in conical tips (Figs. 16b, 17f). The cross bundles were composed of only a few spicules (Figs. 16b, 17f). Live sponges were fragile and easily split from end to end. Spicules were slightly curved thick amphioxea and covered with a small number of spines at their ends (Figs. 16c, 18f); length 234.7–331.2 μ m (mean 271.0 μ m, SD 14.6), width 10.2–18.0 μ m (mean 14.9 μ m, SD 1.4).

Distribution – This species was collected from several stations in the Central and South Basins, such as Listvinichyi, Olkhon Island, Ivanovsky, Ushkanii Island.

Family Spongillidae Gray 1867

(a) Genus *Spongilla* Lamarck 1816

1. *Spongilla lacustris* (Linnaeus)

Description – Mature sponges produced finger-like branches arising from an irregular base. The consistency of live sponges was soft and fragile. When alive,

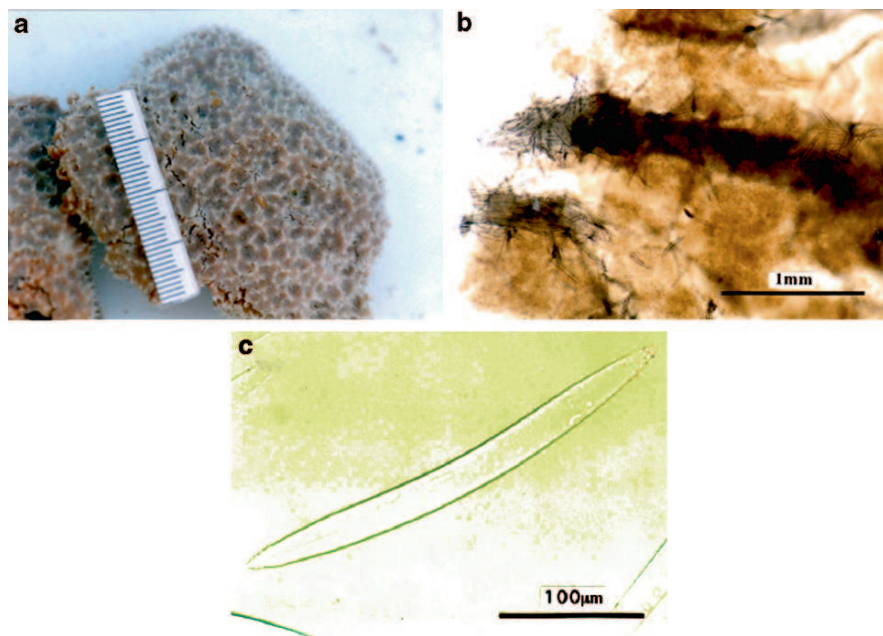


Fig. 16 *Rezhinkovia echinata* Efremova **a** Part of crustal body. Each division of the *scale* = 1 mm. **b** Skeleton (arrangement of spicule). The surface is the left side

color was green due to the presence of a great number of zoochlorellae. The megascleres were slightly curved amphioxea, invariably entirely smooth; length 264.4–346.4 μm (mean 308.2 μm , SD 15.7), width 10.8–20.2 μm (mean 14.9 μm , SD 1.6). The microscleres were slightly curved amphioxea and covered with many spines along the whole length; length 73.5–127.2 μm (mean 95.3 μm , SD 9.5), width 3.1–6.1 μm (mean 4.4 μm , SD 0.6).

The number of gemmoscleres was very small. Though there were some exceptionally smooth spicules, they were generally covered with some spines and the gemmoscleres were rather stout and slightly curved amphioxea or amphistrongyla.

Distribution – This species was collected from one station of an estuary of the North Basin and from three stations in the Little Sea near Olkhon Island (Fig. 1n).

(b) Genus *Eunapius* Gray 1867

1. *Eunapius* sp.

Description – Mature sponges had a crustal form and were attached to submerged tree branches. The consistency of live sponges was soft and fragile. When alive, color was yellowish. The megascleres were slightly curved amphioxea, almost entirely smooth; length 215.2–313.4 μm (mean 246.1 μm , SD 17.8), width 7.2–19.9 μm

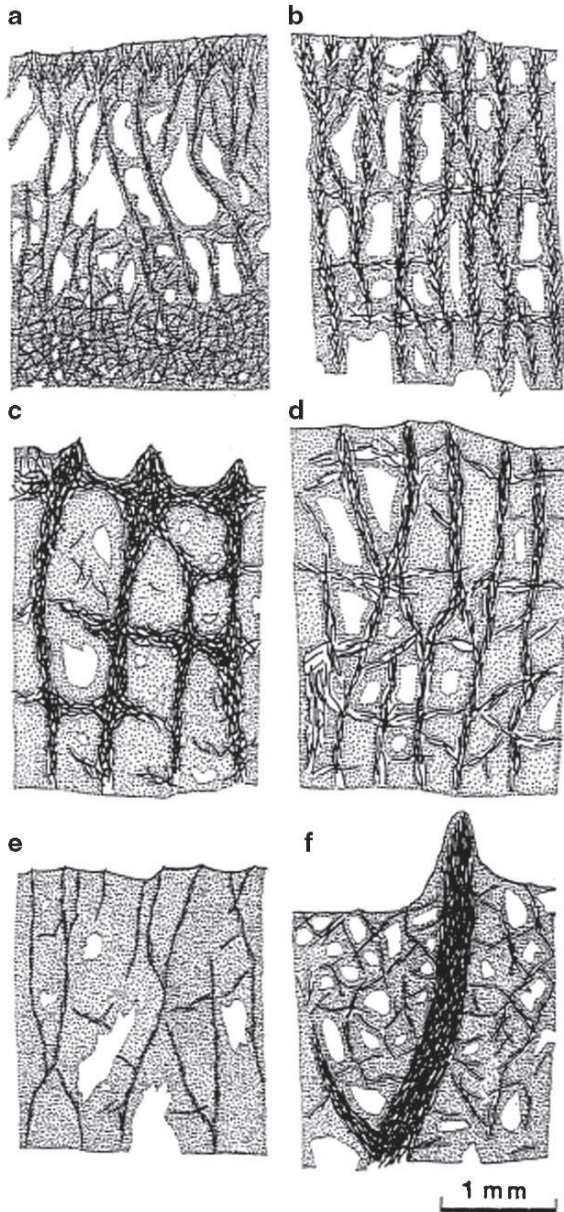


Fig. 17 Skeleton of some species. **a** *Lubomirskia incrustans*; **b** *Baikalospongia martinsoni*; **c** *B. fungiformis*; **d** *B. recta*; **e** *B. intermedia profundalis*; **f** *Rezinkovia echinata*

(mean 10.1 μm , SD 1.2). Microscleres were absent. The gemmoscleres were rather stout and slightly curved amphioxea, covered with many conspicuous spines along the whole length. Many gemmoscleres were attached to the whole surface of the

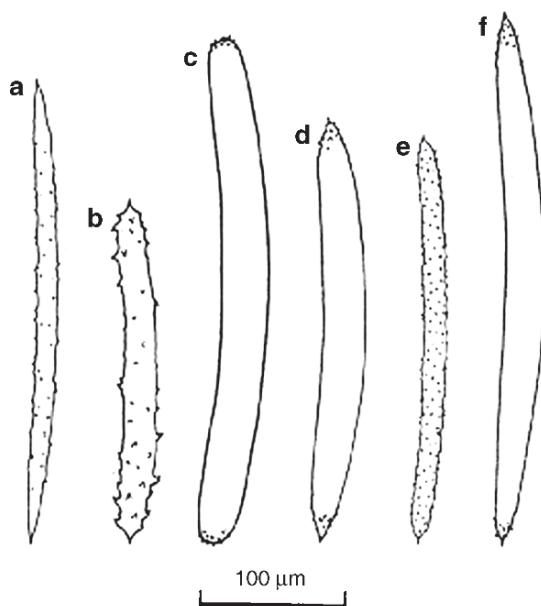


Fig. 18 Spicules of some species. **a** *Lubomirskia incrustans*; **b** *Baikalospongia martinsoni*; **c** *B. fungiformis*; **d** *B. recta*; **e** *B. intermedia profundalis*; **f** *Rezinkovia echinata*

gemmules tangentially; length 59.9–116.0 μm (mean 80.6 μm , SD 10.5), width 4.3–7.5 μm (mean 5.8 μm , SD 0.7).

Distribution – This species was collected from one station; an estuary in the North Basin (Fig. 1o).

(c) Genus *Ephydatia* Lamouroux 1816

1. *Ephydatia muelleri* (Lieberkühn)

Description – The sponges occurred as small crusts attached to the underside of stones. The consistency of live sponges was soft and fragile and, when alive, their color was yellowish. The megascleres were slightly curved amphioxea. Most of the megascleres were covered with small acute spines except at their tips. Some megascleres were entirely smooth; length 198.8–283.2 μm (mean 238.1 μm , SD 17.0), width 6.9–13.9 μm (mean 10.2 μm , SD 1.2). Microscleres were absent. The gemmoscleres were birotulates of one class. They had rotules of equal diameter and were distinctly flat in shape, irregularly and deeply incised into a small number of long rays. Some malformations of gemmoscleres were observed; length 8.4–18.7 μm (mean 13.1 μm , SD 1.5), diameter of rotules 14.4–24.7 μm (mean 18.8 μm , SD 2.3), diameter of shafts 2.0–4.7 μm (mean 3.4 μm , SD 0.6).

Distribution – This species was collected from three stations in the Little Sea near Olkhon Island (Fig. 1p).

2 Horizontal and Vertical Distribution of Freshwater Sponges in Lake Baikal

1. Horizontal distribution

In the summers of 1993–1996, a total of 426 specimens of freshwater sponges were collected from 55 stations (Fig. 1a). Most specimens belonged to the endemic family Lubomirskiidae and were widely distributed in Lake Baikal except on inappropriate substrata. A few specimens with gemmules or microscleres belonged to the Spongillidae and were confined to the Little Sea near Olkhon Island and an estuary in the North Basin (Fig. 1n–p).

The species which were distributed widely along the shore were *L. baicalensis*, *L. incrustans*, *L. fusifera*, and *B. intermedia* (Fig. 1b, c, e, k).

2. Qualitative survey of vertical distribution

During the summers of 1997 and 1998, we surveyed Lake Baikal from the surface to a depth of 45 m in the littoral zone. We analyzed each species' frequency of

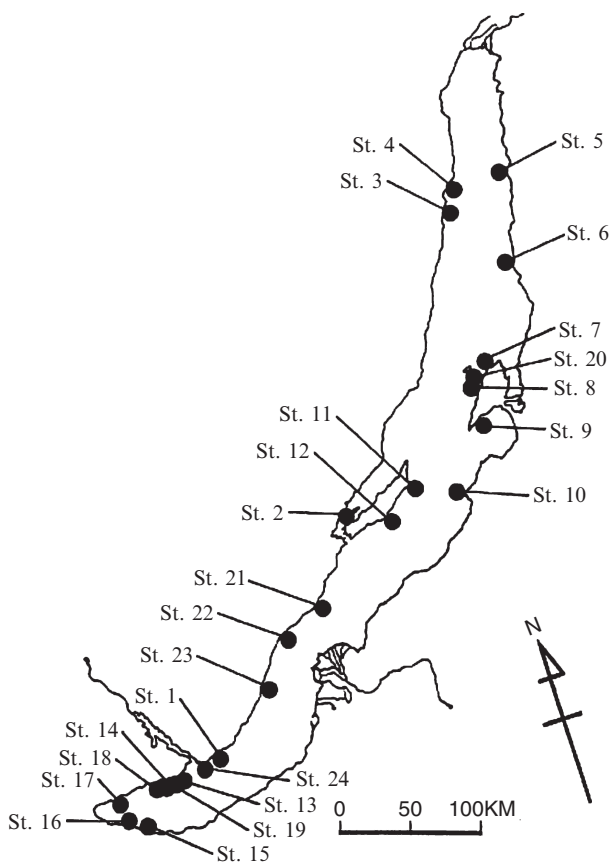


Fig. 19 Sites of vertical distribution survey stations in Lake Baikal (1997–1998)

appearance at the depths of 10, 20, 30, and 40 m, and collected 540 specimens from 92 points at 24 stations (Table 2, Fig. 19). Most specimens belonged to the endemic family Lubomirskiidae and a few to the family Spongillidae.

E. muelleri and *S. lacustris*, which belong to the Spongillidae, were collected from only one point at a depth of 0.5 m. All the Lubomirskiidae species were collected at points less than 1 m deep. Table 3 shows the frequency of each species, but not their quantity. *B. intermedia* had the highest frequency among all species and occurred more often in the shallow zone. *L. baicalensis* was second with regard to frequency and also more often in the shallow zone. *B. fungiformis*, *B. bacillifera*, *L. abietina* and *B. recta* occupied ranks three to six, and all were found more frequently in the deeper zone. The remaining species did not show high frequency either in the shallow zones or in the deeper zones. Though *S. papyracea* had been believed to inhabit only deeper zones, it occurred in shallow zones as well.

3. Quantitative survey of vertical distribution

During the summers of 2000 and 2001, we surveyed Lake Baikal from the surface to a depth of 40 m in the littoral zone and collected 377 specimens from 26 points at 5 stations (Fig. 20). At each station, we put three quadrates (30 × 30 cm) at the shallowest point where sponges were first observed, and at 10, 20, 30, and 40 m depths, respectively. After collecting all specimens in the three quadrates at each point, we put them into a graduated cylinder with enough water to immerse the specimens and measured the volume of each sponge by the rise in water level.

All specimens belonged to Lubomirskiidae. The biomass of sponges at 10 m depth showed maximum value at four stations (Table 4). The biomass of sponges at 20 m depth showed the second largest at three stations.

2.1 Discussion

From 1993 to 2001, we surveyed mainly the littoral zone of Lake Baikal and collected 1,539 specimens of sponges from approximately 60 stations. They were classified into 2 families, 7 genera, and 14 species. Most specimens belonged to the endemic family Lubomirskiidae and the others to the family Spongillidae.

1. Taxonomy

(a) Lubomirskiidae

Lubomirskiidae collected in this survey were classified into 4 genera and 11 species.

Even though Efremova listed 4 genera and 13 species of Lubomirskiidae (Efremova 2001, Table 5), we could not detect *Swartschewskia irregularis* and *Rezinkovia arbuscula* in our collections performed for our survey. Besides, *S. irregularis* was first described by Swartschewski from a single specimen (Swartschewski 1902); unfortunately, the holotype has been lost and thus is unavailable for consultation. In 1990, Efremova collected this species again with

Table 2 List of vertical distribution survey stations in Lake Baikal (1997–1998)

A. Survey in 1997						
Station No.	Name of station	depth of Point 1	depth of Point 2	depth of Point 3	depth of Point 4	depth of Point 5
1	Bolshye Koty	3m	10m	20m	30m	40m
2	Tonik	1m				
3	Cape Muzhinai	3m	18m	25m	33m	
4	Hara Bay	4m	10m	20m	30m	
5	Cape Shignanda	3m	8m	20m	30m	40m
6	Davsha	5m	8m	12m		
7	Cape Orlovsky	5m	20m	30m	40m	
8	Cape Markovo	5m	10m	20m	30m	40m
9	Svyatoy Nos	5m	10m	20m	30m	40m
10	Listvinch Island	20m	30m	40m		
11	Olkhon Island	6m	10m	20m	30m	40m
12	Cape Uhan	4m	10m	20m	30m	40m
13	Katarzhanka	5m	10m	20m	30m	40m
14	Cape Ivanovkkoye	5m	10m	20m	30m	40m
15	Baikalsk	10m				
16	near Utulik River	5m	10m	30m		

B. Survey in 1998						
Station No.	Name of station	depth of Point 1	depth of Point 2	depth of Point 3	depth of Point 4	depth of Point 5
17	Angasolka	1m	10m	20m	30m	40m
18	Tvanovskiy	6m	15m	25m	45m	
19	Tolstiy	3m	40m			
20	Ushkanii Island	4m	6m	10m		
21	Cape Krestovskii	5m	20m	30m	40m	
22	near Krasnyi village	10m	14m	20m	30m	
23	Cape Verkhnie Khomuty	12m	20m	30m		
24	Abuteekha	6m	10m	30m	40m	

Table 3 Frequency at 24 stations (92 points) around Lake Baikal (1997–1998)

Species	Distribution	0–10m	10–20m	20–30m	30–40m	40–45m	0–45m
1. <i>Lubomirskia baicalensis</i>	5–40m	6	10	8	3	1	28
2. <i>L. incrustans</i>	4–40m	2	0	0	1	0	3
3. <i>L. fusifera</i>	4–30m	2	2	1	1	0	6
4. <i>L. abietina</i>	6–40m	1	1	2	3	6	13
5. <i>Baikalospongia bacillifera</i>	5–40m	1	4	3	5	7	20
6. <i>B. martinsoni</i>	10–30m	0	1	0	1	0	2
7. <i>B. fungiformis</i>	5–40m	1	1	6	9	5	22
8. <i>B. recta</i>	10–40m	0	1	2	2	5	10
9. <i>B. intermedia</i>	1–40m	19	17	10	11	7	64
10. <i>B. intermedia profundalis</i>	20–40m	0	0	2	0	1	3
11. <i>Swartschewskaia papyracea</i>	4–40m	3	1	0	1	1	6
12. <i>Rezinkovia echinata</i>	40–45m	0	0	0	0	2	2
13. <i>Ephydatia muelleri</i>	0.5m	1	0	0	0	0	1
14. <i>Spongilla lacustris</i>	0.5m	1	0	0	0	0	1

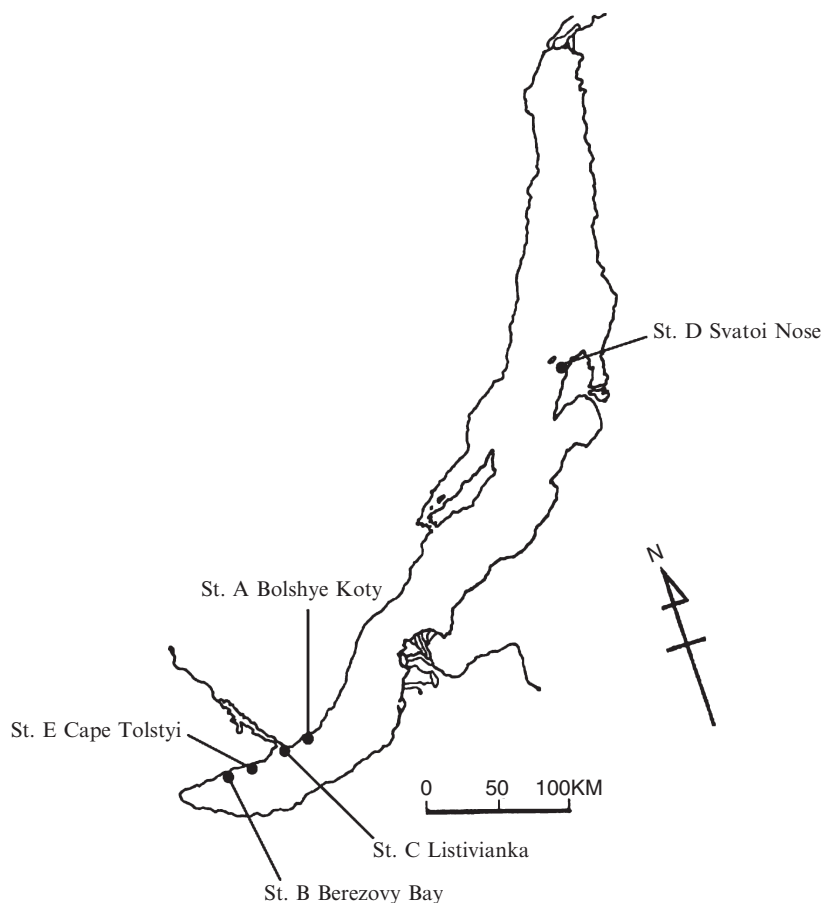


Fig. 20 Sites of vertical quantitative survey stations in Lake Baikal (2000–2001)

a remote controlled manipulator in the canyon opposite pad Chernaya from a depth of 94.5 m (Efremova 2001). She also collected *R. arbuscula* with a remote controlled manipulator from 78 m depth at the same station in 1990; this is the only specimen and holotype. It has been reported that the specimen was considerably damaged during collection (Efremova 2001). Both species are supposed to be very rare and, therefore, more information is required to categorize them.

Also among the specimens collected in our survey there are some whose generic positions are still unclassified. An exhaustive investigation of the sublittoral and deeper zones as well as other littoral zones is required.

(b) Spongillidae

In 1902, Swartschewski collected *S. microgemmata*, *E. olchonensis*, and *E. gorjaevii*, which are synonyms of *S. lacustris*, *E. fluviatilis*, and *E. muelleri*, respectively (Penney

Table 4 Horizontal quantitative survey at five stations (ml/30cm×30cm)

Station A (Bolshye Koty, 3rd, Aug., 2000)					
	5.6m depth	10m depth	20m depth	30m depth	40m depth
<i>L. baicalensis</i>	52	444			
<i>L. incrustans</i>		1.2			
<i>L. fusifera</i>			29.1		
<i>L. abietina</i>			4.6		1
<i>B. bacillifera</i>		16.6	37	14.5	521
<i>B. martinsoni</i>				66	20.5
<i>B. fungiformis</i>			22.8		6
<i>B. recta</i>		2.1	12.7	15.4	
<i>B. tenera</i>			19.1		
<i>B. intermedia</i>	51.1	64.4	2.5		
<i>S. papyracea</i>					0.4
Total	103.1	528.3	127.8	95.9	548.9
Station B (Berezovy Bay, 5th, Aug., 2000)					
	3.7m depth	10m depth	20m depth	30m depth	40m depth
<i>L. baicalensis</i>		1195			
<i>L. incrustans</i>	20				
<i>L. fusifera</i>					
<i>L. abietina</i>			48	5.5	45
<i>B. bacillifera</i>			461.5	134	70
<i>B. martinsoni</i>					5
<i>B. fungiformis</i>					6
<i>B. recta</i>		894			
<i>B. tenera</i>		10		34	
<i>B. intermedia</i>	315	2.5	32		
<i>S. papyracea</i>				1	0.5
Total	335	2101.5	541.5	174.5	126.5
Station C (Listvianka, 6th, Aug., 2000)					
	3.0m depth	10m depth	20m depth	30m depth	40m depth
<i>L. baicalensis</i>		2100			
<i>L. incrustans</i>	18				
<i>L. fusifera</i>			14	25	
<i>L. abietina</i>				10	77
<i>B. bacillifera</i>		36	416	415	362.5
<i>B. martinsoni</i>		20			
<i>B. fungiformis</i>					150
<i>B. recta</i>		9.5	209	80	
<i>B. tenera</i>			20	20	
<i>B. intermedia</i>	56	39			
<i>S. papyracea</i>					
Total	74	2204.5	659	550	589.5
Station D (Cape Tolsty, 8th, Aug., 2001)					
	3.2m depth	10m depth	20m depth	30m depth	40m depth
<i>L. baicalensis</i>		1538			
<i>L. incrustans</i>					
<i>L. fusifera</i>			31		
<i>L. abietina</i>			25.5	27	42.5
<i>B. bacillifera</i>		89	364.5	84.5	87.5
<i>B. martinsoni</i>					

(continued)

Table 4 (continued)

Station D (Cape Tolsty, 8th, Aug., 2001)					
	3.2m depth	10m depth	20m depth	30m depth	40m depth
<i>B. fungiformis</i>			180	42.5	96
<i>B. recta</i>		195	26		
<i>B. tenera</i>					
<i>B. intermedia</i>	310.5	190			
<i>S. papyracea</i>					
Total	310.5	2012	627	154	226
Station E (Svaytoy Nos, Cape Markova, 4-5th, Aug., 2001)					
	2.7m depth	10m depth	20m depth	30m depth	40m depth
<i>L. baicalensis</i>		168	65	100	
<i>L. incrustans</i>					
<i>L. fusifera</i>				59	
<i>L. abietina</i>					
<i>B. bacillifera</i>			4	6	
<i>B. martinsoni</i>					
<i>B. fungiformis</i>			180	6	14.5
<i>B. recta</i>			80	94	
<i>B. tenera</i>					
<i>B. intermedia</i>	105	115	87	12.5	
<i>S. papyracea</i>					
Total	105	283	416	277.5	14.5

Table 5 List of freshwater sponges in Lake Baikal (Efremova, 2001)

Family Lubomirskiidae Rezvoj, 1936

Genus *Lubomirskia*, Dybowski, 1880

- 1) *Lubomirskia baicalensis* (Pallas, 1771)
- 2) *Lubomirskia fusifera* Soukatschhoff, 1895
- 3) *Lubomirskia abietina* (Swartschewski, 1902)
- 4) *Lubomirskia incrustans* Efremova, 2001

Genus *Baikalospongia* Annandale, 1914

- 5) *Baikalospongia bacillifera* (Dybowski, 1880)
- 6) *Baikalospongia fungiformis* (Makuschok, 1927)
- 7) *Baikalospongia recta* Efremova, 2001
- 8) *Baikalospongia martinsoni* Efremova, 2001
- 9) *Baikalospongia intermedia* (Dybowski, 1880)
- 9') *B. intermedia profundalis* (Rezvoj, 1936)

Genus *Swartschewskia* Makuschok, 1927

- 10) *Swartschewskia papyracea* (Dybowski, 1880)
- 11) *Swartschewskia irregularis* (Swartschewski, 1902)

Genus *Rezinkovia* Efremova, 2001

- 12) *Rezinkovia echinata* Efremova, 2001
- 13) *Rezinkovia arbuscula* Efremova, 2001

Family Spongillidae Gray, 1867

Genus *Trochospongilla* Vejdovsky, 1883

- 14) *Trochospongilla* sp.

Genus *Ephydatia* Lamouroux, 1816

- 15) *Ephydatia muelleri* (Lieberkühn, 1855)
- 16) *Ephydatia fluviatilis* (Linnaeus, 1758)

Genus *Spongilla* Lamarck, 1816

- 17) *Spongilla lacustris* (Linnaeus, 1758)

Genus *Eunapius* Gray, 1867

- 18) *Eunapius* sp.

and Racek 1968). Efremova reported that *Trochospongilla* sp. was collected from the South and North basins, in the open Baikal from 1.5 to 80 m depth (Efremova 2001). However, none of the specimens had any gemmules and thus they were identified by megascleres and not by gemmoscleres. Therefore, more information on this species, such as molecular biological analyses, is required.

2. Distribution

(a) Horizontal distribution

Most specimens belonging to the endemic family Lubomirskiidae were distributed widely in Lake Baikal except on inappropriate substrata. A few specimens belonging to the Spongillidae, which had gemmules or microscleres, were confined to the Little Sea near Olkhon Island and to an estuary in the North Basin.

We collected *S. lacustris*, *E. muelleri*, and *Eunapius* sp. which had gemmules or microscleres. *Eunapius* sp. was collected from an estuary that is, strictly speaking, not in Lake Baikal. *S. lacustris* and *E. muelleri* are cosmopolitan species. The other two species were collected from the Little Sea near Olkhon Island. Both sponges were small and some of their spicules showed abnormal forms and smaller dimensions than Japanese ones. We did not collect these species from many other stations in Lake Baikal (Open Baikal). It is supposed that Lake Baikal might be an inappropriate habitat for Spongillidae species which produce gemmules. One reason why Spongillidae species are few in this lake may be its oligotrophy as compared to other lakes which host many Spongillidae species. Though some areas near estuaries of the rivers are not oligotrophic, they are inappropriate habitats for sponges because of sand and pebbles substrata. According to this hypothesis, if Lake Baikal became eutrophic, Spongillidae species would increase. Another reason might be water temperature. Spongillidae species may require higher temperatures for a certain period of the year (summer). The water temperature of the Little Sea near Olkhon Island is higher than that of other areas, especially in summer. More detailed information on differences in the two family habitats is necessary to confirm this presumption.

(b) Vertical distribution

During the summers of 1997 and 1998, we surveyed Lake Baikal from the surface to a depth of 45 m in the littoral zone. We analyzed each species' frequency of appearance at the depths of 10, 20, 30, and 40 m, and collected 540 specimens from 92 points at 24 stations.

(1) Lubomirskiidae

B. intermedia and *L. baicalensis* had the highest frequency, and it was especially high in the moderate zone. In the well-lit zones they had a green body due to many intracellular green algae symbionts; this enables them to adapt to shallower zones. However, they did not occur in depths of less than 1 m; one reason for this may be that most of the water surface of Lake Baikal is frozen in winter and they cannot produce gemmules that can hibernate in the ice. In addition, the strong wave action which often occurs near the surface would damage sponge bodies.

B. intermedia had a thin crustal form or a crustal form with short protuberances. When this species was collected at a depth of 1 m, there were no protuberances. The presence of the protuberances, therefore, is caused by the water current or wave action. That is, having protuberances is a disadvantage in areas of rapid water currents and strong wave actions. This also applies to *L. baicalensis*. In the shallowest zone, *L. baicalensis* had no protuberances, but the protuberances became longer as they inhabited deeper water. A comparison of the protuberances of *L. baicalensis* and of *B. intermedia* collected from the same point showed that the former had much longer protuberances than the latter. This is because the larger amount of spongin in the former gives more elasticity to the skeleton. The abundant spongin of *L. baicalensis* thickly covers the whole skeleton and gives elasticity to the long protuberances so that they can withstand water currents.

Except for *B. intermedia* and *B. intermedia profundalis*, the bodies of *Baikalospongia* were hard, rigid, and brittle and had no protuberances. They were hard due to a great number of thick spicules, and brittle because of a small amount of spongin. *R. echinata* was brittle in the vertical direction because only the main bundles were thick. *B. fungiformis*, *B. bacillifera*, *L. abietina*, and *B. recta* showed a higher frequency in the deeper zone and their bodies were also rigid and brittle, but the consistency of the body did not correlate with the depth of the water. *B. intermedia profundalis* inhabited a deeper zone, but its body was soft and fragile.

Some *Baikalospongia* were green in color due to symbionts. There are chromaic differences in this green color. It is supposed that the difference may not be due to the abundance of symbionts but to their species.

(2) Spongillidae

E. muelleri and *S. lacustris* which belong to Spongillidae were collected from only one point at a depth of 0.5 m. Their bodies were very soft and fragile. Therefore, most of them were attached to the underside of stones and rocks to avoid wave action. Due to intracellular green algae symbionts, *S. lacustris* in the better lit zone was green in color and had some short thin protuberances.

Though habitats of Spongillidae in Lake Baikal are frozen in winter, they can hibernate because of their gemmules, while Lubomirskiidae, which does not have gemmules, cannot.

Acknowledgements We wish to thank Dr. V. B. Itskovich, Dr. E. V. Weinberg, Dr. S. M. Efremova and Dr. V. I. Chernykh for their help to collect samples as well as Dr. M. A. Grachev and Dr. T. D. Evestigneeva for their support of our survey.

References

- Annandale, N., 1913. Notes on some sponges from Lake Baikal in the collection of the Imperial Academy of Sciences, St. Petersburg. *Ann Mus Zool Acad Sci St. Petersburg*:18–101.
- Annandale, N., 1914. Further notes on the sponges of Lake Baikal. *Rec Indian Mus* 10:137–148.

- Dybowski, W., 1882. Studien über die Spongien des Russischen Reiches. Mem Acad Imp Sci St. Petersburg 7(16):61–71.
- Efremova, S. M., 2001. Sponges (Porifera). In: Timoshkin, O. A. (ed.) Index of animal species inhabiting Lake Baikal and its catchment area, vol. I, Lake Baikal, Book 1. Nauka, Novosibirsk, pp. 182–192 (in Russian).
- Efremova, S. M., 2004. New genus and new species of sponges from family Lubomirskiidae Rezvoj, 1936. In: Timoshkin, O. A. (ed.) Index of animal species inhabiting Lake Baikal and its catchment area. vol. I. Lake Baikal, Book 2. Nauka, Novosibirsk, pp. 1261–1278 (in Russian).
- Kozhov, M. M., 1963. Spongia. In: Kozhov, M. M. (ed) Lake Baikal and its life. Dr. W. Junk Publishers, The Hague, pp. 62–68.
- Masuda, Y., Itskovich, V. B., Veinberg E. V. and Efremova, S. M., 1999. Perspective studies of freshwater sponges in Lake Baikal. Berliner geowiss. Abh. E30:329–332.
- Penney, J. T. and Racek, A. A., 1968. Comprehensive revision of worldwide collection of freshwater sponges (Porifera: Spongillidae) United States Nat Mus Bull 272:1–184.
- Rezvoj, P. D., 1936. Freshwater sponges of the USSR. In: The fauna of the USSR2 (2):1–42 (in Russian).
- Swartschewski, B., 1902. Materials on the sponge fauna of Lake Baikal. Mem Soc Natur Kiev 17:329–352 (in Russian).

Towards a Molecular Systematics of the Lake Baikal/Lake Tuva Sponges

Matthias Wiens, Petra Wrede, Vladislav A. Grebenjuk,
Oxana V. Kaluzhnaya, Sergey I. Belikov, Heinz C. Schröder,
and Werner E.G. Müller

1	Introduction.....	112
2	Endemic Freshwater Sponges in Siberia (Lake Baikal and Tuva).....	113
2.1	E. tuva from Lake Chagytai.....	115
2.2	E. altaiensis from Lake Tore-Khol.....	120
3	Molecular Phylogeny of Endemic Freshwater Sponges from Lake Baikal – Tuva Region.....	124
3.1	Molecular Phylogeny According to ITS Analyses.....	126
3.2	Molecular Phylogeny According to Silicatein Analyses.....	134
4	Evolution of Endemic Sponges in Lake Baikal and Lake Chagytai (Tuva-Baikal Region) – An Approach.....	139
5	Conclusion.....	140
	References.....	142

Abstract Lake Baikal is famous for its extensive biodiversity that is equaled only by few other lakes. Fascinatingly, about 80% of all the animals the lake hosts are endemic. Sponges (Porifera) that live in symbiosis with photosynthetic algae are the most abundant animal taxon found in the littoral zone of Lake Baikal and have been grouped to the family Lubomirskiidae. In recent years, several attempts to determine the phylogenetic relationship between Lubomirskiidae and cosmopolitan freshwater sponges have been undertaken. Yet the results obtained remain inconclusive. Here, we strive to determine the phylogeny of freshwater sponges with the focus on endemic Lake Baikal species, also taking into account two poriferan species that were collected during an expedition in 2006 in two other

M. Wiens (✉), P. Wrede, V.A. Grebenjuk, H.C. Schröder, and W.E.G. Müller
Institut für Physiologische Chemie, Abteilung Angewandte Molekularbiologie, Universität,
Duesbergweg 6, D-55099 Mainz, Germany
e-mail: wiens@uni-mainz.de

O.V. Kaluzhnaya and S.I. Belikov
Limnological Institute of the Siberian Branch of Russian Academy of Sciences,
Ulan-Batorskaya 3, RUS-664033 Irkutsk, Russia

isolated Siberian lakes, Lake Chagytai and Lake Tore-Khol. Since its discovery at the beginning of the twentieth century, the Lake Chagytai species was grouped to the Lubomirskiidae and called *Baikalospongia dzhegatajensis*. However, analyses of molecular sequence data [internal transcribed spacer 2 (ITS2), ribosomal DNA (rDNA)] and morphological markers (spicules, habitus) inferred a close relationship to the cosmopolitan genus *Ephydatia* and also to the Lake Tore-Khol species that had not so far been described. Thus, both species were tentatively termed *Ephydatia tuva* (Lake Chagytai) and *E. altaiensis* (Lake Tore-Khol). We hypothesize that these new species might have evolved from Ephydatia-like ancestors through adaptation to the unique environmental conditions of both lakes. To test the ITS data, an unlinked genetic locus was chosen for further phylogenetic analyses, the protein-coding gene silicatein. These analyses provided not only a more robust resolution between the Lubomirskiidae, but also corroborated the grouping of the Lake Chagytai and Lake Tore-Khol species to the genus *Ephydatia*. In addition, the phylogenetic analyses suggest a Spongilla-like founder generation of poriferan species in Lake Chagytai and Lake Tore-Khol. In conclusion, we propose that the process of speciation in Lake Baikal and Lake Chagytai/Lake Tore-Khol, from a cosmopolitan Spongilla-like ancestor to more than ten endemic species follows allopatric speciation patterns and is of the peripatric type.

1 Introduction

It is impressive to dive in Lake Baikal – or other Siberian lakes – and to notice that down to a depth of 30 m, sponges represent the dominant animal taxon. In no other freshwater habitat in the world is the density of poriferan assemblages as high as in Siberian lakes. There, the gorgeously structured animals reach sizes of up to 2 m, are provided with an elaborate body plan, and cover the sandy-gravelly to rocky hard bottom in a forest-like pattern. Lake Baikal, which has been considered to be over 2 million years (MW) old, covers an area the size of one-third of Germany, and is unusually rich in numerous endemic animal species (reviewed in Kozhova and Izmet'eva 1998). It is considered to be an inimitable habitat for rapid evolution (Sherbakov 1999), representing a secluded environment within a unique biotope (see Müller et al. 2006).

Systematics and phylogeny of Lake Baikal sponges were studied as early as 1776 (Pallas) in an effort that continues until today (Efremova 2001), and is mainly based on morphometric datasets [relying in most cases on the morphology of spicules (poriferan synapomorphic skeletal elements)]. Without question – focusing on a morphological dataset such as the specimens' habitus – a number of distinct species exists. However, phylogenetic relationship or even determination of species could frequently not be established conclusively, thus suggesting that further taxonomic decisions based on morphological data require corroboratory support via genotypic data. Nevertheless, analyses of internal transcribed spacers (ITS) and ribosomal DNA (rDNA) sequences have so far not allowed for an unequivocal differen-

tiation between poriferan species and a resolution of phylogenetic relationships (see Schröder et al. 2003a; Müller et al. 2006; Meixner et al. 2007). One approach to overcome this uncertainty is not only to expand the taxon sampling of freshwater sponges by including species found in lakes “close” (i.e., ca. 150 km) to Lake Baikal, but also to integrate analyses of protein-coding genes. Amongst those genes, the silicatein gene in particular appears promising since the protein encoded is a sponge-specific enzyme and crucially involved in the formation of poriferan siliceous spicules that, in their turn, represent standard taxonomic markers. In comparison to marine species, where only two isoforms have so far been discovered, silicatein of freshwater sponges (in particular of Lake Baikal species) has already revealed a striking polymorphism with four known isoforms (Müller et al. 2007a). Considering recent studies on the characteristic association-pattern of silicateins in spicules, Müller et al. (2007b) conclude that silicatein is a key factor involved in the formation of the poriferan body plan.

Here, we describe analyses of endemic sponge species – collected from Siberian lakes – that are based on a combination of molecular (ITS, rDNA, protein-coding genes) and morphological (siliceous spicules) datasets.

2 Endemic Freshwater Sponges in Siberia (Lake Baikal and Tuva)

In order to further investigate the distribution of Siberian sponge species, specimens were sampled in two lakes of the Tuva region, situated in extreme southern Siberia: Lake Chagytai and Lake Tore-Khol. The tissues were subsequently used for isolation of DNA (ITS, rDNA), RNA (silicatein), and spicules. A previous comprehensive description of Lake Chagytai (Greze and Greze 1958) produced the basis for an expedition organized through the Joint Russian–German Laboratory for Biology of Sponges. The Joint Laboratory was established in September 2004 between the Ministries of Research and Science from Germany and Russia (Müller et al. 2006) (Fig. 1b).

The expedition started on 10 September 2006 with three cars, one Russian military truck, one all-purpose minibus (Fig. 1a and b), 15 local crew members (headed by Russian scientist S.I. Belikov), and four invited German scientists (W.E.G. Müller, H.C. Schröder, W. Schiebener, and T. Akly). From Irkutsk, the expedition headed towards Krasnoyarsk via Kansk (11 September 2006), reaching the administrative center of Krasnoyarsk Krai of Russia on 13 September 2006. From thereon the route of the expedition turned south to the Tuva region via Abakan and then Kyzyl, the capital of the Tuvan Republic and geographic center of Asia (14 September 2006). In the Kysyl Conservation Institute of the Russian Academy of Science, final decisions on routes and samplings were made with the colleagues of that institute. Having crossed the Sayan-Mountains, the Tuva Region was entered, in which the rivers Bij-Chem (Big Yenisei) and Ka-Chem (Small Yenisei) dominate the landscape. Here, human population was even less dense and asphalt



Fig. 1 Expedition, organized by the Joint Russian–German Laboratory for Biology of Sponges, to the Tuva region in September 2006. (a, b) Three vehicles were available. (c) Overnight encampments. (d) The untouched countryside astonished us by the beauty of flora and fauna; occasionally wild Bactrian camels (*Camelus bactrianus*) were seen. (e, f) In the Tuvinskaya valley, numerous lakes exist, which are sometimes difficult to reach. (g, h) Lake Chagytaï, the first collection place during the expedition, is located 80 km south of Kyzyl, the geographic center of Asia. (h) Using a rubber dinghy, it was possible to collect sponge specimens by SCUBA diving, even from the center of the 6-km-wide lake, within a depth of 17 m

roads were turned to unsecured/natural paths. Arrival at Lake Chagytai was on 14 September 2006 at midnight. This lake, located 80 km south of the capital of Kyzyl, in the south-east region of the Tuvinskaya valley (836 m above sea level), has a size of 5.0–6.5 km with a maximal depth of 17 m (Fig. 1g and h). An outline of the location and the habitat of Lake Chagytai is given in the chapter by Müller et al. (2008a) in this volume. In general, the Tuvinskaya valley is very rich in lakes of all sizes (Fig. 1e).

Subsequently, the expedition continued towards the central basin of the Evenkijski Autonomous Okrug (district), where Lake Tore-Khol was reached on 18 September 2006. The twin-lake with an average depth of 20 m (maximal depth around 25–27 m) measures in the western part 5.5 km in diameter and in the eastern part, which is more oval, 8 km. Further details are given in the chapter of Wiens et al. (2008) in this volume. The countryside was usually difficult to pass (Fig. 1f). Occasionally, wild Bactrian camels (*Camelus bactrianus*) crossed the way in phalanxes (Fig. 1d). All members of the expedition slept in tents (Fig. 1c). On 21 September 2006 the lake was left behind and the car caravan reached Krasnoyarsk, from where the German members left for home on 24 September 2006.

In both Lake Chagytai and Lake Tore-Khol, sponge species were collected which, according to their skeletons and growth forms, had previously been assigned to the genus *Baikalospongia*. However, here we present evidence for a closer relationship to the genus *Ephydatia*. Thus, the two species described in this study were tentatively termed *Ephydatia tuva* (from Lake Chagytai) and *E. altaiensis* (Lake Tore-Khol) (see below).

2.1 *E. tuva* from Lake Chagytai

The first description of sponges in Lake Chagytai goes back to Rezvoj (1927). He analyzed sponge samples collected in 1915. The samples were described as a new species and termed *Baikalospongia dzhegatajensis*. In parallel, he described a species variety, which he termed *B. dzhegatajensis* var. *lissosclera*. Since this author only had a very small collection of about seven specimens he considered the second form a “variety” instead of an “independent species.” Of interest is the remark (Greze and Greze 1958) that besides *B. dzhegatajensis* the cosmopolitan sponge *Spongilla lacustris* was also found. Here, a coexistence between endemic and cosmopolitan sponge species (Greze and Greze 1958), similar to Lake Baikal communities, was highlighted. It was therefore the initial aim of the 2006 expedition to collect specimens of the proposed genus *Baikalospongia* in Lake Chagytai for a more detailed description.

HABITAT: The description of Lake Chagytai by Greze and Greze (1958) is sufficient to obtain a first impression of the lake. Lake Chagytai is among the largest lakes in the Tuva region. The bottom consists mainly of silt (Fig. 2c and d), found both in the littoral and profundal zone. The absolute mineral concentration in Lake Baikal is low, with ≈ 100 mg/l (Kozhov 1963), compared to ≈ 320 mg/l in Lake Chagytai

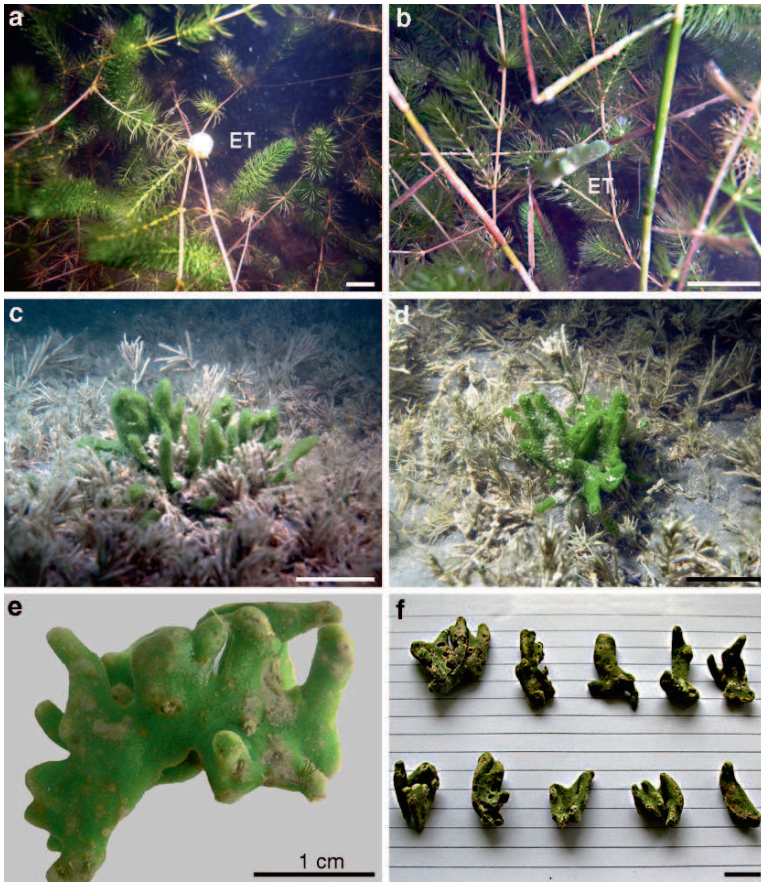


Fig. 2 *Ephydatia tuva* from Lake Chagytai, a bicarbonate lake. (a–d) *E. tuva* (ET) specimens are always associated with *Chara* musk grass specimens. In the littoral, specimens settle on braches of these macro-algae, characterized by their cylindrical, whorled branches. (c, d) In the center of Lake Chagytai, sponges live on smaller branchlets of *Chara*. (e) One larger specimen of *E. tuva*, measuring 35 mm. (f) Growth sizes do not vary much (only 20–30 mm), suggesting a rapid growth of this species; the growth phase ends before September, the collection time during this expedition. All size bars = 10 mm

(Greze and Greze 1958) as summarized recently (Müller et al. 2006). However, the higher concentration of bicarbonate in Lake Chagytai (189 vs 64 mg/ml in Lake Baikal) combined with a lower silica content (0.4 vs 1.1 mg/ml) is striking. This qualifies Lake Chagytai as a bicarbonate lake. The amount of nitrogen is low in both lakes, reflecting an oligotrophic biotope. On the other hand, Lake Chagytai is rich in diatoms (500–600/l), with the cosmopolitan species *Melosira granulata* (also present in Lake Baikal (Popovskaya et al. 2002)) and *Asterionella formosa* prevailing. However, the abundance of zooplankton is lower with ≈ 40 organisms/l. Among plants, the woolgrass *Scirpus* sp. (*Schoenoplectus*), perennial grass-like

plants usually found in wetlands, and especially the muskgrass *Chara* sp. are abundant, which is also highlighted in the only limnological study so far existing (Greze and Greze 1958).

We found that in Lake Chagytai the majority of sponges occur in one habitat and always together with *Chara* specimens (Fig. 2a and b). Based on a morphological phenomenon that uniquely manifests in members of the genus *Baikalospongia*, but not in their closest relatives, the *Lubomirskia*, the Tuva sponges collected might indeed be grouped to the genus *Baikalospongia*: Whereas the size variation of both genera is not very pronounced (Fig. 2e and f), the spicules of *Baikalospongia* are not embedded in an organic matrix, while those of *Lubomirskia* are covered by a bulky organic shell. In fact, the genus *Lubomirskia* comprises a “network of well-defined, compact, strongly coherent series of spicules lying parallel to one another in a thick sheet of chitinoid substance. The vertical fibers branch dichotomously and are joined together by traverse fibers containing fewer spicules than themselves.” In contrast, in the skeleton of the genus *Baikalospongia*, the fibers do not have “horny sheaths and the vertical fibers do not form definite brush-like tufts at their distal extremity” (Annandale 1914). The discrimination between both genera, based on the aforementioned morphological aspects, is still valid today (Masuda et al. 1997).

All specimens of the Lake Chagytai sponge live in association with branches of the algae *Chara* sp. (Greze and Greze 1958) (Fig. 2a and b). The rarely encrusting to globose or short-branched poriferan specimens have a size between 20 and 40 mm in diameter. If present, 3- to 10-mm-thick branches originate from a massive base. Greze and Greze (1958) mentioned a white-gray color for all Lake Chagytai specimens. However, the specimens collected during our 2006 expedition revealed a bright green color, indicative of a symbiotic relationship with zoochlorella. Oscules are present at all lateral surfaces with diameters of 1.5–2.0 mm. They are formed by a torus of densely packed spicules. In the central cavity one diaphragm is usually present. In addition, Lake Chagytai sponges show pronounced growth rings, annuli, in accordance with the observations of Rezvoj (1927, 1936).

The oval–cylindrical body displays a skeleton that is composed of loosely-arranged spicule bundles that never end in conical brush-like structures, as seen on the surface area of the *Lubomirskiidae* (Masuda et al. 1997) (Fig. 3a and b). At higher magnification, the solitary arrangement of spicules at the surface becomes apparent (Fig. 3c and d). The diameter of the axial canal within spicules is comparatively small, measuring 0.3–0.5 μm (Fig. 3f). The body of each Lake Chagytai sponge specimen intimately surrounds *Chara* stems that are characterized by their larger central cells and smaller envelope cells (Müller et al. 2006). In addition to the calcareous algae, siliceous diatoms are frequently seen (Fig. 3h), representing a silicate source for the sponges (Müller et al. 2006).

The spicules of the specimens collected are megascleres of the amphioxea type (Figs. 3e and f, 4). They are most often slightly curved oxeas (or rarely straight), from smooth to microspined (Fig. 4a–h), and have lengths between 100 and 172 μm , with diameters of 11–25 μm . The axial canals of the spicules often comprise unusual ramifications. The majority of spicules shows only one straight axial canal that

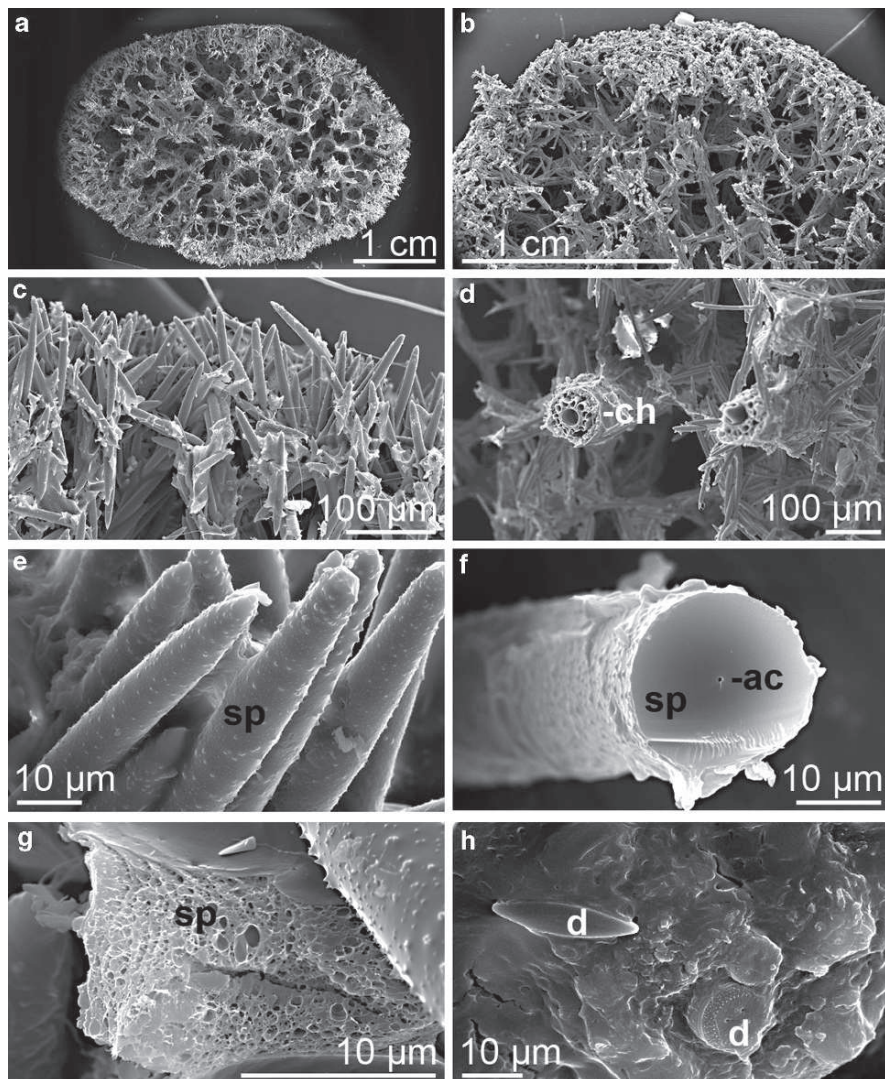


Fig. 3 Spicules of *Ephydatia tuva*; scanning electron microscopy (SEM) analysis. **(a, b)** Cross sections through the specimens show an arrangement of spicules, which are (almost) never connected to bundles by an organic matrix. They are loosely arranged and never end in conical spicule brushes, as seen in Lubomirskiidae. **(c)** At higher magnification, the arrangement of the spicules at the sub-surface region is seen. **(d)** Within the body of *E. tuva*, stems of the macro-algae *Chara* sp. (*ch*) are intimately surrounded by sponge spicules. **(e, f)** Amphioxeas: smooth to microspined megascleres. **(f)** The axial canal (*ac*) within the spicule has a diameter of less than 0.5 μm. **(g)** Frequently, spicules (*sp*) are seen which are in the process of self-absorption. **(h)** Siliceous diatoms (*d*) frequently occur within the body of *E. tuva*

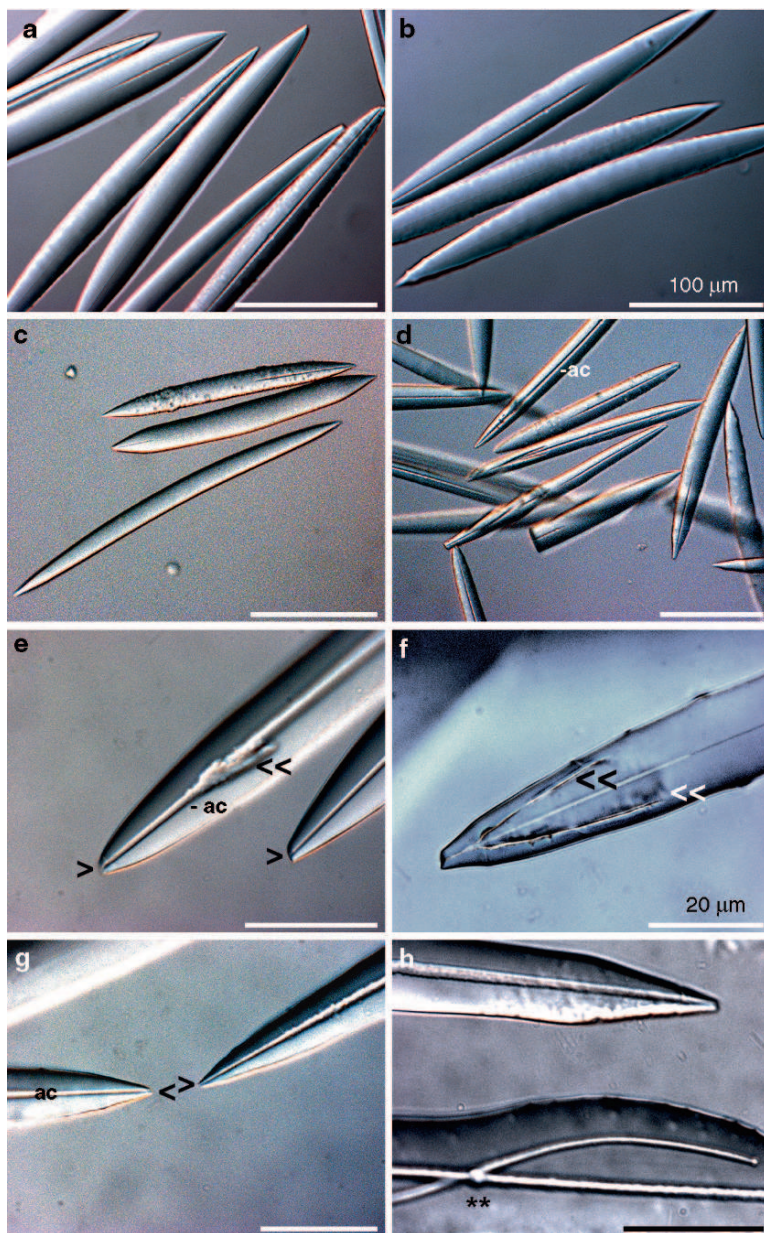


Fig. 4 Amphioxeas from *Ephydatia tuva*; light microscopical observations. (a–d) The slightly curved to rarely straight oxoas, from smooth to microspined, show a straight axial canal. (e, f) A considerable number of spicules comprise at their subterminal region a backward-directed buckler-like cone (<<). (g, h) In addition, in some cases the axial canal of the spicule ends in an opening at the tip (<). Further irregularities, e.g., spliced axial canals, are also seen

ends subterminally at the tip (Fig. 4d). However, a noticeable amount of spicules comprises axial canals that branch close to the tip, with an opening at their very end (Fig. 4e–g). As a further irregularity, spliced axial canals are seen (Fig. 4h). Nevertheless, at present it cannot be excluded that these features – branching of the axial canal and open tips – are artifacts that occurred during preparation of spicules [with acid ($\text{HNO}_3/\text{H}_2\text{SO}_4$) overnight].

Considering the molecular data, which likewise reveal a close relationship to the taxon *Ephydatia* (see below), we tentatively name the Lake Chagytai species *E. tuva*.

It is striking that all sponges collected in Lake Chagytai are rich in the enzyme carbonic anhydrase, which usually controls bicarbonate metabolism. Using the cobalt ion-based assay system (Müller et al. 1984), a high level of carbonic anhydrase was detected in all parts of *E. tuva* specimens, including the algae *Chara* sp. (W.E.G. Müller, unpublished data). In sponges, carbonic anhydrase is additionally involved in burrowing and etching of limestone (Schröder et al. 2003b). Furthermore, it is known from other sponge species as well as from corals that carbonic anhydrase exists not only intracellularly but also extracellularly, and is especially required during autolytic processes (Müller et al. 1984). Therefore, in view of the published data, it is proposed that poriferan carbonic anhydrase is involved in the enzymic degradation of diatoms (Bavestrello et al. 2000). Thus, carbonic anhydrase (and/or the related enzyme silicase, which dissolves siliceous spicules; Schröder et al. 2003b) would be required for the dissolution of diatom frustules and of spicules for subsequent re-utilization of dissolved silicic acid (Fig. 5). On the other hand, in the algae *Chara* sp., carbonic anhydrase is the principal enzyme that is employed for the intracellular conversion of $\text{HCO}_3^-/\text{CO}_2$, probably required during growth of mineralized cell walls (Müller et al. 2006). Interestingly, a dissolution of spicules can frequently be observed adjacent to the stems of *Chara* sp. (Fig. 3g). Here, vesicularly inflated spicules, which are in the process of self-absorption, are often seen.

2.2 *E. altaiensis* from Lake Tore-Khol

To the best of our knowledge, no research team in general and no workgroup concentrating in particular on sponges has ever scientifically explored Lake Tore-Khol. The lake is located between mountains and thus protected against storms, which might contribute to a more moderate climate. However, severe winters, during which the lake is covered with ice, interrupt moderate summers with an average temperature of approximately 15°C.

We focused our interest on the eastern part of the twin-lake (Fig. 6a and b), where diving inspections required dry suits (Fig. 6c). On the southern lakeside, numerous small bays within *Pinus* forests exist, allowing camping, advanced sampling, and preliminary biological determinations (Fig. 6d).

Sponge specimens were collected from hard bottom substrata, covered by flint, at depths of 10–15 m (Fig. 7a). They revealed no strictly defined growth form,

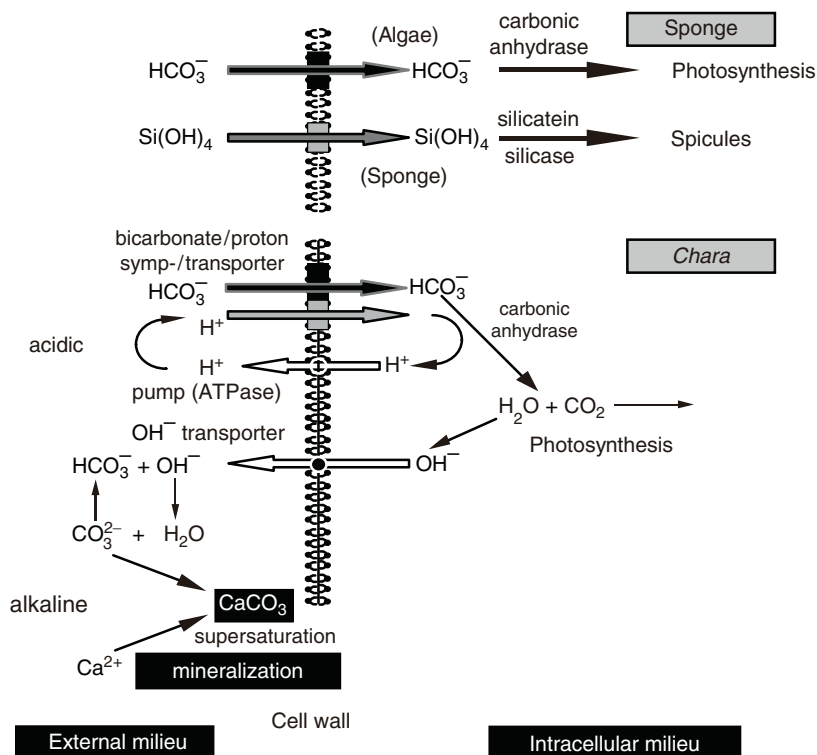


Fig. 5 Scheme of bicarbonate (HCO_3^-) transport into the musk grass *Chara* sp. and into sponges. In both organisms, HCO_3^- is transported into cells via the HCO_3^- symporter. In *Chara* sp., the ion functions as substrate for the carbonic anhydrase and is channeled to the photosynthetic apparatus. Intracellularly-formed hydroxyl anions are transported back to the extracellular milieu and there cause a supersaturation of CaCO_3 , which is subsequently precipitated. In the sponge, a (HCO_3^-) symporter very likely causes the influx of both HCO_3^- and silicic acid (Schröder et al. 2004). HCO_3^- can be considered as a source for symbiotic zoochlorella, which utilize the ions for photosynthesis, while silicic acid is needed for the synthesis of spicules. Carbonic anhydrase is mainly present in zoochlorella, while in the sponge it is the carbonic anhydrase-related enzyme silicase that mediates HCO_3^- -metabolism and dissolution of silica of the spicules

ranging from almost encrusting (Fig. 7b) to arborescent (Fig. 7c and d). Again, the specimens were found in the vicinity of muskgrass (*Chara* sp.). However, in Tore-Khol, this macro-alga is less abundant and less massive than in Lake Chagytai. The specimens reached a maximum size of 40 mm, with an average of ca. 20 mm.

Cross sections through *E. altaiensis* show an arrangement of spicules similar to that described for *E. tuva*. Thus, neither are spicules entrapped in an organic matrix nor do they form well-pronounced bundles nor assemble into brush-like structures underneath the sponge surface (Fig. 8a and b). Megasclere oxeas are predominant, usually thorned (Fig. 9a–c) and slightly curved with sizes between 120 and 200 μm in length and 10–20 μm in diameter. Frequently (we consider them abnormal), spicules possess central slim processi, comprising 1–5 large bulbs (Fig. 8c; Fig. 9d).



Fig. 6 Lake Tore-Khol. (a, b) A view to the eastern part of the twin-lake. (c) Sponge diving. (d) Field work, allowing sampling and conservation of tissue for DNA and RNA isolation

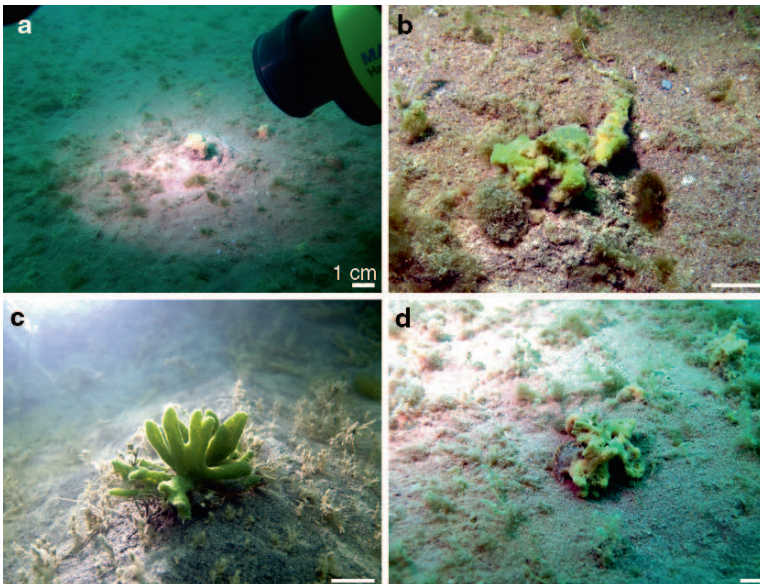


Fig. 7 Habitat of *Ephydatia altaiensis* at Lake Tore-Khol. (a–d) The specimens were found on hard bottom, which is covered by flint. The musk grass (*Chara* sp.) is frequently associated with these specimens but less abundant than in the Lake Chagytai. All scale bars = 1 cm

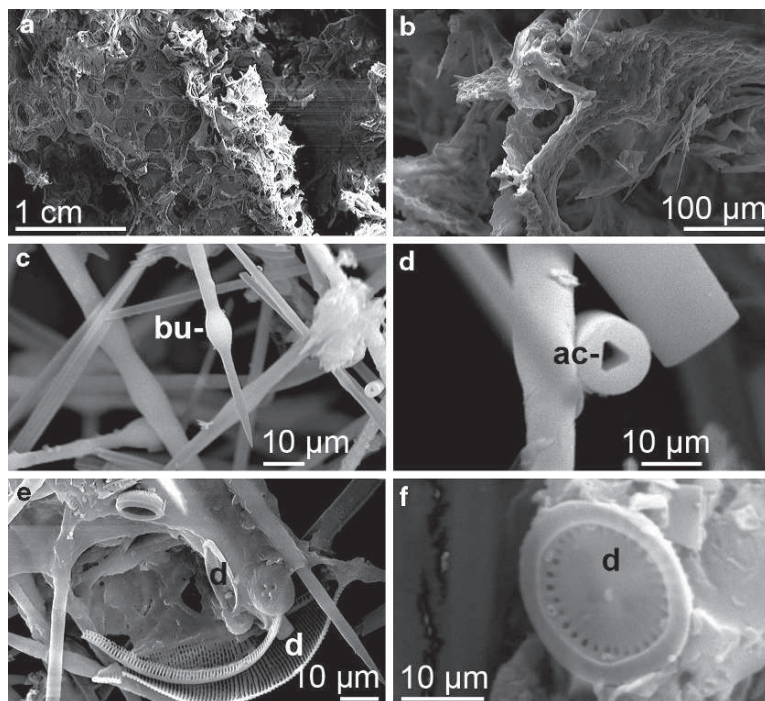


Fig. 8 Spicules of *Ephydatia altaiensis*; scanning electron microscopy (SEM) analysis. (**a, b**) Cross section through a specimen showing that spicules are not joined into bundles through an organic mantle. (**c**) In addition to the dominant megascleres of the regular oxea type, abnormal spicules with large bulbs (*bu*) around the central slim oxea are seen. (**d**) The center of spicules comprises an axial canal (*ac*) that has a triangular shape. (**e, f**) Within the body of *E. altaiensis* numerous diatoms are found with oval, falciform to round-shaped morphologies

In these cases, the megasclere diameter is 2–5 μm, whereas the diameter of bulbs reaches sizes around 10–15 μm. Similar abnormal spicules have been discovered in *E. muelleri* specimens that had been cultivated in medium supplemented with germanium (Simpson et al. 1983). In addition, *E. muelleri* had already been described by Schulze (1923) to form abnormal “peculiar” spicules, spliced axial filaments (such as those of *E. tuva*), and central balls (*E. altaiensis*). Even earlier, Waller (1878) reported comparable abnormal spicules in the closely related freshwater sponge species *S. lacustris*. Specimens that form such unusual spicules have also been termed ecological typi (Simon 1955). *E. altaiensis* spicules are traversed by an axial canal that is wider than that of *E. tuva* spicules (0.5–0.8 μm; Fig. 8d). Additionally, the axial canal has a pronounced triangular shape, prototypic for spicules of demosponges (Uriz et al. 2003). Similarly to *E. tuva*, diatoms are very frequently found, though they reveal a higher morphological diversity, ranging from oval (*Diatoma* sp.) to falciform (*Hannaea* sp.) and round-shaped (*Cyclotella minuta*).

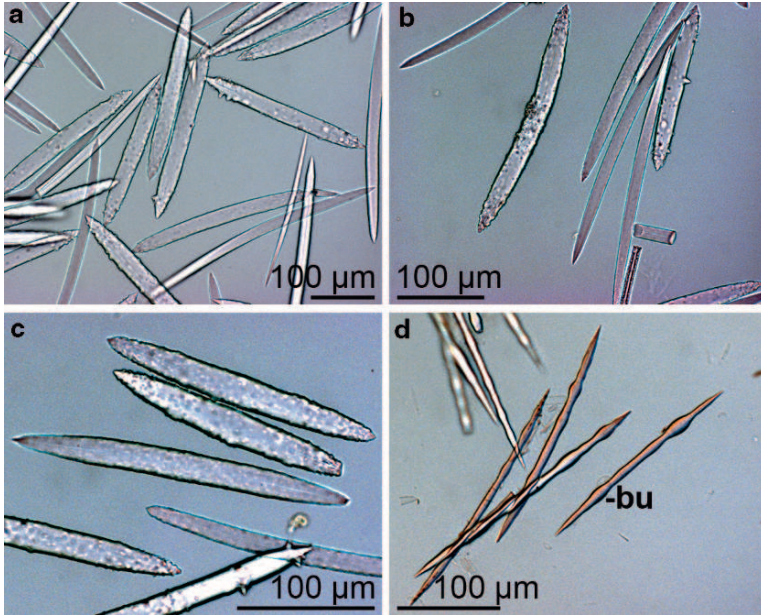


Fig. 9 Amphioxeas from *Ephydatia altaiensis*; light microscopical observations. (a–c) Regular oxeae, the dominant morphology of spicules. Spicules are usually thorned. (d) Abnormal megascleres, which comprise up to five bulbs (*bu*)

3 Molecular Phylogeny of Endemic Freshwater Sponges from Lake Baikal – Tuva Region

Twenty years ago, the phylogenetic position of sponges in the animal tree of life was still enigmatic. Even after the introduction of novel molecular biological data sets [nuclear ribosomal DNA (nrDNA)] subsequent phylogenetic analyses could not unambiguously group the poriferan phylum into the metazoan kingdom (Field et al. 1988). However, based upon common molecular biological characters (i.e., metazoan-specific protein-coding sequences), an unequivocal inclusion of the phylum Porifera within Metazoa soon became possible (Müller 1995). Concurrently, the term Urmetazoa was coined to characterize the first hypothetical ancestral phylum of all Metazoa (Müller 2001), and Porifera was defined as the most basal contemporary metazoan phylum (Müller et al. 2001). Successively, many metazoan specific molecules were identified in sponges (in particular in the poriferan model organism *Suberites domuncula*), including adhesion proteins (Pfeifer et al. 1993), signal transduction molecules (Kruse et al. 1996), proteins of apoptosis, and innate immunity (Wiens and Müller 2006; Wiens et al. 2007), etc. These data provided a solid foundation to re-evaluate rDNA and ITS sequences, which in combination with

enhanced computational resources and refined statistical methods guided inferences of metazoan phylogeny to the next level. During this transition, uncertain rDNA/ITS data, that were collected in order to shed light on the evolution of early-branching Metazoa (using especially poriferan DNA as sources [Lafay et al. 1992]), could be calibrated and applied at a larger scale for phylogenetic analyses (Borchiellini et al. 2001). Having reinstated the value of rDNA/ITS sequence data for phylogenetic disclosure of basal metazoan affiliations (Addis and Petterson 2005), the limitations of the data sets for clarification of evolutionary uncertain relationships became evident, clearly affecting both deep and shallow nodes with obscure/unknown branching events. Regarding this phenomenon, the evolutionary origin of Lake Baikal sponges is exemplary: Lake Baikal sponges are indisputably endemic (Manconi and Pronzato 2002) and, based on their morphological characters and ecological peculiarities, distributed into different species (Efremova 2001; Manconi and Pronzato 2002). Thus, the following valid poriferan genera (and species) have been described; family Lubomirskiidae, including genus *Lubomirskia* with the following species: *Lubomirskia abietina*, *L. baicalensis*, *L. fusifera*, and *L. incrustans*; genus *Baikalospongia* with *B. bacillifera*, *B. fungiformis*, *B. intermedia*, *B. martinsoni*, *B. recta*, and *B. robusta*; genus *Swartschewskia* with *Swartschewskia papyracea*; and genus *Rezinkovia* with *Rezinkovia abietina* and *R. echinata*. In addition, the taxa *Ephydatia*, *Spongilla*, *Eunapius*, and *Trochospongilla* (all family Spongillidae) have been listed. However, despite their greatest efforts the authors could not detect representative specimens of the latter taxa, though one author (S.I. Belikov) sampled *Ephydatia* specimens at several locations in rivers flowing into Lake Baikal, indicating a spatial proximity between cosmopolitan sponges and endemic Baikalian sponges.

Initially, the species *B. dzhegatajensis* was discovered in Lake Chagytai (Tuva region) and subsequently described by Rezvoj (1936; family Lubomirskiidae, genus *Baikalospongia*). Later, *B. dzhegatajensis* was grouped to the family Spongillidae, genus *Ephydatia* (Greze and Greze 1958). The resulting uncertainty concerning its phylogenetic position was recently highlighted (Müller et al. 2006). Even phylogenetic analysis of a cytochrome oxidase subunit I (COI) fragment could not contribute to resolving this discrepancy (Meixner et al. 2007) that in essence prompted the authors to realize the 2006 expedition to Lake Chagytai and Lake Tore-Khol.

Focusing on endemic Lake Baikal sponges, analyses of 18S rDNA, ITS (Itskovich et al. 1999), and COI sequences (Schröder et al. 2003a) and subsequent application of the combined data set were employed to clarify phylogenetic relationships. Thus, the combination with advanced (bio)statistics revealed a frequent and independent emergence of (endemic) freshwater sponge species from a few cosmopolitan founder species. Accordingly, all endemic Lake Baikal sponge species (initially forming the family Lubomirskiidae) have been assigned to the genus *Ephydatia* (Meixner et al. 2007) and were distinguished from a clade that comprises *Trochospongilla*, *Nudospongilla*, and *Pachydictyum* and a further clade including *Spongilla* and *Eunapius*. However, this report (Meixner et al. 2007) also revealed a certain shortcoming of the combined data set: Even though the aforementioned morphological features strongly indicate different Baikalian species, their distinction

across that broad range of sampled taxa and based upon molecular phylogenetic analyses of ITS, rDNA, or COI sequences ultimately remained elusive.

3.1 *Molecular Phylogeny According to ITS Analyses*

Internal transcribed spacers (ITS) represent non-functional RNA sequence stretches between structural ribosomal RNAs (rRNA) on a common polycistronic precursor transcript that consists of a 5' external transcribed sequence (5' ETS), 18S rRNA, ITS1, 5.8S rRNA, ITS2, 28S rRNA, and finally the 3' ETS (read 5'→3'). During processing of the precursor molecule, the non-functional RNA stretches are successively excised and subsequently degraded, resulting in the mature rRNA products (28S, 18S, 5.8S rRNA). Internal transcribed spacers are commonly used in molecular phylogenetic analyses since low evolutionary pressure on non-functional sequences causes a high degree of variation even between closely related species. In contrast, due to significant sequence conservation, the low variability of rRNA sequences limits their value in phylogeny, inherently bearing the risk of creating phylogenetic trees with areas of poor resolution. Rodrigo et al. (1994) conclusively demonstrated that rRNA sequences are unable to resolve patterns of relationships that span more than 500MY, due to the loss of phylogenetic information present in the data.

ITS sequences have often been shown to be suitable phylogenetic markers just below family-rank due to high sequence variability and frequent occurrence of indels. However, following a comprehensive survey of marine sponges, Wörheide et al. (2004) caution against the routine use of ITS analyses even below family-rank due to the frequent presence of divergent paralogs within individual genomes. The frequency of such intragenomic polymorphisms (IGPs) cannot be predicted by taxonomy (Wörheide et al. 2004). In order to test whether ITS sequences are suitable markers for phylogenetic analyses of freshwater sponges, for the present studies only representatives of the closely related families Spongillidae and Lubomirskiidae (which recently had been assigned to the genus *Ephydatia*; Meixner et al. 2007) were taken into account. Using an established oligonucleotide primer combination (forward primer 5'-GTCCCTGCCCTTTGTACACA-3'; reverse primer 5'-CCTGGTTAGTTTCTTTTCCTCCGC-3'; Wörheide et al. 2002), a substantial part of the poriferan polycistronic precursor transcripts was amplified via standard polymerase chain reaction (PCR), embracing 18S rRNA (partial), ITS1, 5.8S rRNA, ITS2, and 28S rRNA (partial) (Table 1). PCR cycling conditions were as follows: 95°C (2.5 min), 35 cycles of 95°C (1 min), 66°C (1.5 min), 74°C (2 min), followed by a final extension step (74°C, 10 min). Amplicons were subsequently subcloned and sequenced. Sequencing was performed on dual laser sequencers (Li-Cor 4300). Each sample was sequenced at least three times.

For phylogenetic analysis, the sequenced fragments were aligned, using the T-Coffee algorithm (<http://www.igs.cnrs-mrs.fr/Tcoffee/tcoffee.cgi/index.cgi>; Notredame et al. 2000) with all pairwise methods (Lalign_pair: 10 best

Table 1 Data set of freshwater sponges analyzed: endemic (e) or cosmopolitan (c). Sequences were elucidate in the course of this study and include 5' ETS, 18S rRNA, ITS1, 5.8S rRNA, ITS2, 28S rRNA and 3' ETS (*). Alternatively, ITS2 containing sequences were obtained from public NCBI database

Family	Genus	Species	Individual	NCBI accession number							
Lubomirskiidae			BBITS2_1MZ	AM949589 (*)							
			BBITS2_2MZ	AM949590 (*)							
			BBITS2_3MZ	AM949591 (*)							
			<i>Baikalospongia bacillifera</i> (e)	BBITS2_4MZ	AM949592 (*)						
			<i>Baikalospongia</i>			BBITS2_5	DQ778319.1				
						BBITS2_6	AY662501.1				
						BBITS2_7	DQ178656.1				
						<i>B. intermedia</i> (e)	BIITS2	AY662500.1			
						<i>B. martinsoni</i> (e)	BMITS2	DQ778320.1			
						<i>B. robusta</i> (e)	BRoITS2	AY662503.1			
						<i>B. recta</i> (e)	BReITS2	DQ778323.1			
						<i>B. fungiformis</i> (e)	BFITS2	DQ778328.1			
						<i>Lubomirskia</i>			LBITS2_1MZ	AM948957 (*)	
									LBITS2_2MZ	AM948958 (*)	
									LBITS2_3MZ	AM949593 (*)	
									<i>Lubomirskia baicalensis</i> (e)	LBITS2_4MZ	AM949594 (*)
									LBITS2_5MZ	AM949595 (*)	
			LBITS2_6	DQ178655.1							
			LBITS2_7	DQ778322.1							
			<i>L. abietina</i> (e)	LAITS2	DQ778321.1						
			<i>L. fusifera</i> (e)						LFITS2_1	DQ778327.1	
									LFITS2_2	AY662504.1	
			<i>L. incrustans</i> (e)			LIITS2	DQ778324.1				
						SPITS2_1MZ	AM950181 (*)				
			<i>Swartschewskia</i>	<i>Swartschewskia papyracea</i> (e)		SPITS2_2MZ	AM950182 (*)				
						SPITS2_3	DQ778325.1				
			<i>Rezinkovia</i>	<i>Rezinkovia abietina</i> (e)		SPITS2_4	AY662499.1				
						RAITS2	AY662502.1				
			<i>Spongillidae</i>	<i>R. echinata</i> (e)		REITS2	DQ778326.1				
<i>Ephydatia altaiensis</i> (e)	EALTAITS2_1MZ	AM950183 (*)									
<i>Ephydatia</i>	<i>Ephydatia tuva</i> (e)		EALTAITS2_2MZ	AM950184 (*)							
			ETUVITS2_1MZ	AM950185 (*)							
			ETUVITS2_2MZ	AM950186 (*)							
			ETUVITS2_3MZ	AM950187 (*)							
			EFITS2_1	DQ178657.1							
			<i>Ephydatia fluviatilis</i> (c)	EFITS2_2	AJ705048.1						

(continued)

Table 1 (continued)

Family	Genus	Species	Individual	NCBI accession number
			EFITS2_3	EF534497.1
			EFITS2_4	EF534498.1
			EMITS2_1	DQ178654.1
		<i>Ephydatia muelleri</i> (c)	EMITS2_2	AY662506.1
			EMITS2_3	EF534500.1
			EMITS2_4	EF534499.1
	<i>Spongilla</i>	<i>Spongilla lacustris</i> (c)	SLITS2_1	DQ178653.1
			SLITS2_2	AJ703890.1
			SLITS2_3	AY662505.1

local alignments. Slow_pair: accurate global alignment. Fast_pair: fast heuristic global alignment. ClustalW_pair: ClustalW pairwise alignment) combined in the T-Coffee library. In order to be able to exploit shorter freshwater sponge sequences obtained from the NCBI database (Table 1), the resulting alignment was trimmed to an overlapping section common to all sequences, encompassing (1) a 3'-segment of 5.8S rRNA, (2) ITS2 (complete), and (3) a 5'-segment of 28S rRNA. Figure 10a depicts the alignment of the trimmed polycistronic sequences of seven

Fig. 10 Phylogenetic analysis of ITS sequences of freshwater Porifera. (a) Alignment of ITS2 sequences and adjoining 5.8S and 28S rDNA fragments from different individuals of endemic and cosmopolitan freshwater sponges with T-Coffee: *Baikalospongia bacillifera* (BBITS2_1MZ: AM949589^{547-998bp}; BBITS2_2MZ: AM949590^{546-998bp}; BBITS2_3MZ: AM949591^{548-999bp}; BBITS2_4MZ: AM949592^{546-996bp}; BBITS2_5: DQ778319.1^{435-885bp}; BBITS2_6: AY662501.1^{1-451bp}; BBITS2_7: DQ178656.1^{29-478bp}), *B. fungiformis* (BFITS2: DQ778328.1^{439-890bp}), *B. intermedia* (BIITS2: AY662500.1^{1-450bp}), *B. martinsoni* (BMITS2: DQ778320.1^{436-888bp}), *B. recta* (BReITS2: DQ778323.1^{439-884bp}), *B. robusta* (BRoITS2: AY662503.1^{1-451bp}), *Ephydatia tuva* (ETUVITS2_1MZ: AM950185^{523-941bp}; ETUVITS2_2MZ: AM950186^{523-941bp}; ETUVITS2_3MZ: AM950187^{476-895bp}), *Ephydatia altaiensis* (EALTAITS2_1MZ: AM950183^{523-944bp}; EALTAITS2_2MZ: AM950184^{523-943bp}), *Ephydatia fluviatilis* (EFITS2_1: DQ178657.1^{29-449bp}; EFITS2_2: AJ705048.1^{2123-2541bp}; EFITS2_3: EF534497.1^{47-467bp}; EFITS2_4: EF534498.1^{47-467bp}), *Ephydatia muelleri* (EMITS2_1: DQ178654.1^{29-436bp}; EMITS2_2: AY662506.1^{1-409bp}; EMITS2_3: EF534500.1^{47-455bp}; EMITS2_4: EF534499.1^{47-455bp}), *Lubomirskia abietina* (LAIMS2: DQ778321.1^{437-880bp}), *L. baicalensis* (LBITS2_1MZ: AM948957^{548-990bp}; LBITS2_2MZ: AM948957^{545-989bp}; LBITS2_3MZ: AM949593^{547-990bp}; LBITS2_4MZ: AM949594^{549-993bp}; LBITS2_5MZ: AM949595^{549-994bp}; LBITS2_6: DQ178655.1^{29-469bp}; LBITS2_7: DQ778322.1^{437-879bp}), *L. fusifera* (LFITS2_1: DQ778327.1^{437-882bp}; LFITS2_2: AY662504.1^{1-446bp}), *L. incrustans* (LIITS2: DQ778324.1^{438-889bp}), *Rezinkovia abietina* (RAITS2: AY662502.1^{1-444bp}), *R. echinata* (REITS2: DQ778326.1^{437-881bp}), *Spongilla lacustris* (SLITS2_1: DQ178653.1^{29-424bp}; SLITS2_2: AJ703890.1^{2117-2510bp}; SLITS2_3: AY662505.1^{1-396bp}), and *Swartschewskia papyracea* (SPITS2_1MZ: AM950181^{547-996bp}; SPITS2_2MZ: AM950182^{544-992bp}; SPITS2_3: DQ778325.1^{436-885bp}; SPITS2_4: AY662499.1^{1-450bp}). The borders between 5.8S rDNA, ITS2, and 28S rDNA are marked.

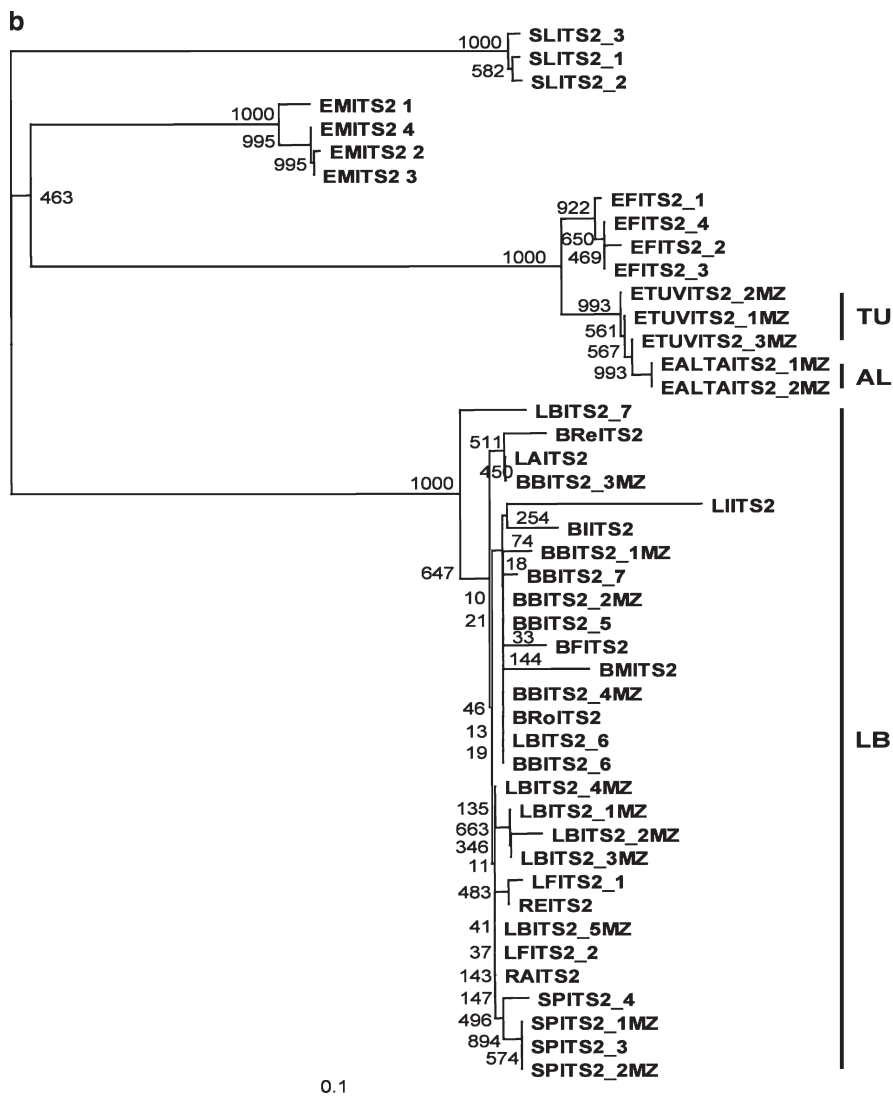


Fig. 10 (b) (continued) Rooted neighbor-joining tree generated after alignment of aforementioned sequences from different individuals of freshwater sponges. The three sequences of *S. lacustris* were used as an outgroup. Numbers at the nodes indicate the level of confidence for the branches as determined by bootstrap analysis (1,000 bootstrap replicates). Sequences from sponges from Lake Baikal (LB), Tuva (Lake Chagytai; TU) and Altai region (Lake Tore-Khol; AL)

L. baicalensis individuals; two *L. fusifera*; one individual of each, *L. abietina*, *L. incrustans*, *R. abietina*, and *R. echinata*; seven individuals of *B. bacillifera*; two *B. fungiformis*; one individual of each of *B. intermedia*, *B. martinsoni*, *B. recta*, and *B. robusta*; three individuals of *E. tuva*; two *E. altaiensis*; four individuals of each

of *E. fluviatilis*, *E. muelleri*, and *S. papyracea*; and three individuals of *S. lacustris*. Already a first glance reveals the high degree of conservation concerning both 5.8S and 28S rRNA sequences, with only a few variable positions between poriferan families (Lubomirskiidae, Spongillidae), genera (*Lubomirskia*, *Rezinkovia*, *Baikalospongia*, *Swartschewskia*, *Ephydatia*, *Spongilla*), and even more invariant nucleotides between species. In contrast, ITS2 demonstrates a much higher degree of sequence variability (occasionally including indels) at every level, even among individual representatives of each species. Thus, sequence identity between families (Lubomirskiidae, Spongillidae) ranges from 67 to 76.3%, between genera from 92.3 to 99.5% (*Lubomirskia*, *Rezinkovia*, *Baikalospongia*, *Swartschewskia*) and from 72 to 99% (*Ephydatia*, *Spongilla*), between species from 97.1 to 98.3% (*E. fluviatilis*–*E. tuva*), from 96.2 to 97.3% (*E. fluviatilis*–*E. altaiensis*), and from 80.4 to 81.3% (*E. fluviatilis*–*E. muelleri*), and between individuals of the same species, e.g., from 98.8 to 100% (*E. fluviatilis*). However, the following sequence pairs are identical: SPITS2_1MZ – SPITS2_3; BBITS2_4MZ – BBITS2_5; ETUVITS2_1MZ – ETUVITS2_2MZ; EFITS2_4 – EFITS2_3; EMITS2_4, EMITS2_3.

Subsequently, based upon this sequence alignment, a neighbor-joining (NJ) tree was calculated via ClustalX (Fig. 10b). Numbers at the nodes indicate the level of confidence for the branches as determined by bootstrap analysis (1,000 bootstrap replicates). The *S. lacustris* sequences were used as outgroup due to the fact that in former studies *S. lacustris* was found to be part of a different clade than the rest of the studied poriferan freshwater species (Meixner et al. 2007). The resulting tree reveals quite unequally resolved clades since sequence identities in the basic dataset range from 66.8% [LIITS2 (*L. incrustans*) to SLITS2_2 (*S. lacustris*)] to 100%. Thus, a clade comprising the genus *Ephydatia* (also including *E. tuva* and *E. altaiensis* that had been initially assigned to the genus *Baikalospongia*; see above) can be distinguished from a clade containing *Lubomirskia*, *Baikalospongia*, *Swartschewskia*, and *Rezinkovia* (i.e., Spongillidae vs Lubomirskiidae). However, within Lubomirskiidae resolution between genera is barely obtained, probably due to (1) sequence identities that are often lower between individuals of the same species than between different species, and (2) variable indels of various length so that homologies cannot be established. Accordingly, the support of branches within Lubomirskiidae is low since nearly half of the bootstrap values are below 100. On the other hand, the phylogenetic tree also revealed a resolution quite robust between species of Spongillidae. Thus, a clade comprising *E. fluviatilis* sequences is separated from a clade consisting of *E. tuva* and *E. altaiensis* sequences with a bootstrap support of 1,000. Less supported is an additional clade containing *E. muelleri* ITS sequences. However, a comparison between *Ephydatia* sequences reveals that there are more different positions between species than between individual representatives, in particular between cosmopolitan *E. fluviatilis* and endemic *E. altaiensis* (96.2–97.3%; Table 2), indicating that in the case of the genus *Ephydatia*, analyses of ITS might be suitable to resolve phylogenetic relationships at the species level. In conclusion, even though a differentiation of the Lubomirskiidae genera is possible based upon morphological characters, quite clearly this is not the case for ITS2 sequence analyses. This phenomenon may be the result of a rather recent separation

Table 2 Sequence identities in a gDNA stretch, encompassing ITS2 and segments of 5.8S and 28S rDNA (total ca. 450 positions), of different species of the genus *Ephydatia*

Species	Sequence identity (%)			
	<i>Ephydatia fluviatilis</i>	<i>Ephydatia tuva</i>	<i>Ephydatia altaiensis</i>	<i>Ephydatia muelleri</i>
<i>Ephydatia fluviatilis</i>	98.8–100	97.1–98.3	96.2–97.3	80.4–81.3
<i>Ephydatia tuva</i>	–	99.7–100	98.5–99.0	79.7–79.9
<i>Ephydatia altaiensis</i>	–	–	99.7–100	80.0–80.6
<i>Ephydatia muelleri</i>	–	–	–	98.2–100

of genera/species in Lake Baikal: After the general cooling at the beginning of the Pleistocene, Lake Baikal became colder and fully oxygenated. These environmental transitions caused a general rearrangement of the Baikalian fauna and concurrently newly unoccupied ecological niches (Sherbakov 1999). After immigration of a poriferan founder species, probably a common ancestor of the Spongillidae, adaptive radiation took place and low selective pressure allowed for fast morphological evolution. Considering the close relationship of *E. tuva* and *E. altaiensis* to *E. fluviatilis*, based on molecular analysis of ITS2-sequences and morphological considerations, we hypothesize that those new species might have evolved from *Ephydatia*-like ancestors through adaptation to the special environmental conditions of Lake Chagytai and Lake Tore-Khol.

3.2 Molecular Phylogeny According to Silicatein Analyses

In order to test the ITS data and the phylogenetic relationships that had not so far unequivocally been established between the different poriferan freshwater species another unlinked genetic locus was chosen for phylogenetic analyses: silicatein. The enzyme silicatein represents an autapomorphic character common to both classes of siliceous sponges, Demospongiae and Hexactinellida (Müller et al. 2008b). It catalyzes the formation of polymeric biosilica from monomeric silicic acid (see Weaver and Morse 2003), thus providing the mechanical support for tissue and the sizes, shapes, and arrangements of siliceous spicules that determine the characteristic bauplan of each sponge species.

Silicatein is closely related to lysosomal members of the papain-like family of proteases, the cathepsins, in particular cathepsin L. Similarly to cathepsins, silicatein is synthesized as a proenzyme and undergoes maturation steps, i.e., release of the signal peptide, activation through limited, autocatalytic proteolysis, and post-translational modification through phosphorylation and glycosylation (Schröder et al. 2007). In addition, silicatein does not only mediate polymerization of silicon, but also displays proteolytic activity similar to cathepsin L, thus underscoring the close relationship of silicatein and cathepsins. Nevertheless, it is distinguished from

cathepsins by replacement of the first amino acid residue in the catalytic triad, cysteine by serine (Shimizu et al. 1998).

Whereas cathepsin L is exclusively found in Metazoa and more distantly related cysteine proteases have been identified in Protozoa (Volkel et al. 1996) or plants (Nakamura et al. 1997), silicatein is restricted to Hexactinellida and Demospongiae. So far, several silicatein isoforms have been found within spicules of demosponges (silicatein- α and silicatein- β of various marine sponges; silicatein a1–a4 of freshwater sponges) as part of a proteinaceous filament that is present in an axial canal (see Müller et al. 2003). This organic filament can be isolated by treatment of spicules with hydrofluoric acid (Kaluzhnaya et al. 2005) and stained with Coomassie brilliant blue (0.25%, dissolved in 10% acetic acid/45% ethanol). In *E. tuva*, the morphology of the axial filament is quite remarkable. While in other demosponges, e.g., *L. baicalensis*, the filament usually appears as a continuous, solid bundle (Belikov et al. 2005), the released filaments of *E. tuva* form a brushy, twinned rope (not shown). Biochemical analysis revealed that this rope is composed of three distinct proteins (22–28 kDa; to be published). This data matches with the silicatein isoforms, characteristic for other demosponge species (Müller et al. 2007b).

Most silicatein sequences described to this point have been discovered in marine sponges (see Müller et al. 2007c) and only few studies so far concentrated on freshwater species (*E. fluviatilis*: Funayama et al. 2005; *L. baicalensis*: Wiens et al. 2006). Phylogenetic analyses based on silicatein, also taking into account genetic structures such as exon/intron boundaries and number of introns, indicate that silicatein and cathepsins arose from a common ancestor among cysteine proteases in the phylum Porifera (Müller et al. 2007c). Therefore, silicatein is a promising candidate to resolve phylogeny of poriferan freshwater species in order to test/complement the ITS data. Accordingly, silicatein sequences were isolated from representative genera of the families Spongillidae and Lubomirskiidae. For this purpose, an oligonucleotide primer combination was used (forward primer: 5'-CAG GGA GAT TGT GGT GCC AGC TAT GC-3'; reverse primer: 5'-ATG CCG CAT TGG TTG TAC TTG TT-3') that targeted the conserved region in the vicinity of the catalytic triad of hitherto known silicatein sequences (aa_{132–321}; *S. domuncula* silicatein- α). The PCR was carried out at an initial denaturation at 95°C for 3 min, followed by 35 amplification cycles at 94°C for 30 s, 58°C (minus 0.1°C per cycle) for 45 s, 72°C for 1.5 min, and a final extension step at 72°C for 10 min. PCR products were subcloned and sequenced. This data set was complemented by silicatein sequences present in the NCBI database (Table 3) and subsequently trimmed to an overlapping section common to all sequences (Fig. 11a).

Based upon an alignment of these sequences, a NJ tree was constructed in which the *S. domuncula* cathepsin L sequence was used as outgroup (Fig. 11b). This tree depicts robust branches and revealed a topology in which all silicatein sequences of freshwater sponge formed a cluster with *S. domuncula* silicatein- α at its base, indicating that silicatein a1–a4 arose from an ancestral α -isoform of marine sponges. Accordingly, the position of *S. domuncula* silicatein- β could not be resolved. However, within the silicatein- α sequences, four clusters can be distinguished, comprising a1-, a2-, a3-, and a4-isoforms, respectively. These four isoforms appear

Table 3 Silicatein/cathepsin data set of freshwater and marine (m) sponges analyzed: endemic (e) or cosmopolitan (c). Protein sequences that were elucidate in the course of this study are marked (*). Alternatively, sequences were obtained from public NCBI database

Family	Genus	Species	Protein	NCBI accession number	
Lubomirskiidae	<i>Baikalospongia</i>	<i>Baikalospongia intermedia</i> (e)	SILICAa1_ BAIKINT_MZ	FM160555 (*)	
			SILICAa4_ BAIKINT_MZ	FM160556 (*)	
			SILICAa1_ LUBAI_MZ	CAI43319.1	
	<i>Lubomirskia</i>	<i>Lubomirskia baicalensis</i> (e)	SILICAa2_ LUBAI_MZ	CAI91571.1	
			SILICAa3_ LUBAI_MZ	CAI91572.1	
			SILICAa4_ LUBAI_MZ	CAI91573.1	
		<i>Swarschewskia</i>	<i>Swarschewskia papyracea</i> (e)	SILICAa4_ SWATPAP	FM160565 (*)
				<i>Ephydatia altaiensis</i> (e)	SILICAa4_ EPHALT2_MZ
			<i>Ephydatia</i>	<i>E. tuva</i> (e)	SILICAa2_ EPHTUV2_MZ
	SILICAa4_ EPHTUV2_MZ	FM160562 (*)			
	<i>E. fluviatilis</i> (c)	SILICAa2_ EPHFLUV			BAE54434.1
	Spongillidae	<i>Ephydatia</i>	<i>E. muelleri</i> (c)	SILICAa2_ EPHMUE_MZ	FM160558 (*)
SILICAa3_ EPHMUE_MZ				FM160559 (*)	
SILICAa4_ EPHMUE_MZ				FM160560 (*)	
SILICAa3_ SPONLAC_MZ				FM160563 (*)	
<i>Spongilla</i>		<i>Spongilla lacustris</i> (c)	SILICAa4_ SPONLAC_MZ	FM160564 (*)	
			<i>Suberites domuncula</i> (c,m)	SILICAa_SUBDO_ MZ	CAI46305.1
				SILICAb_SUBDO_ MZ	CAD67990.1
CATL_SUBDO_MZ	CAH04632.1				

phylogenetically closely related and probably emerged by gene duplication after the separation of freshwater and marine sponges. Hence, silicatein-a3 branched off first from a common ancestor of freshwater sponge silicateins, followed by -a2, -a1, and lastly -a4. Even though the data set of a1 sequences is too limited, the silicatein-a4 data set, the most extensive one, clearly indicates a close relationship between

a

```

SILICAA4_LUBAI_MZ : FAATGALLEGASALSNDKQVILSEQNIIDCSVPYGNHGGSGGDTYTAMKYVIDNGIDTESSYSFOG-----KQSSCOY : 73
SILICAA4_BAIKINT_MZ : FAATGALLEGASALSNDKQVILSEQNIIDCSVPYGNHGGSGGDTYTAMKYVIDNGIDTESSYSFOG-----KQSSCOY : 73
SILICAA4_SWATPAP_MZ : FAATGALLEGASALSNDKQVILSEQNIIDCSVPYGNHGGSGGDTYTAMKYVIDNGIDTESSYSFOG-----KQSSCOY : 73
SILICAA4_EPHTUV2_MZ : FAATGALLEGASALANDKQVILSEQNIIDCSVPYGNHGGSGGDTYTAMKYVIDNGIDTESSYSFOG-----KQLSCQY : 73
SILICAA4_EPHALTA2_MZ : FAATGALLEGASALANDKQVILSEQNIIDCSVPYGNHGGSGGDTYTAMKYVIDNGIDTESSYSFOG-----KQLSCQY : 73
SILICAA4_EPHMUE_MZ : FAATGALLEGASALASDKQVILSEQNIIDCSVPYGNHGGSGGDTYTAMKYVIDNGIDTESSYSFOG-----KQSSCOY : 73
SILICAA4_SPONLAC_MZ : FAATGALLEGASALANDKQVILSEQNIIDCSVPYGNHGGSGGDTYTALKYVIDNGIDTESSCSFOA-----KQSSCOY : 73
SILICAA1_LUBAI_MZ : FAATGALLEGASALANDKQVILSEQNIIDCSVPYGNHGGSGGDTYTAFKYVIDNGIDTESSYSFKG-----KQSSCOY : 73
SILICAA1_BAIKINT_MZ : FAATGALLEGASALANDKQVILSEQNIIDCSVPYGNHGGSGGDTYTAFKYVIDNGIDTESSYSFKG-----KQSSCOY : 73
SILICAA2_EPHFLUV : FAATGTMEGANALSNDKQVALSEQNIIDCSVAYGNHGGSGGDTYTALKYVVDNGIDTESSYSFRG-----KQSSCOY : 73
SILICAA2_EPHTUV2_MZ : FAATGTMEGANALSNDKQVALSEQNIIDCSVAYGNHGGSGGDTYTALKYVVDNGIDTESSYSFRG-----KQSSCOY : 73
SILICAA2_EPHMUE_MZ : FAATGTMEGANALSNDKQVALSEQNIIDCSVAYGNHGGSGGDTYTALKYVVDNGIDTESSYSFRG-----KQSSCOY : 73
SILICAA2_LUBAI_MZ : FAATGTMEGANALSNDKQVLSLEQNIIDCSVPYGNHGGSGGDTYTALKYVVDNGIDTESSYSFRG-----KQSSCOY : 73
SILICAA3_EPHMUE_MZ : FAAAGALEGANALAADKIVALSEQNIIDCSVAYGNHGGSGGDVYTAFKYVVDNGIDTSSYPYKG-----KOYSSCOY : 73
SILICAA3_LUBAI_MZ : FAAAGALEGATATAADKIVALSEQNIIDCSVPYGNHGGSGGDVYTAFKYVVDNGIDTESSYPYKG-----KKSSCOY : 73
SILICAA3_SPONLAC_MZ : FAAVGALLEGASALATDKIVALSEQNIIDCSVPYGNHGGSGGDTYTAFKYVVDNGIDTESSYPYKG-----KQSSCOY : 73
SILICAA SUBDO_MZ : FSAMGALLEGANALAKGNVALSEQNIIDCSVPYGNHGGCGNMDAFLVYVLANEGVDQDSAYPVG-----KQSSCOY : 73
SILICAB SUBDO_MZ : FSAMSLLEGINALSYGSIIVLSEQNIIDCSVPYGNHGGACGQVNRALLVYIENDGVDTWKGYPSGDDPYRSKQYSCKY : 78
CATL SUBDO_MZ : FSATGSLLEGQHALKMGRIVLSLEQNIIMDCSSRFYGNHGGKCGIMDDAFRVVISNHGVDTESSYPYTA-----KDGYCRF : 73

SILICAA4_LUBAI_MZ : SSKNSCASATGVISITASCSETDILFAAVATVGPVAVAVDANTNAFREYOSGVFDSSSCSNTKLNHMLVIGYGSYNGX : 150
SILICAA4_BAIKINT_MZ : SSKNSCASATGVISITASCSETDILFAAVATVGPVAVAVDANTNAFREYOSGVFDSSSCSNTKLNHMLVIGYGSYNGX : 150
SILICAA4_SWATPAP_MZ : SSKNSCASATGVVSHASCSETDILFAAVATVGPVAVAVDANTNAFREYOSGVFDSSSCSNTKLNHMLVIGYGSYNGX : 150
SILICAA4_EPHTUV2_MZ : SSKNSCASATGVISITASCSETDILFAAVATVGPVAVAVDANTNAFREYOSGVFDSSSCSSTKPNHMLVIGYGSYNGX : 150
SILICAA4_EPHALTA2_MZ : SSKNSCASATGVISITASCSETDILFAAVATVGPVAVAVDANTNAFREYOSGVFDSSSCSSTKPNHMLVIGYGSYNGX : 150
SILICAA4_EPHMUE_MZ : SSKNSCASATGVISITASCSETDILFAAVATVGPVAVAVDANTNAFREYOSGVFDSSSCSSTKLNHMLVIGYGSYNGX : 150
SILICAA4_SPONLAC_MZ : NSKNSCASATGVINIAFACESDILFAAVATVGPVAVAVDANTNAFREYOSGVFDSSSCSNTKLNHMLVIGYGSYNGX : 150
SILICAA1_LUBAI_MZ : NNKITSASATGVVSHIGYCESDILFAAVATVGPVAVAVDANTNAFREYOSGVFDSSSCSSTKLNHMLVIGYGSYNGX : 150
SILICAA1_BAIKINT_MZ : NNKITSASATGVVSHIGYCESDILFAAVATVGPVAVAVDANTNAFREYOSGVFDSSSCSSTKLNHMLVIGYGSYNGX : 150
SILICAA2_EPHFLUV : NSKNSCASATGAVSHSYCESDILMSAVATVGPVAVAVDANTNAFREYOSGVFDSSSCSSTKLNHMLVIGYGSYNGX : 150
SILICAA2_EPHTUV2_MZ : NSKNSCASATGAVSHSYCESDILMSAVATVGPVAVAVDANTNAFREYOSGVFDSSSCSSTKLNHMLVIGYGSYNGX : 150
SILICAA2_EPHMUE_MZ : NSKNSCASATGAVSHSYCESDILMSAVATVGPVAVAVDANTNAFREYOSGVFDSSSCSSTKLNHMLVIGYGSYNGX : 150
SILICAA2_LUBAI_MZ : NSKNSCASATGAVHPYCESDILMSAVATVGPVAVAVDANTNAFREYOSGVFDSSSCSSTKLNHMLVIGYGSYNGX : 150
SILICAA3_EPHMUE_MZ : NSKNLCAVATGVVKITSCSETDILLSAVASVGPVAVAVDATVNSEMEYOSGVFDSSSCSSTKLNHMLVIGYSTNGX : 150
SILICAA3_LUBAI_MZ : NSKNVCAISTGVVKITASCSETDILLSAVASVGPVAVAVDASVNAEMEYOSGVFDSSSCSSTKLNHMLVIGYSTNGX : 150
SILICAA3_SPONLAC_MZ : NSKNCATATGVVKITASCSETDILMSAVASVGPVAVAVDASVNSEMEYOSGVFDSSSCSNTKLNHMLVIGYGSYNGX : 150
SILICAA SUBDO_MZ : NSKYKCTSMGMSVSHKSCESDILQAAVSNIPVSVVAIDGANSARELYYSVYDSSRCSSTLNHMLVIGYGSYNGX : 150
SILICAB SUBDO_MZ : ERQYRCASARGIVSHASCSETDILTLTAVANSQPVSVVVDATSTSEQYSDGVLNVVPCSSSTLHGLVVIYGYKLSGQ : 155
CATL SUBDO_MZ : NONNVGATEHSYRDIHARCESSESIQASIQGPIVSVVAIDASHRSEQYKNGVYIYEPSCSSSRLDHLGLVVIYGYKLEGGQ : 150
Ser stretch ===== # CT His

```

Fig. 11 Phylogenetic analysis of silicatein sequences of freshwater Porifera. **(a)** Alignment of partial aa sequences of silicatein- α from *L. baikalensis* (SILICAA1_LUBAI_MZ: CAI43319.1¹³⁷⁻²⁸⁶; SILICAA2_LUBAI_MZ: CAI91571.1¹³⁷⁻²⁸⁶; SILICAA3_LUBAI_MZ: CAI91572.1¹⁵⁵⁻³⁰⁴; SILICAA4_LUBAI_MZ: CAI91573.1¹³⁷⁻²⁸⁶), *S. domuncula* (SILICAA_SUBDO_MZ: CAI46305.1¹⁴¹⁻²⁹⁰), *E. fluviatilis* (SILICAA2_EPHFLUV: BAE54434.1¹³⁷⁻²⁸⁶), *E. muelleri*

(continued)

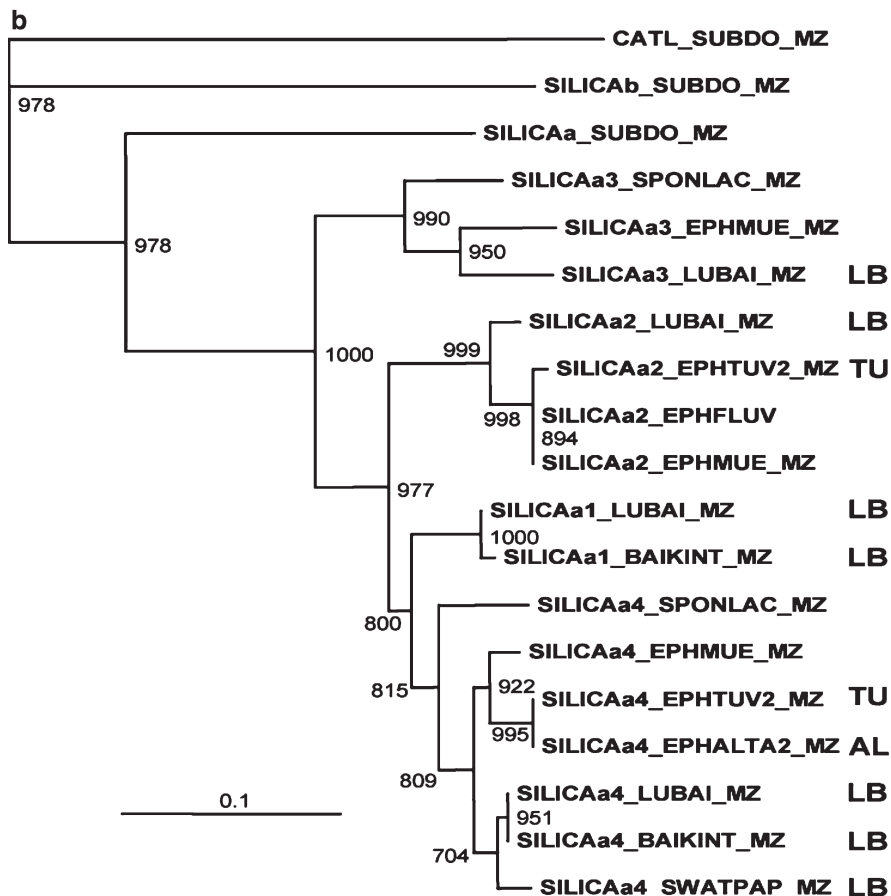


Fig. 11 (continued) (SILICAa3_EPHMUE_MZ: FM160559₁₃₈₋₂₈₇; SILICAa2_EPHMUE_MZ: FM160558₁₅₁₋₃₀₀; SILICAa4_EPHMUE_MZ: FM160560₁₋₁₅₀), *S. lacustris* (SILICAa3_SPONLAC_MZ: FM160563₁₃₈₋₂₈₇; SILICAa4_SPONLAC_MZ: FM160564₁₃₇₋₂₈₆), *B. intermedia* (SILICAa4_BAIKINT_MZ: FM160556₈₋₁₅₇; SILICAa1_BAIKINT_MZ: FM160555₈₋₁₅₇), *S. papyracea* (SILICAa4_SWATPAP_MZ: FM160565₁₋₁₅₀), *E. tuva* (SILICAa2_EPHTUV2_MZ: FM160561₁₀₋₁₅₉; SILICAa4_EPHTUV2_MZ: FM160562₁₀₋₁₅₉), *E. altaiensis* (SILICAa4_EPHALTA2_MZ: FM160557₁₀₋₁₅₉); of the partial aa sequence of *S. domuncula* silicatein- β (SILICAb_SUBDO_MZ: CAD67990.1₁₈₉₋₃₄₃), and of the partial aa sequence of *S. domuncula* cathepsin L (CATL_SUBDO_MZ: CAH04632.1₁₃₅₋₂₈₄). Positions conserved in all sequences are shaded in *black*, over 80% conserved regions are marked in *gray*. *Light gray* shows a conservation of at least 60%. Silicatein specific features are marked: a serine (*Ser*) stretch and the histidine (*His*) residue of the catalytic triad (*CT*) (**b**) Rooted NJ-tree generated after alignment of above-mentioned partial silicatein sequences. The cathepsin L sequence of *S. domuncula* was used as an outgroup. *Numbers* at the nodes indicate the level of confidence for the branches as determined by bootstrap analysis (1,000 bootstrap replicates)

E. tuva and *E. altaiensis*, both forming a group with *E. muelleri*. Together with a second cluster of Lubomirskiidae sequences, these two clades originate from a common ancestor of silicatein-a4, closely related to *S. lacustris* silicatein-a4. Thus, this tree topology suggests a Spongilla-like founder generation of poriferan species in Lake Chagytai and Lake Tore-Khol (whose immediate descendants might still have been present at the time of Rezvoj's sampling of sponges at Lake Chagytai; Rezvoj 1927). The clusters of silicatein-a3 and silicatein-a2 sequences support this assumption to a certain extent, even though the data set is more restricted. In any case, the a2 cluster also reveals a close relationship between *E. tuva* and *E. muelleri*, similar to the a4 cluster, clearly suggesting the species denomination *B. dzhegatajensis* proposed by Rezvoj (1927) should be abandoned in favor of *E. tuva*.

4 Evolution of Endemic Sponges in Lake Baikal and Lake Chagytai (Tuva-Baikal Region) – An Approach

According to the molecular and morphological data presented, we propose a pattern of radiation of Baikalian-Tuva sponges in three stages. The first step was the adaptation to ENVIRONMENTAL CONDITIONS. The northern hemisphere underwent a general cooling period during the Plio-Pleistocene, which superimposed the cooling periods in Central Asia (2.8–2.5 and 1.8–1.5 Ma). During this phase, specimens had to resist increasing environmental stress (i.e., low temperature). Adaptation certainly involved genetic components, e.g., an increase in number and function of stress-resistance molecules (heat shock proteins and other chaperons, etc.). A large array of such genes/proteins is found in sponges in general and in the Baikalian sponge species in particular. Stress-resistance can also be acquired by a reduction of the metabolic activity. Thus, in Lake Baikal and surely also in Lake Chagytai/Lake Tore-Khol, nutritional deprivation and reduction of the intermediary metabolism is compensated in sponges by an extensive symbiosis with photosynthetic algae (zoochlorella) that could also allocate the necessary nutrients during adverse conditions. In this respect, it is important to notice that these algae are also photosynthetically active during winter, when the lakes are covered by ice.

Furthermore, the physical characteristics of the Siberian lakes are highly favorable for sponges in general. The water is oligotrophic, the aeration is high due to significant temperature differences (including the periods of ice coverage), the sedimentation rate is low (with 38 mm/Ka in Lake Baikal), and the visibility is high, favoring the symbiotic relationship between sponges and algae. These parameters greatly contribute to the fact that, in Lake Baikal (Savarese et al. 1997) and also in Lake Chagytai/Lake Tore-Khol, the “photosymbiotic” sponges dominate the photic zone. Thus, they occupy the slopes of the lakes in some regions almost completely, either the available rocky substrates (Lake Baikal) or the *Chara* specimens on the sandy floor (Lake Chagytai/Lake Tore-Khol). This dominance of poriferan populations is exceptional; in other marine (Bergquist 1978) or freshwater environments (Frost 1991) the occurrence of sponges in the ecosystem is much less prevailing.

In the second step, the DOMINANCE OF SEXUAL REPRODUCTION over asexual reproduction (e.g., by gemmules) in sponges, was a further component favorable for the rapid radiation of sponges. In fact, Lake Baikal sponges have been described as forming no gemmules (Efremova 2001). The primary advantage of sexual reproduction can be seen in a greater genetic diversity arising from recombination; success in mating may be considered as a character conferring fitness, rapid development, and longevity. It has been calculated that the life span of *L. baicalensis* exceeds 30 years.

Finally, diversification of the dominant poriferan species in Lake Baikal, Lake Chagytai, and Lake Tore-Khol was driven by DIFFERENCES IN THE HABITATS. Species of the genus *Spongilla* and *Ephydatia* (probably closely related to the common ancestor of poriferan species found in the Siberian lakes) have a hibernant, aestivant, or perennial life cycle (Pronzato and Manconi 2001). However, endemic Baikalian and Chagytai/Tore-Khol species are lacking the property to form gemmules. Since in these lakes the seasonal physical changes do not include drying, the evolutionary pressure to maintain the capability for gemmulation most likely was low. However, intra-species morphological variations do exist, as can be impressively seen in *L. baicalensis*, and might depend primarily on water velocity and depth. Interestingly, in spite of several common characteristics of the Lake Baikal, Lake Chagytai, and Lake Tore-Khol habitats, considerable differences between the respective sponge communities' lifestyles evolved. Whereas the benthic and littoral endemic sponges of Lake Baikal predominantly populate the rocky substratum ("rocky community"), the Lake Chagytai/Lake Tore-Khol communities (almost exclusively live on the algae *Chara* sp. ("algal community").

5 Conclusion

Since the endemic sponges of Lake Baikal, Lake Chagytai, and Lake Tore-Khol are exclusively found in those Siberian lakes and likely originate from the same founder species, it might be concluded that the lowering of temperature initially triggered the evolutionary direction, eventually leading to Siberian speciation. During this process, founder populations arose, which could cope with changing climate. However, during the Rift stage period, habitat differences in the lakes emerged (Ovchinnikova 2005): With the beginning of the Upper Pleistocene the depression of the Baikal basin took place, which was stronger compared to the rifting in the Chagytai/Tore-Khol region. Subsequent increasing selective pressure of abiotic and biotic environments – differing in Lake Baikal and in Lake Chagytai/Lake Tore-Khol – resulted in the development of different species from founder populations that initially might have been similar or identical. Thus, depending on physical (depth, rocky habitats) and biological conditions (existence of mineralizing algae on a sandy ground), in Lake Baikal the family of Lubomirskiidae ultimately evolved, including the genera *Lubomirskia*, *Baikalospongia*, and *Swartschewskia*. Based on the palaeontological data available, the major split of Baikalian Lubomirskiidae from cosmopolitan Spongillidae occurred around the first cold event, 2.8–2.5 Ma.

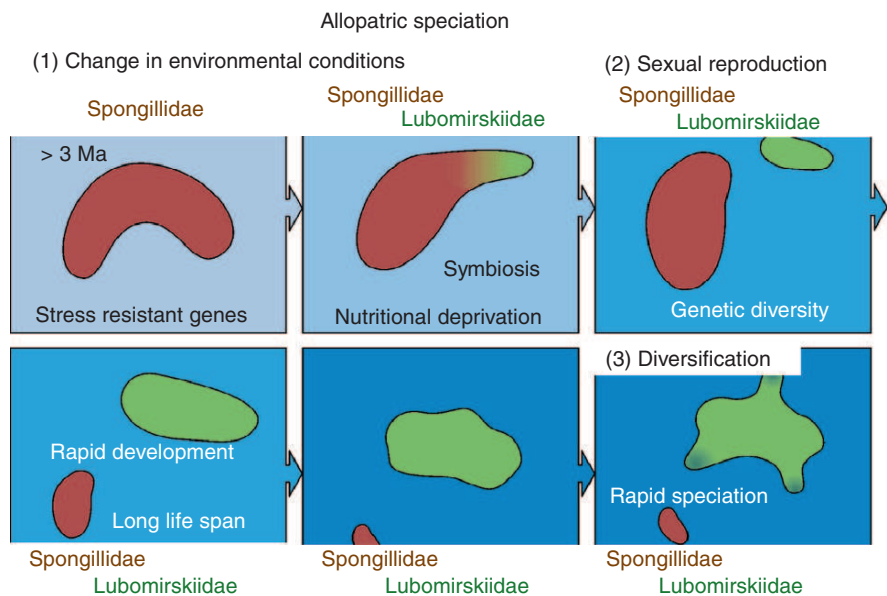


Fig. 12 Proposed allopatric speciation of Baikalian/Chagytai/Tore-Khol sponges. Initially (3–5 Ma) only the cosmopolitan species of the Spongillidae was found in Siberian lakes, including Lake Baikal, Lake Chagytai, and Lake Tore-Khol. During drastic changes of environmental conditions in the Plio-Pleistocene with two major cooling periods (2.8–2.5 and 1.8–1.5 Ma) in Lake Baikal, the Lubomirskiidae and, in Lake Chagytai/Tore-Khol, *Ephydatia tuva* and *E. altaiensis* evolved, very likely in a process of peripatric speciation, from Spongillidae. It is suggested that the Baikalian and Chagytai/Tore-Khol sponges could cope adequately with the changes of temperature through their elaborated genetic repertoire (including, e.g., chaperones). Nutritional deprivation during the cold period, in combination with a reduction of the intermediary metabolism, could be compensated by an extensive symbiosis with algae (zoochlorella). Rapid radiation of the new evolving endemic sponges was further supported by the dominance of sexual reproduction, as is seen in endemic Lake Baikal sponges. Finally, diversification of the dominant sponge species was driven by differences in the habitat

In contrast, in Lake Chagytai and Lake Tore-Khol, *E. tuva* and *E. altaiensis* arose, representing close descendants of the founder species.

In conclusion, the process of speciation in Lake Baikal and Lake Chagytai/Lake Tore-Khol, from a cosmopolitan ancestor closely related to *S. lacustris* to more than 10 endemic species follows allopatric speciation pattern (by climatic “barriers”) and is of the peripatric type (establishment of a founder population beyond the periphery of the preceding species) (Fig. 12). Molecular biological studies are in progress to further assess the evolutionary relationship between Lake Baikal and Lake Chagytai/Lake Tore-Khol sponge fauna.

Acknowledgments This work was supported by grants from the European Commission, the Deutsche Forschungsgemeinschaft (SPP 1174: Deep Metazoan Phylogeny), the Bundesministerium für Bildung und Forschung Germany (project: Center of Excellence *BIOTECmarin*) and the International Human Frontier Science Program.

References

- Addis JS, Petterson KJ (2005) Phylogenetic relationships of freshwater sponges (Porifera, Spongillina) inferred from analyses of 18S rDNA, COI mtDNA, and ITS2 rDNA sequences. *Zool Scr* 34:549–557
- Annandale N (1914) Further notes on the sponges of Lake Baikal. *Rec Indian Mus* 10:137–148
- Bavestrello G, Arillo A, Calcinai B, Cattaneo-Vietti R, Cerrano C, Gaino E, Penna A, Sara M (2000) Parasitic diatoms inside Antarctic sponges. *Biol Bull* 198:29–33.
- Belikov SI, Kaluzhnaya OV, Schröder HC, Krasko A, Müller IM, Müller WEG (2005) Expression of silicatein in spicules from the Baikalian sponge *Lubomirskia baicalensis*. *Cell Biol Int* 29:943–951
- Bergquist PR (1978) Sponges. University of California, Berkeley, CA.
- Borchiellini C, Manuel M, Alivon E, Boury-Esnault N, Vacelet J, Le Parco Y (2001) Sponge paraphyly and the origin of Metazoa. *J Evol Biol* 14:171–179
- Efremova SM (2001) Sponges (Porifera). In: Timoshkin OA (ed) Index of Animal Species Inhabiting Lake Baikal and Its Catchment Area. Novosibirsk Nauka, Novosibirsk, pp. 179–192
- Field KG, Olsen GJ, Lane DJ, Giovannoni SJ, Ghiselin MT, Raff EC, Pace NR, Raff RA (1988) Molecular phylogeny of the animal kingdom. *Science* 239:748–753
- Frost TM (1991) Porifera. In: Thorp JH, Covich AP (eds) Ecology and Classification of North American Freshwater Invertebrates. Academic, Boston, MA, pp. 95–124
- Funayama N, Nakatsukasa M, Kuraku S, Takechi K, Dohi M, Iwabe N, Miyata T, Agata K (2005) Isolation of Ef silicatein and Ef lectin as molecular markers for sclerocytes and cells involved in innate immunity in the freshwater sponge *Ephydatia fluviatilis*. *Zool Sci* 22:1113–1122
- Greze VN, Greze II (1958) Ozero Chagytai. *Izvestija Vsesoyuznogo Geographiceskogo Obscestva* 90:279–284
- Itskovich VB, Belikov SI, Efremova SM, Masuda Y (1999) Phylogenetic relationships between Lubomirskiidae, Spongillidae, and some marine sponges according to partial sequences of 18S rDNA. *Mem Queensl Mus* 44:275–280
- Kaluzhnaya OV, Belikov SI, Schröder HC, Rothenberger M, Zapf S, Kaandorp JA, Borejko A, Müller IM, Müller WEG (2005) Dynamics of skeleton formation in the Lake Baikal sponge *Lubomirskia baicalensis*. Part I: biological and biochemical studies. *Naturwissenschaften* 92:128–133
- Kozhov M (1963) Lake Baikal and Its Life. W. Junk-Verlag, Den Haag
- Kozhova OM, Izmet'eva LR (1998) Lake Baikal – Evolution and Biodiversity. Backhys, Leiden
- Kruse M, Gamulin V, Cetkovic H, Pancer Z, Müller IM, Müller WEG (1996) Molecular evolution of the metazoan protein kinase C multigene family. *J Mol Evol* 43:374–383
- Lafay B, Boury-Esnault N, Vacelet J, Christen R (1992) An analysis of partial 28S ribosomal RNA sequences suggests early radiations of sponges. *Biosystems* 28:139–151
- Manconi R, Pronzato R (2002) Suborder Spongillina subord. nov: Freshwater sponges. In: Hooper JNA, van Soest RWM (eds) *Systema Porifera: A Guide to the Classification of Sponges*. Kluwer, New York, pp. 921–1019
- Masuda Y, Itskovich VB, Veinberg EV, Efremova SM (1997) Studies on the taxonomy and distribution of freshwater sponges in the Lake Baikal. In: Miyazaki N (ed) *Animal Community, Environment and Phylogeny in Lake Baikal*. Otsuchi Marine Center/Ocean Research Institute, Tokyo, Japan, pp. 25–33
- Meixner MJ, Lüter C, Eckert C, Itskovich V, Janussen D, von Rintelen T, Bohne AV, Meixner JM, Hess WR (2007) Phylogenetic analysis of freshwater sponges provide evidence for endemism and radiation in ancient lakes. *Mol Phylogent Evol* 45:875–886
- Müller WEG (1995) Molecular phylogeny of metazoa [Animals]. Monophyletic origin. *Naturwissenschaften* 82:321–329
- Müller WEG (2001) How was the metazoan threshold crossed? The hypothetical Urmetazoa. *Comp Biochem Physiol (A)* 129:433–460

- Müller WEG, Müller I, Zahn RK, Maidhof A (1984) Intraspecific recognition system in scleractinian corals: morphological and cytochemical description of the autolysis mechanism. *J Histochem Cytochem* 32:285–288
- Müller WEG, Schröder HC, Skorokhod A, Bünz C, Müller IM, Grebenjuk VA (2001) Contribution of sponge genes to unravel the genome of the hypothetical ancestor of Metazoa (Urmetazoa). *Gene* 276:161–173
- Müller WEG, Brümmer F, Batel R, Müller IM, Schröder HC (2003) Molecular biodiversity. Case study: Porifera (sponges). *Naturwissenschaften* 90:103–120
- Müller WEG, Schröder HC, Wrede P, Kaluzhnaya OV, Belikov SI (2006) Speciation of sponges in Baikal-Tuva region (an outline). *J Zool Syst Evol Res* 44:105–117
- Müller WEG, Boreiko A, Wang X, Belikov SI, Wiens M, Grebenjuk VA, Schloßmacher U, Schröder HC (2007a) Silicateins, the major biosilica forming enzymes present in demosponges: protein analysis and phylogenetic relationship. *Gene* 395:62–71
- Müller WEG, Schloßmacher U, Eckert C, Krasko A, Boreiko A, Ushijima H, Wolf SE, Tremel W, Schröder HC (2007b) Analysis of the axial filament in spicules of the demosponge *Geodia cydonium*: different silicatein composition in microscleres [asters] and megascleres [oxeas and triaenes]. *Eur J Cell Biol* 86:473–487
- Müller WEG, Boreiko A, Wang X, Belikov SI, Wiens M, Grebenjuk VA, Schlossmacher U, Schröder HC (2007c) Silicateins, the major biosilica forming enzymes present in demosponges: protein analysis and phylogenetic relationship. *Gene* 395:62–71
- Müller WEG, Schröder HC, Belikov SI (2008a) Sustainable exploitation and conservation of the endemic Lake Baikal sponge (*Lubomirskia baicalensis*) for the application in nanobiotechnology. In: Müller WEG, Grachev MA (eds) *Potential of Biosilica in Evolution, Morphogenesis and Nanobiotechnology*. Springer-Verlag, Heidelberg
- Müller WEG, Wang X, Kropf K, Boreiko A, Schloßmacher U, Brandt D, Schröder HC, Wiens M (2008b) Silicatein expression in the hexactinellid *Crateromorpha meyeri*: the lead marker gene restricted to siliceous sponges. *Cell Tissue Res*: Epub ahead of print.
- Nakamura Y, Sato S, Kaneko T, Kotani H, Asamizu E, Miyajima N, Tabata S (1997) Structural analysis of *Arabidopsis thaliana* chromosome 5. III. Sequence features of the regions of 1,191,918bp covered by seventeen physically assigned P1 clones. *DNA Res* 4:401–414
- Notredame C, Higgins DG, Heringa J (2000) T-Coffee: a novel method for fast and accurate multiple sequence alignment. *J Mol Biol* 302:205–217
- Ovchinnikova NS (ed) (2005) *Atlas of Lake Baikal: Past-Present-Future*. Omskaya Kartographicheskaya Fabrik, Omsk
- Pallas PS (1776) *Reise durch die verschiedenen Provinzen des Russischen Reiches*. St. Petersburg
- Pfeifer K, Haasemann M, Gamulin V, Bretting H, Fahrenholz F, Müller WEG (1993) S-type lectins occur also in invertebrates: unusual subunit composition and high conservation of the carbohydrate recognition domain in the lectin genes from the marine sponge *Geodia cydonium*. *Glycobiology* 3:179–184
- Popovskaya GI, Genkal SI, Likhoshway YV (2002) *Diatoms of the Plankton of Lake Baikal*. Nauka, Novosibirsk
- Rezvoj PD (1927) Notes on sponges from the Lake Dzhagataj-kul in the Urjankhaj region. *Doklady Akademii Nauk SSSR* 3/8:296–300
- Rezvoj PD (1936) Freshwater sponges of the USSR. In: Rezvoj PD (ed) *The Fauna of the USSR*. Academy of Sciences, Moscow, Leningrad, pp. 1–42
- Rodrigo AG, Bergquist PR, Bergquist PL, Reeves RA (1994) Are sponges animals: an investigation into the vagaries of phylogenetic inferences. In: Soest RW, Kempen TMG, Braekman, JC (eds) *Sponges in Time and Space*. Balkema, Rotterdam, pp. 47–54.
- Savarese M, Patterson MR, Chernykh VI, Fialkov VA (1997) Trophic effects of sponge feeding within Lake Baikal's littoral zone. 1. In situ pumping rate. *Limnol Oceanogr* 42:171–178
- Schröder HC, Efremova SM, Itskovich VB, Belikov S, Masuda Y, Krasko A, Müller IM, Müller WEG (2003a) Molecular phylogeny of the freshwater sponges in Lake Baikal. *J Zoolog Syst Evol Res* 41:80–86

- Schröder HC, Krasko A, Le Pennec G, Adell T, Hassanein H, Müller IM, Müller WEG (2003b) Silicase, an enzyme which degrades biogenous amorphous silica: contribution to the metabolism of silica deposition in the demosponge *Suberites domuncula*. *Prog Mol Subcell Biol* 33:249–268
- Schröder HC, Perović-Ottstadt S, Rothenberger M, Wiens M, Schwertner H, Batel R, Korzhev M, Müller IM, Müller WEG (2004) Silica transport in the demosponge *Suberites domuncula*: fluorescence emission analysis using the PDMPO probe and cloning of a potential transporter. *Biochem J* 381:665–673
- Schröder HC, Brandt D, Schlossmacher U, Wang X, Tahir MN, Tremel W, Belikov SI, Müller WEG (2007) Enzymatic production of biosilica glass using enzymes from sponges: basic aspects and application in nanobiotechnology (material sciences and medicine). *Naturwissenschaften* 94:339–359.
- Schulze P (1923) Beiträge zur Kenntnis der Kieselnadelbildung besonders bei den Spongilliden. *Arch f Zellforsch* 17:105–130
- Sherbakov DY (1999) Molecular phylogenetic studies on the origin of biodiversity in Lake Baikal. *Trends Ecol Evol* 14:92–95
- Shimizu K, Cha J, Stucky GD, Morse DE (1998) Silicatein alpha: cathepsin L-like protein in sponge biosilica. *Proc Natl Acad Sci USA* 95:6234–6238
- Simon L (1955) Über ökologische Typenbildung bei Süßwasserschwämmen. *Arch f Hydrobiol* 50:136–140
- Simpson TL, Garrone R, Mazzorana M (1983) Interaction of germanium (Ge) with biosilicification in the freshwater sponge *Ephydattia muelleri*: evidence of localized membrane domains in the silicella. *J Ultrastruct Res* 85:159–174
- Uriz MJ, Turon X, Becerro MA, Agell G (2003) Siliceous spicules and skeleton frameworks in sponges: origin, diversity, ultrastructural patterns, and biological functions. *Microsc Res Tech* 62:279–299
- Volkel H, Kurz U, Linder J, Klumpp S, Gnau V, Jung G, Schultz JE (1996) Cathepsin L is an intracellular and extracellular protease in *Paramecium tetraurelia*. Purification, cloning, sequencing and specific inhibition by its expressed propeptide. *Eur J Biochem* 238:198–206
- Waller JG (1878) On variation in *Spongilla lacustris*. *J Quekett Microsc Club* 5:53–62
- Weaver J, Morse DE (2003) Molecular biology of demosponge axial filaments and their roles in biosilicification. *Microsc Res Tech* 62:356–367
- Wiens M, Müller WEG (2006) Cell death in Porifera: molecular players in the game of apoptotic cell death in living fossils. *Can J Zool* 84:307–332
- Wiens M, Belikov SI, Kaluzhnaya OV, Krasko A, Schröder HC, Perovic-Ottstadt S, Müller WEG (2006) Molecular control of serial module formation along the apical-basal axis in the sponge *Lubomirskia baicalensis*: silicateins, mannose-binding lectin and mago nashi. *Dev Genes Evol* 216:229–242
- Wiens M, Korzhev M, Perović-Ottstadt S, Luthringer B, Brandt D, Klein S, Müller WEG (2007) Toll-like receptors are part of the innate immune defense system of sponges (Demospongiae: Porifera). *Mol Biol Evol* 24:792–804
- Wiens M, Grebenjuk VA, Schröder HC, Müller WEG (2008) Identification and isolation of a retrotransposon from the *Lubomirskia baicalensis*: implication in rapid evolution of endemic sponges. In: Müller WEG, Grachev MA (eds) *Potential of Biosilica in Evolution, Morphogenesis and Nanobiotechnology*. Springer-Verlag, Heidelberg
- Wörheide G, Nichols SA, Goldberg J (2004) Intragenomic variation of the rDNA internal transcribed spacers in sponges (Phylum Porifera): implications for phylogenetic studies. *Mol Phylogenet Evol* 33:816–830.

Symbiotic Interaction Between Dinoflagellates and the Demosponge *Lubomirskia baicalensis*: Aquaporin-Mediated Glycerol Transport

Werner E.G. Müller, Sergey I. Belikov, Oxana V. Kaluzhnaya, L. Chernogor, Anatoli Krasko, and Heinz C. Schröder

1	Introduction.....	146
2	Materials and Methods.....	148
2.1	Sponges, Cells/primmorphs, and cDNA Libraries	148
2.2	Glycerol Uptake by Sponge Primmorphs	149
2.3	Identification of Dinoflagellates.....	149
2.4	Determination of Chlorophyll.....	150
2.5	Microscopical Analysis.....	150
2.6	Isolation of cDNA Encoding Aquaporin	150
2.7	EST Sequences	151
2.8	Sequence Analysis	151
2.9	Northern Blotting	151
2.10	In Situ Localization Studies	152
3	Results.....	152
3.1	<i>L. baicalensis</i> Specimens in Winter and Summer.....	152
3.2	<i>L. baicalensis</i> : Localization of Dinoflagellates and Chlorophyll Content	153
3.3	<i>L. baicalensis</i> : Identification of Dinoflagellates	154
3.4	Separation of Dinoflagellates from Sponge Cells and Formation of Primmorphs ...	156
3.5	Uptake of Glycerol by Sponge Cells	158
3.6	Metabolic Studies in Primmorphs Using Molecular Tools.....	158
3.7	<i>L. baicalensis</i> Aquaporin	161
3.8	Expression of Aquaporin	161
4	Discussion.....	163
	References.....	168

Abstract Lake Baikal is rich in endemic sponge species, among them the arborescently growing species *Lubomirskia baicalensis*. During winter when the lake is covered by ice, this species reproduces sexually, reflecting a high metabolic

W.E.G. Müller (✉), A. Krasko, and H.C. Schröder
Institut für Physiologische Chemie, Abteilung Angewandte Molekularbiologie, Universität,
Duesbergweg 6, 55099 Mainz, Germany
e-mail: wmueller@uni-mainz.de

S.I. Belikov, O.V. Kaluzhnaya, L. Chernogor,
Limnological Institute of the Siberian Branch of Russian Academy of Sciences,
Laboratory for Analytical/Bioorganic Chemistry, Ulan-Batorskaya 3, 664033 Irkutsk, Russia

activity. Throughout the year, *L. baicalensis* lives in association with dinoflagellates, which – according to the data presented herein – are symbiotic. The dinoflagellates have been determined on the basis of their rDNA/ITS characteristics and were found to display high sequence similarity to *Gymnodinium sanguineum*. The dinoflagellates give the sponge its characteristic green color, reflecting the high chlorophyll content (chlorophyll-*a* content in March and September of $3.2 \pm 0.6 \mu\text{g/g}$ and $1.9 \pm 0.5 \mu\text{g/g}$ of protein, respectively). With the in vitro cell culture system for sponges, the primmorphs, it could be demonstrated that [^{14}C] glycerol is readily taken up by sponge cells; this process can be inhibited by phloretin, an aquaporin channel blocker. In order to prove the effect of cholesterol on the intermediate metabolism of the sponge cells, molecule probes, cDNAs for key enzymes in gluconeogenesis, glycolysis, and citric acid, have been applied in Northern blot studies. The data revealed that the genes coding for the enzymes citrate synthase and fructose-1,6-bisphosphatase are strongly upregulated after exposure of primmorphs to glycerol. This effect is abolished by phloretin. The genes encoding the phosphoglucose isomerase and pyruvate dehydrogenase do not respond to glycerol supply, suggesting that their expression is not under genetic control in *L. baicalensis*. To prove the assumption that the aquaporin channel is involved in the influx of glycerol in sponge cells, this cDNA was cloned and applied for in situ hybridization studies. The results obtained show that cells surrounding the dinoflagellates become brightly stained after hybridization with the aquaporin this probe. This demonstrates that *L. baicalensis* cells respond to glycerol, a metabolite which might be supplied by the dinoflagellates and imported via the aquaporin channel into the sponge cells.

Note: The sequences from *L. baicalensis* reported here, the aquaporin (*LBAQPr*, accession number AZ231299), as well as the three sequences from the symbiotic dinoflagellates, spanning the 18S rDNA-ITS1–5.8S rDNA region, DINO1_LUBAI (accession number AZ231309), DINO2_LUBAI (AZ231309) and DINO2_LUBAI (AZ231309) have been deposited in the EMBL/GenBank data base.

1 Introduction

Sponges (phyla Porifera) are the phylogenetically earliest taxon which evolved from the hypothetical ancestor of all metazoans, the Urmetazoa (Müller 2001). They evolved approximately 650–665 million years ago (Ma), based on molecular biological data (Schäcke et al. 1994) or 750 Ma according to palaeontological data (Reitner and Wörheide 2002), a period between, or prior to, the Sturtian glaciation (710–680 Ma) and the Varanger-Marinoan ice ages (605–585 Ma). It has been suggested/demonstrated that, during the Proterozoic time, 740 and 580 Ma, global glaciation extended into the equatorial latitude of “snowball Earth.” It is under debate whether during these cooling periods most biotic taxa became extinct (see Corsetti et al. 2006). The sponges could cope with the environmental stress (e.g., low temperature) by their potent genetic abilities for adaptation. It has been demonstrated

that marine and freshwater sponges comprise a surprisingly diverse array of heat shock proteins, including ubiquitins, 14-3-3 proteins, and thioredoxins, as well as enzymes involved in DNA repair, e.g., excision repair proteins, and also apoptotic molecules (Müller et al. 2000; Wiens and Müller 2006).

It remains, however, to be studied from which sources sponges obtain the organic molecules required for the maintenance of their intermediary metabolism during severe cooling periods. Here, the characteristics of sponges to live in symbiosis with bacteria, and very likely also with fungi and algae, can be considered as the major factor that provides them with the ability to overcome periods of food restriction (Wilkinson 1992; Thakur and Müller 2005). The amount of bacteria that sponges ingest and filtrate is enormous; it has been measured that some species daily filtrate through their body tons of water per kg body weight (Reiswig 1974), containing millions of bacteria or viruses (reviewed in Gonzales and Moran 1997; Kennish 1994). It is widely accepted that the major role of symbiotic bacteria is the production of secondary metabolites to eliminate attacking (infectious) bacteria that entered the sponge body with the circulating water (see Proksch 1994). Together with microorganisms, some sponge species also maintain an apparent obligate symbiosis with algae (Wilkinson 1992). Recent molecular cell biological studies support the empirical observations that sponges can recognize gram-positive and gram-negative bacteria as well as fungi, by expression of specific cell-surface receptors (Perović-Ottstadt et al. 2004; Wiens et al. 2005) or defensive enzymes (Thakur et al. 2005).

The role of the secondary metabolites synthesized by bacteria/microorganisms as protection of sponges against invading organisms, has been studied extensively (reviewed in Friedrich et al. 2001). In contrast, the (potential) function of the microorganisms to produce primary metabolites required for energy metabolism of sponges remains uninvestigated by modern techniques. To approach the latter question, we have selected such sponge species that (1) live together with symbiotic algae (zoochlorellae/zooxanthellae), and (2) have to overcome extreme climatic periods. The species of choice are the endemic sponges living in the littoral zone of Lake Baikal (south-central Siberia), primarily the species *Lubomirskia baicalensis*, *Baikalospongia bacillifera*, and *B. intermedia* (Pile et al. 1997). These sponges have a bright green color that is due to the symbiotic zoochlorellae/zooxanthellae living in their external layer (Efremova 1981). Endosymbiotic bacteria seem to be absent in these sponges. It should be stressed that Baikalian sponge species are generally larger than other freshwater species; they grow up to 1.5 m high.

These freshwater sponges (*L. baicalensis* and *B. intermedia*) live for at least 4 months under a closed ice cover around 1 m thick. Maximum temperature of the surface water in August is 12°C, while during the period of ice coverage the water cools down to -0.5°C (February/March; at the site of investigation at Bolshiye Koty). Usually the ice is covered only with thin layers of snow (5–10 cm; Kozhov 1963). Nevertheless, the water in Lake Baikal remains rich in oxygen throughout the year which is the result of the high circulation of the water (Kozhov 1963). It has been estimated that the sponges in Lake Baikal consume the considerable amount of 2 g carbon/day \times m⁻² (Pile et al. 1997). Until now, the contribution of

the symbionts (zoochlorellae/zooxanthellae or other algae) in the metabolism of the Baikalian sponges has not been determined. For marine sponges, it could be demonstrated that their photosynthetic symbionts contribute considerably to the energy budget (Wilkinson 1992), very likely by a transfer of glycerol from the unicellular algae to the multicellular host (Vacelet 1971; Wilkinson 1992).

In the present study, we use the Baikalian sponge *L. baicalensis* to demonstrate that they live in a symbiotic relationship with dinoflagellates; the taxa were determined on the basis of rDNA. In addition, we show that sponge cells are able to take up glycerol from the surrounding medium, most likely through an aquaporin channel. Aquaporins are a family of transmembrane channels, found in bacteria, plants, and animals, that permit osmotically driven movement of water in both directions (Gorin et al. 1984; Pao et al. 1991; Park and Saier 1996; Reizer et al. 1993). A cDNA from *L. baicalensis*, encoding the aquaporin-related channel (AQPr channel), was identified, cloned, and sequenced; the probes were used for in situ hybridization studies in tissue sections through the sponge. Inhibition studies were performed to additionally demonstrate that aquaporin is involved in glycerol transport from dinoflagellates to the sponge cells. In response to the glycerol uptake the sponges upregulate key enzymes involved in glycolysis, glyconeogenesis, and energy production. For these studies, the cDNA probes for the *L. baicalensis* genes, encoding citrate synthase, fructose-1,6-bisphosphatase, pyruvate dehydrogenase and phosphoglucose isomerase were applied. Our in vitro studies were performed with primmorphs, special three-dimensional cell aggregates which contain proliferating and differentiating cells (Müller et al. 1999). We conclude that in the Lake Baikal sponge *L. baicalensis* the dinoflagellates produce glycerol, which is taken up the sponge cells; they metabolize this carbon source for energy production, especially during winter, the ice-cover season.

2 Materials and Methods

2.1 Sponges, Cells/primmorphs, and cDNA Libraries

Specimens of *L. baicalensis* (Porifera, Demospongiae, Haplosclerida) were collected in Lake Baikal near the village Bolshiye Koty (51°58'N, 105°21'E) from depths between 7 and 12 m during September 2005 and March 2006. Cells were prepared by immersing sponge tissue into natural Lake Baikal water, supplemented with 50 mM ethylenediaminetetraacetic acid-Na salt (EDTA). After gentle shaking for 30 min at 16°C on a rotatory shaker, the solution was discarded and new Baikal water/EDTA was added. After 40 min, the supernatant was collected and filtered through a 40-µm mesh nylon net, and shaking in Baikal water/EDTA and filtration were repeated once. The single cells were harvested by centrifugation (500g for

5 min) and washed once. The cells of this pellet were resuspended in Baikal water, supplemented with 100 IE of penicillin and 100 µg/ml of streptomycin). A cell suspension of 10^7 cells was added to 6 ml (final volume) of medium in 10-ml flasks (Nuclon surface; #136196; Nunc Wiesbaden [Germany]). Primmorphs were obtained from these single cells; they reached sizes of 3–7 mm after 2 days.

In the experiments to determine the effect of glycerol on the expression of genes, coding for selected key enzymes of the intermediary metabolism, the primmorphs were incubated in the absence or presence of 100 µM of glycerol for 24h. Subsequently, RNA was isolated and used for Northern blot experiments.

Single cell suspensions obtained after dissociation in Baikal water/EDTA contained dinoflagellates and sponge cells. The algae were separated from the sponge cells by Ficoll discontinuous density gradient centrifugation as described (Müller et al. 1981). The sponge cells were obtained in the pellet below the 25% (v/v) Ficoll layer, while the dinoflagellates were collected on the 15% (v/v) Ficoll. The dinoflagellates could be visualized after illumination with fluorescence light of a wave length of 334/365 nm.

The cDNA library from *L. baicalensis* was prepared in *TriplEx2* vector.

2.2 Glycerol Uptake by Sponge Primmorphs

Primmorphs from *L. baicalensis* were incubated in a volume of 2 ml of culture medium, containing primmorphs and [14 C] glycerol (4.9 GBq/mmol) at room temperature for 2–10 min. The primmorphs were quickly washed five times with ice-cold water. Cell-associated radioactivity was determined by scintillation counting; in parallel aliquots of primmorphs were used for protein determination. Where indicated the primmorphs had been preincubated with 500 µM of phloretin 10 min prior the addition of [14 C] glycerol.

2.3 Identification of Dinoflagellates

The genomic region, spanning the 18S rDNA–ITS1–5.8S rDNA region, was used for the determination of the dinoflagellates. Total DNA of the sponge was isolated (Schröder et al. 2005). Primers were used following the earlier studies (Baillie et al. 2000; Pawlowski et al. 2001). The forward primer was 5′-CGCTCCTACCGATTGAGTGA-3′ and the reverse primer 5′-GTTACGGAGTTCTGCAATTC-3′; the following PCR program was used: initial denaturation at 95°C for 10 min, followed by 40 amplification cycles at 95°C for 30 s, 51°C for 45 s, 74°C for 1.5 min, and a final extension step at 72°C for 2 min.

2.4 Determination of Chlorophyll

Tissue samples from *L. baicalensis* were extracted with 100% acetone for 24h (4°C). After centrifugation (10,000g) the absorbencies were read at 630, 663, and 750nm to determine the chlorophyll concentration (Jeffrey and Humphrey 1975). The means (\pm SE) from six independent experiments are given.

2.5 Microscopical Analysis

Light microscopical images were produced with an Olympus AHB3 light microscope. Digital light micrographs were taken with the VHX-100 Microscope (Keyence, Neu-Isenburg, Germany), equipped with a zoom-lens 25–175 \times . In order to increase the depth of focus, 10- μ m distant images were compiled and computed.

Scanning electron microscopy (SEM) analysis of spicules was performed with a Zeiss DSM 962 Digital Scanning Microscope (Zeiss, Aalen, Germany) as described (Wiens et al. 2006).

For transmission microscopical (TEM) analysis the samples were cut into pieces (2 mm³), incubated in 0.1 M phosphate buffer (supplemented with 2.5% glutaraldehyde, 0.82% NaCl [pH 7.4]) and then washed in 0.1 M phosphate buffer (1.75% NaCl) at room temperature. After treating the samples with 1.25% NaHCO₃, 2% OsO₄ and 1% NaCl, they were dehydrated with ethanol. The dried samples were incubated with propylene oxide, fixed in propylene oxide/araldite (2:1), covered with pure araldite and hardened at 60°C for 2 days prior to cutting to 60nm ultrathin slices (Ultracut S; Leica, Wetzlar, Germany). The samples were transferred onto coated copper grids and analyzed with a Tecnai 12 device (FEI Electron Optics, Eindhoven, Netherlands).

2.6 Isolation of cDNA Encoding Aquaporin

The technique of polymerase chain reaction (PCR) was applied to identify the complete cDNA encoding for aquaporin. Degenerate primers were designed against the conserved aquaporin signature found in mammalian aquaporin, e.g., human aquaporin 9 (accession number BAA24864; Ishibashi et al. 1998), which reads FTAIAGWGW (presence in the sequence between aa₂₂₆ and aa₂₃₂). The forward primer 5'-TTC/T ACI GCI ATA/C/T GCI GGI TGG GGI TGG GAC/T-3' was used; PCR was carried out with this primer and the vector primer at an initial denaturation at 95°C for 5 min, followed by 30 amplification cycles at 95°C for 30 s, 54°C for 45 s, 74°C for 1.5 min, and a final extension step at 74°C for 10 min. Fragments were isolated and cloned into the *pCRII-TOPO* vector in *Escherichia coli* TOP10 cells (Invitrogen). Sequencing was performed with primers directed

to the SP6 promoter and the T7 promoter. The sequence was completed with insert-specific primers in combination with 5'-RACE primer or with 3'-RACE primer using the CapFishing Full-length cDNA Premix Kit. The final sequence was confirmed by an additional PCR using primers directed against the non-translated region of the cDNA, followed by sequencing. The clone encoding the aquaporin-related molecule from *L. baicalensis* *LBAQPr* is 1,248 nucleotides [nts] long (excluding the poly(A) tail).

2.7 EST Sequences

We have established an expressed sequence tag (EST) collection of cDNAs from *L. baicalensis*. Among them partial sequences encoding the following metabolic enzymes also exist and have been used as probes in the Northern blot studies: citrate synthase, fructose-1,6-bisphosphatase, phosphoglucose isomerase and pyruvate dehydrogenase. The EST cDNAs encoding citrate synthase (*CITSYN_LUBAI*), fructose-1,6-bisphosphatase (*FRUC16BISP_LUBAI*), phosphoglucose isomerase (*PGI_LUBAI*) and pyruvate dehydrogenase (*PYDH_LUBAI*) had lengths of 743 nts for the *LUBAICITSYN*, 438 nts for the *LUBAIFRUC16BISP*, 666 nts for the *LUBAIPGI*, and 743 nts for the *LUBAIPYDH*.

2.8 Sequence Analysis

The deduced aa sequence of *L. baicalensis* aquaporin *AQPr_LUBAI* was compared with those of the most closely related proteins, especially those from human, *Drosophila melanogaster*, *Caenorhabditis elegans*, *Saccharomyces cerevisiae* or *Arabidopsis thaliana*, using the neighbor-joining method (Saitou and Nei 1987). The degree of support for internal branches was further assessed by bootstrapping (Felsenstein 1993). Accurate multiple protein sequence alignments were made using the software CLUSTAL W (Thompson et al. 1994). The hydrophobic (potential transmembrane) region was predicted according to the described algorithm (Rao and Argos 1986).

2.9 Northern Blotting

RNA was isolated from the primmorphs. Samples were frozen, pulverized in liquid-nitrogen, and RNA was extracted using the TRIzol Reagent. Two micrograms of total RNA were fractionated by electrophoresis, transferred to a Hybond-N+ nylon membrane, and hybridized overnight at 50°C. The following probes, labeled with the PCR-DIG-Probe-Synthesis Kit, were used: the EST cDNAs *LUBAICITSYN*,

LUBAIFRUC16BISP, *LUBAIPGI*, and *LUBAIPYDH*. As a control to assure that the same amount of RNA was loaded onto the gels, the house keeping gene α -tubulin (*LBTUB*; AJ971711) from *L. baicalensis* was used. After washing, DIG-labeled nucleic acid was detected with anti-DIG Fab fragments conjugated to alkaline phosphatase, and visualized by chemiluminescence technique using CDP-star. Where indicated, the screens were scanned with the GS-525 Molecular Imager (Bio-Rad; Hercules, CA, USA).

2.10 *In Situ Localization Studies*

The method applied bases on a described procedure (Perović et al. 2003). Eight-micrometers-thick frozen sections through tissue were prepared, fixed, treated with Proteinase K and subsequently fixed again with paraformaldehyde. After rehydration, the sections were hybridized with the labeled probe, a 350-nt-long part of the *LBAQPr* cDNA portion. After blocking, the sections were incubated with an anti-digoxigenin antibody conjugated with alkaline phosphatase. The dye reagent NBT/X-Phosphate was used for visualization of the signals. Antisense and sense ssDNA digoxigenin-labeled probes were synthesized by PCR using the “PCR-DIG Probe synthesis Kit.” Sense probes were used in parallel as negative controls in the experiments.

3 Results

3.1 *L. baicalensis Specimens in Winter and Summer*

The species is ubiquitous in the littoral zone of Lake Baikal (Masuda et al. 1997). The morphology and the spatial distribution of *L. baicalensis* does not change seasonally. In September (Fig. 1a) and March (Fig. 1b), the sponges are found at the same sites; their branches reach at depths between 8 and 10 m heights of 80 cm–1 m. In winter, the specimens can be observed by SCUBA diving after cutting holes through the \approx 1-m-thick ice cover (Fig. 1c). Interestingly, during winter under complete ice coverage of the lake, the oscules of the sponges are surrounded by a collar-like dermal border (Fig. 1d). Gemmules are never found (see Kozhova and Izmeteva 1998), *L. baicalensis* reproduces sexually. Oocytes are formed abundantly during September but surprisingly also during the ice-cover period in March (Fig. 2). They are frequently released through the oscules (Fig. 1e).

The oocytes of *L. baicalensis* are found among/between the longitudinal spicule bundles which are embedded in a lectin matrix. Oocytes are produced predominantly in the body at the internal border of the 1- to 2-mm-thick surface zone which contains the dinoflagellates in a dense layer (Fig. 2a). The bundles span the longitudinal branches of the arboreal morphotypes (Fig. 2a). Higher magnification shows the orange color of the oocytes (Fig. 2b); the sizes of oocytes range between 3 and 4 mm. In a more mature stage, the oocytes are attached to a stalk composed of the

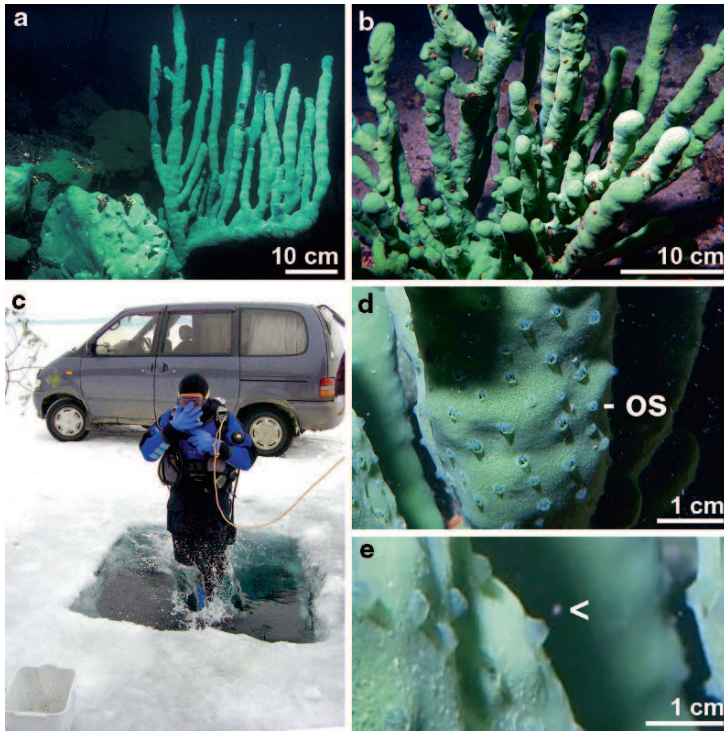


Fig. 1 *L. baicalensis* specimens during the late summer season (September) (a) and during the ice-cover season (March) (b). (c) In winter the specimens are collected by SCUBA diving under a 1-m-thick ice cover. (d) The oscule (*os*) of the specimens in winter are surrounded by a collar-like dermal border. (e) Eggs are frequently produced during the ice-cover period in March and released through the oscules (*arrow head*)

cells that surround the spicule/lectin bundles (Fig. 2c). SEM analysis of an oocyte shows that its surface is wrinkled (Fig. 2d).

Electron microscopical studies (TEM) reveal that besides oocytes spermatogenic cysts also exit in the branches; one of these is shown in Fig. 3e.

3.2 *L. baicalensis*: Localization of Dinoflagellates and Chlorophyll Content

The accumulation of the dinoflagellates in the surface zone of the branches in *L. baicalensis* can be seen by eye inspection (Fig. 3a). Cross sections through branches from a September specimen show a green approximately 1- to 2-mm-thick zone that lines the surface (Fig. 3b). Also, sections through a winter branch revealed that the surface zone is bright green; however, the internal parts of the branches are also greenish (Fig. 3c).

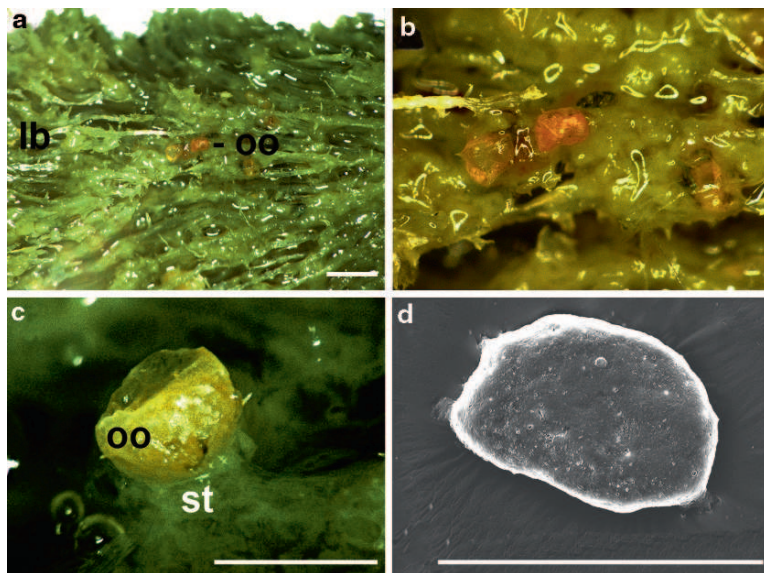


Fig. 2 Oocytes in *L. baicalensis*, formed during the ice-cover season in March (a). The oocytes (oo) are embedded around cells within the longitudinal bundles (lb) (b). Oocytes at higher magnification (c). Oocytes attached in a cavity to a stalk (st) (d) A SEM image of an isolated oocyte

For a more detailed analysis of the dinoflagellates in the tissue, electron microscopical analyses (TEM) were performed (Fig. 3d and e). The dinoflagellates are dominantly present in the outer zone of the branches. They have a round shape with a diameter of approximately 20–40 μm and contain many chloroplasts besides a large central nucleus. For a quantitative assessment of the dinoflagellates in branches from *L. baicalensis* collected in summer and winter, the chlorophyll content was determined. Chlorophyll was determined spectrophotometrically as described under “Materials and Methods.” The March branches had a chlorophyll-*a* content of $3.2 \pm 0.6 \mu\text{g/g}$ of protein, while the content of the September specimens was significant lower ($1.9 \pm 0.5 \mu\text{g/g}$). The content of chlorophyll-*c2* was in general lower; $1.1 \pm 0.3 \mu\text{g/g}$ of protein in March and $0.4 \pm 0.3 \mu\text{g/g}$ in September.

3.3 *L. baicalensis*: Identification of Dinoflagellates

Using the PCR approach mentioned above and primers directed against the rDNA-ITS1-rDNA region, a stretch between 18S rDNA (3'-terminal half of the sequence) via the ITS1 to the 5.8S rDNA (5'-terminal half) was covered. Three sequences, DINO1_LUBAI, DINO2_LUBAI, and DINO2_LUBAI, matching with a high probability score *E* (Coligan et al. 2000) to the dinoflagellates of the taxon *Gymnodinium* have been identified. Highest scores exist to *Gymnodinium sanguineum* (Alveolata; Dinophyceae; Gymnodiniales; Gymnodiniaceae; Gymnodinium; AY831412) with an *E* value of $2 \times e^{-37}$. The sequences of the three *L. baicalensis*

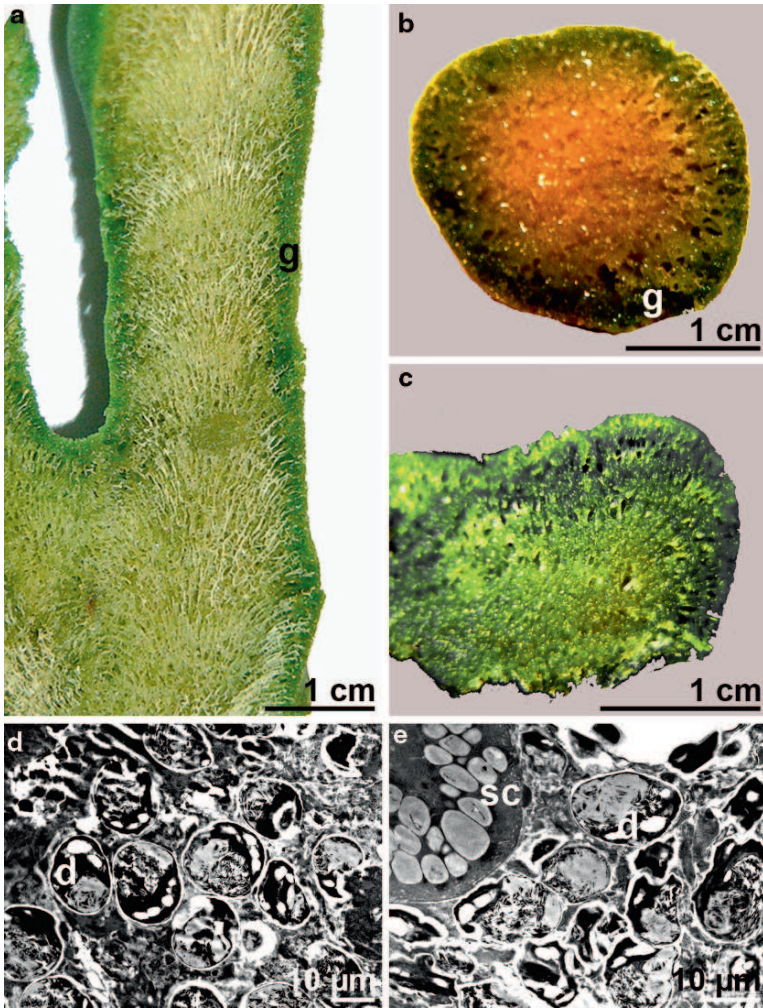


Fig. 3 *L. baicalensis*, and its associated dinoflagellates. (a) Cross section through the longitudinal axis of the branch; the green-colored margin/zone is marked (g). (b) Cross sections through branches from a September specimen; the dinoflagellates are assembled at the rim and turn the tissue green (g). (c) A sections though a winter branch. (d, e) Dinoflagellates associated with the sponge. In the rim zone of the sponge the dinoflagellates (d) are abundantly present. There is also one spermatogenic cyst (sc)

dinoflagellates have been aligned with the corresponding sequence from *G. sanguineum* (Fig. 4a). It is obvious that in the 18S rDNA as well as the 5.8S rDNA regions some differences already exist between the *L. baicalensis* dinoflagellates and *G. sanguineum*. In the ITS1 part, spanning nt₁₅₇ to nt₃₆₇ (in DINO3_LUBAI), the differences are even higher. A phylogenetic tree was constructed (Fig. 4b) which revealed that the three different *L. baicalensis* dinoflagellates are significantly distinct from each other, but all belong to the *Gymnodinium* taxon.

The degree of enrichment of dinoflagellates could also be documented by illuminating the fraction with fluorescence light (Fig. 5e).

From the enriched sponge cells, a primmorph culture was established as described under “Materials and Methods.” Three-day-old primmorphs were used for the experiments (Fig. 5b) and kept in culture flasks (Fig. 5a).

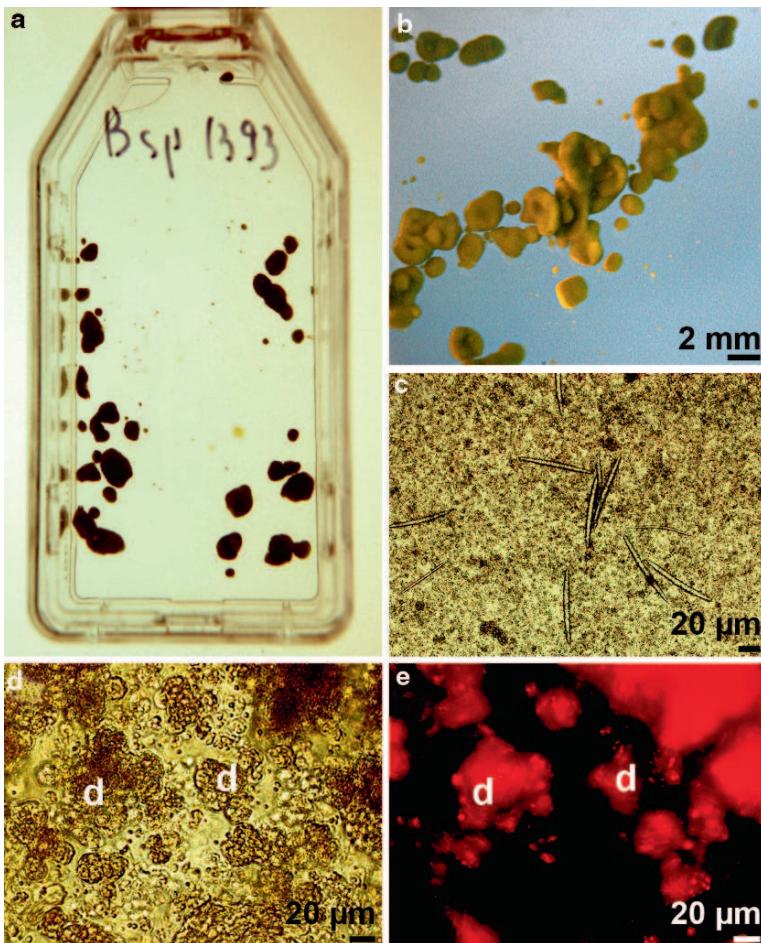


Fig. 5 Primmorph culture cells. (a) Primmorphs were cultivated in 10-ml flasks. (b) These three-dimensional aggregates were obtained from enriched sponge cells after incubation for 2 days. (c) Enriched sponge cells were recovered in the pellet, below the 25% (v/v) Ficoll layer, while (d) the dinoflagellates (d) had been collected on the 15% (v/v) Ficoll layer. (e) Using fluorescence light microscopy the dinoflagellates (d) show a red autofluorescence.

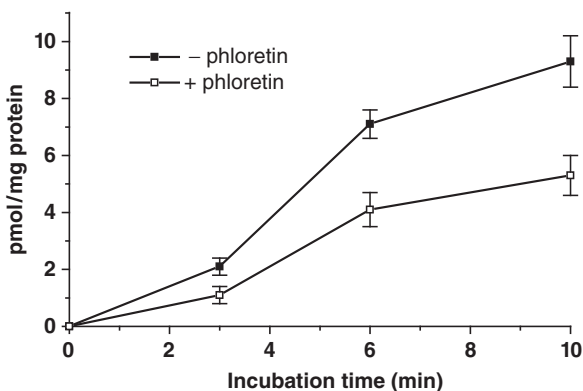


Fig. 6 Glycerol uptake by sponge cells. Primmorphs were incubated with [^{14}C] glycerol for 3–10 min; then the amount of cellular [^{14}C] glycerol was determined as described under “Materials and Methods” (■) and correlated with the amount of protein present in the assays. In one series of experiments, the primmorphs were pretreated with 500 μM of phloretin (□) prior to the addition of [^{14}C] glycerol. The values represent means ($\pm\text{SE}$) of five independent determinations

3.5 Uptake of Glycerol by Sponge Cells

Primmorphs were incubated in the presence of [^{14}C] glycerol for 1–10 min. Then the uptake rates were determined and normalized on the basis of 1 mg of protein. The glycerol uptake within the first 10 min was (almost) linear (Fig. 6); from about 2 pmol/mg (at 3 min) to 10 pmol/mg (at 10 min). Inhibition studies with phloretin, an aquaporin, and L-type Ca^{2+} channel blocker (Gambert et al. 2005) were performed in parallel. Primmorphs were pre-incubated for 10 min with this compound and subsequently incubated with [^{14}C] glycerol for up to 10 min. The results show a decrease of the uptake rate of [^{14}C] glycerol after pretreatment of primmorphs with phloretin by almost 50% (Fig. 6).

3.6 Metabolic Studies in Primmorphs Using Molecular Tools

As molecular tools applicable for the determination of the response of sponge cells to cholesterol, a series of the EST sequences from the *L. baicalensis* EST library were selected. These sequences are not only useful to monitor the effect of cholesterol on the steady-state expression level in Northern blots, but also to clarify whether these sequences are indeed sponge-related and not dinoflagellate-derived.

The following sequences were analyzed: the citrate synthase, an enzyme which catalyzes the condensation of oxalacetate and acetyl CoA, and is the entrance enzyme of the citric acid cycle (Fig. 7a); the fructose-1,6-bisphosphatase, a key

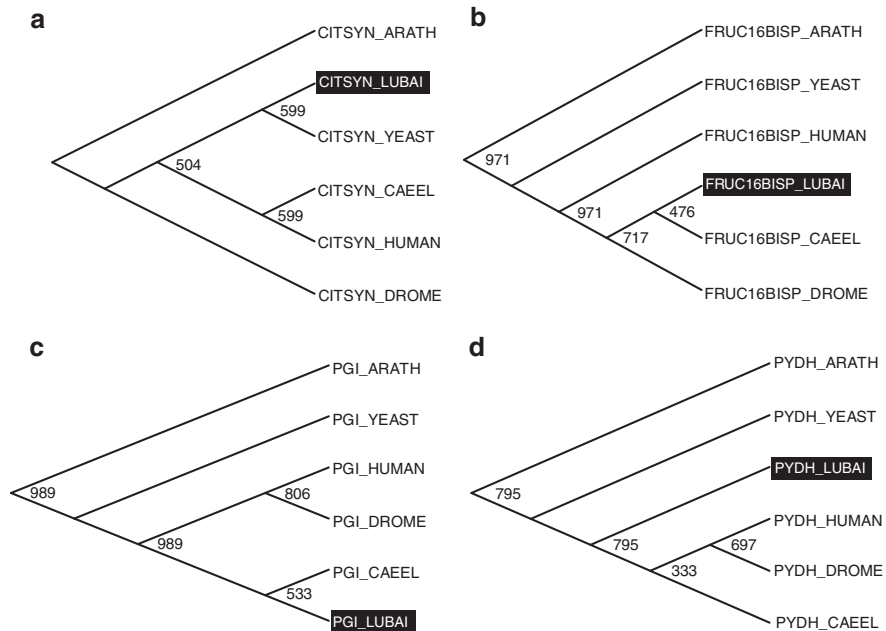


Fig. 7 Sequence relationships of the *L. baicalensis* deduced proteins to sequences, related to other metazoans as well as to the yeast (*S. cerevisiae*) and the plant (*A. thaliana*). (a) Citrate synthase. The following citrate synthase sequences were selected for the alignment of the sponge sequence (CITSYN_LUBAI) and the subsequent construction of the phylogenetic tree: from human (CITSYN_HUMAN; AAP36082.1), *D. melanogaster* (CITSYN_DROME; AAL39405.1), *C. elegans* (CITSYN_CAEL; CAA83004.1), *S. cerevisiae* (CITSYN_YEAST; CAA80781.1) and *A. thaliana* (CITSYN_ARATH; CAB75925.1). (b) Fructose-1,6-bisphosphatase, with the following sequences: from *L. baicalensis* (FRUC16BISP_LUBAI), human (FRUC16BISP_HUMAN; AAA35517.1), *D. melanogaster* (FRUC16BISP_DROME; CG31692-PA), *C. elegans* (FRUC16BISP_CAEL; CAB69047.1), *S. cerevisiae* (FRUC16BISP_YEAST; CAA68723.1) and *A. thaliana* (FRUC16BISP_ARATH; AC009526_2). (c) Cytosolic phosphoglucose isomerase. From *L. baicalensis* (PGI_LUBAI), human (PGI_HUMAN; AAH06342.4), *D. melanogaster* (PGI_DROME; AAA28803.1), *C. elegans* (PGI_CAEL; CAE54920.1), yeast (PGI_YEAST; CAA32158.1) and plant (PGI_ARATH; BAB17639.1). (d) Pyruvate dehydrogenase. The sponge protein (PYDH_LUBAI) was compared with the corresponding proteins from human (PYDH_HUMAN; P11177), *D. melanogaster* (PYDH_DROME; AAK77305.1), *C. elegans* (PYDH_CAEL; AAB92024.2), *S. cerevisiae* (PYDH_YEAST; CAA85184.1) and *A. thaliana* (PYDH_ARATH; AAA52225.1). After alignment the sequences were rooted (slanted) using the plant sequences as outgroups

enzyme of the gluconeogenesis (Fig. 7b); the cytosolic phosphoglucose isomerase which converts glucose 6-phosphate to fructose 6-phosphate at the beginning of the glycolysis pathway (Fig. 7c); and finally the pyruvate dehydrogenase, the enzyme which links the glycolysis pathway with the citric acid cycle (Fig. 7d).

Prior to the application of these sequences for expression studies in Northern blots, phylogenetic trees were constructed to assess the phylogenetic relationships of the sponge-derived genes to the most similar molecules from human

(Deuterostomia), *D. melanogaster*, *C. elegans* (Protostomia) and the yeast *S. cerevisiae* as well as to the plant *A. thaliana*. The sponge citrate synthase was found to share a common sequence ancestry with the yeast and the metazoan molecules (Fig. 7a). With respect to the fructose-1,6-bisphosphatase, the sponge sequence has a significant relationship to the metazoan sequences from *C. elegans*, *D. melanogaster* and human (Fig. 7b). The cytosolic phosphoglucose isomerase likewise shares a high sequence similarity to the other metazoan molecules selected (Fig. 7c). Finally, the pyruvate dehydrogenase again shares with the other metazoan molecules a common ancestor molecule (Fig. 7d). From these comparisons it appears to be highly likely that the sequences selected here are from the sponge host and not from the dinoflagellates.

These cDNA sequences were subsequently applied to assess the steady-state expression of genes encoding key enzymes in the intermediary metabolism. RNA was isolated from primmorphs and analyzed by Northern blotting. In the absence of glycerol the expression of citrate synthase (using *LUBAICITSYN* as a probe) and fructose-1,6-bisphosphatase (*LUBAIFRUC16BISP*) was low, while the expression level of phosphoglucose isomerase (*LUBAIPGI*) and pyruvate dehydrogenase (*LUBAIPYDH*) was comparably higher. However, if the primmorphs were incubated with 100 μ M of glycerol for 24h, the expression of both the *citrate synthase* (transcript size of 1.7kb) and the *fructose-1,6-bisphosphatase* (1.3 kb) increased by 2.5-fold and 4-fold, respectively (Fig. 8). In contrast, the transcript level of

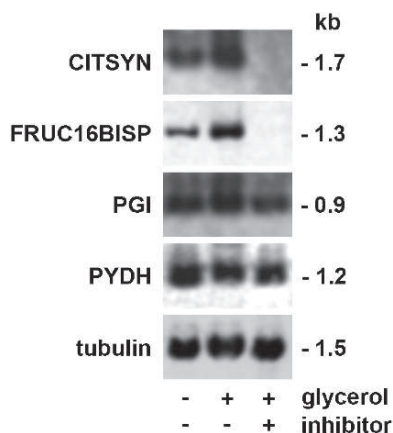


Fig. 8 Expression of the genes encoding citrate synthase (*LUBAICITSYN*), fructose-1,6-bisphosphatase (*LUBAIFRUC16BISP*), phosphoglucose isomerase (*LUBAIPGI*) and pyruvate dehydrogenase (*LUBAIPYDH*) in primmorphs. The primmorphs were incubated for 24h either in the absence (*-glycerol*) or the presence of glycerol (*+glycerol*). In a further series of experiments, the glycerol-treated primmorphs were additionally treated with the aquaporin channel inhibitor phloretin, as described under "Materials and Methods." Then, total RNA was fractionated by electrophoresis, transferred to nylon membrane, and hybridized with the respective labeled probes. After blot transfer, the filters were probed with *LUBAICITSYN*, *LUBAIFRUC16BISP*, *LUBAIPGI*, *LUBAIPYDH*, and also with *tubulin* to verify that the same amounts of RNA had been loaded onto the gels

the *phosphoglucose isomerase* (0.9 kb) and the *pyruvate dehydrogenase* (1.2 kb) remained almost unchanged (Fig. 8). In order to ensure that the same amounts of RNA had been loaded onto the gels, the α -tubulin cDNA was used as a control; the transcript size is 1.5 kb.

The modulation of the expression level was abolished if the aquaporin inhibitor phloretin was co-administered with glycerol. In the presence of phloretin, the expression of *citrate synthase* and of *fructose-1,6-bisphosphatase* was completely blocked (Fig. 8). The effect of this compound on the transcript level of *phosphoglucose isomerase* and *pyruvate dehydrogenase* was negligible.

3.7 *L. baicalensis* Aquaporin

The complete sponge aquaporin cDNA was identified by PCR from the sponge cDNA library. It comprises a length of 1,248 nts. This sequence contains one open reading frame from nt_{178/180} to nt_{1120/1122 (stop)}. The deduced 314 aa long protein (AQP_r_LUBAI; Fig. 9a) has a calculated size of 34,215 Da. Motif scan analysis revealed that it comprises the following characteristic domains for aquaporins. First, the major intrinsic protein (MIP) domain. This signature is found in a series of transmembrane channel proteins (Chrispeels and Agre 1994) and is highly conserved between plant and animal aquaporins. The MIP family proteins contain six transmembrane segments, which are found in the sponge protein at the following sites; #1 at: aa₄₄ to aa₇₅, #2 at: aa₈₀ to aa₁₀₁, #3 at: aa₁₂₆ to aa₁₄₄, #4 at: aa₁₇₈ to aa₂₀₀, #5 at: aa₂₁₄ to aa₂₂₉ and #6 at: aa₂₆₈ to aa₂₉₁ (Fig. 9a). More specific is the aquaporin family consensus (AQPfam) which exists between aa₃₉ to aa₂₉₄. Finally, two further conserved motifs, found also in other mammalian aquaporins (Ishibashi et al. 1997), are also marked in Fig. 9a; they are located between transmembrane segments two and three in the cytosolic region of the molecule (between aa₁₀₄ to aa₁₀₆) and in the outside loops between transmembrane segments five and six (aa₂₃₁ to aa₂₄₈).

A phylogenetic tree was constructed with related aquaporin sequences from the data banks (Fig. 9b). The greatest similarity of the *L. baicalensis* aquaporin exists with the related genes from vertebrates, human (Ishibashi et al. 1998), and fish (*Danio rerio*), as well as from chicken (*Gallus gallus*) and frog (*Xenopus tropicalis*). The branches comprising the vertebrate and the sponge sequences share a common ancestor and are separated from the protostomians *D. melanogaster* and *C. elegans* and also from a yeast (*S. cerevisiae*) and a plant (*A. thaliana*) (Fig. 9b).

3.8 Expression of Aquaporin

To support the assumption that aquaporin is expressed in those cells which surround the dinoflagellates, in situ hybridization studies were performed. The identified

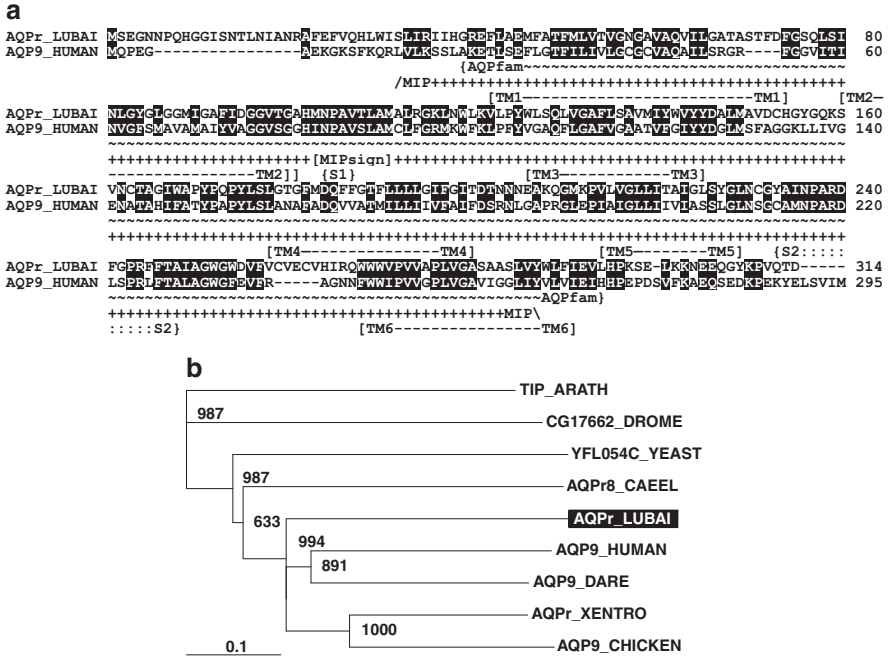


Fig. 9 Aquaporin-related protein in *L. baicalensis*. **(a)** Alignment of the sponge aquaporin-related protein from the sponges (*L. baicalensis*; AQP_r_LUBAI) with the human aquaporin 9 (AQP9_HUMAN, accession number BAA24864; Ishibashi et al. 1998). The characteristic domains within the deduced sponge protein are marked; the major intrinsic protein (MIP) domain [/MIP], including the MIP signature [MUPsign] and the aquaporin family consensus [AQPfam]. Amino acids, similar among the sequences, are in inverted type. The borders of the six transmembrane regions within the deduced sponge protein are marked [TM--TM]. In addition, the two characteristic domains for aquaporins are highlighted {S1/2}. **(b)** Phylogenetic tree is constructed from the two sequences as well as the aquaporin(-related) sequences from *D. rerio* (aquaporin 9, AQP9_DARE, XP_698806), *G. gallus* (aquaporin 7, AQP9_CHICKEN XP_424498), *X. tropicalis* (MGC107875 protein, AQP_r_XENTRO, NP_001015726), *C. elegans* (aquaglyceroporin related protein 8, isoform b, AQP_r8_CAEEL, AAP68935), *D. melanogaster* (deduced protein CG17662-PA, CG17662_DROME, AAF47035), *S. cerevisiae* (deduced protein YFL054C, YFL054C_YEAST, BAA09187.1) and *A. thaliana* (delta tonoplast integral protein, TIP_ARATH, AAC49281). After alignment the tree was built. Scale bar indicates an evolutionary distance of 0.1 aa substitutions per position in the sequence

aquaporin cDNA was used as a probe. Because *L. baicalensis* tissue is extensively traversed by bundles of spicules, most of the slices broke. Nevertheless, the distribution of the signals accumulated in those cells hybridized with the antisense *aquaporin* probe (Fig. 10b, d and f), which did not show the red fluorescence, originating from the dinoflagellates (Fig. 10a, c and e). No reaction could be observed if the sense *aquaporin* probe was used (not shown).

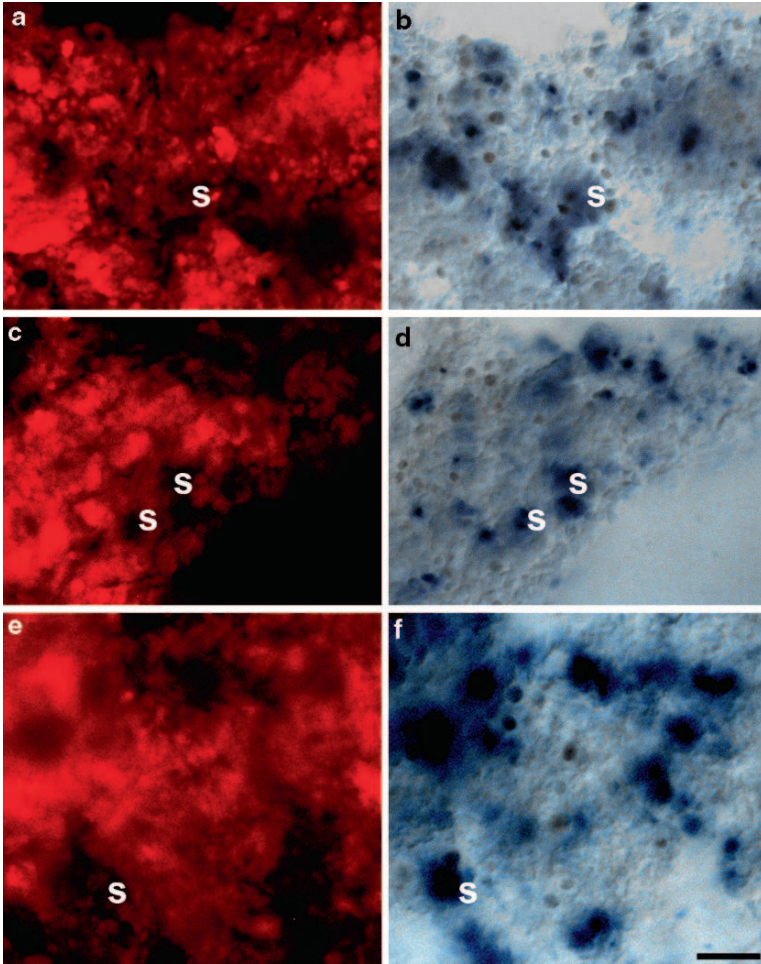


Fig. 10 In situ hybridization analysis applying the antisense probe for aquaporin (*LBAQPr*). (**b**, **d**, and **f**) Sections through tissue were prepared, fixed, treated with Proteinase K and subsequently fixed again with paraformaldehyde. After rehydration the sections were hybridized with the labeled probe. (**a**, **c**, and **e**) In parallel, the slices were inspected by fluorescence light to visualize the chlorophyll-containing dinoflagellates, which appear in *red*. The sponge cells (*s*) become stained with the antisense probe in (**b**, **d**, and **f**), while those areas remained unstained at fluorescent light (**a**, **c** and **e**)

4 Discussion

The Baikalian sponge *L. baicalensis* is an appropriate model to study the interaction between microorganisms and their host, in order to obtain some information on the supply and translocation of primary metabolites from dinoflagellates to

their sponge host. *L. baicalensis* lives throughout the year at ambient temperatures between -0.5°C (March) and 12°C (September) without forming any asexual survival bodies, e.g., buds or gemmules. For marine sponges, it is known that such tissue regression capsules are formed specially to survive extreme physiological and ecological periods (Simpson 1984). Hence, for the Baikalian *L. baicalensis*, it must be postulated that they are provided with some efficient mechanisms to survive these adverse environmental (temperature) conditions. Even more surprising was the finding that during the cold period in March (-0.5°C) these sponges produce sexual reproduction bodies. We could identify oocytes in great abundance in branches of *L. baicalensis* during this season, even by eye inspection. Applying the TEM technique it could be demonstrated that besides the oocytes spermatogenic cysts also exist in the branches. The structures of these cysts are identical to those known from other sponge species, included marine ones (Diaz 1979; Simpson 1984).

To the best of our knowledge it has not been previously described that *L. baicalensis* forms eggs and sperm cells twice a year. While it is well established that during the late summer season egg formation is very frequently observed it was surprising to see that the specimens also form very abundant eggs, in March under the ice cover, at an ambient temperature of -0.5°C . This finding can be explained by the fact that diatoms, which are ingested by the sponge as food (see Kozhova and Izmesteva 1998), also reach greatest abundance during this period (Kozhov 1963). At the end of March, the diatom algae *Melosira baicalensis* and *M. islandica* are dominant, while in September the growth of the species *Cyclotella baicalensis* culminates. Moreover, the oxygen content in Lake Baikal is higher during the ice-cover period than in late summer (Kozhov 1963). This fact together with the high pumping rate (Savarese et al. 1997) supports the supply of oxygen required for the intermediate metabolism. Furthermore, the high abundance of zoochlorellae/dinoflagellates (as shown here) present in the specimens during the ice-cover period observed in the middle of March (under the ice cover) parallels the high transparency of the water and reaches the same values as in September. In both seasons, winter and summer, *L. baicalensis* specimens are characterized by their green appearance. This color has to be attributed to the photosynthetic organisms, zoochlorellae/zooxanthellae (see Kozhova and Izmesteva 1998), and, as shown in the present study, to the dinoflagellates. Using the chlorophyll content as a measure of the abundance of the dinoflagellates, quantitative determinations were performed. It was found that in March the content of both chlorophyll-*a* and chlorophyll-*c2* was higher than in the September samples, suggesting that the abundance of the dinoflagellates is higher during the ice-cover period. This spectrophotometric determination could also be confirmed by eye inspections of the branches. In March, the branches are greenish-colored throughout, while in September only a 2-mm-wide rim has this bright green appearance.

To obtain information about the photosynthetic species harbored by *L. baicalensis*, their 18S and 5.8S rDNA regions together with ITS1 segment were amplified and subjected to the data bases. Based on subsequent sequence comparisons, the highest sequence identity was found with the dinoflagellates from the taxon *Gymnodinium*; more specific to *G. sanguineum*. This dinoflagellate is found worldwide, especially in coastal waters (Steidinger and Tangen 1996). It has been

described that this dinoflagellate species is one component of harmful algal blooms and it has been designated as hemolytic and ichthyotoxic (Garcia-Hernández et al. 2005). Hence, this observation might also have a further implication for the symbionts of the Baikalian sponges, by having the potential to be harmful for some animals living in the Lake. First results with antibodies (Wiens et al. 2003) directed against the toxin okadaic acid revealed that *L. baicalensis* contains this diarrhetic shellfish poison (to be published).

Only a few entrance sites for potential high calorie metabolites from symbionts to a host exist. Firstly, via sugar, preferentially glucose. Through this route sugar can be metabolized in the glycolysis and then in citric acid cycle to reach the respiratory chain for generating ATP. In parallel, sugar can be stored in glycogen. Secondly, via amino acids, e.g., glutamine, which enter the citric acid cycle providing the substrate hydrogen for the respiratory chain. And thirdly, via glycerol. These three routes are also used for parenteral nutrition of human patients (Kong et al. 2000; Zaloga 2006). The additionally required vitamins are likewise delivered by photosynthetic organisms or by microorganisms.

Glycerol holds a central position for delivery of nutrients (Stryer 1995) (Fig. 11). Glycerol can readily enter the glycolysis via the enzymic conversion to glycerol 3-phosphate and dihydroxyacetone phosphate. Fructose-1, 6-bisphosphatase is one key regulatory enzyme required for gluconeogenesis. The enzyme cytosolic phosphoglucose isomerase mediates the reversible conversion of six-membered pyranoses (glucose) to five-membered furanoses (fructose) and is, in vertebrates, not under strong gene expression control. Through the glycolysis, the energy supplying pathways, citric acid cycle, and respiratory chain are linked via the citrate synthase. This protein, which forms citrate, is the key initiator enzyme for the citric acid cycle. Finally, the pyruvate dehydrogenase, which is part of a multienzyme complex, is likewise under allosteric and not under genetic control, and forms the substrate for the citric acid cycle, acetyl CoA.

The steady-state expression level of these four enzymes of the intermediary metabolism (citrate synthase, fructose-1,6-bisphosphatase, phosphoglucose isomerase, and pyruvate dehydrogenase) have been determined by Northern blotting. As molecular probes, the EST cDNAs have been used. The studies revealed that the genes for the two enzymes, citrate synthase and fructose-1,6-bisphosphatase, whose expression in vertebrates is also under genetic control, become strongly upregulated in primmorphs treated with glycerol. In contrast, the two other genes, phosphoglucose isomerase and pyruvate dehydrogenase, coding for enzymes which are primarily not under genetic control, do not respond to glycerol treatment. Interestingly enough, the inhibitor of the aquaporin transport system and of L-type Ca^{2+} channels, phloretin (Gambert et al. 2005), completely abolished the expression of the *citrate synthase* and *fructose-1,6-bisphosphatase* genes. From these expression studies, we conclude that glycerol causes in primmorphs an upregulation of those genes which are controlling gluconeogenesis and citric acid cycle. Even more, they indicate that glycerol enters the sponge cells via an aquaporin transport system.

Based on the results that the cholesterol-mediated upregulation of the genes for *citrate synthase* and *fructose-1,6-bisphosphatase* in primmorphs is inhibited

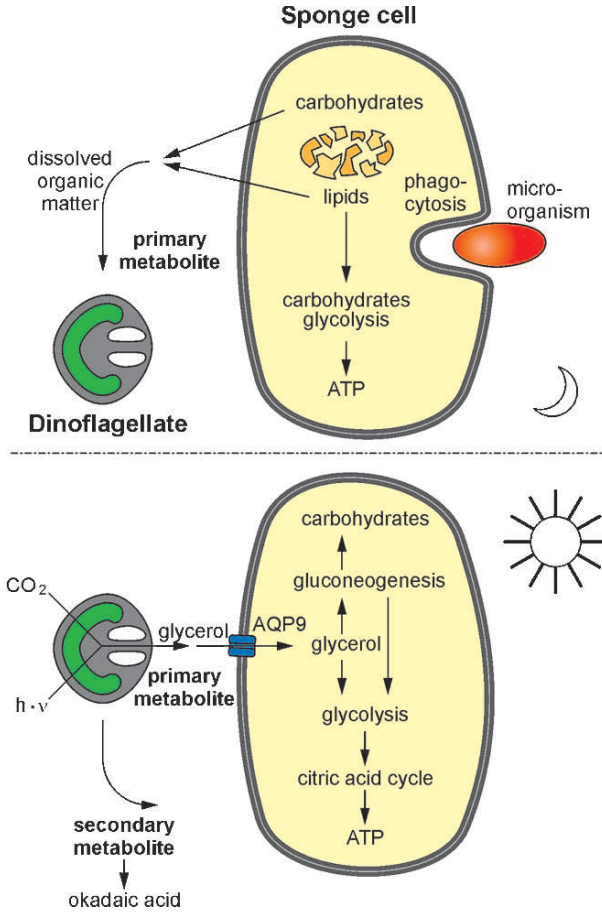


Fig. 11 Proposed symbiotic relationship between sponge cells and dinoflagellates. (*Upper*) At night, at low light intensities, the dinoflagellates are not able to synthesize organic carbon sources for their host. It is suggested that during this period the sponge cells have to rely only on their own metabolic activity; bacteria will be the prime source of organic material. Very likely they release dissolved organic matter which can be utilized by the dinoflagellates (*Lower*) At higher illumination conditions, the dinoflagellates are able to produce organic materials, among those also glycerol. Glycerol is taken up by the sponge cells and converted in the pathways of glycolysis/citric acid and gluconeogenesis for energy production

by the inhibitor of the aquaporin transport system and of L-type Ca²⁺ channels, phloretin, we screened for the presence of the respective gene in the cDNA library of *L. baicalensis*. We especially screened for aquaporin-9 since this channel is known to be a port for glycerol, urea, and a variety of other small uncharged osmolytes (Borgnia et al. 1999; Badaut and Regli 2004). The full-length cDNA for aquaporin-9 was identified and cloned from *L. baicalensis*. The sequence shares the characteristic aquaporin sites with their six transmembrane segments; more specifically, the major intrinsic protein domain, the two further conserved motifs,

comprising within the transmembrane segment two and three in the cytosolic region the Asn-Pro-Ala signature, and between transmembrane segments five and six the Asn-Pro-Ala signature (Borgnia et al. 1999).

After cloning of the *aquaporin-9* gene from *L. baicalensis*, this cDNA was used as a probe to localize the existence of aquaporin-9 transcripts in the sponge tissue. This approach revealed that the cells which surround the dinoflagellates become brightly stained with the labeled antisense probe. This finding – together with the cholesterol uptake inhibition studies – strongly suggests that the existing aquaporin-9 channel in sponge cells, flanking the dinoflagellates, is also involved in glycerol uptake.

Based on these presented data together with the previously reported studies, we conclude that the freshwater sponge *L. baicalensis* is symbiotically associated with dinoflagellates, of the taxon *Gymnodinium*, which produce glycerol via their photosynthetic pathways from carbon dioxide in the presence of light (Fig. 11). This primary metabolite is subsequently taken up by the sponge cell via the aquaporin-9 channel. Glycerol enters the gluconeogenesis to form carbohydrates; in turn, these carbohydrates are fed into the glycolysis and enter the citric acid cycle resulting in the generation of substrate hydrogen. The latter component is channeled into the respiratory chain to generate ATP. No information is available on what advantage the dinoflagellates are provided with by the sponge. It might be proposed that the sponges, as the dominant organism in the littoral zone of Lake Baikal, are the niches where the dinoflagellates can proliferate. In addition, it can be speculated that the sponge cells supply the dinoflagellates with carbohydrates and lipids during the night phase (Fig. 11). From previous studies, it is well established that *L. baicalensis* is a highly active filter feeder (Pile et al. 1997) which engulfs bacteria and fungi (Gil et al. 1997). The property of sponge cells to phagocytose microorganisms has been well established since the studies of Metchnikoff (1892). Furthermore, the potential role of the secondary metabolite okadaic acid as a defense substance needs to be studied in the future.

In conclusion, the presented data show that the endemic sponge *L. baicalensis* lives in a mutual symbiotic relationship with dinoflagellates. There was a surprising finding that these sponges are highly active and also produce eggs during the winter ice-cover period. This high metabolic activity of the sponge during the winter season is – according to the presented data – crucially dependent on the transfer of glycerol from the dinoflagellates to the host sponge cells. Future studies will be undertaken to identify the potential symbionts of those endemic sponges in Lake Baikal which live at a depth below 30 m, e.g., *B. intermedia*; this field is – at present – completely unknown.

Acknowledgements We thank Academician Dr. Michael A. Grachev and Dr. Yelena V. Likhoshway (Limnological Institute, Irkutsk; Russia) very much for very important discussions. This work was supported by grants from the Bundesministerium für Bildung und Forschung Germany (projects: Joint German-Russian Laboratory for Biology of Sponges at the Limnological Institute RAS in Irkutsk; and Center of Excellence *BIOTECmarin*), the European Commission, the Deutsche Forschungsgemeinschaft and the International Human Frontier Science Program; as well as by a grant from the Presidium of the Russian Academy of Science (no. 25.5) and from RFBR (no. 03-04-4985).

References

- Badaut J, Regli L (2004) Distribution and possible roles of aquaporin-9 in the brain. *Neuroscience* 129:971–981
- Baillie BK, Belda-Baillie CA, Maruyama T (2000) Conspecificity and Indo-Pacific distribution of *Symbiodinium* genotypes (Dinophyceae) from giant clams. *J Phycol* 36:1153–1161
- Borgnia M, Nielsen S, Engel A, Agre P (1999) Cellular and molecular biology of the aquaporin water channels. *Annu Rev Biochem* 68:425–458
- Chrispeels MJ, Agre P (1994) Aquaporins: water channel proteins of plants and animal cells. *Trends Biochem. Sci.* 19, 421–425
- Coligan JE, Dunn BM, Ploegh HL, Speicher DW, Wingfield PT (2000) Current protocols in protein science. Wiley, Chichester, pp 2.0.1–2.8.17
- Corsetti FA, Olcott AN, Bakerman C (2006) The biotic response to Neoproterozoic snowball Earth. *Palaogeog Palaeoclimat Pataeoecol* 232:114–130
- Diaz JP (1979) Variations, différenciations et fonctions des catégories cellulaires de la demosponge *Suberites massa* Nardo, au cours du cycle biologique annuel et dans des conditions expérimentales. Thèse de Université de Sciences et Technique Languedoc, pp 1–332
- Efremova SM (1981) The structure and embryonal development of the Baikalian sponge *Lubomirskia baicalensis* (Pallas) and relationships of Lubomirskiidae with other sponges. In: Morphogenesis in sponges. State University, Leningrad, pp 93–107
- Felsenstein J (1993) PHYLIP, ver. 3.5. University of Washington, Seattle
- Friedrich AB, Fischer I, Proksch P, Hacker J, Hentschel U (2001) Temporal variation of the microbial community associated with the Mediterranean sponge *Aplysina aerophoba*. *FEMS Microbiol Ecol* 38:105–113
- Gambert S, Héliès-Toussaint C, Grynberg A (2005) Regulation of intermediary metabolism in rat cardiac myocyte by extracellular glycerol. *Biochim Biophys Acta* 1736:152–162
- García-Hernández J, García-Rico L, Jara-Marini ME, Barraza-Guardado R, Weaver AH (2005) Concentration of heavy metals in sediment and organisms during a harmful algal bloom (HAB) at Kun Kaak Bay, Sonora, Mexico. *Marine Poll Bull* 50:733–739
- Gil TA, Kazarinova TF, Hramtsova TG, Zaitsev IV, Stom DJ (1997) The consumption of microorganisms by the Baikal sponge. *Fresenius Environ Bull* 6:444–449
- Gonzales JM, Moran MA (1997) Numerical dominance of a group of marine bacteria in the alpha-subclass of the class *Proteobacteria* in coastal seawater. *Appl Environ Microbiol* 63:4237–4242
- Gorin MB, Yancey SB, Cline J, Revel JP, Horwitz J (1984) The major intrinsic protein (MIP) of the bovine lens fiber membrane: characterization and structure based on cDNA cloning. *Cell* 39:49–59
- Ishibashi K, Kuwahara M, Gu Y, Kageyama Y, Tohsaka A, Suzuki F, Marumo F, Sasaki S (1997) Cloning an functional expression of a new water channel abundantly expressed in the testis permeable to water, glycerol, and urea. *J Biol Chem* 272:20782–20786
- Ishibashi K, Kuwahara M, Gu Y, Tanaka Y, Marumo F, Sasaki S (1998) Cloning and functional expression of a new aquaporin (AQP9) abundantly expressed in the peripheral leukocytes permeable to water and urea, but not to glycerol. *Biochem Biophys Res Commun* 244:268–274
- Jeffrey SW, Humphrey, GF (1975) New spectrophotometric equations for determining chlorophyll a, b, c1, and c2 in higher plants, algae, and natural phytoplankton. *Biochem Physiol Pflanzen* 17:191–194
- Kennish MJ (1994) Practical handbook of marine science. CRC Press, Boca Raton, IL
- Kong SE, Hall JC, Cooper D, McCauley RD (2000) Glutamine-enriched parenteral nutrition regulates the activity and expression of intestinal glutaminase. *Biochim Biophys Acta* 1475:67–75
- Kozhov M (1963) Lake Baikal and its life. W. Junk, The Hague
- Kozhova OM, Izmesteva LR (1998) Lake Baikal: evolution and biodiversity. Brackhys, Leiden
- Masuda Y, Itskovich VB, Veinberg EV, Efremova SM (1997) Studies on the taxonomy and distribution of freshwater sponges in the Lake Baikal. In: Miyzaki N (ed) Animal community, environment and phylogeny in Lake Baikal. Otsuchi Marine Center/Ocean Research Institute, Tokyo, pp 21–41

- Metchnikoff E (1892) Lecons sur la pathologie comparée de l'inflammation. G Masson, Paris
- Müller WEG (2001) How was metazoan threshold crossed: the hypothetical Urmetazoa. *Comp Biochem Physiol [A]* 129:433–460
- Müller WEG, Zahn RK, Kurelec B, Müller I, Uhlenbruck G, Vaith P (1981) Cell aggregation of the marine sponge *Geodia cydonium*. Identification of the lectin-producing cells. *Eur J Cell Biol* 24:28–35
- Müller WEG, Wiens M, Batel R, Steffen R, Borojevic R, Custodio MR (1999) Establishment of a primary cell culture from a sponge: primmorphs from *Suberites domuncula*. *Marine Ecol Progr Ser* 178:205–219
- Müller WEG, Kozioł C, Wiens M, Schröder HC (2000) Stress response in marine sponges: genes and molecules involved and their use as biomarkers. In: Storey KB, Storey J (eds) *Environmental stressors and gene responses*. Elsevier Science, Amsterdam, pp 193–208
- Pao GM, Wu LF, Johnson KD, Höfte H, Chrispeels MJ, Sweet G, Sanda, NN, Saier MH (1991) Evolution of the MIP family of integral membrane transport proteins. *Mol Microbiol* 5:33–37
- Park JH, Saier MH (1996) Phylogenetic characterization of the MIP family of transmembrane channel proteins. *J Membr Biol* 153:171–180
- Pawlowski J, Holzmann M, Fahrni JF, Pochon X, Lee JJ (2001) Molecular identification of algal endosymbionts in large miliolid Foraminifera. 2. Dinoflagellates. *J Eukaryot Microbiol* 48:368–373
- Perović S, Schröder HC, Sudek S, Grebenjuk VA, Bate, R, Štifanić M, Müller IM, Müller WEG (2003) Expression of one sponge *Iroquois* homeobox gene in primmorphs from *Suberites domuncula* during canal formation. *Evol Dev* 5:240–250
- Perović-Ottstadt S, Adell T, Proksch P, Wiens M, Korzhev M, Gamulin V, Müller IM, Müller WEG (2004) A (1→3)- β -D-glucan recognition protein from the sponge *Suberites domuncula*: mediated activation of fibrinogen-like protein and epidermal growth factor gene expression. *Eur J Biochem* 271:1924–1937.
- Pile AJ, Patterson MR, Savarese M, Chernykh VI, Fialkov VA (1997) Trophic effects of sponge feeding within Lake Baikal's littoral zone. 2. Sponge abundance, diet, feeding efficiency, and carbon flux. *Limnol Oceanogr* 42:178–184
- Proksch P (1994) Defensive role for secondary metabolites from marine sponges and sponge-feeding nudibranchs. *Toxicon* 32:639–655
- Rao J, Argos P (1986) A conformational preference parameter to predict helices in integral membrane proteins. *Biochem Biophys Acta* 869:197–214
- Reiswig HM (1974) Water transport, respiration and energetics of three tropical marine sponges. *J Exp Mar Biol Ecol* 14:231–249
- Reitner J, Wörheide G (2002) Non-lithistid Demospongiae – origins of their palaeobiodiversity and highlights in history of preservation. In: Hooper JNA, Van Soest RWM (eds) *Systema Porifera: a guide to the classification of sponges*. Kluwer/Plenum, New York, pp 52–70
- Reizer J, Reizer A, Saier MH (1993) The MIP family of integral membrane channel proteins: sequence comparisons, evolutionary relationships, reconstructed pathway of evolution, and proposed functional differentiation of the two repeated halves of the proteins. *Crit Rev Biochem Mol Biol* 28:235–257
- Saitou N, Nei M (1987) Neighbor-joining method: a new method for reconstructing phylogenetic trees. *Mol Biol Evol* 4:406–425
- Savarese M, Patterson MR, Chernykh VI, Fialkov VA (1997) Trophic effects of sponge feeding within Lake Baikal's littoral zone. 1. In situ pumping rate. *Limnol Oceanogr* 42:171–178
- Schäcke H, Müller IM, Müller WEG (1994) Tyrosine kinase from the marine sponge *Geodia cydonium*: the oldest member belonging to the receptor tyrosine kinase class II family. In: Müller WEG (ed) *Use of aquatic invertebrates as tools for monitoring of environmental hazards*. Gustav Fischer Verlag, Stuttgart, pp 201–211
- Schröder HC, Perović-Ottstadt S, Grebenjuk VA, Engel S, Müller IM, Müller WEG (2005) Biosilica formation in spicules of the sponge *Suberites domuncula*: synchronous expression of a gene cluster. *Genomics* 85:666–678

- Simpson TL (1984) The cell biology of sponges. Springer-Verlag, New York
- Steidinger, K.A, Tangen K (1996) Dinoflagellates. In: Tomas CR (ed) Identifying marine diatoms and dinoflagellates. Academic, San Diego, CA, pp 387–584
- Stryer L (1995) Biochemistry. Freeman, New York
- Thakur NL, Müller WEG (2005) Sponge-bacteria Association: a useful model to explore symbiosis in marine invertebrates. *Symbiosis* 39:109–116.
- Thakur NL, Perović-Ottstadt S, Batel R, Korzhev M, Diehl-Seifert B, Müller IM, Müller WEG (2005) Innate immune defense of the sponge *Suberites domuncula* against gram-positive bacteria: induction of lysozyme and AdaPTin. *Marine Biology* 146:271–282
- Thompson JD, Higgins DG, Gibson TJ (1994) CLUSTAL W: improving the sensitivity of progressive multiple sequence alignment through sequence weighting, positions-specific gap penalties and weight matrix choice. *Nucleic Acids Res* 22:4673–4680
- Vacelet J (1971) Étude en microscopie électronique de l'association entre une cyanophyceae chroococcale et une éponge du genre *Verongia*. *J Microsc* 12:363–380
- Wiens, M, Müller WEG (2006) Cell death in Porifera: molecular players in the game of apoptotic cell death in living fossils. *Can J Zool/Rev Can Zool* 84:307–321
- Wiens M, Luckas B, Brümmer F, Ammar MSA, Steffen R, Batel R, Diehl-Seifert B, Schröder H C, Müller WEG (2003) Okadaic acid: a potential defense molecule for the sponge *Suberites domuncula*. *Marine Biol* 142:213–223
- Wiens M, Korzhev M, Krasko A, Thakur NL, Perović-Ottstadt S, Breter HJ, Ushijima H, Diehl-Seifert B, Müller IM, Müller WEG (2005) Innate immune defense of the sponge *Suberites domuncula* against bacteria involves a MyD88-dependent signaling pathway: induction of a perforin-like molecule. *J Biol Chem* 280:27949–27959
- Wiens M, Belikov SI, Kaluzhnaya OV, Krasko A, Schröder HC, Perovic-Ottstadt S, Müller WEG (2006) Molecular control of serial module formation along the apical-basal axis in the sponge *Lubomirskia baicalensis*: silicateins, mannose-binding lectin and mago nashi. *Dev Genes Evol* 216:229–242
- Wilkinson CR (1992) Symbiotic interactions between marine sponges and algae. In: Reisser W (ed) Algae and symbioses: plants, animals, fungi, viruses, interaction explored. Biopress, Bristol, pp 111–151
- Zaloga GP (2006) Parenteral nutrition in adult inpatients with functioning gastrointestinal tracts: assessment of outcomes. *Lancet* 367:1101–1111

Silicon in Life: Whither Biological Silicification?

Christopher Exley

1	Life Is Permeable to Silicic Acid	174
2	The Non-selection of Silicon	175
3	Diatoms and Sophisticated Silicic Acid Homeostasis	178
4	Conclusions	182
	References	183

Abstract In my opinion, the last decade or so has seen a golden era of research into the many facets of biological silicification. The contents of this volume are testimony to recent advances in the field (Müller and Grachev 2008). The successes should be carried through into the next 10 years during which time the processes involved in the biomineralisation of silica ought to become as well understood as they are for calcium and iron-based biominerals. Of course, the reason why progress in biological silicification has been relatively slow is an apparent lack of appropriate chemistry to explain myriad forms of seemingly diverse examples of the deposition of silica in biota. In this Chapter, the title of which is a paraphrase of Voronkov et al.'s great work, *Silicon and Life* (1975), I have tried to provide plausible bioinorganic solutions to biological silicification. Ideas are presented in the context of the evolution of biological silicification and are discussed, in the main, naively without specific reference to published research which might either refute or support their validity. (This serves as an apology to the many excellent scientists whose work has not been but should have been cited!) I hope the ideas presented herein demonstrate that, rather than acting as a barrier to understanding biological silicification, the limited, biologically significant, chemistry of silicic acid is actually sufficient to act as a platform for future research in the field.

C.Exley (✉)

Birchall Centre for Inorganic Chemistry and Materials Science,
Lennard-Jones Laboratories, Keele University, Staffordshire, UK
e-mail: c.exley@chem.keele.ac.uk

1 Life Is Permeable to Silicic Acid

Why do living things, including humans, biosilicify? (*Definition: Biosilicification: the movement of silicic acid from environments in which its concentration does not exceed its solubility (<2 mmol/L) to intracellular or systemic compartments in which it is accumulated for subsequent deposition as amorphous hydrated silica.*)

Biosilicification is simply, and often an inevitable consequence of, the presence of silicic acid in the environment combined with an inability in all biota to prevent its systemic and/or intracellular entry. While living things are permeable to silicic acid, it is worth noting at this point that biological processes seem to be largely oblivious to its presence (see Evered and O'Connor 1986). The omnipresence of silicic acid in the environment should make a strong case for the majority of biota to be biosilicifiers. In fact there may well be many as yet unidentified biosilicifiers though the presence of silicic acid is not the only prerequisite to biosilicification. This requires that silicic acid encounters systemic/cellular compartments in which its supersaturation and concomitant autocondensation and deposition are promoted. The polymerisation of silicic acid is not usually a process which is conducive to successful living and, if it is neither constrained within nor controlled by a form of organised framework, it is highly cytotoxic (see Iler 1979). There are clear analogies with the natural selection of calcium as both a signalling molecule ($\text{Ca}^{2+}_{(\text{aq})}$) and a building material (bone) in that polymerising silicic acid is at least as cytotoxic as 10^{-6} M cytosolic $\text{Ca}^{2+}_{(\text{aq})}$ unless, as for the concentration of $\text{Ca}^{2+}_{(\text{aq})}$, it comes under some form of homeostatic control. Is biosilicification a form of homeostatic control of silicic acid concentrations?

Environmental silicic acid is the product of the dissolution of mountains, to which end the younger the geology the higher the ambient concentration of silicic acid (see Aston 1983). The intermediate fate of environmental silicic acid is its sedimentation, as biogenic and non-biogenic silica, before subduction makes it once again available, as silicate melts, for mountain building. The geochemical cycle for silicon predicts peaks and troughs in the concentration of environmental silicic acid which prevail over tens of millions of years (Exley 1998). Pre-biotic environmental silicic acid concentrations were almost certainly much higher than at any time in the post-biotic era and must have exerted significant influence upon the selection of early forms of life. Life is permeable to silicic acid. In some forms of life, systemic or intracellular silicic acid is approximately mirrored by environmental silicic acid concentrations. Providing the latter are not supersaturated with respect to their autocondensation then organisms have no known requirement to 'control' their internal silicic acid concentration. The acidic, reducing environment of the early oceans would have mitigated against the polymerisation of silicic acid while such conditions would have been lost with the advent of dioxygen, photosynthesising organisms and the increasing alkalinisation of the oceans. Concomitant with the changes in ocean chemistry would have been commensurate successions of different life forms, including organisms which through natural selection were enabled with (one could argue, disabled by) some form of biochemical machinery which

coincidentally necessitated the advent of biosilicification. The latter is distinct from the silicification of biota in which non-biosilicifiers, such as blue-green algae, are found entombed within silica deposits. At this point in the evolution of life on Earth, the requirement of an organism to biosilicify was simply a consequence of circumstance which, at least while environmental silicic acid concentrations remained high, may have conferred upon it an evolutionary advantage over other organisms which were not protected against the toxicity of polymerising silicic acid. The early machinery of biosilicification probably only served to lock away precipitated silica in compartments or vesicles in the cell cytosol while further evolutionary change involved the secretion (excretion?) of precipitated silica away from the cell cytosol in the form of rudimentary silica exoskeletons. The transition from rudimentary silica exoskeleton to, for example, the elaborate silica frustules of diatoms (see Werner 1977) must, perhaps akin to the evolution of bone, have involved increased capacities for the modelling and remodelling of silica. These abilities were themselves coincident with the advent of biomolecules (enzymes) which in addition to their genotypically-selected (non-silicon selected) physiological functions also cleaved silica!

2 The Non-selection of Silicon

If, as I am suggesting, environmental (e.g. oceanic) silicic acid concentrations have over evolutionary time contributed towards the diversity of life on Earth right up to the present day, then it is intriguing to speculate on how such selection pressures are operating today at a time when environmental silicic acid concentrations are seemingly much lower. Low concentrations of biologically available silicic acid in some freshwaters and much of the sea are, at least in part, testimony to the successes of the biosilicifiers, and in particular to groups including diatoms and sponges which scavenge silicic acid from waters in which the concentrations are vanishingly low. There exists on Earth today a hierarchy of mechanisms which are either related to or specifically for silicic acid homeostasis. This hierarchy has been borne out of selection pressures due to both the environmental silicic acid concentration and 'normal' biochemical evolution, and in some organisms has achieved a level of sophistication such that we might consider their handling of silicic acid as similar to that of any other essential element or nutrient. The great plant physiologist, Emanuel Epstein, considers silicon as a quasi-essential nutrient in plants (Epstein 1994). Life-forms which over considerable periods of evolutionary time have been subjected to selection pressures related to silicic acid homeostasis, for example the diatoms, have it would seem mastered silica engineering through silicic acid homeostasis to the n^{th} degree, while in biosilicifying newcomers, such as humans, the processes of biological silicification remain rudimentary.

The enigma of silicic acid homeostasis is how it evolved in the absence of complementary silicon biochemistry. Why has silicon not been selected for in any known biochemical reaction or pathway? Why are there not any enzymes

which require silicon as their co-factor? I think that it is unlikely that silicon has been selected out of biochemistry since humans have created diverse and multi-functional silicon biochemistry and in doing so have demonstrated the potential viability of silicon-based life and silicon-catalysed biological processes (see Tacke 1999). Rather than silicon having been selected out of life it would seem that life missed out on selecting for silicon. The non-selection of silicon is contrary to its ubiquity since it is the second most abundant element in the Earth's crust and it was uniquely abundant as silicic acid at the advent of life on Earth. There is, of course, a simple solution to this conundrum of silicon in life and it is as true today as it would have been several thousand million years ago when life was beginning. Silicic acid, the only biologically available form of silicon, is simply too inert to act as a source of biochemically reactive silicon. Silicic acid is an extremely weak acid and only loses its first proton at pH approaching 10. At the pH of much of life on Earth it is ostensibly a small, neutral molecule with almost no inorganic chemistry and no known bioorganic chemistry (see Birchall 1990). It is the inertness of silicic acid which has countered its relative abundance and biological availability and which has resulted in its non-selection in biochemical evolution. I know of only three chemical reactions of silicic acid which are possible under the normal physiological conditions of life: (1) its reaction with itself when its solubility is exceeded to form hydrated amorphous silica; (2) its reaction with aluminium hydroxide to form hydroxyaluminosilicates (HAS); and (3) its reaction with excess molybdate to form the Keggin-like molybdosilicic acid complex. The latter has, as yet, no known biological significance and is the basis for the spectrophotometric determination of silicic acid. The reaction of silicic acid with aluminium, though probably known for many decades, has only recently been fully elucidated such that its significance with respect to the biological availability of aluminium could be explained, while silicic acid's reaction with itself forms the basis for biosilicification. It is interesting to speculate as to how each of these reactions has contributed towards and continues to contribute towards the evolution of sophisticated silicic acid homeostasis in a number of organisms across animal and plant phyla.

The reaction between silicic acid and molybdate is sensitive and is potentiated at acidic pH, and one might have expected to find the molydosilicic acid complex in the acidic and reducing aqueous environments of the early Earth. However, it seems unlikely that such a reaction would have any significant influence upon the availability of environmental silicic acid as it requires a 12-fold excess of molybdate over silicic acid and such a stoichiometric ratio is highly unlikely in any natural water (see Fraústo da Silva and Williams 1991). However, it should not be discounted that such a ratio might be achieved in a specialised intracellular compartment, with the biologically essential molybdenum being transported by an active mechanism into a compartment containing silicic acid to form the molydosilicic acid complex. The formation of the latter might present an opportunity for the storage or transport of silicic acid following which the molybdate could be recycled and re-used in the same application. While I am not aware of any such mechanism operating in biosilicification I am equally unaware of any observation which would preclude it as a possibility.

The reaction between aluminium hydroxide and silicic acid in forming HAS could be influencing silicic acid homeostasis both directly and indirectly. We now know that HAS are important secondary mineral phases in the biogeochemical cycle of aluminium and that they act to keep aluminium out of biota (Exley 2003). The non-selection of aluminium, the third most abundant element in the Earth's crust, as an element of life cannot, unlike silicon, be explained by its chemical inertness. Its non-essentiality comes primarily from a lack of biological availability due in part to its reaction with silicic acid in forming HAS. The probable evolutionary consequence of the exclusion by silicic acid of the biologically reactive aluminium from the natural selection of the elements would have been the positive selection of other metals which though less abundant in the Earth's crust share chemical properties with aluminium. Thus, metals such as magnesium, calcium and iron which ordinarily might not compete effectively with aluminium for certain biochemical ligands would, in its absence, participate in the selection of novel biomolecules and biochemical pathways which in turn could coincidentally form part of the machinery of biosilicification. Interrelationships such as these are excellent examples of what Williams and Fraústo da Silva (1996) call 'the natural selection of the chemical elements'. It is of note that whole-genome expression profiling of the marine diatom *Thalassiosira pseudonana* has identified a common set of 84 genes which were induced by both silicon and iron limitation (Mock et al. 2008). Silicon limitation in any biological system will significantly increase the biological availability of aluminium and potentially the disruption of iron-dependent pathways. By keeping aluminium out of biochemical evolution, silicic acid has helped to direct alternative bioinorganic chemistry and may itself consequentially be affected by its own actions should the advent of a particular biochemical pathway inadvertently catalyse one or more steps in a biosilicification pathway! While the formation of HAS may indirectly influence silicic acid homeostasis by keeping aluminium out of biological processes, it could also have a direct influence by acting as a catalyst for the autocondensation of silicic acid upon an organic framework such as a protein or glycopeptide. For example, while silicic acid cannot bind directly to a 'templating' biomolecule involved in the ordered deposition of silica, the binding of aluminium by such biomolecules could provide a surface of aluminium hydroxide at which the competitive condensation of silicic acid is predicted to take place. The subsequent formation of a silanol-rich surface could then act as a catalyst for the further condensation of silicic acid and the apparently controlled deposition of an amorphous silica surface. While aluminium might be expected to be found occluded within such silica frameworks, it would only require to be present in trace amounts relative to silicon.

The potential cytotoxicity of the polymerisation of silicic acid has already been pointed out and, while the reaction of silicic acid with itself is the chemical basis for biosilicification, if it were to run amok in an intracellular or systemic compartment it could only be damaging to membranous structures and essential biomolecules. In biosilicifiers, the autocondensation of silicic acid and eventual precipitation of an amorphous silica must take place within a controlled environment and without the concomitant formation of dangerous (toxic) polysilicic

acids or silica morphologies. How this level of control is achieved in the absence of a well-defined silicon biochemistry has remained an enigma, and it cannot be adequately modelled in cell-free (abiotic) systems in which numerous biomolecules can be shown to catalyse the formation of silica in supersaturated solutions of silicic acid (see Perry 2008). Silicification is a dynamic and cell-friendly process which is continuous throughout the life of the particular organism. Both its precursor molecule, silicic acid, and its final product, silica, are potentially toxic and yet the transformations which take place in both directions between these forms occur without detriment to the biosilicifier. Of course, what else would one expect from the process of natural selection? However, the natural selection of biosilicifiers is itself a paradox in that we have been unable to explain the existence and immense success of these life-forms in any terms which can be strictly related to the biological essentiality of either silicon or silicification (see, for example, Fauteux et al. 2006). The only experimentally proven mechanism of silicon essentiality in biosilicifiers and non-biosilicifiers alike is to increase the biological availability of phosphorus in algae in the presence of aluminium (Exley et al. 1993).

3 Diatoms and Sophisticated Silicic Acid Homeostasis

Probably one of the most sophisticated examples of the homeostasis of silicic acid is the deposition of silica frustules in diatoms (see Werner 1977). There exists a vast scientific literature on silicification in diatoms, and the casual reader might easily summarise that much of what there is to know on this subject is already known. However, where there are omissions or gaps in our understanding of silicification in diatoms these nearly always have their origin in a lack of appreciation of the inorganic chemistry of silicic acid. (Actually the same criticism might be levelled at all current explanations of biosilicification!) It is perhaps the actual lack, as opposed to appreciation, of such chemistry, inorganic or otherwise, that has proved too great an obstacle for many, and by itself has allowed for frequent speculation upon the biologically available form of silicon. I have lost count of the number of instances where some form of charged silicon species, usually silicate, has been invoked in, for example, the uptake of silicic acid. Some authors have resorted to so-called analogues of silicic acid to support particular ideas or potential biochemical pathways. Many have succeeded in convincing editors and reviewers that, for example, germanic or boric acids are suitable analogues of silicic acid. The former, in particular, has been used extensively in studies concerning silicon 'transport' in diatoms and plants without always taking into account the significant chemistry that germanic acid has, for example, with organic ligands such as citrate (Pokrovski et al. 2000). Clearly, while germanium (IV) has been found substituted for silicon in silica deposits including diatom frustules, this by itself does not make germanic acid an ideal tool for studying biosilicification (Safonova et al. 2007). Quite possibly, the most appropriate analogue for the transport of silicic acid across biological membranes is that of water, and there is burgeoning evidence that aquaporins are permeable to

silicic acid (Raven 2001; Wu and Beitz 2007). It may be of significance to the earlier discussion of the role played by aluminium in the selection for biosilicification that exposure to aluminium has been shown to downregulate the expression of genes for aquaporins in plants (Milla et al. 2002) and animals (Mahieu et al. 2006). We have also observed lower rates of urinary excretion of silicic acid in individuals suffering from aluminium overload (Exley et al. 2006a, b). The role of silicic acid in excluding aluminium from biochemical evolution may have contributed towards the selection of aquaporin-like proteins for the transport of water and, hence, silicic acid.

A number of biomolecules have been identified as facilitating the uptake of silicic acid in diatoms, and evidence has been presented to suggest that uptake involves the active transport of silicic acid. By definition, active transport is both energy-dependent and should, in the case of freely permeable moieties such as silicic acid, involve the movement of the transported species against a concentration gradient. Its evolutionary implication is that without an active mechanism the movement of the transported species would either not take place or would be too slow to sustain function. Neither of these are true for the uptake of silicic acid by diatoms for which normal rates of growth are sustainable by diffusion (Wischmeyer et al. 2003). One might ask which other process of membrane transport would be predicted for a small, neutral and polar molecule? Of course, the energy dependency of the uptake of silicic acid might reflect the recruitment of proteins (aquaporin-like?) into the cell membrane to create silicic acid-permeable channels and/or metabolic processes acting on the internal side of the cell membrane to maintain the diffusive gradient. Until unequivocal evidence of silicon biochemistry is forthcoming, we should apply Occam's razor in acknowledging that silicon crosses biological membranes as silicic acid and we should use this information as the first step in our understanding of biosilicification. The logical next step is to understand how diffusive gradients are maintained for silicic acid uptake across biological membranes.

Silicic acid equilibrates across biological membranes according to a Donnan equilibrium, thereby ensuring a relatively constant intracellular concentration of biologically available silicic acid in all but severely silicon-limiting conditions. However, how can a constant intracellular concentration of silicic acid become a consistent supply of silicic acid for the formation and deposition of amorphous silica? To achieve this, the systemic or intracellular silicic acid has first to be harvested and then stored in a way that it no longer participates in the diffusive gradient that is fuelling its transport. In the case of diatoms, the intracellular (or possibly intramembrane) silicic acid concentration must always be lower than the environmental silicic acid concentration. This poses an immediate problem for biosilicification in that all of the various forms of hydrated amorphous silica which might be involved in biosilicification are quite soluble and, therefore, unsuitable as dynamic stores of silica destined for use in building biogenic silica structures such as frustules in diatoms or spicules in sponges. However, sophisticated biosilicifiers such as these must overcome such problems by, for example, presenting intracellular sinks for silicic acid which act irreversibly to entrap it and thus prevent its equilibration with the environmental silicic acid concentration. In rudimentary forms of biosilicification, these sinks may also represent the final sites of silica deposition,

though in organisms where silicic acid homeostasis has evolved to a higher level of complexity such sinks are probably discrete, membrane-bound compartments which are shuttled to and from sites of silica deposition. If they are membrane-bound structures then they may also incorporate channels which are permeable to silicic acid, similar perhaps to those in the cell membrane, but if so, how is the diffusion gradient for the entry of silicic acid into such intracellular compartments maintained? How might silicic acid be sequestered into these compartments and disguised as something which is chemically dissimilar to silicic acid? From the evolutionary perspective of the non-selection of silicon, it is intriguing to speculate as to the origin of such compartments. Are they pre-existing structures which have completely different roles in non-biosilificiers or are they the consequence of a physiological process which occurs concomitantly with the diffusion of silicic acid into the cell cytosol. Do such 'stores' of silicic acid exist in an apo-form (empty) when silicic acid is not available in the external environment? A consistent feature of nutrient deprivation in general in algae and silicon limitation in particular in diatoms are the appearance of intracellular droplets of lipid (see Werner 1977), and one might speculate that these are the consequence of an environmentally-induced change in the utilisation of lipid in the cell. Thus, in diatoms subjected to very low levels of environmental silicic acid, the appearance of lipid droplets in the cytosol might be the outcome of a change in lipid use rather than an increase in lipid production. In respect of lipid use, this may be indicative in silicic acid-replete diatoms of a role for lipids in the encapsulation of cytosolic silicic acid in micelle-like structures, thereby enabling its removal or exclusion from equilibria with both cytosolic and environmental silicic acid concentrations. The coalescence of silicic acid-filled lipid droplets within, for example, specific constrained environments could provide a mechanism whereby silicic acid is delivered to sites of silica deposition. Clearly, biosilificiers, whether they are algae (diatoms), animals (sponges) or higher plants (horsetail), maintain diffusive gradients for the entry of silicic acid into cellular and systemic compartments, and this is achieved in the absence of its complexation by organic ligands. Theoretically at least, a diffusive gradient could be maintained by ensuring that each molecule of diffused silicic acid is instantaneously removed or transported away from the intracellular or systemic environment which is immediately adjacent to its point of entry. Some form of fluid displacement, such as is found in counter-current flow, would both maintain the uptake of silicic acid and form part of a transport mechanism for delivering the displaced silicic acid towards its eventual site of deposition as amorphous silica. Of course, being able to guarantee a continuous supply of silicic acid does not explain how such can be transformed into amorphous silica. We know that the solubility of silicic acid is approximately 2 mmol/L and that this is often an order of magnitude higher than environmental concentrations of silicic acid. Biosilicification either requires the supersaturation of an undersaturated solution of silicic acid or it requires a lowering of the solubility of silicic acid. The non-selection of silicon as an essential element of life predicts that both of these conditions contribute towards biosilicification. The supersaturation of silicic acid within specific compartments would involve either the transport of

silicic acid into a compartment against a concentration gradient or the transport of solvent, water, out of a compartment without any concomitant (significant) loss of silicic acid. The latter, water removal, is a normal physiological event in compartments as apparently diverse as the xylem vessels of plants and the tubules of mammalian kidneys. It is a mechanism whereby an undersaturated solution of silicic acid could become supersaturated and, as long as the delivery of this solution to a site of silica deposition is sufficiently rapid to preclude the adventitious deposition of silica, it should not present the biosilicifier with any unique problems. Importantly, this mechanism does not require any unknown silicic acid chemistry and could by itself provide a basis for rudimentary forms of silica deposition. However, to achieve the level of sophisticated silicification which is observed in organisms such as diatoms and sponges and to ensure the reproducibility of such structures through the generations there must be roles for proteins/peptides (i.e. genes) in biosilicification. Any such role should enable both a quasi-stable store of supersaturated silicic acid and a mechanism of incorporating such into a prescribed framework, while precluding the requirement for any direct links (bonds, other than hydrogen bonds) between protein/peptide and silicic acid. There are clearly precedents for producing a supersaturated solution of silicic acid within, for example, membrane bound vesicles, by the active removal (pumping out) of water. A potential problem is how to prevent the premature precipitation of silica rendering such vesicles useless as building blocks for higher order silica structures. One possibility is that the vesicles are actually lysosomes (or were originally lysosomes) and those that now function effectively as quasi-stable stores of polymerising silicic acid include hydrolytic peptides such as, for example, esterases (Müller et al. 2008), which, completely coincidentally, are able to cleave Si–O–Si linkages. The presence of such ‘enzymes’ would help to ensure that silica was not deposited adventitiously and that this would be achieved serendipitously without the need to invoke any silicon-specific biochemistry. A final role for proteins/peptides would be in helping to define the structure of the deposited silica framework by acting as specific sites for the nucleation of silicic acid and the subsequent deposition of amorphous silica. Again, following the assumption that there is no direct protein–silicic acid binding then an inorganic linker is required and, based upon what we know about the chemistry of silicic acid, a possible candidate would be aluminium. For example, enzymatic phosphorylation of adjacent hydroxyl groups on the cytosolic side of peptides/proteins which were inserted into a lipid membrane/scaffold would result in avid binding of aluminium and the formation of an hydroxyaluminium ‘surface’ which in turn could bind silicic acid. The silanolisation of such a surface would act as a site for the subsequent deposition of silicic acid as silicic acid-rich lysosomes fused with and lysed at the surface. It is possible that as the silica surface was formed there would be no further requirement for either the bridging aluminium layer or the framework proteins/peptides, and these would probably become occluded within the developing silica structure. The non-selection of silicon as an essential element does not predict a role for aluminium in biosilicification! Of course in natural selection there always have to be some surprises (Fig. 1)!

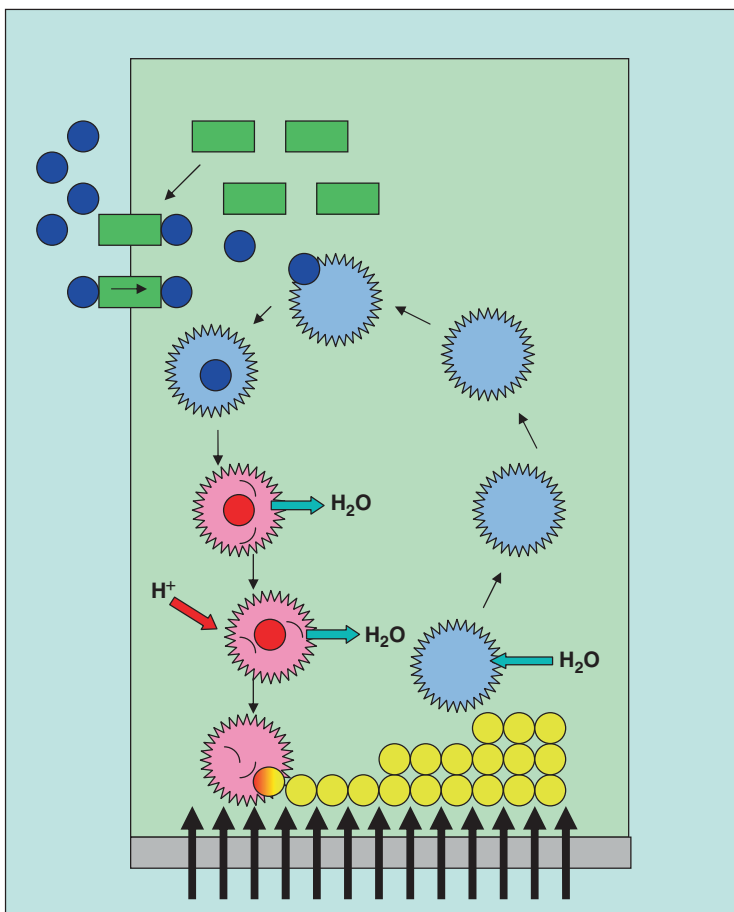


Fig. 1 Bioinorganic biosilicification. Silicic acid-permeable transporters (*bright green rectangle*) are recruited to the cell membrane to support the diffusion of environmental silicic acid (*dark blue circle*) down a concentration gradient to the intracellular/systemic milieu (*light green background*). Lysosomal (or lipid) encapsulation of silicic acid (*light blue star*) helps to maintain the diffusive gradient. Silicic acid is concentrated in the lysosomal vesicle (*red circle*) by active removal of water (*pink star*) and active proton uptake and enclosed hydrolytic peptides (*small arc*) prevent its precipitation as silica. Lysosomal vesicles are lysed at the site of silica deposition (*grey area*) where occluded proteins (*arrow body*) with cytosolic inorganic linker groups (*arrow heads*) catalyse the condensation of silicic acid and the subsequent deposition of silica (*yellow circles*)

4 Conclusions

The non-selection of silicon in the natural selection of the elements of life predicts not one universal mechanism but myriad mechanisms of biosilicification which operate across all biota or biosilicifiers. The common denominators are silicic acid and its inorganic chemistry and not conserved genotypes for proteins involved in

the transport, storage and eventual deposition of silicic acid as silica. The slow but sure emergence of whole genome studies of known biosilicifiers continues to provide support for a lack of evolutionary conservation in the machinery of biosilicification (Armbrust et al. 2004; Mock et al. 2008). However, in conclusion, it is important to emphasise that the non-selection of silicon as an essential element for life on Earth does not preclude biological roles for silicon in biota, only that these roles are underpinned by the bioinorganic chemistry of silicic acid and not an as yet unidentified bioorganic chemistry of silicon.

References

- Armbrust EV, Berges JA, Bowler C, Green BR, Martinez D, et al. (2004) The genome of the diatom *Thalassiosira pseudonana*: ecology, evolution, and metabolism. *Science* 306, 79–85.
- Aston SR (Ed.) (1983) Silicon geochemistry and biogeochemistry. Academic, New York, 248p.
- Birchall JD (1990) The role of silicon in biology. *Chem. Britain Feb.* 141–144.
- Evered D, O'Connor M (Eds) (1986) Silicon biochemistry. *Ciba Found. Symp.* 121, 264p.
- Epstein E (1994) The anomaly of silicon in plant biology. *Proc. Natl. Acad. Sci. USA* 91, 11–17.
- Exley C (1998) Silicon in life: a bioinorganic solution to bioorganic essentiality. *J. Inorg. Biochem.* 69, 139–144.
- Exley C (2003) A biogeochemical cycle for aluminium? *J. Inorg. Biochem.* 97, 1–7.
- Exley C, Tollrvey A, Gray G, Roberts S, Birchall JD (1993) Silicon, aluminium and the biological availability of phosphorus in algae. *Proc. Roy. Soc. Lond. B* 253, 93–99.
- Exley C, Mamutse G, Korchazhkina O, Pye E, Strekopytov S, Polwart A, Hawkins C (2006a) Elevated urinary excretion of aluminium and iron in multiple sclerosis. *Mult. Scler.* 12, 533–540.
- Exley C, Korchazhkina O, Job D, Strekopytov S, Polwart A, Crome P (2006b) Non-invasive therapy to reduce the body burden of aluminium in Alzheimer's disease. *J. Alzh. Dis.* 10, 17–24.
- Fauteux F, Chain F, Belzile F, Menzies JG, Bélanger RR (2006) The protective role of silicon in the *Arabidopsis*-powdery mildew pathosystem. *Proc. Natl. Acad. Sci. USA* 103, 17554–17559.
- Fraústo da Silva JJR, Williams RJP (1991) The biological chemistry of the elements. Oxford University Press, Oxford, 561p.
- Iler RK (1979) The chemistry of silica. Wiley-Interscience, New York, 866p.
- Mahieu S, Millen N, del Carmen Contini M, Gonzalez M, Molinas SM, Elías MM (2006) Urinary concentrating mechanism and aquaporin-2 abundance in rats chronically treated with aluminium lactate. *Toxicology* 223, 209–218.
- Milla MAR, Butler E, Huete AR, Wilson CF, Anderson O, Gustafson JP (2002) Expressed sequence tag-based gene expression analysis under aluminium stress in rye. *Plant Physiol.* 130, 1706–1716.
- Mock T, Samanta MP, Iverson V, Berthiaume C, Robison M, Holtermann K et al. (2008) Whole-genome expression profiling of the marine diatom *Thalassiosira pseudonana* identifies genes involved in silicon bioprocesses. *Proc. Natl. Acad. Sci. USA* 105, 1579–1584.
- Müller WEG, Grachev MA (Eds) (2008) Potential of biosilica in evolution, morphogenesis and nanobiotechnology: Case study Lake Baikal (in press).
- Müller WEG, Schloßmacher U, Wang X, Boreiko A, Brandt D et al. (2008) Poly(silicate)-metabolising silicatein in siliceous spicules and silicasomes of demosponges comprises dual enzymatic activities (silica polymerase and silica esterase). *FEBS J.* 275, 362–370.
- Perry CC (2008) An overview of silica in biology, its chemistry and recent technological advances. In Müller WEG, Grachev MA (Eds) Potential of biosilica in evolution, morphogenesis and nanobiotechnology: Case study Lake Baikal (in press).

- Pokrovski GS, Martin F, Hazemann J-L, Schott J (2000) An X-ray absorption fine structure spectroscopy study of germanium-organic ligand complexes in aqueous solution. *Chem. Geol.* 163, 151–165.
- Raven JA (2001) Silicon transport at the cell and tissue level. In: Datnoff LE, Snyder GH, Korndörfer GH (Eds) *Silicon in agriculture*, Elsevier Science, Amsterdam, The Netherlands, pp. 41–56.
- Safonova TA, Annenkov VV, Chebykin EP, Danilovtseva EN, Likhoshway YV, Grachev MA (2007) Aberration of morphogenesis of siliceous frustule elements of the diatom *Synedra acus* in the presence of germanic acid. *Biochemistry (Moscow)* 72, 1261–1269.
- Tacke R (1999) Milestones in the biochemistry of silicon: from basic research to biotechnological applications. *Angew. Chem. Int. Ed.* 38, 3015–3018.
- Voronkov MG, Zelchan GI, Lukevitz EY (1975) *Silizium und Leben*, transl. by K. Rühlmann, Akademie-Verlag, Berlin, 370p.
- Werner D (Ed.) (1977) *The biology of diatoms*. Botanical Monographs Volume 13, Blackwell Scientific, Oxford, 498p.
- Williams RJP, Fraústo da Silva JJR (1996) *The natural selection of the chemical elements*. Oxford University Press, Oxford, 646p.
- Wischmeyer AG, Del Amo Y, Brzezinski M, Wolf-Gladrow DA (2003) Theoretical constraints on the uptake of silicic acid by marine diatoms. *Mar. Chem.* 82, 13–29.
- Wu B, Beitz E (2007) Aquaporins with selectivity for unconventional permeants. *Cell. Mol. Life Sci.* 64, 2413–2421.

Fossil Sponge Fauna in Lake Baikal Region

Elena Veynberg

1	Introduction.....	186
2	The Martinson Investigations.....	186
3	The Recent Paleontological Investigations.....	187
3.1	The Morphological Peculiarities of the Recent Baikalian Sponge Spicules.....	188
3.2	The Morphological Peculiarities of Fossil Baikalian Sponge Spicules.....	192
3.3	The Sponge Fauna of the Upper Pleistocene and Holocene of the Lake Baikal.....	194
3.4	Baikalian Sponge Fauna of the Late Pliocene (3.2–2.1 Ma).....	194
3.5	The Fossil Sponge Fauna of the Late Miocene.....	200
3.6	The Investigation of Terrigenous Sediment of the Tunka Land Basin.....	200
4	Hypothesis on the Origin of Lubomirskiidae in Lake Baikal.....	200
5	Concluding Remarks.....	202
	References.....	203

Abstract The spicules of almost all the known recent sponges that nowadays inhabit Lake Baikal have been found in the sediments of the Late Pliocene (3.2 Ma). However, the sponge fauna in Late Pliocene (3.2–2.8 Ma) was richer by far than the recent one. Besides the spicules of nearly all the recent sponges, 24 types of spicules belonging to “extinct species,” which have no analogues with recent sponges, have been found.

The species’ composition of the sponge fauna in the Late Pleistocene period (95 Ky) was similar to the recent one.

In the sediments of the Late Miocene (6.50–4.75 and 10 Ma), the well-formed spicules of species of the Lubomirskiidae family can be found. To these belong: *Rezinkovia arbuscula* Efremova, 2001, *Baikalospongia fungiformis* (Makuschok, 1927), *Swartschewskia papyracea* (Dybowski, 1880) and *Lubomirskia incrustans* Efremova, 2001. We can also find here four types of spicules in the genus *Lubomirskia* which have no analogues with the recent sponges. A few types of spicules in the Spongillidae family are also “new.” According to our preliminary brief

E. Veynberg (✉)

Limnological Institute, Siberian Branch of the Russian Academy of Sciences,
Ulanbartorskaya 3, Irkutsk 664033, Russia

investigation of the species' composition in the sediment of this period (6.50–4.75 and 10Ma), the sponge fauna of the Late Miocene is poorer compared to the sponge fauna in Late Pliocene. In the sediments of the Late Miocene (6.50–4.75 Ma) in cold climactic periods, spicules of the family Lubomirskiidae predominate while in warm periods the Spongillidae spicules dominate. Thus, a permanent change in the sponge association took place.

1 Introduction

Baikalian endemic sponge fauna (family Lubomirskiidae) is one of the most interesting and unusual objects of the ancient fauna of Lake Baikal. This flourishing group in the ecosystem of the Lake settled at depths ranging from the littoral to the abyssal. Currently, it co-exists with a few other representatives of another freshwater cosmopolite, the Spongillidae family, which settle mainly in the bays and shallow water of Lake Baikal. Despite the abundance and dominance of Baikalian sponge fauna in benthos populations, its species' variety is relatively small. According to the last taxonomical review, the family of Lubomirskiidae consists of 4 genera, 13 species, and 1 subspecies (Efremova 2001, 2004). The less numerous family of Spongillidae includes 4 genera and 5 species (Masuda et al. 1999; Efremova 2001).

As a result of our studies of more than 1,500 samples of recent sponge fauna from Lake Baikal, 4 groups of the Lubomirskiidae family sponge, which are not analogues with the 14 previously described species, have been discovered. Most probably, they are new species and subspecies of the Baikalian sponges (Weinberg 2005).

The Baikalian sponge can fossilize in sediments in the form of isolated skeleton needles, i.e., spicules, and can be well preserved for millions of years. The paleontological method of investigating the remains of the sponge in sediments is one of the tools used to study the evolution of the sponge fauna. Investigations of the sponges' spicules, buried in the bottom sediments of Lake Baikal, also enable us to study the diversity of the sponge fauna of the latest epochs as well as any modification in its species' composition.

2 The Martinson Investigations

The pioneer of the fossil spicules study in the terrigenous and bottom sediments of Lake Baikal and its region was G.G. Martinson. His studies were carried out in 1936–1948 and were published in several articles (Martinson 1936, 1938, 1940, 1948a, b). After him, this intriguing subject matter has been neglected. Martinson studied the terrigenous deposit near the village of Posolsk (South Baikal). Here, one borehole 1,457.75 m deep was drilled. The age at the bottom of this sediment core was defined as approximately Late Terrias or even Upper Cretaceous by geologist G.E. Ryabuchin. There were spicules of the Spongillidae family: *Ephydatia*

fluviatilis (Linnaeus 1759), *E. muelleri* Lieberkuehn 1856, *Spongilla fragilis* Leidy 1851, and *Spongilla lacustris* L. (Linnaeus 1759); and of the Lubomirskiidae family: *Lubomirskia baicalensis* (Pallas 1772), *L. fusifera* Soukatschoff, 1895, *Baikalospongia intermedia* (Dybowski, 1880), *B. bacilifera* (Dybowski, 1880).

In the lowest layer, at a depth of 1,443.8–1,447.2 m (perhaps in the Paleogene – 36–34 million years ago; Ma) there are solely sole presence of the spicules of the Spongillidae family. Above this layer, there is a layer of coarse sand, where spicules are absent. Only 9 m above this layer, at the depth of 1,332.9–1,275.0 m (aged approximately Early Miocene 34–23 mya) there is a layer with many Lubomirskiidae spicules together with a few spicules of the Spongillidae family. After the second layer of the coarse sand at the depth of 1,275.0 m only, the spicules of the Lubomirskiidae family can be found in the sediments of the core. The spicules of the Spongillidae family disappear and only reappear at the depth of 221 m.

G.G. Martinson described the following scenario of the events: in the Tertrias (perhaps in the Paleogene, and maybe in the Upper Cretaceous period) at this site there existed a shallow freshwater reservoir, characterized by the presence solely of sponges from the Spongillidae family. The layer of the coarse sand, above which only the spicules of the Lubomirskiidae family can be found, testifies for the sudden change in the water conditions and regime of the lake and, as a result, there appear representatives of the endemic fauna of a deep water reservoir. The spicules of Spongillidae appear again only at the depth of 221 m, thus testifying for the fact that throughout this lengthy period there existed conditions typical of a deep freshwater lake. The ongoing increase in Spongillidae spicules in the cross section has shown the respective increasing influence of the shallow water area, which coincides well with the recent conditions in this region of Lake Baikal.

The spicules of the Lubomirskiidae family were found by Martinson in the Tertrias sediments from other regions of Lake Baikal (River Polovinka) (Martinson 1938, 1940). Here, he also found spicules which are not analogous to the spicules from recent species of Lubomirskiidae, and named them *B. fossilis* Martinsoni (Martinson 1938). Lubomirskiidae spicules are also found the Tertrias terrigenous sediments of the Tunka land basin (Martinson 1948a, b). This land basin, which is presently part of the Baikal rift zone, is supposed to have earlier accommodated the waters of the Paleo-Baikal.

3 The Recent Paleontological Investigations

The progress in the modern methods of drilling enables us to obtain Baikalian bottom sediment samples aged a few millions of years. Owing to the international program “Baikal Drilling Project,” long core samples as well as short ones have been obtained. The long cores are named according to the year in which they were obtained: BDP – 93, BDP – 96 (the age of the core bottom is 5 Ma), BDP – 97, BDP – 98 (the age of the core bottom is 10 Ma), and BDP – 99 (Kashiwaya 2003).

All bottom sediment samples were taken on the underwater Academician Ridge, which divides the North part of Lake Baikal from its Central Basin. The Ridge itself is separated from the shores of Lake Baikal by deep cavities, which prevent the transport of terrigenous material from its shores; here, a quiet and isolated regime of sedimentation takes place. The depth of water over the ridge is nowadays at least 300m. The sediment from Academician Ridge is an ideal object to study paleoclimatic and paleoecological conditions from previous epochs (Team of the “Baikal Drilling Project,” 1998).

For our investigations, we used sediments of the deep drilling 200-m core BDP – 96 (53°41'48"N, 108°21'06"E), namely the part aged 3.1–2.1 Ma. The part of 600m core BDP – 98 (53°44'46"N, 108°24'32"E) (aged 6.50–4.75 Ma) and the lower part of this core aged 10Ma. Some samples of the terrigenous sediments from the Tunka land basin (aged approximately Late Miocene) were studied. Also studied were a few short cores (St-18: 53°33'25"N, 107°59'33"E; St-16: 53°42'49"N, 108°22'56"E; St-15: 53°33'19"N, 108°00'43"E; STX – 3GC: 53°40'25"N, 108°21'16"E; ST – 2GC: 53°33'03"N, 107°54'53"E). The age of these cores is no older than Late Pleistocene.

3.1 *The Morphological Peculiarities of the Recent Baikalian Sponge Spicules*

The skeleton architecture is one main criterion for the determination of a sponge species. However, we can find only isolated spicules in the sediments. For the Spongillidae family, it is important to know the structure of their gemules, which are absent in Baikalian sediments. Thus, to divide fossil spicules into two families, genera, and species, one can use morphological and morphometrical characteristics of isolated spicules alone.

For developing reliable criteria for the identification of sponge species according to isolated spicules, we have studied spicules in more than 1,500 samples of recent sponges.

The morphological analysis of recent spicules has shown that the spicules from some species are characterized by very specific features, which do not make the definition of this species according to isolated spicules too difficult (Fig. 1).

This applies to the spicules of *Swartchewskia papyracea*, *Rezinkovia echinata* (Efremova 2001), *R. arbuscula*, *B. fungiformis*, *B. bacillitera*, *B. martinsoni* (Efremova 2001), *B. recta* (Efremova 2001), *B. intermedia profundalis* (Rezvoj 1936), *Lubomirskia baicalensis* ssp.1 (all Weinberg, 2005), *Lubomirskia* sp.1 Weinberg, 2005, *B. martinsoni* ssp.1 Weinberg, 2005, and *B. fungiformis* ssp.1 Weinberg, 2005.

However, some species have spicules with considerably changeable characteristics (*B. recta*, *B. intermedia*, *L. baicalensis*, *L. incrustans*), where certain spicules of one species resemble spicules of other species (*L. abietina*, *L. fusifera*). This is the reason why the diagnosis according to isolated spicules alone of these species can sometimes be difficult. In such cases, we can use one specific feature, which is the direction of the spine in the very top of spicules.

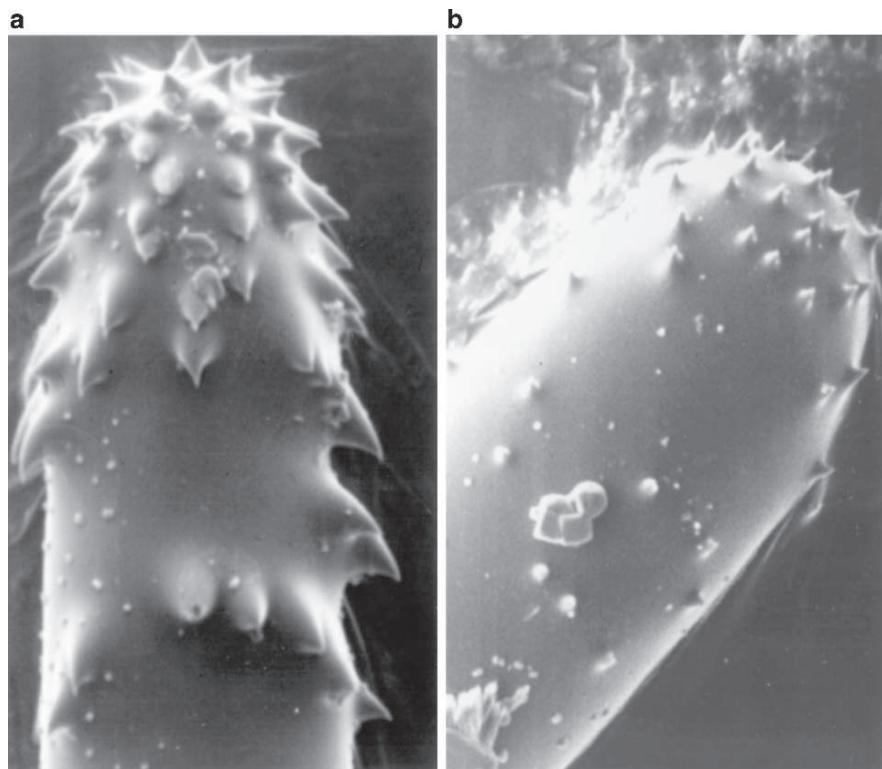


Fig. 1 The spicules of certain species are characterized by specific features, which make the definition of this species according to isolated spicules less difficult. The spicules of (a) *Bakalospongia bacilifera* and (b) *B. fungiformis*. Scale: 1 cm = 10 μ m (Philips SEM 525M)

For example, this feature can be used to distinguish between the spicules from *L. incrustans* and *B. intermedia* (Dybowski, 1880). These two species have spicules with more changeable characteristics. However, the spines on the top of spicules of *L. incrustans* are always perpendicularly directed to the axis of spicules (Fig. 2).

Spines on the tops of the spicules of *B. intermedia* are always oriented towards the top of spicules (Fig. 3).

In the case where qualitative morphological characteristics of the recent spicules coincide (*B. intermedia profundalis* and *B. intermedia*; *L. abietina* (Swartschewsky 1902) and *L. fusifera* (Soukatschoff 1895)) the size of the spicules becomes the determinative character.

To measure the size of spicules we took 100 spicules in a sample. The intra-specific changeability in the size of spicules inside *Lubomirskia* genus has been shown to not be large. This is supported by the low coefficient of variation and small standard deviation as well as small abmodality (Table 1).

The size of spicules in *Baikalospongia* genus is more changeable. The coefficient of variation and standard deviation here is larger (Table 2).

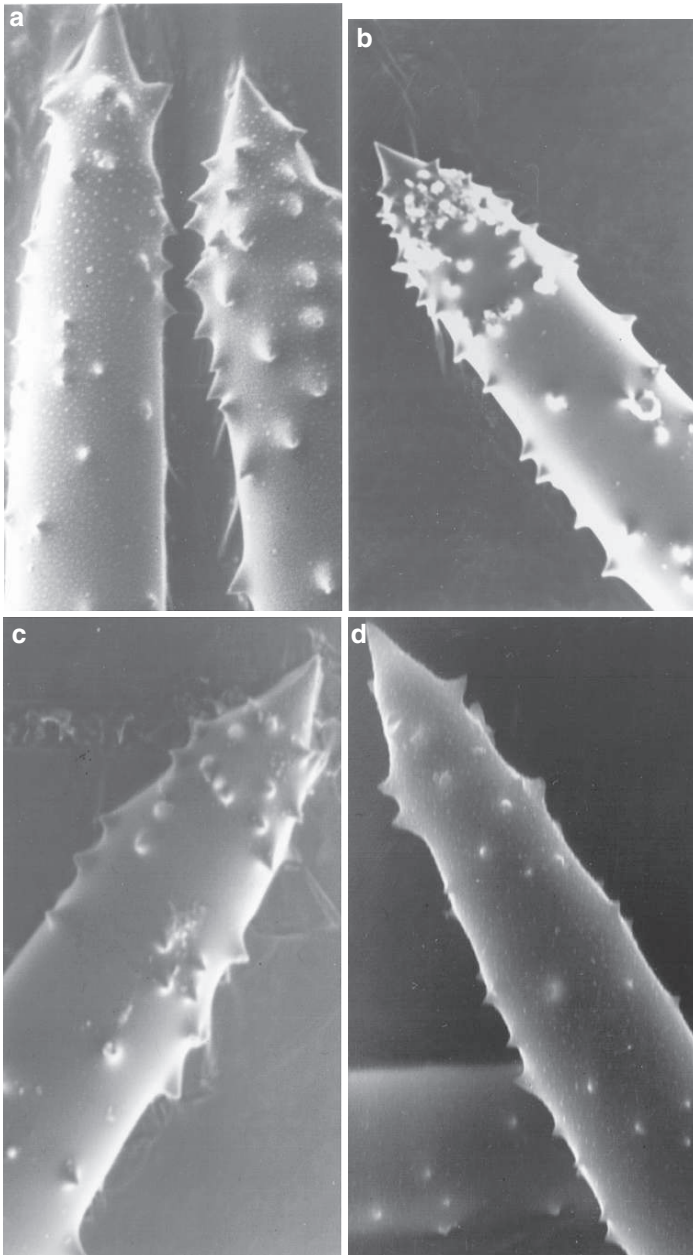


Fig. 2 Characteristic feature of spicules of *Lubomirskia incrustans*. Spines on the top of the spicules of *L. incrustans* are always perpendicularly directed to the axis of spicules. Scale: 1 cm = 10 μ m (Philips SEM 525 M)

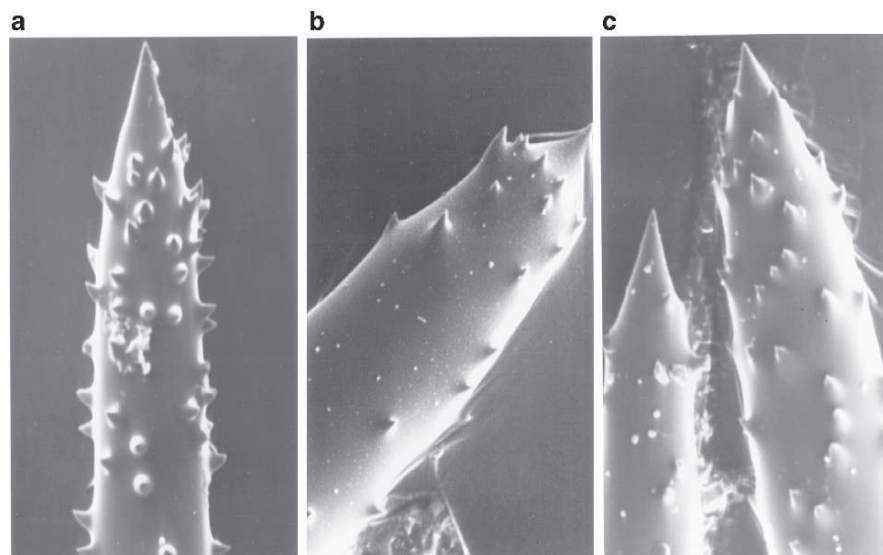


Fig. 3 Characteristic feature of the spicules of *Baikalospongia intermedia*. Spines on the tops of the spicules of *B. intermedia* are always oriented towards the top of spicules. Scale: 1 cm = 10 μ m (Philips SEM 525 M)

Table 1 Average length and average width of spicules of recent sponge *Lubomirskia* genus and sponge *Spongillidae inserta sedis*

Name of species	Average length (μ m)	Standard deviation (μ m)	Coefficient of variation (%)	Average width (μ m)	Standard deviation (μ m)	Coefficient of variation (%)
<i>Baikalospongia intermedia</i>	227 \pm 2	30	8	16 \pm 0.1	3	17
<i>Lubomirskia incrustans</i>	234 \pm 1	25	10	15 \pm 0.1	2	16
<i>L. fusifera</i>	222 \pm 2	18	8	18 \pm 0.2	2	12
<i>L. baikalensis</i>	194 \pm 1	20	10	13 \pm 1	2	17
<i>L. abietina</i>	201 \pm 2	18	9	16 \pm 0.3	3	19
<i>Spongillidae inserta sedis</i>	269 \pm 3	29	11	11 \pm 0.2	2	16

Table 2 Average length of spicules of recent sponges from the genus *Baikalospongia*

Name of species	Average length (μ m)	Standard deviation (μ m)	Coefficient of variation (%)
<i>Baikalospongia recta</i>	254 \pm 4	33	13
<i>B. martinsoni</i>	229 \pm 8	34	15
<i>B. bacilifera</i>	218 \pm 3	26	12
<i>B. fungiformis</i>	262 \pm 3	29	11
<i>B. intermedia</i>	230 \pm 1	23	10

However, the morphological features of spicules of this genus are stable and because of this the definition of these isolated spicules is not difficult.

Thus, the analysis of morphological and morphometrical parameters of recent spicules has shown that both the form and size of Baikalian spicules are relatively stable and that every species has characteristic spicule features of its own.

3.2 *The Morphological Peculiarities of Fossil Baikalian Sponge Spicules*

We have divided all sedimental spicules into four groups. The first group is spicules which are identical to spicules of recent species. We name them “the spicules of transit species.” The second is the spicules from those sediments which have no analogues with the spicules of recent species. We name them “the spicules of extinct species.” The third group can be called “the spicules of conditionally extinct species.” The sponge with this form of spicules has not been found in the recent sponge fauna. However, these spicules have been revealed in both ancient and recent layers of sediments. It is not excluded, however, that the sponge with the third-group spicules could be found in modern sponge fauna following a more thorough study. The fourth group is the spicules which appear in the Holocene sediments alone and are absent in the more ancient ones. They have been named “the spicules of newly appeared species.”

The comparison of spicules' length from recent Lubomirskiidae and fossil – “transit” spicules from the same family show that the size of fossil spicules has not changed much over time (Table 3, Fig. 4).

At the same time, the size of most fossil spicules from extinct species of the Lubomirskiidae family differs greatly from the size of recent spicules. And the

Table 3 The comparison of average spicule length of recent sponges and average spicule length of fossil-transit sponges from sediment aged 3.2–2.1 Ma

Name of species	Recent			Fossil (Pliocene)		
	Average length (μm)	Standard deviation (μm)	Coefficient of variation %	Average length (μm)	Standard deviation (μm)	Coefficient of variation (%)
<i>Baikalospongia recta</i>	254 ± 4	33	13	267 ± 14	31	12
<i>B. martinsoni</i>	229 ± 8	34	15	217 ± 12	42	19
<i>B. bacilifera</i>	218 ± 3	26	12	191 ± 6	6	16
<i>B. fungiformis</i>	262 ± 3	29	11	294 ± 8	50	17
<i>B. intermedia</i>	230 ± 1	23	10	233 ± 6	29	12
<i>Lubomirskia abietina</i>	200 ± 2	18	9	189 ± 8	18	9
<i>L. baikalensis</i>	193 ± 1	20	10	–	–	–
<i>L. fusifera</i>	222 ± 2	18	8	221 ± 4	16	7
<i>L. incrustans</i>	233 ± 1	25	10	255 ± 6	36	14

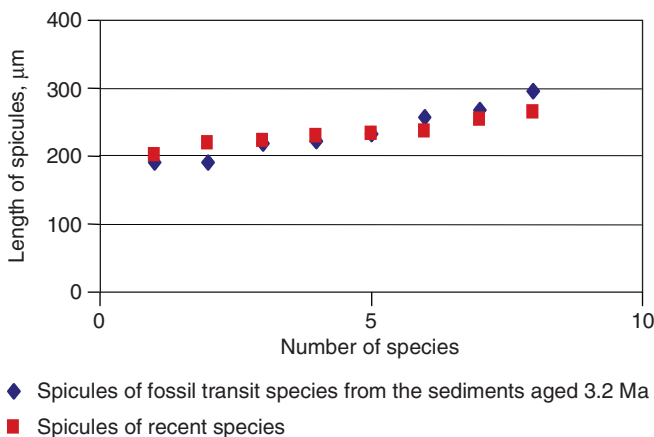


Fig. 4 The comparison of length of recent- and fossil-transit spicules from Lubomirskiidae shows that the size of fossil spicules has not changed much. The measured fossil spicules have been taken from the deposit core BDP – 96 aged as Late Pliocene (3.2–2.1 Ma)

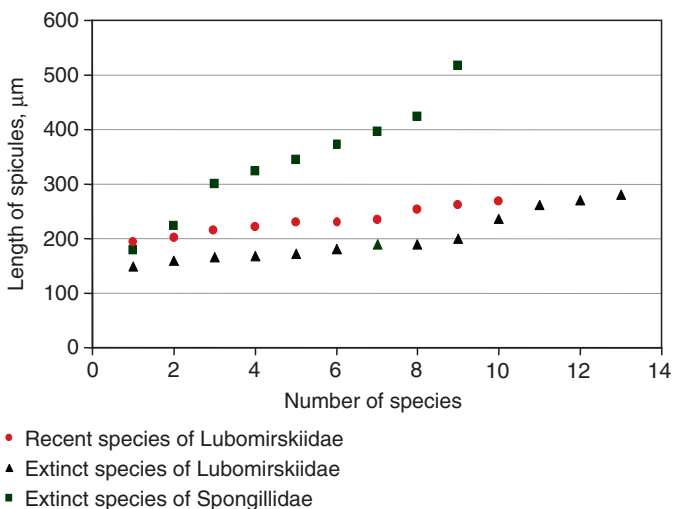


Fig. 5 The comparison of spicule length of recent species of the Lubomirskiidae, extinct species of Lubomirskiidae, and extinct species of Spongillidae. The size of fossil spicules of extinct species of Lubomirskiidae differs greatly from the size of recent spicules. And the size range of fossil spicules of extinct Spongillidae is considerably different from the fossil spicules of extinct Lubomirskiidae, as well as from the recent spicules of the Lubomirskiidae family. The measured fossil spicules have been taken from the deposit core BDP – 96 aged as Late Pliocene (3.2–2.1 Ma)

sizes of fossil spicules of extinct Spongillidae are considerably different both from fossil spicules of extinct Lubomirskiidae species and from recent spicules of the Lubomirskiidae family (Fig. 5).

3.3 The Sponge Fauna of the Upper Pleistocene and Holocene of the Lake Baikal

The investigation of the Pleistocene Baikalian sediments has shown that they are the continuous high-resolution chronicle of the paleo-climate of the Upper Pleistocene and serve only as one of the examples for common regularity, typical of all marine sediments at high latitudes (Bradbury et al. 1994; Colman et al. 1995; Grachev et al. 1998).

In the Paleomagnetic epoch of Brunhes, which lasted 780,000 years, there were ten inter-glacial and nine glacial stages, respectively (MIS – marine isotope stage). This is revealed in the alternation of the layers with high or low concentrations of siliceous elements in oceanic sediments. The former refer to the high productive interglacial period, whereas the latter corresponds to the glacial stages (Imbri et al. 1984; Khursevich et al. 2001)

The quantitative analysis of spicules in the Pleistocene–Holocene sediments (cores St 15, St 16, St 18, ST – 2GC, STX – 3GC) has shown that the quantitative characteristics of the spicules in the sediments also reflect the cycles of climatic alteration (Weinberg et al. 1997; Grachev et al. 1998; Weinberg et al. 1999). The high concentration of spicules in the diatom silt layers (1,500–10,000 spicules/g) coincides with the warm periods, and low quantities in the clay (100–300 spicules/g) correspond to the cold glacial periods. The data obtained for sponges' spicules correlate well with palynological and diatom analyses as well as with the common content of biogenic silica (Fig. 6).

The species' composition of the sponge fauna in the Late Pleistocene period (95 thousand years ago; kya), was similar to the recent one. The spicules of all recent sponges from the Spongillidae and Lubomirskiidae families have been found. However, the fauna was richer in some spicules of the Spongillidae family, which had disappeared in the MIS 2 and MIS 4 glacial period (Fig. 7a). Some of them recovered at the period of Holocene optimum, others became extinct. The species' composition was getting slightly impoverished in the Holocene compared to the Pleistocene. At the same time, we have found here two types of “newly appeared species” from the Lubomirskiidae (Fig. 7b). It can be assumed that in the Lubomirskiidae family the process of speciation took place.

All in all, spicules of 24 species have been revealed in the sediments of Late Pliocene (Table 4).

3.4 Baikalian Sponge Fauna of the Late Pliocene (3.2–2.1 Ma)

For investigation of the Late Pliocene sponge fauna, the sediments from one part (3.2–2.1 Ma) of the deep drilling core BDP 96/1, collected from the underwater Academician Ridg, have been used. This interval has been chosen because at that

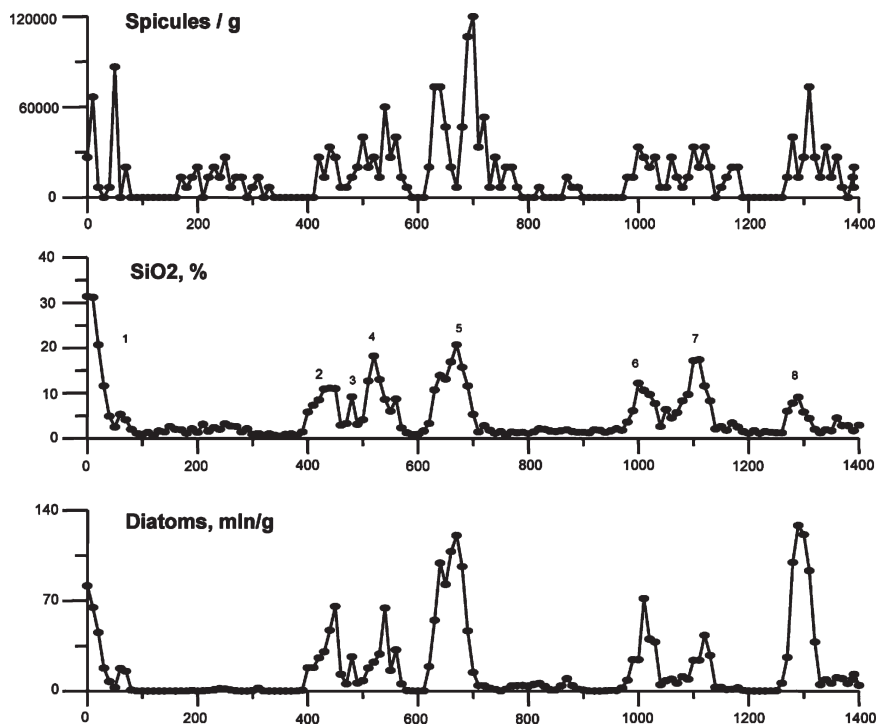


Fig. 6 Distribution of sponge spicules, biogenic silica, and frustules of diatom algae in Pleistocene core ST 16

time, according to the diatom and pollen studies on these sediments, there was a period of considerable cooling which had not previously been noticed in the Siberian climatic scales (Kuzmin et al. 1997; Khursevich et al. 1998; Bezrukova et al. 1999; Karabanov 1999).

In the sediments of the Late Pliocene, the spicules of almost all the known recent sponges that currently inhabit Lake Baikal have been found (Fig. 8).

However, the sponge fauna in the Late Pliocene (3.2–2.8 Ma) was richer by far than the recent one. As well as the spicules of nearly all the recent sponges, i.e., “transit species,” 24 spicules’ types of “extinct species,” which have no analogues with recent ones have been found. All in all, 41 types of spicules have been found (Fig. 9).

It can be assumed that the conditions characteristic of warm-water basins and lower depths compared to modern ones were typical of this period, since at that time (3.2–2.8 Ma) the rate of Spongillidae spicules amounted to 60% and the species composition of the sponge fauna was also richer. During the glacial period (2.8–2.5 Ma) which was accompanied by changes in tectonic conditions of Lake Baikal, dramatic and irreversible transformations took place in both families. The majority of the “extinct species” disappeared (Figs. 10 and 11).

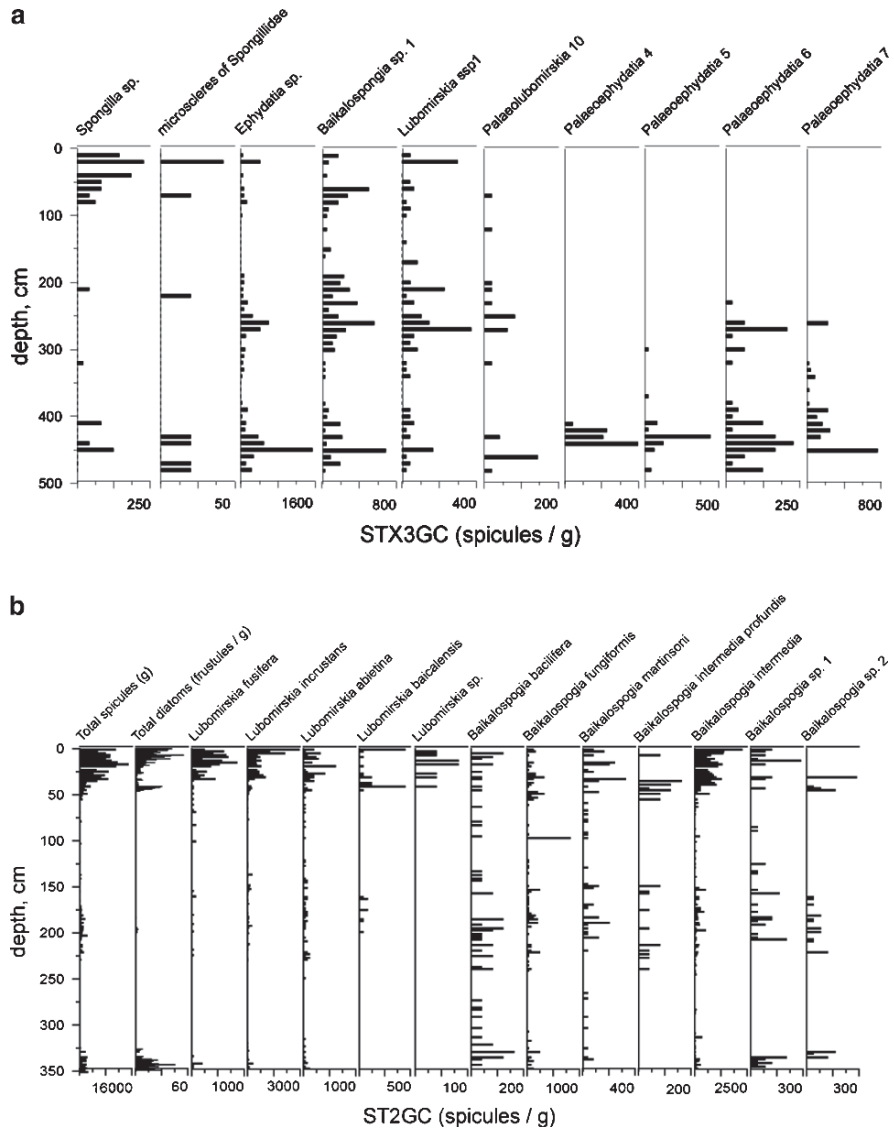


Fig. 7 Distribution of spicules of different fossil sponge species in the sediments of Pleistocene core ST2GC. **(a)** The distribution of sponge spicules in the Pleistocene core STX3GC. The species composition of the fossil sponge fauna in the Late Pleistocene (95 kya) was richer in some spicules of the Spongillidae family, which had disappeared in the MIS 2 glacial period. **(b)** The distribution of sponge spicules in the Pleistocene core ST2GC. Some types of “newly appeared species” from the Lubomirskiidae have been found in the upper part of this core, in the Holocene sediments

Table 4 The number of spicule types in Late Pleistocene bottom sediments

Total	Number of spicules							
	Lubomirskiidae				Spongillidae			
	Transit species	Extinct species	Conditionally extinct species	Newly appeared species	Transit species	Extinct species	Conditionally extinct species	Newly appeared species
24	12	0	2	2	4	2	2	0

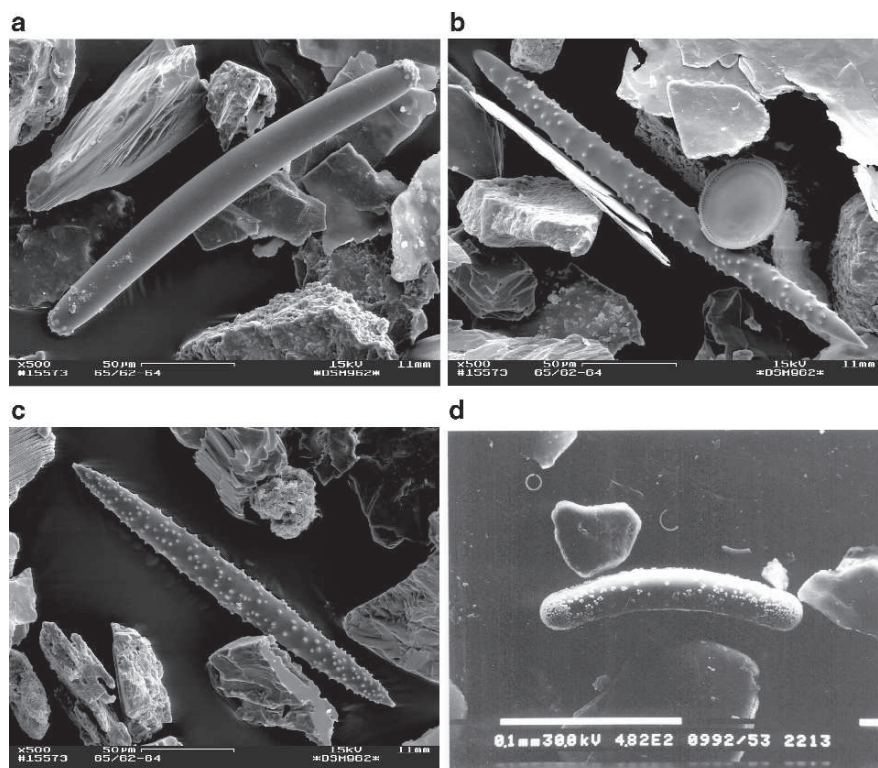


Fig. 8 The spicules of the “transit” species from sediments of BDP 96/1 deep drilling core (interval 3.2–2.8 Ma): (a) *Baikalospongia fungiformis*, (b) *B. intermedia*, (c) *Lubomirskia incrustans*, (d) *Swartschewskia papyracea* (Philips SEM 525 M and Zeiss DSM)

Modern geological research has shown that the underwater Academician Ridge was formerly an on-land formation. It began to gradually sink from the middle of the Miocene. A number of islands remained until the end of the Late Pleistocene (Khlystov et al. 2000; Mats et al. 2001).

To summarize, according to our reconstruction of the fossil sponge fauna development, the recent sponge fauna of Lake Baikal can be regarded as the impoverished fauna of the Late Pliocene.

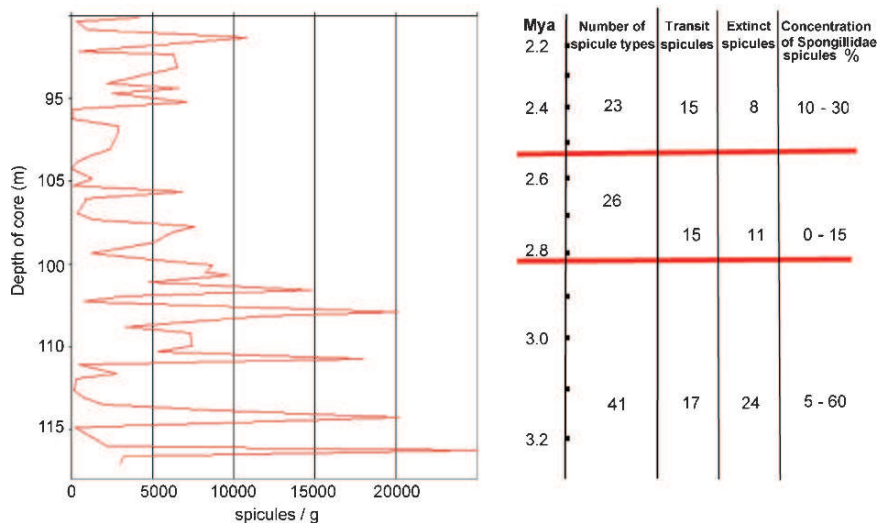


Fig. 9 Total amount of spicules in the sediments of deep drilling core BDP 96/1 (interval 3.2–2.1 Ma) and the number of types of fossil spicules at various time intervals of the Late Pliocene

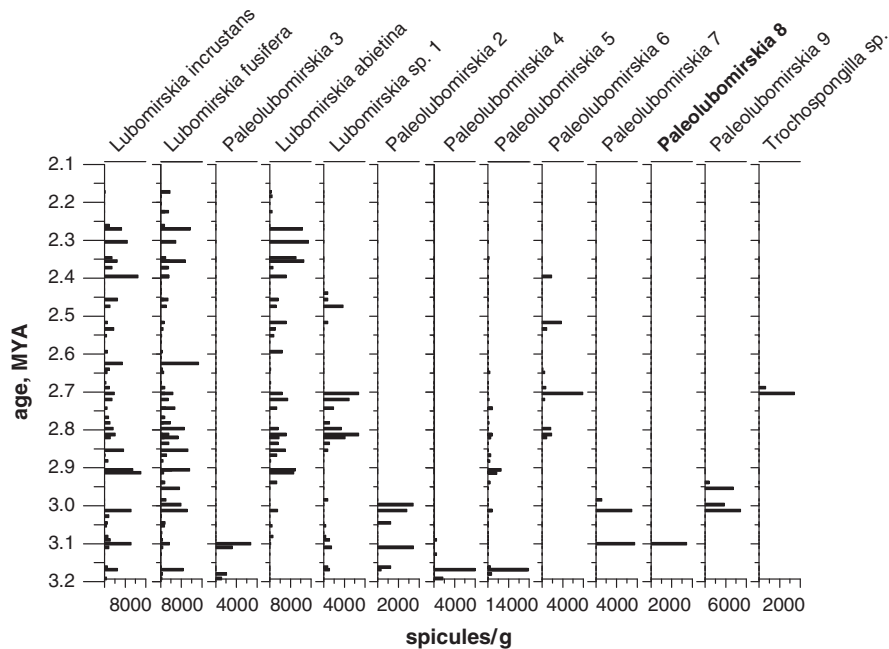


Fig. 10 The distribution of spicules of different fossil sponge species in the sediments of deep drilling core BDP 96/1 (interval 3/2–2/1 Ma)

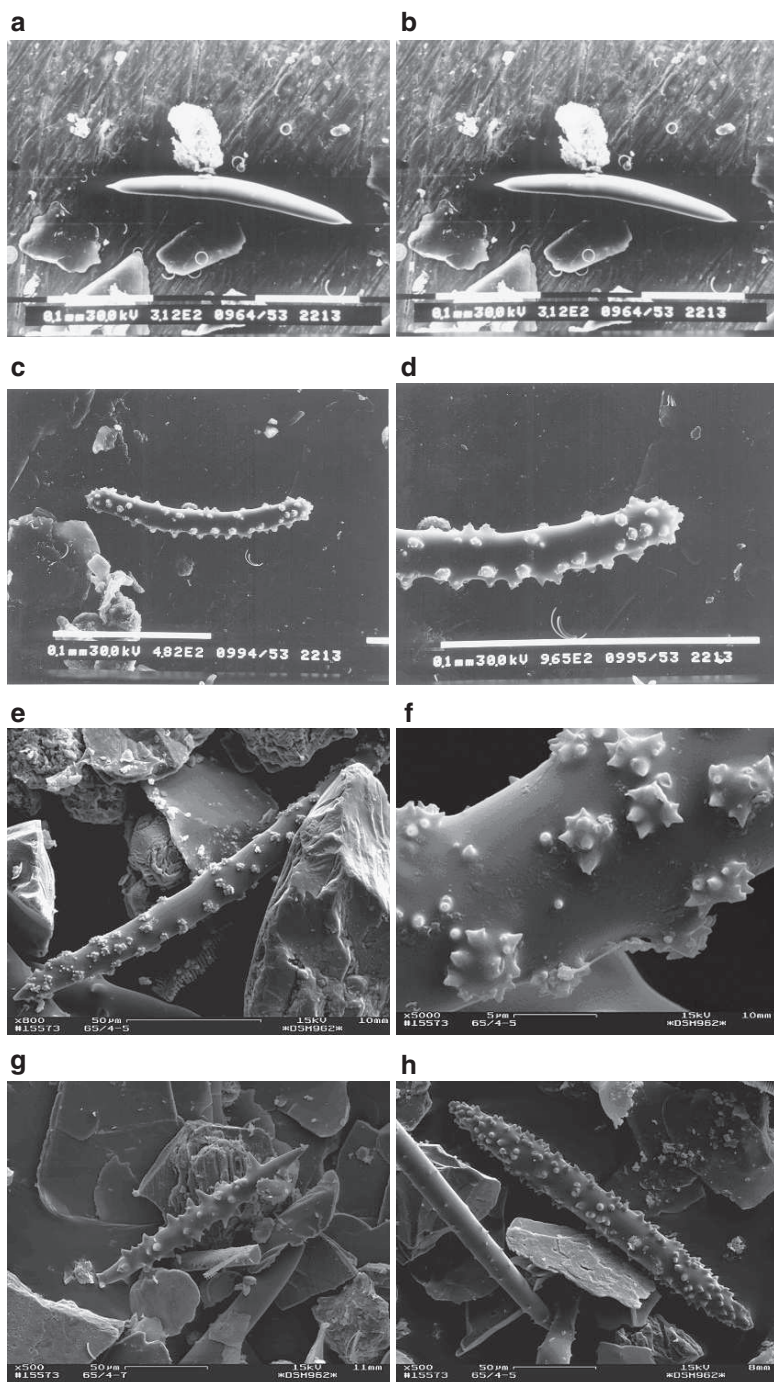


Fig. 11 The spicules of “extinct” species from the sediments of BDP 96/1 deep drilling core, Late Pliocene (interval 3.2–2.8Ma): (a, b) *Paleospongilla 1*, (c, d) *Paleoswartschewskia 1*, (e, f) *Palaeolubomirskia 8*, (g) *Paleolubomirskia 2*, (h) *Paleobaikalospongia 4* (Philips SEM 525M and Zeiss DSM)

3.5 *The Fossil Sponge Fauna of the Late Miocene*

Investigations of sediments of the deep drilling 600-m core BDP 98 has only just begun. For this investigation, we used the part of this core between 301.73 and 197.48 m, which corresponds to the period from 6.50 to 4.75 Ma and the lower part of this core aged at 10Ma. We chose this particular part (6.50–4.75 Ma) because, according to sedimentological studies, dramatic climatic changes, which appear as an alteration of sedimentological regime, took place in that period. The patterns observed and the timing of changes in the sedimentation rates are intriguing and warrant future detailed studies (Antipin et al. 2001).

Our preliminary investigations show that the changes in species composition are dependant on climactic changes. In cold climactic periods, spicules of the Lubomirskiidae family predominate, while in warm periods the Spongillidae spicules dominate. Thus, a permanent change in the sponge association took place.

In these sediments, the well-formed spicules of species of the Lubomirskiidae family can be found. Here belong: *R. arbuscula*, *B. fungiformis*, *Swartschweskia papyracea* and *L. incrustans*. We can also find here four types of spicules in the genus *Lubomirskia* which have no analogues with the recent ones. A few types of spicules in the Spongillidae family are also “new.” According to our preliminary brief investigation of the species’ composition in the sediment of this period, the sponge fauna of the Late Miocene is poorer as compared to the sponge fauna in the Late Pliocene.

3.6 *The Investigation of Terrigenous Sediment of the Tunka Land Basin*

The most ancient spicules of the Lubomirskiidae were found by G.G. Martinson in early Tertrias sediments of the South Baikal terrigenous deposit. Our study of sediments (the age approximately Late Miocene) from the Tunka land basin has shown that in these sediments the known spicules of the Lubomirskiidae family are absent. Here, the spicules of the Spongillidae family and a set of unknown spicules have been found in abundance.

Moreover, the modern investigation (by electron microscopy analysis) of diatom algae from a Tunka Miocene deposit has shown the absence of Baikalian endemic diatoms in the sediments, although in initial studies, using light microscopy analysis, a complex of endemic Baikalian diatom algae was described (Popova et al. 1989). Thus, the conclusion concerning the Miocene age of Baikalian endemic diatom flora was not supported (Lichoshvay et al. 1997)

4 Hypothesis on the Origin of Lubomirskiidae in Lake Baikal

The issue of the origin and evolution of the endemic family of Lubomirskiidae has been studied by many scientists from the beginning of the nineteenth century.

The most contradictory theories have been advanced by two groups of scientists. The first one has put forward the idea of the marine origin of Baikalian sponges (Miklucho-Maklai 1870; Dybowski 1880; Svarchevskii 1901a, b, 1923; Annandele 1913; Rezvoi 1937; Vereschagin 1930, 1937, 1940), while the second one advanced the theory of their freshwater origin (Berg 1922, 1949; Makuchok 1925, 1927a, b; Arndt 1938; Kozhov 1962, 1972; Martinson 1958, 1959, 1967).

P.D. Rezvoy, who published a new taxonomy of Baikalian sponges in 1937, was a supporter of the view of Lubomirskiidae as independent and having a later, as compared with the Spongillidae, origin in the sea. His opinion was based on certain Lubomirskiidae family characteristics which distinguish them from the Spongillidae family, i.e., the absence of gemmules in Baikalian sponges, the absence of the oscular tubes, and their sexual propagation. One of the errors, due to which many scientists classified Baikalian sponges in the marine family, was the idea of their asexual reproduction, which is similar to the one in marine sponges. This way of asexual reproduction by “sorites” – aggregations of somatic cells – which transformed into larvae, was described by B.F. Swartchewski (1925).

The paleontological research of G.G. Martinson (1958, 1967) showed that the sea had not directly participated in the formation of the fauna in Lake Baikal and that ancient continental reservoirs had been inhabited by freshwater hydrobiontes. He considered the Baikalian sponge fauna to be a “mesolimnical” element of fauna, which had originated in the low–upper Cretaceous period in the interior large freshwater basin of Central Asia.

In 1947, G.G. Martinson for the first time described the oscular tubes of Baikalian sponges which were kept in an aquarium. In 1968, the embryological research by M.A. Gureeva (1968a, b, 1972) opened a new epoch in the history of Baikalian sponge study. She described masculine sex cells and the process of oogenesis in the sponge *B. bacilifera*. She showed that “sorites” are the ovules which develop into embryos and that the process of the forming of the larva and its structure did not differ from those of the Spongillidae.

Thus, when it was discovered that the gametogenesis and embryogenesis in the Lubomirskiidae family were similar to those in the Spongillidae family (Gureeva 1968a, b, 1972), and that no sea had ever reached the Baikal region (Martinson 1958), the idea of autochthonous evolution of the Lubomirskiidae and their close connection with cosmopolitan fauna of the Spongillidae was proved (Efremova et al. 1980, 1986; Efremova 1981, 1986).

Modern molecular investigation supports this idea (Itskovich et al. 1999; Efremova et al 2002; Schröder et al. 2003; Itskovich 2005). The investigation on the basis of DNA of different genera has shown that the Spongillidae and Lubomirskiidae have a common ancestor. Estimation of the time of divergence of the Lubomirskiidae family sponges from those of Spongillidae family has been carried out on the basis of succession analysis of the COXI gene and is approximately equal to 1.3–3.8 Ma. The relative adolescence of Baikalian endemic Lubomirskiidae family is testified by the extremely short genetic distance between the species of this family, compared with that to the Spongillidae family (Itskovich 2005).

5 Concluding Remarks

To summarize, according to our studies of the recent and the fossil sponge fauna of Lake Baikal, we can show that fossil spicules are a reliable tool that can be used to investigate the evolutionary history of the Baikalian sponge fauna.

It has been shown that the sponge fauna in Lake Baikal reacted to climatic changes by variations in its quantitative characteristics and species' composition.

The species' composition of the sponge fauna in the Late Pleistocene period (95 kya), was similar to the recent one.

The sponge fauna in the Late Pliocene (3.2–2.8 Ma) was richer by far than the recent one. The recent sponge fauna of Lake Baikal can be regarded as the impoverished fauna of the Late Pliocene.

In the sediments of the Late Miocene period (6.50–4.75 and 10 Ma), the well-formed spicules of species of the Lubomirskiidae family can be found. However, the sponge fauna of the Late Miocene is poorer as compared to the sponge fauna in Late Pliocene.

In spite of all the investigational efforts, some questions on the evolution of Baikalian sponges are still to be answered.

The paleontological investigations (Martinson 1959; Kozhov 1972) support the idea of the ancient age of the Lubomirskiidae and their settlement into Lake Baikal from other regions.

The modern paleontological investigations of Baikal's bottom sediments (Weinberg 2003, 2005) show that some species of the Lubomirskiidae family existed in Lake Baikal as far back as the Late Miocene (10 Ma). However, our investigations also indicate that some spicules, which belong to recent subspecies from the Lubomirskiidae family, appear solely in the Holocene sediments.

The molecular investigation supports the idea of relative adolescence of a Baikalian endemic sponge fauna (1.3–3.5 Ma) and its close relationship with cosmopolitan fauna of the Spongillidae. It also supports the idea of the autochthonous evolution of the Lubomirskiidae family in Lake Baikal.

Thus, certain contradictory data originating from paleontological and molecular investigations are available. Further cooperative efforts by paleontologists and molecular biologists will be able to elucidate this intriguing question.

One needs to carry out further detailed investigations of species' composition of the fossil sponge fauna of the Late Miocene bottom sediments from Lake Baikal and the terrigenous sediments from the Tunka basin, as well as from the shores of Lake Baikal, and to compare these with the data obtained from molecular investigations. These unique dated bottom Baikalian sediments from deep drilling cores BDP 96 and BDP 98 and terrigenous sediments from the southern shore of Lake Baikal and its regions (Tunka basin) contain keep a unique record of the evolution of the Baikalian sponge fauna.

Acknowledgments I am grateful to my teacher and supervisor, Dr. Sofia Efremova from Sankt-Petersburg University, whose support, advice, and encouragement were invaluable and I am also very grateful to my colleague from Kawasaki Medical School (Japan), Dr. Yoshiki Masuda, for the opportunities to take samples and for his support during our team-work. I am also thankful to Mr. Carsten Eckert (Berlin) for kindly providing photos for Fig. 8 (a,b,c) and Fig. 11 (c,d,e,f,g,h).

I would also like to express my gratitude to Prof. Dr. W.E.G. Müller (University of Mainz, Germany) for his useful remarks and opportunity to contribute to this book as well as to Prof. Michail Grachev, director of the Limnological Institute (Irkutsk, Russia), where I did my research.

References

- Annandale N. (1913) Notes on some sponges from Lake Baikal in the collection of the Imperial Academy of Sciences, St.-Petersburg. L'Annuaire du Musée Zoologique de l'Académie Impériale des Sciences de St. Petersburg, 18: 96–101
- Antipin V., Afonina T., Badalov O., Bezrukova E., Bucharov A., et al. (2001) The new BDP – 98 600-m drill core from Lake Baikal: a key late Cenozoic sedimentary section in continental Asia. *Quaternary International* 80–81:19–36
- Berg L.S. (1922) Fauna of Lake Baikal and its origin (in Russian). In: *Climate and Life*. The Academy of Sciences USSR, Moscow, pp. 28–53
- Berg L.S. (1949) Baikal, its nature and its organic world origin. *Essays on Physical Geography*, Moscow-Leningrad, pp. 280–332
- Bezrukova E.V., Kulagina N.V., Letunova P.P., Schestakova O.N. (1999) Direction of changes in the flora and climate of baikalian region for previous 5 Ma (according to the data of the palinological analysis) (in Russian). *Russian Geology and Geophysics* 40: 739–749
- Bradbury J. Platt, Bezrukova Ye.V., Chernyaeva G.P., Colman S.M., Khursevich G., King J.W., Lichoshway Ye.V. (1994) A synthesis of post-glacial diatom records from lake Baikal. *Journal of Paleolimnology* 10: 213–252
- Colman S.M., Peck J.A., Karabanov E.B., Carter S.J. (1995) Continental climate response to orbital forcing from biogenic silica records in Lake Baikal. *Nature* 378:769–771
- Dybowski W. (1880) Studien über die Spongien des Russischen Reiches mit besonderer Berücksichtigung der Spongien-Fauna des Baikal-See. *Memoires de l'academie imperiale des sciences de St Petersburg*, VIIe, XXVII (6): 1–71
- Efremova S.M. (1981) The structure and embryonic development of baikalian sponge *Lubomirskia baikalensis* (Pallas). Connection of Lubomirskiidae family with other sponges. *Morphogenesis of Sponge*, Transaction of Biological Research Institute, 33: 93–107
- Efremova S.M. (1986) The embryology of family Lubomirskiidae and the problems of Lake Baikal sponge fauna origin. *Ontogenesis* 17(14):427–428
- Efremova S.M. (2001) Sponge (Porifera) In: *Annotated register of Baikal Lake fauna* (in Russian). Nauka, Novosibirsk, Vol. 1, pp. 179–192
- Efremova S.M. (2004) New genus and new species of sponge from the family of Lubomirskiidae Rezvoi. In: *Annotated register of Baikal Lake fauna* (in Russian). Nauka, Novosibirsk, Vol. 2, pp. 179–192
- Efremova S.M., Papkovskaya M.V. (1980) Spermatogenesis of baikalian sponge *Lubomirskia baicalensis* (Palass). *Studies of ultrastructure* (in Russian). *Archives of Anatomy, Histology and Embryology* 79(12):88–95
- Efremova S.M., Suchodolskaya A.N., Alekseeva N.P., Papkovskaya M.V. (1986) Common features of spermatogenesis of freshwater sponge from the families of Lubomirskiidae and Spongillidae. In: *Regularities of individual development of animal organisms*, Abstracts of VII Russian Embryology Conference, Nauka, Moscow, Vol. 1, p. 33
- Efremova S.M., Itskovich V.B., Parfenova V., Drucker V.V., Müller W.E.G., Schröder H.C. (2002) Lake Baikal: a unique place to study evolution of sponges and their stress response in an environment nearly unimpaired by anthropogenic perturbation. *Cellular and Molecular Biology* 48:359–371
- Gureeva (1968a) On sexual reproduction of Baikalian Sponge (in Russian). *Transaction of Academy of Science USSR* 80: 1253–1254
- Gureeva (1968b) Reproduction and development of baikalian sponge of Lubomirskiidae family (in Russian). *Short authorized version of the Ph.D. thesis*, Leningrad, 24 p

- Gureeva (1972) "Sorites" and ovogenesis of endemic baikalian sponge. *Cytology* XIV(1):32–45
- Grachev M.A., Vorobyova S.S., Likhoshvay Ye.V., Khlystov O.M., Bezrukova E.V., Veinberg E.V., Goldberg E.L., Granina L.Z., Kornakova E.G., Lazo F.I. (1998) A High-resolution diatom record of the palaeoclimates of East Siberia for the last 2.5 My from Lake Baikal. *Quat Sci Rev* 17: 1101–1106
- Imbrie J., Hays J.D., Martinson D.G. (1984) The orbital theory of Pleistocene climate: support from a revised chronology of the marine $\delta^{18}O$ record. In: Berger A., Imbrie J., Hays J., Kukla G., Saltzman B. (Eds) *Milankovich and Climate, Part I*. Reidel, Dordrecht, The Netherlands, pp. 269–305.
- Itskovich V.B., Belikov S.I., Efremova S.M., Masuda Y. (1999) Phylogenetic relationship between *Lubomirskiidae*, *Spongillidae* and some marine sponges according partial sequences of 18S r DNA. *Mem. Queensland Mus.* 44: 275–280
- Itskovich V.B. (2005) Molecular phylogeny and taxonomy of freshwater sponges. Ph.D. thesis, Vladivostok, 92 p
- Karabanov E. (1999) Geological structure of baikalian deposits and reconstruction of the climate changing of Central Asia in Late Cenozoic (in Russian). Short Authorized Version of the Ph.D. thesis, Moscow, 72 p
- Kashiwaya K., Ochiai S., Tsukahara H., Sakai H., Kawai T. (2003) Long-term Late Cenozoic global environmental changes inferred from Lake Baikal sediments In: *Long Continental Records from Lake Baikal*, Springer, pp. 3–21
- Khlystov O.M., Mats V.D., Vorobeva S.S., Klimanskii A.V., M. de Batist, Cheramikola S. (2000) The structure and development of the underwater Academician Ridge (Lake Baikal). *Russian Geology and Geophysics* 41: 819–824
- Khursevich G.K., Karabanov E.B. (1998) Pliocene-Pleistocene geochronology and bio-stratigraphy of bottom baikalian sediments: new results of Baikal Deep Drilling. In: *Paleoclimates and evolution of paleo-geographical conditions in the geological history of the Earth (in Russian)*. Abstracts of the International Symposium, Petrozavodsk, pp. 87–88
- Khursevich G.K., Karabanov E.B., Prokopenko A.A., Wilams D., Kuzmin M.I., Fedenya S.A., Gvozdkov A.N., Kerber E.V. (2001) Detailed diatomic and bio-stratigraphy of bottom sediments of Lake Baikal in the epoch of Bruness and climatic reasons for specification (in Russian). *Russian Geology and Geophysics* 42:108–129
- Kozhov M.M. (1962) *Biology of Lake Baikal (in Russian)*. Publisher Academy of Science USSR, Moscow, 315 p
- Kozhov M.M. (1972) *Essays on Baikal Lake (in Russian)*. Irkutsk: East-Siberian Publisher, Irkutsk, 254 p
- Kuzmin M.I., Grachev M.A., Wilams D., Kavai T. (1997) The Continuous Record of paleoclimate of previous 4.5Ma from Lake Baikal (first information) (in Russian). *Russian Geology and Geophysics* 38:1021–1023
- Lichoshvai Ye.V., Pomazkina G.V., Nikiteeva T. A. (1997) Centric diatoms in the Miocene deposits in the Baikal rift zone (in Russian). *Russian Geology and Geophysics* 38:1445–1452
- Makuchok M.E. (1925) On the problem of origin of Baikal Sponge fauna. *Russian Zoology Journal* VII(3):50–78
- Makuchok M.E. (1927a) On the taxonomy of baikalian sponge (in Russian). *Russian Zoology Journal* VII(1):5–24
- Makuchok M.E. (1927b) On the taxonomy of baikalian sponge II. On the new genus of baikalian sponge fauna – *Baikalolepis nov. gen.* and new species of this genus (in Russian). *Russian Zoology Journal* VII(1):124–131
- Masuda Y., Itskovich V., Veinberg E.V., Efremova S.M. (1999) Perspective studies of freshwater sponges in Lake Baikal. *Berliner geowiss Abh.* E30:329–332
- Martinson G.G. (1936) The Distribution of sponge spicules in the borehole in the vicinity of the village of Posolsk on the Lake Baikal (in Russian). *Transaction of Academy of Science USSR IV (XIII)(6) (110):261–264*
- Martinson G.G. (1938) The Fossil sponge fauna of the Tertrias deposit in Baikal region (in Russian). *Transaction of Academy of Science USSR* 21(4):212–214

- Martinson G.G. (1940) The materials for the study of fossil sponge fauna of Baikal region (in Russian). Studies of Baikal Limnological Station of Academy of Science USSR, Vol. 10, pp. 425–454
- Martinson G.G. (1947) About oscular tubes of baikalian sponges (in Russian). Transaction of Academy of Science USSR LVIII(1):167–169
- Martinson G.G. (1948a) Remains of animal organisms in the bottom sediments of Lake Baikal (in Russian). Transaction of Academy of Science USSR 59(2):229–302
- Martinson G.G. (1948b) The fossil sponge from Tunka land-basin in Baikal region (in Russian). Transaction of Academy of Science USSR LXI(5):897–900
- Martinson G.G. (1958) The origin of Baikal fauna from the point of view of paleontology (in Russian). Transaction of Academy of Science USSR 120(5):1155–1158
- Martinson G.G. (1959) In search of ancestry of Baikal fauna (in Russian). Issued by Academy of Science USSR, 112 p
- Martinson G.G. (1967) The problem of Baikal fauna origin (in Russian). Russian Zoological Journal XLVI(10):1594–1597
- Mats V.D., Ufimtsev G.F., Mandelbaum M.M. (2001) The Cenozoic of Baikal depression (structure and geological history) (in Russian). Novosibirsk, 253 p
- Miklucho-Maklai N. (1870) Über einige Schwämme des Nördlichen Stillen Oceans und des Eismeeres, welche im Zoologischen Museum der Kaiserlichen Akademie der Wissenschaftlichen in St. Petersburg aufgestellt sind. Ein Beitrag für Morphologie und Verbreitung der Spongien. Memoires de l'academie imperiale des sciences de St. Petersburg VIIe, XV(3):1–24
- Research Team of the “Baikal Drilling Project” (1998) Continuous record of the climatic changes at the deposits of Lake Baikal for the last 5 Ma (in Russian). Russian Geology and Geophysics 39(2):139–156
- Rezvoi P.D. (1937) Freshwater sponge (in Russian). In: Fauna of the USSR, Vol. 2 (Sponge). Academy of Science USSR, Moscow-Leningrad, 124 p
- Schröder H.C., Efremova S.M., Itskovich V.B., Belikov S.I., Masuda Y., Krasko A., Müller I.M., Müller W.E.G. (2003) Molecular phylogeny of the freshwater sponges in Lake Baikal. Journal of Zoological Systematics and Evolutionary Research 41:80–86
- Svarchevskii (1901a) Short studies of Baikal sponge fauna (in Russian). Jubilee collection, Kiev, pp. 1–7
- Svarchevskii (1901b) On the sponge of Lake Baikal (in Russian). Report of Kiev community of Nature Experimentations 14:1–15
- Svarchevskii (1923) Spongiological essays (in Russian). Proceedings of Irkutsk Nature Experimentation Society 1:1–20
- Swartschewski B.F. (1925) Spongiological essays. Asexual reproduction of *Veluspa bacilifera* (Dyb) with the “sorites” (in Russian). Transaction of Irkutsk Nature Experimentation Society 1:11–25
- Vereschagin G.Yu. (1930) On the problem of origin and history of Baikal fauna and flora (in Russian). Transaction of Committee for the Study of Lake Baikal 3:77–116
- Vereschagin G.Yu. (1937) Two types of Baikal biological complex (in Russian). Transaction of Baikal Limnological Station 6:199–212
- Vereschagin G.Yu. (1940) Origin and history of Lake Baikal, its fauna and flora (in Russian). Transaction of Baikal Limnological Station of AS SSSR 10:73–239
- Weinberg E. (2005) Sponge fauna of Pliocene – quaternary sediments of Lake Baikal (in Russian). Ph.D. thesis, Sankt, St. Petersburg, pp. 255
- Weinberg E., Eckert C., Mehl D., Müller J., Masuda Y., Efremova S. (1999) Extant and fossil sponge fauna from the Underwater Academician Ridge of Lake Baikal (Se Siberia), Memoris of the Queensland Museum 44:651–657
- Weinberg E., Weinberg I., Efremova S., Tanichev A., Masuda Y. (2003) Late Pliocene sponge fauna in Lake Baikal (from material from the Deep Drilling Core BDP – 96 – 1) In Long Continental Records from Lake Baikal, Springer, Tokyo, pp. 283–293
- Weinberg E.V., Khlystov O.M., Vorobyuva S.S., Kornakova E.G., Levina O.V., Efremova S.M. and Grachev M.A. (1997) Distribution of sponges spicules in sediments of the underwater Academician Ridge of Lake Baikal, Berliner geowiss. Abh. 20:141–145

Identification and Isolation of a Retrotransposon from the Freshwater Sponge *Lubomirskia baicalensis*: Implication in Rapid Evolution of Endemic Sponges*

Matthias Wiens, Vladislav A. Grebenjuk, Heinz C. Schröder,
Isabel M. Müller, and Werner E.G. Müller

1	Introduction	208
2	Organization of the Contig Silicatein:Baikalum-1 and the Silicatein Gene	210
2.1	Molecular Biological Methods	210
2.2	The Silicatein Gene Sequence Within the Contig Named Silicatein:Baikalum-1	213
3	Organization of the Palindromes in the Silicatein:Baikalum-1 Contig	214
4	Organization of the Retrotransposon Within the Silicatein:Baikalum-1 Contig	214
5	Occurrence of Baikalum-1	217
6	Copy Number of Baikalum-1	221
7	Inter-species Occurrence of Baikalum-1	222
7.1	Animals	222
7.2	Screening for Retrotransposon Baikalum-1	228
8	Conclusion: Evolutionary Ancient Mobile Elements in the Proximity of the Silicatein A1 Gene	229
	References	232

Abstract Transposons are mobile genetic elements that are found in all major branches of life. Similarities to retroviruses concerning genome structure and transposition mechanism suggest a familial relationship. Transposons are important evolutionary drivers that trigger genetic changes such as genomic rearrangement, alteration of gene expression, and gene duplication. And, indeed, now more than ever the effect of transposons on genome evolution represents a dynamic field of research. Since sponges (phylum Porifera) are the phylogenetically oldest still extant meta-

W.E.G. Müller (✉)

Institut für Physiologische Chemie, Abteilung Angewandte Molekularbiologie,
Universität, Duesbergweg 6, D-55099 Mainz, Germany
e-mail: wmueller@uni-mainz.de

*The sequence comprising the *Lubomirskia baicalensis* silicatein gene and retrotransposon Baikalum-1 has been deposited (EMBL/GenBank) under the accession number AM932520.

zoan taxon, the study of poriferan mobile elements contributes to the understanding of the generation of phenotypic diversity and speciation at the base of the metazoan tree of life. This work describes the analyses of the first poriferan mobile genetic element so far identified, the long terminal repeats-retrotransposon Baikalum-1 of *Lubomirskia baicalensis* (Demospongiae; Ceractinomorpha). Baikalum-1 embraces a continuous open reading frame, putatively coding for a polyprotein that consists of nucleocapsid, protease, reverse transcriptase, RNase H, and integrase, all proteins/enzymes characteristic of retrotransposons. Baikalum-1 was discovered in all freshwater sponge species endemic to Lake Baikal, as well as in cosmopolitan sponge species that inhabit a Lake Baikal-feeding rivulet. However, the same cosmopolitan species sampled from lakes and rivers (Siberian and European) with no direct contact to Lake Baikal did not contain this particular mobile genetic element. Thus, Baikalum-1 is probably the result of an evolutionarily ancient retroviral infection that spread exclusively amongst Baikalian sponge species. In addition, the retrotransposon is found in the vicinity of the silicatein-A1 gene. Silicateins are cathepsin-like proteins that catalyze the synthesis of poriferan siliceous skeletal elements (spicules). In *L. baicalensis*, the silicatein-A1 gene is flanked by two palindroms, probably remnants of transposons that might be responsible for the emergence of four different silicatein genes, uniquely present in freshwater but not marine sponges. Adaptation of sponges to the freshwater habitat (with its significantly higher silica content compared to the marine milieu) required the ability to evolve rapidly, which could be conferred by high transpositional activity, accompanied by duplication and diversification of the ancestral silicatein gene of marine species.

1 Introduction

Every genome contains mobile genetic elements, transposable elements (TE) or transposons (“jumping genes”) that can cause mutations and/or change of the amount of DNA in the genome. Transposable elements can be grouped into two classes: Class I mobile genetic elements, also termed retrotransposons, move within the genome via an RNA intermediate that is subsequently reverse transcribed to DNA; Class II mobile genetic elements on the other hand move directly from one position to another within the genome. The enzyme transposase catalyzes the underlying cut-and-paste mechanism (reviewed in Capy et al. 1998).

The abundance of TEs in eukaryotic genomes varies considerably. For example, 3% of the *Saccharomyces cerevisiae* (Kim et al. 1998) and 6% of the *Caenorhabditis elegans* genomes (*C. elegans* Sequencing Consortium 1998; Kidwell 2002) can be attributed to TEs. Even more prominent is the amount of TEs in the genomes of several “higher” eukaryotes (e.g., *Drosophila*, 10–20% (Adams et al. 2000; Hoskins et al. 2002; Kaminker et al. 2002); *Arabidopsis*, 10% (The Arabidopsis Genome Initiative 2000); mouse, 37% (Smit 1999; Waterston et al. 2002); *Homo sapiens*, 43% (Li et al. 2001); and *Vicia* spp., 90% (Flavell 1986; Pearce et al. 1996). Two functions

have been attributed to TEs. They have been viewed as (1) either neutral or deleterious components of genomes (see Orgel and Crick 1980; Charlesworth et al. 1994); thus, located within or in the proximity of genes, TEs are considered to be detrimental to gene function and might be finally removed by natural selection; or (2) TEs might be beneficial to genes, contributing to adaptive evolution (see McDonald 1993, 1995; Brosius 1999; Kidwell and Lisch 2001).

Having these views in mind, the question arose as to whether TEs also exist in the phylum Porifera and might contribute to the evolution and/or adaptation of sponges in a given environment. Lake Baikal sponges represent a brilliant model taxon with which to study those questions, since they are endemic and highly adapted to their freshwater environment in which they are rapidly evolving (reviewed in Müller et al. 2006b).

Sponges are characterized by a complex body plan (Müller et al. 2004; Müller 2005). In most cases, it features a filigree network of skeletal elements (spicules), which are arranged into the species-specific skeleton. One major breakthrough in understanding spicule/body plan formation came through the discovery of the enzymes involved in spiculogenesis. The group of Morse (Shimizu et al. 1998; Cha et al. 1999) discovered that the organic filament in the central canal of spicules is composed of a cathepsin L-related enzyme, which they termed silicatein. In subsequent years, related molecules were identified from many other sponges, among them the marine species *Suberites domuncula* and *Tethya aurantium* (Krasco et al. 2000, 2002; Schröder et al. 2004) as well as the freshwater *Lubomirskia baicalensis* (Wiens et al. 2006). Phylogenetic analyses of silicateins and related cathepsins revealed the latter forming basal branches from which silicatein sequences arose. Furthermore, several silicatein isoforms were discovered in at least five different phosphorylation states (Schröder et al. 2004; Müller et al. 2007). Thus, gene number and sequential post-transcriptional modification processes are indicative of a rather polymorphic enzyme.

In order to understand the evolutionary history of silicatein with respect to its implication in morphogenesis, one poriferan species has been studied in detail, the Lake Baikal sponge *L. baicalensis*. This species has a characteristic body plan that is composed of serial modules, which are arranged along an apical–basal axis (Wiens et al. 2006). In shallow water, *L. baicalensis* occurs only in an encrusting form, yet in deeper environments (>3 m) branches are formed in an arborescent manner. From *L. baicalensis*, four silicatein α isoforms ($\alpha 1$ – $\alpha 4$) have been so far identified that are highly expressed at the top of branches (concurrent with the expression of the regulatory protein mago nashi and the structural protein mannose-binding lectin), whereas only very low expression levels were found at the base. Furthermore, the serial modules are stabilized by bundles of spined oxeas. It was shown that spicule formation (1) starts and is completed inside of the bundles, and (2) occurs simultaneously with the expression of the mannose-binding lectin at the surfaces of the bundles. The data suggested not only a sequential formation of modules but also led to the speculation that the expressions of silicateins and mannose-binding lectin might be controlled by mago nashi (Wiens et al. 2006).

2 Organization of the Contig Silicatein:Baikalum-1 and the Silicatein Gene

Even though the importance of silicatein as a structural protein involved in morphogenesis was revealed relatively early, no information about the genomic background of silicatein was then available. Therefore, a contig of >17.5 kb, including the *L. baicalensis* silicatein gene, was isolated and analyzed.

2.1 Molecular Biological Methods

2.1.1 Isolation of Genomic DNA

To obtain a genomic library, genomic DNA (gDNA) was isolated from 300 mg of *L. baicalensis* living tissue, using the “QIAGEN Genomic DNA Isolation System” (QIAGEN, Hilden, Germany). DNA samples were then dissolved in 5 mM Tris-HCl (pH 8.0) and size-separated on agarose gels. Figure 1, lane b, shows isolated *L. baicalensis* gDNA prior to further purification via agarose gel extraction (lane a). In two extractions, major bands were observed at ca. 23 kb. gDNA isolated from an ethanol-conserved *L. baicalensis* sample appeared shorter and within a greater range of size (lane c–e).

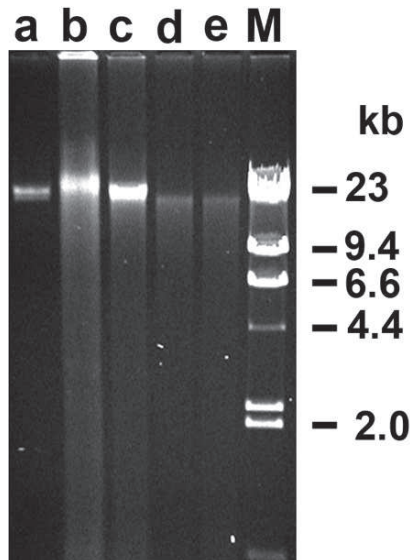


Fig. 1 Genomic DNA isolated from *Lubomirskia baicalensis*. Lane a, purified gDNA, employed for the preparation of a genomic library. Lane b, crude preparation of gDNA after extraction from sponge tissue. Lanes c–e gDNA preparations from ethanol-preserved tissue samples. M Molecular weight marker

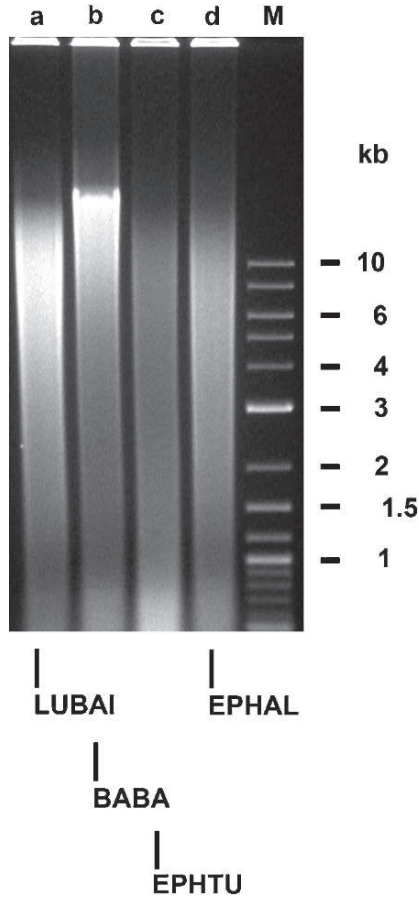


Fig. 2 gDNA isolated from ethanol-preserved tissue samples of the following sponge species: *Lubomirskia baicalensis* (lane a, LUBAI), *Baikalospongia bacillifera* (lane b, BABA), *Ephydatia tuva* (lane c, EPHTU), and *E. altaiensis* (lane d, EPHAL). M Molecular weight marker

For the analysis of further sponge specimens by polymerase chain reaction (PCR), genomic DNA was isolated from 50–100 mg of ethanol-conserved tissue by “QIAGEN DNeasy Blood & Cell Culture DNA Kit,” following the manufacturer’s recommendations. Again, gDNA quality was analyzed by agarose gel electrophoresis (Fig. 2). DNA concentrations were subsequently determined spectrophotometrically (SmartSpec Plus; Bio-Rad, München, Germany).

2.1.2 Preparation of Genomic Library

A *L. baicalensis* genomic library was constructed with the “CopyControl Fosmid Library Production Kit” (Epicentre, Madison, USA) following the manufacturer’s instructions. Briefly, gDNA (Fig. 1, lane a) was sheared mechanically and

size-fractionated by Pulse Field Gel Electrophoresis (PFGE) in low melting point agarose gel (1%), including Crystal Violet (GeneCraft, Münster, Germany) for visualization. A fraction of 40 kb was then excised, recovered with GELase (Epicentre), and ligated with pCC1FOS cosmid vector, using the “Fast-Link Ligation System” (Epicentre). Afterwards, the resulting constructs were packaged with “MaxPlax Lambda Packaging Extract” (Epicentre). Ultimately, the library titer was estimated (using EPI300 plating strain; Epicentre) to be 1×10^6 cfu/ml (4×10^6 cfu/ μ g) with an average insert size of 35 kb.

2.1.3 Homology Screening

Next, 3×10^4 clones of the *L. baicalensis* genomic library were screened with a DIG-labeled cDNA probe (“PCR DIG Labeling Mix Plus Kit,” Roche, Mannheim, Germany) that spans the complete open reading frame (ORF) of *L. baicalensis* silicatein-A1 (AJ872183). Cosmid colonies were lifted onto nylon filters (Duralon-UV Membranes; Stratagene, La Jolla, USA) and hybridized according to standard procedures (Ausubel et al. 1995). Following a successive incubation with anti-DIG-alkaline phosphatase conjugated Fab fragments and nitro blue tetrazolium chloride/5-bromo-4-chloro-3-indolyl phosphate (NBT/BCIP; Roche), more than ten positive colonies were identified. Then, DNA of three selected cosmid clones was digested, either with *Bam*HI or *Eco*RI, or with a combination of both enzymes. Finally, the digests were resolved by electrophoresis and subjected to Southern blot analyses (Ausubel et al. 1995), again applying the DIG-labeled silicatein-A1 probe.

2.1.4 Plasmid and Cosmid DNA Isolation

Plasmid and cosmid clones were routinely grown overnight in LB medium (pH 7.5), supplemented with appropriate antibiotics. In order to obtain high DNA yield following induction of the CopyControl cosmid clones, the medium was supplemented with “Induction Solution” (Epicentre) and grown for an additional 5 h at 37°C. Finally, DNA was isolated by “High Pure Plasmid Isolation Kit” (Roche), with an average cosmid yield of 5 μ g/ml culture.

2.1.5 Sequencing

Cosmid DNA was mechanically sheared, concentrated, and end-ligated in reactions containing 2 μ g DNA, 15U T4 DNA polymerase, 10U *Escherichia coli* DNA polymerase, and 0.5 mM dNTP (MBI Fermentas, Vilnius, Lithuania) (30 min, 15°C). Then the reaction mixtures were desalted and tailed with an additional dAMP residue (30 min, 50°C). For this purpose, 50 μ M each of dCTP, dGTP, and dTTP were added to 2 μ g DNA, as well as 2 mM dATP and 20U *Taq* polymerase (MBI Fermentas). Following size-separations, 2–3 kb fractions were isolated,

purified, and ligated with the cloning vector pGEM-T (Promega, Madison, USA). Subsequently, *E. coli* DH10b cells (Invitrogen, Karlsruhe, Germany) were transformed prior to plasmid preparations on a RoboPrep2500, using the Nucleospin MWG PlasmidPrep96 (MWG, Ebersberg, Germany). Sequencing was performed on an ABI 3700 capillary sequencer, applying the “BigDye Terminator Chemistry” (Applied Biosystems, Foster City, USA). Alternatively, Li-Cor 4200 sequencers were employed, using the “Thermo Sequenase–Fluorescent Labeled Primer Cycle Sequencing Kit” (Amersham Pharmacia Biotech, Freiburg, Germany).

2.1.6 Data Analyses

Compilation of sequences was achieved with the Lasergene software package (DNASTAR, Madison, USA). DNA and deduced protein sequence homology searches were performed via BLASTX and BLASTP software (<http://www.ncbi.nlm.nih.gov/BLAST/>), as well as via the ProDom server (<http://prodom.prabi.fr/prodom/current/html/home.php>). For gene prediction, the HMM-based program FGENESH on the “SoftBerry” home page was used (<http://www.softberry.com>).

2.2 The Silicatein Gene Sequence Within the Contig Named Silicatein:Baikalum-1

Figure 3 gives a schematic outline of the silicatein:Baikalum-1 contig. The complete sequence consists of 17,779 nt, comprising the following notable regions: (1) the silicatein gene (nt_{10,282}–nt_{8,171}), (2) the Baikalum-1 retrotransposon (nt_{12,491}–nt_{17,196}), and (3) two palindromes situated downstream (nt_{4,295}–nt_{4,412}) and upstream (nt_{11,846}–nt_{11,955}) of the silicatein A1 gene. The predicted silicatein gene, running in the opposite direction to the retrotransposon, comprises seven putative

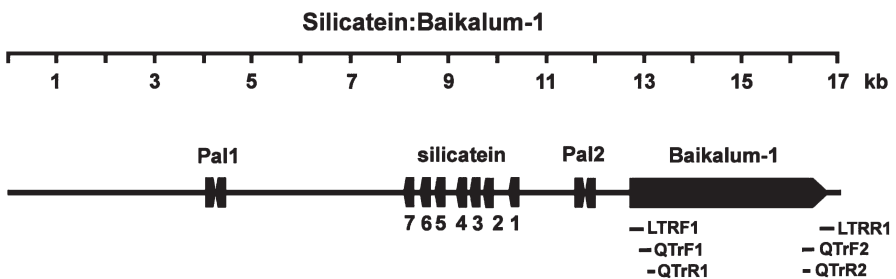


Fig. 3 Schematic outline of the silicatein:Baikalum-1 contig. The 17,779-nt-long sequence comprises the silicatein-A1 gene (*silicatein*, nt_{10,282}–nt_{8,171}) and the *Baikalum-1* retrotransposon (nt_{12,491}–nt_{17,196}). The silicatein gene is enclosed by two palindromes (*Pal1*, *Pal2*) situated downstream (nt_{4,295}–nt_{4,412}) and upstream (nt_{11,846}–nt_{11,955}) of the silicatein-A1. Primers used for screening (LTR-F1/LTR-R1) and real-time PCR (QTrF1/QTrR1 and QTrF2/QTrR2) are marked

exons (nt_{10,282}-nt_{10,004} [exon-1], nt_{9,931}-nt_{9,779} [-2], nt_{9,455}-nt_{9,341} [-3], nt_{8,961}-nt_{8,852} [-4], nt_{8,773}-nt_{8,621} [-5], nt_{8,546}-nt_{8,428} [-6], and nt_{8,344}-nt_{8,171} [-7]), coding for the deduced polypeptide (SILCAaGe_LUBAI) depicted in Fig. 4a. Comparison of the *L. baicalensis* silicatein sequence (SILCAaGe_LUBAI) with sequences of other hitherto identified silicateins (of *L. baicalensis* and *S. domuncula*) revealed the silicatein specific catalytic triad, comprising Ser, His, and Asn (Fig. 4a). In contrast, in the catalytic triad of the closest relative of silicateins, the cysteine protease cathepsin, Ser is exchanged by Cys (Fig. 4a).

It is established that for the formation of mature cathepsins posttranslational processing is required, either by autolysis or by a second protease. Based on comparisons with cathepsins, a similar cleavage site was identified in sponge silicateins, suggesting a processing of the proenzyme (Mr 36kD) to the mature form (23kD). Also, a signal peptide was discovered, ranging from aa₁ to aa₁₅ (Fig. 4a). Phylogenetic analyses were performed, including not only demospongian silicateins (*L. baicalensis*, *T. aurantium*, *S. domuncula*) but also cathepsin L sequences from Porifera (*Geodia cydonium*, *Aphrocallistes vastus*, *S. domuncula*, *L. baicalensis*) and Cnidaria (*Hydra vulgaris*) as well as a plant papain cysteine peptidase (*Arabidopsis thaliana*). The rooted phylogenetic tree thus calculated shows that cathepsin L sequences form basal branches from which silicatein sequences arise. It is noteworthy that the *L. baicalensis* cathepsin L sequence branches off as the last one in the cathepsin cluster, suggesting an evolutionarily rather recent emergence. Similarly, silicatein proteins of the freshwater sponge *L. baicalensis* branch off from marine demosponge sequences. Thus, taken together, the results provide robust evidence that this species is evolutionarily younger than marine demosponges (Fig. 4b).

3 Organization of the Palindromes in the Silicatein: Baikalum-1 Contig

The *L. baicalensis* genomic DNA contig described in this report contains two palindromes (Pal1, Pal2; Fig. 3). Each palindrome consists of two 58-bp conserved inverted-repeats (IR). The first pair of inverted-repeats (A and A') exists within nt₄₂₉₅-nt₄₄₁₂ and the second pair (B and B') within nt_{11,846}-nt_{11,955} (Fig. 5a). The palindromes are directly repeated, flanking a DNA stretch of 7,434 bp that contains the silicatein A1 gene.

4 Organization of the Retrotransposon Within the Silicatein:Baikalum-1 Contig

Upstream of the *L. baicalensis* silicatein A-1 gene, a gDNA stretch revealed the characteristics of a LTR (long terminal repeat)-containing retrotransposon that was subsequently termed Baikalum-1. This putative retrotransposon consists of 4,706 bp,

a

```

SILCAaGe_LUBAI -----HRSILFSLASLAAV--QYVVEEWHLRGQNNRNPASELRLRBAVWLSKKYV--HNRADAFGYTL 69
SILCAa2_LUBAI -----HRSILFSLHGLAAL--NCEAEVHSHKSYGHSRASELRLRBSWLSRKYI--HNSDVFEGYSL 69
SILCAa3_LUBAI MGRDGPCTVKSLEGMLNVFIAQCFCTQVELTYADPDYINLQKSVVHGHGHSRBEQEMRLRBSWLSRKYI--HNNADLFQYTL 89
SILCAa4_LUBAI -----HKLHLLDCAISIMAF--SYVVEEWHLRGQNRNPASELRLRBSWLSRKYI--HNSDVFEGYTL 69
SILCAa_SUBDO -----MIVTVVFDLGFASAAQPKFVVEEWHLRGQNRNPASELRLRDLWLSRKYI--HNNVSHIEGYTL 72
CATL_LUBAI -----HKVLLIILAAVAATAF--DPEEWSRKHGCVNDRLELRLRHWQAARKYVD--HNAEKEGEYV 67
                                     signal peptide >[ propeptide
SILCAaGe_LUBAI MNHLCDLSAEVY---EQLTNARGSNHEHREMKAGLA--KGVQVAELLDWRTRKGVAVTSVYQCCGAYAFAPRATALEGNSALNDKQ 154
SILCAa2_LUBAI MNHPCDMSEVEBK---DAILTHEPGNYTSRGIATPKA--QGMKQVVDLDWRTRKGVAVTSVYQCCGAYAFAPRATALEGNSALNDKQ 154
SILCAa3_LUBAI MNHPCDLSMEBET---ERLLTHKHSQ--RSLGQTPEES--KGVITADLDWRTRGVAVTSVYQCCGCSYAFAPRATALEGNTALADKIL 172
SILCAa4_LUBAI MNHPCDLSMEBET---AMLLTHDPGNVTHHGRKARPT--KGVQVVDLDWRTRKGVAVTSVYQCCGAYAFAPRATALEGNSALNDKQ 154
SILCAa_SUBDO MNPCDLSSEIVANYLGGRIEDKKS--GNYSKTQRDRLQDPEPVDWRTRKGVAVTSVYQCCGAYAFAPRATALEGNTALAKGNA 158
CATL_LUBAI GMINADLESSEEG--RLYNGYNNPKMKKAQSKVST--KVGDLPTVDWRTRKGVAVTSVYQCCGCSWAFSAVAGLEGHFNATGTL 152
                                     propeptide ] [ mature peptide ++++++Ser
SILCAaGe_LUBAI VLSLSEONITDCSVPVGNCGSGGCTTTRFRVYVDN-GIDTESSVSRKHSQSCQANRNTSASATGCVVSTG-YSESLSLDAVAVYGVV 242
SILCAa2_LUBAI VLSLSEONITDCSVPVGNCGSGGCTTTRFRVYVDN-GIDTESSVSRKHSQSCQANRNTSASATGCVVSTG-YSESLSLDAVAVYGVV 242
SILCAa3_LUBAI VLSLSEONITDCSVPVGNCGSGGCTTTRFRVYVDN-GIDTESSVSRKHSQSCQANRNTSASATGCVVSTG-YSESLSLDAVAVYGVV 260
SILCAa4_LUBAI VLSLSEONITDCSVPVGNCGSGGCTTTRFRVYVDN-GIDTESSVSRKHSQSCQANRNTSASATGCVVSTG-YSESLSLDAVAVYGVV 242
SILCAa_SUBDO VLSLSEONITDCSVPVGNCGSGGCTTTRFRVYVDN-GIDTESSVSRKHSQSCQANRNTSASATGCVVSTG-YSESLSLDAVAVYGVV 246
CATL_LUBAI VLSLSEONITDCSVPVGNCGSGGCTTTRFRVYVDN-GIDTESSVSRKHSQSCQANRNTSASATGCVVSTG-YSESLSLDAVAVYGVV 241
*****Ser*****
SILCAaGe_LUBAI AVAVDNTNLERLYSGVF--SSGSSSLNHEMVAVGYSYGIDYWLKNSGKNGGSGYDVRNKNOCGLIASALHFM 326
SILCAa2_LUBAI AVAVDNTNLERLYSGVF--SSGSSSLNHEMVAVGYSYGIDYWLKNSGKNGGSGYDVRNKNOCGLIASALHFM 326
SILCAa3_LUBAI AVAVDNTNLERLYSGVF--SSGSSSLNHEMVAVGYSYGIDYWLKNSGKNGGSGYDVRNKNOCGLIASALHFM 344
SILCAa4_LUBAI AVAVDNTNLERLYSGVF--SSGSSSLNHEMVAVGYSYGIDYWLKNSGKNGGSGYDVRNKNOCGLIASALHFM 326
SILCAa_SUBDO SVAVDCAVNSLERLYSGVF--SSGSSSLNHEMVAVGYSYGIDYWLKNSGKNGGSGYDVRNKNOCGLIASALHFM 330
CATL_LUBAI SVAVDNTNLERLYSGVF--SSGSSSLNHEMVAVGYSYGIDYWLKNSGKNGGSGYDVRNKNOCGLIASALHFM 327
*****Ser*****His Asn
                                     ++++++mature peptide ]

```

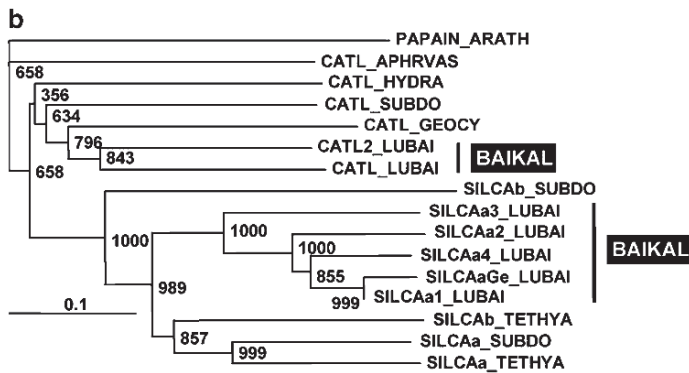


Fig. 4 Silicatein polypeptide deduced from putative exons present in the silicatein:Baikalum-1 contig. (a) The deduced *Lubomirskia baicalensis* silicatein protein (SILCAaGe_LUBAI) sequence was aligned with the presently known isoforms of silicatein- α from *L. baicalensis* (SILICAa2_LUBAI, AJ968945; SILICAa3_LUBAI, AJ968946; SILICAa4_LUBAI, AJ968947), with silicatein- α from *Suberites domuncula* (SILICAa_SUBDO; CAC03737.1), as well as with the cathepsin L sequences from *L. baicalensis* (CATL_LUBAI, AJ96849). Residues conserved (similar or related with respect to their physico-chemical properties) in all sequences are shown in *white on black*, and those in at least five sequences in *black on gray*. The characteristic sites in the sequences, i.e. the catalytic triad amino acids, His (#), Asn (#), Ser (#) in silicateins and Cys in cathepsins respectively, as well as the segments of the propeptide (-) and of the mature peptide (+) are marked. Finally, the serine cluster (*Ser*) and the putative cleavage site of the signal peptide are marked (>). (b) Phylogenetic relationship of silicateins and cathepsin L. The sequences mentioned above were analyzed, including additionally *L. baicalensis* cathepsin L (CATL2_LUBAI, AJ968951), silicatein- α of *Tethya aurantium* (SILICAa_TETHYA, AAD23951), silicatein- α 1 from *L. baicalensis* (SILICAa1_LUBAI, CAI43319), silicatein- β of *S. domuncula* (SILICAb_SUBDO, AJ547635.1) and *T. aurantium* (SILICAb_TETHYA, AF098670), cathepsin L of *S. domuncula* (CATL_SUBDO, AJ784224), *G. cydonium* (CATL_GEOCY, Y10527), *A. vastus* (CATL_APHRVAS, AJ968951), *Hydra vulgaris* (CATL_HYDRA, AAO65603), and the related papain-like cysteine peptidase XBCP3 of *Arabidopsis thaliana* (PAPAIN_ARATH, AAK71314) (outgroup). The phylogenetic tree was constructed applying the neighbor-joining method to distance matrices that were calculated using a Dayhoff PAM matrix model. Numbers at the nodes are an indication of the level of confidence for the branches as determined by bootstrap analysis (1,000 bootstrap replicates) (Dayhoff et al. 1978; Felsenstein 1993; Nicholas and Nicholas 1997)

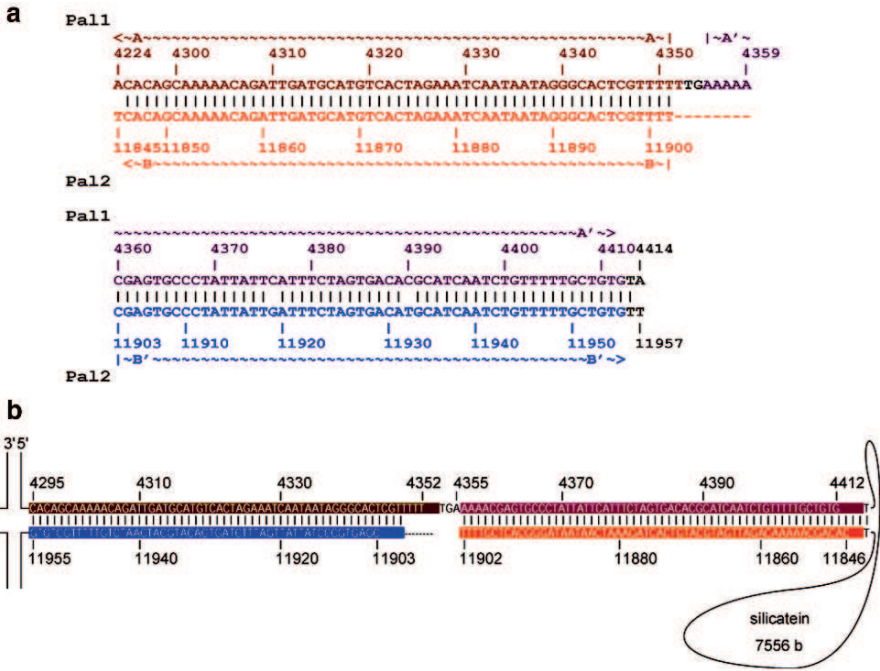


Fig. 5 Palindromes (inverted-repeat tandems) found within the silicatein:Baikalum-1 contig. (a) Nucleotide sequences comprising palindrome-1 (*Pal1*) and palindrome-2 (*Pal2*). *Pal1*: upper line, the first inverted-repeat (IR) unit is marked in brown (A), the second unit is in violet (A'). *Pal2*: bottom line, the first IR unit is in orange (B), the second IR unit in blue (B'). The numbering is consistent with the one used in Fig. 3. (b) Schematic outline of the two palindromes enclosing the silicatein gene. Color coding according to (a)

containing 202-bp LTRs (LTR-5', nt₁-nt₂₀₂; LTR-3', nt₄₅₀₅-nt₄₇₀₆). Furthermore, the sequence comprises two TATA signals (nt₁₀₃-nt₁₁₀, nt₃₃₅-nt₃₄₂) as well as a 4,275-bp ORF, including the following predicted features: nucleocapsid motif [Gag; aa₂₂₁-aa₂₃₅ (nt₈₇₀-nt₉₂₀)], protease domain [Pro; aa₂₉₄-aa₃₉₃ (nt_{1,095}-nt_{1,394})], reverse transcriptase domain [RT; aa₅₂₁-aa₆₉₆ (nt_{1,776}-nt_{2,303})], ribonuclease H domain [RH; aa₇₉₁-aa₉₀₆ (nt_{2,586}-nt_{2,933})], and integrase domain [Int; aa_{1,071}-aa_{1,216} (nt_{3,426}-nt_{3,863})] (Figs. 6 and 7). However, a chromodomain, C-terminally located of the integrase and present in several of the closest relatives of Baikalum-1 (*Ty3/gypsy* retrotransposons; see below), is not detected.

The *L. baicalensis* protein sequence, deduced from the Baikalum-1 ORF, is most closely related to those encoded by members of the *Ty3/gypsy* family, in particular the *Schistosoma mansoni* LTR-containing retrotransposons *Saci-5* and *Saci-2* [Expect value (*E*) was calculated to be $E = 8e^{-58}$; Coligan et al. 2000]. *Saci-2* (4,946 bp) also contains one single ORF (Gag, Pro, RT, RH, Int); its estimated copy number in the *S. mansoni* genome is 70–850 (DeMarco et al. 2004). A similar

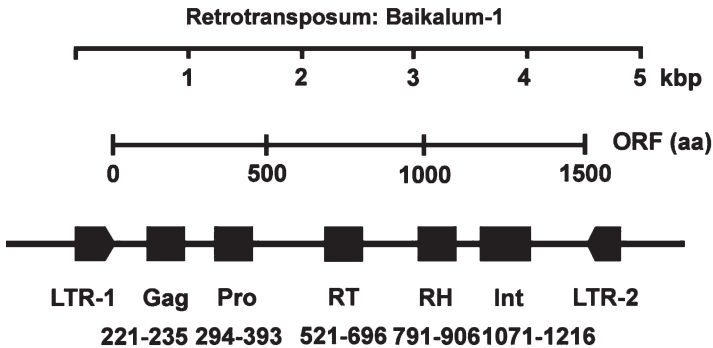


Fig. 6 Schematic representation of conserved domains present within the retrotransposon Baikalum-1. The margins of the predicted features are given: nucleocapsid motif (*Gag*), protease domain (*Pro*), reverse transcriptase domain (*RT*), ribonuclease H domain (*RH*), integrase domain (*Int*), and long terminal repeat-1 (*LTR-1*) and repeat-2 (*LTR-2*). The numbering refers to aa, the first translated aa of the Baikalum-1 ORF

organization has been described for Saci-5 (4,257 bp) that is present with 60–600 copies within the genome.

A phylogenetic tree based on analyses of RT sequences of closely related retrotransposons (including *S. mansoni* Saci-5 and Saci-2; DeMarco et al. 2004) revealed a topology in which Baikalum-1 RT clusters with the corresponding sequences of *S. mansoni* and other aquatic organisms, whereas RT of insects, yeast, and plants appeared more distantly related (Fig. 8).

5 Occurrence of Baikalum-1

Mobile elements such as retrotransposons often exist in the host genome as numerous copies of different sizes. Some copies are complete and include at least RT while others are truncated. The ratio of the number of short copies to the number of complete ones is characteristic for each mobile element. PCR with primers to LTR allows simultaneous detection of all retrotransposon sizes. However, due to the competitive nature of PCR, shorter products are amplified most efficiently. PCR success does not only rely on the choice of polymerase but is also affected by the quality of template DNA (the shorter the DNA template the lower the yield of long-sized PCR products). In our hands, best results were obtained with the “FailSafe PCR PreMix–D Selection Kit” (Epicentre).

Thus, to investigate whether Baikalum-1 also exists in other specimens of *L. baicalensis* and to find possible variants of this retrotransposon gDNA was screened via PCR, employing primers that target LTRs: forward primer LTR-F1 5'-CGGGTATTTCTCGTTGTCAAGC-3' (positions nt_{12,626}–nt_{12,647}) and reverse primer LTR-R1 5'-GAATGTTCTACTTGGTCATCCG-3' (nt_{17,077}–nt_{17,056}) (Fig. 9).

BAIKALUM-1_LUBAI	MAASNHVSIPEP-----FQSGNISEWFTRFDICDANEVNDNRRAIILPPTLEGLALAVINDLS	59
SACI-2_SCHIMA	MEVFTTKRDEMINEPPIVVKPTTCSAPROPPLLENSDVTYVTK-ERVMAALRKRVPASQDFYLYSYL	67
BAIKALUM-1_LUBAI	AEERKKSYSARKV-----ETTVS---RITPNTTSMITE-----QFROKRLIPGEALSIFLHDKRQTLDDQA	113
SACI-2_SCHIMA	SDSATKRAIVNGFAADNTTAQNWKILDDCSPTVPDPQQAIRLRLSHQTEGENPMPYFNSLQQAQVQA	135
BAIKALUM-1_LUBAI	MFKLDAGAREQLIHTHSLAGLPGVVSQOLRAAGDTTKIQTTLDRAKLLMSLEDEQVLAIVSTBAEKPR	181
SACI-2_SCHIMA	FECLDATTGDEILIKRSFVIGLSSSLKEHFLLNPTDINSILKRVFRMAALRKRVPASQDFYLYSYL	203
BAIKALUM-1_LUBAI	VSENRVVEQLVEQVAALSKQVEALSTRPENQOQDFREVCFFCGKPGCHIRN-GRVLSFQPDARNQQ	247
SACI-2_SCHIMA	VQPTKASRFLNFORIISNVTSSHWNSR-RQFNPTKRWKPTNS---YHGRQSECFYQSRFGKNAKCC	267
BAIKALUM-1_LUBAI	GN---FRGMSAAGNSHPRKLLSPHKPIVIALKSEVSTIIGITGDKEIDVMLDSSGSSVLSLRKBAIAGV	313
SACI-2_SCHIMA	CHNRFGNTSKPYIFHLSYSYANHVREPTIKAR-----VQGDIDVFLLDTGASVSLIRSEFISLGR	325
BAIKALUM-1_LUBAI	NAIVKDKP SLNVRVVTAAGENPPLHYHTARVKLNMDVRVHDSLVENIVAAALGVDFLRQGLLLD	381
SACI-2_SCHIMA	NRKVC-QTRHPSTLLTASDPPKRVNSKVVLDLMLIDRHSFRGCFVCPITLWDMILGVDFRLEH----	387
BAIKALUM-1_LUBAI	FRTPTVTVSPPNASETQSYSDDGHSLNLEKIWARAKKRDACSVABITQDDTIVQVDEKIPAFGD	449
SACI-2_SCHIMA	-R---ACDFMSLSEARFGETRIRLHHTNTP-----FRVSYVIGSDLVRVQVNDKPRKEK-D	439
BAIKALUM-1_LUBAI	QTGLEPAPYVRPCNSVVRKFNDFLLSNPQVKAATHEHNVGPF-BAVRPFRRIPVHFQEEVHEQIRN	516
SACI-2_SCHIMA	R---HPTIAVQOQSSVFEES-----HSGNRSTVQHTICGHDHRLQPPRRVPEVHYQVQDITMIDK	499
BAIKALUM-1_LUBAI	MLQKCTIESSSEPVVAEYAVYRKRKTEIRLCVDYRELLKRRHKDAVPLFLDEVDRLSCGTVFTKID	584
SACI-2_SCHIMA	MLDGNLIVSSSPVAEILVKKKDSRLRLCIDYRRLNATLRDSDPPEPRIDAILSGACWFLSD	567
BAIKALUM-1_LUBAI	HSGYQVQVNCEDQKTAFFSPGPMGLFOFYRMPFGLCCASSFQRLMNIIRGLP--YVTTQDDV	650
SACI-2_SCHIMA	HASCYQVQVVRPQDRKKTAFVVPN---GLYEEQVMPFGLTINAPATFORLQVQLQDVTVPHKCLILDDI	633
BAIKALUM-1_LUBAI	ITHSPSEFHHKHKHEAATVTRQAGTLTRGSKQCGVAVQVYVGLGVFAEGMTPDNSKVOAVWQVWF	718
SACI-2_SCHIMA	ILVYGSFPEQBNANKAVIHELQHNLRVKSQRKRLQKREVFLEGRIRVADGKTRKRVQVWVWF	701
BAIKALUM-1_LUBAI	SDATEVROPTGLASYRRTYQHFADTARPLHRIITKDTTCWSECEQAFRLNKTKLKAPITLAVRF	786
SACI-2_SCHIMA	RSPEDEVRSPLGLASYRVRVDFASLSAAPLHRIITKGRKSLWTECOQAFDALKTRISSPILAVVDT	769
BAIKALUM-1_LUBAI	DKEASPLVITDASLITGLGAVLEQ---NGC---VTIAYASRLTISEVNSVIOREKCLAVVWGTQREHY	849
SACI-2_SCHIMA	SANGGEFIDDDSSALGAVLSQVAPDGOEVRTIAYASRLTISEVNSVIOREKCLAVVWGTQREHY	837
BAIKALUM-1_LUBAI	LLGRPEQVTDHPEPRKIVGQK-MEGLTICRWALAOEYTVIILYKRGALINGNADALSRRADEKPKYPA	916
SACI-2_SCHIMA	LLKRPFRVTDHRAIQVLSFREPQGVARQWERLOEDDTCFYPFGSRHYNADALSR--TEQTAGTV	903
BAIKALUM-1_LUBAI	ATAVQVNVYMERIRHAQHDDITKHLMEDIKATN-PLSKPQRCQLQPWRVYQIWSQLSVVDGVVCR	983
SACI-2_SCHIMA	NAVDSAVPVDWPSLQADDPDQIITYQROIQGNRRESMRLKQSLTTRRICTKSNLRTYGDITFLI	971
BAIKALUM-1_LUBAI	YTPDPTGDVVTVVPLKCLQHKAVVECHDHPAAGHQSQRTLHRQQAIVVNSMAQDVDQCRGQK	1051
SACI-2_SCHIMA	NEARQP--DI---VVVRITKVESIVRQVHRK--LGEACRRREYAVRQREWILSMHEDVQIQRKQNTC	1032
BAIKALUM-1_LUBAI	QCSK-LCTETRAPLPTIGRFPQVAVDVLQVPSVNN-NKYLVMQDYFTKADAKTKDQALAVI	1117
SACI-2_SCHIMA	CRFSRPROSRAPLTPVVTTCBQRVGHDMGPLTTRKGNRILVLMWDYFTKKECAVPLPQDQALAVI	1100
BAIKALUM-1_LUBAI	STELVLELQVYGLPEIITHSDQANFESTLIGTLEAFGVKKSHTVYHPEGDMGVERENRITLQITR	1184
SACI-2_SCHIMA	ARAFIDHIVSRKCAFSLHSDQCAPAESRLAICQLLVKRVKRTVAHYHPEGGLVPERNRSIKALIQ	1168
BAIKALUM-1_LUBAI	TYVKK--KPEERKYLDELAFVYRTAVHSSVGVTEPKMLYCRFP--SNCHTFSFPGHEAN---QSPAVT	1245
SACI-2_SCHIMA	AEVSRSSQELDDVLEQCLLYAYRSTVHSGTGFSPATLLFCHELRLEPHEQVPLPCEQEHVPIRITL	1236
BAIKALUM-1_LUBAI	QSKLKLQDVEBNAHNAACRQKSHYDKTSSRHHVADGVVLSITFG---GLDPTQCRWRKKS	1308
SACI-2_SCHIMA	RRLADAYRLVSSNLRKASEHOKDLYDRRVHGVFVKVQDRVWVRRMSSGSCSKFHQFQVQVPEVIL	1304
BAIKALUM-1_LUBAI	VKSPLEIVETDCEK----TKIVHVNVRHROVENDTPGNPSSHQGTYPWSESVVDHCEIETTTTHLH	1372
SACI-2_SCHIMA	HRSTDFVIRNLQSPQDDVITVHVNQHKPDRVTVSSDAQGANPPATTFYVPESEGGTAYCPRPGTE	1372
BAIKALUM-1_LUBAI	VQGEPTQDQDDREVPDEPQDPTNIQVMPRRYPDRTRHPPERYGRGSSSGRAAN	1425
SACI-2_SCHIMA	DSAYLRGAV	1382

Fig. 7 Alignment of the deduced polyprotein encoded by the Baikalum-1 ORF with the polyprotein sequence encoded by the closely related retrotransposon Saci-2 of *Schistosoma mansoni* (SACI-2_SCHIMA; accession number DAA04499.1). Residues conserved (similar/related with respect to their physico-chemical properties) in both sequences are shown in white on black. The conserved regions protease (*Pro*), reverse transcriptase (*RT*), RNase H (*RH*), and integrase (*Int*) are marked

Each reaction contained 50% two-fold concentrated PCR PreMix-D, 10 picomols of each primer, and 5–10 ng of *L. baicalensis* gDNA.

Cycling conditions (iCycler; Bio-Rad) were as follows: 2 min initial denaturation at 95°C, followed by 35 cycles of denaturation (95°C, 20 s), annealing (appropri-

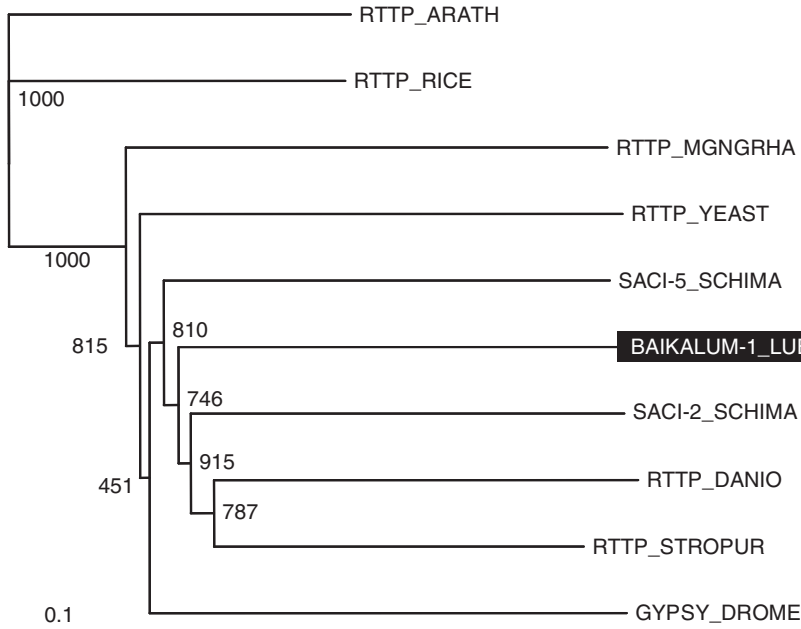


Fig. 8 Phylogenetic analysis of the deduced reverse transcriptase (RT) encoded by the *Lubomirskia baicalensis* retrotransposon Baikalum-1. Baikalum-1 RT (BAIKALUM-1_LUBAI) was aligned with the retrotransposon-encoded RT of *Schistosoma mansoni* SACI-5 (SACI-5_SCHIMA; aa₄₄₁-aa₆₁₅; CAJ00251) and SACI-2 (SACI-2_SCHIMA; aa₃₀₄-aa₆₈₀; DAA04499.1), as well as the related sequences from *Danio rerio* (RTTP_DANIO; aa₇₇₆-aa₉₅₁; XP_688848), *Magnaporthe grisea* [Grasshopper] (RTTP_MGNGRHA; aa₃₈₇-aa₅₆₄; M77661.1), *Strongylocentrotus purpuratus* (RTTP_STROPUR; aa₂₂₅-aa₄₀₁; XP_786277), *Drosophila melanogaster* (GYPSY_DROME; aa₂₀₈-aa₃₉₀; P10401), *Saccharomyces cerevisiae* (RTTP_YEAST; aa₆₄₉-aa₈₂₃; Q7LHG5), *Oryza sativa* (RTTP_RICE; aa₅₆₃-aa₇₃₉; AAV31274), and *Arabidopsis thaliana* (RTTP_ARATH; aa₆₈₆-aa₈₆₂; AAD20658). The phylogenetic tree was constructed based on distance matrices and rooted with the *A. thaliana* sequence. Scale bar indicates an evolutionary distance of 0.1 aa substitutions per position in the sequence

ate *T*, 20s), and elongation (70°C, 5 min). However, for the first five cycles, the annealing temperature was 60°C, followed by five cycles at 59°C, and 25 cycles at 58°C. Eventually, the amplified DNA was A-tailed at 70°C (20 min) and ligated with the cloning vector pGEM-T. At least three clones were sequenced for each PCR product.

Analyses of four *L. baicalensis* specimens produced three major bands of 1.4, 3.0, and 4.5 kb (Fig. 10). In some instances, other bands were visible, but no band exceeding 4.5 kb was observed. Since sequencing revealed that the 4.5 kb product corresponds to the transposon copy already found in the cosmid clone described above, it is considered as a full-sized complete copy. However, the remaining PCR products appeared truncated between identical LTRs, thus displaying different sizes, resulting in frame-shifts and the emergence of stop codons (Fig. 9).

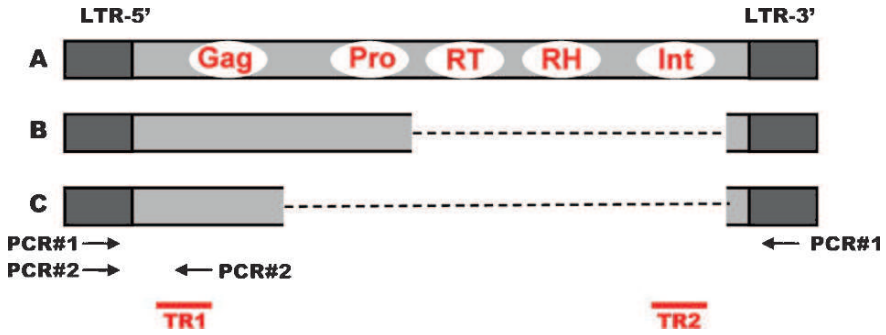


Fig. 9 Schematic representation of Baikalum-1. Three variations of the retrotransposon were discovered in *Lubomirskia baicalensis* specimens. (A) Full length copy (17,779 nt), comprising long terminal repeats (LTR-5', LTR-3') and an ORF coding for the conserved domains/motifs of nucleocapsid (Gag), protease (Pro), reverse transcriptase (RT), ribonuclease H (RH), and integrase (Int). (B, C) Truncated copies of Baikalum-1 (ca. 3.0 and 1.4 kb, respectively), also identified in *L. baicalensis* individuals, resulting in frame-shift and premature stop of translation. Primer combinations to detect full-sized and truncated copies are indicated, PCR#1 and PCR#2, respectively

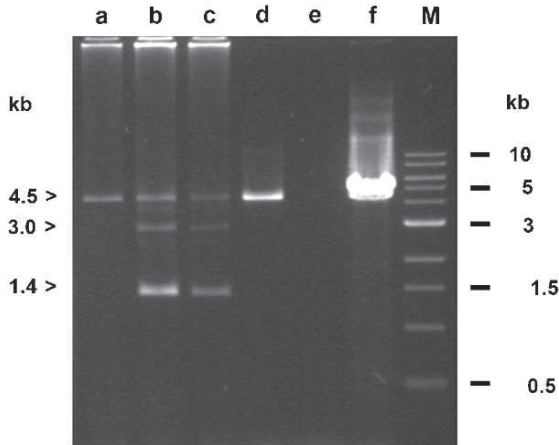


Fig. 10 Identification of full-length and truncated copies of Baikalum-1. gDNA of four *Lubomirskia baicalensis* specimens was analyzed for the presence of the retrotransposon via PCR, employing the primer combination QTrF1/QTrR1. The resulting amplicons enclose the region between LTR-5' and LTR-3'. Lanes a–d, amplicons of four individual *L. baicalensis* DNA samples. Lane a, template DNA shown in Fig. 1 lane c. Lane b, template DNA shown in Fig. 1 lane d. Lane c, template DNA shown in Fig. 1 lane e. Lane d, template DNA shown in Fig. 1 lane b. Lane e, negative control (no template DNA). Lane f, positive control (cosmid genomic clone as a template). Copy sizes are given in kb. M Molecular weight standard

6 Copy Number of Baikalum-1

The copy number of any repetitive element in a given genome can be determined as the ratio to the number of copies of any single (unique) gene present in the sample. For reliable quantification by Real-Time PCR, the efficiency of amplification must be equal for all targets – reference and query. To achieve equal efficiency, PCR conditions were optimized using control templates (i.e., cloned targets) with known concentrations. As reference, the silicatein-A1 gene was used, and as a control, the genomic cosmid clone, containing one copy of silicatein-A1 as well as of Baikalum-1. This template provides exactly a 1:1 gene to mobile element ratio, which is not affected by possible errors due to unwanted differences in template quantity and quality. Since truncated and full-sized copies of Baikalum-1 were identified, two target sites were applied for qPCR in order to quantify the copy number selectively (Fig. 9). Target site Tr1, located at the 5'-terminus of the ORF (within gag), allows quantification of all copies, whereas Tr2 (located at the ORF 3'-terminus) uniquely allows detection of full-sized copies. As reference, a target within exon-2 of silicatein-A1 was chosen (Sil). The sites read: QPCR Target#1 “Tr1” (116 bp amplicon) – all transposon copies, QTrF1 5'-GGGCTTCCTGGCACCGTTAG-3' (nt_{13,102}–nt_{13,121}). QTrR1 5'-GCCACCGTCTGCTCATCCTC-3' (nt_{13,217}–nt_{13,198}), as well as QPCR Target#2 “Tr2” (129 bp amplicon) – longest transposon copies, QTrF2 5'-TTTGGAGTAAAGAAATCGCACAC-3' (nt_{16,165}–nt_{16,187}), QTrR2 5'-GGTACTTTTCCACTCCTCTTTC-3' (nt_{16,294}–nt_{16,272}), and Reference Target “Sil” (92 bp amplicon) – Lb Silicatein-A1 gene (exon-2), QLbSil1F 5'-GCCGAAGAATATGTGGAGCAG-3' (nt_{9,928}–nt_{9,908}), QLbSil1R 5'-TGGAC-CCCTTTCGGAGCTAG-3' (nt_{9,837}–nt_{9,856}).

Since *L. baicalensis* contains four different silicatein genes, the silicatein-A1 specific binding of the primers had to be verified. Therefore, silicatein-A2, -A3, and -A4 coding cDNAs were used as template. However, with the primer set chosen, no amplification through qPCR could be observed. All experiments were performed on two separate five-fold dilution series for each individual genomic DNA sample. qPCR conditions and template dilution rates were optimized until the obtained quantification results within the series matched the dilution factor.

qPCR was performed via “Absolute QPCR SYBR Green Mix” (Abgene, Hamburg, Germany) in an iCycler PCR machine. The two-fold concentrated PCR premixes contained 5 picomoles of each primer and 0.02–2.0 ng template DNA. Cycling conditions were as follows: initial denaturation/enzyme activation (95°C, 15 min), followed by 40 cycles (95°C, 30 s; 59°C, 30 s; 72°C, 30 s). Fluorescence data was collected at 72°C during elongation. All calculations were done by the data analysis module that is part of Bio-Rad's iCycler software package.

The qPCR results revealed a total of 8–22 Baikalum-1 copies per *L. baicalensis* genome (with an average of 13), among them 6–10 full-sized copies (average 8).

Thus, 38.5% of all copies are incomplete and the ratio of total copy number to full-sized copy number is 1.62.

7 Inter-species Occurrence of Baikalum-1

Since the retrotransposon described in this report is the first mobile element identified in Porifera, different sponge taxa were screened for its presence, in particular taxa found within the Lake Baikal habitat. However, the studies were also extended to marine sponges as well as to cosmopolitan freshwater species.

7.1 Animals

7.1.1 Marine Species

Representatives of the marine class of Demospongiae were collected in the vicinity of Rovinj (Croatia, Mediterranean Sea) and in the nearby Limski Canal. This fjord-like canal is located about 15 km to the north of the marine station in Rovinj. Limski is ecologically unique in that it is separated from the open sea by a sediment barrier which prevents fluctuation of biotic and abiotic parameters (reviewed in Müller et al. 2003; Schröder et al. 2004). Its meandering course hampers the organismal life from mixing with that in the open sea. Hence, this canal represents an ecological situation allowing for the evolution of “endemic” species, with the example of *T. limski* (Demospongiae; Hadromerida; Tethyidae) (Müller and Zahn 1968). This species is closely related to the orange-yellow *T. lyncurium* (*T. aurantium*), which is ubiquitously distributed throughout the Mediterranean Sea. Three individuals of *T. limski* were collected. In addition, from the open sea, two individuals of *S. domuncula* (Demospongiae; Hadromerida; Suberitidae), four individuals of *G. cydonium* (Demospongiae; Astrophorida; Geodiidae), and two individuals of *Timea unistellata* (Demospongiae; Hadromerida; Timeidae) were studied. In addition, three individuals of one representative of the poriferan class of Calcarea were included (*Sycon raphanus*; Calcarea; Calcaronea; Leucosolenida; Sycettidae).

7.1.2 Cosmopolitan Freshwater Species

From the River Rhine (near Mainz, Germany), the following widely occurring species were collected: one individual of *Trochospongilla horrida* (Demospongiae; Haplosclerida; Spongillina; Spongillidae), and two individuals of *Spongilla lacustris* (Demospongiae; Haplosclerida; Spongillina; Spongillidae). In addition, two individuals of *Ephydatia fluviatilis* (Demospongiae; Haplosclerida; Spongillina;

Spongillidae) from Lake Constance (near Constance, Germany) were included in this study.

7.1.3 Endemic Freshwater Species of Lake Baikal

From Lake Baikal (Figs. 11 and 12), the following endemic species were chosen: *L. baicalensis* (Demospongiae; Haplosclerida; Spongillina; Lumobirskiidae; five individuals) (Fig. 12c–f), *Baikalospongia bacillifera* (Demospongiae; Haplosclerida; Spongillina; Lumobirskiidae; six individuals) (Fig. 12b), and *Swartschewska papyracea* (Demospongiae; Haplosclerida; Spongillina; Lumobirskiidae; five individuals) (Fig. 12a). *L. baicalensis* individuals were collected from Bolshye Koty, Olhon Island, and Cape Orlovsky sites; *B. bacillifera* and *S. papyracea* from Bolshye Koty and Olhon Island.

7.1.4 Freshwater Species from a Lake Baikal Feeding Rivulet

In addition to the species populating Lake Baikal, sponge specimens were collected from a rivulet that flows into the lake (Fig. 11; Listvinch site). There, a non-determined species was collected. Closer inspection revealed megascleres of the acanthoxeas type, covered by small spines, very similar to those described for *E. mülleri*, while microscleres are absent (Penney and Racek 1968). Seven individuals were studied. Furthermore, a second species was discovered that appears closely related to *S. lacustris* since it is rich in microscleres (fusiform oxeads) with dense spines or asterose-like skeletal elements. Also, the megascleres have an appearance typical for smooth and fusiform oxeads (Penney and Racek 1968); five individuals were studied.

7.1.5 Species from Lake Chagytai in South Siberia/Northwest Mongolia

During an expedition in September 2006, sponge specimens from south Siberia/northwest Mongolia were collected in the Tuva region, focusing on Lake Chagytai and Lake Tore-Khol (Fig. 10). Lake Baikal and the Tuva lakes are separated by a high mountain range, which acts as a barrier against the spreading of species living on either side (Kashiwaya et al. 2000; Müller et al. 2006b). The Tuva region, which remained largely undiscovered until the 1940s (Leimbach 1936, 1949; Greze and Greze 1958), comprises many lakes, among them Lake Chagytai. Furthermore, it is the headwater region of the great Jenisej River that runs towards the northwest. Lake Chagytai is located in the southeast region of the Tuvinskaya Valley, approximately 750 km to the west of Lake Baikal and the Hovsgol basins. This area had been formed during the Eocene period at the rims of the Eurasian Platform/Siberian Craton and the Central Asian Deformation Zone (Sankov et al. 2003). The descrip-



Fig. 11 Lake Baikal, Lake Chagytai, Lake Tore-Khol and surrounding areas. The border between Russia/Siberia and Mongolia is marked in *blue*. Lake Chagytai is located south of the city Kyzyl, the capital of Republic Tuva; it is connected with the River Jenisej through the rivulet Mozhalik. The lower map represents an enlargement of this region, including the second sampling site in Lake Tore-Khol

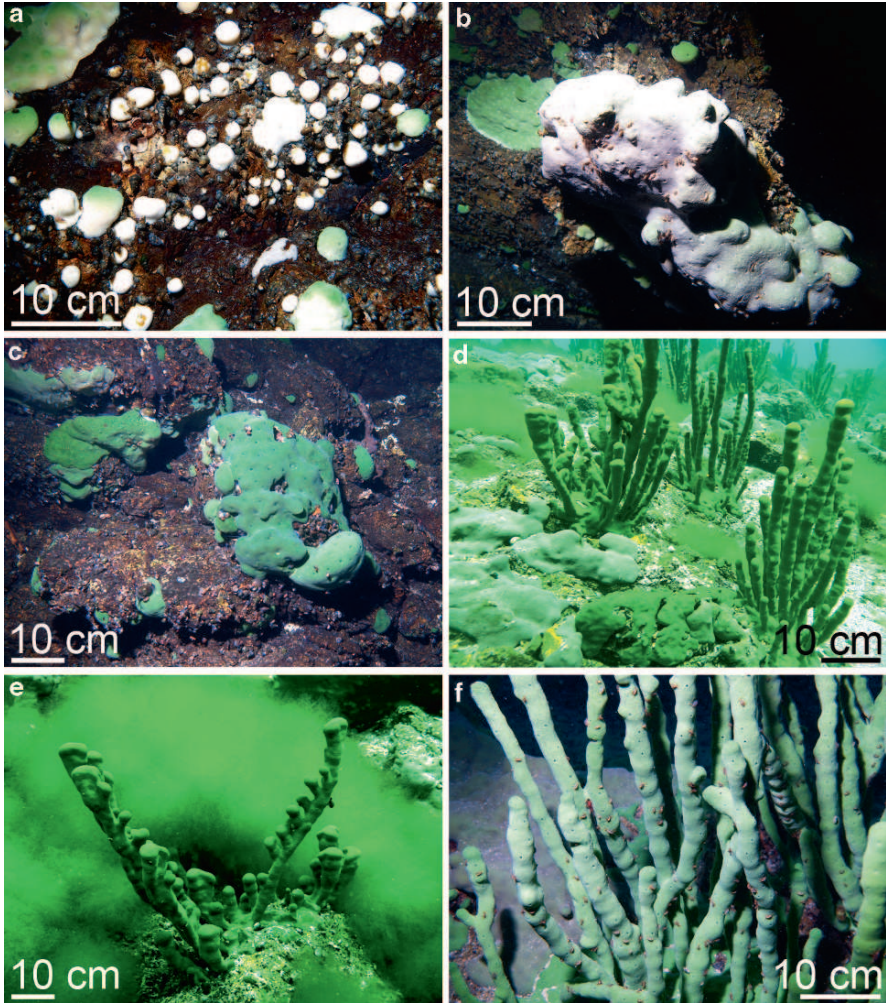


Fig. 12 Endemic Lake Baikal species. (a) *Swartschewskia papyracea* is a 2- to 5-cm-sized spherical species, living secluded under ledges in a depth of 8–15 m. *S. papyracea* has a white color, in contrast to the co-existing *Lubomirskia baicalensis* specimens, which are green and display in this depth a bark-like growth form. (b) *Baikalospongia bacillifera* specimens with a spherical appearance, showing mostly a whitish color; depth 6 m. (c–f) The most abundant species in the lake is *L. baicalensis*. This species has various growth forms, ranging from spherical (c; depth 4 m) to arborescent (d–f; depth 8–15 m). The arborescently growing specimens can reach sizes of over 1 m

tion of Lake Chagytai by Greze and Greze (1958) is already reasonably comprehensive. This lake is located at 51°N, 94°40'E and has a diameter of 5–6.5 km; its maximum depth is 17 m. Its bottom is composed of silt, found both in the littoral and profundal zones. The climate is typically continental, with relative warm summers

(20°C in July; water temperature of 18°C) and cold winters (−20°C in March; water temperature of 1°C); winds are mostly from the north and east. Because of the low temperatures in winter it can be assumed that the lake is then covered completely by ice. The visibility in the lake is low (only 6.5 m), compared to the extremely high visibility in Lake Baikal of ca. 40 m. Lake Chagytai sponge specimens were collected from depths of 7–15 m. The visibility of the water was poor, reflecting the high load of diatoms. In general, Lake Chagytai is rich in diatoms, with the cosmopolitan species *Melosira granulata* dominating.

The first description of sponges in Lake Chagytai dates back to Rezvoj (1927). During the September 2006 expedition, the southeast shore in the vicinity of the rivulet Mozhalik, a sandy region, was chosen as a major collection site (Fig. 13a–c). The ionic compositions of Lake Baikal and Lake Chagytai differ in some crucial aspects: The absolute mineral concentration in Lake Baikal is lower with approximately 100 mg/l compared to 320 mg/l in Lake Chagytai (Greze and Greze 1958). Also striking is the higher concentration of bicarbonates in Lake Chagytai compared to Lake Baikal (189 vs 64 mg/ml). Nitrogen is low in both lakes, reflecting an oligotrophic biotope.

Only in 1927 were the Lake Chagytai sponge specimens collected in 1915 analyzed (Rezvoj 1927). These samples were described as a new species and termed *B. dzhegatajensis* Rezvoj 1927. An interesting remark in this description is that *B. dzhegatajensis* co-exists with the cosmopolitan sponge *S. lacustris* (Greze and Greze 1958). In contrast to the endemic Lake Baikal species, the Lake Chagytai specimens have either a less pronounced arborescent growth form, as is the case for *L. baicalensis*, or a spherical appearance combined with a hard consistency, as is the case for *B. bacillifera* and *S. papyracea* (Fig. 12). Based on skeleton, growth form, and resemblance to the genus *Ephydatia*, the current classification of the Lake Chagytai sponge specimens to the genus *Baikalospongia* has to be rejected. Thus, for the present study, it was preliminarily termed *E. tuva*.

7.1.6 Species from Lake Tore-Khol in South Siberia/Northwest Mongolia

To the best of our knowledge, no geographic information on Lake Tore-Khol is available – at least in English literature. Only the report of Granö (1910), from his expedition, gives some insight into the harsh climate and living conditions of this region. The lake is located at 50°N, 95°E and basically represents a twin-lake with an average depth of 20 m. Whereas the western part is small and horseshoe shaped with a diameter of 5.5 km, the eastern part is more oval, with a longer axis of 8 km and a smaller one of 5 km. It is here where samples were collected. The sponge specimens, most abundantly found in the southern part of the lake (depth of 7–12 m), revealed a habitus more rigid than that of the Lake Chagytai specimens (*E. tuva*). Furthermore, they displayed an intense green color, originating from colonization with green dinoflagellates that are related to *Gymnodinium sanguineum*

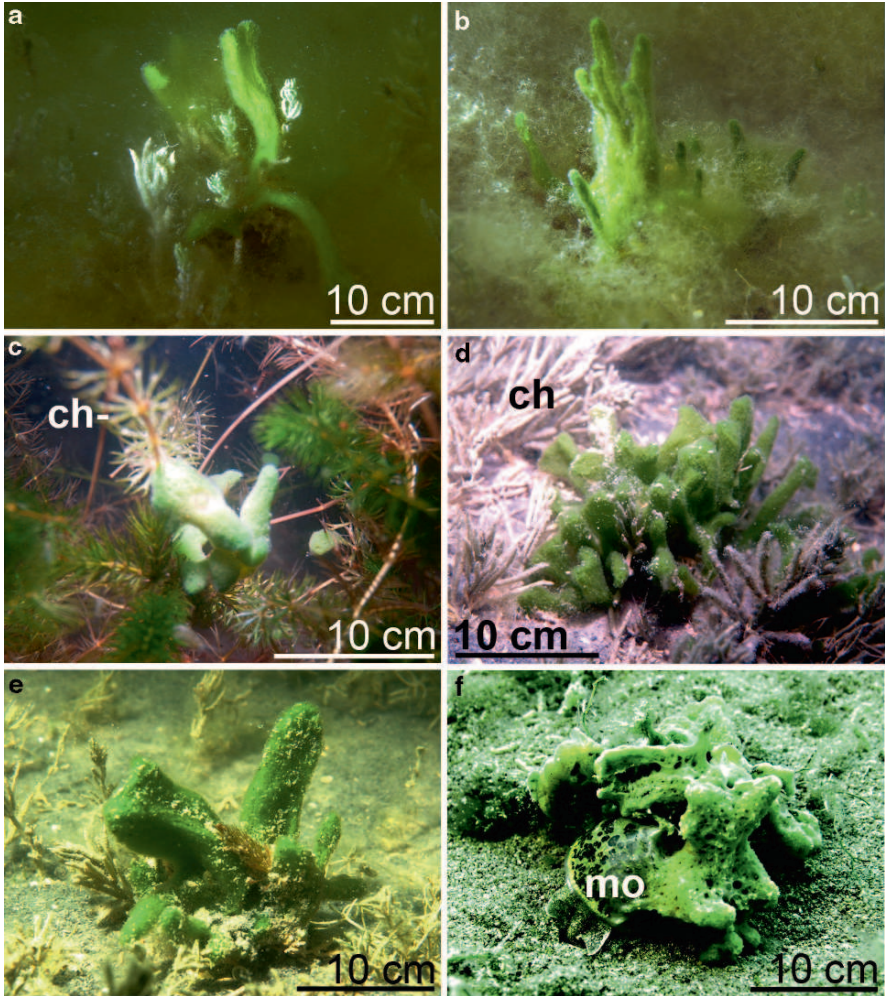


Fig. 13 Species from two lakes in south Siberia/northwest Mongolia: Lake Chagytai and Lake Tore-Khol. (a–c) Specimens collected in Lake Chagytai, preliminarily termed *Ephydatia tuva*. Most of these specimens grow on gray-green branched multicellular algae, preferentially on *Chara* (ch). (d–f) Specimens collected in Lake Tore-Khol, temporarily termed *E. altaiensis*. Whereas this species also grows on *Chara* (ch), many individuals are also found on the mollusk *Baicalia herderiana* (mo). The *Ephydatia* species described here usually reach average sizes of 5–10 cm

(see Müller et al. 2006a), and which are abundantly located in the tissue close to the surface of the specimens (Fig. 13d–f). The animals reach sizes of up to 65 mm. Again, based on spicule size and shape as well as on their habitus, these specimens were grouped to the genus *Ephydatia* and subsequently tentatively termed *E. altaiensis*.

7.2 Screening for Retrotransposon *Baikalum-1*

In order to verify whether *Baikalum-1* is present in different sponge species, PCRs were performed with primers targeting 5'-LTR ("LTR-F1") and gag ("QTrR1"; 5'-GCCACCGTCTGCTCATCCTC-3', nt₁₃₂₁₇-nt₁₃₁₉₈) (Fig. 9). This primer combination allowed amplification of a fragment (592 bp), present in all *Baikalum-1* variants found in the *L. baicalensis* genome. PCR reactions contained the two-fold concentrated FailSafe PCR PreMix, 10 pmol of each primer and 5–10 ng of sponge gDNA. Cycling conditions were as follows: initial denaturation (95°C, 2 min) and 35 cycles of denaturation (95°C, 20 s), annealing (59°C, 20 s), and extension (72°C; 1 min). Cloning was done as described above. At least three clones were sequenced for each PCR product.

Surprisingly, *Baikalum-1* was detected exclusively in sponges from Lake Baikal and the Lake Baikal rivulet (Listvinch site). Thus, 560- to 590-bp PCR products were identified in all the Lake Baikal endemic species, i.e., from five *L. baicalensis* individuals, six *B. bacillifera* individuals, and five *S. papyracea* individuals (Fig. 14). Also, *Baikalum-1* was identified in the *S. lacustris* and *E. mülleri*-related species of the Lake Baikal rivulet. In contrast, no signals were detected in any specimen collected at Lake Tore-Khol and Lake Chagytai, even though they are also clearly *Ephydatia*-related (i.e., *E. tuva* and *E. altaiensis*; Fig. 14). Furthermore, the retrotransposon could also not be detected in the cosmopolitan freshwater sponges collected in Europe: *T. horrida*, *S. lacustris*, and *E. fluviatilis*. In addition, no amplification products were obtained from the marine demosponges *T. limski*,

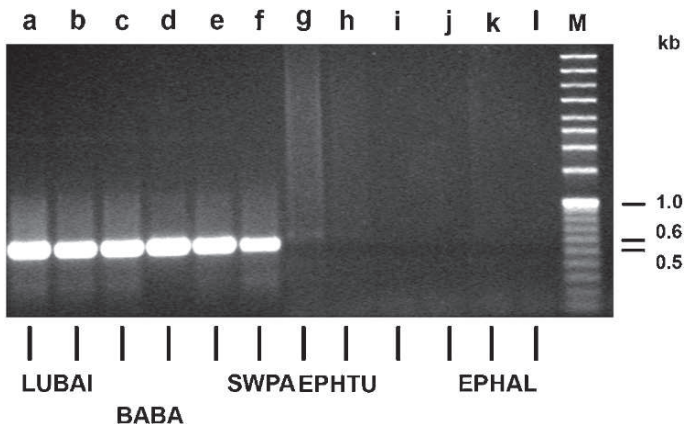


Fig. 14 Retrotransposon *Baikalum-1* detection in different sponge species. Several poriferan freshwater species were screened for the presence of *Baikalum-1* via PCR, employing the primer combination LTR-F1/QTrR1. The retrotransposon was detected not only in *Lubomirskia baicalensis* (LUBAI), but also in other Lake Baikal sponge species (i.e., *B. bacillifera* [BABA] and *S. papyracea* [SWPA]) but was not identified in the Lake Chagytai/Lake Tore-Khol species, *E. tuva* (EPHTU) and *E. altaiensis* (EPHAL). For each species tested, representative results of, respectively, two–three specimens are shown

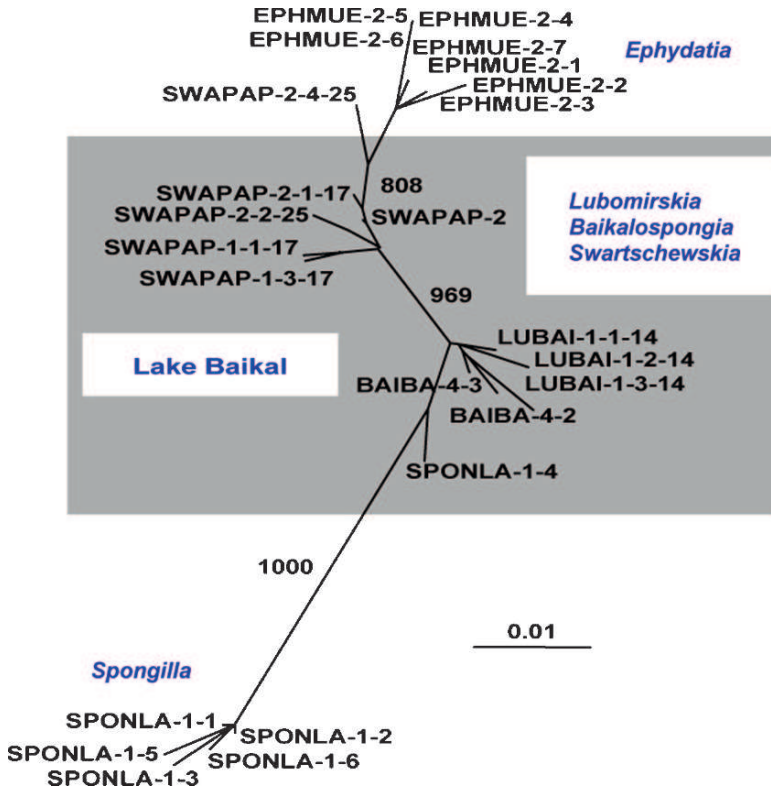


Fig. 15 Phylogenetic relationship of the Baikalum-1 sequences obtained from different Lake Baikal endemic sponge species; *Lubomirskia baicalensis* (LUBAI), *Baikalospongia bacillifera* (BAIBA) and *Swartschewskia papyracea* (SWAPAP), also including the cosmopolitan species *Ephydatia muelleri* (EPHMUE) and *Spongilla lacustris* (SPONLA), collected near Lake Baikal. Fragments of 560–590bp, between 5'-LTR and Gag region, have been amplified, cloned, sequenced, and aligned. Based on NJ analyses, an unrooted tree was constructed

T. lyncurium, *S. domuncula*, *G. cydonium*, and *T. unistellata*. Finally, no signal was seen in the calcarean species *S. raphanus*. A preliminary phylogenetic relationship (unrooted tree) is given in Fig. 15.

8 Conclusion: Evolutionary Ancient Mobile Elements in the Proximity of the Silicatein A1 Gene

The genomic contig isolated from the endemic (Lake Baikal) freshwater sponge species *L. baicalensis* contains the silicatein A1 gene, one of four different silicatein A isoform genes discovered in the *L. baicalensis* genome (Wiens et al. 2006), as well as several mobile genetic elements surrounding the silicatein A1 gene.

Mobile elements can be grouped according to their mechanism of transposition into class I and class II transposons, both of which have been shown to contribute considerably to gene evolution, thus representing important evolutionary drivers (e.g., Ganko et al. 2003; Makalowski 2003; Hedges and Batzer 2005). *Ty3/gypsy* retrotransposons are part of long terminal repeats (LTR)-bearing class I transposable elements that are present in many plant, fungal, and metazoan genomes. Since phylogenetic analyses found significant similarities between reverse transcriptase (RT) domain sequences of retrovirus and *Ty3/gypsy* retrotransposons (Xiong and Eickbush 1990), and furthermore since all *Ty3/gypsy* transposable elements contain in addition to gag sequences pol gene domains in the order protease (P) – RT – ribonuclease H (RH) – integrase (I), they were classified as viruses (Metaviridae) (Malik and Eickbush 1999). Metaviridae have been divided into three genera based on the presence/absence of envelope (*env*) and chromointegrase genes (Marin and Llorens 2000).

The LTR-containing retrotransposon Baikalum-1 first discovered in the sponge *L. baicalensis* (2.2kb upstream of the silicatein A1 gene) encodes a single large ORF that features significant sequence similarities to all protein domains characteristic for Metaviridae class, including gag, P, RT, RH, and I. Sequence homologies were found in particular to the *S. mansoni* LTR-containing retrotransposons Saci-2 and Saci-5 (DeMarco et al. 2004, 2005).

The parasitic platyhelminth (flatworm) *S. mansoni* (subclass Digenea) is mainly found in tropical/subtropical areas. Even though its life cycle includes an intermediate snail host, not all platyhelminths are parasitic and characterized by mollusk associations. Since Lake Baikal harbors a wealth of flatworms (Goldman 2003), horizontal transfer of ancestral Baikalum-1 from/to a platyhelminth ancestor (possibly even via a molluskan vector) at some time during recent evolution appears conclusive.

Baikalum-1 is represented in the *L. baicalensis* genome by a relatively low copy number (though mostly full-sized), whereas the most closely related retroelements, Saci-2 and Saci-5, were found in the *S. mansoni* genome in a one order of magnitude higher copy number. Copies of the retrotransposon Baikalum-1 were identified in all sponge species endemic to Lake Baikal (i.e., not only *L. baicalensis* but also *S. baicalensis* and *B. bacilifera*). Furthermore, the retrotransposon was discovered in cosmopolitan freshwater sponge species (*Spongilla* sp. and *Ephydatia* sp.), though uniquely in specimens that populated rivers with direct contact to Lake Baikal. In contrast, *Spongilla* and *Ephydatia* specimens collected in waters with no contact whatsoever to Lake Baikal [e.g., Tuva lakes (south Siberia/northwest Mongolia), Lake Constance (south Germany), or River Rhine (west Germany)] did not carry a single copy of retrotransposon Baikalum-1. Therefore, we conclude that this transposable element represents the result of an evolutionary ancient retroviral infection of freshwater sponges that uniquely spread amongst closely related poriferan species (suborder Spongilina) inhabiting Baikalian waterbodies, and occurred after the geohistorical emergence of Lake Baikal.

In contrast to class I mobile genetic elements that move within the genome of their host via the enzyme reverse transcriptase and an RNA intermediate, class II mobile elements (DNA transposons) relocate mainly via a cut-and-paste mechanism, using

the transposase enzyme encoded by them (Curcio and Derbyshire 2003). During this process, the transposase first recognizes both ends of the DNA transposable element (comprising inverted terminal repeats (ITR)). Subsequently, not only is a recipient DNA site cleaved (generating cohesive ends) but so also is the transposon cut out (double strand breaks) and ligated with the thus prepared target DNA. Afterwards, a DNA-polymerase and -ligase fill the gaps and reestablish the phosphoester bonds of the sugar-phosphate backbone, generating short direct repeats that flank the transposon at its new position (Brillet et al. 2007). DNA transposons are doubtlessly involved in gene transduction, duplication, and exon shuffling. For example, Pack-MULE transposon-mediated gene duplication in *Arabidopsis* gave rise to genes retaining functional coding capacity with putative novel function (Hoen et al. 2006).

The *L. baicalensis* silicatein A1 gene is embraced by two palindromes with structural similarity to bacterial insertion sequences (Pal1 and Pal2, ca. 3,800bp downstream and 1,600bp upstream, respectively). They probably represent the evolutionary remnants of two DNA (class II) transposons: At one point during evolution, functional DNA transposons probably invaded the poriferan host DNA at positions flanking the last common ancestor of poriferan silicateins. Instead of each insertion sequence (IS) element moving separately, the entire length of DNA spanning from one IS element to the next following might then have formed one unit, rendering the intervening region mobile. Thus, a composite transposon, including genomic DNA sequences that contain the silicatein gene, was then excised due to the enzymatic activity of a transposase that recognized the outer repeats. This process might have involved intermediary stem-loop-like structures already described for miniature inverted-repeat transposable elements (MITE) (Izsvak et al. 1999).

Because of DNA gap repair via homologous recombination during the S phase of the cell cycle, the excised element might then have been restored at the original site, using the sister chromatid as template (Feschotte and Pritham 2007). Multiple transposition events within the sponge genome would then have led to the generation of one or more copies of the silicatein ancestor that evolved independently to the present-day silicatein isoforms A1–A4 that can be found in the endemic sponge species of Lake Baikal (family Lubomirskidae). Furthermore, as a result of aborted gap repair, the transposons lost their ability to synthesize transposase (resulting in only a few remaining nucleotides between the ITR) (Rubin and Levy 1997). Though this modification precludes autonomous transposition, internally deleted nonautonomous elements may still transpose by using enzymes, encoded elsewhere in the genome by an autonomous copy, that only require to recognize the inverted terminal repeats (Craig et al. 2002).

Acknowledgments We thank Professor F. Brümmer (Biologisches Institut/Zoologie, Universität Stuttgart, Germany) for providing us with the samples from the German freshwater sponges. Professor S.I. Belikov (Limnological Institute of the Siberian Branch of Russian Academy of Sciences, Irkutsk, Russia) helped us to collect the endemic sponges in the Lake Baikal region during our expeditions 2003–2007. This work was supported by grants from the Bundesministerium für Bildung und Forschung Germany (Center of Excellence: BIOTECmarin) and the Deutsche Forschungsgemeinschaft (SPP 1174: Deep Metazoan Phylogeny).

References

- Adams MD, Celniker SE, Holt RA et al. (2000) The genome sequence of *Drosophila melanogaster*. *Science* 287:2185–2195
- Ausubel FM, Brent R, Kingston RE, Moore DD, Smith JA, Seidmann JG, Struhl K (1995) *Current Protocols in Molecular Biology*. Wiley, New York
- Brillet B., Bigot Y, Auge-Gouillou C (2007) Assembly of the Tc1 and mariner transposition initiation complexes depends on the origins of their transposase DNA binding domains. *Genetica* 130:105–120
- Brosius J (1999) Genomes were forged by massive bombardments with retroelements and retrosequences. *Genetica* 107:209–238
- Caenorhabditis elegans* Sequencing Consortium (1998) Genome sequence of the nematode *C. elegans*: a platform for investigating biology. *Science* 282:2012–2018
- Capy P, Bazin C, Higuier D, Langin T (1998) Dynamics and evolution of transposable elements. Landes Bioscience, Austin, TX
- Cha JN, Shimizu K, Zhou Y, Christiansen, SC, Chmelka, BF, Stucky, GD, Morse, DE (1999) Silicatein filaments and subunits from a marine sponge direct the polymerization of silica and silicones *in vitro*. *Proc Natl Acad Sci USA* 96:361–365
- Charlesworth B, Sniegowski P, Stephan W (1994) The evolutionary dynamics of repetitive DNA in eukaryotes. *Nature* 371:215–220
- Coligan JE, Dunn BM, Ploegh HL, Speicher DW, Wingfield PT (2000) *Current Protocols in Protein Science*. Wiley, Chichester, pp. 2.0.1–2.8.17
- Craig NL, Craigie R, Gellert M, Lambowitz AM (2002) *Mobile DNA II*. American Society of Microbiology Press, Washington, DC
- Curcio MJ, Derbyshire KM (2003) The outs and ins of transposition: from mu to kangaroo. *Nat Rev Mol Cell Biol* 4:865–877
- Dayhoff MO, Schwartz RM, Orcutt BC (1978) A model of evolutionary change in protein. In: Dayhoff MO (ed) *Atlas of Protein Sequence and Structure*. National Biomedical Research Foundation, Washington, DC, pp. 345–352
- DeMarco R, Kowaltowski AT, Machado AA, Soares MB, Gargioni C, Kawano T, Rodrigues V, Madeira AM, Wilson RA, Menck CF, Setubal JC, as-Neto E, Leite LC, Verjovski-Almeida S (2004) Saci-1, -2, and -3 and Perere, four novel retrotransposons with high transcriptional activities from the human parasite *Schistosoma mansoni*. *J Virol* 78:2967–2978
- DeMarco R, Machado AA, Bisson-Filho AW, Verjovski-Almeida S (2005) Identification of 18 new transcribed retrotransposons in *Schistosoma mansoni*. *Biochem Biophys Res Commun* 333:230–240
- Felsenstein, J, 1993 PHYLIP, ver. 3.5. University of Washington, Seattle
- Feschotte C, Pritham EJ (2007) DNA Transposons and the evolution of eukaryotic genomes. *Annu Rev Genet* 41:331–368
- Flavell RB (1986) Repetitive DNA and chromosome evolution in plants. *Philos Trans R Soc Lond B Biol Sci* 312:227–242
- Ganko EW, Bhattacharjee V, Schliekelman P, McDonald JF (2003) Evidence for the contribution of LTR retrotransposons to *C. elegans* gene evolution. *Mol Biol Evol* 20:1925–1931
- Goldman E (2003) Puzzling over the origin of species in the depths of the oldest lakes. *Science* 31:654–655
- Granö, JG (1910) *Beiträge zur Kenntnis der Eiszeit in der Nordwestlichen Mongolei*. Helsingfors: J. Simelii.
- Greze VN, Greze II (1958) Ozero Chagytai. *Izvestija Vsesoyuznogo Geographiceskogo Obscestva* 90:279–284
- Hedges DJ, Batzer MA (2005) From the margins of the genome: mobile elements shape primate evolution. *BioEssays* 27:785–794
- Hoen DR, Park KC, Elrouby N, Yu Z, Mohabir N, Cowan RK, Bureau TE (2006) Transposon-mediated expansion and diversification of a family of ULP-like genes. *Mol Biol Evol* 23:1254–1268

- Hoskins RA, Smith CD, Carlson JW, et al. (2002) Heterochromatic sequences in a *Drosophila* whole-genome shotgun assembly. *Genome Biol* 3:RESEARCH0085–0085
- Izsvák Z, Ivics Z, Shimoda N, Mohn D, Okamoto H, Hackett PB (1999) Short inverted-repeat transposable elements in teleost fish and implications for a mechanism of their amplification. *J Mol Evol* 48:13–21
- Kaminker JS, Bergman CM, Kronmiller B et al. (2002) The transposable elements of the *Drosophila melanogaster* euchromatin: a genomics perspective. *Genome Biol* 3:RESEARCH0084–0084
- Kashiwaya K, Tanaka A, Sakai H, Kawai T (2000) Paleoclimatic signals printed in Lake Baikal sediments. In: Minoura K (ed) *Lake Baikal*. Elsevier, Amsterdam, pp. 53–70
- Kidwell MG (2002) Transposable elements and the evolution of genome size in eukaryotes. *Genetica* 115:49–63
- Kidwell MG, Lisch DR (2001) Perspective: transposable elements, parasitic DNA, and genome evolution. *Int J Org Evol* 55:1–24
- Kim JM, Vanguri S, Boeke JD, Gabriel A, Voytas DF (1998) Transposable elements and genome organization: a comprehensive survey of retrotransposons revealed by the complete *Saccharomyces cerevisiae* genome sequence. *Genome Res* 8:464–478
- Krasko A, Batel R, Schröder HC, Müller IM, Müller WEG (2000) Expression of silicatein and collagen genes in the marine sponge *Suberites domuncula* is controlled by silicate and myotrophin. *Eur J Biochem* 267:4878–4887
- Krasko A, Schröder HC, Batel R, Grebenjuk VA, Steffen R, Müller IM, Müller WEG (2002) Iron induces proliferation and morphogenesis in primmorphs from the marine sponge *Suberites domuncula*. *DNA Cell Biol* 21:67–80
- Leimbach W (1936) *Die Landeskunde von Tuwa – das Gebiet des Jenissei-Oberlaufes*. Julius Perthes Verlag, Gotha
- Leimbach W (1949) Neue Beiträge zur Geomorphologie von Tuwa. *Petermanns geographische Mitteilungen [Gotha]* 93:66–75
- Li WH, Gu Z, Wang H, Nekrutenko A (2001) Evolutionary analyses of the human genome. *Nature* 409:847–849
- Makalowski W (2000) Genomic scrap yard: how genomes utilize all that junk. *Gene* 259: 61–67
- Makalowski W (2003) Genomics. Not junk after all. *Science* 300:1246–1247
- Malik HS, Eickbush TH (1999) Modular evolution of the integrase domain in the Ty3/Gypsy class of LTR retrotransposons. *J Virol* 73:5186–5190
- Marin I, Llorens C (2000) Ty3/Gypsy retrotransposons: description of new *Arabidopsis thaliana* elements and evolutionary perspectives derived from comparative genomic data. *Mol Biol Evol* 17:1040–1049
- McDonald JF (1993) Evolution and consequences of transposable elements. *Curr Opin Genet Dev* 3:855–864
- McDonald JF (1995) Transposable elements: possible catalysts of organismic evolution. *Trends Ecol Evol* 10:123–126
- Müller WEG (2005) Spatial and temporal expression patterns in animals. In: Meyers, RA (ed) *Encyclopedia of Molecular Cell Biology and Molecular Medicine*, Vol 13. Wiley-VCH, Weinheim, pp. 269–309
- Müller W, Zahn RK (1968) *Tethya limski n.sp.*, eine Tethyide aus der Adria (Porifera: Homosclerophorida: Tethyidae). *Senckenbergiana Biol.* 49:469–478
- Müller WEG, Brümmner F, Batel R, Müller IM, Schröder HC (2003) Molecular biodiversity. Case study: Porifera (sponges). *Naturwissenschaften* 90:103–120
- Müller WEG, Wiens M, Adell T, Gamulin V, Schröder HC, Müller IM (2004) Bauplan of Urmetazoa: basis for genetic complexity of Metazoa. *Int Rev Cytol* 235:53–92
- Müller WEG, Belikov SI, Kaluzhnaya OV, Perović-Ottstadt S, Fattorusso E, Ushijima H, Krasko A, Schröder HC (2006a) Cold stress defense in the freshwater sponge *Lubomirskia baicalensis*: role of okadaic acid produced by symbiotic dinoflagellates. *FEBS J* 274:23–36
- Müller WEG, Schröder HC, Wrede P, Kaluzhnaya OV, Belikov SI (2006b) Speciation of sponges in Baikal-Tuva region (an outline). *J Zool Syst Evol Res* 44:105–117

- Müller WEG, Boreiko A, Wang X, Belikov SI, Wiens M, Grebenjuk VA, Schloßmacher U, Schröder HC (2007) Silicateins, the major biosilica forming enzymes present in demosponges: protein analysis and phylogenetic relationship. *Gene* 395:62–71
- Nicholas KB, Nicholas HB Jr (1997) GeneDoc: a tool for editing and annotating multiple sequence alignments. Version 1.1.004. Distributed by the author; cris.com/~ketchup/genedoc.shtml; Internet
- Orgel LE, Crick FHC (1980) Selfish DNA: the ultimate parasite. *Nature* 284:604–607
- Pearce SR, Harrison G, Li D, Heslop-Harrison J, Kumar A, Flavell AJ (1996) The Ty1-copia group retrotransposons in *Vicia* species: copy number, sequence heterogeneity and chromosomal localisation. *Mol Gen Genet* 250:305–315
- Penney JT, Racek AA (1968) Comprehensive revision of a worldwide collection of freshwater sponges (Porifera: Spongillidae). Smithsonian Institution Press, Washington
- Rezvoj P (1927) Notes on sponges from the Lake Dzhegataj-kul in the Urjankhaj region. *Doklady Akademii Nauk SSSR* 3/8:296–300
- Rubin E, Levy AA (1997) Abortive gap repair: underlying mechanism for Ds element formation. *Mol Cell Biol* 17:6294–6302
- Sankov VA, Parfeevets AV, Miroschnichenko AI, Likhnev A, Arzhannikova AV (2003) Cenozoic dynamics of Baikal and Khubsugul basins. *Berliner Paläontol Abh* 4:49–54
- Schröder HC, Grebenjuk VA, Binder M, Skorokhod A, Batel R, Hassanein H, Müller WEG (2004) Functional molecular biodiversity assessment of the immune status of two sponge populations (*Suberites domuncula*) on the molecular level. *Mar Ecol* 25:93–108
- Shimizu K, Cha J, Stucky GD, Morse DE (1998) Silicatein alpha: cathepsin L-like protein in sponge biosilica. *Proc Natl Acad Sci USA* 95:6234–6238
- Smit AF (1999) Interspersed repeats and other mementos of transposable elements in mammalian genomes. *Curr Opin Genet Dev* 9:657–663
- The Arabidopsis Genome Initiative (2000) Analysis of the genome sequence of the flowering plant *Arabidopsis thaliana*. *Nature* 408:796–815
- Thompson JD, Higgins DG, Gibson TJ (1994) CLUSTAL W: improving the sensitivity of progressive multiple sequence alignment through sequence weighting, positions-specific gap penalties and weight matrix choice. *Nucleic Acids Res* 22:4673–4680
- Waterston RH, Lindblad-Toh K, Birney E et al. (2002) Initial sequencing and comparative analysis of the mouse genome. *Nature* 420:520–562
- Wiens M, Belikov SI, Kaluzhnaya OV, Krasko A, Schröder HC, Perovic-Ottstadt S, Müller WEG (2006) Molecular control of serial module formation along the apical-basal axis in the sponge *Lubomirskia baicalensis*: silicateins, mannose-binding lectin and Mago Nashi. *Dev Genes Evol* 216:229–242
- Xiong Y, Eickbush TH (1990) Origin and evolution of retroelements based upon their reverse transcriptase sequences. *EMBO J* 9:3353–3362

Modelling the Skeletal Architecture in a Sponge with Radiate Accretive Growth

Jaap A. Kaandorp

1	Introduction	237
2	Skeletal Architectures in Sponges	239
3	Radiate Accretive Growth	240
4	The Aquiferous System in a Sponge	241
5	Gene Regulation of the Deposition of the Skeleton.	242
6	Modelling Radiate Accretive Growth in a Sponge	243
7	Conclusions	246
	References	246

Abstract A mathematical model of the skeletogenesis and the influence of the physical environment on the morphogenesis of a branching sponge, for example, *Haliclona oculata* or *Lubomirskia baikalensis*, is presented. In the model, we assume that the radiate accretive growth process is nutrient limited. With this model we can generate in a simulated accretive growth process branching objects with a similarity to the branching sponges.

1 Introduction

In this Chapter, we want to present a model for generating skeletal architectures as found in certain sponges. We use here sponges with radiate accretive growth as a case study. Typical examples of sponges with radiate accretive growth are *Haliclona oculata* (see for example, details on growth and morphology of this sponge in Kaandorp and Kübler 2001) and *Lubomirskia baikalensis* (see also Kaluzhnaya et al. 2005a, b). In Fig. 1, examples are shown of the sponge *H. oculata*. Within the

J.A. Kaandorp
Section Computational Science, Faculty of Science, University of Amsterdam,
Kruislaan 403, 1098 SJ Amsterdam, The Netherlands,
e-mail: jaapk@science.uva.nl

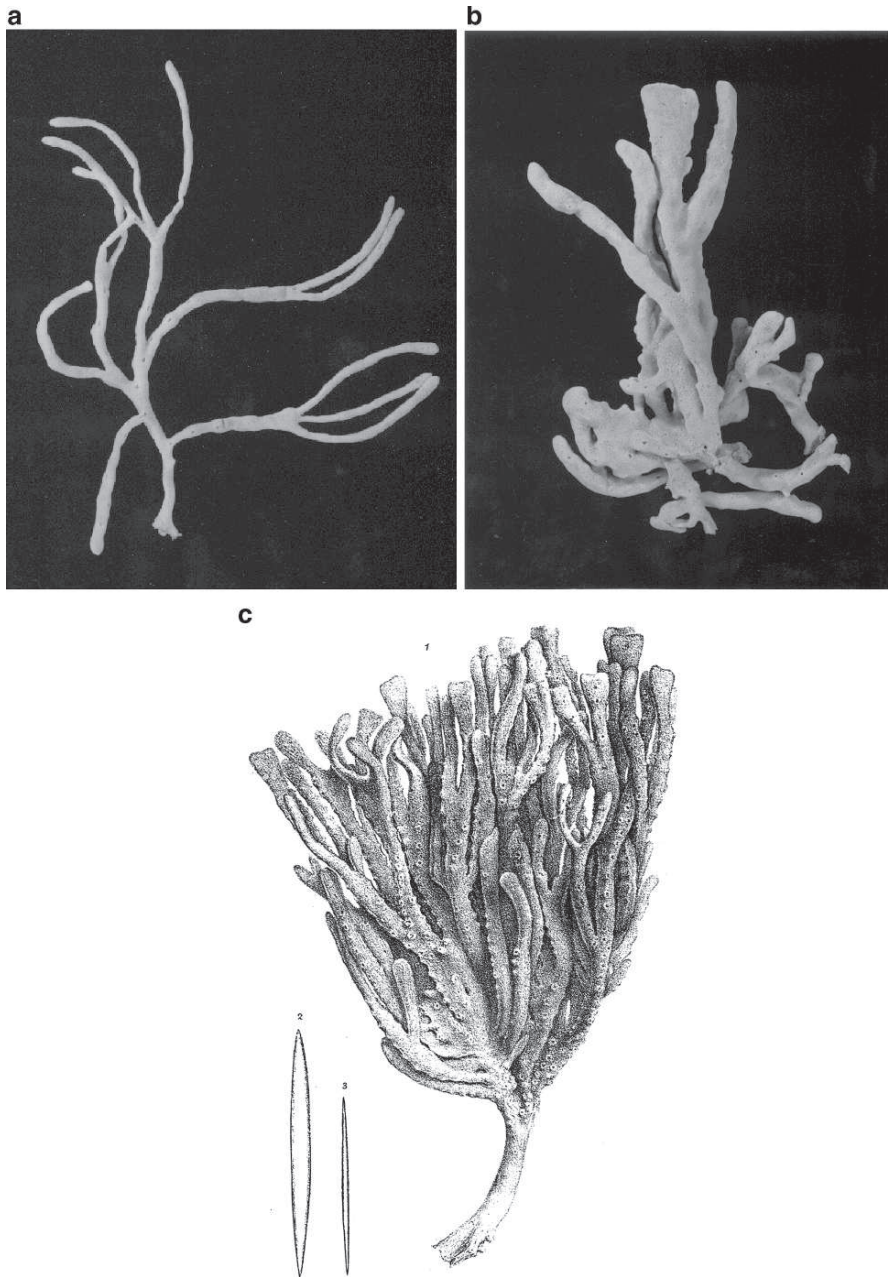


Fig. 1 Example of a branching sponge *Haliclona oculata* with radiate accretive growth. (a) Growth form from an environment exposed to water movement. (b) Growth form originating from a sheltered environment. (c) Drawing of *H. oculata* (Bowerbank, 1876) showing the arrangement of oscula at the lateral sides of the branches (lateral with respect to the upstream downstream direction of the governing flow)

metazoans, sponges represent the phylum with the simplest body plan. Recently, much information has become available about the regulatory network controlling the skeletogenesis and development in sponges (Le Pennec et al. 2002; Adell et al. 2003; Müller 2003, 2004; Perovic et al. 2003). This makes these organisms an excellent case study for understanding morphogenesis and the physical translation of the genetic information into a growth form, using a combination of a biomechanical model of the growth form and a model of the physical environment.

The aim of this Chapter is to present a mathematical model of skeletogenesis and the influence of the physical environment on the morphogenesis of a branching sponge (e.g., *H. oculata* or *L. baikalensis*). This model consists of a biomechanical component (a model of the deposition of the skeleton and the aquiferous system) and an environmental component (a model of the distribution of nutrients in the immediate environment of the sponge). In the following sections, we will discuss the various components, and in the last section, we will discuss how we can combine these model components.

2 Skeletal Architectures in Sponges

In sponges, only species with a certain kind of skeleton architecture can develop erect tree-like growth forms, as shown in Fig. 1. In Fig. 2, three major different types of skeleton architectures (Wiedenmayer 1977) are shown, i.e., a radiate accretive architecture (e.g., *H. oculata*, *H. simulans* and *L. baikalensis*), an

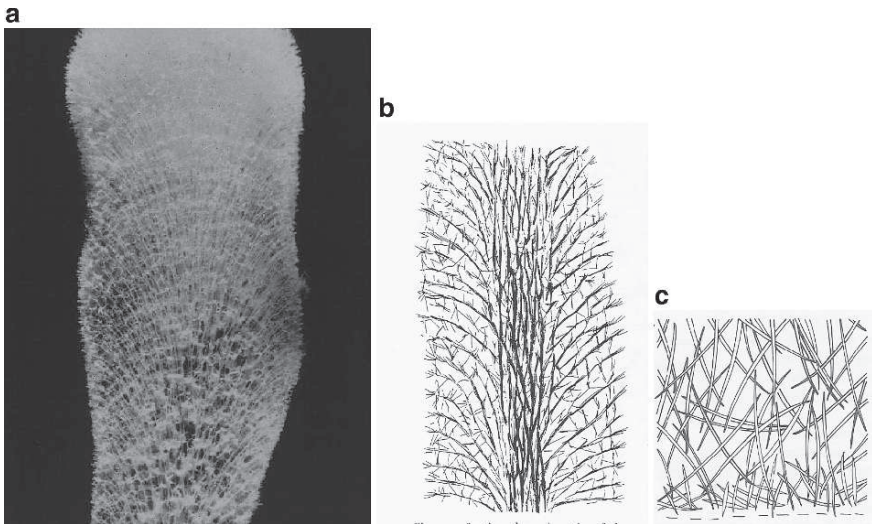


Fig. 2 Three major types of skeleton architectures in sponges. (a) radiate accretive architecture (*Haliclona oculata*). (b) Axinellid architecture (*Axinella polypoides*) (After Vosmaer 1912). (c) Halichondrid architecture (*Halichondria panacea*) (After Boury-Esnault and Ruetzler 1997)

axinellid architecture (e.g., *Axinella polypoides* and *Raspailia inaequalis*) and a halichondrid architecture (e.g., *Halichondria panicea*). In all three, the growth process can be described as an accretive process: new layers are deposited on top of the previous layers, while the previous growth stages remain unchanged. In the case of a halichondrid architecture, where the spicules are organized in a random fashion (sometimes indicated as a ‘confused’ skeleton) only quite irregular (often encrusting) growth forms emerge. Only in the case of a radiate accretive and a axinellid architecture can branching forms develop in the growth process. The branching forms of sponge with an axinellid architecture tend to be more ‘stiff-looking’ (see Abraham 2001), while sponges with a radiate accretive structure tend to show a resemblance with some abiotic growth processes [e.g., growth of ammonium chloride crystal (Brener et al. 1992) or ‘viscous-fingering’-like growth processes]. The type of skeleton architecture has a predominating impact on the type of growth forms which can develop in the growth process.

3 Radiate Accretive Growth

In some stromatolites and algae, as well as many sponges, hydro corals, and scleractinian corals, if we study the growth at the level of deposition of individual skeleton elements, the growth process can be described as a relatively simple accretive growth or surface normal deposition process (Kaandorp and Kübler 2001). Growth of the branches of these organisms proceeds by the deposition of new layers on top of the previous growth stages. The underlying reason why this type of growth process is found in various kingdoms, and also in abiotic growth processes, can be a physical explanation. In radiate accretive growth, the basic elements (e.g., the spicules in a sponge) are deposited in the direction of the physical forces. The result is that the basic elements are deposited in a minimal energy configuration, where the elements in a tangential surface are organized in pattern of polygons (see Fig. 3), the pattern resembling a Voronoi tessellation. The longitudinal elements (see Fig. 2a) are deposited along the normal vectors which can be constructed at the surface of the tangential layers.

For the formation of a regular radiate accretive architecture in a sponge, it is required that there is a mechanism by which spicules are secreted in the direction of a physical force; if there is no such mechanism controlling the direction of skeleton material, the growth process would result in a ‘confuse’ halichondrid architecture (Fig. 2c) in which spicules seem to be secreted in all directions. The result of the radiate accretive growth process is a highly efficient structure; with a minimal amount of material, a very stable and strong structure can be created. The structure is comparable with the architecture of bone trabeculae, where elements are formed in the direction of the forces (van Rietbergen et al. 1999), and where stresses and strains are distributed evenly over the trabecular architecture. The entire structure consists of discrete elements, and a direct consequence is that the growth proceeds in discrete steps and layers of material cannot have an infinitesimal thickness. The exact mechanisms of how spicule secreting cells are able to detect forces in

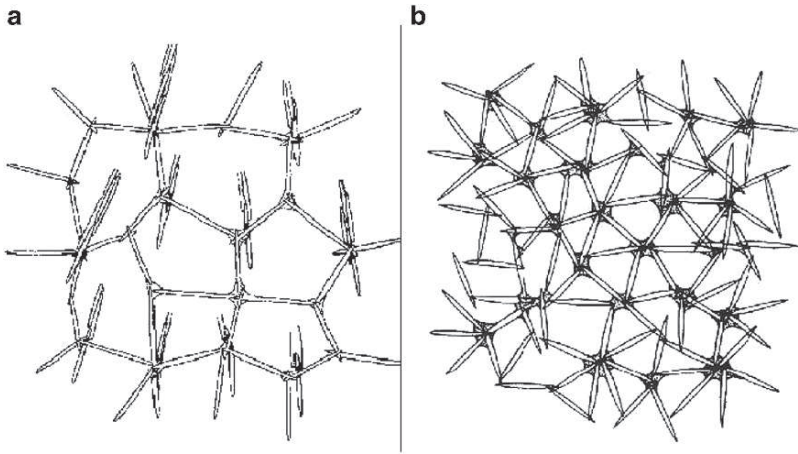


Fig. 3 Tangential arrangements of spicules in (a) polygonal tessellation in *Haliclona oculata*, and (b) triangular tessellation in *H. simulans* (de Weerd 1986), where the triangles are again organized in polygons

the extracellular environment, how spicules are secreted in the direction of the force, and why spicules in the halichondrid architecture (Fig. 2c) do not seem to be secreted in the direction of a force are, to our knowledge, still unknown.

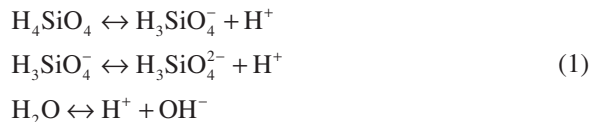
4 The Aquiferous System in a Sponge

Another major component in the growth process of a sponge is the pump system with which suspended material is collected from the environment and transported through the sponge tissue, the aquiferous system. The aquiferous system of *H. oculata* is poorly developed in comparison to a related species such as *H. simulans* where the oscula are very clearly visible as holes in the growth form. In *H. oculata*, macroscopic evidence of canals is only found close to the oscula. In *H. simulans*, the aquiferous system is far more evolved and visible as an extensive system of canals. The aquiferous system of *H. oculata* is probably also strongly supported by external water movements (compare Vogel 1974). In conditions with strong water movements, plate-like growth forms are possible, whereas in sheltered conditions a decrease of food supply will occur in the tissue, unless it is in short-distance contact with the environment; in this case, only thin-branching forms will occur in *H. oculata* (Kaandorp and Kübler 2001). In the related species *H. simulans* with a more evolved aquiferous system, relatively wide branches and more globular forms are found. The development of the aquiferous system is a species-specific pattern which is another major component determining the resulting growth form. In many sponges, it can be observed that the oscula tend to be positioned at locations with strong water currents. In, for example, *H. oculata*, it can be seen that in high-flow morphs the oscula tend to be located at

the lateral sides. Note that lateral is defined here as the sides of the plane in which the branches of the sponge develop; this plane is usually perpendicular with respect to the upstream–downstream direction of the governing flow. This phenomenon is, for example, very well demonstrated in a drawing by Bowerbank (1876) of *H. oculata* (shown in Fig. 1c). The oscula in this picture are arranged in rows at the lateral sides of the branches. The distance between neighboring oscula in one row is quite regular and varies about a certain constant value. By positioning the oscula at strong water current locations, the sponge can exploit the external water movement for inducing a current within the canal system. Under sheltered conditions, the oscula in sponges like *H. oculata* and *H. simulans* are more or less evenly distributed over the surface of the sponges where the distance, measured at the surface of the sponge, between neighboring oscula is more or less regular and varies about a certain constant value.

5 Gene Regulation of the Deposition of the Skeleton

For building a skeleton, nutrient (silicate) is absorbed from the environment. Two species of silicate (silicic acid) are absorbed by the sponge: the silicic acid chemical equilibria can be described by the following equations:



The rates in these reactions are dependent on temperature (see Wischmeyer et al. 2003). Silicate is being transferred over the diffusive boundary layer around the sponge, and locally silicate is depleted. When it is assumed that there is a constant supply of silicate from the environment and silicate is continuously being absorbed, silicate gradients will emerge in the direct neighborhood of the sponge.

In the paper by Le Pennec et al. (2002), it was demonstrated that high concentrations of silicate (or ferric ions) induce spicule formation and upregulate the silicatein, collagen, and myotrophin genes. The upregulation of the genes activates the production of spicules in the sponge, the deposition of the skeleton. The second major morphogenetic event is formation of the oscula and aquiferous system. Both events, the deposition of the skeleton and the formation of the oscula and aquiferous system, are separated in time and space. Only after the skeleton is built, can the aquiferous system be constructed. In Perovic et al. (2003) and Müller (2004), it is described that the expression of the gene *Iroquois* is induced by an increased water current and activates the formation of oscula and aquiferous system. During the formation of this canal system, some material has to be removed from the original skeleton and skeletogenesis is stopped in the regions of the sponge where the aquiferous system is formed. Furthermore, both the skeletogenesis and the formation of oscula (where some material has to be removed from the original skeleton) are processes occurring more or less at the surface of the sponge. In Adell et al. (2003), it is demonstrated that *Frizzled* works as polarity factor; in the sponge *Suberites domuncula*,

Frizzled is expressed at the surface (the pinacoderm) of the sponge. It is hypothesized here that Frizzled can work as a positional information system, indicating the ‘up’-direction (the direction towards the external environment in a branching sponge).

The oscula are formed near the surface (with high concentrations of Frizzled product). In the sponge, the oscula are formed at more or less regular distances. Under stagnant conditions, the oscula will be about evenly distributed over the surface of the sponge (see Fig 1a). Figure 1b and c demonstrate the effect of strong water currents at the system regulating the position of the oscula; the oscula tend to move towards regions with a strong water movement, and more or less regular distribution of oscula over the surface is tweaked, causing the oscula to be arranged in rows.

6 Modelling Radiate Accretive Growth in a Sponge

The model is divided into two coupled components: (1) the geometric representation of the growth form, and (2) the model of the distribution of nutrient in the environment. We assume that this is a diffusion-limited growth process. For our simulation models, we use a differential accretive growth model (Kaandorp and Kübler 2001; Kaandorp et al., 2005). The growth process is modeled as a surface-normal deposition process, where new material is deposited along the normal vectors that are constructed on the surface of the previous growth stage (Fig. 4). In Fig. 2a, it can be seen that the longitudinal fibres with spicules tend to be set normally with respect to the previous growth layers, while the growth layers consist of a network of spicules organized in a polygonal pattern (see Fig. 3). For the simulation model, it is therefore assumed that in the areas in which skeletogenesis is activated new layers of material are deposited on top of the previous layers, which remain unchanged. The thickness l_{i+1} of the new layer, the distance between the vertices V_i and V_{i+1} in Fig. 4, is determined by a growth function. In this Chapter, we will use a growth function which includes the influence of the local available amount of simulated silicate.

The accretive growth model of Fig. 4 can be combined with a growth function:

$$l_{i+1} = \bar{n}_i c_i s \quad (2)$$

where \bar{n}_i is the average normal vector in vertex V_i , c_i is the amount of absorbed simulated nutrient in vertex V_i and s is the maximal thickness of a growth layer (Kaandorp et al. 2005). In this growth function, we assume that there is a linear relationship between the local deposited amount of material and the local amount of absorbed nutrient from the environment. If in the accretive growth simulation the assumption is made that the nutrient is absorbed at the surface of the object, while nutrient is exclusively distributed by diffusion and the source of nutrient is located at the top plane, it can be demonstrated that this model is sufficient to obtain branching objects as an emergent phenomenon in the model and no additional rules are required to explain the branching process (see Merks et al. 2004; Kaandorp et al. 2005). Details on the model used to compute the distribution of nutrients in a three-dimensional diffusion limited growth process of a branching object are discussed elsewhere (Merks et al. 2004; Kaandorp et al. 2005). In Fig. 5, a section

Fig. 4 Small detail of the accretive growth model showing the construction of a new layer (layer $i + 1$) on top of the previous layer (layer i). The thickness l_{i+1} of the new layer, the distance between the vertices V_i and V_{i+1} is determined by a growth function

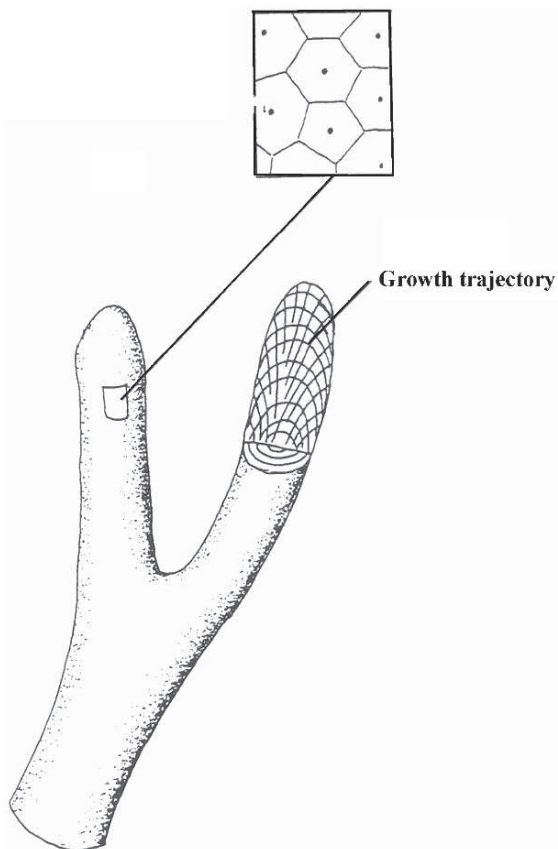
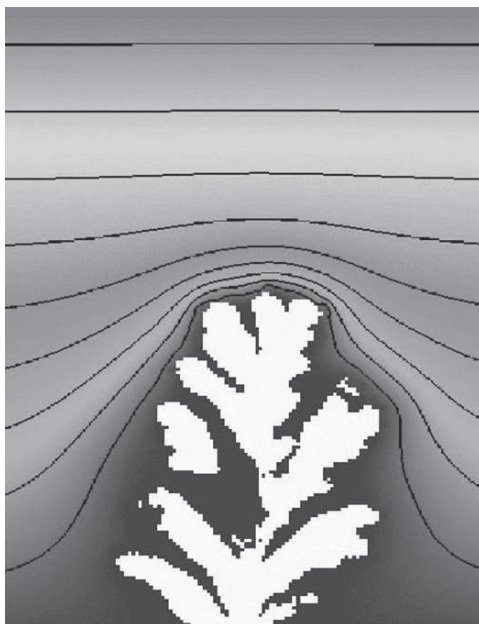


Fig. 5 A section through a (simulated) three-dimensional nutrient distribution. The areas depleted from nutrient are visualized in *black*, while the region with high concentrations are shown in *white*. In the simulation, the assumption was made that the nutrient is absorbed at the surface of the object, while nutrient is exclusively distributed by diffusion and the source of nutrient is located at the top plane



through a simulated branching object is shown together with a visualization of the external simulated nutrient distribution. The areas depleted from nutrient are visualized in black, while the region with high concentrations are shown in white. Very close to the object, regions depleted of nutrient occur, while the steepest gradients are located at some of the tips of the object. From this simulated nutrient distribution, it can be predicted that the steepest gradients, and the highest supply of nutrient, will occur at the tips of the object. In Fig. 6, two views of a simulated

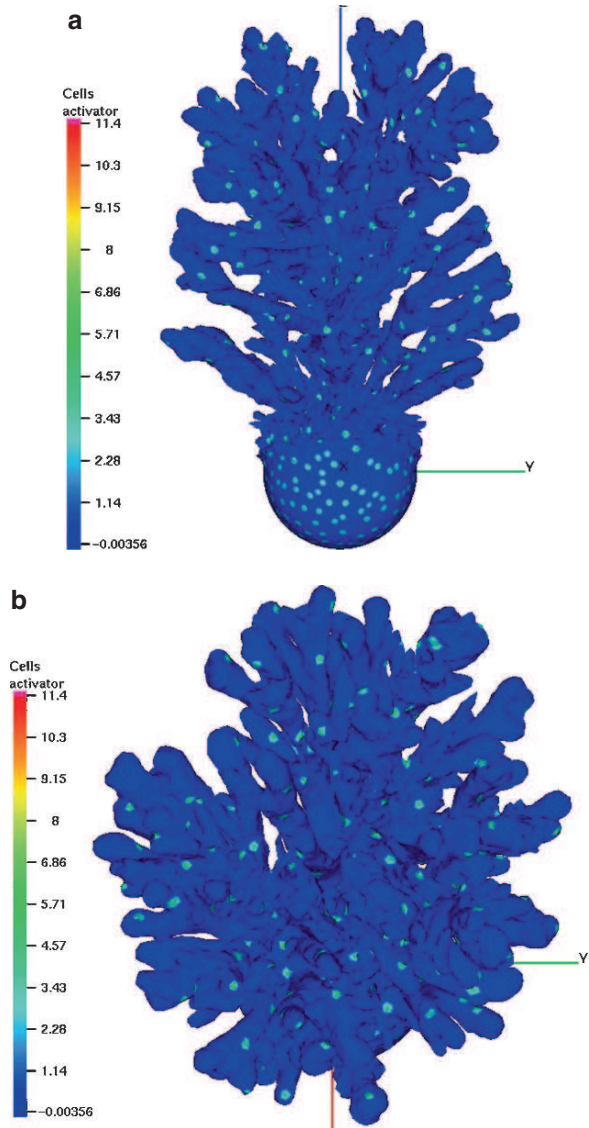


Fig. 6 Two views of an object generated in the diffusion-limited simulated accretive growth process. The simulation started with an initial spherical object. The simulated growth form was generated within 80 accretive steps

branching object are shown. The simulation started with an initial spherical object and was generated within 80 accretive steps.

In the model, we assume that silicate in the reactions shown in Eq. 1 is the main factor limiting skeletogenesis and growth of the sponge. In the model, we assume, for simplicity reasons, that silicate is only distributed in the environment of the sponge by diffusion and that advection of silicate does not play a role. Furthermore, we assume that there is one source of silicate, the top plane in the three-dimensional simulation box, and we also assume that all silicate is absorbed at the surface of the simulated growth form. If we make the assumption that the diffusion of silicate is much faster compared to growth of the sponge, then we can describe the local concentrations of silicate around the simulated object using a Laplace equation. After every growth step, the silicate concentration needs to be recomputed.

7 Conclusions

In the models we have presented, many simplifications have been made. A very simple model is used for the skeletogenesis; we assume that this process is only regulated by the local available silicate. From recent work (Le Pennec et al. 2003), it is known that high concentrations of silicate induce spicule formation and upregulate the silicatein, collagen, and myotrophin genes. In the models shown in this Chapter, we did not include this gene regulation. Furthermore, another major component in the growth process of a sponge, the aquiferous system with which suspended material is collected from the environment and transported through the sponge tissue, is not yet present in this model. The other major assumption we have made is that silicate is exclusively distributed through the environment by diffusion. The samples in Fig 1. clearly show that advection has a major impact on the growth form. Although we made these major simplifications we can generate, in a simulated nutrient-limited accretive growth process, branching objects which show a similarity to branching sponges with accretive growth.

References

- E.R. Abraham. The fractal branching of an arborescent sponge. *Mar. Biol.* **138**, 503–510 (2001).
- T. Adell, I. Nefkens, and W.E.G. Müller. Polarity factor ‘frizzled’ in the demosponge *Suberites domuncula*: identification, expression and localization of the receptor in the epithelium/pinacoderm. *FEBS* **554**, 363–368 (2003)
- N. Boury-Esnault and K. Ruetzler, Thesaurus of sponge morphology. *Smithson. Contr. Zool.* **596**, 1–55 (1997)
- J.S. Bowerbank. A monograph of the British Spongiadae VIII, London Royal Society, London, 1876
- E. Brener, K. Kassner, and H. Mueller-Krumbhaar. Pattern formation in first order phase transitions. *Int. J. Modern Phys. C* **3**, 825–851 (1992)
- W.H. de Weerd, A systematic revision of the north-eastern Atlantic shallow-water Haplosclerida (Porifera, Demospongiae), part (II): (C)halinidae, Beafortia **36**, 81–165 (1986)

- J.A. Kaandorp and J.E. Kübler. *The algorithmic beauty of seaweeds, sponges and corals*. Springer-Verlag, Heidelberg, 2001
- J.A. Kaandorp, P.M.A. Sloom, R.M.H. Merks, R.P.M. Bak, M.J.A. Vermeij, and C. Maier. Morphogenesis of the branching reef coral *Madracis mirabilis*. *Proc. Roy. Soc. Lond. B* **272**, 127–133, 2005
- G. Le Pennec, et al. Cultivation of primmorphs from the marine sponge *Suberites domuncula*: morphogenetic potential of silicon and iron a review. *J. Biotechnol.* **100**, 93–108 (2003)
- R.M.H. Merks, A.G. Hoekstra, J.A. Kaandorp, and P.M.A. Sloom. Branching and morphologic plasticity in corals: the polyp oriented approach. *J. Theor. Biol.* **228**, 559–576, 2004
- W.E.G. Müller, et al. Molecular mechanism of spicule formation in the demosponge *Suberites domuncula*: silicatein – collagen- myotrophin. *Prog. Mol. Subcell. Biol.* **33**, 195–231 (2003)
- W.E.G. Müller, et al. Bauplan of urmetazoa: basis for genetic complexity of metazoa. *Int. Rev. Cytol.* **235**, 53–92 (2004)
- B. van Rietbergen et al. Tissue stresses and strain in trabeculae of a canine proximal femur. *J. Biomech.* **32**, 443–451 (1999)
- C.J. Vosmaer On the distinction between the genera *Axinella*, *Phakelia*, *Acantella* a.o. Abdruck aus den Zoologischen Jahrbüchern, Verlag von Gustav Fischer, Jena, 1912
- F. Wiedenmayer. *Shallow-water sponges of the western Bahamas*. Birkhäuser, Basel, 1977
- A.G. Wischmeyer et al. Theoretical constraints on the uptake of silicic acid species by marine diatoms. *Mar. Chem.* **29**, 13–29 (2003)

Silicatein: Nanobiotechnological and Biomedical Applications

Heinz C. Schröder, Ute Schloßmacher, Alexandra Boreiko, Filipe Natalio, Malgorzata Baranowska, David Brandt, Xiaohong Wang, Wolfgang Tremel, Matthias Wiens, and Werner E.G. Müller

1	Introduction	252
2	Biocatalytic Formation of Silica: Silicateins	253
2.1	Post-translational Modification	255
2.2	Silicatein Assembly	255
2.3	Enzymatic Activities of Silicatein	257
3	Degradation of Silica: Silicase	258
4	Recombinant Proteins	258
5	Immobilization of Silicatein: Preparation of Biosilica Coatings	259
6	Biocatalytic Formation of Titania and Zirconia	260
7	Formation of Au and Ag Nanoparticles	260
8	Nanowires: Biocatalytic Formation of Nanocomposite Materials	261
9	Nanolithography Approaches	261
10	Synthesis of Core-Shell Materials	262
11	Bone Replacement Materials/Bone Regeneration Scaffolds	264
12	Encapsulation of Bacteria	265
13	Microstructured Optical Fibers	267
14	Conclusions	268
	References	269

Abstract Silica-based materials are used in many high-tech products including microelectronics, optoelectronics, and catalysts. Siliceous sponges (Demospongiae and Hexactinellida) are unique in their ability to synthesize silica enzymatically. We

H.C. Schröder (✉), Ute Schloßmacher, A. Boreiko, F. Natalio, M. Baranowska, D. Brandt, and W.E.G. Müller
Institut für Physiologische Chemie, Abteilung Angewandte Molekularbiologie, Universität, Duesbergweg 6, D-55099 Mainz, Germany
e-mail: hschroed@uni-mainz.de

X. Wang
National Research Center for Geoanalysis, 26 Baiwanzhuang Dajie, CHN-100037 Beijing, PR China

W. Tremel
Institut für Anorganische Chemie und Analytische Chemie, Universität, Duesbergweg 10–14, D-55099 Mainz, Germany

W.E.G. Müller and M.A. Grachev (eds.), *Biosilica in Evolution, Morphogenesis, and Nanobiotechnology*, Progress in Molecular and Subcellular Biology, Marine Molecular Biotechnology 47, DOI: 10.1007/978-3-540-88552-8, © Springer-Verlag Berlin Heidelberg 2009

have cloned the silica-forming enzymes, silicateins, from both demosponges (marine and freshwater sponges) and hexactinellid sponges. The recombinant enzymes allow the synthesis of silica under environmentally benign ambient conditions, while the technical (chemical) production of silica commonly requires high temperatures and pressures, and extremes of pH. Silicateins can be used for the fabrication of highly-ordered inorganic–organic composite materials with defined optical, electrical, and mechanical properties. The simple self-assembly properties of silicateins which are able to form silica and other metal oxides in aqueous solution allow the development of novel products in nano(bio)technology, medicine, and dentistry.

1 Introduction

In nature, silicon is found in the form of silicon dioxide (silica) and silicate in many minerals occurring in rocks, sand, and clay. Silicon is also the principal constituent of many technical products such as glass and cement. More recently, silicon has become of increasing importance as the basic element of many high-tech products such as silicon wafers (manufacture of transistors and other electronic devices) and integrated circuits (development of computer chips).

The chemistry of silicon shows some similarities but also striking differences to the chemistry of carbon, the principle element of all living organisms on Earth. Silicon and carbon belong to the same group (group IV) in the periodic table of elements. Like carbon, silicon combines with four hydrogen atoms to form silane (SiH_4), a tetrahedral molecule like methane (CH_4). Both elements can form long-chain polymers containing a backbone of alternating atoms of silicon and oxygen (polysilicates and silicones) or carbon and oxygen (polyacetals).

Based on these similarities, it has been proposed that life must not be inevitably associated with carbon and carbon compounds but could also be based – at least theoretically – on the element silicon. This idea can be traced back to the German astrophysicist, Julius Scheiner, who, in 1891 most likely as the first person, discussed the possibility of “silicon-based life.” Later proponents of this idea were the British chemist, James Emerson Reynolds, who stressed the heat stability of silicon compounds allowing life to exist at higher temperatures (Reynolds 1893), Robert S.W. Ball who speculated about the existence of silicon–aluminium-based organisms (Ball 1894), and the science fiction writer, Herbert George Wells, (“The living things that may be”; Wells 1894). Later, the hypothesis of the existence of silicon-based life was taken up by the biochemist, John B.S. Haldane, who speculated about the origin of life inside a planet based on partly molten silicates (Haldane 1928)

However, despite the structural similarity of many silicon and carbon compounds, there are strong differences in the reactivity of these compounds, which limit the suitability of silicon as an alternative of carbon in living systems. Silanes, in contrast to alkanes, are highly reactive with water. In metabolism, the final oxidation product of carbon is carbon dioxide, which is a gaseous compound that can be easily removed from the organism, while oxidation of silicon yields silica (silicon dioxide) which is

a solid. Because of their larger size, silicon atoms cannot easily form double or triple covalent bonds, in contrast to carbon. In addition, there is no evidence that silicon compounds such as silanes or silicones are present somewhere in the universe (in contrast to their oxidized compounds such as silicates), and, therefore, there is no evidence for the existence of silicon-based prebiotic chemicals or silicon-based life.

Nevertheless, silica is used to a large extent by many unicellular and multicellular organisms, including diatoms, radiolaria, choanoflagellates, sponges, and higher plants, to build up their skeleton. Even more importantly, these organisms possess biomolecules including proteins which interact with silica. There are even enzymes which are able to synthesize or to degrade silica (silicateins and silicase in sponges). Moreover, silicon is an essential element in animals and human, which plays a critical role in bone (hydroxy-apatite) formation and in the development of the extracellular (collagen) matrix (Schwarz and Milne 1972; Carlisle 1978; Reffitt et al. 2003; Jugdaohsingh et al. 2004). It has also been proposed that clay crystals formed from silicates in solution may have determined the preferred handedness (left-handedness of amino acids and right-handedness of carbohydrates) of the first prebiotic carbon compounds (“Clay theory”; Cairns-Smith 1968, 1982, 2008). Thus, silicon is an integral part of life, although silicon metabolism seems only to involve the oxidized forms of silicon: silica and silicates.

In the last few years, biosilicification in living organisms has come into the spotlight by the discovery of the principle molecules involved in this process both in diatoms (silaffins and polyamines) and sponges (silicateins) (for a review, see Schröder et al. 2008). In sponges, these molecules turned out to be enzymes which are able to metabolize silicon compounds, and this fact made them of extreme interest for application in nanobiotechnology, medicine, and dentistry. Here, some recent advances in research towards nanobiotechnological/medical applications of silicateins are reviewed. These enzymes are present both in marine and freshwater sponges and are at the center of interest of the German Center of Excellence BIOTECmarin (<http://www.biotechmarin.de>) and the German-Russian collaboration programme (“Joint Lab Baikal”; Müller et al. 2006a; <http://www.deutsch-russische-partnerschaft.de>).

2 Biocatalytic Formation of Silica: Silicateins

The discovery of enzymes that catalyze the formation of silica (an inorganic polymeric material) from water soluble inorganic precursors was a great breakthrough both in inorganic chemistry and biochemistry. The existence of these novel enzymes which link two worlds – inorganic chemistry and biochemistry – was unexpected and opens new possibilities in material sciences, medicine, and dentistry.

Silicateins were first described by the group of Morse (Shimizu et al. 1998; Cha et al. 1999), who discovered that the axial filament of the sponge needle-like spicules is composed of a protein which turned out to be an enzyme (reviewed in Weaver and Morse 2003). This enzyme, which has been termed silicatein, is related

to the cysteine protease, cathepsin L. The existence of such a protease in a sponge has been described before by our group (Krasko et al. 1997).

Several isoforms of silicatein have been identified and characterized, both in marine sponges and freshwater sponges. The first silicatein cDNAs comprising two isoforms (silicatein- α and silicatein- β) have been isolated from the marine demosponge *Tethya aurantium* (Shimizu et al. 1998; Cha et al. 1999; Müller et al. 2007c); the possible existence of a third isoform (silicatein- γ) has not been confirmed on the cDNA level. The genes/cDNAs encoding silicatein- α and silicatein- β have also been cloned from other marine sponges, including *Suberites domuncula* (Krasko et al. 2000, 2002; Schröder et al. 2004a, b, 2005b; Müller et al. 2006b) and *Petrosia ficiformis* (Pozzolini et al. 2004). In addition, silicateins have been isolated and characterized from the freshwater sponges *Ephydatia fluviatilis* (Funayama et al. 2005) and *Lubomirskia baicalensis* (Belikov et al. 2005; Kaluzhnaya et al. 2005). In *L. baicalensis*, at least four isoforms of silicatein- α (silicatein a1–a4) exist (Kaluzhnaya et al. 2005; Wiens et al. 2006, 2008). More recently, silicatein has also been discovered and isolated from a hexactinellid sponge, *Crateromorpha meyeri* (Müller et al. 2008d). This result demonstrates that these enzymes are not restricted to demosponges but are a general feature of siliceous sponges. In demosponges (*S. domuncula*), the silicatein- α and silicatein- β genes comprise six exons (Müller et al. 2003a; Schröder et al. 2005b).

Various substrates have been used to measure silicatein activity. The most commonly used substrate is tetraethoxysilane (TEOS) which is relatively stable in aqueous solution. However, the reaction kinetics are difficult to follow by quantitation of the insoluble silica formed in the course of the reaction (usually done by a molybdate-based assay after dissolution of the precipitated silica in NaOH solution). Recently, we introduced a novel substrate, bis(*p*-aminophenoxy)-dimethylsilane, allowing determinations of catalytic constants (see below). The natural substrate of the enzyme is most likely silicic acid or silicate. Silica deposition in living cells, but also in in vitro systems, is influenced by a number of inorganic factors including ferric ions and selenite (Müller et al. 2005a). Silicatein is also able to catalyze the formation of organically modified polysiloxanes (silicones; Cha et al. 1999, and to be published).

The silicateins are related to the cathepsin family of proteases; the highest similarity is shared with cathepsin L (Müller et al. 2003b, 2006d; Shimizu et al. 1998; Krasko et al. 2000). Cathepsins do not precipitate silica. The catalytic center of these cysteine proteases consists of the three amino acids, Cys, His, and Asn (“catalytic triad”). In the catalytic center of the silicatein molecules, the cysteine residue present in cathepsins is replaced by a serine residue. This serine residue is essential for the catalytic mechanism of the enzyme (Shimizu et al. 1998; Krasko et al. 2000). Another feature of silicateins not found in cathepsins is the presence of a serine cluster which might act as a template for biosilica deposition.

Applying homology modeling, the presumptive 3D structure of silicatein has been obtained (Fig. 1a; Schröder et al. 2007a). First, a model of the mature human cathepsin based on the X-ray structure was constructed. This model was then used as a template for the mature silicatein of *S. domuncula*. In Fig. 1b, the distribution of distinct hydrophobic domains on the surface of the silicatein molecule is shown.

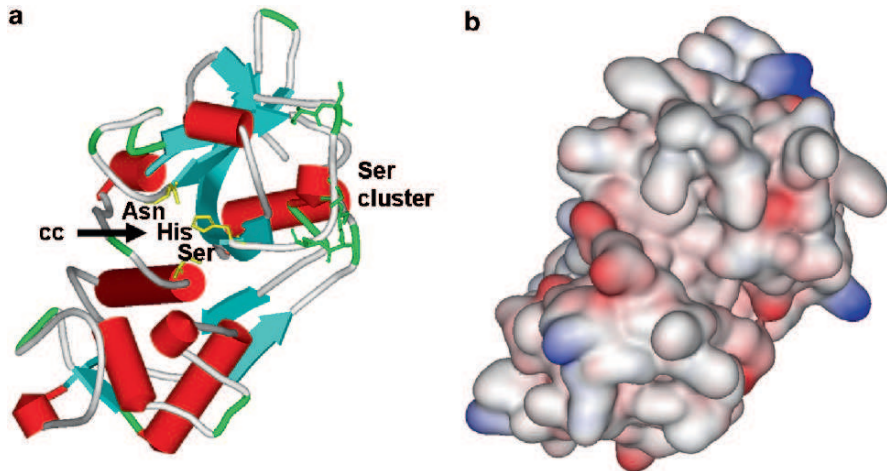


Fig. 1 Three-dimensional modeling of silicatein- α (*Suberites domuncula*). The published X-ray structure of cathepsin S was used as a reference for modeling the silicatein- α structure. (a) Secondary structure elements are marked in red (α -helices) or blue (β -strands). (b) Electrostatic charge distribution; red, positive charges; blue, negative charges; white, hydrophobic areas. The catalytic center (cc) of the enzyme comprising the amino acids Ser, His, and Asn (yellow) and the localization of the Ser residues (green) of the serine-rich cluster (Ser cluster) are marked

2.1 Post-translational Modification

Analysis of native silicatein isolated from axial filament protein both from marine sponges (*S. domuncula*; Müller et al. 2005b) and freshwater sponges (*L. baicalensis*, to be published) by 2D electrophoresis revealed that silicatein undergoes post-translational modification steps. Five phospho-isoforms have been identified (Müller et al. 2005b, 2007b, i); similar post-translational modifications have been detected in the hexactinellid sponge *Monorhaphis chuni* (Müller et al. 2008a). Further post-translational modifications (e.g., de-hydroxylation from tyrosine to phenylalanine) have been identified by electrospray ionization (ESI)-mass spectrometry (MS) (Müller et al. 2007i).

2.2 Silicatein Assembly

Using a new extraction procedure, we succeeded to isolate silicatein from axial filaments which was able to polymerize under formation of long filaments (Müller et al. 2007b). The native silicateins isolated by this procedure from the demosponge *S. domuncula* are monomeric, but readily form non-covalently linked dimers. The filament/aggregate formation from disassembled silicatein could be visualized by transmission electron microscopy (TEM); the filaments reach sizes

of several μm (Fig. 2a, b). This self-assembly process is initiated after transfer of the disassembled silicatein which is present in a glycerol-containing buffer to a glycerol-free assembly medium. Polymerization of silicatein, which is accompanied by an increase in catalytic activity of the protein, proceeds through formation of fractal-like intermediates (Fig. 2a), which subsequently form the filaments (Fig. 2b; Müller et al. 2007b).

These self-assembly features were not observed if silicatein was isolated from spicules using the common extraction procedure with hydrofluoric acid (HF). This procedure induces cross-linking of silicateins with each other to form dimers,

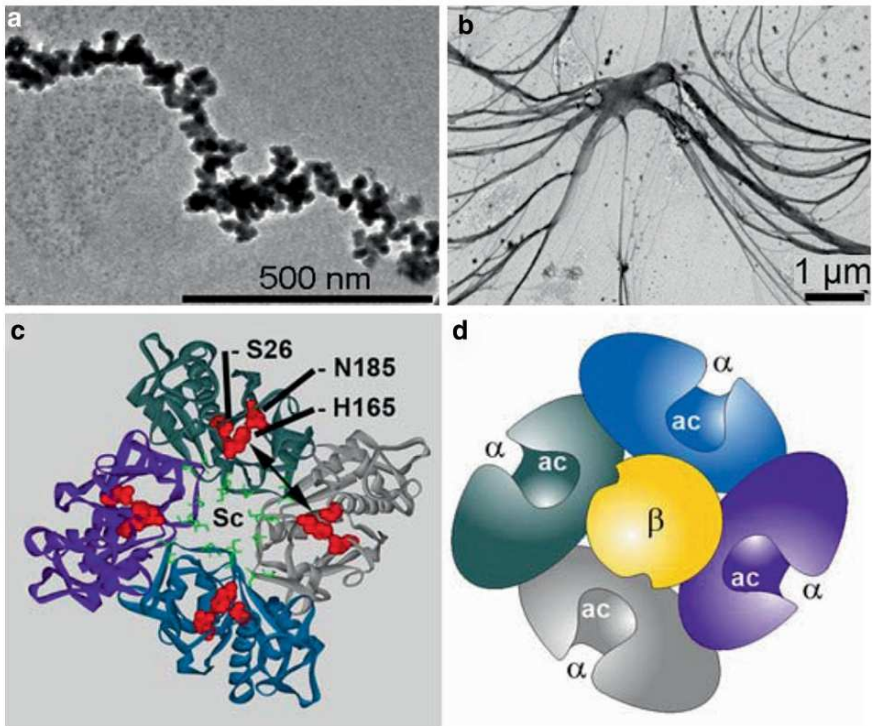


Fig. 2 (a, b) Self-assembly of silicatein. Electron microscopical analysis of silicatein filaments/aggregates formed by polymerization of silicatein monomers/dimers in glycerol-free buffer (assembly buffer) after an incubation period of 60 (a) and 320 min (b). (c) Silicatein tetramer with con-axial orientation of the silicatein molecules (the entrances of the active centers of the silicatein molecules are located in the plane of the tetramer). The amino acids of the catalytic centers of the silicatein molecules (serine *S26*; histidine *H165*; and asparagine *N185*) are marked (red). The serine clusters (*Sc*; green) are directed towards the center of the tetramer. (d) Schematic representation of the planar silicatein- α tetramer (green-grey-blue-pink) with the silicatein- β (yellow) in the center. The active (catalytic) centers of the silicatein- α molecules are marked (*ac*). The distortion of the silicatein- α molecules within the plane of the tetramer is visible

trimers, or tetramers (Murr and Morse 2005). Axial filaments, obtained after HF-extraction, require harsh conditions (treatment with urea) to obtain monomeric silicatein (Müller et al. 2007b).

Based on sodium dodecyl sulfate polyacrylamide gel electrophoresis (SDS-PAGE) analyses the ratio of silicatein- α form to silicatein- β -form in the filaments is 4:1. A computer model for the proposed arrangement between the two isoforms of silicatein has been developed (Müller et al. 2007b). In this model, the silicatein- α molecules form a tetramer, in which the Ser-clusters of these proteins direct towards the center of the oligomer (Fig. 2c). In order to reach the optimal configurations the silicatein- α molecules are distorted to some extent (Fig. 2d). It is assumed that one silicatein- β molecule is bound in the center of the platform formed by the four silicatein- α molecules (Fig. 2d). This arrangement also allows an understanding of the directional growth of the filaments. It should be noted that the pattern of silicatein isoforms may differ in different types of spicules or different sponge species; for example, the axial filament of the microscleres of the marine demosponge *Geodia cydonium* only contains one silicatein molecule in contrast to the megascleres of the same sponge species (Müller et al. 2007g). In addition, binding to other proteins (e.g., galectin; Schröder et al. 2006) may affect self-assembly of silicatein molecules.

2.3 Enzymatic Activities of Silicatein

Recently, we succeeded in demonstrating for the first time that silicatein comprises a dual enzymatic function: the enzyme acts both as silica polymerase and silica esterase (Müller et al. 2008c). In order to monitor the kinetics of silicatein esterase activity, we introduced a new substrate: bis(*p*-aminophenoxy)-dimethylsilane. This substrate comprises two ester-like bonds between silicon and *p*-aminophenol and two methyl silane linkages. The hydrolysis of the ester-like bonds can be monitored spectroscopically on the basis of the release of *p*-aminophenol.

Using this substrate, the enzymatic parameters of the silica-esterase activity of silicatein- α (recombinant protein) from *S. domuncula* were determined (Müller et al. 2008c). The Michaelis constant (K_m) is 22.7 $\mu\text{mol/l}$ and the turnover number is 5.2 (molecules of converted substrate per one enzyme molecule per second). The temperature coefficient (Q_{10}) above the temperature optimum of 25°C decreases by 2.5-fold; it increases below the temperature optimum of 25°C by 2.9-fold. The esterase activity of silicatein can be blocked by Na-hexafluorosilicate and the cysteine proteinase inhibitor E-64.

In addition, we demonstrated that polymerization reaction catalyzed by the silica-polymerase activity of silicatein occurs by successive addition of single silica monomeric units (Müller et al. 2008c). Using dimethyl-dimethoxy-silane as substrate, a stepwise (74–75 Da) increase in mass due to a stepwise polymerization of $-\text{Si}(\text{Me})_2\text{-O-}$ units to the starter silane molecule was recorded, as analyzed by matrix-assisted laser desorption/ionization mass spectrometry (MALDI-MS).

3 Degradation of Silica: Silicase

Enzymes which degrade silica may also be of interest for nanobiotechnological applications (Müller et al. 2007f). Sponges like the marine sponge *S. domuncula* indeed possess such an enzyme, termed silicase (Schröder et al. 2003; Eckert et al. 2006). The silicase is able to depolymerize amorphous silica but does not affect crystalline silica (quartz). The silicase is closely related to the carbonic anhydrases, which are a family of zinc metal enzymes (Sly and Hu 1995). The three conserved histidine residues which are characteristic for these enzymes are also found in the sponge protein (Schröder et al. 2003; Eckert et al. 2006). These histidine residues bind a zinc ion which is essential for the catalytic mechanism of the enzyme. In aqueous solution, a hydroxide ion is bound to the zinc ion, which performs a nucleophilic attack at one of the silicon atoms of the polymeric silica. The transiently formed zinc-bound silica is then hydrolyzed by water, resulting in the release of the silicic acid.

4 Recombinant Proteins

The prerequisite of the nanobiotechnological exploitation of the biosilicification machinery in sponges is the availability of enzymatically active recombinant proteins involved in silica formation and dissolution. We applied both prokaryotic and eukaryotic expression systems to obtain recombinant silicateins. Silicatein- α and silicatein- β were expressed in *Escherichia coli* using the Qiaexpress expression system (Qiagen), pET 41A + (Novagen), pBAD/Myc-His (Invitrogen), and pGEX (Amersham). The purification of the recombinant proteins comprising a histidine-tag was performed on a Ni-NTA matrix. To prepare larger quantities of the recombinant proteins, isolation of the proteins was performed using the Profinia™ protein purification system which allows the automated affinity purification and desalting of histidine- or glutathione S-transferase (GST)-tagged proteins in a single run. The eukaryotic systems used for the expression of recombinant silicatein included pCDNA 3.1 (Invitrogen) and pCDNA4V5 (Invitrogen).

To provide silicatein with additional biological properties, we synthesized fusion proteins, e.g., comprising a silicatein sequence and a silk fibroin sequence (Müller et al. 2006c). Silk fibroin may be used as an adhesive protein (“underwater glue”) to attach silicatein and silica nanoparticles formed by silicatein to surfaces. Such proteins, like the foot proteins mfp-1 and mfp-3 from mussels *Mytilus edulis*, have raised increasing interest because of their potential application as water-resistant adhesives (Lin et al. 2007). Further strategies involve adhesive protein from Cuvierian tubules of sea cucumber *Holothuria forskali* (Müller et al. 1972; Baranowska et al., in preparation).

The silicase has been expressed in *E. coli* using the glutathione S-transferase (GST) fusion system; the fusion protein was cleaved with thrombin to separate GST from the recombinant silicase (Schröder et al. 2003).

5 Immobilization of Silicatein: Preparation of Biosilica Coatings

Silicateins provide an attractive tool with which to prepare silica coatings or coatings made of other metal oxides (see below) both on inorganic and organic surfaces. The advantage of this procedure relies on the enzymatic properties of silicatein, which allow biosilification to occur under mild, enzymatic conditions, at low temperature and at near-neutral pH. These properties are important, in particular, for coating heat-sensitive materials or materials which are damaged under alkaline or acidic pH conditions. Recombinant silicatein containing a histidine-tag affinity sequence remains biocatalytically active when immobilized to surfaces (Tahir et al. 2004). The histidine-tag on the silicatein molecule provides a binding site to tether the protein via a linker to the surface. In the following, some examples are given.

Gold surfaces. Silicatein molecules can be immobilized on gold (111) surfaces after functionalization with the chelator nitrilotriacetic acid (NTA) alkanethiol (Tahir et al. 2004). The recombinant protein binds through its His-tag affinity sequence to the NTA group of the linker via Ni^{2+} complex formation (Tahir et al. 2004). Both molecules, the two histidine residues of the His-tag of silicatein and the carboxylate groups and the nitrogen of the NTA head-group of the linker, are involved in the formation of a hexagonal complex. Binding of silicatein can be monitored by atomic force microscopy, SEM, and surface plasmon resonance spectroscopy. The formation of interconnected silica nanospheres with a diameter about 70–300 nm by the immobilized silicatein has been observed (Tahir et al. 2004).

Immobilization of silicatein on gold surfaces can also be achieved by using a reactive ester polymer which specifically reacts with primary amines (Tahir et al. 2005). The amine groups are created on the gold (111) surface by exposure to a cysteamine solution. The reactive ester polymer then allows the binding of ω -terminated NTA amine molecules. These linkers bind at one end to the histidine-tagged silicatein by Ni^{2+} complexation, and at the other end to the amine group of the reactive ester polymer.

Metal oxide surfaces. Surface functionalization of metal oxides such as TiO_2 and Fe_2O_3 can be achieved using a multifunctional polymeric ligand which contains dopamine (catechol) residues used as anchor groups to attach the polymer onto the surface of the metal oxide and a NTA linker to immobilize the His-tagged protein (Tahir et al. 2006). This method has been used to immobilize His-tagged silicatein onto TiO_2 nanowires (Tahir et al. 2006) and $\gamma\text{-Fe}_2\text{O}_3$ nanoparticles (Shukoor et al. 2007a, b, 2008a, b).

Silica surfaces. Silicatein molecules can also be immobilized onto the surface of silica, e.g., organic-layer free spicules, after functionalization (Schröder et al. 2007b). The silica surface (of the spicules) is functionalized with 3-aminopropyltriethoxysilane. The amino groups created on the silica surface allow binding of a reactive ester polymer which serves as a matrix for silicatein. Finally, the recombinant His-tagged silicatein is linked to the functionalized spicules via nickel complexation. Immobilization of silicatein onto the NH_2 -functionalized spicules is

checked by incubation of the spicules with the anti-silicatein antibodies. The immobilized enzyme can be used for the synthesis of a new biosilica layer.

6 Biocatalytic Formation of Titania and Zirconia

Silicatein does not only mediate the synthesis of biosilica but also the formation of other metal oxides such as titania (TiO_2 ; Sumerel et al. 2003; Tahir et al. 2005), zirconia (ZrO_2 ; Bansal et al. 2004; Tahir et al. 2005), and GaOOH/spinel gallium oxide (Kisailus et al. 2005) from water stable precursors at room temperature and neutral pH. This property of silicatein opens further potential areas of application of this enzyme. These metal oxides are known to exhibit semiconductor, piezoelectric, dielectric, and/or electrooptic properties. TiO_2 , a wide-bandgap semiconductor, is used in optoelectronics, solar cells, and photocatalysis. ZrO_2 is applied for the fabrication of piezoelectric, dielectric, and electrooptic materials. The chemical synthesis of these oxides requires extreme pH and temperature conditions, while silicatein is able to form these metal oxides enzymatically using the water stable substrates titanium(IV) bis(ammonium-lactato) dihydroxide and anionic hexafluorozirconate (ZrF_6^{2-} ; Tahir et al. 2005); gallium(III) nitrate is used as precursor in silicatein-mediated catalytic formation of GaOOH and spinel gallium oxide (Kisailus et al. 2005).

7 Formation of Au and Ag Nanoparticles

Silicatein has been shown to possess a side activity which may be of nanobiotechnological relevance, besides its silica esterase activity/silica polymerase activity. Silicatein is able to facilitate the reductive formation of gold or silver nanoparticles in solution (Tahir et al. 2006). Formation of Au nanoparticles has been observed after incubation of silicatein with an aqueous solution of tetrachloroaurate anions (AuCl_4^-) at room temperature. The reduction of AuCl_4^- anions to Au^0 most likely involves the sulfhydryl groups which are hidden below the surface of the protein. The nanoparticles formed are thought to be stabilized by the NH_2 groups of the basic amino acid residues at the surface of the protein. Electron microscopical investigations revealed that the colloidal gold nanoparticles further aggregate to form gold nanocrystals which have a triangular shape. This triangular shape of the surface bound Au nanocrystals has been explained by chiral induction through the protein during the nucleation of the nanocrystals based on the chirality of the nucleation centers at the surface of the silicatein protein (Tahir et al. 2006).

Silicatein is also able to form silver nanoparticles by reduction of AgNO_3 in aqueous solution (Tahir et al., to be published). Silver nanoparticles show antimicrobial activity. Silicatein-mediated formation of silver nanoparticles may provide a method applicable in the fabrication of wound dressings or coatings of biomedical instruments.

8 Nanowires: Biocatalytic Formation of Nanocomposite Materials

Nanotubes and nanowires have become increasingly important building blocks in nanotechnology based on their unique electronic and mechanical properties (Katz and Willner 2004). These properties depend on their constituents (e.g., TiO_2 , V_2O_5 , WS_2 , and others) and morphology. Functionalization of nanotubes and nanowires opens the possibility for binding additional components and thus considerably increases their physical–chemical properties.

Immobilization of His-tagged silicatein to functionalized nanotubes and nanowires presents an attractive method to fabricate novel nanodevices and nanocomposite materials. We described a procedure to immobilize His-tagged silicatein onto TiO_2 nanowires (see above; Tahir et al. 2006). Binding of silicatein to the surface of the nanowires was visualized by high magnification confocal laser scanning microscopy using antibodies against the bound protein and a fluorophore-labeled secondary antibody. The immobilized silicatein was used for the fabrication of Au nanoparticles at the surface of the nanowires by exploiting the reducing activity of the protein (see above). High resolution electron microscopical studies of the Au-decorated TiO_2 nanowires revealed a triangular or hexagonal morphology of Au nanoparticles obtained by the bioreduction of AuCl_4^- (Tahir et al. 2006). Using other oxide/chalcogenide nanotubes/nanowires, this methodology can be used for the synthesis of a wide range of nanocomposite materials.

9 Nanolithography Approaches

Soft lithographical procedures have gained increasing importance in the manufacture of microelectronics (Xia and Whitesides 1998; Pisignano et al. 2005). However, none of these procedures takes advantage of enzyme-catalyzed reactions. Silicateins exhibit two properties which make them of interest for the fabrication of silica patterns. Silicateins are (1) biocatalytically active; they are able to form silica and other metal oxides from water-soluble precursors, and (2) they show structure-directing activity. Silicatein molecules are able to self-assemble to form protein templates that can be employed to synthesize defined patterns of silica and other metal oxides. Silicatein templates may be created not only on various surfaces (metal, metal oxide, or glass) but silicatein protein filaments may also form 3D scaffolds which may serve as template for the biocatalytic formation of 3D silica structures. These unique properties of silicatein are exploited in an ongoing research programme (<http://www.bio-litho.de>). The potential impact of silicatein-mediated biomineralization processes for the controlled realization of silica patterns applying soft lithography procedures also relies on the ability of silicatein to synthesize silica at low temperature and near-neutral pH, allowing new fabrication processes for microelectronic devices under gentle, environmentally benign, conditions.

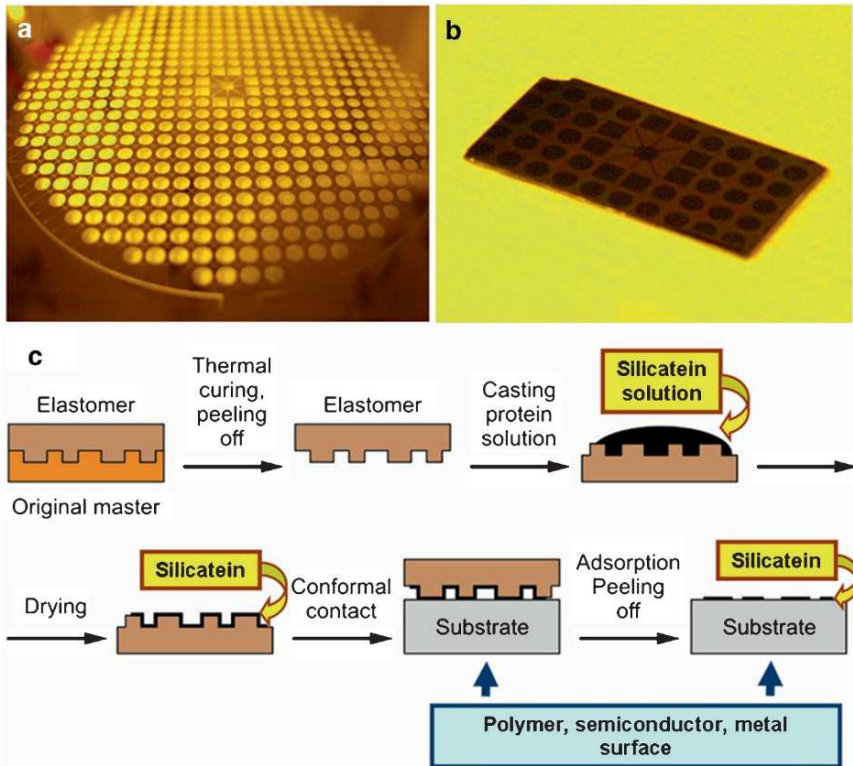


Fig. 3 Application of silicatein on substrate surfaces by microcontact printing (μ CP). (a) Master plate. (b) Wafer after development. (c) Schematic representation

Various soft lithography techniques are available for the controlled patterned deposition of silicatein molecules, including microcontact printing (μ CP; Fig. 3; Bernard et al. 2000; Sgarbi et al. 2004) and micromolding in capillaries (MIMIC). Further procedures include the use of polymer nanofibers in soft lithography (Pisignano et al. 2005). The realization of electrically insulating patterns for micro-electronic devices, fabricated by silicatein-controlled biosilicification, is thought to be an extremely innovative step in the opto- and microelectronics industry.

10 Synthesis of Core-Shell Materials

A fascinating approach would be to use the biosynthetic abilities of silicatein to synthesize materials which imitate the lamellar architecture with its unique physicochemical properties found in sponge spicules. Such a biomimetic approach, using “Nature as model,” was indeed found to be feasible. Using recombinant silicatein immobilized on

the surface of spicules freed of organic material, fabrication of spicule-like core-shell materials of alternating metal and metal oxide layers with complex architectures and properties turned out to be possible (Schröder et al. 2007b).

Purified recombinant silicatein was linked onto spicules after amino-group-functionalization of the silica surface with aminopropyltriethoxysilane as described above (Fig. 4a). The NH_2 -functionalized spicules were reacted with a reactive ester polymer which allows binding of the recombinant protein, with its His-tag, via Ni(II). We demonstrated that the immobilized enzyme synthesized a new silica lamella using TEOS as substrate (Schröder et al. 2007b). SEM analysis revealed that the spicules that were covered with silicatein have a wrinkled surface caused by the proteinaceous layer (Fig. 4b). Backscattered SEM images showed a 200- to 500-nm-thick additional surface layer at the surface of spicules; EDX analysis of this layer showed a distinct silicon peak which was absent in reference samples. The presence of silicatein molecules at the surface of the spicules could also be visualized using antibodies against this protein, as revealed by fluorescence microscopical analysis (Fig. 4c). Functionalized spicules which had been treated with the polymer but not with silicatein (controls) showed a completely smooth surface (Fig. 4d).

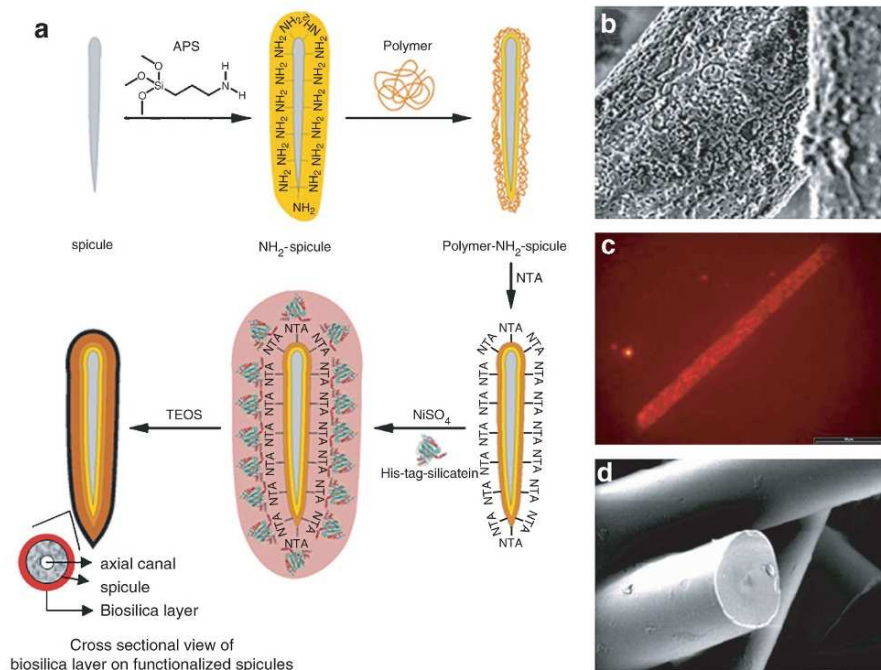


Fig. 4 (a) Schematic representation. Functionalization of spicule surface and formation of biosilica mediated by immobilized recombinant silicatein. The NH_2 -functionalized spicules are reacted with the polymer and then with the His-tagged silicatein. (b) SEM analysis of spicules of *Suberites domuncula* with biosilica layer. (c) Immunostaining of spicule of *S. domuncula* with immobilized silicatein. (d) Non-functionalized spicules

Functionalization of His-tagged silicatein, which synthesizes gold nanoparticles from auric acid by the reductive action of the protein, has also been performed onto core-shell colloids (Lange et al. 2007). Gold nanoparticles were formed after addition of aqueous tetrachloroauric acid to the silicatein-functionalized core-shell colloids, resulting in a change of the color of the solution from pale yellow (auric acid) to red (gold nanoparticles).

11 Bone Replacement Materials/Bone Regeneration Scaffolds

Biosilicification has become a promising approach in the design of novel biomimetic nanoscale composites used in surgery and dentistry. Biological hard tissues are nanocomposite hybrid materials. The fact that they consist of both inorganic and organic phases provide them with excellent mechanical properties. Silica is a constituent of many materials used as scaffolds in tissue engineering of bone and cartilage (Hench and Wilson 1984; Yamamuro et al. 1990). Biosilica which contains an organic component shows significant advantages over existing composite materials (Müller et al. 2008e). In addition, biosilica exhibits osteogenic, osteoblast-stimulating, activity. We showed that mineralization (formation of mineralized calcium phosphate nodules) of human bone-forming cells (human osteosarcoma SaOS-2 cells) significantly increases if the cells were grown on surfaces coated with enzymatically (via silicatein) synthesized biosilica (Schröder et al. 2005a). In addition, we showed that biosilica has an effect on the expression of genes that are crucial for the control of formation of tooth enamel: amelogenin, ameloblastin, and enamelin (Müller et al. 2007d).

Silicatein may provide a promising approach for preparation of biosilica coatings of metal implants used in surgery (Fig. 5). Metal implants made of titanium (Fig. 5a), titanium alloys, or CoCr may be coated with biosilica using silicatein bound to the metal surface (Fig. 5b). Binding of silicatein to the surface can be achieved by simple adsorption or the use of chemical linkers. SaOS-2 cells grown on a biosilica-coated titanium implant show an increase in mineralization (Fig. 5c). The biocatalytically-formed biosilica layer is expected to increase the biocompatibility of the implant. Besides biocompatibility, the formation of a mechanically stable, interfacial bond between the bone and the implant is of critical importance. We are still far away from a satisfactory solution of this problem, but coating the metal surface with biosilica may provide a promising strategy.

The biosilica-modified metal surface could also be used as a binding site for bioactive substances which may be either physically entrapped or chemically bound to the biosilica layer (after functionalization). Formation of biosilica under mild (enzymatic) conditions may be a suitable method for encapsulation of proteins (e.g., bone morphogenic protein) and drugs which are heat-sensitive or sensitive to caustic chemicals.

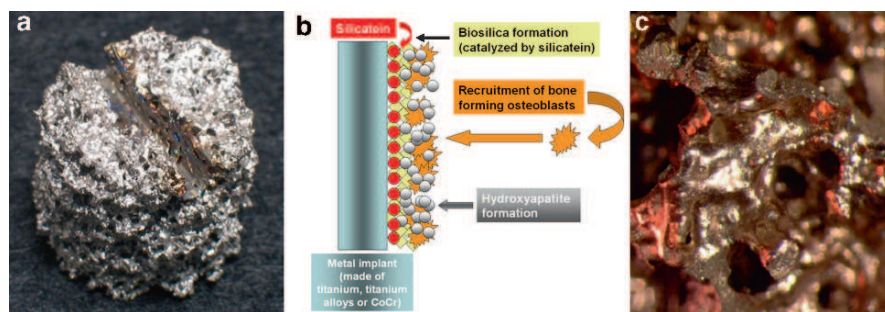


Fig. 5 Bioactive, osteoblast-stimulating surface generated by coating of surface of metal implants with silicatein and subsequent enzymatic formation of biosilica. **(a)** Titanium implant (screw). **(b)** Scheme showing recruitment of bone-forming cells (osteoblasts) and formation of hydroxyapatite on the bioactive silicatein/biosilica-coated metal surface. **(c)** Mineralizing culture of SaOS-2 cells grown on a biosilica-modified surface

12 Encapsulation of Bacteria

Bioencapsulation of enzymes or cells into hydrogels has gained increasing interest in biotechnology. Bioencapsulated molecules or cells can be applied, for example, as scaffolds in tissue engineering, as sustained-release delivery systems, and biosensors.

Major tasks are the control of the process of gelation of silicate or silicon alkoxide to prevent the formation of monolithic gels. Smaller-sized particles are more convenient to handle and to apply for encapsulation; those biotechnological processes require additional steps such as extrusion or the use of linkers.

Previous approaches to encapsulate cells and molecules in poly(silicate) (reviewed in Coradin and Livage 2007) include: (1) hydrolysis and condensation reactions of metal alkoxides (Brinker and Scherrer 1990), and (2) utilization of the gel-forming ability of aqueous salts of metals (Iler 1979). Silicon alkoxide-based sol-gel chemistry makes use of an alcohol which is required as a cosolvent to water for solubilization of the precursor. However, alcohol is a disadvantage if used for encapsulations of biological molecules or cells. It has been shown that alcohol is not needed as an additive in the silicon alkoxide sol-gel process (Avnir and Kaufman 1987), but alkoxide monomers release alcohol molecules in aqueous solution. Accordingly, techniques based on the use of aqueous precursors, e.g., silicates and/or colloidal silica, have been developed for encapsulation of cells or biomolecules (Liu and Chen 1999; Bhatia et al. 2000; reviewed in Coradin and Livage 2007).

Physiological conditions for encapsulation of cells or molecules require the use of non-toxic silicic acid monomers or silicon alkoxides at neutral pH and ambient temperature in aqueous solutions. The availability of an enzyme, i.e., silicatein, that

forms silica under mild (enzymatic) conditions provides a new tool in this important area of biotechnology.

We demonstrated that bacteria (*E. coli*) can be transformed with the silicatein- α gene from *S. domuncula* (Müller et al. 2008a). The procedure is summarized in Fig. 6a. The expression of the silicatein- α gene induced by isopropyl β -D-thiogalactoside (IPTG) was found to be markedly increased after addition of silicic acid. Silicatein is transported onto the bacterial cell surface where it retains its catalytic activity. Electron microscopic analysis revealed that the transformed bacteria which were grown in the presence of silicic acid form a silica cover which encapsulates the whole bacteria (Fig. 6b, c). Surprisingly, the growth kinetics of the bacteria were not affected by the formation of the silica shell (Müller et al. 2008a). The silicatein-mediated encapsulation of the bacterial cells seems rather to increase the resistance of the bacteria against a number of external stressors (to be published). We assume that this procedure might improve the stability and extend the range of application of bacteria in industrial biotechnology (“White Biotechnology”; e.g., for the production of fine chemicals or recombinant proteins).

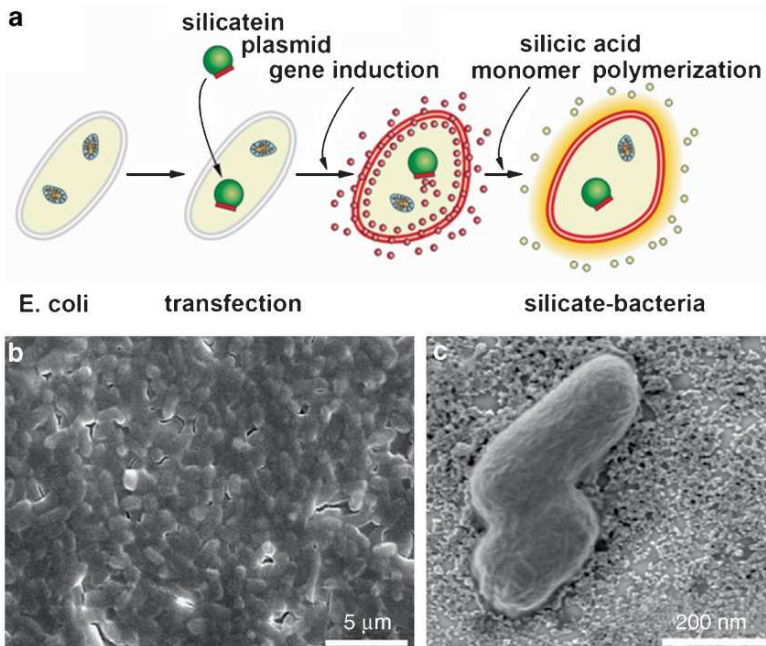


Fig. 6 Encapsulation of *Escherichia coli* with biosilica. (a) Schematic representation. *E. coli* are transformed with the silicatein gene. After induction with IPTG, the bacteria express the silicatein protein. This protein is deposited on the surface of the bacteria. The bacteria are encapsulated in a biosilica layer mediated by silicatein on the bacterial cell surface after incubation with silicic acid. (b) Scanning electron microscopic analysis of silicatein-gene-transformed *E. coli* grown in medium for 48 h supplemented with 60 μ M silicic acid. (c) Higher magnification

13 Microstructured Optical Fibers

The introduction of fiber-optic communication systems has revolutionized telecommunication. Optical fibers consist of a core and a lower-refractive-index cladding, which are made of silica glass, and a protective outer coating (Fig. 7, upper panel left). The light is transmitted in the core by total internal reflection (Fig. 7, upper panel right). Such optical fibers show a striking similarity with the spicules of siliceous sponges, in particular the spicules of Hexactinellida (Fig. 7, lower panel). The spicules of these sponges can reach a length of up to 3 m and a diameter of up to 1 cm (*M. chuni*); they are composed of up to 500 silica lamellae (Müller et al. 2007a, f, 2008e; Wang et al. 2007). Sponge spicules have been shown to act as optical glass fibers which transmit light with high efficiency; these light transmission properties of sponge spicules have been demonstrated first in *Rossella racovitzae* (Cattaneo-Vietti et al. 1996) and later also in other hexactinellid sponges, *Euplectella aspergillum* (Aizenberg et al. 2004), *Monorhaphis* (Wang et al. 2007), and *Hyalonema sieboldi* (Müller et al. 2006e). The stalk spicules of the latter sponge are composed of ~40 siliceous layers which surround the central axial filament (thickness, 1 µm). The innermost siliceous layer, the protosiphon, is more flexible and less fragile than the outer layers (siphons). We demonstrated that these spicules (length, 30 cm) act as sharp high- and low-pass filters. Only light

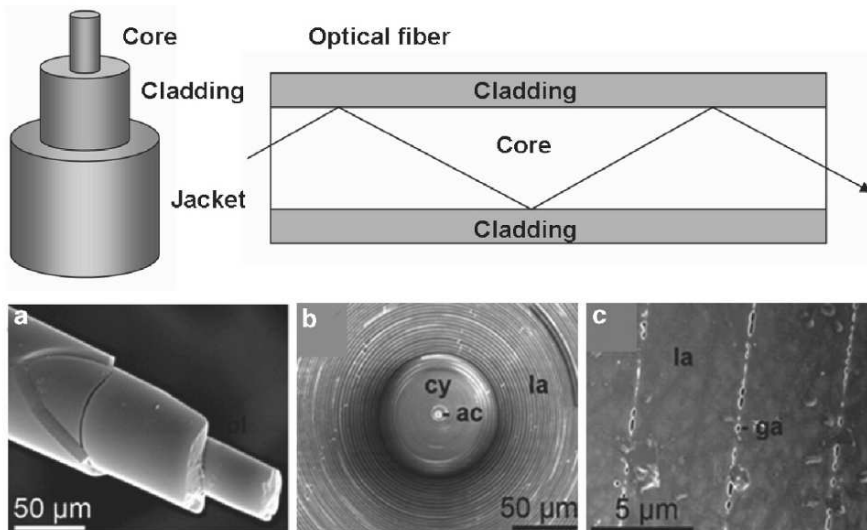


Fig. 7 Similarity in the construction of technical optical fibers and sponge spicules. *Upper panel* Schematic representation of a technical optical fiber used in telecommunication. Optical fibers are cylindric dielectric waveguides that transmit light along their axis by total internal reflection. The fiber consists of a core surrounded by a cladding layer, as well as a protective outer coating (jacket). *Lower panel (a–c)* Concentric arrangement of the silica layers of the comitalia (a) and the stalk spicule (b, c) of the glass sponge *Monorhaphis chuni*; rapid-SEM analysis

with wavelengths between 615 and 1,310nm can pass through the spicule fiber, while wavelengths <615 and >1,310nm are filtered out (Müller et al. 2006e). One advantage of sponge optical fibers is their higher stability compared to technical optical fibers. Technical optical fibers which only consist of an inorganic (glass) phase easily break if bent too sharply, while sponge optical fibers are made of a composite consisting of both an inorganic (silica glass) and organic (protein) phase and are therefore much more stable against mechanical forces.

14 Conclusions

The innovative potential of novel technologies based on the understanding of biomineralization processes seems to be enormous. Silicon and silica are basic elements/materials used in nanotechnology which is considered as a key technology and powerful economic force in this century. The availability of enzymes involved in silica (“biosilica”) metabolism, silicatein and silicase (protected by patents; e.g., Müller et al. 2004, 2007h), opens a variety of novel applications and products in nano(bio)technology and medicine/dentistry. Silica-based materials are present in many high-tech products such as microelectronics, optoelectronics, (bio)sensors, and catalysts. The extreme interest in biosilica and the enzymes involved in biosilica formation is based on the fact that the enzymatic (silicatein)-mediated fabrication of biosilica glass occurs under mild, ambient conditions (low temperature and pressure, near-neutral pH), whereas conventional technical (chemical) procedures require high temperatures and pressures, and the use of caustic chemicals. In addition, biosilica is a composite material consisting of both an inorganic (silica) phase and an organic (protein) phase, which provide this material with unique physiochemical properties. The enzymatic formation of biosilica glass is particularly advantageous for the fabrication of silica coatings on organic (bio) material surfaces. In addition, silicatein molecules are able to self-assemble, either alone or together with other (protein) molecules, to defined structures which may act as a template for silica deposition (or the formation of other metal oxides). Thus, silicateins can be used for the design of specific nanodevices, the preparation of coatings on diverse surfaces including metals, metal oxides, and glass, and the encapsulation of (bio)molecules such as drugs and proteins, as well as for the synthesis of novel biomimetic biosilica-containing nanocomposites. There is at present a great interest in alternative bone replacement materials due to the disadvantages of bone autografts. The recombinant silicateins are also of particular interest for the preparation of bioactive coatings of medical implants, which promote new bone formation, as well as in dentistry. This novel technology which exploits the ability of sponges to form (bio)silica enzymatically, is bioinspired, i.e., nature is used as model, and combines for the first time two chemistries – silicon and carbon – and two areas of technology – biotechnology and micro/optoelectronics – via a unique enzyme – silicatein.

Acknowledgments This work was supported by grants from the European Commission (BIO-LITHO project), the Deutsche Forschungsgemeinschaft, and the Bundesministerium für Bildung und Forschung Germany (project: Joint-Lab Baikal and Center of Excellence *BIOTECmarin*).

References

- Aizenberg J, Sundar V, Yablon AD, Weaver JC, Chen G (2004) Biological glass fibers: correlation between optical and structural properties. *Proc Natl Acad Sci USA* 101:3358–3363
- Avinir D, Kaufman VR (1987) Alcohol is an unnecessary additive in the silicon alkoxide sol-gel process. *J Non-Cryst Solids* 192:180–182
- Ball RSW (1894) The possibility of life in other worlds. *Fortnightly Rev* 78:676
- Bansal V, Rautaray D, Ahmad A, Sastry M (2004) Biosynthesis of zirconia nanoparticles using the fungus *Fusarium oxysporum*. *J Mater Chem* 14:3303–3305
- Belikov SI, Kaluzhnaya OV, Schröder HC, Krasko A, Müller IM, Müller WEG (2005) Expression of silicatein in spicules from the Baikalian sponge *Lubomirskia baicalensis*. *Cell Biol Int* 29:943–951
- Bernard A, Renault JP, Michel B, Bosshard HR, Delamarche E (2000) Microcontact printing of proteins. *Adv Mater* 12:1067–1070
- Bhatia RB, Brinker CJ, Gupta AK, Singh AK (2000) Aqueous sol-gel process for protein encapsulation. *Chem Mater* 12:2434–2441
- Brinker CJ, Scherrer G (1990) *Sol-Gel Science: The Physics and Chemistry of Sol-Gel Processing*. Boston, MA: Academic
- Cairns-Smith AG (1968) An approach to a blueprint for a primitive organism. In: Waddington CH (ed.). *Towards a Theoretical Biology*, vol 1. Edinburgh: Edinburgh University Press, pp 57–66
- Cairns-Smith AG (1982) *Genetic Takeover and the Mineral Origins of Life*. Cambridge: Cambridge University Press
- Cairns-Smith AG (2008) Chemistry and the missing era of evolution. *Chemistry* 14:3830–3839
- Carlisle EM (1978) Essentiality and function of silicon. In: Bendz G, Lingvist I (eds) *Biochemistry of Silicon and Related Problems*. New York: Plenum, pp 231–253
- Cattaneo-Vietti R, Bavestrello G, Cerrano C, Sarà A, Benatti U, Giovine M, Gaino E (1996) Optical fibres in an Antarctic sponge. *Nature* 383:397–398
- Cha JN, Shimizu K, Zhou Y, Christianssen SC, Chmelka BF, Stucky GD, Morse DE (1999) Silicatein filaments and subunits from a marine sponge direct the polymerization of silica and silicones *in vitro*. *Proc Natl Acad Sci USA* 96:361–365
- Coradin T, Livage J (2007) Aqueous silicates in biological sol-gel applications: new perspectives for old precursors. *Acc Chem Res*. 40:819–826
- Eckert C, Schröder HC, Brandt D, Perovic-Ottstadt S, Müller WEG (2006) A histochemical and electron microscopic analysis of the spiculogenesis in the demosponge *Suberites domuncula*. *J Histochem Cytochem* 54:1031–1040
- Funayama N, Nakatsukasa M, Kuraku S, Takechi K, Dohi M, Iwabe N, Miyata T, Agata K (2005). Isolation of Ef silicatein and Ef lectin as molecular markers for sclerocytes and cells involved in innate immunity in the freshwater sponge *Ephydatia fluviatilis*. *Zool Sci* 22:1113–1122
- Haldane JBS (1928) *Possible Worlds and Other Essays*. Harper & Brothers, New York/London; Chatto & Windus 1937 edition, Transaction Publishers 2001
- Hench LL, Wilson JW (1984) Surface-active biomaterials. *Science* 226:630–636
- Hildebrandt M, Wetherbee R (2003) Components and control of silicification in diatoms. *Prog Mol Subcell Biol* 33:11–57
- Iler RK (1979) *The Chemistry of Silica*. Wiley, New York

- Jugdaohsingh R, Tucker KL, Qiao N, Cupples LA, Kiel DP, Powell JJ (2004) Dietary silicon intake is positively associated with bone mineral density in men and premenopausal women of the Framingham Offspring cohort. *J Bone Miner Res* 19:297–307
- Kaluzhnaya OV, Belikov SI, Schröder HC, Wiens M, Giovine M, Krasko A, Müller IM, Müller WEG (2005) Dynamics of skeleton formation in the Lake Baikal sponge *Lubomirskia baicalensis*. Part II. Molecular biological studies. *Naturwissenschaften* 92:134–138
- Katz E, Willner I (2004) Integrated nanoparticle-biomolecule hybrid systems: synthesis, properties, and applications. *Angew Chem Int Ed* 43:6042–6108
- Kisailus D, Choi JH, Weaver JC, Yang W, Morse DE (2005) Enzymatic synthesis and nanostructural control of gallium oxide at low temperature. *Adv Mater* 17:314–318
- Krasko A, Gamulin V, Seack J, Steffen R, Schröder HC, Müller WEG (1997) Cathepsin, a major protease of the marine sponge *Geodia cydonium*: purification of the enzyme and molecular cloning of cDNA. *Mol Mar Biol Biotechnol* 6:296–307
- Krasko A, Lorenz B, Batel R, Schröder HC, Müller IM, Müller WEG (2000) Expression of silicatein and collagen genes in the marine sponge *Suberites domuncula* is controlled by silicate and myotrophin. *Eur J Biochem* 267:4878–4887
- Lange B, Metz N, Tahir MN, Fleischhaker F, Theato P, Schröder HC, Müller WEG, Tremel W, Zentel R (2007) Functional polymer-opals from core-shell colloids. *Macromol Rapid Commun* 28:1987–1994
- Lin Q, Gourdon D, Sun C, Holten-Andersen N, Anderson TH, Waite JH, Israelachvili JN (2007) Adhesion mechanisms of the mussel foot proteins mfp-1 and mfp-3. *Proc Natl Acad Sci USA* 104:3782–3786
- Liu DM, Chen JW (1999) Encapsulation of protein molecules in transparent porous silica matrices via an aqueous colloidal sol-gel process. *Acta Mater* 47:4535–4544
- Müller WEG, Zahn, RK, Schmid K (1972) The adhesive behaviour in Cuvierian tubules of *Holothuria forskali*: biochemical and biophysical investigations. *Cytobiologie* 5:335–351
- Müller WEG, Krasko A, Le Pennec G, Schröder HC (2003a) Biochemistry and cell biology of silica formation in sponges. *Microsc Res Tech* 62:368–377
- Müller WEG, Krasko A, Le Pennec G, Steffen R, Wiens M, Ammar MSA, Müller IM, Schröder HC (2003b) Molecular mechanism of spicule formation in the demosponge *Suberites domuncula*: silicatein – collagen – myotrophin. *Prog Mol Subcell Biol* 33:195–221
- Müller WEG, Schröder HC, Lorenz B, Krasko A (2004) Silicatein-mediated synthesis of amorphous silicates and siloxanes and use thereof. European Patent No. EP1320624
- Müller WEG, Borejko A, Brandt D, Osinga R, Ushijima H, Hamer B, Krasko A, Xupeng C, Müller IM, Schröder HC (2005a) Selenium affects biosilica formation in the demosponge *Suberites domuncula*: effect on gene expression and spicule formation. *FEBS J* 272:3838–3852
- Müller WEG, Rothenberger M, Borejko A, Tremel W, Reiber A, Schröder HC (2005b) Formation of siliceous spicules in the marine demosponge *Suberites domuncula*. *Cell Tissue Res* 321:285–297
- Müller WEG, Belikov SI, Schröder HC (2006a) *Science – First Hand* 3:26–35
- Müller WEG, Belikov SI, Tremel W, Perry CC, Gieskes WWC, Borejko A, Schröder HC (2006b) Siliceous spicules in marine demosponges (example *Suberites domuncula*). *Micron* 37:107–120
- Müller WEG, Geurtsen WK, Schröder HC (2006c) Biosilica-adhesive protein nanocomposite materials: synthesis and application in dentistry. US Patent Application No. US60/839,601
- Müller WEG, Schröder HC, Wrede P, Kaluzhnaya OV, Belikov SI (2006d) Speciation of sponges in Baikal-Tuva region: an outline. *J Zool Syst Evol Res* 44:105–117
- Müller WEG, Wendt K, Geppert C, Wiens M, Reiber A, Schröder HC (2006e) Novel photoreception system in sponges? Unique transmission properties of the stalk spicules from the hexactinellid *Hyalonema sieboldi*. *Biosens Bioelectron* 21:1149–1155
- Müller WEG, Eckert C, Kropf K, Wang X, Schloßmacher U, Seckert C, Wolf SE, Tremel W, Schröder HC (2007a) Formation of giant spicules in the deep-sea hexactinellid *Monorhaphis chuni* (Schulze 1904): electron-microscopic and biochemical studies. *Cell Tissue Res* 329:363–378

- Müller WEG, Boreiko A, Schloßmacher U, Wang X, Tahir MN, Tremel W, Brandt D, Kaandorp JA, Schröder HC (2007b) Fractal-related assembly of the axial filament in the demosponge *Suberites domuncula*: relevance to biomineralization and the formation of biogenic silica. *Biomaterials* 28:4501–4511
- Müller WEG, Boreiko A, Wang X, Belikov SI, Wiens M, Grebenjuk VA, Schloßmacher U, Schröder HC (2007c) Silicateins, the major biosilica forming enzymes present in demospo- nges: protein analysis and phylogenetic relationship. *Gene* 395:62–71
- Müller WEG, Boreiko A, Wang X, Krasko A, Geurtsen W, Custódio MR, Winkler T, Lukić-Bilela L, Link T, Schröder HC (2007d) Morphogenetic activity of silica and bio-silica on the expression of genes controlling biomineralization using SaOS-2 cells. *Calcif Tissue Int* 81:382–393
- Müller WEG, Schröder HC, Krasko A (2007e) Decomposition and modification of silicate and silicone by silicase and use of the reversible enzyme. European Patent No. EP1546319
- Müller WEG, Li J, Schröder HC, Qiao L, Wang X (2007f) The unique skeleton of siliceous sponges (Porifera; Hexactinellida and Demospongiae) that evolved first from the Urmetazoa during the Proterozoic: a review. *Biogeosciences* 4:219–232
- Müller WEG, Schloßmacher U, Eckert C, Krasko A, Boreiko A, Ushijima H, Wolf SE, Tremel W, Müller IM, Schröder HC (2007g) Analysis of the axial filament in spicules of the demosponge *Geodia cydonium*: different silicatein composition in microscleres (asters) and megascleres (oxeas and triaenes). *Eur J Cell Biol* 86:473–487
- Müller WEG, Schröder HC, Lorenz B, Krasko A (2007h) Silicatein-mediated synthesis of amor- phous silicates and siloxanes and use thereof. United States Patent No. US 7,169,589 B2
- Müller WEG, Wang X, Belikov SI, Tremel W, Schloßmacher U, Natoli A, Brandt D, Boreiko A, Tahir MN, Müller IM, Schröder HC (2007i) Formation of siliceous spicules in demospo- nges: example *Suberites domuncula*. In: Bäuerlein E (ed) *Handbook of Biomineralization*, vol. 1: Biological Aspects and Structure Formation. Weinheim: Wiley-VCH, pp 59–82
- Müller WEG, Boreiko A, Schloßmacher U, Wang X, Eckert C, Kropf K, Li J, Schröder HC (2008a) Identification of a silicatein (-related) protease in the giant spicules of the deep sea hexactinellid *Monorhaphis chuni*. *J Exp Biol* 211:300–309
- Müller WEG, Engel S, Wang X, Wolf SE, Tremel W, Thakur NL, Krasko A, Divekar M, Schröder HC (2008b) Bioencapsulation of living bacteria (*Escherichia coli*) with poly(silicate) after transformation with silicatein- α gene. *Biomaterials* 29:771–779
- Müller WEG, Schloßmacher U, Wang X, Boreiko A, Brandt D, Wolf SE, Tremel W, Schröder HC (2008c) Poly(silicate)-metabolizing silicatein in siliceous spicules and silicasomes of dem- ospo- nges comprises dual enzymatic activities (silica-polymerase and silica-esterase). *FEBS J* 275:362–370
- Müller WEG, Wang X, Kropf K, Boreiko A, Schloßmacher U, Brandt D, Schröder HC, Wiens M (2008d) Silicatein expression in the hexactinellid *Crateromorpha meyeri*: the lead marker gene restricted to siliceous sponges. *Cell Tissue Res* (in press), doi:10.1007/s00441–008–0624–6
- Müller WEG, Wang X, Kropf K, Ushijima H, Geurtsen W, Eckert C, Tahir MN, Tremel W, Boreiko A, Schloßmacher U, Li J, Schröder HC (2008e) Bioorganic/inorganic hybrid com- position of sponge spicules: matrix of the giant spicules and of the comitalia of the deep sea hexactinellid *Monorhaphis*. *J Struct Biol* 161:188–203
- Murr MM, Morse DE (2005) Fractal intermediates in the self-assembly of silicatein filaments. *Proc Natl Acad Sci USA* 102:11657–11662
- Pisignano D, Maruccio G, Mele E, Persano L, Di Benedetto F, Cingolani R (2005) Polymer nanofibers by soft lithography. *Appl. Phys Lett* 87:123109
- Pozzolini M, Sturla L, Cerrano C, Bavestrello G, Camardella L, Parodi AM, Raheli F, Benatti U, Müller WEG, Giovine M (2004) Molecular cloning of silicatein gene from the marine sponge *Petrosia ficiformis* (Porifera, Demospongiae) and development of primmorphs as a model for biosilicification studies. *Mar Biotechnol* 6:594–603
- Reffitt DM, Ogston N, Jugdaohsingh R, Cheung HF, Evans BA, Thompson RP, Powell JJ, Hampson GN (2003) Orthosilicic acid stimulates collagen type 1 synthesis and osteoblastic differentiation in human osteoblast-like cells *in vitro*. *Bone* 32:127–135
- Reynolds JE (1893) Notes. Section B. Chemistry. *Nature* 48:477–481

- Schröder HC, Krasko A, Batel R, Skorokhod A, Pahler S, Kruse M, Müller IM, Müller WEG (2000) Stimulation of protein (collagen) synthesis in sponge cells by a cardiac myotrophin-related molecule from *Suberites domuncula*. *FASEB J* 14:2022–2031
- Schröder HC, Krasko A, Le Pennec G, Adell T, Wiens M, Hassanein H, Müller IM, Müller WEG (2003) Silicase, an enzyme which degrades biogenous amorphous silica: contribution to the metabolism of silica deposition in the demosponge *Suberites domuncula*. *Prog Mol Subcell Biol* 33:250–268
- Schröder HC, Perović-Ottstadt S, Rothenberger M, Wiens M, Schwertner H, Batel R, Korzhev M, Müller IM, Müller WEG (2004a) Silica transport in the demosponge *Suberites domuncula*: fluorescence emission analysis using the PDMPO probe and cloning of a potential transporter. *Biochem J* 381:665–673
- Schröder HC, Perović-Ottstadt S, Wiens M, Batel R, Müller IM, Müller WEG (2004b) Differentiation capacity of the epithelial cells in the sponge *Suberites domuncula*. *Cell Tissue Res* 316:271–280
- Schröder HC, Boreiko O, Krasko A, Reiber A, Schwertner H, Müller WEG (2005a) Mineralisation of SaOS-2 cells on enzymatically (silicatein) modified bioactive osteoblast-stimulating surfaces. *J Biomed Mater Res Part B: Appl Biomater* 75B:387–392
- Schröder HC, Perović-Ottstadt S, Grebenjuk VA, Engel S, Müller IM, Müller WEG (2005b) Biosilica formation in spicules of the sponge *Suberites domuncula*: synchronous expression of a gene cluster. *Genomics* 85:666–678
- Schröder HC, Boreiko A, Korzhev M, Tahir MN, Tremel W, Eckert C, Ushijima H, Müller IM, Müller WEG (2006) Co-expression and functional interaction of silicatein with galectin: matrix-guided formation of siliceous spicules in the marine demosponge *Suberites domuncula*. *J Biol Chem* 281:12001–12009
- Schröder HC, Brandt D, Schloßmacher U, Wang X, Tahir MN, Tremel W, Belikov SI, Müller WEG (2007a) Enzymatic production of biosilica glass using enzymes from sponges: basic aspects and application in nanobiotechnology (material sciences and medicine). *Naturwissenschaften* 94:339–359
- Schröder HC, Natalio F, Shukoor I, Tremel W, Schloßmacher U, Wang X, Müller WEG (2007b) Apposition of silica lamellae during growth of spicules in the demosponge *Suberites domuncula*: biological/biochemical studies and chemical/biomimetical confirmation. *J Struct Biol* 159:325–334
- Schröder HC, Wang X, Tremel W, Ushijima H, Müller WEG (2008) Biofabrication of biosilica-glass by living organisms. *Nat Prod Rep* 25:455–474
- Schwarz K, Milne DB (1972) Growth-promoting effects of silicon in rats. *Nature* 239:333–334
- Sgarbi N, Pisignano D, Di Benedetto F, Gigli G, Cingolani R, Rinaldi R (2004) Self-assembled extracellular matrix protein networks by microcontact printing. *Biomaterials* 25:1349–1353
- Shimizu K, Cha J, Stucky GD, Morse DE (1998) Silicatein alpha: cathepsin L-like protein in sponge biosilica. *Proc Natl Acad Sci USA* 95:6234–6238
- Shukoor MI, Natalio F, Ksenofontov V, Tahir MN, Eberhardt M, Theato P, Schröder HC, Müller WEG, Tremel W (2007a) Double-stranded RNA polyinosinic-polycytidylic acid immobilized onto γ -Fe₂O₃ nanoparticles by using a multifunctional polymeric linker. *Small* 3:1374–1378
- Shukoor MI, Natalio F, Tahir MN, Ksenofontov V, Therese HA, Theato P, Schröder HC, Müller WEG, Tremel W (2007b) Superparamagnetic γ -Fe₂O₃ nanoparticles with tailored functionality for protein separation. *Chem Commun* 2007:4677–4679
- Shukoor MI, Natalio F, Metz N, Glube N, Tahir MN, Therese HA, Ksenofontov V, Theato P, Langguth P, Boissel JP, Schröder HC, Müller WEG, Tremel W (2008a) dsRNA-functionalized multifunctional γ -Fe₂O₃ nanocrystals: a tool for targeting cell surface receptors. *Angew Chem Int Ed Engl* 47:4748–4752
- Shukoor MI, Natalio F, Tahir MN, Divekar M, Metz N, Therese HA, Theato P, Ksenofontov V, Schröder HC, Müller WEG, Tremel W (2008b) Multifunctional polymer-derivatized γ -Fe₂O₃ nanocrystals as a methodology for the biomagnetic separation of recombinant His-tagged proteins. *J Magn Magn Mater* 320:2339–2344

- Sly WS, Hu PY (1995) Human carbonic anhydrases and carbonic anhydrase deficiencies. *Annu Rev Biochem* 64:375–401
- Sumerel JL, Yang W, Kisailus D, Weaver JC, Choi JH, Morse DE (2003) Biocatalytic structure-directing synthesis of titanium dioxide. *Chem Mater* 15:4804–4809
- Tahir MN, Théato P, Müller WEG, Schröder HC, Janshoff A, Zhang J, Huth J, Tremel W (2004) Monitoring the formation of biosilica catalysed by histidine-tagged silicatein. *Chem Commun* 2004:2848–2849
- Tahir MN, Théato P, Müller WEG, Schröder HC, Borejko A, Faiß S, Janshoff A, Huth J, Tremel W (2005) Formation of layered titania and zirconia catalysed by surface-bound silicatein. *Chem Commun* 28:5533–5535
- Tahir MN, Eberhardt M, Therese HA, Kolb U, Theato P, Müller WEG, Schröder HC, Tremel W (2006) From single molecules to nanoscopically structured functional materials: Au nanocrystal growth on TiO₂ nanowires controlled by surface bound silicatein. *Angew Chem Int Ed* 45:4803–4809
- Wang X, Li J, Qiao L, Schröder HC, Eckert C, Kropf K, Wang Y, Feng Q, Müller WEG (2007) Structure and characteristics of giant spicules of the deep sea hexactinellid sponges of the genus *Monorhaphis* (Hexactinellida: Amphidiscosida: Monorhaphididae). *Acta Zool Sinica* 53:557–569
- Weaver J, Morse DE (2003) Molecular biology of demersal sponge axial filaments and their roles in biosilification. *Micr Res Techn* 62:356–367
- Wells HG (1894) The living things that may be. *Pall Mall Gazette* 58:4
- Wiens M, Belikov SI, Kaluzhnaya OV, Krasko A, Schröder HC, Perovic-Ottstadt S, Müller WEG (2006) Molecular control of serial module formation along the apical-basal axis in the sponge *Lubomirskia baicalensis*: silicateins, mannose-binding lectin and mago nashi. *Dev Genes Evol* 216:229–242
- Wiens M, Belikov SI, Kaluzhnaya OV, Adell T, Schröder HC, Perovic-Ottstadt S, Kaandorp JA, Müller WEG (2008) Regional and modular expression of morphogenetic factors in the demersal sponge *Lubomirskia baicalensis*. *Micron* 39:447–460
- Yamamuro T, Hench LL, Wilson J (eds) (1990) *Handbook on Bioactive Ceramics, vol I: Bioactive Glasses and Glass-Ceramics*. Boca Raton, FL: CRC Press
- Xia Y, Whitesides GM (1998) Soft lithography. *Angew Chem Int Ed* 37:550–575

Role of Biosilica in Materials Science: Lessons from Siliceous Biological Systems for Structural Composites

George Mayer

1	Background	278
2	Mechanical Testing of Fine Fibers	280
3	Materials	281
3.1	Melt-Processed Silica	281
3.2	Biogenic Silica	282
3.3	Silica Composite Spicules	282
4	Mechanical Behavior	283
4.1	Concepts of Toughness and Work-to-Failure	283
4.2	Energetic Considerations	286
4.3	The Role of Thin Adhesive Organic Phases in Enhancing the Mechanical Behavior of Siliceous Composites	287
4.4	Comparison of Mechanical Behavior of Melt-Drawn Silica Fibers with Biogenic Silica Spicule Fibers	288
4.5	Effects of Loading Rate on Mechanical Behavior	290
5	Considerations for New Synthetic Composites	292
	References	293

Abstract The unique mechanical response of spicules of Hexactinellid sponges, notably, *Euplectella aspergillum*, are reviewed and related to the structure, architecture, and failure modes of those natural rigid composite materials. In particular, exceptional levels of resilience, damping capacity, and the ability to dissipate mechanical energy prior to failure have been observed, all these properties greatly exceeding those of synthetic melt-fabricated glass. How these observations can be related to the design of new structural composites that are based on glass are described.

G. Mayer
Department of Materials Science and Engineering, University of Washington, Seattle,
WA 98195-2120, USA
e-mail: gmayer@u.washington.edu

1 Background

The occurrence and formation of biosilica in sponges has been discussed at length by Hartman (1981), Garrone et al. (1981), Perry and Keeling-Tucker (2000), Müller et al. (2003), Uriz et al. (2003), Uriz (2006), and others, in substantive detail.

Interest in the structure–mechanical property relationships in Hexactinellid sponges was kindled by a paper by Levi et al. (1989). In this brief and important paper, the authors reported on the existence of both remarkable resilience and toughness that was observed in a large spicule of *Monorhaphis chuni*, the failed surfaces of which are shown in the scanning electron microscopy (SEM) image in Fig. 1. This attractive combination of properties, in a material with such a large proportion of silica in its structure, has been of strong interest to the materials science community. In comparison, silica rods of like diameters (about 2 mm in thickness) typically show much lower resilience and low toughness, as shown in Fig. 2.

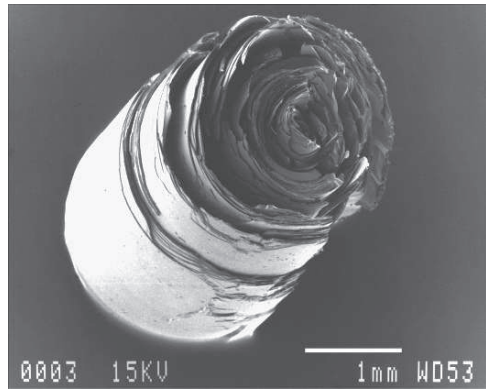


Fig. 1 SEM image of a broken spicule of a *Monorhaphis chuni* sponge (courtesy of P. Lehuede)

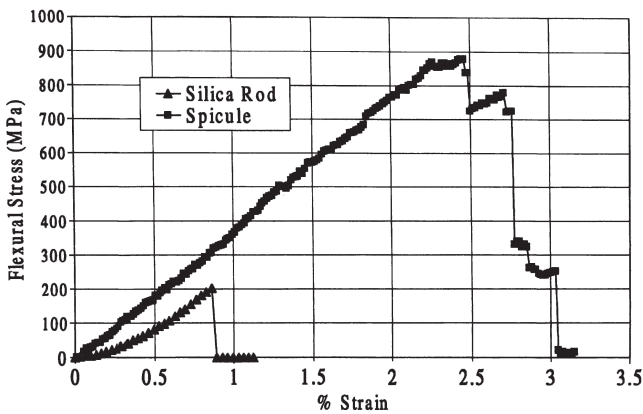


Fig. 2 Flexural stress versus strain of Hexactinellid sponge spicule compared to that of glass rod (Sarikaya et al. 2001)

The purpose of this Chapter is to summarize the mechanical behavior of the interesting and potentially important composite structure that is found in Hexactinellid sponges, with emphasis on studies of the skeletal spicules of the sponge *E. aspergillum* (Fig. 3). A schematic diagram of a smooth cylindrical filamentary spicule of this sponge, on the order of 30–70 μm diameter, is shown in Fig. 4. The major component, of the order of 97–98 vol%, is a hydrated silica, $\text{SiO}_2 \cdot n\text{H}_2\text{O}$, and the remainder is organic, mainly proteinaceous. In essence, it may be considered to be a glass/organic composite material. Such structures are present in all Hexactinellid sponges.

In sponges of classes Hexactinellida and Demospongiae, there is evidence of an axial organic ordered (crystalline) core that has been studied in several species of Demosponges and one Hexactinellid by Croce et al. (2004), and described as complex structures of various proteins, probably including a type of silicatein that stimulates the establishment of the sequential layered ring structure indicated in Fig. 4. The thin layers of organic constituent, of the order of 10–25 nm, are

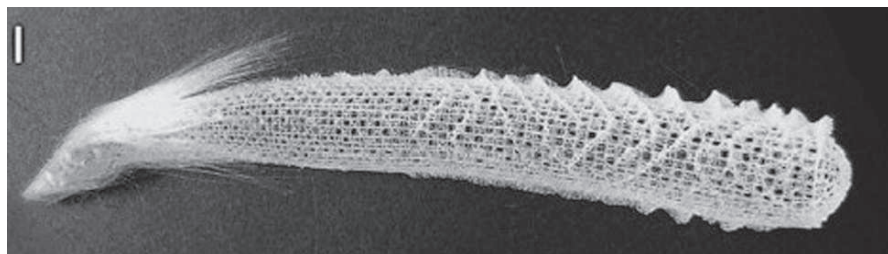
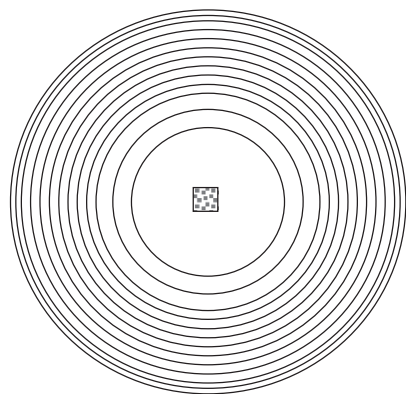


Fig. 3 Skeleton of *E. aspergillum*. Length can range from 6–32 cm with a diameter of 1.5–5 cm. Scale bar = 1 cm. Most of the smooth filaments seen toward the left side of this photo were taken from this area for testing. Going toward the basal end of the skeleton (left), the filaments become barbed or begin to branch (see Fig.9)



Cross-section of *E. aspergillum* spicule

- Spicule fibers ~30-70 μm in diameter
- Rings generally increase in thickness (~0.1-1 μm) from outer to inner cylinders
- Solid silica cylinder is 30-40% of diameter
- Axial cylinder with ~1 μm square core of protein & other organic constituents
- Number of rings varies
- Organic layers between silica cylinders ~10nm in thickness

Fig. 4 Schematic drawing of cross-section of spicule of *Euplectella aspergillum*. Note, drawing not to scale, and only a smooth section of the spicule is illustrated

interposed with concentric cylinders of varying thickness and varying numbers of hydrated amorphous silica. The thicknesses are of the order of 0.1–1 μm , and generally (but not always) increase in thickness from outside to inside, where they stop at a thick (of the order of 20 μm) cylindrical core that contains the axial filament. The inner section of solid hydrated silica in Hexactinellid sponges have been reported by Sarikaya et al. (2001), Aizenberg et al. (2004), Müller et al. (2006), and others, to exhibit optical transmission characteristics. It has been found that the concentric rings and cylindrical solid silica core, together with the major role of thin organic layers, also have a controlling influence on the mechanical behavior of the spicules of Hexactinellid sponges such as *E. aspergillum* (Mayer et al. 2005; Walter et al. 2007a,b).

The structural hierarchy of *Euplectella* sp. has been reported in an informative paper by Aizenberg and colleagues (2005). The authors described the intricate structure of the skeleton through seven levels from the nanoscale, where they reported on the observation of silica nanospheres that ranged from 50 nm to 200 nm in diameter, to the network of regular interconnected latticework on the macroscale level. Knowledge about the detailed mechanisms by which those spheres cohere and make up the siliceous portions of the spicules is presently incomplete, there being no clear concept about strength or porosity in the thin biogenic siliceous cylinders.

The mechanical behavior of the spicules of *E. aspergillum* has been extensively studied, compared with the mechanical behavior of synthetic silica fibers that were fabricated by conventional melting and drawing procedures and reported recently (Walter et al. 2007a, b). In the case of biosilica, organic precursors have always been involved in the formation of biogenic silica (Lowenstam and Weiner 1989). Mann (2001) notes “Organic frameworks play an important role in the mechanical design of biomineralized tissues such as bones, shells, and teeth. Many of the general functions of these biominerals – movement, protection, cutting, and grinding – are dependent on mechanical properties, such as strength and toughness, which are specifically associated with inorganic–organic composites.”

Thus, the mechanical properties of monolithic silica formed at high temperatures are very different from biogenic silica, which is really a composite comprising a very small volume fraction (albeit, well-distributed) of organic constituents, of the order of 2–3 vol%. Nonetheless, that small amount of organic component is often considered to be the matrix, and it controls the growth and form of systems such as the sponge spicule, as well as the hierarchical structure of the Hexactinellid siliceous sponge.

2 Mechanical Testing of Fine Fibers

Tensile tests were done utilizing procedures for mounting and testing fine brittle fibers that were developed at Oak Ridge National Laboratory, Oak Ridge, TN, per ASTM standard C1557-03, *Standard Test Method for Tensile Strength and Young's Modulus of Fibers*. This procedure required extreme care in handling and attaching fibers onto tabs, assuring fastening of both spicule and glass fibers to tabs

Fig. 5 A DMA fixture for testing in static or dynamic bending. The spicule specimen (not visible) sits across the channel in the solid aluminum base, and is loaded in bending by the triangular anvil above it



with strong adhesives. Even then, because of slippage, special procedures were necessary for measuring strain, employing a laser extensometer.

Subsequently, realizing that sponges experience bending and torsion in the ocean, a simplified, and faster, technique was employed for characterizing both spicule fibers and synthetic glass fibers in bending. This used a dynamic mechanical analysis (DMA) apparatus in the static mode; the unit is shown in Fig. 5. The spicule fibers were placed carefully just below the triangular loading anvil and across the narrow slot that was machined in the aluminum disc-shaped basal holder. This method allowed the use of either static or dynamic mode of loading, and loading rate could be controlled over 3 decades. Oscillatory loading was performed with the DMA apparatus over a range of frequencies to assess mechanical losses in the fibers due to viscoelastic processes.

3 Materials

3.1 *Melt-Processed Silica*

Glasses that are utilized in conventional applications are amorphous solids and comprise only inorganic materials. Fibers are produced by drawing from a melt through a die (for size control) without crystallization. It should be noted that the

mechanical properties of synthetic glass fibers vary greatly with diameter, and both strength and flexibility increase as the sizes decrease (Gordon 1976).

First, silica fibers of an electronic glass (EMGO360, with small contents of Ba_2O_3 and Na_2O in SiO_2) were specially fabricated at the National Institutes of Standards and Technology (NIST), Gaithersburg, MD, USA, in order to provide a baseline material to test for comparison with the spicule fibers. Such silica fibers are produced from a melt at high temperatures of the order of 1,400–1,600°C, and drawn through dies for diameter control. Typically, when a glass fiber is spun, a “sizing,” or thin polymeric coating is deposited on the freshly made fiber, and this prevents damage during subsequent handling. For the purposes of the comparative study, no sizing was used on the synthetic fiber surfaces, but they were carefully handled for transport after coating with a thin water-soluble coating at NIST. This coating was removed just before mechanical testing.

3.2 *Biogenic Silica*

A wide variety of organisms deposit silica (Lowenstam and Weiner 1989). The mechanisms of deposition, including the nucleation and growth of tiny spheres of amorphous hydrated silica in the sponge skeleton of *Euplectella*, has been discussed by several investigators (Aizenberg et al. 2005; Woesz et al. 2006). They have noted the sphere sizes as being 50–200 nm. The mechanical properties of biogenic silica (without an organic component) have not been realistically compared with those of synthetically melt-grown silica, although Woesz et al. (2006) have presented a nano-hardness study employing atomic force microscopy (AFM) on *M. chuni*. However, the measurements made therein represent the properties of the composite, since the organic layers that separate the cylinders of silica should be viscoelastic, and the nano-hardness of such a material would be difficult to interpret. A true test of the nano-hardness of biogenic silica would involve the removal of at least the organic phases, and perhaps also removal of the water of hydration. An illustration of how complicated such a removal process would be is shown in Fig. 6, which shows a collapsed spicule of a Hexactinellid sponge (*H. sieboldi*). The thin organic layers between the silica cylinders had been burned out. This may not be a fair test, however, since fracture by stresses due to differential thermal stresses may have been involved.

3.3 *Silica Composite Spicules*

The spicules of sponges that were examined in a series of studies (Mayer et al. 2005; Walter et al. 2007) came from at least five different skeletons of *E. aspergillum*, and were collected from deep water off the Phillipine Islands.¹ A schematic diagram of

¹Donated by Nature's Creations, of Sammamish, WA, USA.

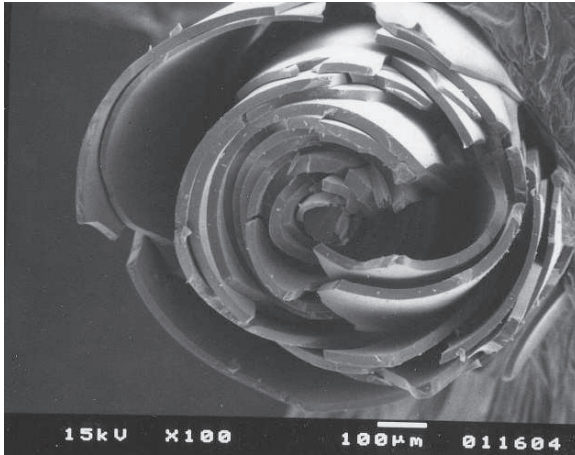


Fig. 6 SEM image of burnt Hexactinellid spicule fiber (*H. sieboldi*)

a typical spicule fiber was shown in Fig. 4. The structure consists of a series of concentric rings, numbering from 15 to 40, and there has been no correlation between the external fiber diameter and the number of rings. It was found (Aizenberg 2004) that the morphology of the spicules varied from the bottom of the skeleton to the top. Only smooth sections of fibers were subjected to the mechanical tests discussed in detail here. In the central core of each multi-layered spicule fiber (*H. sieboldi*), there is a square core, of diameter $\sim 1\ \mu\text{m}$. The square core signifies order, or crystallinity, and, it is assumed, transports to the thin (of the order of 10 nm) layers that separate cylinders of amorphous hydrated silica ($\text{SiO}_2 \cdot n\text{H}_2\text{O}$). It is known that the thin layers behave as adhesives. What is unknown at present is whether the minor organic matrix behaves as a scaffold, or may be a loosely interconnected framework that contains transport pathways through the hydrated silica rings from the central core to the outermost layers of the spicules.

4 Mechanical Behavior

4.1 Concepts of Toughness and Work-to-Failure

In conventional brittle materials, such as synthetic glass that is formed by high-temperature means, fracture strength can be found from a simple calculation using the Griffith equation:

$$\sigma = 2\gamma E / \pi c \quad (1)$$

where: σ is the fracture strength, γ is the surface energy, E is the Young's modulus, and c is the crack length.

This assumes that the energy of fracture is taken up by the creation in completely brittle fashion of (often) two new surfaces, without any other means to dissipate energy. If the stored energy levels are very high (because of diminution of crack size by chemical dissolution during testing), brittle solids have been observed to break at very high stress levels into many tiny fragments, probably by propagation of stress waves (Mayer 1963).

Recent work has discussed possible reasons for the attractive mechanical properties of the biogenic silica that is encountered in skeletons of Hexactinellid sponges, such as *E. aspergillum* and of the anchoring spicule of *M. chuni* (Woesz et al. 2006). In essence, it was argued that the critical crack length at the nanometer scale was very small (of the order of 30 nm), thereby resulting in high strengths, and that toughening was also aided by the structural configuration encountered at the micrometer level.

It is important here to discuss the toughness of natural composites that have a high volume fraction of what is normally considered a brittle phase (such as a glass or a ceramic), and that are coupled architecturally with layers of a very thin organic adhesive phase(s).

In the general case, fracture toughness is estimated to be the resistance to propagate an existing crack, and is estimated from the so-called R-curves (denoting resistance to crack propagation) of both brittle and ductile materials. However, such curves characterize materials during slow and stable crack propagation, where the crack growth is fairly linear. In the cases of both mollusks and sponges, crack growth is certainly not linear, nor is the concern about growth per se, but about crack tolerance. In fact, it has been concluded that, for rigid biological systems, i.e., siliceous sponges (Walter et al. 2007a), as well as for mollusks (Mayer 2006), fracture mechanisms aid in the dissipation of energy of systems undergoing mechanical loading. The processes that take part in this energy dissipation, or work-to-failure, include cracking and microcracking, delamination of the organic adhesive phase from the glass phase, crack arrest and diversion (see Fig. 7), crack bridging by fibrils of the organic adhesive, energy

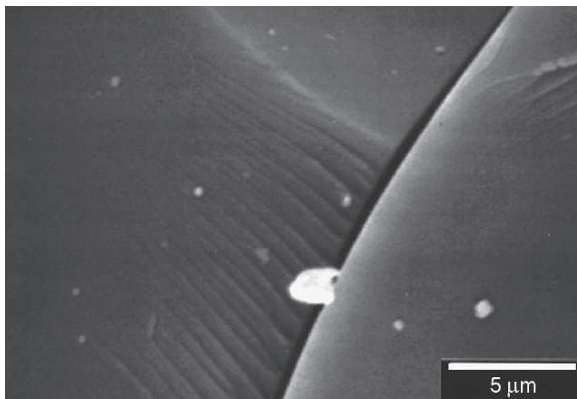


Fig. 7 Example of crack arrest at interface between two hydrated silica cylinders in spicule of a Hexactinellid sponge (Walter et al. 2007b)

dissipation by viscoelastic processes in the adhesive, and possible changes in the molecular configuration of the adhesive organic component.

Thus, the use of work-to-failure, or energy dissipation, to the point of final failure is a more reasonable concept than fracture toughness when considering siliceous biogenic composites. In such materials that are “fracture-tolerant,” fracture assists the toughening process.

In a prior work (Mayer et al. 2005), the mechanisms noted above have been described as occurring during the failure process in glass/organic natural composites such as sponge spicules. Two representative failures are shown in Figs. 8 and 9. These SEM images show that the failure mechanisms are quite complex. Figure 8 shows a failed smooth-sided spicule that represents the skeletal portion away from

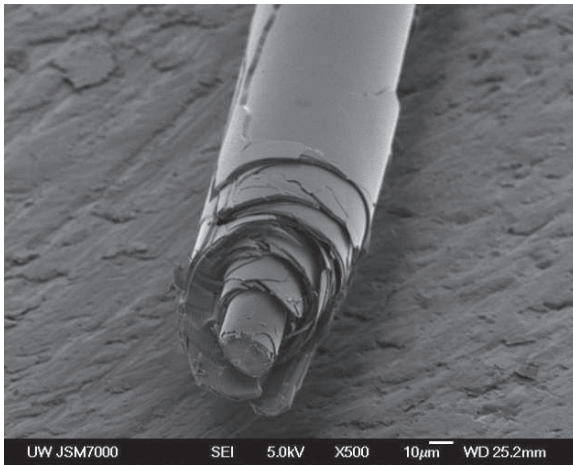


Fig. 8. SEM image of failure of spicule fiber in bending; tested in static mode using DMA apparatus

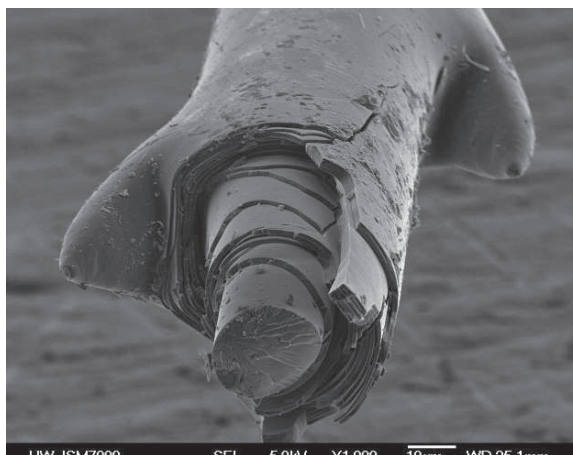


Fig. 9 SEM image of a branched spicule of *E. aspergillum* failed in bending (DMA test)

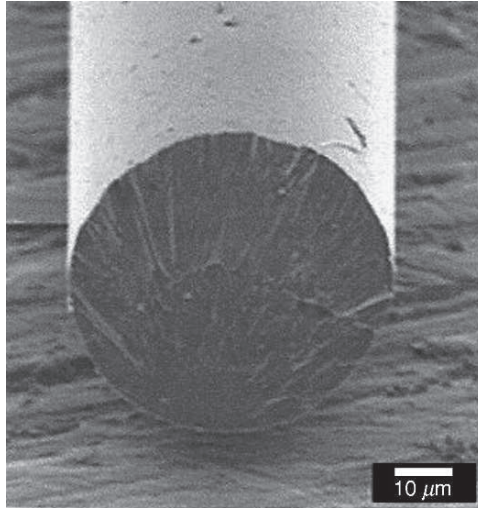


Fig. 10 SEM image of failure of synthetic glass fiber in bending; static test using DMA apparatus

the anchoring end, but before the woven skeletal tube begins. Figure 9 shows a failed lower spicule portion, and the branched or barbed segments assist in anchoring the spicule to the sediment of the ocean floor. In the latter image, evidence is seen on the branches of the central axial filament, and what appears to be a solid cylinder surrounding that filament. These, and other examples of failures in branched areas, are indications that the branches have quite similar structures to the main filaments, and show the characteristic axial core and cylinder at the tips of the branches. Failure of a synthetic glass filament is shown for reference in Fig. 10.

It should be noted that Gordon and colleagues (Cook et al. 1964) did quite pertinent work on the problem of toughening of brittle composites by crack diversion. What nature has done in the case of siliceous rigid composites has been to refine, even further, with more ways to absorb energy, what is known as the “Cook-Gordon” mechanism. In fact, the thin rings near the outer periphery of Hexactinellid spicules use the Griffith theory as part of the enhancement of work-to-failure. This is accomplished by sacrificing the thin outer layer to early fracture, proceeding through other micromechanisms of energy dissipation, and losing layers along the way to final separation of the spicule into two parts. Thus, there are controlled failures and other processes, such as molecular rearrangements and viscoelastic damping, that do not, in themselves, constitute instability along the path to complete separation of the spicule into two or more portions.

4.2 Energetic Considerations

The criticality of the small volume fraction of the organic phase in ceramic/organic or glass/organic composites that have structures such as the nacre structure of mollusks

or in the spicules of Hexactinellid sponges is likely related to how energy is partitioned among the various mechanisms that are involved in deformation and fracture during energy dissipation. The relationship:

$$dE_{T|_{t,\dot{\gamma}}} = dE_S + dE_{div} + dE_{del} + dE_{CB} + dE_{VF} + dE_{FR} + dE_Q + dE_{MR}, \quad (2)$$

where:

- $dE_{T|_{t,\dot{\gamma}}}$ = total energy dissipated at constant temperature and strain rate, and
- dE_S = surface energy created, including multiple microcracks
- dE_{div} = energy associated with crack divergence
- dE_{del} = energy associated with delamination
- dE_{CB} = energy associated with crack bridging
- dE_{VF} = energy associated with void formation
- dE_{FR} = work dissipated against frictional constraints
- dE_Q = work dissipated as heat
- dE_{MR} = energy dissipated via molecular rearrangements in the organic adhesive phase(s)

The foregoing shows the complexity of the failure processes in these composite materials where the primary phase is a ceramic or a glass, that are normally quite brittle in their monolithic forms. Thus, the toughness of such materials cannot be interpreted as resistance to crack propagation, or thought of in terms of fracture toughness. Rather, the area under the work-to-failure curve is a more reasonable measure of “toughness” in such materials. These arguments have been discussed by Mayer (2004) and Walter et al. (2007a).

4.3 The Role of Thin Adhesive Organic Phases in Enhancing the Mechanical Behavior of Siliceous Composites

Recently, the mechanics of the molecular rearrangements of proteins in natural materials have been studied by Qi et al. (2005), and serrated stress–strain curves have been shown to result from kinking and associated mechanisms during the deformation of some proteins. How such behavior would manifest itself during the constrained deformation of ceramic/organic or glass/organic composites, where the organic constituent is proteinaceous and appears as very thin (of the order of tens of nanometers) layers, sandwiched and constrained between much stiffer and thicker constraining materials, is an important matter for future work.

Our concern with extremely thin layers of organic constituents in structures such as siliceous sponge skeletons and the nacre structure of mollusks stems from a number of considerations. The first is that these small constituents, that may comprise only 1–3 vol% of a composite structure, have the unusual ability to dissipate mechanical energy without catastrophic failure, that is a key element of toughness in materials that have formerly been thought of as extremely brittle in their monolithic forms. The second point is the matter of thin layers of proteins as adhesives and their

superior structural performance in ceramic/organic or glass/organic composites. The study and characterization of the interfaces and anchoring of the adhesives to their inorganic substrates have been key facets of prior and on-going study. These thin layers provide both resilience and damping characteristics to the composite, and, if the mechanisms underlying that adhesion, resilience, and damping can be discovered, superior bio-inspired synthetic adhesives should be achievable.

4.4 Comparison of Mechanical Behavior of Melt-Drawn Silica Fibers with Biogenic Silica Spicule Fibers

The mechanical behavior of the structure of the biogenic composite silica fibers of *E. aspergillum* has been compared directly with those of synthetic fibers of silica that were drawn from the melt (Walter et al. 2007a). Under static loading, the work-to-failure for the spicule fibers greatly exceeded those of the synthetic silica fibers under various experimental conditions, in both tension and in bending, by a factor of nearly six. This has been attributed primarily to the influence of the thin organic layers between the concentric rings of hydrated silica in the spicule systems. Those thin organic rings have a multitude of functions. First, they can divert cracks that form and propagate in the cylindrical rings of silica (Fig. 4); second, they may dissipate energy through delamination; and, third, they have been shown to dissipate energy through damping. The great differences between the failures in bending of typical glass fibers and spicules can be seen in Figs. 8 and 10. Note the tortuous crack paths evident in the failure of the spicules, and the uncomplicated failure of the synthetic glass fiber.

Figure 11 shows the damping characteristics, expressed by the $\tan \delta$ versus frequency characteristics of spicules of the *E. aspergillum*, that were measured with the aid of a dynamic mechanical analyzer (DMA) apparatus (Walter et al. 2007a). Because most materials have elements of both elastic and viscoelastic behavior in their response to a dynamic oscillating load, there is a phase lag, δ , between the sinusoidal force imposed and the material response (Menard 1999). Briefly, E'' is defined as the energy loss associated with the internal loss response, and E' is the elastic response, and

$$\tan \delta \text{ (or tangent of } \delta) = E''/E' \quad (3)$$

Thus, $\tan \delta$ represents the damping of a fiber (glass or spicule), and is measured over a range of frequency. It is an indicator of how efficiently a material dissipates energy by molecular rearrangements and through internal friction.

A model of the deformation behavior of a spicule of *E. aspergillum* in tension has been suggested (Mayer et al. 2005). It is shown in Fig. 12. In this model, the concentric cylinders break at various places during tensile deformation, and extend in the form of the telescoping shaft of a telescope. However, the cylinders of hydrated glass are constrained by thin tenacious organic layers (not shown). After final separation of the spicule fiber, the cylindrical organic layers would relax elastically and viscoelastically.

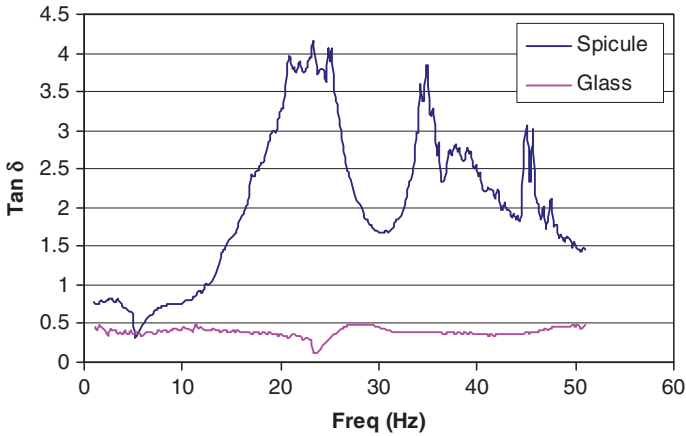


Fig. 11 DMA spectra of $\tan \delta$ plotted against frequency for spicules of *E. aspergillum* and for glass fibers of similar diameters (Walter et al. 2007b)

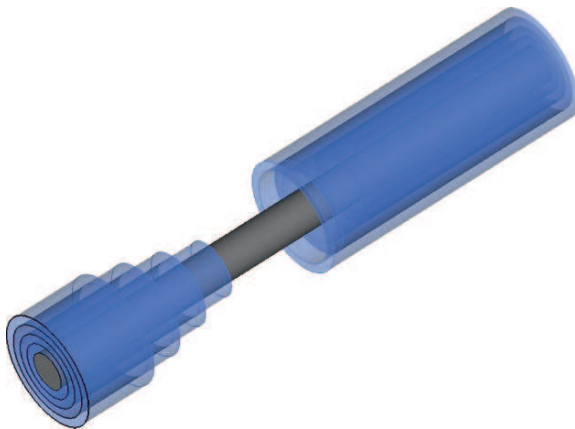


Fig. 12 Telescoping model for deformation of spicule of *E. aspergillum* in tension (Mayer et al. 2005)

Nonetheless, the foregoing comparison of biogenic silica and synthetic (melt-grown) silica fibers of similar size may be much more complicated than what has been discovered thus far. It must be recognized that what has been tested is a composite of organic/hydrated silica material in the case of the spicule of a larger Hexactinellid sponge (*H. sieboldi*) by exposure. Up to this point, it has not been possible to interrogate the mechanical properties of the hydrated silica alone, without the presence of the organic constituent, and it has been uncertain how the organic constituent can be entirely stripped from the siliceous component without creating damage. In an extreme case, the dried protein was burned out from an end of a large-diameter of the spicule of a Hexactinellid sponge (*H. sieboldi*) larger by exposure to an open flame. The resultant structure was seen to have collapsed, probably due to the thermal stresses, together with the elimination of the organic constituent (Fig. 6).

4.5 Effects of Loading Rate on Mechanical Behavior

The influence of loading rate variations done with the DMA apparatus over 3 decades of loading, ranges from 1 through 100 mN/min. The results are shown in Fig. 13 for the glass and Fig. 14 for the spicule specimens. The glass fibers showed little variation of stress versus strain over the 3 decades of loading. Since the areas of the glass fibers did not change, the stress–strain relations can be either engineering stress–strain, or true stress–strain. However, in the case of the spicules, the cross-section decreased during the bending tests, and thus, true stress–strain estimates had

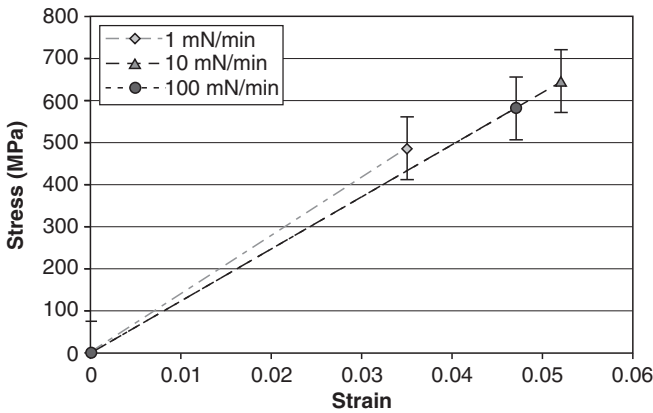


Fig. 13 Loading rate effects on glass fiber stiffness and fracture strength. Results of five tests at each rate noted (Walter et al. 2007b)

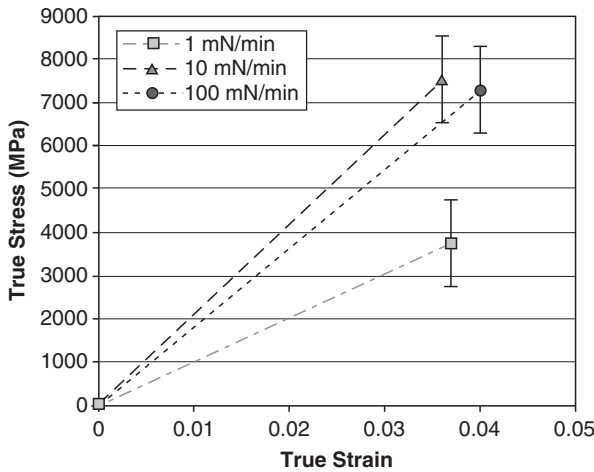


Fig. 14 Loading rate effects on mechanical response of spicule fibers in bending. Results of five tests at each rate are shown (Walter et al. 2007b)

to be made from the final areas that supported the load before catastrophic failure. The appearances of the failures are shown in the SEMs indicated as Fig. 15. The glass failures, from low to high loading rates, showed increasing elements of shear, while, for the spicules, the reverse appears to be true. These behaviors are probably related to the energetic considerations expressed in bending, and Eq. 2, above, for the spicule. For the glass, the increased ductility in evidence at higher loading rates was somewhat surprising, although no other published data could be found for

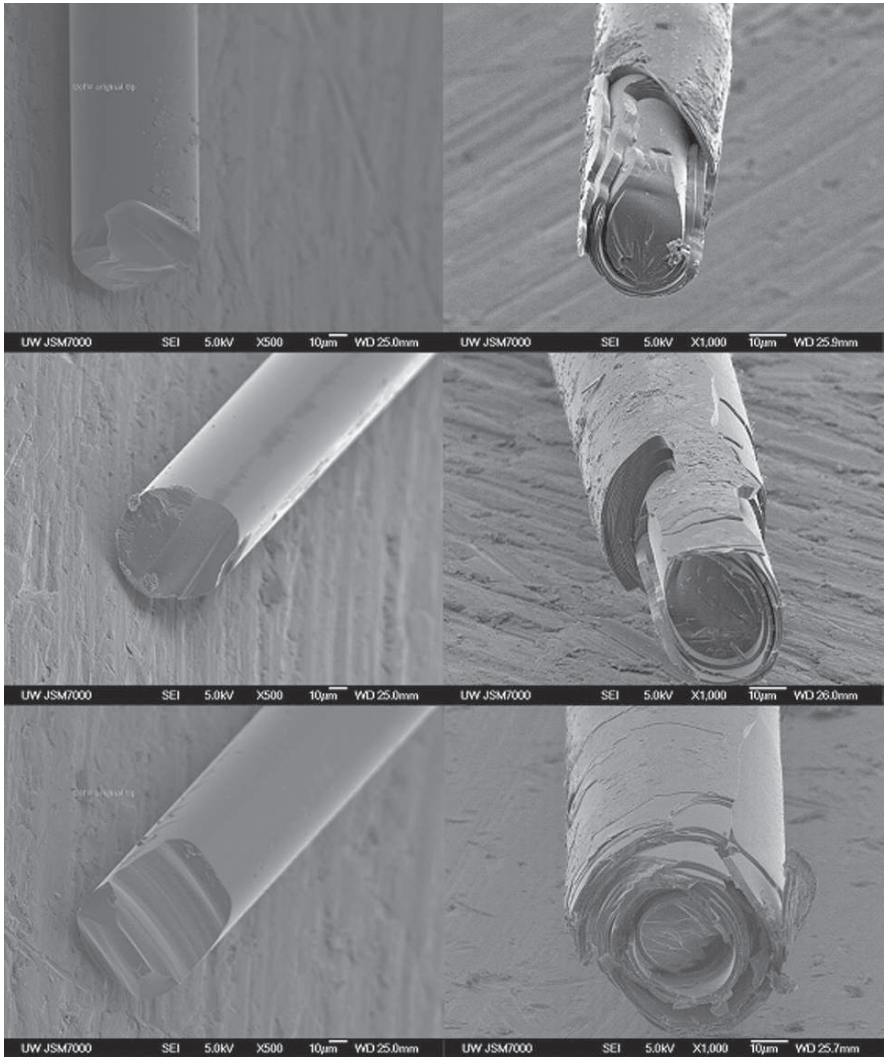


Fig. 15 SEM images of failure surfaces of glass fibers (*left*) and spicule fibers (*right*) (Walter et al. 2007b). Loading rates increase from 1mN/min to 10mN/min to 100mN/min, top to bottom, as indicated in Figs. 13 and 14

loading rate effects on glass. The ductilities and strengths of the glass fibers seemed to increase at the higher rates, although the stiffnesses remained approximately the same. Thus, the work-to-failure was seen to increase with increasing loading rate. For the spicules, true stress–true strain curves were plotted. The stiffness was seen to increase, and then decreased slightly, as loading rate increased. The stresses at failure were seen to increase substantially at the higher rates of loading for the spicules. A higher loading rate than 100 mN/min (150–200 mN/min – at the limit of the DMA apparatus) showed that the decrease in the stress at failure was real. The root cause of this effect has been suggested as related to adiabatic softening in the thin organic layers (Walter et al. 2007b). If adiabatic shear does, in fact, occur at higher loading rates in the spicules, there would be little or no transfer of the shear stresses during bending in the cross-section, and this may explain the differences in the appearances of failure between the low and high loading rates.

5 Considerations for New Synthetic Composites

We have learned a number of important lessons from the studies that have been performed on the natural rigid silica/organic composites with very large proportions of silica (as contained in Hexactinellid sponges such as *E. aspergillum*), architectures that include a concentric layered configuration, with alternating hydrated silica and thin organic constituent(s), and important combinations of mechanical contributions of the latter. First, it is necessary to recognize that fracture toughness, or resistance to crack propagation, should not be used for assessing the toughness of such brittle-matrix composites, because non-linear fracture processes and other complex effects of deformation play such important parts in energy dissipation. Second, very thin layers of organic materials, on the order of tens of nanometers, are effective in stopping and diverting cracks; they probably bridge cracks, and hinder them from opening, dissipate energy by delamination, yet remain tenaciously adherent to their silica substrates. Furthermore, the organic layers damp out mechanical vibration by viscoelastic means, affording yet another way to dissipate energy. These are practical lessons that would be of benefit when designing and building synthetic structures of brittle-matrix composites. Thinness and tenacity of adhesives to their normally brittle substrates, and both resilience and damping characteristics of those adhesives would also be desirable and necessary. As for the glass employed, it should have sufficient strength yet provide for a variety of crack modes and paths. At the present time, not a great deal of attention has been devoted to the fine structure of the biomineralized glass, the description of the interfaces with the organic constituents, and their relationship to the mechanical behavior of these interesting composites. The development of adhesives that are tenacious with glass substrates, the preparation of the glass surfaces, and the tailoring of interface conditions are key to the design of composites that have high volume fractions of silica. Promotion of the various micromechanisms that delay final failure in natural glass/organic composites are the key steps that will lead to the development of synthetic glass/adhesive composites with superior mechanical properties.

Acknowledgments The author wishes to thank Sara Walter, Brian Flinn, Bob Smith, Tom Murray, and Maria Rodriguez for their extensive efforts at the University of Washington in a large part of the work reported here. In addition, the perception and assistance of Dr. Edgar Lara-Curzio of Oak Ridge National Laboratory is gratefully acknowledged. Finally, this work could not have been done without the continuing support, encouragement, and assistance of his wife, Jane Mayer.

References

- Aizenberg J, Sundar VC, Yablon AD, Weaver JC, Chen G (2004) Biological glass fibers: correlation between optical and structural properties. *Proc. Natl. Acad. Sci. USA* 101:3358–3363
- Aizenberg J, Weaver JC, Thanawala MS, Sundar VC, Morse DE, Fratzl P (2005) Skeleton of *Euplectella* sp.: structural hierarchy from the nanoscale to the macroscale. *Science*, 309:275–278
- Cook, J, Gordon JE, Evans CC, Marsh DM (1964) A Mechanism for the control of crack propagation in all-brittle systems. *Proc. Roy. Soc. Lond. A* 282:508–520
- Croce G, Frache A, Milanesio M, Marchese L, Causa M, Viterbo D, Barbaglia A, Bolis V, Bavestrello G, Cerrano C, Benatti U, Pozzolini M, Giovine M, Amenitsch H (2004) Structural characterization of siliceous spicules from marine sponges. *Biophys. J* 86:526–534
- Garrone R, Simpson TL, Pottu-Boumendil J (1981) Ultrastructure and Deposition of Silica in Sponges. In: Simpson TL, Volcani BE (eds) *Silicon and Siliceous Structures in Biological Systems*. Springer-Verlag, New York, pp 495–525
- Gordon, JE, *The New Science of Strong Materials*, Penguin Books, Harmondsworth, UK, 1976, p. 75
- Hartman WD (1981) Form and Distribution of Silica in Sponges. In: Simpson TL, Volcani BE (eds) *Silicon and Siliceous Structures in Biological Systems*, Springer-Verlag, New York, pp 454–493
- Levi C, Barton JL, Guillemet C, LeBras E, Lehuède P (1989) A remarkably strong natural glassy rod: the anchoring spicule of the *Monorhaphis* sponge. *J. Mater. Sci. Lett.* 8:337–339
- Lownstam HA, Weiner S (1989) *On Biomineralization*, Oxford University Press, Oxford, pp 7–15
- Mann S (2001) *Biomineralization: Principles and Concepts in Bioinorganic Materials Chemistry*. Oxford University Press, Oxford, p 91
- Mayer G (1963) unpublished report: the fracture of brittle solids under bending stresses in reactive solutions and in ultrahigh vacuum. Iikon Corp., Natick, MA
- Mayer G (2004) Toughening of ceramic materials. *Cer. Bull.* 83:9301–9307
- Mayer G, Trejo R, Lara-Curzio E, Rodriguez M, Song H, Ma WH (2005) Lessons for new classes of inorganic/organic composites from the spicules and skeleton of the sea sponge *Euplectella aspergillum*, in *Mechanical Properties of Bioinspired and Biological Materials*, Warrendale, PA, MRS Symp. Proc. 844:79–86
- Mayer G (2006) New classes of tough composite materials—Lessons from natural rigid biological systems. *Mater. Sci. Eng.-C* 26:1261–1268
- Menard KP (1999) *Dynamic Mechanical Analysis*, CRC Press, Boca Raton, FL, pp 61–65
- Müller WEG, Krasko A, Le Penec G, Schroeder HC (2003) Biochemistry and cell biology of silica formation in sponges. *Micros. Res. Tech.* 62:368–377
- Müller WEG, Wendt K, Geppert C, Wiens M, Reiber A, Schroeder HC (2006) Novel photoreception system in sponges? Unique transmission properties of the stalk spicules from the hexactinellid *Hyalonema sieboldi*. *Biosens. Bioelec.* 21:1149–1155
- Perry CC, Keeling-Tucker T (2000) Biosilicification: the role of the organic matrix in structure control. *J. Biol. Inorg. Chem.* 5:537–550
- Qi HJ, Ortiz C, Boyce MC (2005) Protein forced unfolding and its effects on the finite deformation stress–strain behavior of biomacromolecular solids. *Mater. Res. Soc. Symp. Proc.* 874:L4.3.1

- Sarikaya M, Fong H, Sunderland N, Flinn BD, Mayer G (2001) Biomimetic model of a sponge-spicular optical fiber-mechanical properties and structure. *J. Mater. Res.* 16:1420–1428
- Uriz M-J, Turon X, Becerro MA, Agell G (2003) Siliceous spicules and skeleton frameworks in sponges: origin, diversity, ultrastructural patterns, and biological functions. *Micros. Res. Tech.* 62:279–299
- Uriz M-J (2006) Mineral skeletogenesis in sponges. *Can. J. Zool.* 84:322–356
- Walter SL, Flinn BD, Mayer G (2007a) Mechanisms of toughening of a natural rigid composite. *Mater. Sci. Eng.-C* (in press)
- Walter SL, Flinn BD, Mayer G (2007b) Effects of loading rate on the mechanical behavior of a natural rigid composite. *Acta Biomat.* (in press)
- Woesz A, Weaver JC, Kazanci M, Dauphin Y, Aizenberg J, Morse DE, Fratzl P (2006) Micromechanical properties of biological silica in skeletons of deep-sea sponges. *J. Mater. Res.* 21:2068–2078

An Overview of Silica in Biology: Its Chemistry and Recent Technological Advances

Carole C. Perry

1	Silica Structure: Molecules, Materials and Methods of Analysis	296
2	Silicification in Sponges	298
3	Silicification in Diatoms	300
4	Silicification in Plants	301
5	Role of Silica in Stress Relief	302
6	Laboratory Studies of Silica Condensation, Polymerisation and Materials Formation. . .	303
7	The Effect of Biologically Relevant Solution Additives on Condensation, Polymerisation and Materials Formation.	304
8	Applications Using the Biomolecules as Identified from Diatoms, Sponges and Higher Plants	305
9	Technological and Model Advances Utilising Diatoms	306
	References	309

Abstract Biomineralisation is widespread in the biological world and occurs in bacteria, single-celled protists, plants, invertebrates and vertebrates. Minerals formed in the biological environment often show unusual physical properties (e.g. strength, degree of hydration) and often have structures that exhibit order on many length scales. Biosilica, found in single cell organisms through to higher plants and primitive animals (sponges), is formed from an environment that is undersaturated with respect to silicon and under conditions of around neutral pH and low temperature, ca. 4–40°C. Formation of the mineral may occur intra- or extra-cellularly, and specific biochemical locations for mineral deposition that include lipids, proteins and carbohydrates are known. In most cases, the formation of the mineral phase is linked to cellular processes, understanding of which could lead to the design of new materials for biomedical, optical and other applications. This Chapter briefly describes the occurrence of silica in biology including known roles for the mineral

C.C. Perry
School of Science and Technology, Nottingham Trent University, Clifton Lane, Nottingham
NG11 8NS
e-mail: carole.perry@ntu.ac.uk

phase, the chemistry of the material, the associated biomolecules and some recent applications of this knowledge in materials chemistry.

The terminology which is used in this and other contributions within this volume is as follows:

Si: the chemical symbol for the element and the generic term used when the nature of the specific silicon compound is not known.

Si(OH)₄: orthosilicic acid, the fundamental building block used in the formation of silicas.

SiO₂·nH₂O or SiO_{2-x}(OH)_{2x}·2H₂O: amorphous, hydrated, polymerised material.

Oligomerisation: the formation of dimers and small oligomers from orthosilicic acid by removal of water. For example, $2\text{Si(OH)}_4 \leftrightarrow (\text{HO})_3\text{Si-O-Si(OH)}_3 + \text{H}_2\text{O}$

Polymerisation: the mutual condensation of silicic acid to give molecularly coherent units of increasing size.

Organosilicon compound: must contain silicon covalently bonded to carbon within a distinct chemical species

Silane: a compound having silicon atom(s) and organic chemical groups often connected through an oxygen linkage; e.g. tetrethoxy or tetramethoxysilane

Silanol: hydroxyl group bonded to silicon atom

Silicate: a chemically specific ion having negative charge (e.g. SiO₃²⁻), term also used to describe salts (e.g. sodium silicate Na₂SiO₃)

Opal: the term used to describe the gem-stone and often used to describe the type of amorphous silica produced by biological organisms. The two are similar in structure at the molecular level (disordered or amorphous), but at higher levels of structural organisation are distinct from one another.

1 Silica Structure: Molecules, Materials and Methods of Analysis

Plants and primitive organisms, such as diatoms, choanoflagellates, radiolaria through to primitive animals such as sponges and molluscs such as limpets, are capable of accumulating, storing and processing 'silicon' to create ornate hierarchical patterned biosilicas. The production of silica by biological organisms is carried out in an aqueous environment from under-saturated solutions of silicic acid, at atmospheric pressure and with temperatures ranging between 4°C and 40°C, and this production, amounting to gigatons per annum, vastly outweighs that produced industrially. The methods by which this can be achieved in organisms have been the subject of immense study and debate; however, it is apparent that the organic environment, including a vast range of proteins, carbohydrates, lipids,

metal ions and, in plants, phenolic compounds, is likely to play a fundamental role (Perry 2003).

The simplest form of silica, the monomer orthosilicic acid, is a weakly acidic molecule (pK_a 9.8) with silicon tetrahedrally coordinated to four hydroxyl groups (Iler 1979). This monomeric unit is found universally (seawater, freshwater, soil water) at low concentrations (a few parts per million; ppm). It is most likely that it is in this form that all organisms are able to take silica into their bodies although it is known that, at least for exemplars of the three main classes (the most well studied) of silicified organisms (diatoms, sponges and higher plants), silicic acid transporters are available to at least transport silicic acid into the organism (Hildebrand et al. 1997, 1998; Schröder et al. 2004; Ma et al. 2006). Beyond this, the exact transport mechanism for all these classes of organism through to the final place of deposition is largely unknown.

In all organisms, where the concentration of silicic acid is in excess of 100–200 ppm, auto polycondensation reactions occur that lead to the formation of stable nuclei with critical size, growth of nuclei to form spherical particles and aggregation of particles to form branched chains or structural motifs (Perry and Keeling-Tucker 2000). An interesting feature of silicic acids is that although the pK_a of the silanol groups in the monomer is mildly basic, the pK_a of silanol groups on the outside of oligomers ca. 1 nm in size is 6.8. This means that, as the silica particles grow and approach a couple of nanometres in size (as found in nature), they will carry a surface negative charge, and it is these particles what will be interacting with the cell wall or the environment in which they are found. Many factors affect the process of silica condensation from the molecular level upwards, including concentration, temperature, pH and the presence of other ions, small molecules and polymers (Iler 1979), but in all cases the materials that form are built up from SiO_4 tetrahedra with variable Si–O–Si bond angles and Si–O bond distances that are amorphous at the 1 nm length scale (Mann and Perry 1986). The materials contain hydroxyl groups and, according to the reaction environment in which the mineral forms, silica from different organisms/precipitation conditions can vary greatly with regard to density, hardness, solubility, viscosity and composition (Perry and Keeling-Tucker 2000). This can also be true for silica formed within a single cell of an organism with evidence for this being observed in diatoms (Wetherbee et al. 2000) and plant hairs (Perry et al. 1990).

The mineralised structures are built up from nanosized particles intermixed with organic material. The structure that the composite adopts arises from a complex interplay between inorganic chemistry (silica formation) and cellular biology (biomolecule structure and location of both phases), analysis of which should yield information on the pathway/mechanism by which the mineral has formed. Although the mineral phase that forms is amorphous, there are now a wide range of techniques that are being used to probe the structure of these complex materials (Perry 2003). The techniques that provide information on the nanoscopic through to the microscopic length scales include the following: electron microscopy (scanning and transmission modes) which is used to identify the sizes of fundamental particles and their interconnection to one another and, in conjunction with energy

dispersive X-ray analysis (EDXa), can be used to locate the mineral within an organism as well as locate co-localised inorganic species and additionally, the extent of hydration of a particular mineral form can be explored by use of reactive heavy metal compounds that react with hydroxyl groups (Perry et al. 1990); small angle, ultra small angle and wide angle X-ray diffraction (SAXS, USAXS and WAXS) that can detect order at the nm level; none of these techniques has identified any crystallinity within biosilicas but USAXS has been used successfully to identify structures on different length scales including pore structures (Vrieling et al. 2002). Atomic force microscopy (AFM) with a range of viewing modes can be used to great effect to measure particle sizes in three dimensions, including height (Wetherbee et al. 2000).

Another technique which gives information on bulk samples is nitrogen (or other gas) adsorption analysis and this can be used to provide evidence on porosity, including the distribution of pore sizes. There are also a wide range of spectroscopic techniques that provide information at the molecular level and these include ^{29}Si nuclear magnetic resonance (NMR) spectroscopy, Fourier transform infrared (FTIR) spectroscopy and Raman spectroscopy. NMR spectroscopy (solution and solid state) provides information on the immediate local environment around the chosen nucleus and by judicious use of single pulse and multiple pulse methods can give information on speciation (including level of hydroxylation) and the extent of interaction between the inorganic phase and any organic material present. Silicon-29 only occurs at 4.67% natural abundance which means that, in order to obtain information on direct connections between the inorganic and organic phase, isotopically enriched Si sources must be used. At present, the costs of preparing enriched samples are prohibitive and very few experiments have been performed. It is to be hoped that if costs reduce then more experiments will be performed to provide information on the extent of and molecular nature of any interactions occurring between the mineral phase and associated biomolecules within the composite material as it forms. Infrared spectroscopy and Raman spectroscopy are both molecular spectroscopies that probe vibrational motion and can be used to provide information on the internal structure of siliceous phases as well as on the composition and conformation of components of the organic phase. The use of these instruments in 'mapping' modes can be used to identify any co-localisation of the mineral with specific molecule types (protein, carbohydrate, etc.) that can be of great use in planning further biochemical investigations.

2 Silicification in Sponges

Sponges are one class of organisms known to make structural objects out of silica and for which much is known concerning the mineral phase, associated biomolecules and the biology of mineralisation. Of the three classes of sponges, two produce silicified spicules as their body support (Hexactinellida and

Demospongiae) with the silica being deposited around an axial filament largely made up of protein, although most recent studies have indicated that there is organic material intimately associated with the silica throughout the width of the spicule (Pisera 2003). Spicules are synthesised by special cells, the sclerocytes, with synthesis occurring in a membrane (silicalemma)-bounded compartment (Simpson 1984). The spicules range in size over several length scales with the largest measuring ca. 8 mm in diameter by 3 m in length (Levi et al. 1989) and the smallest having dimensions on the micron scale. Furthermore, although some sponge species only generate one spicule type, others are known to produce many different spicule forms, with the diversity thought to be affected by the amount of silicon available to the organism (Maldonado et al. 1999). The smallest silica particles that have been measured by electron microscopy are of the order of 2–3 nm in size with little space between the particles. These particles are then arranged into larger scale structures admixed with the biomolecules that include silicatein, silicase, galectin, sponge collagen and other proteins. Papers by Morse and coworkers and Muller and coworkers provide great detail on the structure and function of the principal protein, silicatein, a relatively small protein of molecular weight ca. 23 kDa involved in silica formation. The axial filament contains silicatein molecules organised into a filamentous form. Silicatein is enzymatically active (Shimizu et al. 1998; Cha et al. 1999) and able to catalyse the formation of silica from alkoxysilanes. Silicatein is a hydrolytic enzyme that has some structural analogies with cathepsin for which crystal structures are known. The catalytic centre contains three amino acids, serine, histidine and asparagine, all required for activity (Shimizu et al. 1998; Zhou et al. 1999) as well as a cluster of hydroxyl containing amino acids and hydrophobic patches on the surface that are probably used in the self-assembly of the protein molecules to form the axial filament. It is reported that, at least for *Suberites domuncula*, only the phosphorylated form of silicatein is able to oligomerise to form silicatein dimers and trimers (Müller et al. 2005). Silicatein has also been detected in the extracellular space during spicule formation as a pro-enzyme of molecular weight ca. 36.3 kDa (Muller et al. 2005) which is inactive until cleavage of a signal peptide and a propeptide occurs. Application of molecular biology techniques to the production of recombinant silicatein have used both *Escherichia coli* and the bacterial expression vector pQE-30 with some success and His-tag labelled and non His-tag labelled recombinant silicatein has been produced for biotechnological applications, see later in this Chapter for an overview (including appropriate references) and elsewhere in the book for other chapters containing more detailed information.

Other proteins identified from silicified spicules, at least from *S. domuncula* include silicase (ca. 43.1 kDa) (Schröder et al. 2003), an enzyme that has been proposed to depolymerise amorphous silica, a selenoprotein (ca. 14 kDa), a silicatein-associated protein (26 kDa), a galectin (Schröder et al. 2006) and collagen (Schröder et al. 2000). In addition to this, a putative silicic acid transporter has been isolated (Schröder et al. 2004) with high sequence similarity to the $\text{Na}^+/\text{HCO}_3^-$ cotransporter.

3 Silicification in Diatoms

More than 100,000 species of single-celled algae (diatoms) are currently known. They occur in both freshwater and in seawater and different species contain different amounts of amorphous silica in their cell walls that are known as frustules. The frustule has two halves with the upper half being known as the epitheca and the lower half as the hypotheca. Both halves of the frustule are known as valves and the structures that overlap the two valves are known as the girdle bands. The valve structures are composed of a range of organic molecules and silica and can be porous with each diatom species having a very specific pattern of mineral/pore structures. Reproduction involves division of the cell and the formation of new mineralised valves within a membrane-bounded compartment known as the silica deposition vesicle (SDV). The mineral structures are formed from ca. 5 nm amorphous particles that initially appear to form small aggregates ca. 40 nm in diameter that are then packed in specific patterns within the developing structure. Electron microscopy studies of the early stages of valve development and studies by others (Wetherbee et al. 2000) using mild etching methods in conjunction with AFM analysis have shown that the packing density of the silica particles varies between different parts of the mineralised structure. All these observations indicate that the silica formation process is regulated. Early experimental studies on cultures of diatoms found that silica formation occurred when cells were also synthesising proteins (Coombs and Volcani 1968). Biochemical analysis of cell wall isolates identified unusual amino acids including a dihydroxyproline and a trimethylated lysine derivative as well as its phosphorylated analogue (Nakajima and Volcani 1969, 1970). This information combined with the fact that chemical inhibition of protein synthesis during valve development produced structural irregularities (Blank and Sullivan 1983) all pointed to the fact that protein synthesis is an essential part of the silicified valve formation process. More recently, a variety of biomolecules have been found specifically associated with the mineral phase of the diatom *Cylindrotheca fusiformis* that include silaffins and polyamines. These families of molecules are all of low molecular weight, ca. 4–17 kDa for the silaffins and 0.6–1.25 kDa for the polyamines (Kröger et al. 2000). The silaffin that has been most studied is Sil-1 which contains a series of repeating units containing high levels of posttranslationally-modified lysine and serine. The serine units are modified by phosphorylation (Kröger et al. 2002) and the lysine units by dimethylation, by methylation and hydroxylation or by the incorporation of an oligomeric structure built up from *N*-propylamine units showing various levels of methylation (Kröger et al. 1999, 2001). The peptide sequence derived from the *sillp* gene is known as R5 and has been used in model studies of silica formation as well as in nanobiotechnological applications. The further class of molecules identified in a range of diatoms are low molecular weight (by comparison with proteins) linear polyamines composed of *N*-methylaminopropyl or aminopropyl units (Kröger et al. 2000), although a wider range of functionality has been identified and now includes tertiary ammonium groups (Sumper et al. 2005).

Molecular biology approaches to the understanding of silica formation in diatoms have identified silicic acid transporters (Hildebrand et al. 1997, 1998) which are coupled with the transport of sodium but beyond this little is known concerning transport within the diatom itself.

Silica deposition in diatoms occurs within the silica deposition vesicle which itself is surrounded by a membrane, the silicalemma. A very elegant study by Hildebrand and co workers (Frigeri et al. 2006) has probed the synthesis of membrane-associated proteins, and through the use of synchronised cultures and the measurement of mRNA levels they were able to identify many (>10) proteins that correlated with mRNA levels of silaffin synthesis (taken as a marker for cell wall formation) during cell growth. One specific enzyme, glutamate acetyltransferase, was identified. Application of a specific enzymic inhibitor for ornithine decarboxylase resulted in dramatic changes to the silica structures produced, providing evidence for the direct involvement of this enzyme in the formation of the silica frustule. Although biomolecules are clearly involved in the formation of the patterned silica deposits it should be remembered that the shape of the SDV is also governed by microtubules derived from actin and that microfilaments are also involved (Chiappino and Volcani 1977; Van der Meene and Pickett-Heaps 2002). Their role in the growth of the SDV, the manipulation of its shape and their relationship to the biomolecules such as the silaffins and polyamines remains to be determined.

4 Silicification in Plants

Silica deposition occurs in many plant families though the highest levels are found in the primitive plants such as the Equisetaceae and the Gramineae (>4% Si), Cucurbitales, Urticales and Commelinaceae show intermediate Si accumulation (2–4% Si), while most other species demonstrate little accumulation (Epstein 1994). Plants deprived of silicon are often weaker structurally and more prone to abnormalities of growth, development and reproduction (Epstein 1999). Silica can occur in cell walls, cell lumens, intracellular spaces, roots leaves and other spaces, and different parts of the same plant can show large differences in Si accumulation; a good example is the variation between 0.5 g/kg in polished rice through 50 g/kg in rice bran, 130 g/kg in rice straw, 230 g/kg in rice hulls to 350 g/kg in rice joints (found at the base of the grain) (Van Hoest 2006). There have been few detailed studies of Si-uptake, but for rice, the uptake of silicon from solution is the result of the operation of two different transport mechanisms. In the lateral roots, a low affinity transporter (*Lsi1*) is responsible for the uptake of silicic acid from the external solution to the root cortical cells (Ma and Yamaji 2006). The second transporter is responsible for xylem loading of Si (Mitani and Ma 2005). Studies of cucumber (moderate accumulator) and tomato (low level accumulator) have shown much lower levels of *Lsi1* with further transport of any silicic acid into the xylem being by passive diffusion.

The silica structures formed and their localisation show great variation between individual plant families. Even within single hair cells more than one type of silica

can be identified. For example, in detailed studies of plant hairs on the lemma of the grass *Phalaris canariensis* L., three distinct types of silica have been identified (sheet-like, fibrillar and globular) that differ in terms of their fundamental particle size, aggregation characteristics, extent of hydration and location within the plant hair (Perry et al. 1984). Similar structures and others have also been observed in other plant species such as members of the Equisetaceae family and in nettle hairs (Perry and Fraser 1991). In many other plants, notably those that produce food crops, silica infills certain cells such as silica cells, dumb-bell-shaped cells located on vascular bundles, and silica bodies found for example on bulliform cells of rice leaves. These gross silica structures (known as phytoliths) when found at archaeological sites have proved useful in identifying the plant species used by a population at a given time. Progress in the understanding of plant silicification is not as far advanced as for sponges and diatoms, but studies in the early 1990s identified that plant silicas contained protein and carbohydrate-containing biomolecules intimately associated with the mineral phase (Harrison 1996). The cell wall is the site of deposition for most plant silica deposits and is a highly complex matrix that contains cellulose, more complex polysaccharides such as hemicelluloses and pectins rich in galacturonic acid residues that are cross linked by the coordination of Ca ions, proteins and phenolic compounds including lignin. This biochemical environment may be capable of modifying the solubility and binding possibilities of the silica phase as it develops (Perry and Keeling-Tucker 1998, 2003). Much experimental work is still required to increase our understanding of the relationship between the silica deposits and the biochemical environment in which they are found.

5 Role of Silica in Stress Relief

In all three main classes of silicifying organisms, the silica structures so formed perform a structural role (Currie and Perry 2007). Beyond this, however, studies on plants containing 'silicon' have shown that the presence of the element in some form has been found to alleviate many abiotic and biotic stresses. As a consequence of this, silicates are incorporated into many fertilisers. It is not known how the presence of silicon exerts such a protective effect although roles including provision of a physical and/or biochemical defence system have been proposed. The deposition of silica as a physical barrier to penetration and reduction in the susceptibility to enzymatic degradation by fungal pathogens has been explored (Yoshida et al. 1962; Cherif et al. 1992). An alternative hypothesis is that silicon is a biologically active element capable of triggering a broad range of natural defences. This was first demonstrated in cucumbers whereby silicon-treated plants demonstrated enhanced activity of a range of enzymes such as chitinases, peroxidases and polyphenoloxylases as well as flavenoid phytoalexins to protect against fungal pathogens (Cherif et al. 1994; Fawe et al. 1998). Similar biologically active defence agents (increased production of glycosylated phenolics and antimicrobial products such as flavonoid phytoalexins) have been induced in the presence of silica for wheat and rice blast

(Bélanger et al. 2003; Rodrigues et al. 2003). Experiments performed on cucumber leaves following fungal infection identified that further resistance to infection is acquired by expression of a proline-rich protein together with the presence of silica at the site of attempted penetration (Kauss et al. 2003). The c-terminal end of this protein contained a high density of lysine and arginine residues that were proposed to catalyse the localised deposition of silica at the site of vulnerability, with clear analogies being observed with the composition of the R5 peptide found within the silica of selected diatom species (Currie and Perry 2007).

In addition, silicon application has been found to alleviate metal toxicity, salinity, drought and temperature stresses (Liang et al. 2007). The proposed mechanism for the alleviation of Mn, Cd, Al and Zn toxicities is through accumulation of Zn as a silicate (Neuman and zur Nieden 2001), increased enzymatic (e.g. superoxide dismutase; SOD) and non-enzymatic antioxidant production (e.g. ascorbate) against Mn toxicity (Shi et al. 2005), and increased release of phenolics with a strong Al chelating ability for Al tolerance (Kidd et al. 2001). Application of silicon (usually as a soluble silicate) can also bring about drought tolerance possibly as a result of decreased transpiration (Epstein 1999), and the presence of silicified structures in plants has also been shown to improve plant tolerance to high temperatures (Wang et al. 2005). The resistance to salt stress has been found to be due to the enhancement of antioxidants such as SOD and catalase preventing oxidative membrane damage (Zhu et al. 2004; Moussa 2006).

6 Laboratory Studies of Silica Condensation, Polymerisation and Materials Formation

In order to understand how silica-associated biomolecules affect silicic acid polymerisation and materials formation, several laboratory-based model systems have been developed. A variety of silicic acid precursors including salts of silicates (e.g. diluted and buffered Na_2SiO_3 ; Coradin and Livage 2001), salts of silicon complexes (e.g. $\text{K}_2[\text{Si}(\text{C}_6\text{H}_4\text{O}_2)_3] \cdot x\text{H}_2\text{O}$; Perry and Lu 1992 and all later publications from the Perry group), alkoxy silanes (e.g. $\text{Si}(\text{OCH}_3)_4$ (TMOS); Kröger et al. 1999; and $\text{Si}(\text{OC}_2\text{H}_5)_4$ (TEOS)), and alkylsilanes (e.g. $\text{CH}_3\text{Si}(\text{OCH}_3)_3$; Cha et al. 1999; Zhou et al. 1999) have been used. All biological silica forms from an aqueous environment, but many of the experiments designed to understand the process are performed in largely non-aqueous solutions using alkoxy silanes as the silicon precursor. If we only consider the differences in the molecules available for silica formation, then for reaction in an aqueous environment the building block is orthosilicic acid ($\text{Si}(\text{OH})_4$) or its anion ($\text{Si}(\text{OH})_3\text{O}^-$), but in solutions of alkoxy silanes, e.g. tetraethoxysilane ($\text{Si}(\text{OC}_2\text{H}_5)_4$), hydrolysis yields a mixture of monomers ($\text{Si}(\text{OC}_2\text{H}_5)_3\text{OH}$, $\text{Si}(\text{OC}_2\text{H}_5)_2(\text{OH})_2$, $\text{Si}(\text{OC}_2\text{H}_5)(\text{OH})_3$ and $\text{Si}(\text{OH})_4$), all of which show different reactivity towards condensation and hence polymerisation. All species present in the reaction mixture have some effect on the silica formation process (Iler 1979) and this fact should not be ignored. All the silicic acid precursor

systems listed above have their disadvantages; presence of methanol, ethanol or catechol as breakdown products, very fast kinetics preventing detailed analysis of kinetics (alkoxysilanes), or incomplete breakdown to monomeric silicic acid (silicate solutions). Colorimetric methods (molybdenum yellow and blue, which are most sensitive to low concentrations), atomic absorption and inductively coupled plasma analysis are all methods that have been used to measure silicon concentrations in solution (Iler 1979; Perry 2003). Analysis of the materials formed is possible by a number of methods including dynamic light scattering, gas adsorption, FTIR, solid state ^{29}Si NMR and electron microscopy in order to determine particle sizes, aggregate characteristics, porosity, surface area, and surface and local molecular chemistry, as well as morphological characteristics on a range of length scales as described earlier in this chapter.

7 The Effect of Biologically Relevant Solution Additives on Condensation, Polymerisation and Materials Formation

In vitro studies of silica formation using molecules extracted from biosilica have shown that silicatein (sponge protein), either as the extracted axial filament or as single molecules, catalyses the hydrolysis and condensation of alkoxysilanes (Cha et al. 1999); the silaffins (diatom cell wall proteins) and long-chain polyamines of diatoms (Sumper and Kroger 2004) influence both the rate of silicate polymerisation and also the structures formed, while plant intrasilica isolates modify condensation kinetics and silica form (Perry and Keeling-Tucker 1998, 2003). Such studies have indicated that all these bioextracts can act as catalysts and/or as templating agents and, partly because of the very limited quantities available, other researchers have used chemical mimics of these biomolecules to further explore the capacity of these and similar molecules to modify silica condensation, polymerisation and aggregation behaviour.

Complementary in vitro studies using peptides, amino acids and recombinant proteins have also been performed (e.g. Coradin and Livage 2001; Belton et al. 2004; Tomczak et al. 2005; Patwardhan et al. 2006, 2007; Tilburey et al. 2007). Coradin and Livage (2001) have studied the effect of four amino acids (lysine, serine, aspartic acid and proline) and their homopeptides ($n = \text{ca. } 50$ for poly(-L-)lysine, aspartic acid and proline, and $n = \text{ca. } 130$ for poly(-L-)serine) on silica formation using buffered solutions of diluted sodium silicate over a range of pH values. Belton et al. (2004) explored the effect of eleven amino acids (lysine, arginine, asparagine, glutamine, threonine, serine, tyrosine, glycine, alanine, glutamic acid and proline) together with homopeptides of glycine (1–5 amino acid units) and lysine (1–5 amino acid units) on silica formation from solutions containing monomeric silicic acid derived from a silicon catecholate complex. The nature of the side chain and the number of these within a peptide both affect the silica formation process. Charged side chains have the most effect, with positively charged side chains showing the largest effect via electrostatic interactions between positively charged

amino acid side chains and negatively charged silica species. The pI of the side chain functionality correlates positively with acceleration of the early stage reaction kinetics and the hydrophobicity of the side chain with the surface area of the silica material formed. Reactions using nitrogen-containing amino acids modified the morphology of the silica formed with granular structures being created suggesting their ability to stabilise aggregates. The addition of L-lysine homopeptides of increasing length ($n = 1-5$) to the model reaction system showed increases in rates of oligomer formation and aggregate growth, together with reduced silica surface area as n increased (Belton et al. 2004). The small positively charged peptides are thought to be able to bridge particles to produce extended structures. Studies with longer chain poly-L-lysines (Tomczak et al. 2005; Patwardhan et al. 2006) have demonstrated the ability of this macromolecule to form silica hexagons with either TMOS or waterglass as the silicic acid precursors. The hexagons are composed of amorphous silica templated on packed arrays of alpha helical poly-L-lysine molecules. Detailed studies have also been performed with recombinant silicatein (26kDa) and with three highly basic recombinant proteins pYT320 (alpha helical), pYT338 (beta sheet) and pYT287 (random coil) (Patwardhan et al. 2007). All the recombinant proteins investigated affected the early stages of silica formation, with particularly strong effects on the dissolution process suggesting the promotion of structural reorganisation. In solution, all of the proteins exhibited self-assembled structures that were disrupted by the presence of the negatively charged, early stage, silica particles. Analysis of silicas produced by thermogravimetric analysis and nitrogen gas adsorption showed a decreasing trend in surface area, pore volume and average pore diameter that could be correlated with increasing amounts of organic material entrapped within the precipitated silica (alpha helical < beta sheet < random coil, R5 < silicatein). Similar studies on highly hydroxylated proteins (sericin) and other hydroxyl-containing molecules found little effect on silica formation in highly aqueous media due to competition with water for hydrogen bonded interactions between the additives used and the forming silica structures (Tilburey et al. 2007).

Other molecules of biological relevance that have been examined in model reaction systems are the polyamines, spermine, spermidine and putrescine, which are sometimes found conjugated to phenolic acids. Putrescine, a simple alkyldiamine, was able to increase the rate of condensation and the rate of particle aggregation (Belton et al. 2005a). Longer chain amines, spermidine and spermine, influenced aggregation according to molecule length. While only two natural polyamines were examined, these conclusions were verified by the analysis of a number of synthetically produced homologues (Belton et al. 2005b).

8 Applications Using the Biomolecules as Identified from Diatoms, Sponges and Higher Plants

Materials scientists, bioengineers, chemists and theoretical chemists have begun to utilise the molecules isolated from the silica of mineralised organisms, as well as recombinant proteins and synthetic peptides based on the biomolecules

previously identified by others, to perform experiments (including *in silico*) aimed at understanding the biological process of silicification or for developing new materials using a biomimetic approach.

9 Technological and Model Advances Utilising Diatoms

The scientists who identified the presence of silaffins or isolated and characterised them from *C. fusiformis* showed that the naturally occurring protein was able to generate spheres (sphere diameter size range 50–700 nm depending on whether single silaffins or mixtures of silaffins were used) *in vitro* from metastable solutions of silicic acid generated from alkoxysilanes at neutral pH (Kröger et al. 1999, 2002). Silaffin-1A, isolated or prepared without the posttranslational modifications was found to promote sphere formation down to pH 4 provided that phosphate ions were present in the reaction medium. The presence of the highly positively charged side chains is thought to be required for the formation of silica under mildly acidic conditions with the presence of the phosphate groups providing an intrinsic source of anions. The first application of the R5 (repeating peptide sequence within Sil-1A) peptide was to create an ordered organic/inorganic array of silica nanospheres within a polymer hologram originally created by two-photon-induced polymerisation, with the R5 peptide being used to promote localised condensation under pH neutral reaction conditions that were compatible with the polymer matrix (Brott et al. 2001). The incorporation of a regular array of silica nanospheres in the polymer hologram lead to a nearly 50-fold increase in diffraction efficiency, and the authors proposed that the adopted experimental approach may find use in photonic applications. The formation of silica under physiologically compatible (benign) reaction conditions has also been exploited by the same group in the encapsulation of enzymes (Luckarift et al. 2004) to produce composite materials with improved stability of the enzyme and no loss of activity. The peptide has also been used to generate unusual silica morphologies including arched and elongated structures (Naik et al. 2003).

More recently, the R5 peptide has been attached as a fusion to a protein from *Nephila clavipes* spider dragline silk to generate a novel family of chimeric proteins for use in model materials-forming reactions (Foo et al. 2006). The chimeric proteins have been used to generate silica polymer nanocomposites in the form of films and fibers whose composite morphology and structure can be regulated by changes to processing conditions. These materials have potential use in the biomaterials field including replacement bone and dental materials.

A synthetic site-directed mutagenesis study of non-posttranslationally-modified R5 has explored the effect of amino acid sequence on the activity of the peptides on silica formation *in vitro* (Knecht and Wright 2003). The authors found that the presence of the RRIL motif in the peptide was crucial for activity and that this was related to the ability of the peptide to form a supramolecular self-assembled structure.

More recently, theoretical chemists using a coarse-grained simulation model have looked at the self-assembly of model peptides (e.g. R5) under a range of volume fractions (concentrations). In the simulations, the model peptides self-assemble to form spherical clusters, networks of strands or bicontinuous structures with characteristic length scales from 12 to 45 nm. The authors suggest that the self-assembled structures act as either nucleation points or scaffolds for the deposition of the 10- to 100-nm silica building blocks from which diatom skeletons and synthetic nanospheres are constructed (Lenoci and Camp 2006).

Most recent uses to which R5 have been put include the synthesis of amorphous titania from titanium bis(ammonium lactate)dihydroxide (Sewell and Wright 2006) and the synthesis of amorphous titanium phosphate in the form of spheres and fused structures (Cole et al. 2006) with entrapment of the peptide in both materials as formed. Thermal treatment to 600°C was still required for conversion to crystalline anatase, but the temperature at which conversion to rutile occurred was some 125°C lower than found for similar experiments performed with silicatein from sponges (Sewell and Wright 2006).

Many similar studies have been made using peptides of simpler composition that retain a key feature of the R5 peptide, namely the presence of charged amine groups. For example, polylysine (PLL) of different chain lengths (Coradin and Livage 2001; Tomczak et al. 2005; Patwardhan et al. 2006), polymers such as poly(allylamine hydrochloride) (PAH), polyethylenimine (PEI) (Patwardhan and Clarkson 2002), poly(2-(dimethylamino)ethyl methacrylate) (poly(DMAEMA)) (Kim et al. 2004) and polypropyleneimine (PPI) amine terminated dendrimers (Knecht and Wright 2004), as well as small molecules such as amino acids and small peptide oligomers (Belton et al. 2004), together with diamines of various chain length (Belton et al. 2005a) and amines with varied spacing (Belton et al. 2005b), and synthetic propylamines built from the *N*-methyl propylamine as found in diatom silica (Annenkov et al. 2006), have all been found to affect the silica formation process at physiological pH. In some instances, the mechanism by which this happens has been identified and should lead to greater predictive ability in the generation of silica with different structure including particle sizes, density, porosity and surface chemistry.

In a totally different chemical approach, diatom silica frustules have been used to fabricate a range of different materials using the frustule as the shaped template which is then converted into a different material at high temperatures (at least compared with biological synthesis) whilst retaining the shape of the organism. The technique has the acronym BaSIC (biosculpting and shape-preserving inorganic conversion) (Dickerson et al. 2005), and whilst the earliest studies used silica generated in the presence of the R5 peptide, later studies have utilised diatoms with a wide range of morphologies to generate a range of ceramics (MgO, Cai et al., 2005; ZrO₂, Shian et al., 2006; BaTiO₃; Weatherspoon et al., 2006), the element silicon (Baö et al., 2007) and boron nitride (Kusari et al., 2007) with complex shapes for potential use in environmental, aerospace, biomedical, chemical, telecommunications, automotive and defence applications.

Native silicateins, as extracted from sponges such as *Tethya aurantia* and *S. domuncula*, have been explored as catalysts and templates in the formation of

silica (Cha et al. 1999) and, more latterly, a whole range of different inorganic materials, including oxides of titanium (Sumerel et al. 2003), zirconium (Tahir et al. 2005) and gallium (Kisailus et al. 2005), as well as phosphates of titanium (Curnow et al. 2005), the metals silver (Schröder et al. 2007) and gold (Tahir et al. 2006) and organic materials such as poly (L-lactide) (Curnow et al. 2006), have been generated. It is clear from the data accumulated to date that the hydrolytic activity of silicatein is somewhat unspecific! In all cases, water-soluble precursors were used and reactions performed under approximately physiological conditions. Silicatein, by structural analogy with the cathepsin family of enzymes, probably has an active site that recognises substrates primarily through main chain and side chain interactions (Curnow et al. 2005) which is why reactions with substrates having significant organic mass (e.g. ethyl, isopropoxide, bis(ammonium lactato)) have perhaps been successful. It is less clear how precursors such as nitrates of gallium and silver, fluoride anions of zirconium and chloride containing anions of gold fit the same proposed mechanism although interaction of active silicatein with a metal and its precursor ligands with modification of the partial charges on species present has been used to explain the activity of silicatein in the generation of oxides and oxyhydroxides of gallium. (Kisailus et al. 2005).

The use of silicatein in nano(bio)technology is expanding due to the ability of scientists to produce recombinant material, albeit without the posttranslational modifications found in nature. It is possible using different methods of extraction to produce filaments of silicatein alone by HF treatment or by use of lysis media combined with urea to retain the intricate assembly of proteins that includes silicatein, galectin, collagen and other as yet unidentified proteins that make up the mineralising environment into which silica forms and is moulded (Schröder et al. 2007). Another difference between the naturally occurring silicatein and that produced by recombinant methods is that it can be produced with a His-tag at the c-terminus. This tag can be cleaved enzymatically during purification using an enterokinase (Schröder et al. 2007) or can be used to advantage in the preparation of surfaces functionalised with the protein. Silicatein-functionalised surfaces been used in the formation of metals (gold: Tahir et al. 2006; and silver: Schröder et al. 2007) and oxides (silica, titania and zirconia: Tahir et al. 2005). Silicatein attached to culture plate plastic has been used to generate silica which was then used to culture human osteosarcoma SaOS-2 cells that were found to generate more calcium phosphate in the presence of the silica (Schröder et al. 2005) However, other less expensive methods could be used to prepare the silica under the same biocompatible conditions!

Problems with expression and reconstitution of recombinant silicatein due to its high degree of hydrophobicity have limited the applications to date as efficient expression to generate large quantities of protein has not been possible. Several routes are currently being explored by scientists to surmount this problem. One approach has been to use molecular biology techniques to create whole cell biocatalysts for inorganic and organic/polymer applications through the recombinant expression and presentation of folded functional silicatein-alpha at the external surfaces of cells (Curnow et al. 2005, 2006). The initial study generated layered titanium phosphates at the outer membrane of the silicatein-displaying cells at

physiologically relevant temperature and pH (Curnow et al. 2005), and a later study generated amorphous poly (L-lactide) through the polymerisation of the PLA precursor (Curnow et al. 2006). Poly (L-lactide) is one of a family of biocompatible and biodegradable polymers that can be used as scaffolds for tissue engineering and as an encapsulant, and this study may form the starting point for the generation of new cell-based materials and therapies.

Proposed applications for silicatein include uses in the biomedical field as a surface modifier of materials routinely used including metals, in the preparation of bone replacement materials and in the generation of encapsulating materials for the carriage and release of biomolecules. Other roles envisaged lie in the synthesis of nanostructured amorphous silica and in the synthesis of semiconductors, biosensors and catalysts in the form of nanowires, nanotubes and nanoparticles.

It is clear that silicateins, silaffins and polyamines that have been isolated from sponges and diatoms and other simpler molecules retaining some of the same chemical characteristics will find use in the generation of a wide range of simple and complex materials that may find application in a great variety of fields. In time, other molecules associated with the mineral phases of these and other classes of organism may likewise find application; only further experimentation and time will tell.

References

- Annenkov VV, Patwardhan SV, Belton D, Danilovtseva EN, Perry CC (2006) A new stepwise synthesis of a family of propylamines derived from diatom silaffins and their activity in silicification. *Chem. Commun.* 14:1521–1523
- Bao ZH, Weatherspoon MR, Shian S, Cai Y, Graham PD, Allan SM, Ahmad G, Dickerson MB, Church BC, Kang ZT, Abernathy HW, Summers CJ, Liu ML, Sandhage KH (2007) Chemical reduction of three-dimensional silica micro-assemblies into microporous silicon replicas. *Nature* 446(7132):172–175
- Bélangier RR, Benhamou N, Menzies JG (2003) Cytological evidence of an active role of silicon in wheat resistance to powdery mildew (*Blumeria graminis* f. sp. tritici). *Phytopathology* 93:402–412
- Belton DJ, Paine G, Patwardhan SV, Perry CC (2004) Towards an understanding of (bio)silicification: the role of amino acids and lysine oligomers in silicification. *J. Mater. Chem.* 14:2231–2241
- Belton DJ, Patwardhan SV, Perry CC (2005a) Putrescine homologues control silica morphogenesis by electrostatic interactions and the hydrophobic effect. *Chem. Commun.* 3475–3477
- Belton DJ, Patwardhan SV, Perry CC (2005b) Spermine, spermidine and their analogues generate tailored silicas. *J. Mater. Chem.* 15:4629–4638
- Blank GS, Sullivan CW (1983) Diatom mineralization of silicic acid. VI. The effects of microtubule inhibitors on silicic acid metabolism in *Navicula saprophila*. *J. Phycol.* 19:39–44
- Brott LL, Naik RR, Pikas DJ, Kirkpatrick SM, Tomlin DW, Whitlock PW, Clarson SJ, Stone MO (2001) Ultrafast holographic nanopatterning of biocatalytically formed silica. *Nature* 413(6853):291–293
- Cai Y, Allan SM, Sandhage KH (2005) Three-dimensional magnesia-based nanocrystal assemblies via low temperature magnesiothermic reaction of diatom microshells. *J. Am. Ceram. Soc.* 88(7):2005–2010

- Cha JN, Shimizu K, Zhou Y, Christiansen SC, Chmelka BF, Stucky GD, Morse DE (1999) Silicatein filaments and subunits from a marine sponge direct the polymerization of silica and silicofenones *in vitro*. Proc. Natl. Acad. Sci. USA 96:361–365
- Chérif M, Benhamou N, Menzies JG, Bélanger RR (1992) Silicon induced resistance in cucumber plants against *Pythium ultimum*. Physiol. Mol. Plant Pathol. 41:411–425
- Chérif M, Asselin A, Bélanger RR (1994) Defense responses induced by soluble silicon in cucumber roots infected by *Pythium spp.* Phytopathology 84:236–242
- Chiappino ML, Volcani BE (1977) Studies on the biochemistry and fine structure of silica shell formation in diatoms. VIII. Sequential cell wall development in the pennate *Navicula pelliculosa*. Protoplasma 93:205–221
- Cole KE, Ortiz AN, Schoonen MA, Valentine AM (2006) Peptide- and long-chain polyamine-induced synthesis of micro- and nanostructured titanium phosphate and protein encapsulation. Chem. Mater. 18(19):4592–4599
- Coombs J, Volcani BE (1968) Studies on the biochemistry and fine structure of silica-shell formation in diatoms. Chemical changes in the wall of *Navicula pelliculosa* during its formation. Planta 82:280–292
- Coradin T, Livage J (2001) Effect of some amino acids and peptides on silicic acid polymerisation. Coll. Surf. B: Biointerfaces 21:329–336
- Curnow P, Bessett PH, Kisailus D, Murr MM, Daugherty PS, Morse DE (2005) Enzymatic synthesis of layered titanium phosphates at low temperature and neutral pH by cell-surface display of silicatein- α . J. Am. Chem. Soc. 127(45):15749–15755
- Curnow P, Kisailus D, Morse DE (2006) Biocatalytic synthesis of poly(L-lactide) by native and recombinant forms of the silicatein enzymes Angew. Chem. Int. Ed. 45(4):613–616
- Currie HA, Perry CC (2007) Silica in plants. Annals in Botany 100:1383–1389, doi: 10.1093/aob/mcm247
- Dickerson MB, Naik RR, Sarosi PM, Agarwal G, Stone MO, Sandhage KH (2005) Ceramic nanoparticle assemblies with tailored shapes and tailored chemistries via biosculpting and shape preserving inorganic conversion. J. Nanosci. Nanotechnol. 5(1):63–67
- Epstein E (1994) The anomaly of silicon in plant biology. Proc. Natl. Acad. Sci. USA 91:11–17
- Epstein E (1999) Silicon. Ann. Rev. Plant Physiol. Plant Mol. Biol. 50:641–664
- Fawe A, Abou-Zaid M, Menzies JG, Bélanger RR (1998) Silicon-mediated accumulation of flavinoid phytoalexins in cucumber. Phytopathology 88:396–401
- Foo CWP, Patwardhan SV, Belton DJ, Kitchel B, Anastasiades D, Huang J, Naik RR, Perry CC, Kaplan DL (2006) Novel nanocomposites from spider silk-silica fusion (chimeric) proteins. Proc. Natl. Acad. Sci. 103(25):9428–9433
- Frigeri LG, Radabaugh TR, Haynes PA, Hildebrand M (2006) Identification of proteins from a cell wall fraction of the diatom *Thalassiosira pseudonana* – Insights into silica structure formation. Mol. Cell. Proteomics 5(1):182–193
- Harrison CC (1996) Evidence for intramolecular macromolecules containing protein from plant silicas. Phytochemistry 41:37–42
- Hildebrand M, Volcani BE, Gassmann W, Schroeder JI (1997) A gene family of silicon transporters. Nature 385:688–689
- Hildebrand M, Dahlin K, Volcani BE (1998) Characterization of a silicon transporter gene family in *Cylindrotheca fusiformis*: sequences, expression analysis, and identification of homologs in other diatoms. Mol. Gen. Genet. 260:480–486
- Iler RK. 1979. The chemistry of silica. Wiley, New York
- Kauss H, Seehaus, K, Franke R, Gilbert S, Dietrich RA, Kröger N (2003) Silica deposition by a strongly cationic proline-rich protein from systemically resistant cucumber plants. Plant J 33:87–95
- Kidd PS, Llugany M, Günsé B, Barceló J (2001) The role of root exudates in aluminium resistance and silicon induced amelioration of aluminium toxicity in three varieties of maize (*Zea mays* L.). J. Exp. Bot. 52:1339–1352
- Kim DJ, Lee KB, Chi YS, Kim WJ, Paik HJ, Choi IS (2004) Biomimetic formation of silica thin films by surface-initiated polymerisation of 2-(dimethylamino) ethyl methacrylate and silicic acid. Langmuir 20(19):7904–7906

- Kisailus D, Choi JH, Weaver JC, Yang WJ, Morse DE (2005) Enzymatic synthesis and nanostructural control of gallium oxide at low temperature. *Adv. Mater.* 17(3):314–318
- Knecht MR, Wright DW (2003) Functional analysis of the biomimetic silica precipitating activity of the R5 peptide from *Cylindrotheca fusiformis*. *Chem. Commun.* 24:3038–3039
- Knecht MR, Wright DW (2004) Amine-terminated dendrimers as biomimetic templates for silica nanosphere formation. *Langmuir* 20(11):4728–4732
- Kröger N, Deutzmann R, Sumper M (1999) Polycationic peptides from diatom biosilica that direct silica nanosphere formation. *Science* 286:1129–1132
- Kröger N, Deutzmann R, Bergsdorf C, Sumper M (2000) Species-specific polyamines from diatoms control silica morphology. *Proc. Natl. Acad. Sci. USA* 97:14133–14138
- Kröger N, Deutzmann R, Sumper M (2001) Silica-precipitating peptides from diatoms, the chemical structure of silaffin-1a from *Cylindrotheca fusiformis*. *J. Biol. Chem.* 276:26066–26070
- Kröger N, Lorenz S, Brunner E, Sumper M (2002) Self-assembly of highly phosphorylated silaffins and their function in biosilica morphogenesis. *Science* 298:584–586
- Kusari U, Bao Z, Cai Y, Ahmad G, Sandhage KH, Sneddon LG (2007) Formation of nanostructured, nanocrystalline boron nitride microparticles with diatom-derived 3-D shapes. *Chem. Commun.* 11:1177–1179
- Liang YC, Sun WC, Zhu YG, Christie P (2007) Mechanisms of silicon-mediated alleviation of abiotic stresses in higher plants: a review. *Environ. Pollut.* 147(2):422–428
- Lenoci L, Camp PJ (2006) Self-assembly of peptide scaffolds in biosilica formation: Computer simulation of a coarse-grained model. *J. Am. Chem. Soc.* 128(31):10111–10117
- Levi C, Barton JL, Guillemet C, le Bras E, Lehuède P (1989) A remarkably strong natural glassy rod- the anchoring spicule of the monorhaphis sponge. *J. Mater. Sci. Lett.* 8(3):337–339
- Luckarift HR, Spain JC, Naik RR, Stone MO (2004) Enzyme immobilization in a biomimetic support. *Nat. Biotechnol.* 22(2):211–213
- Ma J-F, Yamaji N (2006) Silicon uptake and accumulation in higher plants. *Trends Plant Sci.* 11:392–397
- Ma J-F, Tamai K, Yamaji N, Mitani N, Konishi S, Katsuhara M, Ishiguro M, Murata Y, Yano M (2006) A silicon transporter in rice. *Nature* 440:688–669
- Maldonado M, Carmona MC, Uriz MJ, Cruzado A (1999) Decline in Mesozoic reef-building sponges explained by silicon limitation. *Nature* 401:785–787
- Mann S, Perry CC (1986) Structural aspects of biogenic silica. *Ciba Found. Symp.* 121:40–58
- Mitani N, Ma J-F (2005) Uptake system of silicon in different plant species. *J. Exp. Biol.* 56:1255–1261
- Moussa HR (2006) Influence of exogenous application of silicon on physiological response of salt stressed maize (*Zea mays* L.). *Int. J. Agric. Biol.* 8:293–297
- Müller WEG, Rothernberger M, Boreiko A, Tremel W, Reiber A, Schröder HC (2005) Formation of siliceous spicules in the marine demosponge *Suberites domuncula*. *Cell Tissue Res.* 321:285–297
- Naik RR, Whitlock PW, Rodriguez F, Brott LL, Glawe DD, Clarson SJ, Stone MO (2003) Controlled formation of biosilica structures *in vitro*. *Chem. Commun.* 24:238–239
- Nakajima T, Volcani BE (1970) Eta-N-trimethyl-L-gamma hydroxylysine phosphate and its non-phosphorylated compound in diatom cell walls. *Biochem. Biophys. Res. Commun.* 39:28–33
- Nakajima T, Volcani BE (1969) 3,4-dihydroxyproline: a new amino acid in diatom cell walls. *Science* 164:1400–1401
- Neuman D, zur Nieden U (2001) Silicon and heavy metal tolerance of higher plants. *Phytochem.* 56:685–692
- Patwardhan SV, Clarson SC (2002) Silicification and Biosilicification Part 3: role of synthetic polymers and polypeptides at neutral pH. *Silicon Chem.* 1(3):207–214
- Patwardhan SV, Maheshwari R, Mukherjee N, Kiick KL, Clarson SJ (2006) Conformation and assembly of polypeptide scaffolds in templating the synthesis of silica: an example of a polylysine macromolecular ‘switch’. *Biomacromolecules* 7:491–497
- Patwardhan SV, Shiba K, Schröder HC, Müller WEG, Clarson SC, Perry CC (2007) The interaction of ‘silicon’ with proteins: part 2. The role of bioinspired peptides and recombinant proteins in silica polymerization ACS. *Symp. Ser.* 964:328–347

- Perry CC (2003) Silicification: the processes by which organisms capture and mineralize silica. *Rev. Miner. and Geochem.* (Dove PM, De Yoreo JJ, Weiner S, eds) 54:291–327
- Perry CC, Fraser MA (1991) Silica deposition and ultrastructure in the cell wall of *Equisetum arvense*: the importance of cell wall structures and flow control in biosilicification? *Phil. Trans. Roy. Soc. Lond. B* 334:149–157
- Perry CC, Keeling-Tucker T (1998) Crystalline silica prepared at room temperature from aqueous solution in the presence of intrasilica bioextracts. *Chem. Commun.* 2587–2588
- Perry CC, Keeling-Tucker T (2000) Biosilicification: the role of the organic matrix in structure control. *J. Biol. Inorg. Chem.* 5:537–550
- Perry CC, Keeling-Tucker T (2003) Model studies of colloidal silica precipitation using biosilica Extracts from *Equisetum telmatia*. *Coll. Polym. Sci.* 281:652–664
- Perry CC, Lu Y (1992) Preparation of silicas from silicon complexes: role of cellulose in polymerisation and aggregation control. *Farad. Trans.* 88:2915–2921
- Perry CC, Mann S, Williams RJP (1984) Structural and analytical studies of the silicified macrohairs from the lemma of the grass *Phalaris canariensis* L. *Proc. Roy. Soc. Lond. B* 222:427–438
- Perry CC, Moss EJ, Williams RJP (1990) A staining agent for biological silica. *Proc. Roy. Soc. Lond. B* 241:47–50
- Pisera A (2003) Some aspects of silica deposition in Lithistid demosponge desmas. *Microsc. Res. Tech.* 62:312–326
- Rodrigues FA, Benhamou N, Datnoff LE, Jones JB, Bélanger RR (2003) Ultrastructural and cytochemical aspects of silicon-mediated rice blast resistance. *Phytopathology* 93:535–546
- Shian S, Cai Y, Weatherspoon MR, Allan SM, Sandhage KH (2006) Three-dimensional assemblies of zirconia nanocrystals via shape-preserving reactive conversion of diatom microshells. *J. Am. Ceram. Soc.* 89(2):694–698
- Schröder HC, Krasko A, Batel R, Skorokhod A, Pahler S, Kruse M, Müller IM, Müller WEG (2000) Stimulation of protein (collagen) synthesis in sponge cells by a cardiac myotrophin-related molecule from *Suberites domuncula*. *FASEB J.* 14:2022–2031
- Schröder HC, Krasko A, Le Pennec G, Adell T, Wiens M, Hassanein H, Müller IM, Müller WEG (2003) Silicase, an enzyme which degrades biogenous amorphous silica: contribution to the metabolism of silica deposition in the demosponge *Suberites domuncula*. *Prog. Mol. Subcell. Biol.* 33:250–268
- Schröder HC, Perović-Ottstadt S, Rothenberger M, Wiens M, Schwertner H, Batel R, Korzhev M, Müller IM, Müller WEG (2004) Silicon transport in the demosponge *Suberites domuncula*: fluorescence emission analysis using the PDMPO probe and cloning of a potential transporter. *Biochem. J.* 381:665–673
- Schröder HC, Boreiko O, Krasko A, Reiber A, Schwertner H, Müller WEG (2005) Mineralization of SaOS-2 cells on enzymatically (silicatein) modified bioactive osteoblast-stimulating surfaces *J. Biomed. Mater. Res. Part B Appl. Biomater.* 75B(2):387–392
- Schröder HC, Boreiko A, Korzhev M, Tahir MN, Tremel W, Eckert C, Ushijima H, Müller IM, Müller WEG (2006) Co-expression and functional interaction of silicatein with galectin. *J. Biol. Chem.* 281(17):12001–12009
- Schröder HC, Brandt D, Schlobmacher U, Wang X, Tahir MN, Tremel W, Belikov SI, Müller WEG (2007) Enzymatic production of biosilica glass using enzymes from sponges: basic aspects and application in nanobiotechnology (material sciences and medicine) *Naturwissenschaften* 94:339–359
- Sewell SL, Wright DW (2006) Biomimetic synthesis of titanium dioxide utilizing the R5 peptide derived from *Cylindrotheca fusiformis*. *Chem. Mater.* 18(13):3108–3113
- Shi Q, Bao Z, Zhu Z, He Y, Qian Q, Yu, J (2005) Silicon mediated alleviation of Mn toxicity in *Cucumis sativus* in relation to activities of superoxide dismutase and ascorbate peroxidase. *Phytochemistry* 66:1551–1559
- Shimizu K, Cha J, Stucky GD, Morse DE (1998) Silicatein α : cathepsin L-like protein in sponge biosilica. *Proc. Natl. Acad. Sci. USA* 95:6234–6238
- Simpson TL (1984) *The cell biology of sponges*. Springer, Berlin/Heidelberg/New York

- Sumerel JL, Yang WJ, Kisailus D, Weaver JC, Choi JH, Morse DE (2003) Biocatalytically templated synthesis of titanium dioxide. *Chem. Mater.* 15(25):4804–4809
- Sumper M, Kröger N (2004) Silica formation in diatoms: the function of long chain polyamines and silaffins. *J. Mater. Chem.* 14:2059–2065
- Sumper M, Brunner E, Lehmann G (2005) Biomineralization in diatoms: characterisation of novel polyamines associated with silica. *FEBS Lett.* 579(17):3765–3769
- Tahir MN, Theato P, Müller WEG, Schröder HC, Janshoff A, Zhang J, Huth J, Tremel W (2004) Monitoring the formation of biosilica catalysed by histidine-tagged silicatein. *Chem. Commun.* 24:2848–2849
- Tahir MN, Theato P, Müller WEG, Schröder HC, Borejko A, Faiss S, Janshoff A, Huth J, Tremel W (2005) Formation of layered titania and zirconia catalysed by surface-bound silicatein. *Chem. Commun.* 44:5533–5535
- Tahir MN, Eberhardt M, Therese HA, Kolb U, Theato P, Müller WEG, Schröder HC, Tremel W (2006) From single molecules to nanoscopically structured functional materials: Au nanocrystal growth on TiO₂ nanowires controlled by surface-bound silicatein. *Angew. Chem. Int. Ed.* 45(29):4803–4809
- Tilburey GE, Patwardhan SV, Huang J, Kaplan DL, Perry CC (2007) 'Are hydroxyl containing biomolecules important in (bio)silicification? A model study'. *J. Phys. Chem. B* 111(17) 4630–4638
- Tomczak MM, Glawe DD, Drummy LF, Lawrence CG, Stone MO, Perry CC, Pochan DJ, Deming TJ, Naik RR (2005) Polypeptide templated synthesis of hexagonal silica platelets. *J. Am. Chem. Soc.* 127:12577–12582
- Van der Meene AML, Pickett-Heaps JD (2002) Valve morphogenesis in the centric diatom *Proboscia alata Sundstrom*. *J. Phycol.* 38:351–363
- Van Hoest PJ (2006) Rice straw, the role of silica and treatments to improve quality. *Anim. Feed Sci. Technol.* 130:137–171
- Vrieling EG, Beelen TPM, van Santen RA, Gieskes WWC (2002) Mesophases of (bio)polymer-silica particles inspire a model for silica biomineralization in diatoms. *Angew. Chem. Int. Ed.* 41:1543–1546
- Wang L, Nie Q, Li M, Zhang F, Zhuang J, Yang W, Li T, Wang Y (2005) Biosilicified structures for cooling plant leaves: a mechanism of highly efficient midinfrared thermal emission. *Appl. Phys. Lett.* 87:194105
- Weatherspoon MR, Haluska MS, Cai Y, King JS, Summers CJ, Snyder RL, Sandhage KH (2006) Phosphor microparticles of controlled three-dimensional shape from phytoplankton. *J. Electrochem. Soc.* 153(2):H34–H37
- Wetherbee R, Crawford S, Mulvaney P (2000) The nanostructure and development of diatom biosilica. In: Bauerlein E (ed) *Biomineralization, from Biology to Biotechnology and Medical Applications*. Wiley VCH, Weinheim, Germany, pp189–206
- Yoshida S, Ohnishi Y, Kitagishi K (1962) Histochemistry of silicon in rice plant III. The presence of cuticle silica-double layer in the epidermal tissue. *Soil Sci. Plant Nutr.* 8:1–5
- Zhou Y, Shimizu K, Cha JN, Stucky GD, Morse DE (1999) Efficient catalysis of polysiloxane synthesis by silicatein α requires specific hydroxy and imidazole functionalities. *Angew. Chem. Int. Ed.* 38:780–782
- Zhu Z, Wei G, Li J, Qian Q, Yu J (2004) Silicon alleviates salt stress and increases antioxidant enzymes activity in leaves of salt-stressed cucumber (*Cucumis sativus* L.). *Plant Sci.* 167:527–533

Optical and Nonlinear Optical Properties of Sea Glass Sponge Spicules

Yu. N. Kulchin, A.V. Bezverbny, O.A. Bukin, S.S. Voznesensky,
A.N. Galkina, A.L. Drozdov, and I.G. Nagorny

1	Introduction	316
2	Structural Peculiarities of Glass Sponge Spicules	317
3	Optical Properties of Biological Silica Spicules of Glass Sponges	320
4	Glass Sponge Spicules as Natural Photonic Crystals: Waveguide and Photonic Crystal Properties of Glass Sponge Spicules	322
4.1	Waveguide Properties of Spicules of Glass Sponges	322
4.2	Propagation of Ultra-Short Pulses in Spicules of Glass Sponges	331
5	Fluorescent Properties of Glass Sponge Spicules	336
6	Conclusion	338
	References	338

Abstract Originating in nature, the combination of spongin protein with silicon dioxide extracted from seawater by silicatein protein presents a natural nanocomposite material of unique optical and mechanical properties. Mechanically, it combines the elasticity of protein with the flexibility and durability of silica. The light propagation inside spicules of glass sponges is of substantial interest for developing novel elements for photonics applications. The glass sponge spicules have remarkable light guiding properties. Our experimental research on passing laser pulses through spicules of *Hyalonema sieboldi* and *Pheronema* sp. reveals a concentration of guided light in the paraxial region. The multi-layer cladding of glass sponge spicules produced by nature has an obvious analogy with some contemporary artificial microstructured optical fibers. Our researches have shown that the core diameter and cladding layers thickness of the

Yu. N. Kulchin (✉) A.V. Bezverbny, O.A. Bukin, S.S. Voznesensky,
A.N. Galkina and I.G. Nagorny
Institute for Automation and Control Processes of Far Eastern Branch of RAS, Radio Str. 5,
690041 Vladivostok, Russia
e-mail: kulchin@iacp.dvo.ru

A.L. Drozdov
Institute of Marine Biology of Far Eastern Branch of RAS, Palchevsky Str. 17, 690041
Vladivostok, Russia

spicules of *H. sieboldi* and *Pheronema* sp. glass sponges are appropriate for causing photonic bandgaps in the infrared, visible, and ultraviolet wavelength regions. This enables singlemode waveguide and Bragg light propagation regimes in the spicules and provides exciting prospects of using them for the development of fundamentally new integrated optical elements based on peculiar waveguide properties of such structures, e.g., single-way waveguides (optical diodes) with increased mode field diameter and unique frequency and dispersion characteristics. Also, we have investigated the dynamics of propagation of intensive ultra-short pulses with durations $T_0 < 40$ fs through various patterns of spicules. Comparative analysis of the spectra of the output signals has shown that chromatic dispersion in spicules is considerably reduced, which can be explained by waveguide dispersion prevailing over material dispersion because of the multilayer structure of the cladding.

1 Introduction

In the course of evolution, biological systems have evolved unique survival techniques ranging from means of frightening predators and achieving mechanical rigidity to complex photosynthesis processes. One example is sea organisms whose skeletons are built from diverse minerals: calcite, aragonite, apatite, and silica (Aizenberg et al. 2004; Drozdov 2005). Particularly attractive in practical terms are the following sea organisms: diatomaceous, radiolarian, and sponges, whose skeletons are built from silica (Müller et al. 2006, Schröder et al. 2007, 2008). This is because silicon and its oxides are very widely used in micro- and optoelectronics for a wide range of applications.

Nowadays, optical telecommunications based on fused silica optical fibers play an essential part in our everyday life. However, the idea of using glass fibers had been realized in nature long before it came to create the human being (Müller et al. 2007a, b). *Hexactinellida* (*Porifera*) glass sponges represent a group of the most ancient multicellular organisms dwelling mostly in deep sea areas of the oceans at depths of 30–5,000m. There are some 5,000 species of sea sponges known nowadays with about 500 species being classified as six-ray glass sponges. The skeleton of such a sponge is composed of peculiar structures: siliceous six-ray spicules. The dimensions of such spicules, depending on their kind and age, vary considerably: diameter ranges from 0.01 to 30mm and length from some millimeters to several meters (Aizenberg et al. 2005; Müller et al. 2008a). Therefore, although science knows quite a few natural minerals with peculiar optical properties, spicules of glass sponges represent unique light-conducting objects of natural origin (Kulchin et al. 2006).

The most practically attractive objects for scientific investigation are the sea sponges whose skeleton is formed of long spicules (of the order of centimeters) representing hydrated quartz structures deposited around a protein core. This is because understanding of growth mechanisms of such structures (Müller et al. 2008b, c), as well as light propagation processes inside them, is of substantial interest in terms of creating a new, low-temperature technology for optical fiber production, as well as developing novel functional elements for photonics applications (Schröder et al. 2007, 2008; Kulchin et al. 2008).

The emphasis in this Chapter is laid on the results of studying two genera of glass sponges dwelling in the southern seas of the Pacific Ocean: I, *Hyalonema sieboldi* (Fig. 1; basal spicules), and II, *Pheronema* sp. (Fig. 2; skeletal spicules) (Kulchin and Voznesensky 2007; Kulchin et al. 2007a).

2 Structural Peculiarities of Glass Sponge Spicules

The choice of the two above mentioned species of glass sponges is due to a peculiar structure of their skeletons. As is known (Uriz et al. 2003; Aizenberg et al. 2005), sponge spicules are classified into basal (anchor) and skeletal spicules. Basal spicules represent thin threads consisting of a central organic thread and silica layers around it (Figs. 3 and 4). Supposedly, the basic function of these spicules consists

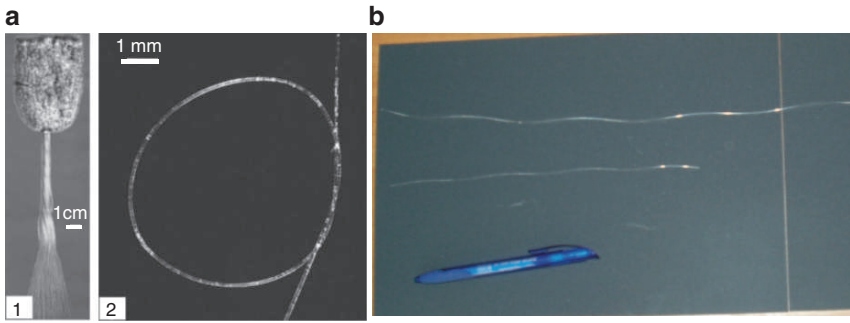


Fig. 1 Basal spicules of glass sponge *Hyalonema sieboldi*, obtained at a depth of about 200 m

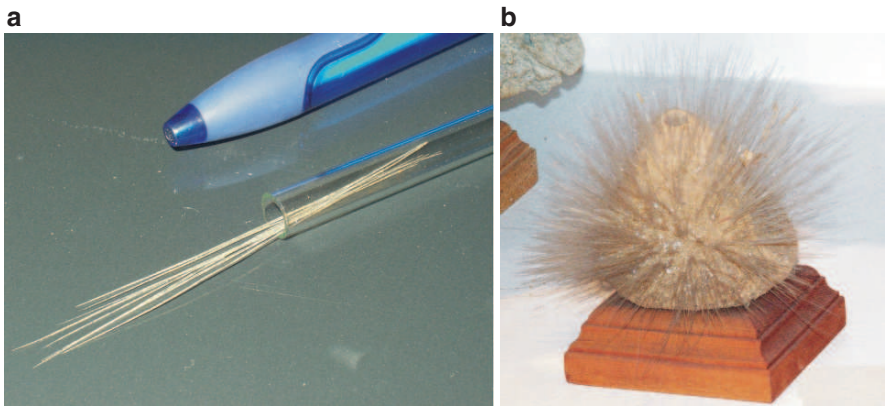


Fig. 2 Skeletal spicules of glass sponge *Pheronema* sp. obtained at a depth of 215 m

in ensuring mechanical linkage with the environment and reacting to changes in the environmental conditions. The skeletal spicules also have a complex mechanical structure with an axial channel containing a protein filament (Figs. 5 and 6). These spicules function as a shaping element of the skeleton ensuring its strength and mechanical protection of the sponge (Uriz et al. 2003).

In-depth microscopic examination of basal and skeletal spicules end-faces shows them to consist of numerous coaxial crystal layers, with their number ranging from tens to several hundreds depending on the spicule type and diameter as well as on the age of the sponge (Müller et al. 2007a, b).

Microscopic investigation also reveals that spicules are formed around a central protein filament 1–2 μm in diameter built up from 50–120 nm silicon dioxide particles which then combine together to form micron-sized particles making up a solid layer of silicon dioxide. This structure is clearly seen in Fig. 3. A spicule grows in the course of biosilification process which constitutes a periodic natural

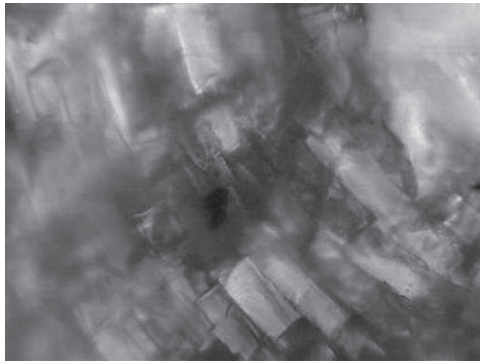


Fig. 3 Microscopic photo of cross section of *Hyalonema siebody* sponge spicule (magnification 1,157 \times)



Fig. 4 Photo of *Hyalonema siebody* basal spicule end-face, etched in HF solution and polished, obtained by scanning electron microscopy (scale 100 μm)

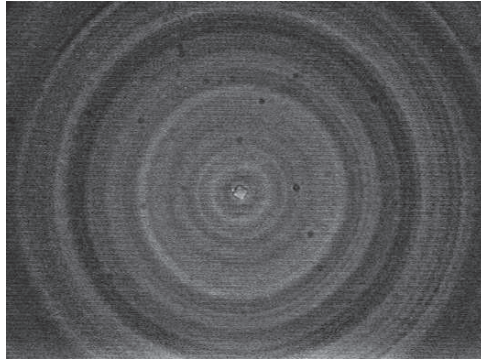


Fig. 5 Microscopic photo of cross section of *Pheronema* sp. spicule (magnification 1,157 \times)

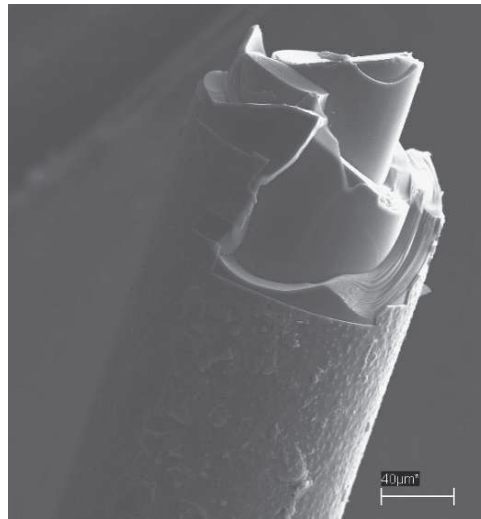


Fig. 6 Scanning electron microscopy photo of a cleaved end of *Pheronema* sp. skeletal spicule (scale 40 μm)

technological process during which silicon dioxide and protein layers are formed alternately one over the other. As a result of the process, basal and skeletal spicules are produced presenting complex composite formations with a central channel surrounded by 100- to 400-nm-thick cylindrical silicon dioxide layers with nano-sized protein layers between them (Sundar et al. 2003; Schröder et al. 2007, 2008).

Detailed investigation into such important mechanical properties as microhardness and Young modulus by dynamic microhardness measurement techniques using Berkovsky's pyramids (Kulchin et al. 2007b) disclosed that both kinds of sea sponges have nearly the same values of microhardness and Young modulus as that of fused silica (Samsonov 1978). However, the distribution of these parameters

over spicule cross section is non-uniform and they tend to decrease from the center towards the periphery. This is explained by the layered structure of spicules (Figs. 2–6) as well as by the layers becoming thinner towards the outer surface of the spicule. On the other hand, the layered structure of spicules ensures their mechanical strength and flexibility which allows one to actually tie them into a knot without breaking them (Fig. 1).

3 Optical Properties of Biological Silica Spicules of Glass Sponges

An important parameter, which defines light-guiding properties of optical fibers, is refractive index and its spatial distribution in the waveguide structure. Measurement of refractive index distribution in glass sponge spicules was carried out in accordance with the interferometric technique proposed in Sundar et al. (2003). The measurements revealed (Kulchin et al. 2006, 2007b) that the refractive index of the spicule core 2–3 μm in diameter lies in the range 1.45–1.48 at $\lambda = 633 \text{ nm}$ which is very close to the refractive index of fused silica and is in a good agreement with the data given in Sundar et al. (2003). The region around the core of the spicule 15–20 μm in diameter (which is clearly seen in Figs. 4 and 5) proved to be of a lower refractive index, ~ 1.4 , which is explained by a high concentration of organic matter and the quartz content being less. Then, there is a gradual increase in the refractive index from 1.4 to 1.45 in the region from 20 to 35 μm in diameter which is concerned with a progressive change in composition of the spicule material and an increase of the silicon dioxide layers' diameter. Further towards the outer layers of the spicule the refractive index tends to decrease changing in the range of 1.4 to 1.35–1.39. Refractive index variations in those regions are also associated with the protein layers thickness separating the layers of silicon dioxide, and they correlate with the variations in microhardness distribution over the cross section of the basal spicule (Fig. 7).

The investigation of transmission spectrum of basal and skeletal spicules of glass sponges I and II in the range of 400–900 nm using a halogen lamp disclosed that the spicules being studied transmit light in the visible and near infrared regions (Kulchin et al. 2006, 2008), which is in close agreement with the results of studying other genera of glass sponges (Maslov et al. 2006). Figure 8 presents the transmission spectrum of *H. sieboldi* basal spicule. As seen from the graph, there is a considerable absorption in the range of 400–450 nm. At the same time, a good transmission of light is observed in the region from 500 to 900 nm. In this spectral range, transmission loss is sufficiently low and at 633 nm amounts to 0.1 dB/km. This proves glass sponge spicules to have remarkable light-guiding properties.

Experimental research on passing white light through basal spicules 100–1,500 μm in diameter (sponges I and II) revealed a concentration of guided light in the paraxial region of the spicule (Kulchin et al. 2006, 2007b, 2008) and a distinct white-to-red color gradient along the spicule (Fig. 9). The experimental results presented above initiated further studies which are reviewed in the following sections.

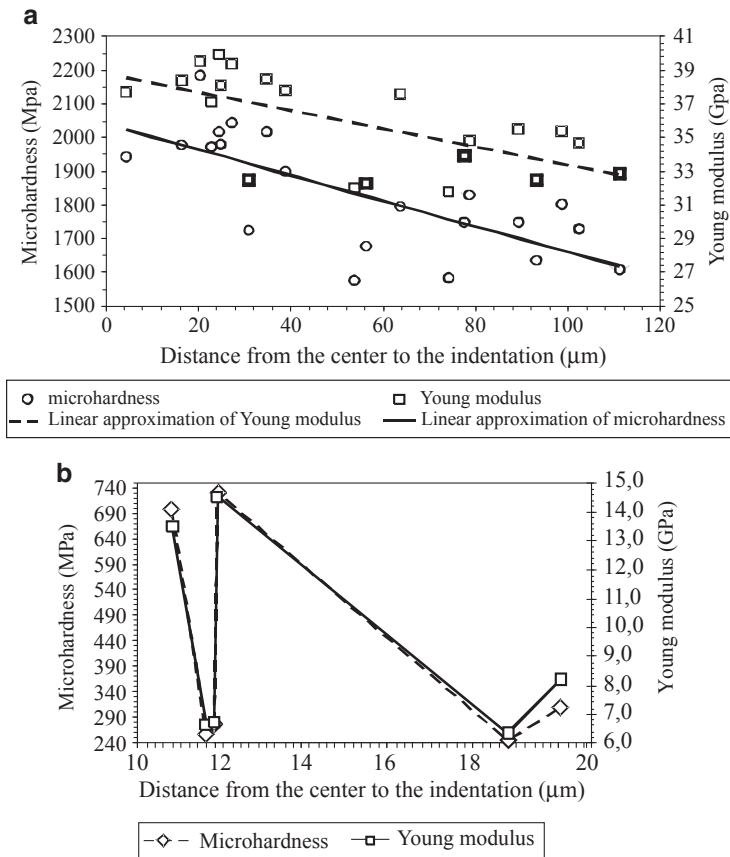


Fig. 7 Young modulus and microhardness distribution over cross section of a basal spicule of sponge I (a) and a skeletal spicule of sponge II (b)

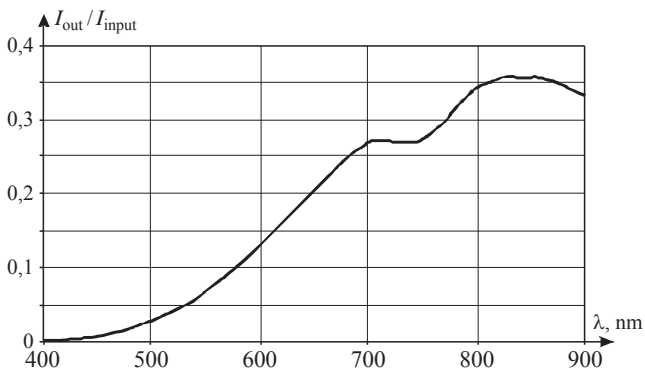


Fig. 8 Transmission spectrum of the *Hyalonema sieboldi* basal spicule

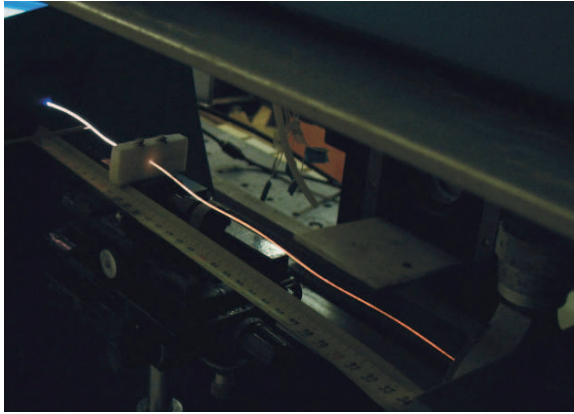


Fig. 9 Spectral transformation of light passing through a long spicule

4 Glass Sponge Spicules as Natural Photonic Crystals: Waveguide and Photonic Crystal Properties of Glass Sponge Spicules

Waveguide properties of glass sponge spicules make it possible to use the wave theory of electromagnetic field (Marcuse 1974; Solimeno et al. 1986) to describe the specifics of light propagation processes in such biological objects.

4.1 Waveguide Properties of Spicules of Glass Sponges

As is seen from the above results, the spicules of glass sponges are in many ways an analogue of fiber optical waveguides used in optical telecommunication systems. The main differences are that spicules are cone-shaped (Fig. 10) and consist of very numerous alternating coaxial cylindrical layers with different dielectric constant surrounding the core and composed of silica (amorphous silicon dioxide) and protein (Kulchin et al. 2007b, 2008). In this connection, the waveguide properties of spicules will depend essentially on their geometry, thickness, number of layers, and their refractive indices.

This section discusses light propagation process in a multiple-layer spicule approximated to be cylindrical, thus leaving out of consideration its true cone-shaped configuration. However, such an approximation is generally quite adequate for basal spicules of glass sponges longer than ~ 1 cm and larger than $200\ \mu\text{m}$ in diameter.

Several publications have addressed different types of waveguide modes in multi-layer cylindrical dielectric waveguides ranging from monographs (Marcuse

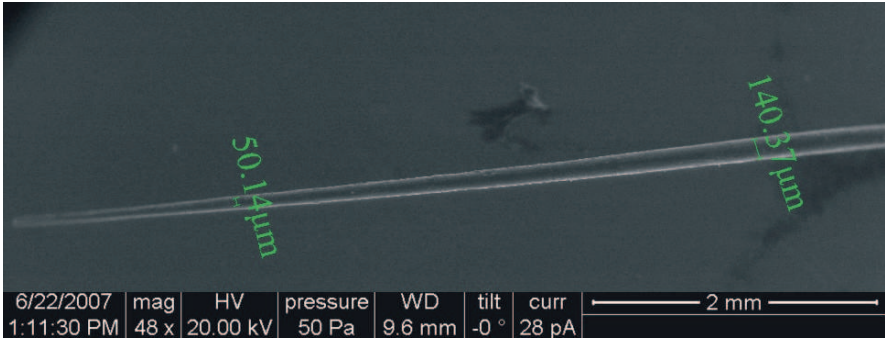


Fig. 10 SEM photo of a glass sponge spicule

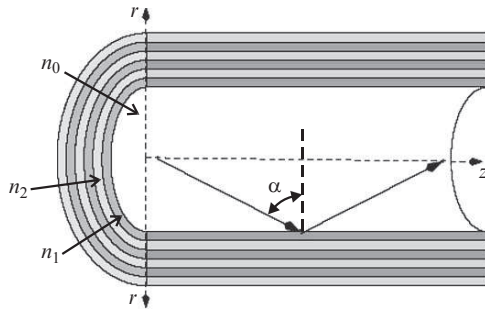


Fig. 11 Cylindrically layered waveguide

1974; Solimeno et al. 1986), where guided modes of waveguides with few layers in cladding are discussed in much detail, to the topical researches on Bragg waveguide regimes in fibers with a hollow core. The structure of waveguide modes has been investigated (Johnson et al. 2001; Argyros 2002; Ibanescu et al. 2003) in the case of a high contrast of refractive indices of adjacent layers of the cladding (so-called omniguide fibers). The waveguide properties of hollow-core fibers with coaxial cylindrical silica layers separated by nano-sized support bridges have been considered by Vienne et al. (2004).

The schematic of a multi-layer cylindrical waveguide is shown in Fig. 11, which corresponds to the elementary model of spicule structure. Here, (\bar{r}, z) are cylindrical coordinates, n_0 is refractive index of the waveguide core, n_1 and n_2 are refractive indices of alternating layers of cladding ($n_1 < n_0, n_2$), \vec{k} is the wave vector of the light field, and α is the angle of incidence upon the cladding of the waveguide mode propagating through the core.

As follows from the above assumptions, when $\sin \alpha \leq \sin \alpha_0 = n_{out} / n_0$, where α_0 is the critical angle at the interface spicule–outside media with refractive index n_{out} ,

total internal reflection of the light wave will occur at the interface spicule–outside media. Since the waves of this kind are totally confined within the spicule they can travel long distances without attenuation as eigenmodes of the waveguide.

If $\alpha \leq \alpha_0$, the waves propagating along the spicule are only reflected in part from the boundary which causes leaky modes to emerge with their intensity decreasing as the wave propagates through the spicule. However, due to the low leakage of light field through the cladding into the outer media, the modes with incidence angles corresponding to Fresnel reflection coefficients close to 1 (Born and Wolf 2005) can propagate rather a long distance $L_e \approx 10$ cm, where L_e is the waveguide attenuation length – the length of the waveguide corresponding to the attenuation of the input light intensity by a factor of e^2 .

Of particular interest is the case when Bragg guided modes emerge in the spicule within the incidence angle range $0 < \alpha < \alpha_0$. Here, a different guiding mechanism is employed based on multiple coherent wave scattering at alternating cladding layers with different refractive indices (Yeh et al. 1977, 1978). Effectiveness of Bragg reflection depends on the cladding geometry, core radius, cladding layers number, and refractive index contrast $n_1 - n_2$. As will be shown in the course of further consideration, these modes are dramatically different from ordinary leaky modes with respect to optical field distribution in the core and cladding layers of the spicule.

We analyzed the mode structure of the layered cylindrical waveguide based on the model described in Yeh et al. (1978) and Solimeno et al. (1986). The matrix method proposed in Yeh et al. (1978) for the calculation of electric and magnetic components \vec{E} , \vec{H} in concentric layered fiber waveguide allows definition of light modes characteristics using supplementary boundary conditions at the axis and on the outside of the waveguide cladding. As a result, each guided mode is represented in the form of a propagating wave along the spicule axis (named z) and at the same time as a standing cylindrical wave in the transverse plane.

4.1.1 Guided Modes of a Layered Cylindrical Waveguide

Among the guided waves of a multi-layer waveguide, the boundary condition on the outside surface of the cladding corresponds to the wave with evanescent decay of radial components of electrical and magnetic amplitudes that is $E_r, H_r \sim e^{-\gamma r}$

with $r \rightarrow \infty$, where damping constant $\gamma = \sqrt{\beta^2 - \left(\frac{2\pi n_0}{\lambda}\right)^2}$ is expressed in terms of wavelength λ and propagation constant β .

Let us consider the specifics of guided modes at $\lambda = 750$ nm using a relatively simple model treating a spicule to consist of a core of radius $R_0 = 0.5 \mu\text{m}$ and refractive index $n_0 = 1.49$, and cladding of four layers $h_1 = 20$ nm and $h_2 = 60$ nm in thickness with corresponding refractive indices $n_1 = 1.1$ and $n_0 = n_2 = 1.49$. The patterns of spatial distributions of electrical vector E_z longitudinal component and of the absolute value of energy flux vector P are given in Figs. 12 and 13 for the fundamental mode \mathbf{HE}_{11} , which is confined within the core of the waveguide and corresponds to the angle of incidence $\alpha = 73^\circ.55$, and for the mode \mathbf{EH}_{41} ,

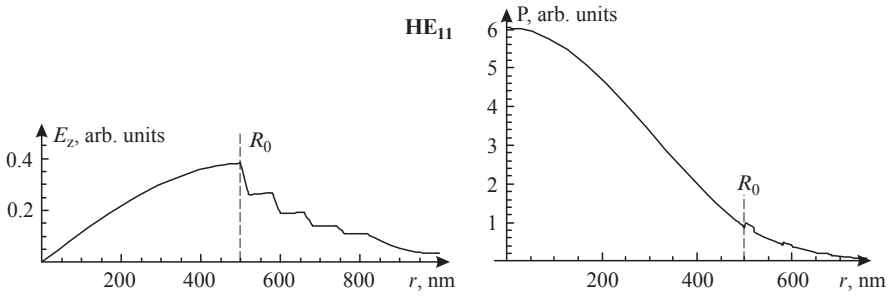


Fig. 12 Spatial distributions of longitudinal component of electrical field E_z and absolute value of energy flux vector for the fundamental mode HE¹¹

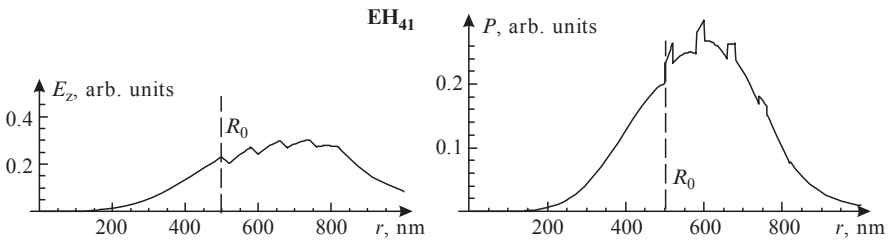


Fig. 13 Spatial distributions of longitudinal component of electrical field E_z and absolute value of energy flux vector for the cladding mode EH⁴¹

which propagates through the cladding and corresponds to the angle of incidence $\alpha = 49^\circ.2$. Though the total number of propagating modes within the given model is equal to 15, only a few core modes are of practical interest since the numerous cladding modes suffer drastic power losses because of strong scattering and absorption at spatial inhomogeneities of spicule layers. One can estimate the number of the core modes from the well-known evaluation formula for normalized frequency V (or cylindrical fiber waveguide number V) $V = \frac{2\pi R_0}{\lambda} \sqrt{n_0^2 - n_{\text{clad}}^2}$ (Agrawal 2001).

The effective refractive index of the cladding is determined by the following approximate relationship, $n_{\text{clad}} \approx \sqrt{\frac{n_1^2 h_1 + n_2^2 h_2}{h_1 + h_2}}$, as an effective refractive index of a

layered structure (Yariv and Yeh 1984). The above equations give $V \sim 2 \div 3$ which corresponds within our model to the single-mode regime of light propagation through the spicule.

The parameters of spicules are typically within the following ranges: $R_0 \sim 5 \div 50 \mu\text{m}$, $h_1 \sim 20 \div 100 \text{nm}$, $h_2 \sim 200 \div 2000 \text{nm}$, and $n_0 \approx n_2 \sim 1.45 \div 1.49$. Consequently, a spicule guides only a few core modes because of the small refractive index difference $n_0^2 - n_{\text{clad}}^2$.

4.1.2 Leaky Modes

Leaky and Bragg guided modes experience propagation losses because of partial leakage of light energy in the outside media in the form of an expanding cylindrical wave $\sim H^{(2)}(\tilde{k}r)$, where Hankel function $H^{(2)}(k_{\perp}r) \sim \frac{e^{-ik_{\perp}r}}{\sqrt{r}}$ has outgoing wave asymptotics tending to zero with $r \rightarrow \infty$, whereas the structure of electromagnetic field longitudinal components inside the spicule are described by:

$$E_z(r) = (AJ_L(k_{\perp}r) + BY_L(k_{\perp}r)) \cdot e^{-\beta z}$$

$$H_z(r) = (CJ_L(k_{\perp}r) + DY_L(k_{\perp}r)) \cdot e^{-\beta z}$$

where $k_{\perp} = \sqrt{(2\pi/\lambda \cdot n)^2 - \beta^2}$ means the absolute value of transverse component of the wave vector, n is the refractive index of the layer, $J_L(x)$ and $Y_L(x)$ are Bessel and Neumann functions, respectively (Bateman and Erdelyi 1953), and β is the propagation constant. In this case, an efficient method of calculation of leaky and Bragg modes can be implemented based on the minimization of the following coefficient (Konorov et al. 2003):

$$X = \frac{A_N^2 + B_N^2 + C_N^2 + D_N^2}{A_0^2 + C_0^2}$$

The physical interpretation of the coefficient is that it determines the ratio of the light energy outside the waveguide (in the last layer of the cladding) to the light energy at the axis of the waveguide (Argyros 2002).

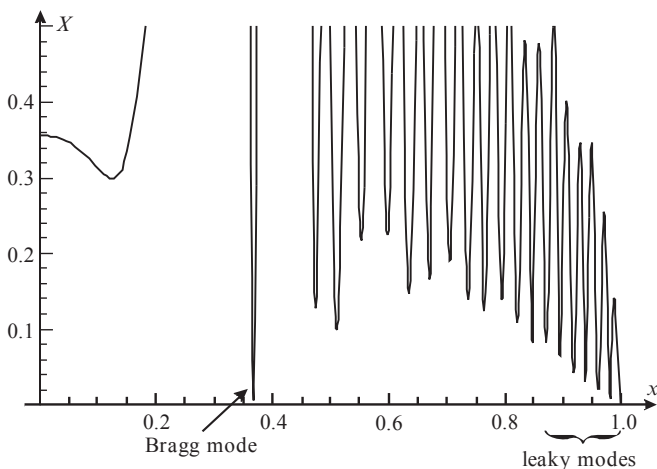


Fig. 14 The plot of the function $X(x)$

Figure 14 demonstrates the function $X(x)$ at $\lambda = 600\text{ nm}$, where $x = n_0 \cdot \sin \alpha$, for the fundamental mode TE_{01} calculated for a cylindrical layered waveguide with the following parameters: the radius of the core $R_0 = 5\ \mu\text{m}$ and the cladding consists of 50 double layers of thickness $h_1 = 20\text{ nm}$, $h_2 = 200\text{ nm}$.

The minima of $X(x)$ correspond to leaky modes in the vicinity of $x = 1$. For comparison, another minimum is marked in Fig. 14 corresponding to the Bragg mode. Qualitative difference between these two kinds of modes is clearly seen from the different character of their intensity distribution in the cladding layers. As it follows from the calculated dependencies depicted in Fig. 15, there is an exponential decay of light intensity of the Bragg mode towards the outer boundary of the cladding, whereas the intensity distribution of leaky modes at the cladding layers has a perfectly regular character, which corresponds to the coherent superposition of several cylindrical standing waves. Thus, a significant part of light intensity of leaky modes is distributed in the cladding, unlike Bragg modes, which are confined essentially within the core of the waveguide.

4.1.3 Bragg Modes

The Bragg modes are of particular interest in modern laser physics and non-linear optics since Bragg reflection as a coherent process can be realized without considerable optical power loss in so-called photonic crystals (Joannopoulos et al. 1995). In that way, the creation of totally reflecting dielectric structures has been made possible, which holds much promise in terms of the development of various devices operating in optical, ultra-violet, and X-ray wavelength ranges, where metallic reflective structures are inefficient due to the significant absorption losses. Particularly, layered waveguide structures representing one-dimensional (1D) photonic crystals are now being actively used in studying non-linear optical properties of gases (Zheltikov 2004) as well as in generation of ultra-short optical pulses with predefined spectral and temporal characteristics (Zheltikov 2007).

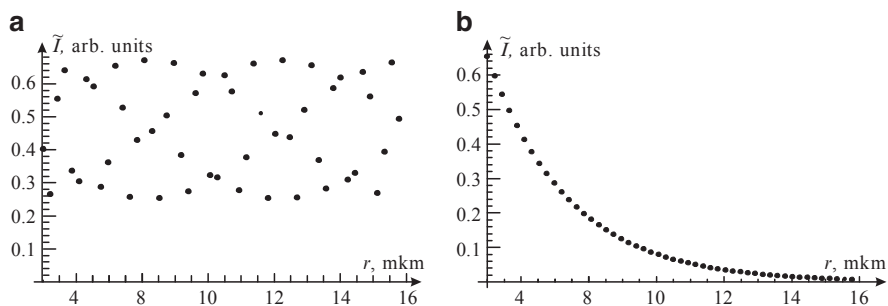


Fig. 15 Calculated intensity distributions of a leaky mode (a) and Bragg mode (b) with normalized intensity $\tilde{I} = 1$ at the center of the core

Let us consider the above-mentioned example of a layered fiber consisting of the cladding made up of 50 double layers with the following parameters: $n_0 = 1.425$, $R_0 = 5 \mu\text{m}$, $n_1 = 1.2$, $h_1 = 20 \text{ nm}$, $n_2 = 1.435$ and $h_2 = 200 \text{ nm}$. The calculations carried out made it clear that the highest values of waveguide attenuation length L_e belong only to the fundamental mode TE_{01} among all possible Bragg modes, whereas the leakage and corresponding power loss of TM_{01} -modes and lower-order hybrid modes are at least one order of magnitude higher. The results obtained are in good agreement with the outcome of earlier theoretical studies (Argyros 2002). The waveguide attenuation length can be calculated using a standard procedure (Konorov et al. 2003). The computed dispersion curve $\alpha(\lambda)$ and attenuation length $L_e(\lambda)$ of the layered waveguide for the most efficient Bragg mode TE_{01} are presented in Fig. 16.

The peculiarities of the Bragg modes are the following:

1. Single-mode regime of light propagation occurs even in large-core ($R_0 > 10\lambda$) waveguides because other Bragg modes have significantly smaller values of L_e in comparison with the fundamental mode TE_{01} .
2. The effective refractive index of the mode complies with the relation $n_{\text{eff}} = n_0 \cdot \frac{\beta}{k} < 1$, which makes its properties markedly different from that of ordinary guided modes with $n_{\text{eff}} > 1$.

As a consequence of multi-layer structure of glass sponge spicules, the existence of Bragg modes is possible though the characteristics of those such as attenuation length L_e are worse as compared to the above model and contemporary microstructured optical fibers such as omniguide fibers (Ibanescu et al. 2003) or silica photonic crystal fibers (Johnson et al. 2001; Konorov et al. 2003). There are several reasons for that:

1. The cross section geometry of layers in a spicule has a quasiperiodic structure because of variations in growth conditions, therefore the existence of more than one Bragg mode is possible, which involves Bragg reflection from different layer groups comprised of sufficient number of double layers ($N \sim 10$) with nearly the same values of h_2 and n_2 .
2. The refractive index contrast for n_1 and n_2 is rather low in spicules as compared to that of microstructured fibers and it depends on the spicule condition. For example,

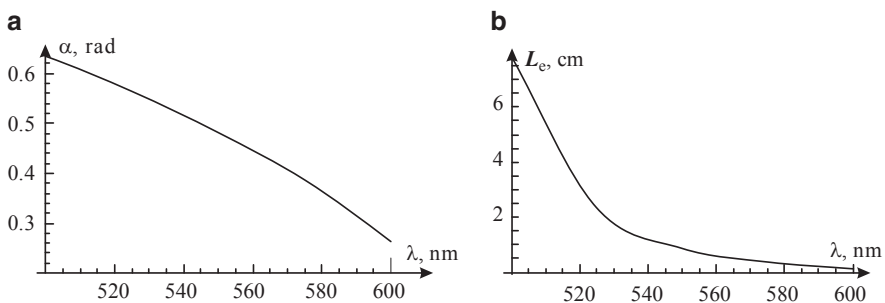


Fig. 16 Dispersion curve $\alpha(\lambda)$ (a) and attenuation length curve $L_e(\lambda)$ (b)

the contrast does not exceed 0.01 in the newly obtained sponges (Aizenberg et al. 2004; Kulchin et al. 2006, 2007b) because of the presence of water in the layers, whereas it can be much higher for old and well-dried sponges.

3. The condition of the most efficient Bragg reflection (Yeh et al. 1978) from an individual double layer $k_1 h_1 = k_2 h_2 = \frac{\pi}{2}$ can't be realized in a spicule due to the small thickness of protein layers which are of nano-metric scale ($h_1 \ll \lambda$).

We have been investigating the presence of Bragg modes in glass sponge spicules having taken as an example a basal spicule of a museum sample of *H. sieboldy*. SEM-photography of an obliquely cut and polished end of the spicule is presented in Fig. 17.

The core radius of this spicule amounted to $R_0 = 19.68 \mu\text{m}$, the thickness h_2 of silica layers varied from $10.3 \mu\text{m}$ near axis to $1.95 \mu\text{m}$ in the outer layers of the cladding, and the number of double layers totals $N = 45$. The thickness of separating protein layers between silica ones ranged from 20 to 100 nm.

So as to detect Bragg modes and to estimate the possible values of h_1 and n_1 , a series of experiments has been carried out aimed at measuring the intensity of laser radiation transmitted through the spicule at $\lambda = 632 \text{ nm}$. The experimental setup is presented in Fig. 18. Here, the slant of polished spicule end-face amounted to

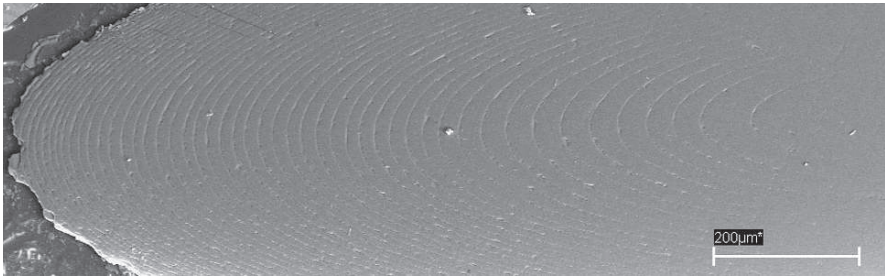


Fig. 17 Scanning electron microscopy photo of a slanted polished end-face of *Hyalonema sieboldy* spicule

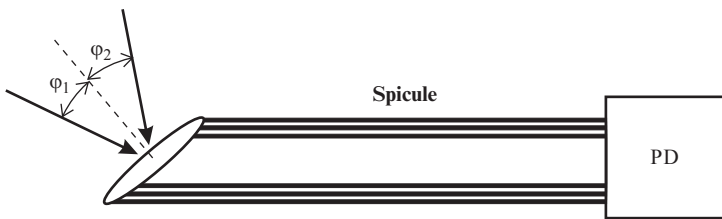


Fig. 18 The layout of the experimental setup: *PD* photodetector, φ_1 and φ_2 incidence angles of laser beams

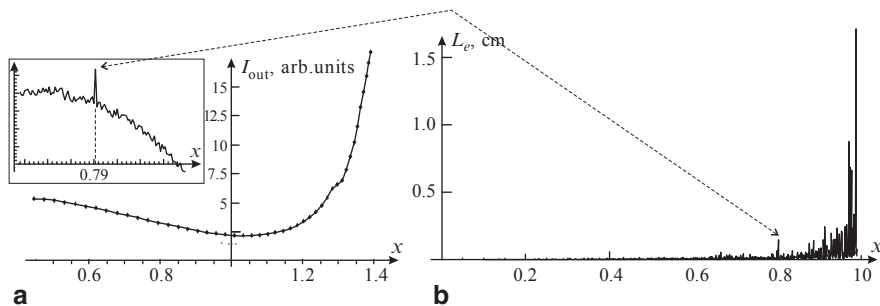


Fig. 19 ((a) Experimental dependence of the output light intensity on the angle of incidence; (b) calculation results of attenuation length $L_e(x)$)

45° with respect to the spicule axis. To prevent unwanted light from reaching the photodetector, it was diaphragmed by a pinhole aperture. The incidence angle of the laser beam upon the end-face of the spicule was being varied in the range of $0 < \varphi_{1,2} \leq 40^\circ$.

The measurement results of the laser intensity at the output of the spicule are shown in Fig. 19a as the dependence $I_{out}(x)$ (where $x = n_0 \cdot \sin \alpha$) taking into account Fresnel reflection on the input end of the spicule. In this experiment, values $x > 1$ correspond to the angles of incidence between 0 and φ_1 , and the values $x < 1$, when Bragg modes can be excited inside the spicule core, correspond to the angles of incidence between 0 and φ_2 . It should be noted that the decline of the curve observed in the region of $\alpha \sim \alpha_0$ (where the angle of internal reflection α_0 corresponds to $\varphi \sim 0^\circ$) can be related to the inefficiency of excitation of leaky modes and guided modes with large mode field diameters because of the above-mentioned strong scattering and absorption of light inside the cladding. On the other hand, the increase of $I_{out}(x)$ occurs with decreasing $x < 1$. In the close-up of this part of the curve $I_{out}(x)$ shown in the inset to Fig. 19a, one can see noticeable variations of the output intensity with the change of the input angle φ .

Figure 19b presents the calculation results of attenuation length L_e of the spicule as a multi-layer waveguide with the following parameters: $h_1 = 20 \text{ nm}$ and $n_1 = 1.2$. As is seen from both plots in Fig. 19a, b, a maximum in transmission is observed in the vicinity of $x = 0.79$, which confirms the presence of Bragg modes in the spicule.

The experimental data have also demonstrated that Bragg modes account only for a small part of the total transmitted intensity (a few percent). This is explained by non-efficient excitation of Bragg modes in a quasiperiodic multi-layer media.

The calculated distribution of light intensity I of the most effective Bragg mode at double layers of the spicule is represented in Fig. 20. As can be seen from the distribution, the double layers with exponential decay of light intensity are grouped in a nonuniform manner. This is quite different from the results obtained for the case of strictly periodic cladding presented in Fig. 15b.

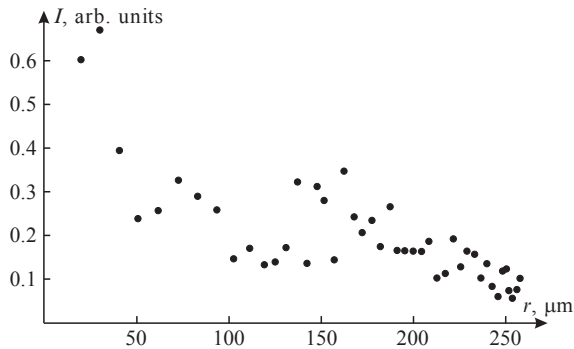


Fig. 20 The distribution of light intensity I at the layers of the spicule cladding

4.2 Propagation of Ultra-Short Pulses in Spicules of Glass Sponges

The dynamics of propagation of intensive ultra-short pulses (USP) with duration $T_0 < 100$ fs through microstructured optical fibers is of considerable interest in terms of investigations into nonstationary nonlinear processes in optical fiber waveguides, as well as for multiple practical applications of USP with predefined spectral and temporal properties in optical telecommunications (Smirnov et al. 2006), optical frequency metrology (Holzwarth et al. 2000), and optical coherence tomography (Hartl et al. 2001).

Physical mechanisms of dramatic nonlinear variations in temporal, spatial, and spectral characteristics of USP propagating through a transparent medium have attracted much attention in recent years (Gaeta 2000). Among them, are such well-studied phenomena in optical fibers as absorption and chromatic dispersion, as well as nonlinear effects: self-phase modulation, spatial self-focusing, and non-stationary stimulated Raman self-scattering of USP (Agrawal 2001). The interplay between different linear and nonlinear phenomena brings about such important effects as USP time splitting, space compression with filamentation, spectral broadening with generation of supercontinuum, etc. For example, supercontinuum generation and filamentation are essentially nonlinear phenomena, products of synergy between all the above-mentioned fundamental nonlinear processes.

One can derive a general wave equation, which provides an accurate description of the evolution of the optical pulse envelope $A(z, t)$ down to the duration of a few femtoseconds (Boyd 2003). In the approximation of moderate intensities of USP, the effects of self-focusing, plasma formation, multiphoton absorption, chromatic dispersion, and nonlinear susceptibilities of an order higher than the third can be neglected. Then, the envelope evolution equation (nonlinear envelope equation) in Kerr media can be expressed as (Kodama and Hasegawa 1987):

$$\frac{\partial A}{\partial z} + \beta_1 \frac{\partial A}{\partial t} + \frac{i}{2} \beta_2 \frac{\partial^2 A}{\partial t^2} - \frac{1}{6} \beta_3 \frac{\partial^3 A}{\partial t^3} + \frac{\alpha}{2} A = i\gamma |A|^2 A - \frac{2\gamma}{\omega_0} \frac{\partial (|A|^2 A)}{\partial t} - i; \quad (1)$$

where z is the distance of pulse propagation along the axis of the spicule, ω_0 is the central frequency of the pulse, $\beta_{1,2,3}$ are the coefficients of propagation constant β expansion in Taylor's series in the vicinity of ω_0 (β_2 is the group-velocity dispersion), α is absorption factor, γ is the coefficient of nonlinearity, and T_R is the lag time of media response (polarization) to the pulse. These parameters present important information about optical properties of the material under investigation. For reference, the parameters of fused silica at $\lambda = 800$ nm are $\alpha = 2 \cdot 10^{-3} \text{ m}^{-1}$, $\beta_2 = 44.6 \cdot 10^{-3} \frac{\text{ps}^2}{\text{m}}$, $\beta_3 \approx 10^{-4} \frac{\text{ps}^3}{\text{m}}$, $\gamma = 20 \cdot 10^{-3} (\text{W} \cdot \text{m})^{-1}$, $T_R \approx 2 \div 4 \cdot 10^{-3} \text{ ps}$ (Agrawal 2001; Boyd 2003). It must be noted that silica structure in the core and especially in the cladding layers of glass sponge spicules is quite different from that of fused silica: SiO_2 -globules measure 50–120 nm in spicules, whereas the cluster sizes in fused silica are ~ 2 nm in size according to the results of spectral analysis of combination Rayleigh scattering (Gorelik 2007).

In Eq. 1, linear effects of propagation are on the left and they describe absorption (the term including α) and the processes of temporal broadening of the pulse due to the group velocity dispersion (the terms including second and third time derivatives). Other terms on the right side of Eq. 1 describe nonlinear effects: the first term deals with nonlinear acquisition of phase, the second one can be identified as an intensity-dependent contribution to the group velocity leading to the effects of self-steepening and optical shock formation on trailing edge of the envelope (Boyd 2003), and the last term describes nonstationary stimulated Raman self-scattering of USP (Agrawal 2001).

Laser complex Spitfire Pro 40F (Spectra Physics, USA) with femtosecond Ti:Sapphire oscillator was used in our experiments on propagation of USP in spicules. Input pulse duration amounting to < 40 fs was controlled by a standard technique of nonlinear autocorrelation with second harmonic generation. Other parameters of USP were as follows: maximum pulse energy ~ 1 mJ, repetition rate 100 Hz, and pulse spectrum was centered at 800 nm with FWHM $\Delta\lambda_{\text{FWHM}} = 35$ nm.

In the course of the first series of experiments (Kulchin et al. 2006, 2008), pulse duration amounted to $T_0 \approx 40$ fs with relatively low pulse energies of $Q < 8 \cdot 10^{-6}$ J. The experimental spectrums of output USP are presented in Fig. 21 for the different samples of spicules (curves 2, 3, 4) in comparison with input spectrum (curve 1). The shape of spectrums 3–4 demonstrates minor changes indicating nonlinear self-phase modulation to be a dominating factor in the formation of the spectrums (Agrawal 2001), whereas curve 2 for spicule sample 2 40 mm long and 190 μm in diameter demonstrates a markedly strong anti-Stokes component in the output spectrum. The ratio of input and output spectrums (Fig. 22) shows that stimulated Raman self-scattering for certain nearly equidistant frequencies is possibly of resonant character in this spicule sample. These resonant frequencies indicate potential effect of Bragg reflection of pulses from the layered cladding, which can result in the amplification of resonant frequency components in the output spectrum.

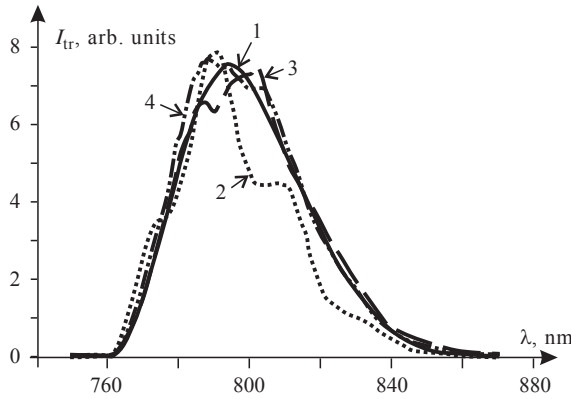


Fig. 21 Spectra of USP: 1 spectrum of the input pulse, 2–4 spectra of output pulses passed through different samples of spicules

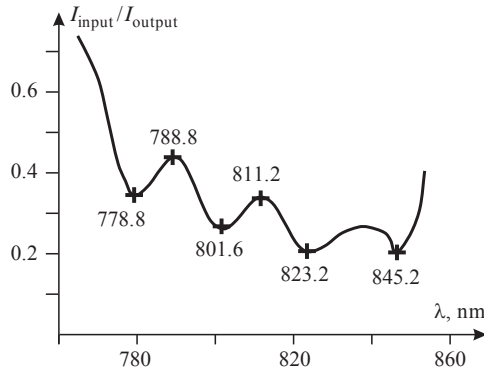


Fig. 22 Ratio of input and output pulse spectra of sample 2

In the second series of experiments, pulse energy was increased to $Q = 0.1 \cdot 10^{-3} \text{ J}$, which brought about qualitative changes in the spectrum of the output signals. It should be noted that typical propagation distances necessary for chromatic dispersion and self-phase modulation to manifest themselves are defined by dispersion length $L_D = \frac{T_0^2}{\beta_2}$ and nonlinear length $L_{FM} = (\gamma \cdot |A|^2)^{-1}$ (Boyd 2003). For our experimental layout, these lengths amounted to $L_D \sim 3 \text{ cm}$ and $L_{FM} \sim 1 \text{ cm}$. In other words, dispersion and self-phase modulation effect have significant influence upon the propagation of high-intensity USP in the spicules samples of length $L \sim 1.5 \div 7 \text{ cm}$. For the duration of pulses $T_0 \approx 35 \text{ fs}$ and the above-mentioned values of energy Q , the peak input intensity comes to $I = 7 \cdot 10^{10} \frac{\text{W}}{\text{cm}^2}$, and the influence of such nonstationary nonlinear optical effects as generation of optical “shock wave” at the back edge of

the light pulse which brings about intensification of the higher-frequency part of the pulse spectrum (Agrawal 2001; Boyd 2003), multiphoton absorption, spatial self-focusing, and noninstantaneous contribution to the nonlinear refractive index increase dramatically. As a result, shock formation due to space-time focusing and self-steepening leads to the appearance of an extremely broad pedestal in the blue part of the transmitted pulse spectrum (so-called supercontinuum generation) as well as to the formation of filaments in the medium that was initially transparent.

In Fig. 23, the spectrums of USP are presented for the cases of transmitting pulses through quartz optical fiber and a thick sample of spicule of length $L_1 = 7$ cm and diameter $500\mu\text{m}$ (the slanted end-face of the spicule is shown in Fig. 7). In Fig. 24,

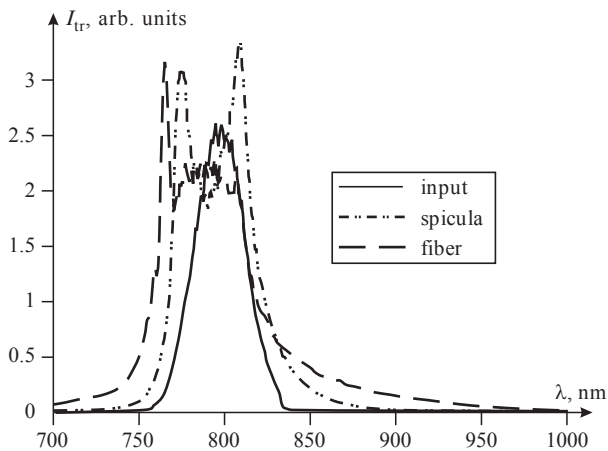


Fig. 23 Spectrums of the input ultra-short pulse and the pulses transmitted through an ordinary quartz fiber and a thick spicule of length 7 cm and diameter $\sim 500\mu\text{m}$

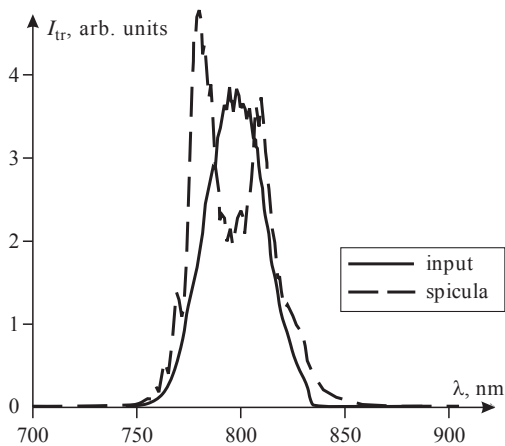


Fig. 24 Spectrums of input USP and the transmitted pulse through a thin spicule of length 1.5 cm and diameter $\sim 200\mu\text{m}$

USP spectrum is shown for the case of passing through a thin sample of spicule of length $L_1 = 1.5$ cm and diameter $\sim 200 \mu\text{m}$. Comparative analysis of the experimental plots makes it clear that spicules exhibit much stronger nonlinear optical properties than quartz optical fibers, whereas light-transmission capacity of the ordinary optical fiber is far better than that of spicules. This conclusion also follows from numerical simulation of the envelope dynamics $A(z,t)$ based on Eq. 1, which can be integrated by applying both the split-step Fourier method (Agrawal 2001) and the finite difference method. Figure 25 depicts the spectral distribution of transmitted USP intensity calculated on the basis of Eq. 1, assuming that $\beta_2 = 4.6 \cdot 10^{-3} \frac{\text{ps}^2}{\text{m}}$, which being one order of magnitude lower than β_2 of fused silica, gives good agreement of the calculated spectrum with the experimental data shown in Figs. 23 and 24. Thus, chromatic dispersion in spicules is considerably reduced which can be explained by waveguide dispersion prevailing over material dispersion because of the multilayer structure of the cladding. In this respect, spicules are similar to such light guides as free-strand (cobweb) fibers (Apolonski et al. 2002), which are composed of quartz core attached to the cladding by a cobweb-like structure of thin bridges. The free-strand fibers are a special type of photonic crystal fibers (PCF). It is well known that by adjusting refractive index of the cladding at different wavelengths and by arranging capillaries in a certain way at the time of manufacture, one can create PCF with flat dispersion profile of $\beta_2(\lambda)$ and shift zero dispersion wavelength λ_0 (by definition $\beta_2(\lambda_0) = 0$) in the visible region of electromagnetic spectrum.

A more efficient generation of supercontinuum (SC) in transmitted USP as compared to quartz optical fibers is an additional experimental verification of the above-mentioned dispersion properties of spicules as a one-dimensional PCF. SC generation indicates that dispersion profile $\beta_2(\lambda)$ of spicule is flat which allows generation of flat and wide SC spectra in such fibers. The photograph in Fig. 26

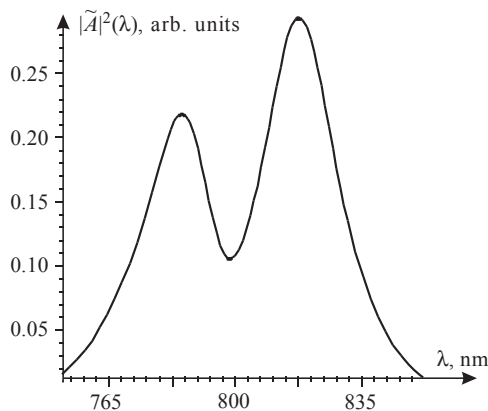


Fig. 25 Calculated intensity spectrum of output USP

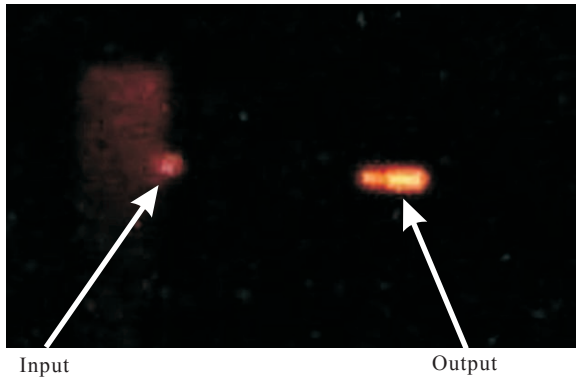


Fig. 26 Generation of supercontinuum in the spicule

illustrates the transformation of focused laser radiation into SC with the following parameters of the laser: central wavelength of the pulse $\lambda_0 = 800$ nm, duration $T_0 = 35$ fs, and energy $Q = 0.9 \cdot 10^{-3}$ J. The parameters of focusing lens are: 3 mm thickness and, 200 mm focal length.

Here, an input pulse of infrared radiation was transformed into SC extending to the visible region up to $\lambda_{\min} \sim 400$ nm. A spicule 200 μm in diameter and 1.5 cm in length was used in the experiment.

5 Fluorescent Properties of Glass Sponge Spicules

Present-day fluorescence spectroscopy opens up exciting experimental prospects by providing researchers with improved instrumentation of increased sensitivity and well-developed data processing techniques. This enables extensive multi-component analysis of a wide range of biological systems because most organic substances exhibit intrinsic fluorescent properties, which can be measured using fluorometric technique.

We use the second harmonics at $\lambda = 532$ nm of YAG: Nd-laser for the excitation of basal spicules by pulses with duration 12 ns, repetition rate 10 Hz, and variable energy up to 30 mJ. Experimental fluorescence spectrums were analyzed for various pulse energies in perpendicular geometry of the output signal to the input one (Kulchin et al. 2006, 2007b). A strong increase of fluorescence intensity was observed in the long-wavelength region of the optical spectrum. Normalized experimental curves of fluorescence spectrums $I_{\text{fluor}}(\lambda)$ for various pumping intensities are presented in Fig. 27, where $E = I_{\text{input}} / I_{\text{max}}$ is the relative value of laser intensity and I_{max} corresponds to the pulse energy $Q = 30$ mJ. Here, basal spicule samples with diameter 140 μm and length 5 cm of glass sponge I were used. As can be seen from Fig. 27,

fluorescent peaks are not dependent on the input pumping intensity and are observed at about $\lambda = 770\text{ nm}$. It is noteworthy that the pattern of fluorescence variation differs from that of ordinary multimode quartz optical waveguides (Agrawal 2001), which is evidently related to the presence of large organic complexes on the basis of spongin in the glass sponge spicules. The follow-up fluorescence measurements with varied light intensity at $\lambda = 770\text{ nm}$ made it clear that saturation of fluorescence intensity occurs upon reaching the maximum of laser intensity. According to (Maslov et al. 2006), this is the evidence of the nonlinear nature of light energy transformation in spicules concerned with a high content of those organic complexes.

Another characteristic feature of fluorescence in spicules consists in the delayed character of fluorescence decay kinetics. Fluorescence duration measurements yield values of the order of $10\mu\text{s}$ for basal spicules whereas the similar parameters of marine zooplankton or quartz fibers amount to $\sim 10^{-10}\text{--}10^{-9}\text{ s}$ (Fig. 28).

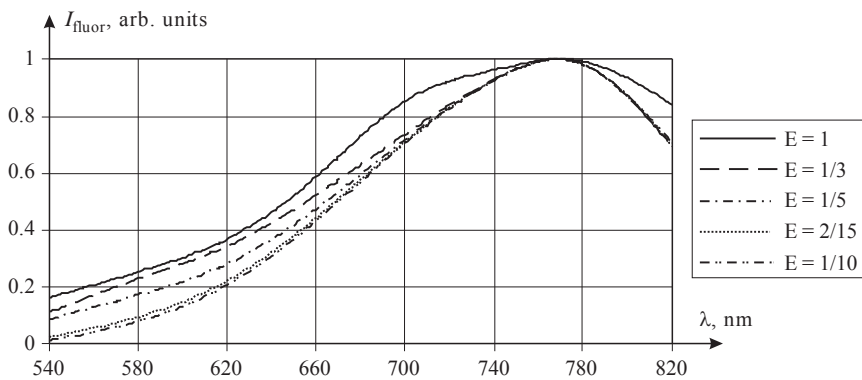


Fig. 27 Normalized experimental fluorescence spectra for various intensities of input laser radiation

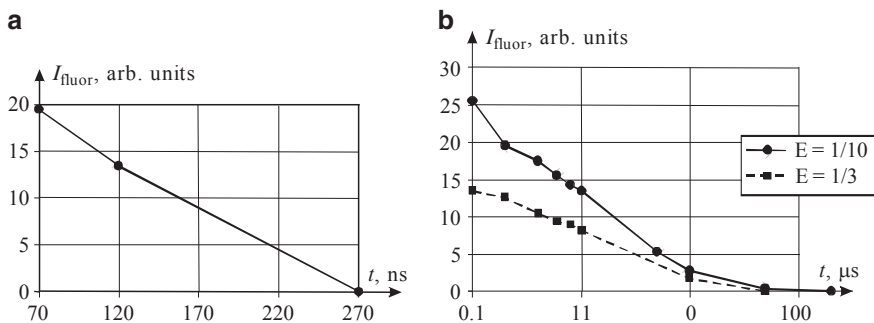


Fig. 28 Fluorescence durations for quartz fibers (a) and for basal spicules (b) under various intensities of input laser radiation

6 Conclusion

Thus, the studies carried out showed that the combination, originated in nature, of spongin protein with silicon dioxide extracted from seawater by silicatein protein presents a natural nanocomposite material of unique optical and mechanical properties.

Mechanically, it combines the elasticity of protein with flexibility and durability of silica. In terms of optical properties the material is of markedly weaker birefringence as compared with quartz optical fibers. The multi-layer cladding of glass sponge spicules produced by nature has an obvious analogy with some contemporary artificial microstructured optical fibers. Our researches have shown that the core diameter and cladding layers thickness of the spicules of *Hyalonema sieboldi* and *Pheronema* sp. glass sponges are appropriate for causing photonic bandgaps in the infrared, visible, and ultraviolet wavelength regions. This enables singlemode waveguide and Bragg light propagation regimes in the spicules and provides exciting prospects for using them for the development of fundamentally new integrated optical elements based on the peculiar waveguide properties of such structures, e.g., single-way waveguides (optical diodes) with increased mode field diameter and unique frequency and dispersion characteristics. The nonlinear character of the fluorescence spectrum makes glass sponge spicules a promising material for implementation of active optoelectronic devices such as optical fiber amplifiers and lasers.

References

- Agrawal G.P. (2001) Nonlinear fiber optics. Academic, San Diego, CA
- Aizenberg J., Sundar V.C., Yablon A.D., Weaver J.C., Chen G. (2004) Biological glass fibers: correlation between optical and structural properties. *Proceedings of the National Academy of Sciences of the USA* 10: 3358–3363
- Aizenberg J., Weaver J.C., Thanawala M.S., Sundar V.C., Morse D.E., Fratzl P. (2005) Skeleton of *Euplectella* sp.: structural hierarchy from the nanoscale to the macroscale. *Science* 309: 275–278
- Apolonski A., Povazay B., Unterhuber A., Drexler W., Wadsworth W.J., Knight J.C., Russell P.S.J. (2002) Spectral shaping of supercontinuum in a cobweb photonic-crystal fiber with sub-20-fs pulses. *Journal of Optical Society of America B* 19: 2165–2170
- Argyros A. (2002) Guided modes and loss in Bragg fibres. *Optics Express* 10: 1411–1417
- Bateman H., Erdelyi A. (1953) Higher transcendental functions, Vol. 2. McGraw-Hill, New York
- Born M., Wolf E. (2005) Principles of optics. Cambridge University Press, Cambridge
- Boyd R.W. (2003) Nonlinear optics. Academic Press, San Diego, CA
- Drozdov A.L. (2005) Biology for physicists and chemists. Far Eastern National University Press, Vladivostok (in Russian)
- Gaeta A.L. (2000) Catastrophic collapse of ultrashort pulses. *Physical Review Letters* 84: 3582–3585
- Gorelik V.S. (2007) Optics of globular photonic crystals. *Quantum Electronics* 37: 409–432
- Hartl I., Li X.D., Chudoba C., Ghanta R.K., Ko T.H., Fujimoto J.G., Ranka J.K., Windeler R.S. (2001) Ultrahigh-resolution optical coherence tomography using continuum generation in an air–silica microstructure optical fiber. *Optics Letters* 26: 608–610
- Holzwarth R., Udem T., Hansch T.W., Knight J.C., Wadsworth W.J., Russell P.S.J. (2000) Optical frequency synthesizer for precision spectroscopy. *Physical Review Letters* 85: 2264–2267

- Ibanescu M., Johnson S.G., Soljačić M., Joannopoulos J.D., Fink Y., Weisberg O., Engeness T.D., Jacobs S.A., Skorobogatiy M. (2003) Analysis of mode structure in hollow dielectric waveguide fibers. *Physical Review E* 67: 046608-1–046608-8
- Joannopoulos J.D., Meade R.D., Winn J.N. (1995) *Photonic crystals: molding the flow of light*. Princeton University Press, Princeton, NJ
- Johnson S.G., Ibanescu M., Skorobogatiy M., Weisberg O., Engeness T.D., Soljačić M., Jacobs S.A., Joannopoulos J.D., Fink Y. (2001) Low-loss asymptotically single-mode propagation in large-core OmniGuide fibers. *Optics Express* 9: 748–779
- Kodama Y., Hasegawa A. (1987) Nonlinear pulse propagation in a monomode dielectric guide. *IEEE Journal of Quantum Electronics* 23: 510–524
- Konorov S.O., Kolevatova O.A., Fedotov A.B., Serebryannikov E.E., Sidorov-Biryukov D.A., Mikhailova J.M., Naumov A.N., Beloglazov V.I., Skibina N.B., Mel'nikov L.A., Shcherbakov A.V., Zheltikov A.M. (2003) Waveguide modes of electromagnetic radiation in hollow-core microstructure and photonic-crystal fibers *Journal of Experimental and Theoretical Physics* 96: 857–869
- Kulchin Yu.N., Voznesensky S.S. (2007) (in Russian) In: Kulchin Yu.N. (ed) *Selected works on "Promising Trends on Nanotechnology Development in the Far East of Russia"*. Dalnauka, Vladivostok, pp. 10–42
- Kulchin Yu.N., Voznesensky S.S., Bukin O.A., Bagaev S.N., Pestriakov E.V. (2006) Optical Properties of Natural Biominerals-the Spicules of the Glass Sponges. *Optical Memory and Neural Networks (Information Optics)* 16: 189–197
- Kulchin Yu.N., Bukin O.A., Voznesensky S.S., Galkina A.N., Gnedenkov S.V., Drozdov A.L., Kuryavy V.G., Maltseva T.L., Sinebruchov S.L., Therednichenko A.I. (2007a) Biological species of fiber-optic waveguides. "Nonlinear Waves" – 2006, Nizhny Novgorod, IAP RAS Press, pp. 548–559
- Kulchin Yu.N., Voznesensky S.S., Galkina A.N., Gnedenkov S.V., Drozdov A.L. (2007b) *Bulletin of Far Eastern Branch of RAS* 1: 27–41 (in Russian)
- Kulchin Yu.N., Bukin O.A., Voznesensky S.S., Galkina A.N., Gnedenkov S.V., Drozdov A.L., Kuryavy V.G., Maltseva T.L., Nagorny I.G., Sinebruchov S.L., Therednichenko A.I. (2008) Fiber-optic waveguides on the base of natural biominerals – siliceous spicules of sea sponges. *Quantum Electronics* 38: 51–55
- Marcuse D. (1974) *Theory of dielectric optical waveguides*. Academic, New York
- Maslov D.V., Ostroumov E.E., Fadeev V.V. (2006) Saturation fluorimetry of complex organic compounds with a high local concentration of fluorophores (by the example of phytoplankton). *Quantum Electronics* 36: 163–168
- Müller W.E.G., Wendt K., Geppert Ch., Wiens M., Reiber A., Schröder H.C. (2006) Novel photoreception system in sponges? Unique transmission properties of the stalk spicules from the hexactinellid *Hyalonema sieboldi*. *Biosensors and Bioelectronics* 21: 1149–1155
- Müller W.E.G., Eckert C., Kropf K., Wang X., Schloßmacher U., Seckert C., Wolf S.E., Tremel W., Schröder H.C. (2007a) Formation of giant spicules in the deep-sea hexactinellid *Monorhaphis chuni* (Schulze 1904): electron-microscopic and biochemical studies. *Cell and Tissue Research* 329: 363–378
- Müller W.E.C., Wang X., Belikov S.I., Tremel W., Schloßmacher U., Natoli A., Brandt D., Boreiko A., Tahir M.N., Muller I.M., Schröder H.C. (2007b) Formation of siliceous spicules in demosponges: example *suberites domuncula*. In: Baeuerlein E. (ed) *Handbook of biomineralization. Biological aspects and structure formation*. Wiley-VCH, Weinheim, pp. 59–82
- Müller W.E.G., Wang X., Kropf K., Ushijima H., Geurtsen W., Eckert C., Tahir, M.N., Tremel W., Boreiko A., Schloßmacher U., Li J., Schröder H.C. (2008a) Bioorganic/inorganic hybrid composition of sponge spicules: matrix of the giant spicules and of the comitalia of the deep sea hexactinellid *Monorhaphis*. *Journal of Structural Biology* 161: 188–203
- Müller W.E.G., Boreiko A., Schloßmacher U., Wang X., Eckert C., Kropf K., Li J., Schröder H.C. (2008b) Identification of a silicatein(-related) protease in the giant spicules of the deep-sea hexactinellid *Monorhaphis chuni*. *The Journal of Experimental Biology* 211: 300–309
- Müller W.E.G., Schloßmacher U., Wang X., Boreiko A., Brandt D., Wolf S.E., Tremel W., Schröder H.C. (2008c) Poly(silicate)-metabolizing silicatein in siliceous spicules and sili-

- casomes of demosponges comprises dual enzymatic activities (silica polymerase and silica esterase). *FEBS Journal* 275: 362–370
- Samsonov G.V. (1978) Physical and chemical properties of oxides. Metalurgia Press, Moscow (in Russian)
- Schröder H.C., Brandt D., Schloßmacher U., Wang X., Tahir M.N., Tremel W., Belikov S.I., Müller W.E.G. (2007) Enzymatic production of biosilica glass using enzymes from sponges: basic aspects and application in nanobiotechnology (material sciences and medicine). *Naturwissenschaften* 94: 339–359
- Schröder H.C., Wang X., Tremel W., Ushijima H., Müller W.E.G. (2008) Biofabrication of biosilica-glass by living organisms. *Natural Product Report* 25: 455–474
- Smirnov S.V., Ania-Castanon J.D., Ellingham T.J., Kobtsev S.M., Kukarin S., Turitsyn S.K. (2006) Optical spectral broadening and supercontinuum generation in telecom applications. *Optical Fiber Technology* 12: 122–147
- Solimeno S., Crosignani B., Di Porto P. (1986) Guiding, Diffraction, and Confinement of Optical Radiation. Academic, San Diego, CA
- Sundar V.C., Yablon A.D., Grazul J.L., Ilan M., Aizenberg J. (2003) Fiber-optical features of a glass sponge. *Nature* 424: 899–900
- Uriz M.-J., Turon X., Becerro M.A., Agell G. (2003) Siliceous spicules and skeleton frameworks in sponges: origin, diversity, ultrastructural patterns, and biological functions. *Microscopy Research and Technique* 62: 279–299
- Vienne G., Xu Y., Jakobsen Ch., Deyerl H.-J., Jensen J.B., Sorensen T., Hansen T.P., Huang Y., Terrel M., Lee R.K., Mortensen N.A., Broeng J., Simonsen H., Bjarklev A. and Yariv A. (2004) Ultra-large bandwidth hollow-core guiding in all-silica Bragg fibers with nano-supports. *Optics Express* 12: 3500–3508
- Yariv A., Yeh P. (1984) Optical waves in crystals. Wiley, New York
- Yeh P., Yariv A., Hong C.S. (1977) Electromagnetic propagation in periodic stratified media. I. General theory. *Journal of Optical Society of America* 67: 423–438
- Yeh P., Yariv A., Marom E. (1978) Theory of Bragg fiber. *Journal of Optical Society of America* 68: 1196–1201
- Zheltikov A.M. (2004) Nonlinear optics of microstructure fibers. *Physics-Uspekhi* 47: 69–98
- Zheltikov A.M. (2007) Microstructure optical fibers for a new generation of fiber-optic sources and converters of light pulses. *Physics-Uspekhi* 50: 705–729

Nanobiotechnology: Soft Lithography

Elisa Mele and Dario Pisignano

1	Introduction	342
2	Key Elements of Soft Lithography	343
2.1	Replica Molding	343
2.2	Elastomeric Materials	345
3	Microcontact Printing	347
3.1	DNA and Protein Microarrays	349
4	Microfluidic Lithography	351
4.1	Patterning Strategies	353
4.2	Analytical Devices	355
5	Conclusions and Perspectives	356
	References	356

Abstract An entirely new scientific and technological area has been born from the combination of nanotechnology and biology: nanobiotechnology. Such a field is primed especially by the strong potential synergy enabled by the integration of technologies, protocols, and investigation methods, since, while biomolecules represent functional nanosystems interesting for nanotechnology, micro- and nano-devices can be very useful instruments for studying biological materials. In particular, the research of new approaches for manipulating matter and fabricating structures with micrometre- and sub-micrometre resolution has determined the development of soft lithography, a new set of non-photolithographic patterning techniques applied to the realization of selective proteins and cells attachment, microfluidic circuits for protein and DNA chips, and 3D scaffolds for tissue engineering. Today, soft lithographies have become an asset of nanobiotechnology. This Chapter examines the biological applications of various soft lithographic techniques, with particular attention to the main general features of soft lithography and of materials commonly employed with these methods. We present approaches particularly suitable

E. Mele and D. Pisignano (✉)

National Nanotechnology Laboratory of Istituto Nazionale di Fisica della Materia-Consiglio Nazionale delle Ricerche, Distretto Tecnologico ISUFI, Università degli Studi di Lecce, via Arnesano, I-73100 Lecce, Italy
e-mail: Dario.pisignano@unile.it

for biological materials, such as microcontact printing (μ CP) and microfluidic lithography, and some key micro- and nanobiotechnology applications, such as the patterning of protein and DNA microarrays and the realization of microfluidic-based analytical devices.

1 Introduction

The progress of the electronic industry, accomplished in the last decades in terms of both more efficient and less expensive miniaturized circuits, has been the consequence of the implementation and the development of micro- and nano-fabrication techniques. This development, in its turn, has encouraged a novel research field, investigating the possible integration of nanotechnology and biology. In fact, a large number of scientists have investigated the advantages offered by nanotechnology when applied to biological and medical purposes, and an entirely new scientific and technological area has been born from the combination of nanotechnology and biology: nanobiotechnology.

Such a field has been primed especially by the strong potential synergy enabled by this integration of technologies, protocols, and investigation methods, since on the one hand biomolecules represent functional nanosystems interesting for nanotechnology, and on the other hand micro- and nano-devices can be very useful instruments for studying biological materials. In particular, to achieve a full and satisfactory integration between these sciences, one would need to design new approaches for manipulating matter and for fabricating structures with micrometre- and sub-micrometre resolution, thus developing specific micro-nano-manufacturing technologies, highly compatible with biomolecules. Photolithography, electron- and focused-ion-beam and X-ray lithographies, together with scanning probe methods, are well-established and high-resolution approaches conventionally employed, with various degrees of reproducibility and complexity, for micro- and nanofabrication in the semiconductor field, but they are generally unsuitable for application to biological compounds. In addition, for many of these patterning approaches, the costs are still unaffordable for large-scale industry. In particular, serial lithographies such as electron-beam writing provide too low a throughput. This can be increased by a specific optimization of the process and of the exposed compounds; however, the cost per device very often still remains too high for production.

For these reasons, in the 1990s, G. M. Whitesides and co-workers have proposed a new set of non-photolithographic patterning techniques, collectively named as soft lithography (Xia and Whitesides 1998). These methods are characterized by the use of an elastomeric element to transfer a pattern to a target material. Soft lithographic approaches have been applied to the realization of patterned surfaces for selective proteins and cells attachment, microfluidic circuits for protein and DNA chips, and 3D scaffolds for tissue engineering (Whitesides 2006). Today, soft lithographies have become an asset of nanobiotechnology.

This Chapter examines the biological applications of various soft lithographic techniques. The main general features of soft lithography and of the materials commonly employed with these methods are described in Section 2. Some soft lithographic approaches which are particularly suitable for biological materials, such as microcontact printing (μ CP) (Section 3) and microfluidic lithography (Section 4) are then introduced, together with some key micro- and nanobiotechnology applications, such as the patterning of protein and DNA microarrays and the realization of microfluidic-based analytical devices.

2 Key Elements of Soft Lithography

Among the different lithographic techniques, developed over the past decade as alternatives to optical lithography for realizing high-quality micro- and nanostructures, have been electron and ion beams, X-rays, scanning probes (Ross et al. 1993), imprinting lithographies (Chou et al. 1995, 1996), self-assembling (Kumar and Whitesides 1993), atom lithography (Mutzel et al. 2002), and micro-plasma discharges (Chai et al. 2005). Soft lithography represents a low-cost and high-throughput method, which is directly applicable onto biomolecules. Soft lithography includes a series of patterning approaches, all of them characterized by the use of elements fabricated by texturing elastomeric polymers, to transfer a pattern to a substrate: replica molding (Xia et al. 1996), microcontact printing (Kumar and Whitesides 1993), microtransfer molding (Zhao et al. 1996), micromolding in capillaries (Kim et al. 1995), and solvent-assisted micromolding (Kim et al. 1997). The key feature of the soft techniques is the use of poly(dimethylsiloxane) (PDMS), or other elastomeric compounds, to replicate the geometry of a starting master. This operation principle offers the possibility to produce faithful copies (replicas) of complex features of the master, and to accomplish sub-100 nm resolution without the drawbacks related to optical diffraction, which affect photolithography. Even more importantly, the chemical and physical properties of the employed elastomers have a large number of advantages, conferring on these technologies an unequalled chemical flexibility, moreover being easy and inexpensive. These characteristics make soft lithography an excellent technological tool for biomaterials with potential applications in proteomics, medical diagnostics, biological assays (Mrksich and Whitesides 1995), and in the formation of tissue engineering templates (Patel et al. 1998).

2.1 *Replica Molding*

The Replica molding (REM), namely the generation of elastomeric replicas of a previously fabricated master structure, is the enabling technique of soft lithography (Xia et al. 1996). The scheme of the overall REM process is shown in Fig. 1

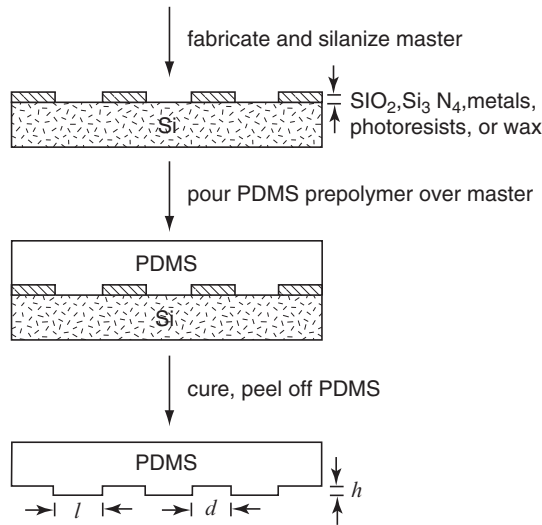


Fig. 1 Scheme of the replica molding (REM) procedure for realizing poly(dimethylsiloxane) (PDMS) replicas (Image reproduced from Xia and Whitesides 1998. With permission)

(Xia and Whitesides 1998). The surface of a master, containing relief micro- or nano-features, is coated by an elastomeric prepolymer in the liquid state. After the complete, in situ, polymerization of the elastomer, generally performed by thermal curing, the replica can be peeled off from the master by slightly reversible deformations. The final result is a faithful negative copy of the master pattern. The high quality of the replication is guaranteed by the elastic nature of the polymer, which allows one to replicate the initial master structure many times without damage, and also 3D structures in a single step. REM technology is incomparably inexpensive in comparison with all the other fabrication approaches, and it can be carried out in ambient laboratory conditions, without clean-room facilities. These characteristics make REM a sub-micrometre patterning method particularly accessible for biological laboratories. The rapid prototyping method of REM allows the cost of the fabrication of the master to be spread over tens of final samples; this makes possible the use of high-resolution advanced lithographies (particularly electron-beam writing) for producing the initial structure, then for it to be replicated many times almost without additional cost. The REM processes are a direct demonstration that *soft nanotechnology* (besides producing patterns and devices for generation, processing, transmission and detection of signals) *is able to replicate the information* provided by the master features.

The elastomer conventionally used is PDMS, exhibiting a Young's modulus of about 3 MPa. Recently, other polymeric compounds with different physical properties (Young's modulus of about 9 MPa) have been developed for high-resolution patterning, such as a polymeric composite based on vinyl and hydrosilane (Schmid and Michel 2000), or photocurable polymers (Choi and Rogers 2003). The basic property of all the elastomers used in REM is their capability to prime and propagate a conformal contact over large areas of the target substrates of interest. The intimate

contact between the elastomeric stamp and the substrate, both at macroscopic and microscopic level, is common to all the soft lithographic techniques, and important for favoring the pattern transfer in microcontact printing, the reversible or irreversible sealing of channels in microfluidics, or for structuring non-planar surfaces.

The chemico-physical properties of PDMS, and especially its biocompatibility, make it highly useful for biotechnology. Moreover, its surface can be treated in different ways in order to change the interfacial free energy, as described in the following section. The possibility of modifying the surface chemistry of PDMS allows one to design elastomeric stamps for specific applications, and, for example, to realize microdimensional force sensor arrays for cell attachment and motion, consisting of discrete arrays of PDMS micropillars (Du Roure et al. 2005), as shown in Fig. 2.

2.2 Elastomeric Materials

The PDMS is the most used polymer in soft lithography. It is a linear polymer, with a Si–O backbone and two methyl side-groups for each Si atoms. PDMS exhibits a series of properties useful for biological applications: it is chemically

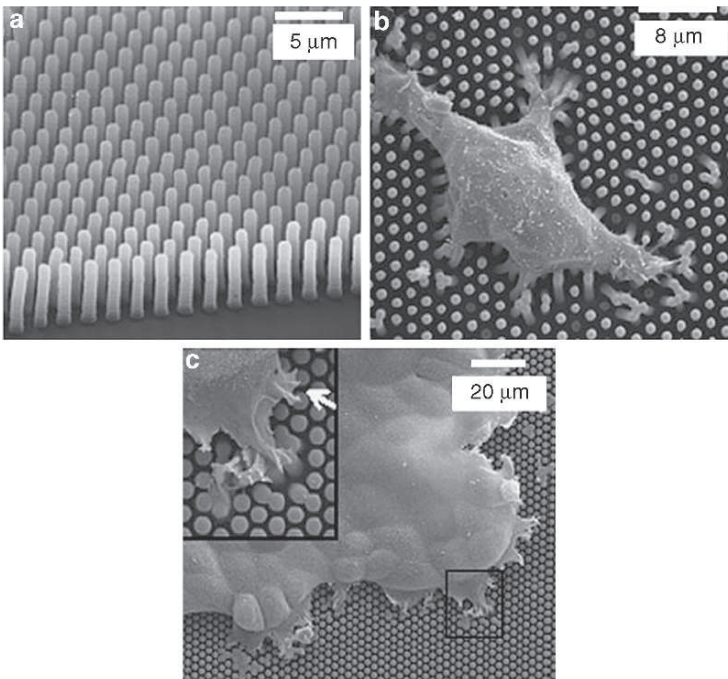


Fig. 2 (a) Array of poly(dimethylsiloxane) (PDMS) pillars. (b) Individual cells lying. (c) Cell monolayer. (c inset): magnified view of the area delimited by the *black square* (Image reproduced from Du Roure et al. 2005. With permission)

inert, transparent for wavelengths from the near UV to the near-IR (300–800 nm), thus being compatible with optical detection, non toxic to proteins (Delamarche et al. 1997), and gas-permeable (Merkel et al. 2000). Moreover, it is stable at the temperatures required for biological procedures (40–95°C).

The commercially available PDMS is generally composed by a base and a curing agent. It is in the liquid state at room temperature, with a typical viscosity ranging from 10^{-3} to 10^3 Pa s, and its polymerization is typically carried out by thermal curing. The low value of the Young's modulus (3 MPa) guarantees the conformal contact with different target substrates, although reducing the mechanical stability of the elastomeric features, with a possible loss of resolution. The molds can suffer distortions, collapse of high-aspect ratio (>2) features, and sagging of low-aspect ratio (<0.2) ones by mutual adhesion and by gravity and replica-substrate adhesion, respectively (Xia and Whitesides 1998; Zhou et al. 2005; Hsia et al. 2005). For high-resolution (sub-micrometre) templates, new types of elastomers have been proposed, exhibiting larger Young's modulus, such as the so-called hard PDMS (*h*-PDMS), which is obtained by blending siloxanes with vinyl and hydride groups, cross-linking via a platinum catalyzed hydrosilylation reaction (Schmid and Michel 2000).

The surface properties of the elastomeric replicas are particularly important. PDMS is characterized by a surface energy value of around 22 mN/m, being hydrophobic (water contact angle about 110°). Small hydrophobic molecules, biopolymers, and cells can irreversibly adsorb to the surface. Methods have therefore been developed to tailor the surface energy, in order to render the PDMS more hydrophilic. Plasma oxygen treatments have been widely validated as methods for creating superficial silanol functional groups (Duffy et al. 1998) that can be used as reactive sites for subsequently bonding organic groups (Makamba et al. 2003; Hu et al. 2002). Other techniques include UV-exposure (Vasilets et al. 1998), UV/ozone irradiation (Ouyang et al. 2000), photograft polymerization (Wang et al. 2005), and attachment of hydrophobic molecules onto the surface (Boxshall et al. 2006).

The elastomeric polymers employed in soft lithography also present another important advantage over glass, silicon, and hard plastics, namely the capability to be bonded, reversibly or irreversibly, to different substrates. For instance, the sealing of PDMS is easy, because high temperatures, pressures, or voltages are not required. The bonding of glass to glass or silicon to silicon requires, instead, temperature values in the range of 600–1,000°C, or anodic bonding with voltages up to 500 V. Moreover, PDMS can be sealed to PDMS, glass, silicon, polystyrene, polyethylene, and other materials, thus allowing one to realize both monolithic and hybrid devices, which are particularly useful for microfluidic applications.

The reversible sealing is mediated by van der Waals forces that allow PDMS elements to provide conformal contact with other surfaces. This is a fast method, simply consisting in placing the stamp onto the target surface; it occurs at room temperature and it is watertight. The removal of PDMS replica from the target surface breaks the seal, which can be again accomplished on other substrates without damage in the PDMS features.

The irreversible sealing can be obtained in different ways, depending on the target surfaces to be bonded. A common approach relies on exposing functional chemical groups on the surface of both PDMS and the substrate by oxygen plasma.

The plasma treatment determines the formation of silanol groups on PDMS, and –OH- containing functional groups on the other materials. When the two surfaces are brought into contact, there is the formation of covalent –O–Si–O-bonds that irreversibly seal the oxidized replica to the substrate (Owen and Smith 1994). Whenever sealing involves two PDMS stamps, a thermal approach can also be used. The PDMS elements can be realized by using different relative ratios of monomer and curing agent, which are then placed in mutual contact and thermally cured together, thus obtaining an irreversible bond.

3 Microcontact Printing

The microcontact printing (μ CP), originally proposed to realize self-assembled monolayers of alkanethiolates onto gold surfaces (Kumar and Whitesides 1993), is nowadays used for patterning onto solid supports complex biomolecules, such as proteins (Bernard et al. 1998, 2000; James et al. 1998) and DNA (Smith et al. 2001), and to control the spatial distribution of living cells on surfaces (Kane et al. 1999). In particular, the μ CP technology is suitable for directly immobilizing proteins in well-defined, spatially and geometrically controlled areas of the substrate.

The μ CP is based on the *localized delivery of molecules able to self-assemble onto a suitable surface, by means of the contact of raised features of the elastomeric replicas inked with a solution of the molecules and acting as dry reservoir*. The basic idea is the use of elastomeric templates with relief features to transfer molecules of a molecular ink onto a target surface by mechanical contact (Fig. 3) (Biasco et al. 2005). Importantly, soft lithography can template the self-assembling of molecules. Self-assembling systems are characterized by relatively weak attractive interactions, often balanced by other forces tending to disrupting the inter-components bonds (such as repulsive intermolecular forces, thermal agitation, etc.), which are of the same order of magnitude as the attraction. *This is a basic prerequisite of the self-assembly, since it guarantees that the inter-components associations are not irreversible*, thus leaving a *high degree of adjustability* to the system, which is able to find the most favored (i.e., the ordered) energetic configurations. Templating self-assembling molecules against elastomeric elements, during the evaporation of solvents and the subsequent sandwiching in contact with the target surface, turned out to be a powerful method to obtain ordered nanostructures.

Briefly, the process steps are the following: after the realization of an elastomeric stamp by REM, the replica is wetted with a solution of the biological material of interest, for example proteins. After drying the solution in excess, a layer of proteins remains on the surface of the stamp. Then, the replica is placed in conformal contact, for times ranging from a few seconds to many minutes, with a surface (glass slides, Petri dishes, silicon, metals, etc., possibly functionalized with proper bonding groups) and, upon peeling off, the proteins are transferred to the substrate. The anchoring mechanism can be aspecific (mainly electrostatic), such as that of proteins on glass, or strongly specific (covalent), such as the adhesion of streptavidin on biotinylated species. In this way, only selected regions of the target

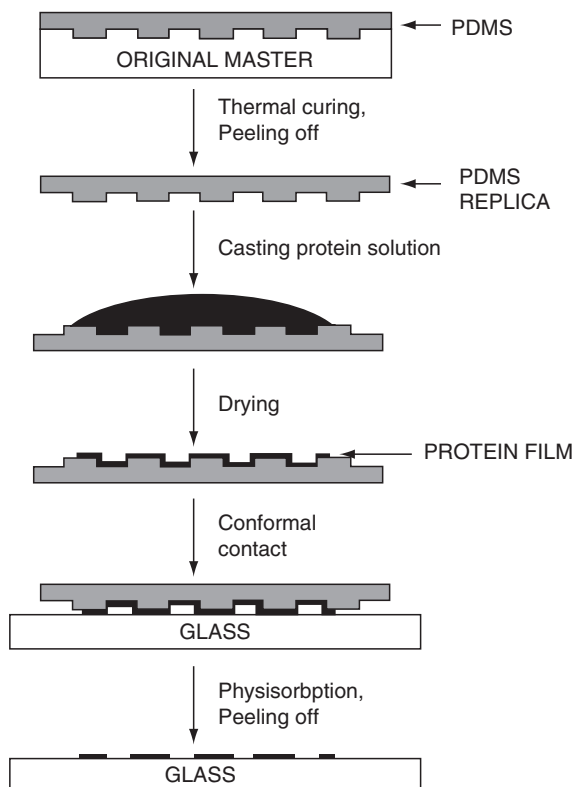


Fig. 3 Schematic diagram of the microcontact printing (μ CP) procedure (Image reproduced from Biasco et al. 2005. With permission)

surface are covered by the protein layer, i.e., the areas corresponding to the relief features in the replica, thus resulting in an accurate control of the spatial arrangement of the deposited biomolecules.

Although a lot of work has been carried out in the direct printing of biomolecules onto surfaces, the evaluation of the possible structural changes induced on proteins has not yet been fully addressed. The drying process and the interaction of the biomaterial with the solid surface, in fact, could determine aggregation phenomena and a partial or complete loss of functionality of the used biomaterial. However, it seems that, in the most cases, the μ CP preserves the biological activity of the involved species, since the process is carried out entirely working at room temperature and using only the solvent compatible with the molecule of choice for casting. For instance, physiological patterns of the extracellular matrix protein, laminin-1, have been obtained on glass substrates by physisorption-assisted μ CP (Sgarbi et al. 2004). Besides the well-retained antigenicity, which has been tested by means of immunofluorescence assays, the characteristic protein self-assembling in polygonal networks has been found with the well-defined sub-100-nm quaternary structures of laminin. These physiological mesh-like protein matrices were obtained by one-step

μ CP, without preliminary functionalization of the involved surfaces, and have many potential applications for cell cultures and biomolecular devices.

Finally, the μ CP can be straightforwardly combined with the standard detection and characterization procedures employed in biology, in particular with fluorescent microscopy. Because this patterning technology is compatible with fluorescence labelling, the involved species can be marked with optically responsive dyes. In this way, it is possible to carefully characterize the patterned surfaces to check the success of the inking and the printing procedures.

3.1 DNA and Protein Microarrays

The μ CP has been applied to the patterning of a wide range of biomaterials and it has good potentialities also for the fabrication of microarrays. It allows one to stamp large areas with high-density patterns of biomolecules, which offers a series of advantages in genomics and proteomics. Miniaturization means, in fact, the increasing of the rate of data generation. The development of DNA microarrays, in particular, has made possible the simultaneous monitoring of the expression of thousands to tens of thousands of genes in a single experiment. Figure 4 shows

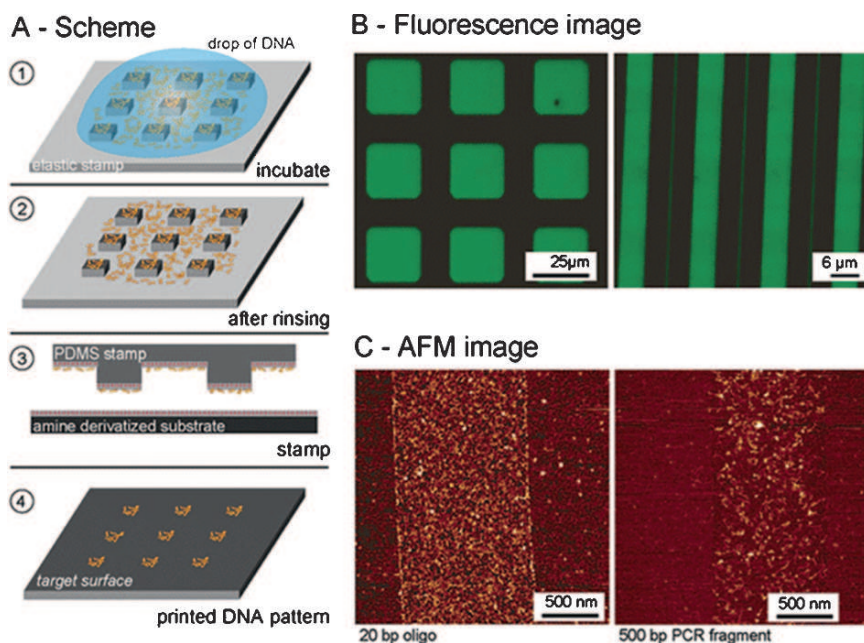


Fig. 4 Microcontact printing (μ CP) of DNA molecules. (a) Scheme of DNA printing. Fluorescence images of patterned oligonucleotides on a glass surface (*top*). One micrometre lines of oligonucleotides, imaged by atomic force microscopy (*bottom*) (Image reproduced from Lange et al. 2004. With permission)

patterns of DNA molecules onto solid surfaces fabricated by μ CP. It has been demonstrated that the realizing DNA arrays with micrometre-resolution favors the realization of a functional hybridization assay (Lange et al. 2004).

The transfer of proteins onto surfaces is interesting, for example, in drug-discovery, analytical assays, and proteomics. Different approaches can be used to fabricate arrays of proteins, such as ink-jet printing (Roda et al. 2000) and electrospray through a dielectric grid mask (Morozov and Morozova 1999). In any case, the challenge in the fabrication of protein microarrays is the ability to work in parallel with many different proteins. The μ CP method offers the possibility to carry out subsequent patterning steps on the same substrate with a large number of different proteins, as shown in Fig. 5 (Bernard et al. 2000), because the patterning of molecules from the elastomeric stamp to the target surfaces can be made practically

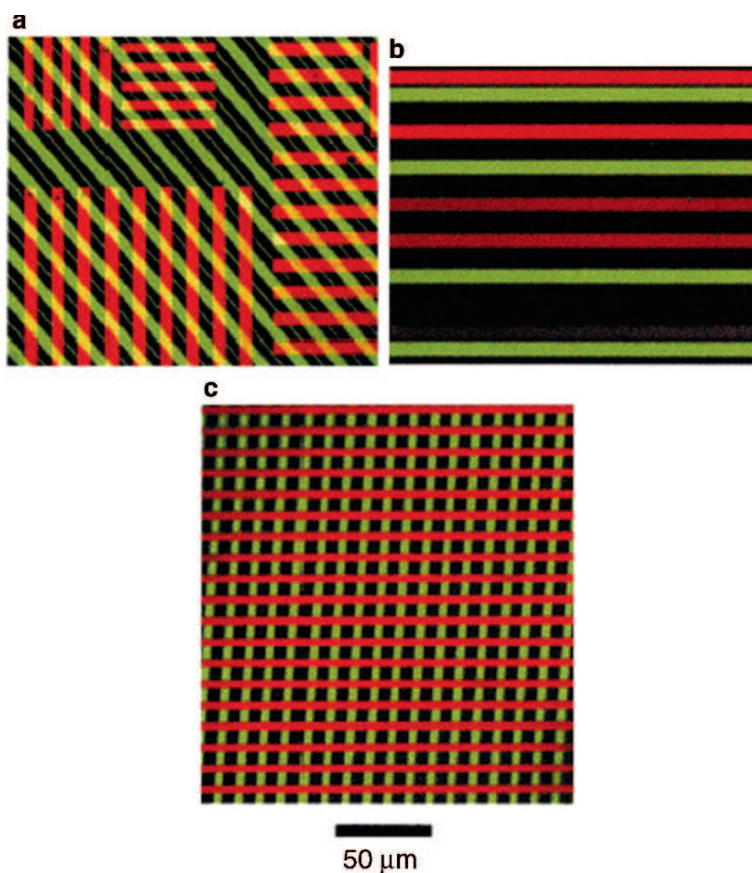


Fig. 5 Immunofluorescence images of proteins transferred onto a substrate by microcontact printing (μ CP). (a) Two-protein pattern. (b) Pattern of 16 different proteins. (c) Three-protein pattern (Image reproduced from Bernard et al. 2000. With permission)

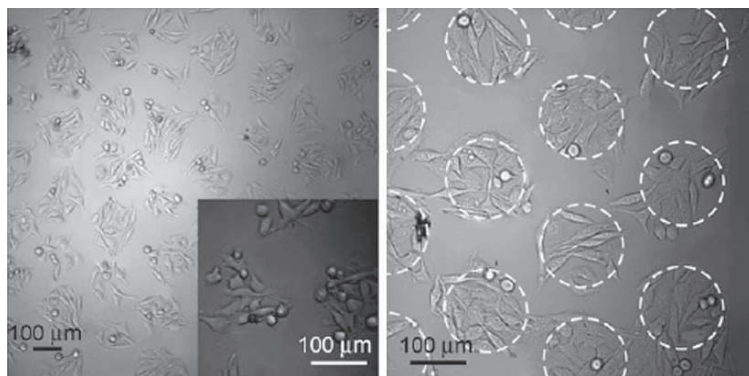


Fig. 6 Patterns of cells obtained by microcontact printing (μ CP) of proteins (Image reproduced from Rozkiewicz et al. 2006. With permission)

unidirectional. In this way, the patterning strategy simply consists in printing many times on the same substrate, using different stamps having different patterns or various inks without loss of contrast or resolution. Finally, the spatially localized immobilization of proteins onto a substrate surface can also be interesting in view of the direct adhesion of cells. As illustrated in Fig. 6, μ CP has also been employed for controlling locally cell attachment by the adsorption of extracellular matrix proteins onto selected areas of a substrate (Rozkiewicz et al. 2006).

4 Microfluidic Lithography

Microfluidic lithography, also called micromolding in capillaries, is one of the most interesting lithographic technique for biological applications and for the realization of analytical devices. The pattern formation is the result of the motion of a liquid (biomolecule solutions, buffers, fluid prepolymers, etc.) driven by capillarity into micro- or nanochannels (Xia and Whitesides 1998; Kim et al. 1996). The manipulation of very minute fluid volumes (in the nanolitre to picolitre range) in capillaries offers many advantages: reduction in reagent and sample and waste volumes, more homogeneous reaction conditions and shorter times for diffusion-driven reactions, the possibility of high integration with automation, and massive parallel processing. By analogy with electronic integrated circuits, microfluidic functional elements (fluid injectors, filters, pumps, valves, mixers, separation elements, detectors) can be used and assembled as building blocks for lab-on-chips specifically designed for genomics and proteomics (Whitesides 2006).

The lithographic procedure is schematized in Fig. 7 (Kim et al. 1996). Similarly to other soft lithographies, the first step is fabricating an elastomeric replica of a master, constituted by a network of hydraulically connected capillaries, by REM. The stamp is manually or automatically cut to expose the micro/nano-channels,

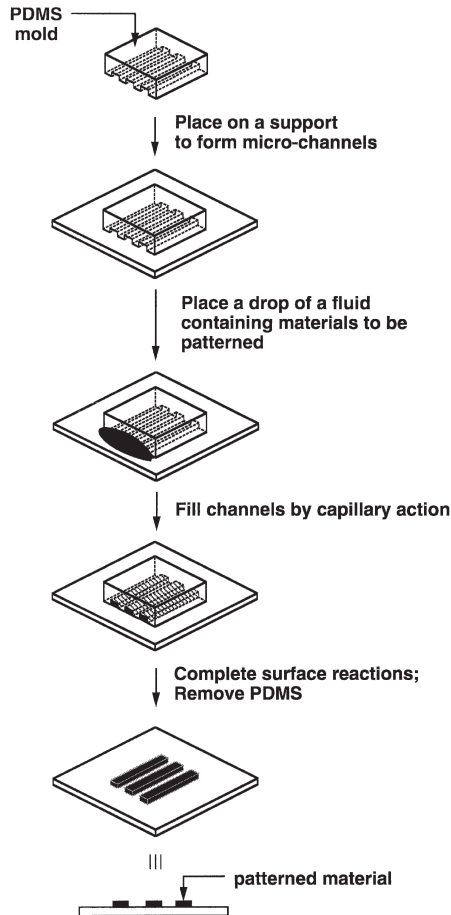


Fig. 7 Schematic illustration of the microfluidic lithographic procedure (Image reproduced from Kim et al. 1996. With permission)

and placed in contact with the target substrate under its own weight. A liquid drop is deposited at the edge of the mold, in order to make the channels spontaneously filled by capillary action. After a surface reaction, assisted by the solvent evaporation, or by the curing of the prepolymer in the case of monomer solutions, the template is peeled off and the pattern is stably transferred to the substrate.

The pressure difference between the initial and the final part of the capillary is responsible for the liquid penetration. For many liquids, the filling rate of the capillary is described by the equation (Kim et al. 1996):

$$\frac{dz}{dt} = \frac{R\gamma \cos \Theta}{4\eta} \quad (1)$$

where η , R , γ and Θ indicate the liquid viscosity, the hydraulic radius of the capillary, the liquid–vapor interfacial free energy of the fluid, and the contact angle

between the liquid and the surface of the capillary, respectively. Hence, the velocity of a fluid inside a microchannel strongly depends on the geometry of the adopted fluidic network.

In addition to spontaneous capillarity, other methods have been developed to drive liquids inside microchannels, including capillary electrophoresis (Jacobson et al. 1996), electro-osmotic flow (Pennathur and Santiago 2005), and mechanical syringes or pumps (Kopp et al. 1998). The use of external pumping devices, such as syringe pumps, offers a high control of the flow rate (down to a few tens of nanolitres/minute), and of the delivered volumes of liquid, which is almost impossible relying on spontaneous capillarity only. Moreover, a constant fluid velocity can be obtained in microchannels, thus overcoming the drawback of the intrinsic slowness of microfluidics, that has previously limited its application to large-area patterning.

Microfluidic lithography has been shown to be suitable for a number of applications, including the realization of polymeric and optically amplified waveguides (Yang et al. 2000), fully plastic field-effect transistors (Beh et al. 1999), and directional carbon nanotube strings (Chen and Weimer 2002). It is a remarkably simple procedure and, unlike conventional exposure-development-etching lithographies, and similar to μ CP, it is additive, thus minimizing the material wastes.

4.1 Patterning Strategies

The unique characteristics of microfluidics in terms of manipulation of liquids into spatially separated microchannels offer the possibility of guiding solutions of bio-materials over different regions of a substrate, and of localizing biochemical reactions on a surface with high resolution and contrast. This technique is interesting for simultaneously patterning lines of proteins (Delamarche et al. 1998) or antigens (Bernard et al. 2001) onto a surface. In Fig. 8, a micromosaic immunoassay realized by microfluidics is displayed (Bernard et al. 2001).

Another property of microfluidics, making it very appealing for biotechnology, is the occurrence of laminar fluid flow inside microchannels. A liquid flow is laminar when adjacent streams of fluids are mutually parallel, and mixing occurs only by diffusion; vice versa, in turbulent flows, turbulence mixes the streams. The parameter that describes these two regimes is the Reynolds number: $Re = vl\rho/\eta$, where v is the velocity of the fluid, l is the channel cross-section, ρ is the density of the fluid, and η is the viscosity of the fluid. For typical microfluidic channels (cross section of about $100\mu\text{m}$), Re is down to 1, which indicates that the flow is laminar. Consequently, parallel liquid streams can be used for patterning in a single channel different materials simultaneously, without inter-mixing. In this way, it possible to arrange proteins and cells within selective patterns (Takayama et al. 1999).

Interesting microfluidic devices that exploit the laminar flow are the T sensors (Kamholz et al. 1999) and the H filters (Brody et al. 1996). In a T sensor, two streams of different liquids flow inside a channel. When the solute molecules in each stream diffuse into the other, an interdiffusion zone is formed. An example of

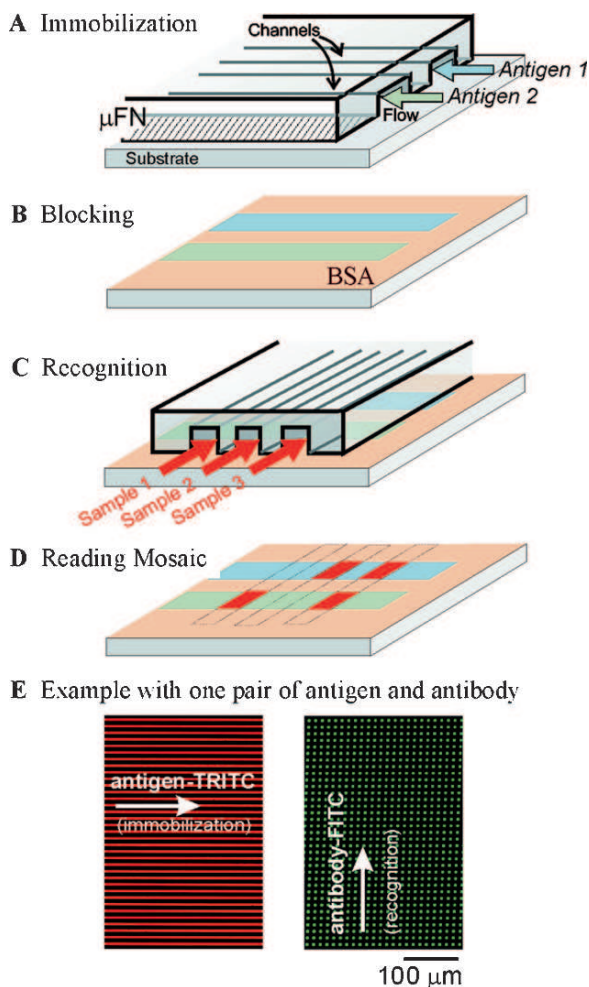


Fig. 8 Strategy for performing biological patterning by microfluidic lithography. (a) Pattern of different antigens along single lines on a substrate. (b) The unpatterned area of the substrate is blocked with albumin to prevent aspecific protein binding in subsequent steps. (c) Antibodies flowing through the channels of a second pattern locally bind to the patterned antigens. (d) Reading the binding pattern reveals the amount of present antibodies. (e) A mosaic can be read by fluorescence microscopy (Image reproduced from Bernard et al. 2001. With permission)

a T sensor application is the injection of an antibody solution alongside a solution of known, labeled antigen. The antigen–antibody binding occurs only in the inter-diffusion region, where there is an accumulation of the marked species, whereas the unmarked antigen can be detected differentially (Hatch et al. 2001). H-filters are instead based on the continuous extraction of molecular analytes from fluids without a membrane (Brody et al. 1996). With an H filter, for example, the lysis of a cell membrane has been demonstrated (Schilling et al. 2002).

4.2 Analytical Devices

Lithography has been recently employed also for the realization of multifunctional, microfluidic-based devices, which offer a high degree of integration, presenting potential applications in biomolecular separations, enzymatic assays, polymerase chain reaction (PCR), and immunohybridization reactions. Many biotechnology and pharmaceutical researchers have employed microfluidic chips, especially in the area of high-throughput drug screening, DNA sequencing, gene-expression profiling, protein analysis, and cell-based assays (Auroux et al. 2002).

The realization of lab-on-chips or micro-total analysis systems (μ TAS) requires the integration of all the functional components necessary for carrying out conventional, macroscopic analytical, procedures, within a highly portable chip. The first expertise needed for fabricating μ TAS is the ability to seal irreversibly the patterned layer, containing the microfluidic networks, with a flat surface that operates as support. As described in Section 2.3, PDMS and others elastomers employed in soft lithography offer a high flexibility and ease of bonding both with other polymers and with silicon and glass. Hence, the realization of monolithic and hybrid devices with these polymers is facilitated. Moreover, microfluidic chips can be interconnected with external pumps and valves, in order to achieve a good control of the flow rate of the injected biological solutions, and with optical devices and detection elements, sensors, and heaters. All these elements are necessary for accomplishing and detecting bio-chemical reactions: for instance, lab-on-chip devices for PCR integrate microfluidic networks and heaters for reaching the temperature values required for denaturation, extension, and annealing (Fig. 9) (deMello 2003).

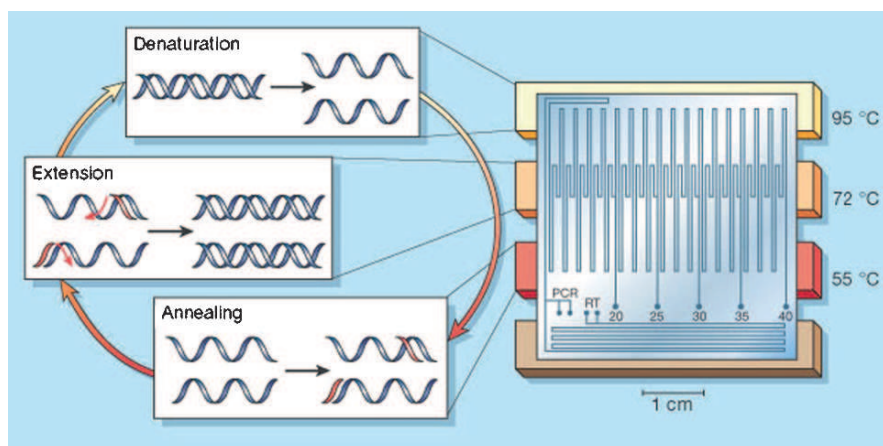


Fig. 9 Scheme of a microfluidic chip for PCR, characterized by three regions at different temperature for the required PCR steps (Image reproduced from deMello 2003. With permission)

5 Conclusions and Perspectives

Soft lithographies such as μ CP and microfluidics are simple, versatile, and high-throughput patterning techniques, suitable for a wide range of molecules of interest for biotechnological applications. Some issues need to be investigated in more depth, particularly the achievable degree of reproducibility in patterning organics and biomaterials at the sub-micrometre scale, and the capability of performing multilevel lithographic processes (layer by layer) despite the distortions inevitably occurring in the employed plastic materials. However, the flexibility, ease of use, and biocompatibility of these technologies certainly deserve to be fully exploited in nanobiotechnology.

New possibilities, in terms of concepts and devices, can be opened up by the applications of these methods to biomaterials, and particularly to biomineralization processes. By virtue of their intrinsic compatibility with proteins and other biomolecules, soft printing and microfluidic networks can be fruitfully specialized to the case of bio-mimetic materials. Since the main mission of nanotechnologies is the realization of nanostructured materials exhibiting novel properties and high performances, the integration of patterning methods and controlled biomineralization is particularly intriguing aiming at mimicking the nature capability of positioning molecules and assembling complex supramolecular structures with order ranging from the nanoscopic to the macroscopic scale. One of the most important goals of this research is obtaining nanomaterials and nanocomposites under mild physiological conditions, and with well-defined hierarchical architectures, similar to the way in which biosilica is produced by many marine organisms.

References

- Auroux P-A, Iossifidis D, Reyes D R, Manz A (2002) Micro total analysis systems. 2. Analytical standard operations and applications. *Anal Chem* 74:2637–2652
- Beh W S, Kim I T, Qin D, Xia Y, Whitesides G M (1999) Formation of patterned microstructures of conducting polymers by Soft Lithography, and applications in microelectronic device fabrication. *Adv Mater* 11:1038–1041
- Bernard A, Delamarche E, Schmid H, Michel B, Bosshard H R, Biebuyck H (1998) Printing patterns of proteins. *Langmuir* 14:2225–2229
- Bernard A, Renault J P, Michel B, Bosshard H R, Delamarche E (2000) Microcontact Printing of proteins. *Adv Mater* 12:1067–1070
- Bernard A, Michel B, Delamarche E (2001) Micromosaic immunoassays. *Anal Chem* 73:8–12
- Biasco A, Pisignano D, Krebs B, Pompa P P, Persano L, Cingolani R, Rinaldi R (2005) Conformation of microcontact-printed proteins by atomic force microscopy molecular sizing. *Langmuir* 21:5154–5158
- Boxshall K, Wu M-H, Cui Z, Cui Z, Watts J F, Baker M A (2006) Simple surface treatments to modify protein adsorption and cell attachment properties within a poly(dimethylsiloxane) micro-bioreactor. *Surf Interface Anal* 38:198–201
- Brody J P, Yager P, Goldstein R E, Austin R H (1996) Biotechnology at low Reynolds numbers. *Biophys J* 71:3430–3441
- Chai J, Li B, Kwok D Y (2005) Selective surface modification and patterning by a micro-plasma discharge. *Appl Phys Lett* 86:034107-1-3

- Chen J, Weimer W A (2002) Room-temperature assembly of directional carbon nanotube strings. *J Am Chem Soc* 124:758–759
- Choi K M, Rogers J A (2003) A photocurable poly(dimethylsiloxane) chemistry designed for soft lithographic molding and printing in the nanometer regime. *J Am Chem Soc* 125:4060–4061
- Chou S Y, Krauss P R, Renstrom P J (1995) Imprint of sub-25 nm vias and trenches in polymers. *Appl Phys Lett* 67:3114–3116
- Chou S Y, Krauss P R, Renstrom P J (1996) Imprint lithography with 25-nanometer resolution. *Science* 272:85–87
- Delamarche E, Bernard A, Schmid H, Michel B, Biebuyck H (1997) Patterned delivery of immunoglobulins to surfaces using microfluidic networks. *Science* 276:779–781
- Delamarche E, Bernard A, Schmid H, Bietsch A, Michel B, Biebuyck, H A (1998) Microfluidic networks for chemical patterning of substrates: design and application to bioassays. *J Am Chem Soc* 120:500–508
- deMello A J (2003) DNA amplification moves on. *Nature* 422:28–29
- Duffy D C, McDonald J C, Schueller J A, Whitesides G M (1998) Rapid prototyping of microfluidic systems in poly(dimethylsiloxane). *Anal Chem* 70:4974–4984
- Du Roure O, Saez A, Buguin A, Austin R H, Chavrier P, Siberzan P, Ladoux B (2005) Force mapping in epithelial cell migration. *Proc Natl Acad Sci USA* 102:2390–2395
- Hatch A, Kamholz A E, Hawkins K R, Munson M S, Schilling E A, Weigl B H, Yager P (2001) A rapid diffusion immunoassay in a T-sensor. *Nat Biotechnol* 19:461–465
- Hsia K J, Huang Y, Menard E, Park J-U, Zhou W, Rogers J, Fulton J M (2005) Collapse of stamps for soft lithography due to interfacial adhesion. *Appl Phys Lett* 86:154106-1-3
- Hu S, Ren X, Bachman M, Sims C E, Li G P, Allbritton N L (2002) Surface modification of poly(dimethylsiloxane) microfluidic devices by ultraviolet polymer grafting. *Anal Chem* 74:4117–4123
- Jacobson S C, Ramsey J M (1996) Integrated microdevice for DNA restriction fragment analysis. *Anal Chem* 68:720–723
- James C D, Davis R C, Kam L, Craighead H G, Isaacson M, Turner J N, Shain W (1998) Patterned protein layers on solid substrates by thin stamp microcontact printing. *Langmuir* 14:741–744
- Kamholz A E, Weigl B H, Finlayson B A, Yager P (1999) Quantitative analysis of molecular interaction in a microfluidic channel: the T-sensor. *Anal Chem* 71:5340–5347
- Kane R S, Takayama S, Ostuni E, Ingber D E, Whitesides G M (1999) Patterning proteins and cells using soft lithography. *Biomater* 20:2363–2376
- Kim E, Xia Y, Whitesides G M (1995) Polymer microstructures formed by moulding in capillaries. *Nature* 376:581–584
- Kim E, Xia Y, Whitesides G M (1996) Micromolding in capillaries: applications in materials science. *J Am Chem Soc* 118:5722–5731
- Kim E, Xia Y, Zhao X-M, Whitesides G M (1997) Solvent-assisted microcontact molding: a convenient method for fabricating three-dimensional structures on surfaces of polymers. *Adv Mater* 9:651–654
- Kopp M U, de Mello A J, Manz A (1998) Chemical amplification: continuous-flow PCR on a chip. *Science* 280:1046–1048
- Kumar A, Whitesides G M (1993) Features of gold having micrometer to centimeter dimensions can be formed through a combination of stamping with an elastomeric stamp and an alkanethiol ‘ink’ followed by chemical etching. *Appl Phys Lett* 63:2002–2004
- Lange S A, Benes V, Kern D P, Holrber J K H, Bernard A (2004) Microcontact printing of DNA molecules. *Anal Chem* 76:1641–1647
- Makamba H, Kim J H, Lim K, Park N, Hahn J H (2003) Surface modification of poly(dimethylsiloxane) microchannels. *Electrophoresis* 24:3607–3619
- Merkel T C, Bondar V I, Nagai K, Freeman B D, Pinnau I (2000) Gas sorption, diffusion, and permeation in poly(dimethylsiloxane). *J Polym Sci Part B: Polym. Phys* 38:415–434
- Morozov V N, Morozova T (1999) Electrospray deposition as a method for mass fabrication of mono- and multicomponent microarrays of biological and biologically active substances. *Anal Chem* 71:3110–3117

- Mrksich M, Whitesides G M (1995) Patterning self-assembled monolayers using microcontact printing: a new technology for biosensors? *Trends Biotechnol* 13:228–235
- Mutzel M, Tandler S, Haubrich D, Meschede D, Peithmann K, Flaspohler M, Buse K (2002) Atom lithography with a holographic light mask. *Phys Rev Lett* 88:083601-1-4
- Ouyang M, Yuan C, Muisener R J, Boulares A, Koberstein J T (2000) Conversion of some siloxane polymers to silicon oxide by UV/ozone photochemical processes. *Chem Mater* 12:1591–1596
- Owen M J, Smith P J (1994) Plasma treatment of polydimethylsiloxane. *Adhesion Sci Technol* 8:1063–1075
- Patel N, Padera R, Sanders G H W, Cannizzaro S M, Davies M C, Langer R, Roberts C J, Tendler S J B, Williams P M, Shakesheff K M (1998) Spatially controlled cell engineering on biodegradable polymer surfaces. 112:1447–1454
- Pennathur S, Santiago J G (2005) Electrokinetic transport in nanochannels. 1. Theory *Anal Chem* 77:6772–6781
- Roda A, Guardigli M, Russo C, Pasini P, Baraldini, M (2000) Protein microdeposition using a conventional ink-jet printer. *BioTechniques* 28:492–496
- Ross C B, Sun L, Crooks R M (1993) Scanning probe lithography. 1. Scanning tunneling microscope induced lithography of self-assembled n-alkanethiol monolayer resists. *Langmuir* 9: 632–636
- Rozkiewicz D I, Kraan Y, Werten M W T, De Wolf F A, Subramaniam V, Jan Ravoo B, Reinhoudt D N (2006) Covalent Microcontact Printing of proteins for cell patterning. *Chem Eur J* 12:6290–6297
- Schilling E A, Kamholz A E, Yager P (2002) Cell lysis and protein extraction in a microfluidic device with detection by a fluorogenic enzyme assay. *Anal Chem* 74:1798–1804
- Schmid H, Michel B (2000) Siloxane polymers for high-resolution, high-accuracy soft lithography. *Macromolecules* 33:3042–3049
- Smith E A, Wanat M J, Cheng Y, Barreira S V P, Frutos A G, Corn R M (2001) Formation, spectroscopic characterization, and application of sulfhydryl-terminated alkanethiol monolayers for the chemical attachment of DNA onto gold surfaces. *Langmuir* 17:2502–2507
- Sgarbi N, Pisignano D, Di Benedetto F, Gigli G, Cingolani R, Rinaldi R (2004) Self-assembled extracellular matrix protein networks by microcontact printing. *Biomaterials* 25:1349–1353
- Takayama S, McDonald J C, Ostini E, Liang M N, Kenis P J A, Ismagilov R F, Whitesides G M (1999) Patterning cells and their environments using multiple laminar fluid flows in capillary networks. *Proc Natl Acad Sci USA* 96:5545–5548
- Vasilets V N, Nakamura K, Uyama Y, Ogata S, Ikada Y (1998) Improvement of the micro-wear resistance of silicone by vacuum ultraviolet irradiation. *Polymer* 39:2875–2881
- Wang Y, Lai H-H, Bachman M, Sims C E, Li G P, Allbritton N L (2005) Covalent micropatterning of poly(dimethylsiloxane) by photografting through a mask. *Anal Chem* 77:7539–7546
- Whitesides G M (2006) The origins and the future of microfluidics. *Nature* 442:368–373
- Xia Y, Whitesides G M (1998) Soft lithography. *Angew Chem Int Ed Engl* 37:550–575
- Xia Y, Kim E, Zhao X-M, Rogers J A, Prentiss M, Whitesides G M (1996) Complex optical surfaces formed by replica molding against elastomeric masters. *Science* 273:347–349
- Yang P, Wirsberger G, Huang H C, Corsero S R, McGehee M D, Scott B, Deng T, Whitesides G M, Chmelka B F, Buratto S K, Stucky G D (2000) Mirrorless lasing from mesostructured waveguides patterned by Soft Lithography. *Science* 287:465–467
- Zhao X-M, Xia Y, Whitesides G M (1996) Fabrication of three-dimensional micro-structures: microtransfer molding. *Adv Mater* 8:837–840
- Zhou W, Huang Y, Menard E, Aluru N R, Rogers A, Alleyne A G (2005) Mechanism for stamp collapse in soft lithography. *Appl Phys Lett* 87:251925-1-3

The Application of Silicon and Silicates in Dentistry: A Review

A.-K. Lührs and Werner Geurtsen

1	Introduction	360
2	Glass-Ionomer Cements.	360
2.1	Resin-Modified Glass-Ionomer Cements	362
2.2	Compomers (“Polyacid-Modified Composite Resins”)	362
2.3	Composite Resins	364
2.4	Adhesive Systems	370
2.5	Flowable Composite Resins	372
2.6	Composite cements	372
2.7	Tribochemical Silication.	375
2.8	Dental Ceramics	375
2.9	MTA	377
2.10	Toothpastes	377
	References	377

Abstract Silicates and silicate-based compounds are frequently used materials in dentistry. One of their major applications is their use as fillers in different dental filling materials such as glass-ionomer cements, compomers, composites, and adhesive systems. In these materials, the fillers react with acids during the setting process or they improve the mechanical properties by increasing physical resistance, thermal expansion coefficient and radiopacity in acrylic filling materials. They also reduce polymerization shrinkage, and increase esthetics as well as handling properties. Furthermore, silicates are used for the tribochemical silication of different surfaces such as ceramics or alloys. The silicate layer formed in this process is the chemical basis for silanes that form a bond between this layer and the organic composite matrix. It also provides a micromechanical bond between the surface of the material and the composite matrix. Silicates are also a component of dental ceramics, which

A.-K. Lührs and W. Geurtsen(✉)
Department of Conservative Dentistry, Periodontology & Preventive Dentistry,
Medical University Hannover, Hannover, Germany.
e-mail: Geurtsen.Werner@mh-hannover.de

are frequently used in dentistry, for instance for veneers, inlays, and onlays, for denture teeth, and for full-ceramic crowns or as crown veneering materials.

1 Introduction

Silicon is a relatively inactive, half-metallic element, which reacts with oxygen to silicon dioxide at high temperatures (SiO_2). Silicates are defined as salts and esters of mono silicic acid (H_4SiO_4). The tetrahedral structured anions $[\text{SiO}_4]^{4-}$ can be connected in different ways.

Silicon-based compounds are frequently used in dentistry, but silicate cement, which was previously used for filling purposes, is no longer applied due to its pronounced pulp toxicity and poor mechanical properties.

Main present applications of silicon/silicates are:

- As synthetic silica gel in tooth pastes
- In the powder of glass-ionomer cements as calcium–aluminum–silicate–glass
- As filler in adhesive systems, compomers, composite resins, resin-based cements, and in ormocers
- As component of mineral trioxides
- As structural component in ceramics
- As powder for intro-oral silication
- As colloidal silicate in phosphoric acid gels for the conditioning of dental hard substances, in particular enamel
- As bioactive glasses with antimicrobial properties

These main indications and applications and the associated groups of materials will be briefly discussed in the following sections.

2 Glass-Ionomer Cements

The development of glass-ionomer cements (GICs) as dental filling materials was initiated in by Wilson and Kent at the end of the 1960s (Kent et al. 1973). The first product was launched on the market in the middle of the seventies. Glass-ionomer cements were developed based on carboxylate and silicate cements. They consist of a powder and a liquid component (Gasser 1987). The powder of these materials contains calcium-aluminum-silicate and strontium-fluoro-silicate glasses, respectively, which are mixed with polyacrylic or polycarbonic acids. Subsequently, an acid-base reaction takes place. During this reaction, calcium and aluminum ions are released from these glasses, which generate a silica gel matrix based upon a bridge formation with the carboxylate groups from the polyacrylic acid around the glass particles (Nicholson et al. 1988). These materials set in two phases. During the initial phase, primarily calcium carboxylate is generated. In the second hardening phase, aluminum-polycarboxylates are being formed that are sterically

better cross-linked and thus form a more stable final setting product (Hickel and Kunzelmann 1999) (Figs. 1 and 2).

The fillers are produced through a simultaneous melting of the individual components at 1,200–1,550°C (Hill et al. 1988). A shockwise cooling of the melted glass causes coarse frits, which are ground with mills to generate final fillers with a diameter between 15 and 45 µm dependent on the application of the cement. A further surface treatment additionally reduces the reactivity of the glass powder.

GICs can adhere to the dental hard tissues through interactions generated by the carboxylate groups of the chain-like acid molecules. The adhesion of GICs to dental hard tissues, however, is inferior to the bond of modern composite resin-based adhesive systems to the tooth. Furthermore, glass-ionomers may release fluoride,

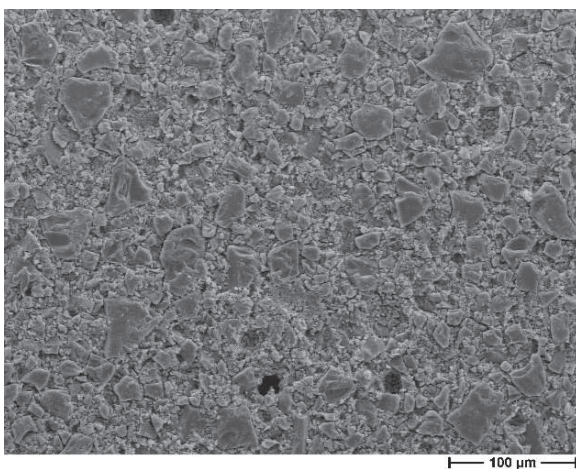


Fig. 1 Scanning electron microscopic image of a glass-ionomer (Ketac Fil, 3M Espe, Seefeld (300×))

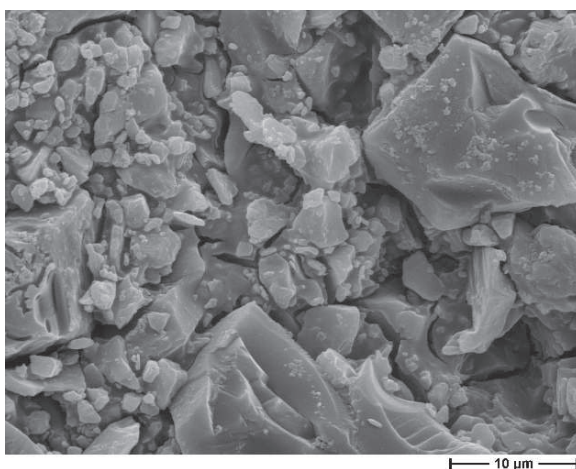


Fig. 2 Higher magnification of the glass-ionomer surface from Fig. 1 (3,000×)

which might cause a certain cariostatic effect. This, however, is still controversially discussed in the literature.

Conventional GICs are used for many applications, such as base materials, for cementation of indirect restorations, for fillings, or for build-ups. Due to a relatively high failure rate (annual mean: 7.2%), conventional GICs cannot be considered as definitive filling materials in posterior teeth with a high masticatory load (Manhart et al. 2004). In addition, mechanical characteristics, like high brittleness and pronounced surface degradation, limit their use in loaded posterior teeth.

2.1 Resin-Modified Glass-Ionomer Cements

This type of material sets also through a polymerization reaction in addition to the original acid-base reaction of conventional GICs due to polymerizable components and side chains. Hickel and Kunzelmann (1999), therefore, prefer the term “hybrid ionomers” or resin-modified glass-ionomer cements contrary to the expression light-curable glass-ionomer cements. The mechanical properties of these materials are improved based on the addition of polymerizable compounds in comparison to conventional GICs.

Furthermore, the mechanical properties of resin-modified GICs can be improved by an addition of spheroid silicate fillers. The compressive strength is increased by the addition of silanized particles by 17%, whereas the use of non-silanized particles increases the compressive strength only by 9%. Both filler types increase the flexural strength by 17% (Tjandrawinata et al. 2004).

2.2 Compomers (“Polyacid-Modified Composite Resins”)

Compomers or polyacid-modified composite resins (McLean et al. 1994) were introduced onto the market in 1993. They consist primarily of a light-curable composite component and to a lesser degree of GICs. Therefore, their chemical and mechanical characteristics are very similar to conventional composite resins. Their matrix consists of polymerizable macromolecules (base monomers) like Bis-GMA as well as bis-carbonic acids with polymerizable double bonds. The fillers of the majority of the products, which are available on the market, are derived from composite resins (e.g., quartz, silicon dioxide particles) as well as GICs (fluoro-silicate glasses) (Attin et al. 1995; Eliades et al. 1998). A bond between fillers and matrix is caused by a silanization of the filler particles (Ruse 1999). But contrary to conventional glass-ionomer cements, an autonomous adhesion of compomers to dental hard tissues is not possible (Martin et al. 1997; Moodley et al. 2003). However, a certain fluoride release was identified based on the proportion of fluoro-silicate glasses among the entire filler content. This is similar to GICs, but the total amount of released fluoride is much smaller (Shaw et al. 1998). The presence of a “glass-ionomer-phase” in compomers was found by Tay et al. (2001) using transelectron

microscopy (TEM). But this phase or layer was very thin (<200nm) and was only determined after storage in water, but not after storage in air at a humidity of 100%. The share of fillers in the total volume also influences the mechanical properties of the material. Viscosity of non-polymerized compomers is directly correlated to their filler content. A filler content of more than 20–30 vol%, however, did not further improve certain mechanical properties, such as pressure resistance (Schulze et al. 2003). Furthermore, an inverse reaction between filler content and thermal expansion of compomers was found. However, micro-hardness was directly dependent of the filler content (Kwon et al. 2002) (Figs. 3–6).

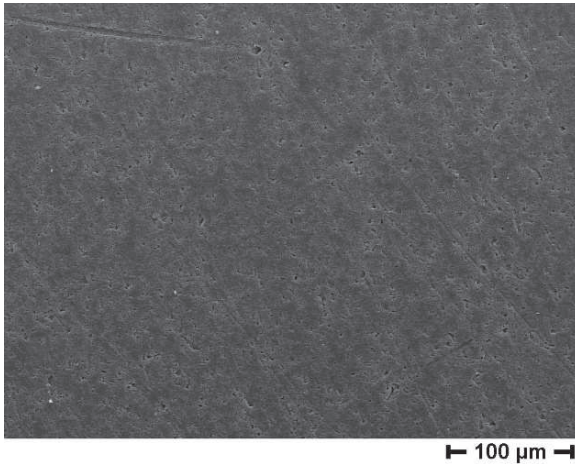


Fig. 3 Scanning electron microscopic image of a compomer (Dyract Xtra; Dentsply, Konstanz) (300 \times)

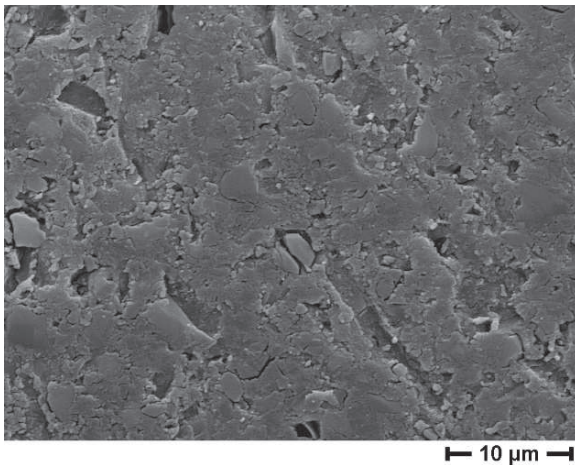


Fig. 4 Higher magnification of the compomer from Fig. 3 with irregularly shaped silicate-based fillers that are embedded into the compomer matrix. The size distribution of the particles appears to be more homogenous in comparison to the glass-ionomer cement (3,000 \times)

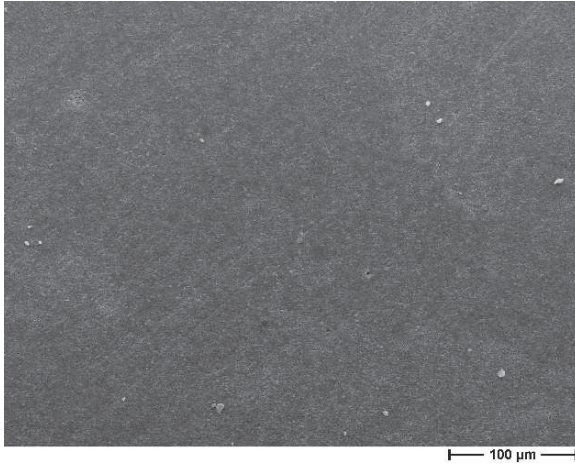


Fig. 5 Scanning electron microscopic image of a compomer (Compoglass F; Ivoclar Vivadent, Ellwangen) (300×)

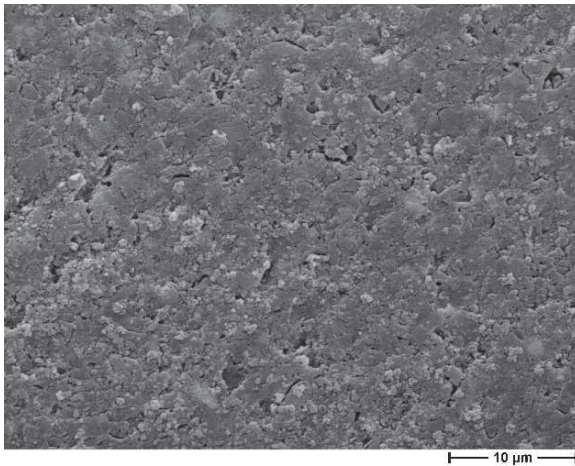


Fig. 6 Higher magnification of the compomer from Fig. 5. Besides irregular shaped fillers that are embedded into the compomer matrix, spheroidal filler agglomerates are visible (3,000×)

2.3 Composite Resins

Composite resins are complex oral biomaterials, which consist of macro and micro particles (Figs. 7–12). These particles are chemically completely different. The three main components of composite resins are the organic matrix, consisting of monomers, co-monomers and various additives and the inorganic phase (fillers). A silane is used as coupling agent to connect the organic and the inorganic phase (Geurtsen 1999).

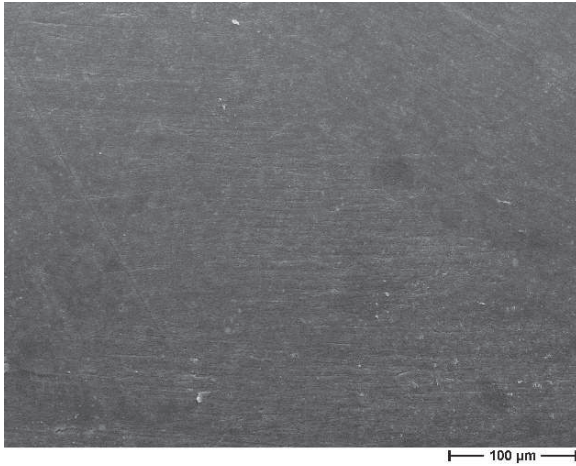


Fig. 7 Scanning electron microscopic image of a composite resin (Tetric EvoCeram; Ivoclar Vivadent, Ellwangen), which can be classified as (nano-)hybrid material (300×)

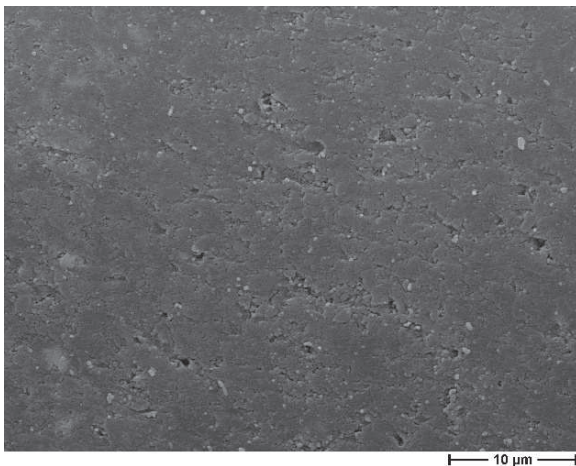


Fig. 8 Higher magnification of the composite resin from Fig. 7. Besides irregular shaped prepolymerized particles that are embedded in the composite matrix, individual spheroidal fillers are visible (3,000×)

Silanization of filler particles improves the physical/mechanical properties of the composite resins. An increasing filler content improves pressure resistance and diametrical fracture resistance. Fracture analyses indicated that fractures of composite resins containing silanized fillers occurred primarily within the matrix, whereas composites with non-silanized fillers fractured predominantly adjacent to the filler particles (Lin et al., 2000). In addition, wear increases in correlation with a decreasing share of silanized fillers (Condon et al. 1997).

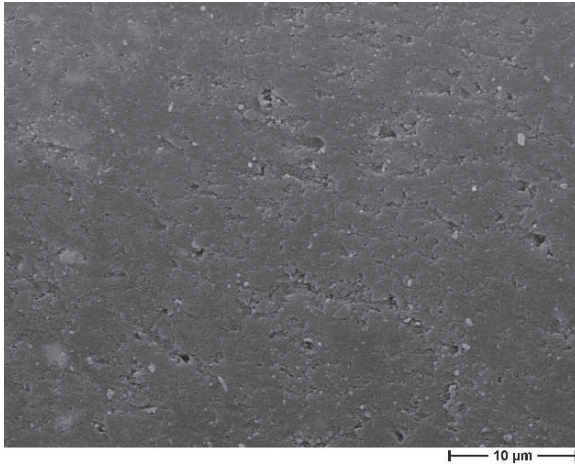


Fig. 9 Scanning electron microscopic image of a composite resin (Venus; Heraeus, Hanau), which can be classified as (ultrafine particle) hybride material (300×)

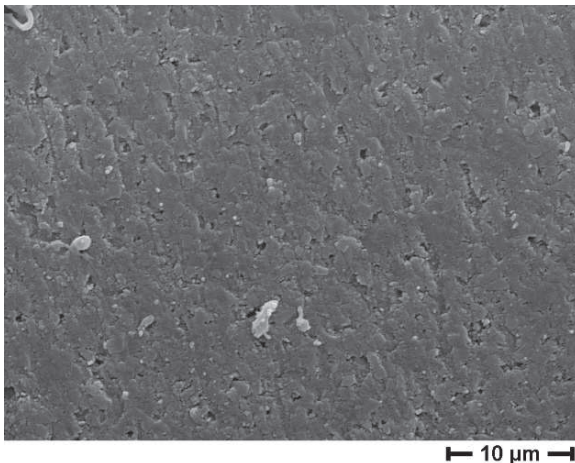


Fig. 10 Higher magnification of the composite resin from Fig. 9. The image is similar to materials from Figs. 7 and 8 since this composite belongs to the same classification (3,000×)

The mechanical properties of composite resins are primarily determined by inorganic filler particles. Since the organic polymer matrix of composite resins is characterized by poor mechanical and physical characteristics, the highest possible amount of fillers is added to the matrix in order to improve the mechanical properties of composite resins (Hervas-Garcia et al. 2006). There is a direct correlation between the amount of filler particles that are added to a plastic material and improved mechanical properties (Ferracane 1989; Fortin et al. 2000; Kim et al.

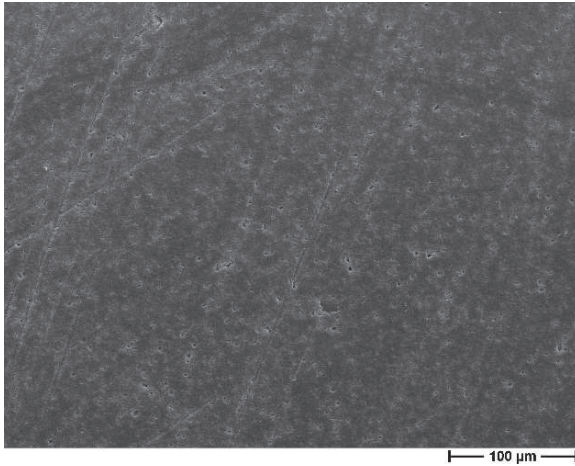


Fig. 11 Scanning electron microscopic image of a composite resin (Filtek Supreme; 3M Espe, Seefeld), which can be considered as nano-composite (300×)

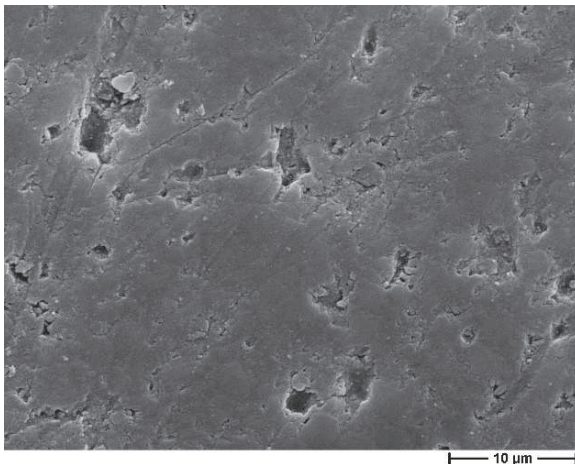


Fig. 12 Higher magnification of the composite resin from Fig. 11. This material reveals a more homogenous surface compared to Figs. 8 and 10 due to its smaller spheroidal filler particles (300×)

2002). Fillers increase resistance, thermal expansion coefficient and radiopacity in plastic filling materials, reduce polymerization shrinkage, and increase esthetics as well as handling properties of the materials (Ferracane 1995). The filler content of condensable composite resins varies between 65.5 and 79.8 wt% in dependence of the product. Filler amounts in micro-filled materials vary between 41.7 and 59.8 wt%, hybrid-type materials between 69.7 and 85.2 wt% (Sabbagh et al. 2004).

The surface wear of experimental composite resins is increasing with decreasing filler content (e.g., strontium glass), below a percentage of 48 wt%, wear increases significantly (Condon et al. 1997).

Furthermore, a direct correlation was determined between the filler content and the viscosity of the respective material: The higher the share of fillers of the total volume of the individual material, the higher the flexural strength, the modulus of elasticity, and the hardness. Only fracture resistance is not correlated with maximum filler content, instead revealing the highest value at a filler content of 55 vol% (Kim et al. 2002). Experimental restorative materials with a filler content of up to 78 vol% revealed an exponential correlation between filler content and flexural strength or the modulus of elasticity as well as the adhesive bond to dentin (Inoue et al. 1994).

Mechanical properties are also influenced by the shape of the filler particles in addition to the amount of fillers. Spherical filler particles allow a denser packing and thus an increase of the share of fillers on the total volume, whereas round filler particles increase fracture resistance of the restorative material. Irregularly shaped filler particles can trigger stress peaks during load and, therefore, may initiate or cause fractures (Bayne et al. 1994; Suzuki et al. 1995). However, no correlation exists between shape of fillers (spherical, round, square-edged), and the type or classification of material (Sabbagh et al. 2004).

Another direct influence exists between filler type and radiopacity of the filling material. Pure quartz fillers are not radiopaque. Therefore, elements like barium, strontium, zinc, and zirconium have to be added to the inorganic filler phase in order to secure a sufficient radiopacity (van Dijken et al. 1989).

Various materials are used as filler particles (van Dijken et al. 1989; Ferracane 1989; Hervas-Garcia et al. 2006). The main filler component is silicon dioxide. Other fillers consist, for instance, of quartz, glasses (e.g., boron-silicate glasses, aluminum-silicate-glasses), or ceramics (lithium-aluminum-silicate).

Atai M et al. (2007) analyzed the influence of various filler types in relation to their chemical composition on the wear of composite resins. Leucite-containing ceramic fillers were compared to the frequently used ceramic fillers and aluminum-barium-silicate glass fillers. A commercial hybrid-type composite resin served as control. The experimental composite resin containing leucite-based fillers showed a higher wear resistance compared to hybrid-type material and the experimental composite resin with glass fillers.

Pure quartz fillers were only added to the first commercial composite resins. It was a significant disadvantage of these materials that small filler particles cannot be made of pure quartz due to its hardness. Consequently, pure quartz fillers are comparably big. Although the first composite resins were very hard, they disappeared from the market since a satisfying surface finishing was not possible due to the size of the quartz particle. In addition, the disproportion between hardness of matrix and fillers increased wear of these products. If the large filler particles were quarried out of the composite resin, the soft polymer matrix was exposed without reinforcing inorganic fillers and was thus susceptible to an increased and rapid wear. This resulted in composite resins that were difficult to process and polish (Fortin et al. 2000).

The size of the filler particles as well as filler content/degree allows a classification of these restorative materials (Lutz et al. 1983; Willems et al. 1992; Bayne et al. 1994). Filler particles that are made by mechanical milling show a size between 0.1 and 100 μm (Phillips et al. 1991).

The most common classification proposed by Lutz et al. (1983) considers only the size of filler particles and classifies composite resins in conventional composites (filler size: 1 to 15 μm), hybrid-type composites containing glass- and micro fillers (particle size: between 5 and 0.04 μm) as well as micro-filled composites (mean particle size: 0.04 to 0.1 μm). Micro-filled materials may be further sub-classified due to an advanced characterization of the filler types in more, sub-classes'.

'Micro-filled composites' (according to the classification of Lutz et al. 1983) contain amorphous silicon dioxide, which is added as individual filler particles or as so-called "pre-polymerized" particles (size appr. 25 μm). Pre-polymerized particles allow to increase the filler share compared to the share of the matrix. Consequently, the filler content can be increased from appr. 35 wt% to 50 to 60 wt% (Ferracane 1995). The resulting materials are called homogenous or inhomogenous micro-filler composite resins that can be better polished and reveal excellent esthetic characteristics. But their mechanical properties are not satisfying (Geurtsen 1999).

Micro-filled composite resins with an experimental filler content of 20 to 35 vol% reveal the lowest wear at a filler content of 30 to 35 vol%. A surface treatment with functional silanes results in less abrasion compared to a treatment with non-functional silanes. The latter group tends to cause an agglomeration of fillers with sizes of more than 1 μm (Lim et al. 2002).

Hybrid-type composites contain ultrafine silicon dioxide (appr. 7 to 15%) besides glass fillers (ca. 7–15%), to improve mechanical and processing properties.

Bayne et al. (1994) classify composite resins dependent on the biggest filler size into three sub-types:

- Microfills (mean size: 0.01 to 0.1 μm)
- Minifills (0.1 to 1 μm)
- Midfills (1 to 10 μm)

Contrary to the two aforementioned classifications, Willems et al. (1992) consider the further development of composite resins with regard to a non-uniform size distribution of the added filler particles and sub-divide the materials according to the share of filler content on the total volume. Composite resins with a filler content of less than 60 vol% are called "midway-filled", and those with a share of more than 60 Vol% as "compact-filled". Based on the filler size, an additional sub-classification is used: "fine" (mean size > 3 μm) and "ultrafine" (<3 μm). Since the share of the filler content of the total volume is considered by this classification, a correlation exists between classification and the properties of the material.

During the further development of composite resins, the filler material itself (pure silicates – quartz vs. glass vs. ceramics) was modified as well as specifically the filler size, which was reduced from originally 20 μm to less than 0.4 μm . Another approach is the production of so-called "nano fillers", which are not made by grinding of large particles rather than by chemical synthesis of water-soluble

colloidal silica gel particles with a diameter of appr. 25 nm (Mitra et al. 2003). Nano-filled composite resins contain individual nanofillers as well as nano-aggregates (diameter: 75 nm), which consist of zircon or silicates. This special type of filler particles made it possible, to increase the filler content of these materials to more than 79%. But due to their particle size, these materials do not represent a special type of micro-filled composite resins. However the addition of single nanofillers (nanomers) and agglomerated nanofillers (nanoclusters) allowed a further increase of the filler content compared to conventional micro-filled composite resins. Therefore, composites based on nanofillers can be called highly filled micro-filled composites (Ernst, 2003).

The composition of filler particles or their silanization does not influence the organic matrix of a composite regarding the release of TEGDMA from composite resins based on a BisGMA/TEGDMA- or a UEDMA/TEGDMA-matrix. Composites based on a BisGMA/TEGDMA matrix release more TEGDMA into distilled water compared to a UDMA/TEGDMA based material if the TEGDMA concentration is equivalent (Müller et al. 1997).

2.4 Adhesive Systems

Since the sole adhesion of composite resins and compomers to dental hard tissues is insufficient, specific adhesion mediators are used to increase their bonding to the tooth structure (Figs. 13 and 14). The adhesion to dental hard tissues, which is based on enamel etching using an appropriate phosphoric acid gel, has been clinically successful since its introduction in 1955 (Buonocore 1955; Inoue et al. 1999;

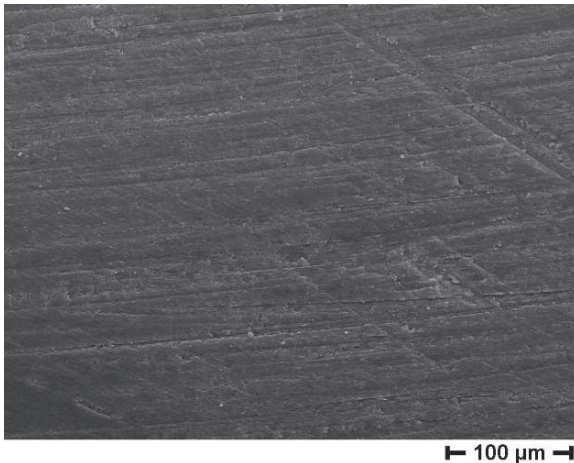


Fig. 13 Scanning electron microscopic image of a filled adhesive (Prime & Bond NT; Dentsply, Konstanz). Due to the lower filler content, superficial grooves were generated during surface finishing (300×)

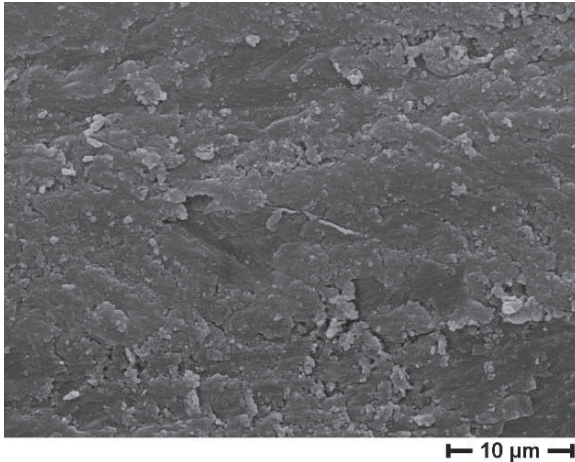


Fig. 14 Higher magnification of the adhesive from Fig. 13. Individual filler particles are visible (300 \times)

Wang et al. 2005). However, dentin adhesion compared to the enamel etch technique is much more complex due to the tubular micro structure, the intrinsic humidity of dentin, and the higher share of organic components in dentin. Furthermore, treatment of dentin, in particular subsequently to phosphoric acid etching, is much more technique sensitive compared to the conditioning of enamel (Ferrari et al. 2003). The further development of the adhesive technique towards simpler self-etch adhesives, which are easier to use, resulted in a “co-existence” of various generations of dentin adhesives. Dentin adhesives can be classified based on their interaction with the smear layer and the underlying dentin into three groups: (1) self-etch systems modify the smear layer, (2) selective etch-, or (3) total etch-systems cause a partial or complete removal of the smear layer (Inoue et al. 1999; van Meerbeek et al. 2003). Factors that impair the adhesion of composites or compomers to enamel or dentin, such as thermal expansion, polymerization shrinkage or polymerization, stress on the cavity wall can be considerably compensated for by an adhesive bonding and an appropriate layering technique. Besides the simplification of the handling of dentin adhesives through shorter application times of the individual components, various products meanwhile contain silicate-based fillers to increase their mechanical properties.

The comparison of two unfilled “total etch-systems,” which were loaded with filler particles did not result in increased material properties, such as bond strength. Only the type or product of dentin adhesive was of significant influence rather than the potential filler content (Lee et al. 2006). However, PRG-Ca fillers that were synthesized by means of an acid-base reaction from calcium-fluoro-silicate glasses with polyacrylic acid improved the material properties of conventional self-conditioning dentin adhesives. A filler content of 17 wt% causes an optimal adhesion to bovine enamel and dentin (Ikemura et al. 2003).

The bond of UDMA-based adhesives, which are used for orthodontic brackets, can be improved by adding SiO₂-fillers (Faltermeier et al. 2007).

Adhesives containing nanofillers (P&B NT) revealed in vitro in class V-cavities of bovine teeth an increased micro-leakage after the application of two layers. Use of unfilled systems (P&B 2.1, SB) was not associated with an influence of the applied layers on the microleakage.

A study that investigated the micro tensile bond strength (μ TBS) of adhesives based on their composition revealed inconsistent results when fillers were added. For example, a significant reduction of the μ TBS of one product was found when fillers were added (Nunes et al. 2001).

After infiltration of filled adhesives into the dentin surface (P&B NT) and their subsequent polymerization an accumulation of nano-fillers (dispersed SiO₂) in the orifices of open dentin tubules or a penetration into the collagen network within the hybrid layer was not identified. This may be due to an aggregation of fillers (amongst others) which might prevent the infiltration of filler clusters (Tay 1999).

2.5 Flowable Composite Resins

These materials are based on composite resin or compomer technology and are characterized by a lower viscosity (Hervas-Garcia et al. 2006). Compared to regular composite resins, flowable composites contain a lesser amount of fillers between ca. 45–66 wt% (Sabbagh et al. 2004) (Figs. 16 and 17).

In general, the mechanical properties of these materials are inferior to those of conventional composite resins. Some products contain a filler amount, which is 20% lower compared to hybrid-type composite resins. This is, of course, associated with increased polymerization shrinkage (Sabbagh et al. 2004). The lower filler content is responsible for a higher degree of wear due to attrition/abrasion (Clelland et al. 2005). Therefore, they should only be applied in very small cavities or for the repair of fillings and cast/ceramic restorations (Bayne et al. 1998). Since flowable composites reveal a lower modulus of elasticity than conventional composite resins or polyacid-modified composites (“compomers”). They are more flexible and thus more resistant to fractures. Therefore, these materials could improve the marginal sealing of cervical fillings (Li et al. 2006).

2.6 Composite cements

Dual curing composite cements are used to fix indirect restorations made of ceramic, composite, or casting alloys. The idea of dual curable materials is to reduce the setting time and to allow for a sufficient polymerization of the resin in deeper cavity areas where light polymerization is limited.

The silicon-based fillers that are added to the resin matrix are very differently shaped, varying between round, angular, or spheroid (Inokoshi et al. 1993). The

Fig. 15 Scanning electron microscopic image of a “flowable” composite resin (Tetric EvoFlow; Ivoclar Vivadent, Ellwangen) (300×)

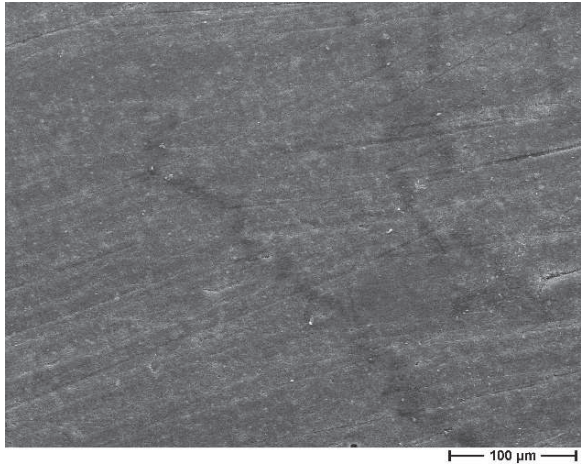


Fig. 16 Higher magnification of the flowable composite from Fig. 15 containing spheroidal filler particles (300×)

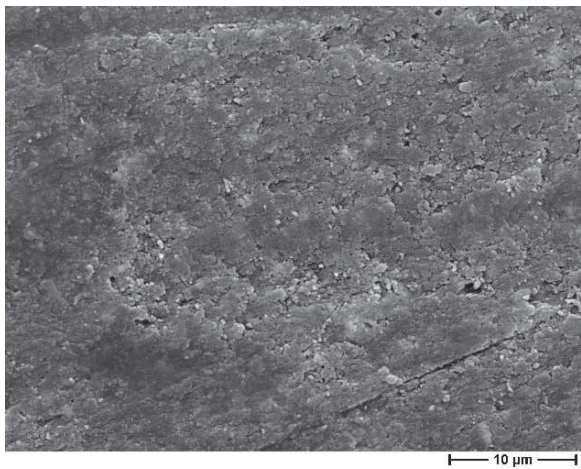
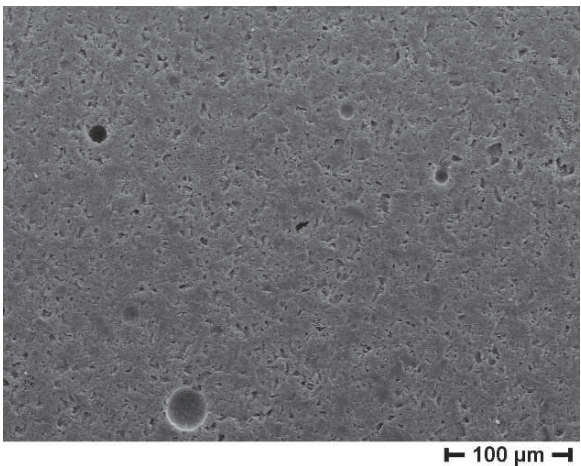


Fig. 17 Scanning electron microscopic image of a self-adhesive cement (RelyX Unicem; 3M Espe, Seefeld) (300×)



filler particles are based on silicon dioxide, glasses containing barium, ytterbium trifluoride, etc. The filler content of composite-based cements varies significantly. Peutzfed (1995) determined a filler content between 31 and 66 vol%. Inokoshi et al. (1993) could also demonstrate that the filler content of dual-curing resin cements varies between 36 and 77 wt%. This variation applies also to filler sizes with a range between 1 and 250 μm . The majority of the materials, however, contain fillers with a maximum size of less than 25 μm . The curve of the size distribution of the fillers is bell-shaped. Therefore, the majority of the fillers in a material are always smaller than the maximum size (Figs. 17 and 18).

No correlation was found between the maximum filler size and layer thickness of the material on one side and consistency and filler share of the total weight on the other side (van Meerbeek et al. 1994). Wear resistance, however, increases with increasing filler content. (Peutzfed 1995). If CAD/CAM-fabricated ceramic restorations are cemented with experimental dual-curing cements (silanized Ba-Si-fillers), it can be found that cements with a filler share of more than 70 wt% are more wear resistant than cements with 60 wt% fillers (Torii et al. 1999).

Composite cements can be classified based on filler size. Materials with a filler size of less than 0.1 μm are called micro-filled, particle sizes between 0.1 and 1 μm are classified as XXfine, between 1 and 5 μm as Xfine, and sizes between 5 and 25 μm are characteristic for fine filled products. Materials with particle sizes of more than 25 μm are called macro-filled (Inokoshi et al. 1993). The newest development of this type of products are self-adhesive cements, which are supposed to provide an adhesive bond to dental hard tissues, for instance by adding phosphoric acid modified acrylates that cause a lower pH after mixing.

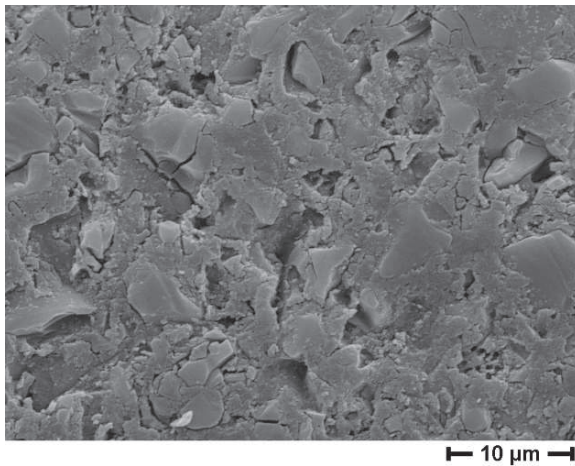


Fig 18 Higher magnification of the self-adhesive cement from Fig. 17 whose irregular shaped filler particles are similar to those contained in glass-ionomer cements (Fig. 2)

2.7 *Tribochemical Silication*

Tribochemical silication is based on specific silica-coated aluminum-oxide particles ($[Al_2O_3]_x \times [SiO_3X]_y$), which impinge at high speed on the surface that is going to be silicated and thus turn their entire kinetic energy into thermal energy. This may cause temperature peaks of up to 1,200°C. During this process, a silicate layer is embedded into the surface of the substrate (Guggenberger 1989). The silicate layer is the chemical basis for silanes that form a bond between the silicate layer and organic composite matrix through $\equiv Si-O-Si\equiv C$ -linkers (Matinlinna et al. 2007). Furthermore, silication also provides a micromechanical bond between the surface of the material and composite matrix. Systems that are appropriate for an intra-oral application are used for the intraoral repair of ceramic, composite resin, or cast restorations and the silication of aluminum- and zirconium-dioxide ceramics, which cannot be conditioned with conventional acids like hydrofluoric acid (HF). No significantly different marginal quality was found in vitro when porcelain inlays made of leucite-reinforced glass ceramic were repaired using intra-oral silication versus a conditioning with HF that cannot be applied intra-orally (Frankenberger et al. 2006). Intra-oral silication using silanization may also cause higher bond strengths between a pre-existing composite surface and freshly applied repair material compared to a conditioning with phosphoric acid (Özcan et al. 2007). Silication of zirconium-dioxide ceramics with subsequent silanization causes higher bond strength values to composite cements compared to conditioning with pure Al_2O_3 and silanization (Amaral et al. 2006). Edelhoff et al. (2000) could also demonstrate the efficiency of a combined silication/silanization of aluminum-oxide and zirconium-dioxide ceramics. This technique, which is used during the application of dual-curing cementation composites, provides higher bond strengths values compared to other pre-treatment procedures such as conditioning with HF, grinding with diamond burs, and sand-blasting with corundum. But the efficiency of a pre-treatment of such ceramics is dependent on the applied air pressure. The highest shear bond strength after silication was found at the highest air pressure applied (450 kPa) (Heikkinen et al. 2007).

Furthermore, composite-based core build-up materials can also be silicated prior to cementation of lithium-disilicate ceramic, which results in higher shear bond strength in comparison to non-treated surfaces of HF-conditioned material (Bitter et al. 2006).

2.8 *Dental Ceramics*

Ceramics are frequently used in dentistry, for instance for veneers, inlays, and onlays, for denture teeth, and for full-ceramic crowns or as crown veneering materials. Contrary to household ceramics/porcelain, dental ceramics do not contain kaolin but instead ca. 65% feldspath and ca. 25% quartz (van Noort 2002).

Full-ceramic systems can be classified as silicate ceramics and oxide-based ceramics. Silicate ceramics are multiphase materials as compared to oxide-based ceramics that contain a crystalline phase and a glass phase.

Glass and feldspathic ceramics belong to the group of silicate ceramics, which reveal excellent esthetic properties. Feldspathic ceramics are produced by a powder–liquid slurry. This technique allows the use of individual color layers. Processing-related flaws, however, like porosities, can impair the hardness of the ceramic. Glass ceramics consist of a glass matrix, which contains embedded single crystals. Conventional glass ceramics are cast and subsequently transferred into crystalline structures by a targeted thermal treatment. Glass ceramics can be processed by casting or heat pressing. The restorations can be colored by using stains or sintered ceramics.

Ceramics can be sub-classified either based on chemical aspects or according to the type of processing, e.g., ceramics that are individually layered or sintered using fire-proof duplicated dies. Pressed ceramics are heat-pressed from pre-sintered blanks. Other systems are based on CAD/CAM technology. For this, the restoration is milled out of a ceramic blank. The big advantage of this technique is the high quality of the industrially made ceramic blanks, since these are produced under controlled conditions and thus are much more uniform than manually sintered ceramics.

The mechanical properties depend on the size and density of the crystals as well as their interaction with the matrix. Different moduli of elasticity and a different thermal expansion of the various phases also influence the material properties (van Noort 2002). Small crystals and a higher volume proportion of crystals results in an increased stability/resistance of the material. Leucite-reinforced glass ceramics contain an optimized share of leucite crystals in order to improve the mechanical properties. Therefore, they reveal a much higher fracture stability (up to 180 MPa) compared to veneering ceramics (30–40 MPa). Meanwhile, systems have been developed that allow the use of ceramics for smaller full-ceramic bridges in the anterior region up to the second premolar tooth. These materials are based on a crystalline phase of lithium-disilicate ($\text{SiO}_2\text{-Li}_2\text{O}$). In contrast to leucite-reinforced glass ceramics, systems based on lithium-disilicate reveal a bending strength of up to 400 MPa (McLean et al. 1965; Höland et al. 2000; van Noort 2002).

Therefore, leucite- or lithium-disilicate reinforced glass ceramics reveal improved mechanical properties compared to conventional glass ceramics. Leucite is a potassium-aluminum-silicate ($\text{K}_2\text{O} \times \text{Al}_2\text{O}_3 \times 6\text{SiO}_2$), which has a high coefficient of thermal expansion (Mackert et al. 1986). Most ceramics that are used for metal-ceramic restorations contain 15–25% leucite. Originally, leucite was added to veneering ceramics in order to adapt the coefficient of thermal expansion to the metal framework and thus to avoid tensions in the restoration.

Ceramics are not shapeable and are less resilient to tension and bending but more resilient to pressure. The mean bending stability of silicate-based ceramics is approximately 250 MPa. Oxide-based ceramics reveal much higher stabilities varying between 400 and 1,200 MPa depending on the type and product. Therefore, restorations made of silicate-based ceramics have to be adhesively cemented, which will cause a stabilization of tooth hard substance and ceramic restoration (Burke et al. 2002). Ceramic restorations that were fixed with glass-ionomer cement revealed failure rates of up to 15% within 2 years compared to a loss of only 2% of adhesively cemented ceramic restoration within the same time frame (Höglund

et al. 1992). If CAD/CAM-fabricated MOD-inlays are adhesively cemented, then the fracture stability of the restored teeth is similar to non-restored sound teeth. However, a decreasing thickness of the restored cusps is linked to a significantly higher proportion of marginal gaps (Mehl et al. 2004).

The long-term survival rate of ceramic restorations is high. The yearly loss rate of conventional ceramic restorations was determined to be 1.7%; CAD/CAM-fabricated restorations showed loss rates 1.4% (Manhart et al. 2004).

2.9 MTA

Mineral trioxide aggregate (MTA) consists of various oxide compounds, such as silicon oxide. MTA initially forms a colloidal gel in the presence of water with a pH of 12.5 and sets after approximately 4 h (Torabinejad et al. 1995). MTA is applied in dentistry for the treatment/closure of root perforations, apexification, retrograde root canal filling after an apical root resection, and for the capping of the vital pulp (Schwarze 2004)

2.10 Toothpastes

Silicates are applied as abrasive/cleaning particles in toothpastes. They facilitate the removal of plaque and debris from the tooth surface. The cleaning particles differ in form and dimension, they can be spherical or disc-shaped, for example, and have a size up to 15 μm . The abrasiveness of different toothpastes can be measured by the “radioactive dentine abrasion” (RDA), their cleaning performance by the “pellicle cleaning ratio” (PCR). A high RDA-level is correlated to a high PCR. The RDA-level can be low, medium, or high, but there is a limited transferability of these levels to the oral situation (Hefferren 1976). A recent study by Moore et al. (2005) showed that the abrasivity of a toothpaste is not only the result of the contained abrasive/cleaning particles because a loss of dentine occurred with all detergents. Regarding whitening toothpastes, no significantly different enamel or dentin wear was caused by toothpastes that contain either calcium carbonate/perlit or SiO_2 (Joiner et al. 2004).

References

- Amaral R, Ozcan M, Bottino MA, Valandro LF (2006) Microtensile bond strength of a resin cement to glass infiltrated zirconia-reinforced ceramic: the effect of surface conditioning. *Dent Mater* 22:283–290
- Atai M, Yassini E, Amini M, Watts DC (2007) The effect of a leucite-containing ceramic filler on the abrasive wear of dental composites. *Dent Mater* 23:1181–1187
- Attin T, Buchalla W, Kielbassa AM, Hellwig E (1995) Curing shrinkage and volumetric changes of resin-modified glass ionomer restorative materials. *Dent Mater* 11:359–362

- Bayne SC, Heymann HO, Swift EJ Jr (1994) Update on dental composite restorations. *J Am Dent Assoc* 125:687–701
- Bayne SC, Thompson JY, Swift EJ Jr, Stamatias P, Wilkerson M (1998) A characterization of first-generation flowable composites. *J Am Dent Assoc* 129:567–577
- Bitter K, Paris S, Hartwig C, Neumann K, Kielbassa AM (2006) Shear bond strength of different substrates bonded to lithium disilicate ceramics. *Dent Mater J* 25:493–502
- Buonocore MG (1955) A simple method of increasing the adhesion of acrylic filling materials to enamel surfaces. *J Dent Res* 34:849–853
- Burke FJ, Fleming GJ, Nathanson D, Marquis PM (2002) Are adhesive technologies needed to support ceramics? An assessment of the current evidence. *J Adhes Dent* 4:7–22
- Clelland NL, Pagnotto MP, Kerby RE, Seghi RR (2005) Relative wear of flowable and highly filled composite. *J Prosthet Dent* 93:153–157
- Condon JR, Ferracane JL (1997) In vitro wear of composite with varied cure, filler level, and filler treatment. *J Dent Res* 76:1405–1411
- Edelhoff D, Abuzayeda M, Yildirim M, Spiekermann H, Marx R (2000) Adhäsion von Kompositen an hochfesten Strukturkeramiken nach unterschiedlicher Oberflächenbehandlung. *Dtsch Zahnärztl Z* 55:617–623
- Eliades G, Kakaboura A, Palaghias G (1998) Acid-base reaction and fluoride release profiles in visible light-cured polyacid-modified composite restoratives (compomers). *Dent Mater* 14:57–63
- Ernst, CP (2003) Eine aktuelle Standortbestimmung zahnärztlicher Füllungskomposite. *Zahnärztliche Mitteilungen* 93:30–40
- Faltermeier A, Rosentritt M, Faltermeier R, Reicheneder C, Mussig D (2007) Influence of filler level on the bond strength of orthodontic adhesives. *Angle Orthod* 77:494–498
- Ferracane JL (1989) In vitro evaluation of composite resins. Structure-property relationships. Development of assessment criteria, *Trans Acad Dent Mater* 2:6–35
- Ferracane JL (1995) Current trends in dental composites. *Crit Rev Oral Biol Med* 6:302–318
- Ferrari M, Tay FR (2003) Technique sensitivity in bonding to vital, acid-etched dentin. *Oper Dent* 28:3–8
- Fortin D, Vargas MA (2000) The spectrum of composites: new techniques and materials. *J Am Dent Assoc* 131:26S–30S
- Frankenberger R, Taschner R, Lohbauer U, Krämer NH, Rosenbusch S, Reich SM (2006) Aktuelle Aspekte der intraoralen Keramikreparatur. *ZWR* 115:70–75
- Gasser O (1987) Glass ionomer cements: the present and future from the viewpoint of the science of materials *Schweiz Monatsschr Zahnmed* 97:328–335
- Geurtsen W (1999) Kunststofffüllung. In: *Praxis der Zahnheilkunde Band 2, Kariologie und Füllungstherapie*, Urban & Schwarzenberg Verlag München, pp 179–211
- Guggenberger R (1989) Rocatec system – adhesion by tribochemical coating. *Dtsch Zahnärztl Z* 44:874–876
- Hefferen JJ (1976) A laboratory method for assessment of dentifrice abrasivity. *J Dent Res* 55:563–573
- Heikkinen TT, Lassila LV, Matinlinna JP, Vallittu PK (2007) Effect of operating air pressure on tribochemical silica-coating. *Acta Odontol Scand* 65:241–248
- Hervas-Garcia A, Martinez-Lozano MA, Cabanes-Vila J, Barjau-Escribano A, Fos-Galve P (2006) Composite resins. A review of the materials and clinical indications. *Med Oral Patol Oral Cir Bucal* 11:E215–20
- Hickel R, Kunzelmann KH (1999) Glasionomer- und Kompomerfüllung, in: *Praxis der Zahnheilkunde Band 2, Kariologie und Füllungstherapie*, Urban & Schwarzenberg Verlag München, pp 155–172
- Hill RG, Wilson AD (1988) Some structural aspects of glasses used in ionomer cements. *Glass Technol* 29:150–188
- Höglund C, van Dijken J, Olofsson AL (1992) A clinical evaluation of adhesively luted ceramic inlays. A two year follow-up study. *Swed Dent J* 16:169–171
- Höland W, Schweiger M, Frank M, Rheinberger V (2000) A comparison of the microstructure and properties of the IPS Empress 2 and the IPS Empress glass-ceramics. *J Biomed Mater Res* 53:297–303

- Ikemura K, Tay FR, Kouro Y, Endo T, Yoshiyama M, Miyai K, Pashley DH (2003) Optimizing filler content in an adhesive system containing pre-reacted glass-ionomer fillers. *Dent Mater* 19:137–146
- Inokoshi S, Willems G, Van Meerbeek B, Lambrechts P, Braem M, Vanherle G (1993) Dual-cure luting composites: Part I: filler particle distribution. *J Oral Rehabil* 20:133–146
- Inoue M, Finger WJ, Mueller M (1994) Effect of filler content of restorative resins on retentive strength to acid-conditioned enamel. *Am J Dent* 7:161–166
- Inoue S, Van Meerbeek B, Vargas M, Lambrechts P, Vanherle G (1999) Adhesion mechanism of self-etching adhesives. *Advanced Adhesive Dentistry Proceedings book. 3rd International Kuraray Symposium Granada. Kuraray Europe GmbH, Medical Division*, pp 131–148
- Joiner A, Weader E, Cox TF (2004) The measurement of enamel wear of two toothpastes. *Oral Health Prev Dent* 2:383–388
- Kent BE, Lewis BG, Wilson AD (1973) The properties of a glass ionomer cement. *Br Dent J* 135:322–326
- Kim KH, Ong JL, Okuno O (2002) The effect of filler loading and morphology on the mechanical properties of contemporary composites. *J Prosthet Dent* 87:642–649
- Kwon YH, Kwon TY, Ong JL, Kim KH (2002) Light-polymerized compomers: coefficient of thermal expansion and microhardness. *J Prosthet Dent* 88:396–401
- Lee YK, Pinzon LM, O'Keefe KL, Powers JM (2006) Effect of filler addition on the bonding parameters of dentin bonding adhesives bonded to human dentin. *Am J Dent* 19:23–27
- Li Q, Jepsen S, Albers HK, Eberhard J (2006) Flowable materials as an intermediate layer could improve the marginal and internal adaptation of composite restorations in Class-V-cavities. *Dent Mater* 22:250–257
- Lim BS, Ferracane JL, Condon JR, Adey JD (2002) Effect of filler fraction and filler surface treatment on wear of microfilled composites. *Dent Mater* 18:1–11
- Lin CT, Lee SY, Keh ES, Dong DR, Huang HM, Shih YH (2000) Influence of silanization and filler fraction on aged dental composites. *J Oral Rehabil* 27:919–926
- Lutz F, Phillips RW (1983) A classification and evaluation of composite resin systems. *J Prosthet Dent* 50:480–488
- Mackert JR Jr, Butts MB, Fairhurst CW (1996) The effect of the leucite transformation on dental porcelain expansion. *Dent Mater* 2:32–36
- Manhart J, Chen H, Hamm G, Hickel R (2004) Buonocore Memorial Lecture. Review of the clinical survival of direct and indirect restorations in posterior teeth of the permanent dentition. *Oper Dent* 29:481–508
- Martin R, Paul SJ, Luthy H, Scharer P (1997) Dentin bond strength of Dyract Cem. *Am J Dent* 10:27–31
- Matinlinna JP, Vallittu PK (2007) Bonding of resin composites to etchable ceramic surfaces – an insight review of the chemical aspects on surface conditioning. *J Oral Rehabil* 34:622–630
- McLean JW, Hughes TH (1965) The reinforcement of dental porcelain with ceramic oxides. *Br Dent J* 119:251–267
- McLean JW, Nicholson JW, Wilson AD (1994) Proposed nomenclature for glass-ionomer dental cements and related materials. *Quintessence Int* 25:587–9
- Mehl A, Kunzelmann KH, Folwaczny M, Hickel R (2004) Stabilization effects of CAD/CAM ceramic restorations in extended MOD cavities. *J Adhes Dent* 6:239–245
- Mitra SB, Wu D, Holmes BN (2003) An application of nanotechnology in advanced dental materials. *J Am Dent Assoc* 134:1382–1390
- Moodley D, Grobler SR (2003) Compomers: adhesion and setting reactions. *SADJ* 58:21, 24–28
- Moore C, Addy M (2005) Wear of dentine in vitro by toothpaste abrasives and detergents alone and combined. *J Clin Periodontol* 32:1242–1246
- Müller H, Olsson S, Söderholm KJ (1997) The effect of comonomer composition, silane heating, and filler type on aqueous TEGDMA leachability in model resin composites. *Eur J Oral Sci* 105:362–368
- Nicholson JW, Brookman PJ, Lacy OM, Wilson AD (1988) Fourier transform infrared spectroscopic study of the role of tartaric acid in glass-ionomer dental cements. *J Dent Res* 67:1451–1454

- Nunes MF, Swift EJ, Perdigao J (2001) Effects of adhesive composition on microtensile bond strength to human dentin. *Am J Dent* 14:340–343
- Özcan M, Barbosa SH, Melo RM, Galhano GA, Bottino MA (2007) Effect of surface conditioning methods on the microtensile bond strength of resin composite to composite after aging conditions. *Dent Mater* 10:1276–1282
- Peutzfeldt A (1995) Dual-cure resin cements: in vitro wear and effect of quantity of remaining double bonds, filler volume, and light curing. *Acta Odontol Scand* 53:29–34
- Phillips RW (1991) Skinner's science of dental materials, 9th edition. Philadelphia: WB Saunders, pp 215–48
- Ruse ND (1999) What is a "compomer"? *J Can Dent Assoc* 65:500–504
- Sabbagh J, Ryelandt L, Bacherius L, Biebuyck JJ, Vreven J, Lambrechts P, Leloup G (2004) Characterization of the inorganic fraction of resin composites. *J Oral Rehabil* 31:1090–1101
- Schulze KA, Zaman AA, Söderholm KJ (2003) Effect of filler fraction on strength, viscosity and porosity of experimental compomer materials. *J Dent* 31:373–382
- Schwarze T (2004) Mineral Trioxide Aggregate (MTA) – Eine Literaturübersicht, *Endodontie* 13:211–221
- Shaw AJ, Carrick T, McCabe JF (1998) Fluoride release from glass-ionomer and compomer restorative materials: 6-month data. *J Dent* 26:355–359
- Suzuki S, Leinfelder KF, Kawai K, Tsuchitani Y (1995) Effect of particle variation on wear rates of posterior composites. *Am J Dent* 8:173–178
- Tay FR, Moulding KM, Pashley DH (1999) Distribution of nanofillers from a simplified-step adhesive in acid-conditioned dentin. *J Adhes Dent* 1:103–117
- Tay FR, Pashley EL, Huang C, Hashimoto M, Sano H, Smales RJ, Pashley DH (2001) The glass-ionomer phase in resin-based restorative materials. *J Dent Res* 80:1808–1812
- Tjandrawinata R, Irie M, Yoshida Y, Suzuki K (2004) Effect of adding spherical silica filler on physico-mechanical properties of resin modified glass-ionomer cement. *Dent Mater J* 23:146–154
- Torabinejad M, Hong CU, Pitt Ford TR (1995) Physical properties of a new root end filling material. *J Endod* 21:349–353
- Torii Y, Itou K, Itota T, Hama K, Konishi N, Nagamine M, Inoue K (1999) Influence of filler content and gap dimension on wear resistance of resin composite luting cements around a CAD/CAM ceramic inlay restoration. *Dent Mater J* 18: 453–461
- Van Dijken JW, Wing KR, Ruyter IE (1989) An evaluation of the radiopacity of composite restorative materials used in Class I and Class II cavities. *Acta Odontol Scand* 4: 401–407
- Van Meerbeek B, Inokoshi S, Davidson CL, De Gee AJ, Lambrechts P, Braem M, Vanherle G (1994) Dual cure luting composites – Part II: clinically related properties. *J Oral Rehabil* 21:57–66
- Van Meerbeek B, De Munck, Yoshida Y, Inoue S, Vargas M, Vijay P, Van Landuyt K, Labrechts P, Vanherle G (2003) Buonocore Memorial Lecture. Adhesion to enamel and dentin: current status and future challenges. *Oper Dent* 28–3:215–235
- Van Noort R (2002) Dental Ceramics. In: Van Noort R (ed) *Introduction to Dental Materials*, 2nd edition. St Louis: Mosby, pp 231–246
- Wang Y, Spencer P (2005) Hybridization efficiency of the adhesive/dentin interface with wet bonding. *J Dent Res* 82:141–145
- Willems G, Lambrechts P, Braem M, Celis JP, Vanherle G (1992) A classification of dental composites according to their morphological and mechanical characteristics. *Dent Mater* 8:310–319

Sustainable Exploitation and Conservation of the Endemic Lake Baikal Sponge (*Lubomirskia baicalensis*) for Application in Nanobiotechnology

Werner E.G. Müller, Heinz C. Schröder, and Sergey I. Belikov

1	Introduction	384
2	History of the Discovery of Lake Baikal	387
3	Geology and the Unique Biotope	390
4	Morphological Characteristics of <i>L. baicalensis</i>	390
5	Different Morphotypes of <i>L. baicalensis</i>	392
6	Spicules of <i>L. baicalensis</i>	393
7	Genetic Characteristics of <i>L. baicalensis</i> : The EST Database	396
8	Evolution of Metazoa in Lake Baikal: <i>L. baicalensis</i> , a Prominent Example	399
9	Evolution in Action: Another New Sponge Species from the Lake	400
10	Biosilica from <i>L. baicalensis</i> for Human Benefit: Silicatein	401
11	Sustainable Production of Biosilica: Silicatein	404
12	(Potential) Applications of <i>L. baicalensis</i> silicateins: Nanobiotechnology	406
13	(Potential) Applications of <i>L. baicalensis</i> Silicateins: Biomedicine	409
14	Conclusion: The Joint Laboratory for Molecular Biodiversity of Endemic Sponge	410
	References	412

Abstract The large sub-continent of Siberia is one of the richest mineral and oil resources on Earth. In its center, one region has gained prominence: Lake Baikal. It is one of the oldest, the deepest, and the lake with the greatest volume on Earth and is inhabited by more than 1,500 endemic species. It was Pallas (1771) who discovered in the lake a sponge species, *Lubomirskia baicalensis* (Porifera: Demospongiae), which dominates Lake Baikal's littoral-zone benthos. This sponge species has a distinguished, pronounced body plan which is composed of modules. The application of molecular biological and cell biological techniques has allowed

W.E.G. Müller(✉) and H.C. Schröder
Institut für Physiologische Chemie, Abteilung Angewandte Molekularbiologie,
Universität, Duesbergweg 6, 55099 Mainz, Germany
e-mail: wmueller@uni-mainz.de

S.I. Belikov
Limnological Institute of the Siberian Branch of Russian Academy of Sciences,
Laboratory for Analytical/Bioorganic Chemistry, Ulan-Batorskaya 3, 664033 Irkutsk, Russia

an insight into the richness of the genomic regulatory systems of *L. baicalensis*. Predominantly present are those genes which are involved in body plan formation, e.g., signal transduction, stress response, and morphogenesis. The value of this species for the understanding of the evolutionary processes is reflected by recent studies on the monophyly of Lake Baikal endemic sponge species; *L. baicalensis* is a reference animal for other endemic sponges of this area, such as in the Tuva region (Lake Dzhagataj). In addition, *L. baicalensis* gained special interest for biomedicine after the identification of the enzyme, silicatein, which catalyzes biosilica formation for the synthesis of the siliceous skeletal elements, the spicules. The sustainable use of this enzyme became feasible after the achievement of recombinant preparations. The huge impact of the recombinantly prepared biosilica for nanotechnology in general cannot yet be quantified, e.g., in the field of new materials (biozirconia and biotitania) or in semiconductor technology.

1 Introduction

In the last 10 years, a distinct paradigm change took place in the field of evolution, especially as a result of the introduction of new technologies, such as molecular biology and bioinformatics. Until recently, it had been assumed that the shift from the eukaryotic Protozoa to multicellular animals occurred due to one simple evolutionary novelty, the formation of an extracellular adhesive glycoprotein. The first taxon which arose from the hypothetical ancestor of all metazoans, the Urmetazoa (Müller 2001; Müller et al. 2001), were the sponges (phylum Porifera). Not long ago, they had been considered to be mere clumps of unicellular flagellates that secrete adhesive glycoproteins which bind them together (e.g., Loomis 1988). This assumption had been a reiteration from older views, but can still be found in modern textbooks (e.g., Pechenik 2000). There, one can read that sponges are “more remarkable for the characteristics they lack than those they possess.” Hence, the Porifera had been classified as Parazoa (“alongside” animals) or Mesozoa (“middle” animals). The latter terms imply qualitative assessments that – in view of the molecular data compiled – proved not to be helpful anymore for a further understanding of the evolution of Metazoa. At present, it is well established that the diversity and richness of the sponge toolkit means that the roots for every metabolic, morphogenetic, and developmental pathway can be traced back to the Porifera (Müller et al. 2004b; Pilcher 2005). Very much influenced by the discoveries of the Ediacaran fossils (period between 620 and 550 million years ago; Ma) and then by the Burgess Shale fossils (metazoan swimmers and floaters, 520Ma; see Conway Morris 1998) we became aware that early metazoans already had a complex body plan. The present-day knowledge on the diversification of body plans of the oldest still extant metazoans from that period, the sponges, came from the elucidation of the architecture of the genetic regulatory hierarchies, primarily elucidated using the marine sponge *Suberites domuncula* (Müller 1995; Müller et al. 2004b). The results of those molecular cell biological studies replaced the old views that these organisms were animal–plants or plant–animals, Zoophyta or Mesozoa, and finally Parazoa, from the assumption that

Porifera have to be grouped monophyletically together with the other metazoan phyla. The first strong support came from the discovery that cell–cell and cell–matrix adhesion molecules that were cloned from sponges (mainly the demosponges *S. domuncula* and *Geodia cydonium*) and were subsequently expressed, share high DNA sequence and protein function similarity with the corresponding molecules from other metazoans (Müller 1998a, b). Besides the evolutionary novelties for Metazoa, sponges also have morphogens, transcription factors (e.g., T-box/homeodomain proteins/retinoid X receptor) in common with the other metazoan phyla (Adell et al. 2003a). To our surprise, Porifera even possess those elements which are characteristic for pattern and axis formation (e.g., Frizzled receptor; Adell et al. 2003b). Recent studies have even shown that the epithelial layers of sponges are sealed against the extracellular milieu through tight junction proteins (Adell et al. 2004). Further progress came from the development of the technique to culture sponge cells in vitro (Müller et al. 1999). This cell culture system from sponges, the primmorphs, is a suitable tool for the understanding of morphogenetic events (e.g., canal formation initiated by the Iroquois transcription factor, or spicule formation). Finally, stem cell marker genes were isolated, which underscores the fact that the sponge cells have the capacity to differentiate (Müller 2006). The complex immune system (see Müller and Müller 2003) and the apoptotic machinery (reviewed in Wiens and Müller 2006) must also be highlighted, qualifying the sponges as animals comprising an individuality. Hence, the body plan of the hypothetical Urmetazoa can now be deduced from the genomic regulatory system, which is similar to those found in higher Metazoa. All these data together initiated a paradigm change: Porifera are complex and simple but certainly not primitive.

The Porifera evolved with three major taxa/classes: Hexactinellida, Demospongiae, and Calcarea. The spicules, the skeletal elements of the sponges grouped to the classes of Demospongiae and Hexactinellida, are composed of hydrated, amorphous, noncrystalline silica while those of the class Calcarea are formed from calcium carbonate (reviewed in Simpson 1984). The Demospongiae and Hexactinellida are the only two taxa within the kingdom of Metazoa which utilize silica instead of calcium in their mineral skeleton; calcium is otherwise the dominant inorganic skeletal component in the Metazoa. The present study will focus solely on siliceous sponges, primarily demosponges.

The evolution of the Porifera proceeded during a period between, or prior to, the Sturtian glaciation (710–680 Ma) and the Varanger-Marinoan ice ages (605–585 Ma). According to molecular biological data, the appearance sponges can be dated back to 650–665 Ma (Schäcke et al. 1994), or to 750 Ma considering palaeontological data (Reitner and Wörheide 2002). Very likely during these two cold periods, the Earth was almost completely covered by ice. Supposedly as a consequence of these ice ages most organisms went extinct (Hoffman et al. 1998). Since the sponges survived these periods it is reasonable to assume that they were provided with highly efficient metabolic systems to resist these abiotic stresses, such as heat shock proteins (ubiquitins, 14-3-3 proteins, thioredoxins) and also enzymes involved in DNA repair (excision repair proteins, as well as apoptotic molecules) (Müller et al. 2000; Wiens and Müller 2006).

Usually it is assumed – and it holds true – that the metabolic pathways and their adaptation as sessile filter feeders made the sponges not only so highly successful,

but also to slowly evolving animals during the last 700 million years. The basic body plan of the sponges has not changed from the Proterozoic/Phanerozoic period, 700 Ma, until today. The oldest sponge fossils (Hexactinellida) have been described from Mongolia and were assessed to have lived coeval with the diverse Ediacara fauna of Namibia more than 540 Ma (Brasier et al. 1997). In addition, the Hexactinellida are the oldest group of sponges, as documented there and later, in fossil records of the Sansha section in Hunan (Early Cambrian; China; Steiner et al. 1993), where more or less completely preserved sponge fossils, e.g., *Solactiniella plumata* (Fig. 1b), have been found. This fossil is noteworthy since it also shows, besides the unusual body preservation, very intact spicules; the approximately



Fig. 1 Siliceous sponges. (a, b) Earliest sponges in body preservation are known from the Lowermost Cambrian Sansha section (Hunan, China); *Solactiniella plumata* (Hexactinellida). (a) Some spicules are broken and show the internal axial canals; size of the spicules 0.5–5 mm cm. (b) *S. plumata*; size of the specimen 40 mm. (c) The fossil freshwater sponge *Spongilla gutenberiana* from the Middle Eocene (Lutetian) near Messel (Darmstadt, Germany). Spicule assembly is reminiscent of a complete animal. Size 4 mm. (d) A cup-shaped organization is more prevailing; this organization pattern is already known from the Jurassic (Swabian Alb; Germany) e.g. from *Tragos* sp; size 40 mm

40-mm-across specimen comprises 0.5- to 5-mm-long spicules with a diameter of 0.1 mm (Fig. 1a). Some of them are broken and show the open axial canals (Fig. 1a). The oil-shales of the Messel pit, near Darmstadt (Germany), are very rich in fossil freshwater sponges; among them is *Spongilla gutenbergiana* from the Middle Eocene (Lutetian), approximately 50 Ma (Fig. 1c). In some areas, spicule assemblies are found, which are very reminiscent of complete animals. Most spicules found in these bundles are 160- to 230- μ m-long oxeas; many of them show the brightly lit axial canals in the center. Cup-shaped organization of species, e.g., *Tragos* sp (Jurassic) *Synops neptuni* (Fig. 1d), prevails in the Porifera.

Even though Porifera in general, especially the marine ones, have a high level of conservation and a slow evolutionary progress, there is one exceptional location where the sponges (Demospongiae) show an unusually rapid evolution; this is in the world's largest freshwater lake, Lake Baikal.

2 History of the Discovery of Lake Baikal

Lake Baikal is located in the center of Siberia (Russia) (Fig. 2). It is the deepest body of freshwater (maximum 1,637 m) on Earth, one of the oldest lakes (according to some estimations >2.5 million years old), and is 636 km in length and

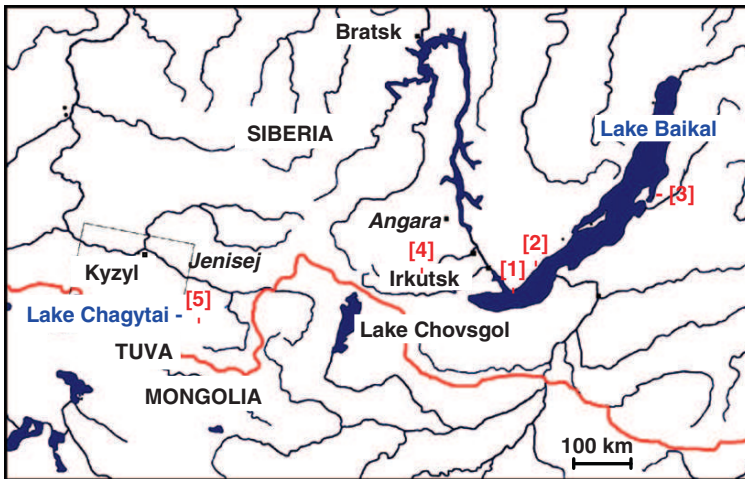


Fig. 2 Regions of Lake Baikal – Lake Chagytai. The border between Russia/Siberia and Mongolia is marked in red; the region around the city of Kyzyl (Tuva region) is boxed. The main sites for the studies on Lake Baikal sponges are around the village Listvianka in depths between 2 and 12 m [1], Bol. Kolokalnyj (2 and 25 m) [2] and Civyркуjskij Zaliv (2 and 12 m) [3]. Lake Chagytai, which harbors a further endemic freshwater sponge species, *Baikalospongia dzhegatajensis*, is located south of the city of Kyzyl [5]. This area is connected with the Jenisej River through the rivulet Mozhalik. The Joint Russian–German Laboratory for Biology of Sponges is located at the Limnological Institute of the Siberian Branch of Russian Academy of Sciences in Irkutsk [4]

up to 80 km wide; it appeared on maps in the seventeenth/eighteenth century (Fig. 3). In 1779, Müller reported on the occupation in 1656 of the Lake Baikal region around Irkutsk (founded in 1661) by Paschkow together with Pokhabov, and gave an impressive picture on the pain/agony of both the conquerors and the occupants. Detailed descriptions of the geographical location of the Lake Baikal were given by Gmelin (1751) and Pallas (1771). Sporadic reports came from the discoverers/founders of Tomsk in 1604 or Jenisseisk in 1618 (see Johansen 1925). The scientific discovery of Lake Baikal started with the expedition of Messerschmidt 1720–1727 (Winter et al. 1968). This scientist (physician) reached Lake Baikal on 8 April 1725, and crossed the frozen lake with great caution. However, Messerschmidt was only interested in land plants, not in animals. Since his notes from the expedition had been confiscated by Czar Peter the Great and also partially stolen by Strahlenberg, who published some of them (1730), they remained unknown to the public. Gmelin (1751) was more successful and performed during his 1733–1743 expedition extensive zoological and botanical investigations in Central Asia and also at Lake Baikal. In parallel, Müller (1732–1764) performed ethnographical and historical studies in this region which gained a rapid impact and attraction and were quickly translated (William 1814). Among the first inhabitants around Lake Baikal were the Tungoose (Fig. 3), who lived as nomads and hunters and reindeer breeders.

While most of the expeditions, on reaching Irkutsk, took the route along the River Lena and did not cross Lake Baikal, e.g., Lesseps (1791), it was Pallas (1771) who crossed Lake Baikal and studied the fauna and flora in depth. He also gave the first description of the endemic freshwater sponges in Lake Baikal, which he termed *Spongia baikalensis*. He mentioned that this species has an arborescent/fan-shaped morphology and mentioned its distinct green color. He also described the oscules as a water current regulatory structure, which contracts and opens, depending on the surrounding water current. Georgi (1797) should also be mentioned; he gave a comprehensive geographical and natural historical description of the Lake Baikal region. He recognized the Lake Baikal endemic sponges, which he called *S. baikalensis*. However, primarily, he presented an amazingly modern description of the medicinal herbs, among them *Digitalis*, and the birch trees from which the still-famous birch-wine (vodka) is produced. A further important scientist contributed to the exploration of Siberia: Humboldt (1844). He is the founder of geography in this region. Driven by the expectation of commercially exploiting the natural resources in Siberia, especially initiated by Czar Peter the Great, Pallas (1771) had already described the gold and silver mines in Smeinogorsk and the permafrost in Irkutsk, a line which was extended by Humboldt. In his global comparative approaches, he succeeded in identifying rich gold deposits, contributed to the improvement of the traffic infrastructure, and introduced the barometer readings as well as centers for the determination of earth magnetism.

Since Pallas, Lake Baikal has been the target for intensive scientific studies on evolution of the fauna and flora, because of its extreme richness in endemic organisms. Over 2,565 endemic animals and over 1,000 plants have been described from

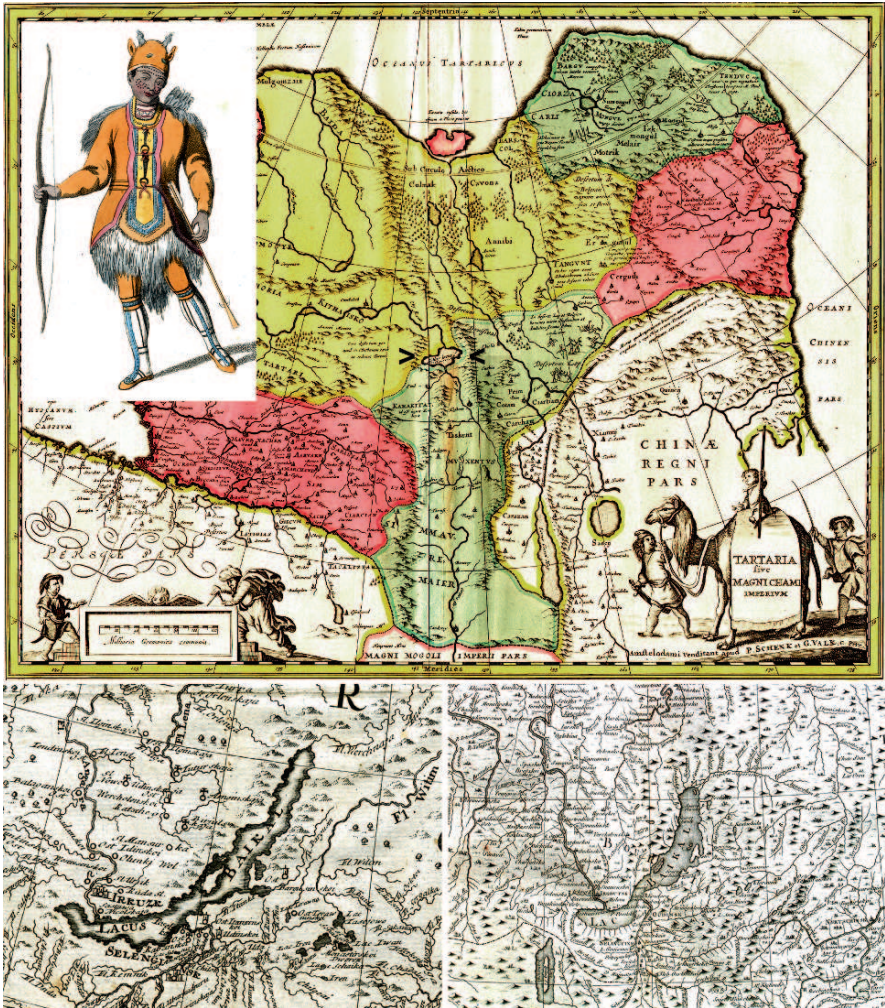


Fig. 3 Appearance of Lake Baikal on maps. (*Upper*) Map by A.P. Schenk and G. Valk (around 1750; Tartaria sive magni chami imperium); Lake Baikal is marked by *arrowheads*. Gmelin (1751) (*lower left*) gave a detailed description which was subsequently perfected by Georgi (1797) (*lower right*). (*Inset top left*) A Tungusic; they inhabited the region around the rivers Angara and Lena Aldan and also settled at Lake Baikal

the Lake (Timoshkin 2001). This fact resulted, in 1925, in the foundation of the “Baikal Limnological Station/Institute,” which is at present headed by Professor M. Grachev. While the Institute is located in Irkutsk (Fig. 2: [4]), the sampling sites for *L. baicalensis* are in the Southern or Middle part of the Lake (Fig. 2: [1]–[3]).

3 Geology and the Unique Biotope

In the Upper Cretaceous (50 Ma) the Baikal area was a plain. The temperature in that period averaged 15–20°C, which is reflected by the rich occurrence of pollen from Myrtaceae, *Araucaria*, palms, and cedars. The rift stage started about 3.5 Ma and is subdivided into the Proto-Baikal (35–3.5 Ma) and Neo-Baikal stages (3.5–0 Ma); Mats (1990). During the Proto-Baikal stage, the lake basin deepened in depth down to several hundreds of meters. The shore of the Lake was framed only by hilly mountains. During the Pliocene (3 Ma), the lake basin in the North started to be formed and the Barguzin River developed (see Mats et al. 2000). With the beginning of the Pliocene, the average temperature dropped to 10–12°C. The Neo-Baikal stage can be further subdivided into the Upper Pliocene (3.5–0.8 Ma), Pleistocene (0.8–0.01 Ma) and Holocene (0.01–0 Ma). During the Upper Pliocene, an uplifting of the Baikal arch has been recorded, resulting in a deepening of the lakes, resulting in the joining of the then separate southern and central parts. Finally, during the course of further depressions, the northern lake also almost joined with the southern one and the modern coastline of Lake Baikal was formed. In the late Pliocene, the temperature dropped to an average of 5°C. The depression continued during the Pleistocene resulting in a deepening of the Lake and the formation of high mountains around the Lake reached maximum size. During the Middle Pleistocene (0.3 Ma), a glaciation of the mountains occurred (Burkharov and Fialkov 1996); however, Lake Baikal never completely froze the whole year round. At the end of the Pleistocene, today's coastline of Lake Baikal was attained. The temperature was 2–3°C. Nowadays, the mid-annual temperature in the southern hollow of the Lake is –0.7°C, in the middle part –1.6°C, and in northern part –3.6°C (Galaziy 1988).

The most outstanding characteristic of Lake Baikal is its pristine clear water. The visibility in the Lake is extraordinarily high (Kozhov 1963); light can penetrate over 100 m down. The average temperature of the Lake is 3.5°C and it never has ice cover all year round. In summer, the surface layer (first 50 cm) reaches a maximum temperature of 12–16°C; usually, a sharp drop of the temperature takes place at 4–5 m. Ice cover starts forming in December/January and reaches a thickness of up to 120 cm. During May, the Lake becomes free of ice. In general, Lake Baikal water is poorly mineralized, but reaches a silicon concentration of 18 µM (Kozhov 1963). This level is unusually high and it undergoes a pronounced annual change, also due to the appearance of diatom blooms (Goldberg et al. 2005). Due to the high tectonic activity around Lake Baikal, it is not surprising that this region is rich in very popular spas, e.g., the sulfur springs around Turkinsk (Scherer 1820).

4 Morphological Characteristics of *L. baicalensis*

One major family of endemic sponges exists in Lake Baikal, the Lubomirskiidae (Masuda et al. 1997). Among this family, *L. baicalensis* is a species which is found on every hard bottom down to at least 15 m (Efremova 2001). As reported by Savarese et al. (1997), it is one of the most abundant Lake Baikal sponge species in the littoral

zone. The initial description of this species came from Pallas (1771) and Georgi (1797), with the precise description by Dybowski (1880). *L. baicalensis* grows in some locations to over 120 cm high, such specimens have a dichotomous morphology comprising branches of between 1 and 3 cm in diameter. The oscules are located at the lateral surfaces of the branches and have a diameter of 3–4 mm. The spicules of *L. baicalensis* are slightly curved amphioxea which are covered by many spines. Only this type of spicule is found; they measure 150–210 μm in length and 8–15 μm in diameter (Dybowski 1880; Masuda et al. 1997). The spicules of *Lubomirskia* are – in contrast to the related genus *Baikalospongia* – embedded into a horny sheet (Annandale 1914).

This organic support allows a regular construction of the bundles within the sponge tissue. X-ray analysis reveals a highly ordered arrangement of the spicules within the body of the specimens; the arrangement of the 150- to 220- μm -long spicules into longitudinal bundles becomes visible. These structures are, to some extent, interrupted by transversal lines which demarcate 1-cm growth annuli (Kaluzhnaya et al. 2005a).

Longitudinal cross-sections through the skeleton of *L. baicalensis* (Fig. 4a) show the pronounced apical-basal organization of the branches into modules of

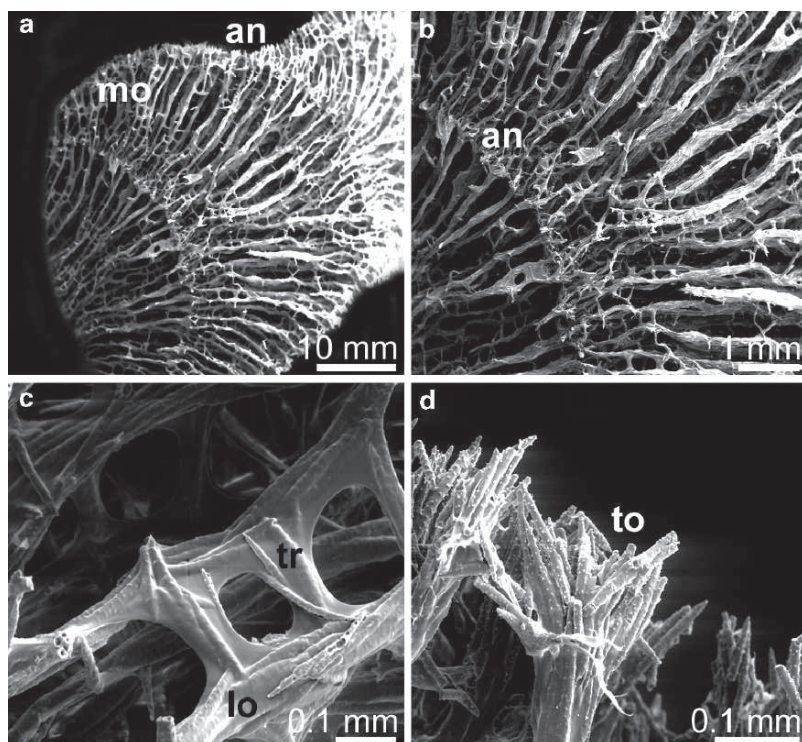


Fig. 4 Microscopical analysis of the skeleton (*Lubomirskia baicalensis*). SEM images through a longitudinal section of a branch. (a) The lower magnification shows the two modules (*mo*) which are separated from each other by an annulus (*an*). (b–d) At higher magnification, it is seen that the longitudinal bundles (*lo*) are fortified by transverse bundles (*tr*). The top of one branch is marked (*to*). Size bars are given

approximately 1 cm in length. The modular organization is constructed and determined by the arrangement of spicule bundles. The ascending, longitudinal bundles of one module originate from the annulus, a demarcation zone between modules which is formed by a dense fusiform arrangement of the bundles. This zone is concavely curved towards the tip of the branch. Annuli are composed of a ramified network of longitudinal and traverse bundles which appear very bright in cross-sections (Fig. 4b, c). This network is also seen at the top of the branches (Fig. 4d). Within the branches, the spicules are embedded in an organic matrix through which they are fixed in the ordered skeleton. At the tips of branches, the spicules protrude freely into the environment and are not embedded into any organic matrix (Fig. 4d).

5 Different Morphotypes of *L. baicalensis*

Dybowski (1884) noticed that *L. baicalensis* occurs in several morphotypes, depending on the habitats in which they grow. He subdivided them into crust forms, arborescent specimens, and bush-like animals. It is amazing that this scientist even analyzed *L. baicalensis* from mobile bottoms at a depth of 100 m. *L. baicalensis*, which can reach a size of over 1 m, exists as an encrusting form in depths between 3 and 7 m (Figs. 5B-a, B-b and 6c) while, at greater depths, branches with rounded tips, which can dichotomize, grow from the encrusting base (Fig. 5B-b, B-c and 6b). A transition of the growth form from crusts to arborescent is frequently seen at depths between 4 and 6 m (Fig. 6b, c). Already by eye inspection, it becomes evident that the branches (diameter of 1–2 cm) of such specimens are composed of 1- to 2.5-cm-long septate modules, which are arranged along the growing axis of the branch (Fig. 6b, c). This growth pattern is underscored by X-ray analysis of the branches of the skeleton and also by longitudinal cross-sections (Fig. 7b) (Müller et al. 2006b).

A scheme of the longitudinal section is given in Fig. 7a, which shows that the longitudinal bundles of spicules originate from the apex of the earlier module. From there, newly formed spicular bundles protrude. Slightly delayed, the tip of the branch changes from cone-shaped to cap-like, very probably by the outgrowth of spicular bundles from the lateral surface adjacent to the apex. This transition of the tips from cone-shaped to capped can frequently be seen in the natural environment in the same specimen (Fig. 7c), thus ruling out that module-formation within the branches is primarily seasonally controlled.

Another impressive feature of *L. baicalensis* is its bright green appearance (Fig. 6a, b). This color stems from the close symbiotic relationship of *L. baicalensis* with zoochlorella. It can be assumed that this interaction of sponges and algae allows *L. baicalensis* to survive adverse environmental conditions by also obtaining nutrients during the winter when the Lake is covered by ice.

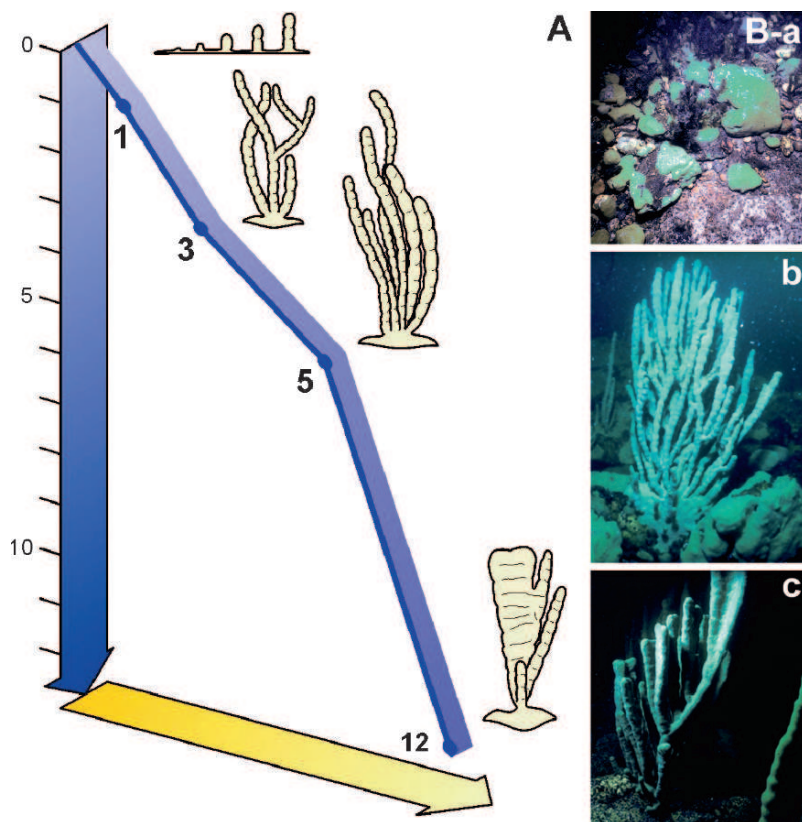


Fig. 5 Correlation of the morphology of *Lubomirskia baicalensis* with depth. (A) A profile is given which shows the habitus at different depths in Lake Baikal. Irregular crusts are formed in depths between 2 and 4 m. The arborescent growth pattern is seen below 4 m; from the 2-cm-thick crusts, branches emerge which show the modular arrangement of the tissue units. Fusion of the branches starts below 7 m, and the bases of the specimens are still embedded in the crusts from where the branches develop. (B-a) Crust; (B-b) arborescent growth form; (B-c) arborescent to laminar growth

6 Spicules of *L. baicalensis*

The spicules, fusiform amphioxea, are characteristically slightly curved and covered with many spines (Fig. 8a). Their average length is 180 μm with a width of 10 μm . Often, spicules that have not been completely liberated from the cells are associated with pronounced 15- to 20- μm -thick sclerocytes. In transmitted light, axial canals can be seen, which in approximately 20% of the spicules are dichotomous and follow/cause bifurcation of the spicules. Higher magnification (scanning electron microscopy; SEM) shows the spines at the surface of the spicules (Fig. 8a, b). If

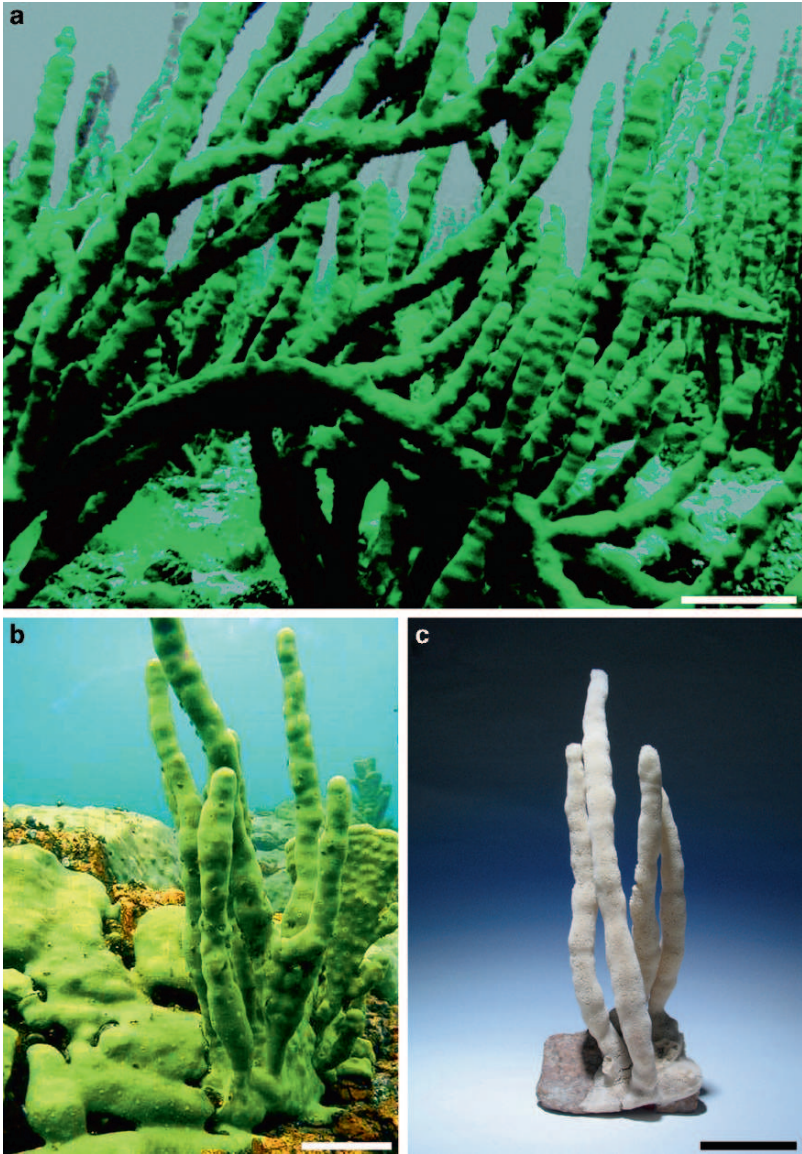


Fig. 6 Bush-like growth form of *Lubomirskia baicalensis* (a). (b) A specimen from a depth of 5 m, showing the transition from the crust growth form to the arborescent pattern organization. (c) A skeleton from a specimen of the same depth, showing the transition of the two growth forms. *Size bars*: 10 cm

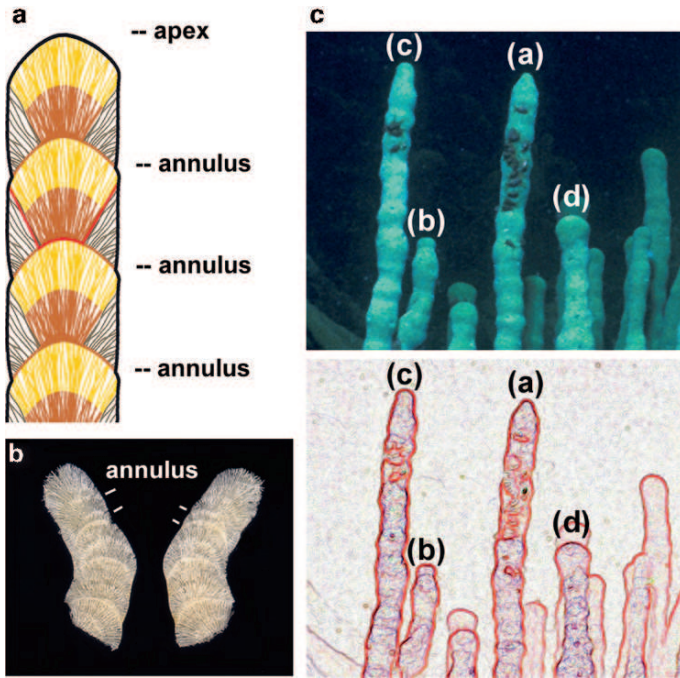


Fig. 7 Serial module formation in *Lubomirskia baicalensis*. (a) Schematic representation of serial module formation. It is outlined that from the surface of an earlier growth stage a small apex is formed (in *brown*). It is proposed that from this region new spicule bundles originate (fibers in *brown*, and at the later stage in *yellow*). In time, bundles adjacent to the apex region also appear which form the socket and reach the surface of the skeleton of one serial module (in *black*). One serial module is delimited by two annuli; one of these transversal lines is formed from the surface of an earlier growth stage and the second one from the successive module. (b) Cross-section through a tip of a branch reveals that the top module originates from an annulus. (c) The different forms of the tips of the branches: *above*, life view; *below*, contours of the surfaces of these branches. In the natural environment, the apical end of the branches appear in the following developing order; *a*, as apex on the surface of a newly developing module; *b* and *c*, a cap-like tip; and finally *d*, the massive dome-like end of a branch

broken spicules are analyzed by SEM, the transversal sections often show that they are formed from a silica shell composed of different layers of biosilica; in Fig. 8b, two layers are visible. The spicules contain in the center an axial canal (Fig. 8c, d). Usually, fractures through a spicule show tightly packed biosilica (Fig. 8c); however, the axial canal is often also surrounded by loosely packed biosilica (Fig. 8d), composed of densely packed but granular silica. The diameters of those particles are 20–50 nm. In the axial canal in the center of the spicules, a 0.5- to 4- μm -thick proteinaceous filament is found, which is composed of the enzyme silicatein (Fig. 8e, f). If such filaments are incubated with monomeric inorganic ortho-silicate, silicatein mediates the deposition of biosilica onto the filaments (Fig. 8f).

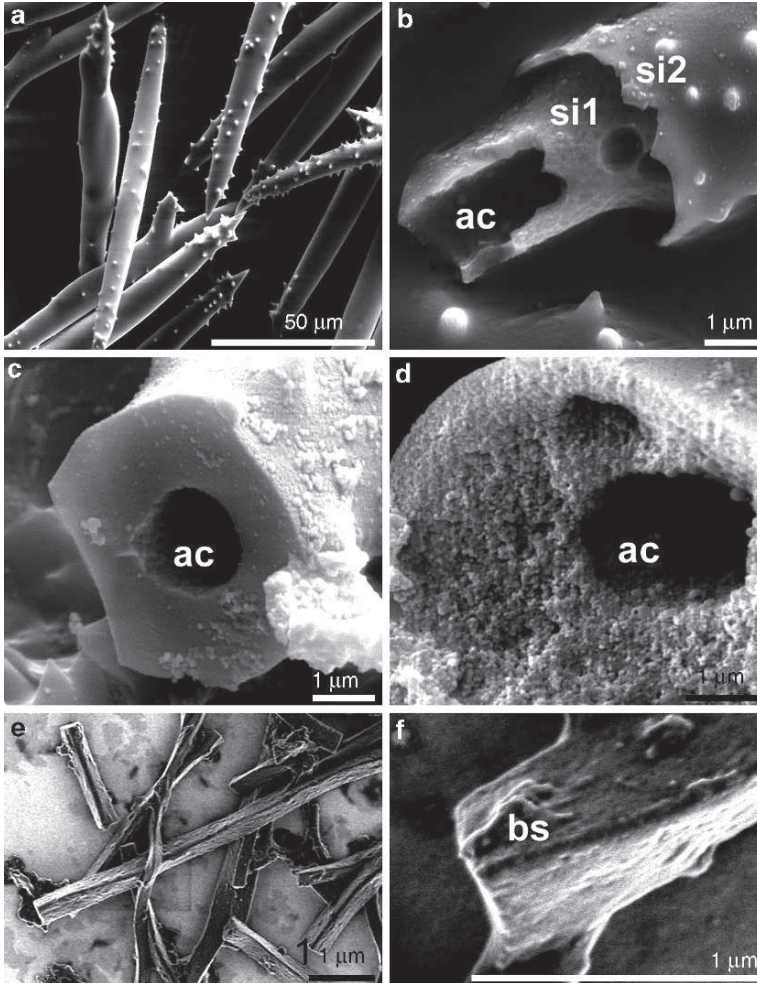


Fig. 8 SEM micrographs of amphioxiae from *Lubomirskia baicalensis*. (a) The thorned spicules. (b) A fracture through an amphioxiae showing that the axial canal (*ac*) is surrounded by two layers of biosilica (*si1* and *si2*). It can be seen that layer 1 is perforated by a hole through which the silicatein protrudes to the thorns. (c) The fracture through a spicule showing tightly packed biosilica. (d) Broken spicule showing the granular silica composition; in the center is the axial canal (*ac*). (e, f) The axial canal harbors the organic axial filament, composed of silicatein. In the presence of inorganic ortho-silicate, silicatein mediates the deposition of biosilica (*bs*) onto the filament

7 Genetic Characteristics of *L. baicalensis*: The EST Database

It is already a trend, and one that will surely accelerate in the future, that molecular biology/genetics will dominate biomedicine and biology. Based on this awareness, it was an effective and fruitful decision to establish an EST (expressed sequence tag)

database of sponge genes in general (*S. domuncula*; <http://spongebase.genoserv.de/>), and in particular of the sponge *L. baicalensis* (Baikal) and of *Baikalospongia dzhegatajensis*, the endemic sponge of Lake Chagytai (Tuva region). The collection of *L. baicalensis* comprises approximately 3,000 ESTcDNA-sequences that have been analyzed and classified according to their functional categories (Fig. 9). A large proportion (14%) can be grouped to putative cell adhesion molecules and to signal transduction proteins (22%). Importantly, the percentage fraction coding for enzymes involved in intermediary metabolism is comparatively low (15%). Transcripts coding for proteins participating in DNA/RNA metabolism (9%) and the formation and assembly of ribosomes (5%) are in the expected range. However, the comparatively high percentages of expressed genes involved in biotic and abiotic stress response (15%) and morphogenesis (7%) are unexpected. Also remarkable is the finding that 9% of the polypeptides deduced from the sponge ESTs do not show significant similarity to sequences from organisms outside their phylum Porifera. Especially within this fraction, genes can be expected which firstly execute sponge-specific functions, and/or secondly are suspected to be the source for novel biomedical processes.

Previously, it could be demonstrated that the intron lengths within the sponge genes are unusually short. This also holds true for *L. baicalensis*; on average, the size is between 150 and 1,000nts. As an example, the genomic structure for silicatein (from *L. baicalensis*), which governs the synthesis of the dominant structural elements of sponges, is given (Müller et al., submitted). The silicatein gene comprises seven exons and six introns (Fig. 10a). In order to elucidate the potential allelic variance among different specimens, intron-5 was sequenced in different *L. baicalensis* specimens. In silicatein- α 1, intron-5 is approximately 250bp long,

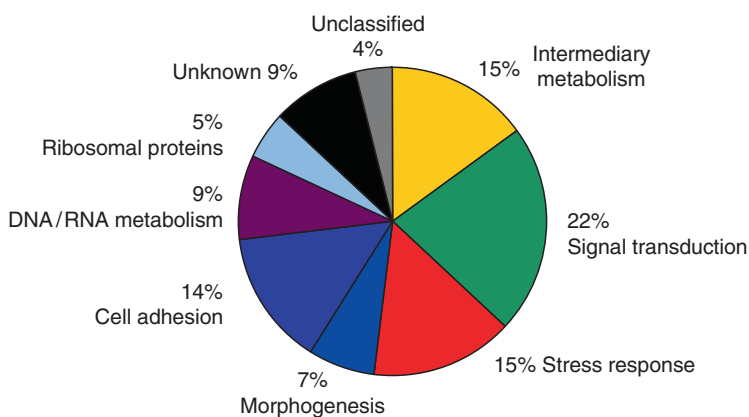


Fig. 9 Distribution of the biological functions attributed to the deduced proteins from EST sequences isolated from the sponge *Lubomirskia baicalensis*. The unknown category contains sequences with no significant sequence similarities to those cloned from other phyla comprises about 9%; those sequences are candidate molecules to be used for biomedical exploitations. The percentage of sequences, coding for proteins, involved in signal transduction, morphogenesis, and stress response, is unexpectedly high

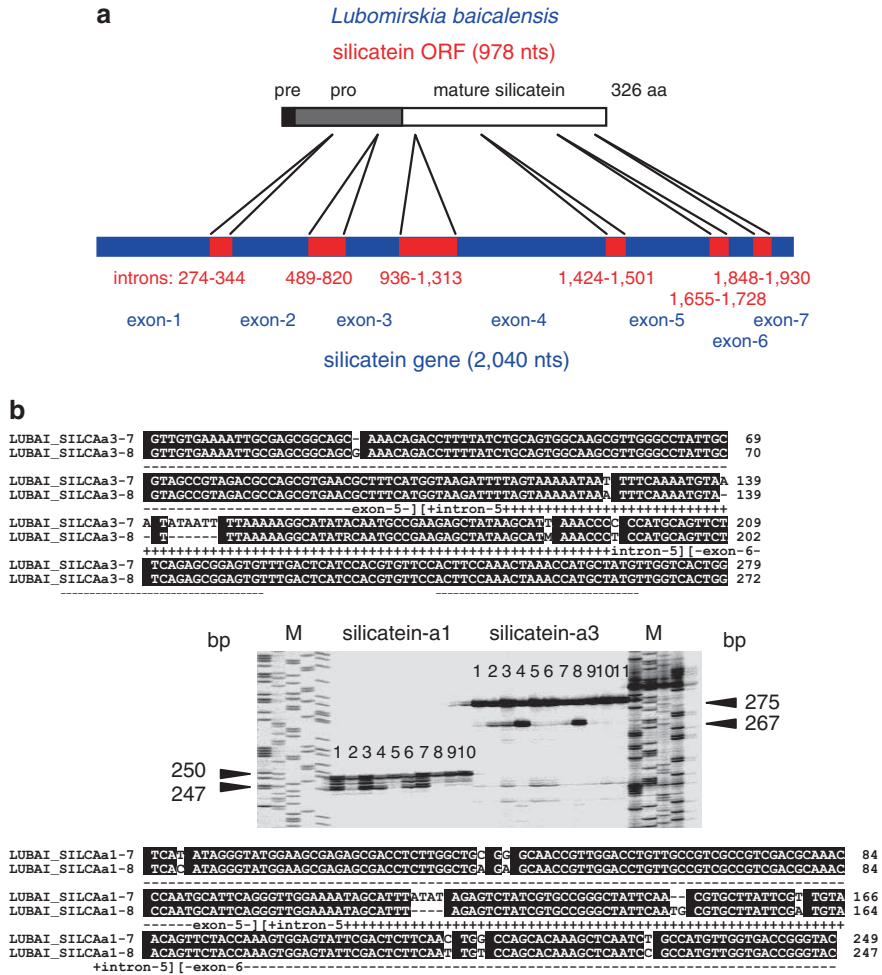


Fig. 10 Genomic organization of the silicatein gene (*Lubomirskia baicalensis*). (a) The sizes and the borders of the introns/exon for silicatein silicatein- α 1 are given, with the open reading frame (ORF) of the respective transcript schematically outlined at the top. The processing sites at the deduced protein are highlighted. (b) PCR analysis of intron-5 in 10 or 11 different specimens for silicatein- α 1 [silicatein- α 3] gene[s]. The different specimens are marked 1 to 10 or 1 to 11. Representative sequences, spanning exon-5 to exon-6 region for silicatein- α 1 (*LUBAI_SILCAa1*) and silicatein- α 3 (*LUBAI_SILCAa3*) are given for specimens 7 and 8. *M* Size markers on the sequencing gel

while in silicatein- α 3 this region spans 270bp (Fig. 10b). The intron-5 in the α 1 isoform had been sequenced from ten different specimens, collected around Listvianka, and those from the α 3 isoform from 11 specimens. After isolation of DNA, conventional polymerase chain reactions (PCR) were performed (Müller et al., submitted). The results are of interest and are summarized in Fig. 10b. It is

very obvious that the introns in both genes (silicatein- α 1 and silicatein- α 3) exist only in two variations; for silicatein- α 1 (below the gel used for analysis of the PCR product), the sizes are 250 bp and 247 bp, respectively, and for silicatein- α 3 (above the image) 275 bp or 267 bp. Likewise remarkable is that these alleles exist either just once, e.g., for silicatein- α 1 in animal nos. 2, 5, and 8–10, or twice as in the rest of the animals. No additional allele could be identified. Similarly, in silicatein- α 3, only two alleles can be identified on the basis of the sequence polymorphism; here, animal nos. 1, 5, 6, 7, and 9–11 have only one allele (Fig. 10b). This finding is a first strong indication that *L. baicalensis* has a diploid chromosome set.

8 Evolution of Metazoa in Lake Baikal: *L. baicalensis*, a Prominent Example

Several important contributions have been published in the past addressing the question how those factors which displayed evolutionary pressure on the cosmopolitan freshwater sponges, e.g., *Ephydatia fluviatilis* or *S. lacustris*, allowed the emergence of an array of endemic sponge species in Lake Baikal (e.g., Dybowski 1880, 1884; Annandale 1913; Rezvoj 1936; Martinson 1948; Röpstorf and Reitner 1994; Timoshkin 1997; Mehl-Janussen et al. 2000). Progress in those studies was hampered by the lack of molecular biological methods to be applicable as comparative tools. It was the groups of Belikov and Masuda (Itskovich et al. 1999) which first implemented these modern approaches. Even though only preliminary data could be given, they provided the basis for subsequent studies which demonstrated that the Lake Baikal sponges are of monophyletic origin (Schröder et al. 2003a). In the frame of the “Joint Russian–German Laboratory for Biology of Sponges (Irkutsk)”, it had been established, by sequence data coding for informative molecules, e.g., the mitochondrial cytochrome oxidase subunit I gene, the exon/intron sequences framing the intron-2 of the sponge tubulin gene of those sponges (Schröder et al. 2003a) and also of silicatein (a major enzyme involved in the synthesis of spicules; Müller et al. 2006c), that a monophyletic evolutionary scenario for the endemic Baikal sponge species is most likely.

Operationally, we deduce from the currently available data that the radiation of Baikalian sponges is a consequence of the following three factors (see Müller et al. 2006c). The first factor is adaptation to *environmental conditions*. The northern hemisphere underwent a general cooling period during the Plio-Pleistocene which brought about the cooling periods in Central Asia (2.8–2.5 Ma and 1.8–1.5 Ma). During this phase, the specimens had to resist environmental stress (low temperature). Adaptation involved genetic components, e.g., an increase in number and function of stress-resistance molecules (e.g., the heat shock proteins). The variety of genes also identified in *L. baicalensis* supports the notion that these Baikalian sponges are provided with a rich array of resistance proteins against environment stress. In Lake Baikal and surely also in other lakes of this region, e.g., Lake Chagytai, nutritional deprivation and the reduction of the intermediary

metabolism are additionally compensated for by an extensive symbiosis with algae (*Zoochlorella*), which are rich in chlorophyll and which will also provide the specimens with the necessary nutrients during adverse conditions. The algae are also photosynthetically active during the winter, when the lakes are covered by ice (usually without snow). Furthermore, the geomorphological/ecological characteristics of the lakes are highly favorable for sponges in general. The water is oligotrophic, the aeration is high due to strong temperature differences including the periods of ice coverage, the sedimentation rate is low, and the visibility is very high, favoring the symbiotic relationship between sponges and algae. These parameters surely contribute considerably to the fact that in Lake Baikal (Savarese et al. 1997) as well as in Lake Chagytai the “photosymbiotic” sponges dominate the photic zone.

Second, the dominance of *sexual reproduction* (Röpstorf and Reitner 1994) over asexual reproduction in sponges, e.g., by gemmules, is a further component that favored a rapid radiation of the sponges. The primary advantage of sex can be seen in a greater genetic diversity arising from recombination. It has been calculated that the life span of *L. baicalensis* is longer than 30 years.

Finally, diversification of the dominant sponge species in the lakes (Lake Baikal and Lake Chagytai) was driven by *differences in the habitats*. Species of the genus *Spongilla* (in Lake Baikal: *S. lacustris*) and *Ephydatia* (*E. muelleri*) have a hibernant, aestivant, or perennial life cycle (Pronzato and Manconi 2001). Since in the two lakes the seasonal, physical changes do not include drying out, the pressure to maintain gemmule-formation is low; an exception is perhaps the biotope around Olkhon Island (Lake Baikal) where these species may produce dry-resistant asexual gemmules. No endemic Baikalian (family Lubomirskiidae) and Chagytai species forms gemmules (Kozhov 1963; Manconi and Pronzato 2000). Intra-species variations in morphology exist, as can be impressively seen in *L. baicalensis*, and these depend very likely primarily on water current and depth.

9 Evolution in Action: Another New Sponge Species from the Lake

It was not surprising that in lakes tectonically connected with Lake Baikal similar endemic sponges are present. Our team selected for their study the Tuva region, located approximately 750 km to the west of Lake Baikal. This area had been formed during the Eocene period at the rims of the Eurasian Platform/Siberian Craton and the Central Asian Deformation Zone (Sankov et al. 2003). The Tuva region, which remained largely undiscovered until 1940 (see Greze and Greze 1958), comprises many lakes, among them Lake Chagytai.

The first description of sponges in Lake Chagytai goes back to Rezvoj (1927). The lake is located 80 km south of the capital of Tuva, Kyzyl, in the southeast region of the Tuvinskaya valley (Fig. 2: [5]). He determined sponge samples collected in 1915 and described a new species, *B. dzhegatajensis*. It is notable that the habitat of Lake Chagytai is different from that in Lake Baikal. Lake Chagytai

is located 836m above sea level and has a diameter of 5–6.5 km; its maximum depth is 17 m. The bottom of the lake consists of silt, found both in the littoral and profundal zones. The climate is typical continental, with relatively warm summers (20°C in July; water temperature 18°C) and cold winters (–20°C in March). The visibility in the lake is low (only 6.5 m) compared to the extremely high visibility in Lake Baikal. The ionic compositions of Lake Baikal and Lake Chagytai differ in some crucial aspects. The absolute mineral concentration in Lake Baikal is, at ≈ 100 mg/l (Kozhov 1963) lower compared to the ≈ 320 mg/l in Lake Chagytai (Greze and Greze 1958). The “hardness” of the water is soft, as usually found in silicate-enriched aqueous systems. The higher concentration in bicarbonate in Lake Chagytai compared to Lake Baikal (189 vs 64 mg/ml), combined with a lower silica content [0.4 (7 μ M) vs 1.1 mg/ml] is striking. This qualifies Lake Chagytai as a bicarbonate lake. The lake is also rich in diatoms (Popovskaya et al. 2002).

According to their structure and the form of the fibers (see Annandale 1914; Müller et al. 2006c), the Tuva sponges should be grouped to the genus *Baikalospongia*. Like the sponges in Lake Baikal, almost all specimens of *B. dzhegatajensis* also live in an association with branches of the algae *Chara* sp. (Greze and Greze 1958). The skeleton of *B. dzhegatajensis* is made of spicules, which are (almost) never assembled together by an organic matrix; they are of the oxeas type and are uniformly spined (thorned) and between 100 and 172 μ m long with diameters of 11–25 μ m (Rezvoj 1927, 1936).

10 Biosilica from *L. baicalensis* for Human Benefit: Silicatein

Wöhler (1828) performed a revolutionary experiment by showing that, in the presence of acidic cyanic silver-oxide, liquid ammonia can be converted to urea. This first demonstration of a conversion of inorganic compounds to organic substances revolutionized chemistry and opened the way towards biochemistry. In 1999, Cha et al. demonstrated for the first time that organic molecules (enzymes) can be used for the synthesis of an inorganic material; biosilica. Biosilica is the material which forms the sponge skeletal elements, their spicules. Hence, siliceous sponges provide the morphogenetic and genetic blueprints for the production of this new biomaterial, and also provides basic hints for its application. Biomaterials of inorganic composition will surely become one of the leading innovations of this century (Morse 1999; Müller et al. 2005a). The basis of this biotechnological revolution was the finding of silicatein, the enzyme which converts silica monomers into amorphous glass. It had been already anticipated by Eberhard (1751) that complex inorganic materials, like pearls, require the complex synthetic machinery of an organism. However, it took until very recently before a more comprehensive understanding of the enzymic/biochemical/molecular biological bases of the metazoan biomineralization, e.g., spicule synthesis, was reached (see Müller et al. 2006a).

The formation of the spicules is a surprisingly rapid process; in the freshwater sponge *E. fluviatilis*, the 100- to 300- μm -long spicules are synthesized under optimal conditions within 40h (Weissenfels 1989). The rate of appearance of new spicules is apparently correlated with the growth of the oscular tube, implying that an efficient relocation system must be active to place spicules to their functional destination. The group of Morse (Shimizu et al. 1998; Cha et al. 1999) discovered that the organic filament in the central canal of the spicules is composed of a cathepsin L-related enzyme, which they termed silicatein. They cloned two of the proposed three isoforms of silicateins, the α - and β -form, from the demosponge *Tethya aurantium* (Cha et al. 1999). In subsequent years, these molecules were also cloned from other sponges, among them *S. domuncula* (Krasko et al. 2000, 2002; Schröder et al. 2004), and also, of course, from *L. baicalensis* (Kaluzhnaya et al. 2005a, b). The silicatein molecules share highest sequence similarity to the catabolic enzyme cathepsin L. The catalytic triad of cysteine proteases, like cathepsin L, comprise the three aa Cys, His, and Asn; these amino acids are also present in the sponge cathepsins at the expected sites. However, in the sponge silicatein sequences, the cysteine residue is replaced by serine. In addition, like the other silicateins, the proteins from *L. baicalensis* also comprise a signal peptide, a cleavage site which converts the inactive enzyme into the enzymic, functional one (Fig. 11a). The outstanding

Fig. 11 Phylogenetic relationship of the silicateins, the enzyme which catalyzes the polymerization process of biosilica in the sponge spicules. (a) Alignment of the three deduced silicatein sequences of the isoform silicatein- α (α -2, α -3, and α -4) from *Lubomirskia baicalensis* (SILICAa2_LUBAI, accession number AJ968945; SILICAa3_LUBAI, AJ968946; SILICAa4_LUBAI, AJ968947). Residues conserved (similar or related with respect to their physico-chemical properties) in all sequences are shown in white on black and those in at least two sequences in black on gray. The characteristic sites in the sequences are marked; the catalytic triad (CT) amino acids, Ser (#) in silicateins and Cys in cathepsin, as well as His (#) and Asn (#), and the processing site for the conversion of the proenzyme to the mature enzyme ([] PRO). Finally the serine cluster ([=Ser=]) and the cleavage site of the signal peptide are marked “[{}].” (b) These three silicatein sequences were additionally aligned with *L. baicalensis* silicatein- α -1 (SILICAa1_LUBAI, AJ872183) and the two cathepsin L sequences (CATL1_LUBAI, AJ96849; CATL2_LUBAI, AJ968951) and with silicatein- α from *Suberites domuncula* (SILICAa_SUBDO; CAC03737.1) and from *Tethya aurantium* (*T. aurantium*) (SILICAa_TETYA, AAD23951) and with the β -isoenzymes from *S. domuncula* (SILICAb_SUBDO, AJ547635.1) and *T. aurantium* (SILICAb_TETYA, AF098670), as well as with the cathepsin L sequences from sponges *S. domuncula* (CATL_SUBDO, AJ784224), *Geodia cydonium* (CATL_GEOCY, Y10527) and *Aphrocallistes vastus* (CATL_APHRVAS, AJ968951) as well as from higher Metazoa: human (CATL_HUMAN, X12451), *Drosophila melanogaster* (CATL_DROME, S67481) and from *Caenorhabditis elegans* (CATL_CAEEL, NP_507199.1) and the related papain-like cysteine peptidase XBPC3 from *Arabidopsis thaliana* (PAPAIN_ARATH, AAK71314) (outgroup). Additionally the deduced silicateins from the cosmopolitan freshwater sponges *Ephydatia fluviatilis* (SILCA1_EPHYDAT and SILCA2_EPHYDAT) and *Spongilla lacustris* (SILCA_SPONGILLA) are included in this analysis. Furthermore, the new sequences from *Baikalospongia dzhegatajensis* (from Tuva region); the two silicateins- α (α -1 and α -7) (SILICA1_TUVA and SILICA7_TUVA) and also the cathepsin L sequence from the same species (CATL_TUVA) had been included. The silicatein sequences from *L. baicalensis* are boxed (black) and those from *B. dzhegatajensis* are in grey. The numbers at the nodes are an indication of the level of confidence for the branches as determined by bootstrap analysis (1,000 bootstrap replicates). The slanted phylogenetic tree was constructed after the alignment of these sequences and had been rooted with the plant enzyme (papain from *A. thaliana*) as an outgroup

feature, the beauty, and the scientific value of the Baikalian sponges must be seen in the fact that they possess many more silicatein genes than sponges found in the marine environment (Wiens et al. 2006).

In addition, our group was also successful in isolating the first genes/cDNAs of the Lake Dzhegataj endemic sponge *B. dzhegatajensis*. This achievement is of basic and applied importance. First, the new sequences from *B. dzhegatajensis* and *L. baicalensis* contributed to a deeper understanding of the phylogenetic position of the endemic Siberian sponges and the sequence of emergence of those species. In order to demonstrate this relationship, a slanted tree was constructed after alignment of the sequences (Fig. 11b). Besides the silicatein sequences, the cathepsins L from this species was also included. The founder enzyme, papain from *Arabidopsis thaliana*, was used as an outgroup. The phylogenetic tree shows that the cathepsin L sequences form the basic branches from which the silicatein sequences originate.

a

SILCAa2_LUBAI	-----MRST DF GLIGLAAALNC Q F A EW HS W R GS Y G K S V A S LEELERHS V W L S	50
SILCAa3_LUBAI	MGDRG P CT V KS L E G M L N V F I A L G F I Q VEL T Y A A P D R Y E N L Q E W S V R K G H H O R S V E S Q L O E M R H S I W V A	70
SILCAa4_LUBAI	-----MK L I D L G L A S I S M A F S Y E F V E W H L W K G O H O K S Y S L E L E R H S I W L S	50
SIGNAL {}		
SILCAa2_LUBAI	S R K Y I E H N A H S D V F G Y S L A M N H F G D M S E V E K D A L T H E P G N I T S R E L A T E R A F O G K V D S I D W R T K G	120
SILCAa3_LUBAI	N K K Y I E H N A N A D I F G Y T L A M N H F G D L M S A E E T E R M L T H R K H S --Q R S L O T E S P K G V T A D S L D W R T R G	138
SILCAa4_LUBAI	N K K Y I E H N A H S D V F G Y T L A M N H F G D L S T E F E N A M Y L T H D P G N I T H H E R K A B E R T E K G V O V D S I D W R T K G	120
PRO {}		
SILCAa2_LUBAI	A V T S V K N O C C A S Y A F A A C M E G A N A L E N D K O V L S E Q N I I D C S V P Y G N H G C S G G D I Y T A K Y V D N G	190
SILCAa3_LUBAI	V V T S V Q S O C C S S Y A F A A G A L E G A T A A A D K L V A L S E Q N I I D C S V P Y G N H G C S G G D I Y T A K Y V D N G	208
SILCAa4_LUBAI	A V T S V K Y O C C A S Y A F A A G A L E G A S A L S N D K O V L L S E Q N I I D C S V P Y G N H G C S G G D I Y T A K Y V D N G	190
CT# Ser		
SILCAa2_LUBAI	S I D T E S S Y S F R G K O S S C O Y N S K N S G A S A T C A V G I P Y G S E S D L M A V A T V G P V A V A V A D A N N A F R F Y O S G V	260
SILCAa3_LUBAI	S I D T E S S Y P Y R G K K S S C O Y N S K N V G A I S T G V K I A S G S E T D L S A V A S V G P I A V A V D A S V N A F M F Y O S G V	278
SILCAa4_LUBAI	S I D T E S S Y S F O G K O S S C O Y S S K N S G A S A T C A V I S I A S G S E T D L F A V A T V G P V A V A V D A N N A F R F Y O S G V	260
CT# His		
SILCAa2_LUBAI	F D S S T C S S T K L N H A M L V T G Y G S N G K D Y L V R K N S K Y W C D N G Y I M V R N K Y N O C C I A S D A L Y P M L	326
SILCAa3_LUBAI	F D S S T C S S K L N H A M L V T G Y G S N G K D Y L V R K N S W T G W C E S G Y I K M V R N K Y N O C C I A S D A L Y P M L	344
SILCAa4_LUBAI	F D S S S C S S T K L N H A M L V T G Y G S N G K D Y L V R K N S S K N W C D N G Y I M V R N K Y N O C C I A S D A L Y P T L	326
CT# Asn		

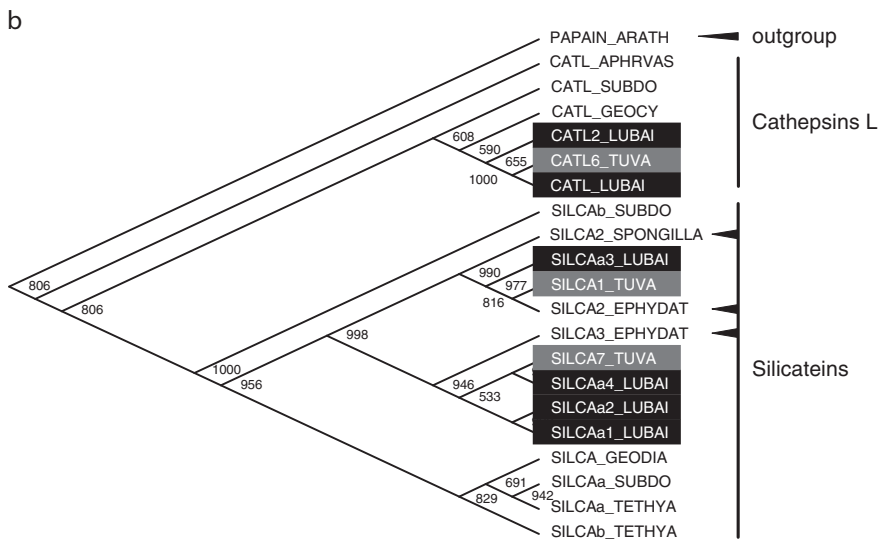


Fig. 11 (continued)

This analysis also suggests that the silicateins derive from a common ancestor with the cathepsin L sequences from marine demosponges, *S. domuncula* and *G. cydonium*. Interestingly enough, this tree also discloses that Hexactinellida, here with the example of the cathepsin L sequence from *Aphrocallistes vastus*, are phylogenetically older than the Demospongiae. In addition, the tree comprising the silicatein sequences also shows that the silicateins from the cosmopolitan freshwater species *S. lacustris* and *E. fluviatilis* form the basal branch from which the polypeptides of the Lake Baikal sponges *L. baicalensis* emerge (Fig. 11). Interestingly enough, and also supporting the geological finding, it is seen that the Lake Dzhegataj species is younger than those in Lake Baikal. Both the cathepsin L sequences and the silicatein proteins from *B. dzhegatajensis* branch off either together or later from a common ancestor with the cosmopolitan freshwater sponges. Again, these molecular biological approaches (together with the earlier ones on mitochondrial genes and the introns of tubulin; Müller et al. 2006c) demonstrate that the endemic sponges in Lake Baikal evolved monophyletically from a common ancestor with the cosmopolitan freshwater sponges. Furthermore, it can now be postulated that the Lake Dzhegataj species is evolutionarily younger.

One difference of the spicules produced by *B. dzhegatajensis* to those found in Baikalian sponges or marine species is the physical property that their biosilica is softer. Hence, it can be expected that silicatein in those species produce biosilica glass composed of a higher percentage of water. This property will surely be of importance for the application for those biomedical processes for which water-rich biosilica is favorable, e.g., for the encapsulation of drugs.

11 Sustainable Production of Biosilica: Silicatein

The central canal of the spicules contains a proteinaceous axial filament (Fig. 8e, f). This structure can be released from the silica shell by treatment with hydrofluoric acid (Fig. 12). It was O.V. Kaluzhnaya (Müller et al. 2006b) who succeeded in demonstrating that the filament can be visualized under the light microscope by simultaneous staining with Coomassie brilliant blue. Optical micrographs were taken within a time lapse of 1–3 min (Fig. 12). At the beginning, the surfaces of the partially broken spicule samples still show spines. With progressing time, the

Fig. 12 Dissolution of the polymerized silica of the spicules with hydrofluoric acid in a time lapse period. The dissolution of the siliceous “shell” of the spicules was achieved by addition of hydrofluoric acid (2M HF/8M NH₄F; pH 5) at room temperature (Kaluzhnaya et al. 2005a), in the presence of Coomassie brilliant blue. A photograph was taken every 3 min through a light microscope to demonstrate the appearance of the pure axial filament, producing the sequences of six images. (A-a) Dissolution of fossil spined amphioxea from a species related to *Lubomirskia baicalensis*; the samples were obtained from the Baikal Drilling Project (site 96) (age of the sample approximately 2Ma). In the fifth image of the series, the axial filaments (af) of the spicules, composed of silicatein can be distinguished. (B-a) Liberation of the axial filament from spicules of recent *L. baicalensis* specimens. The thin filaments are already apparent after 6 min. *Size marker*: 10 μm

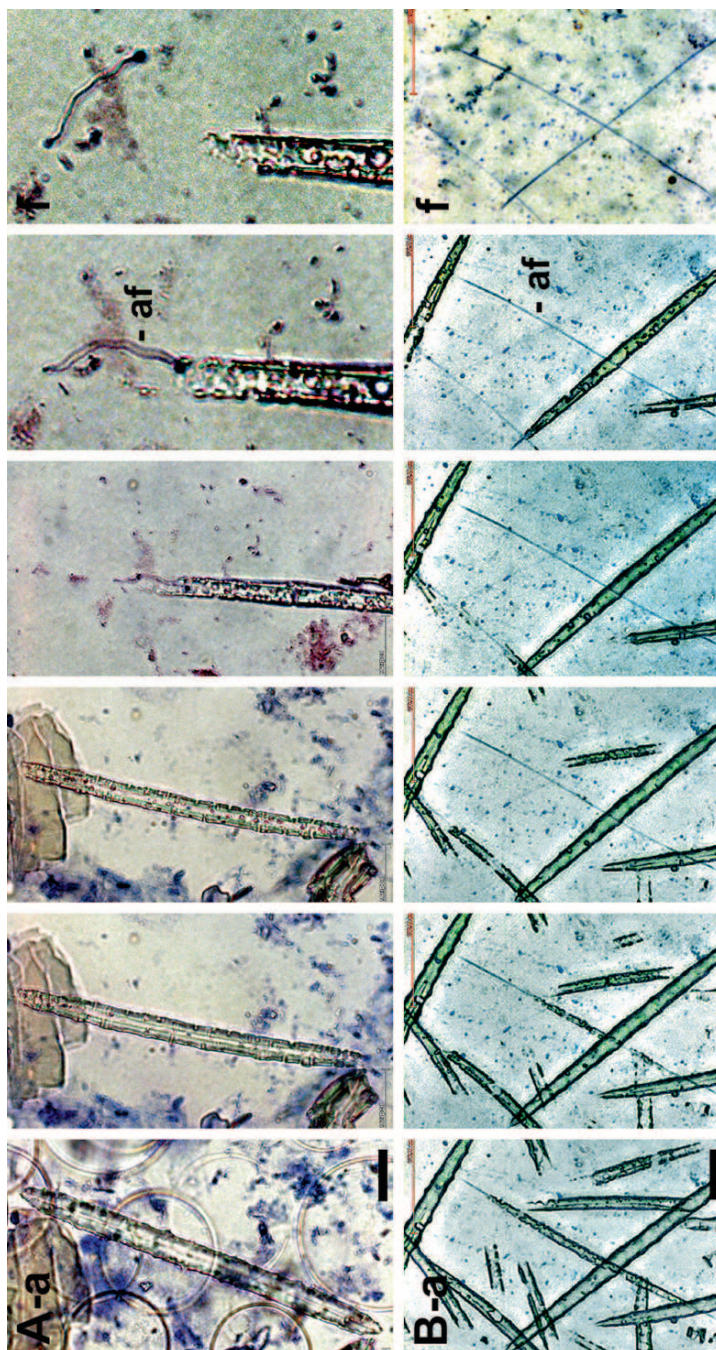


Fig. 12 (continued)

silica is dissolved, showing first the perforation of the silica mantle at the sites where spines had protruded. Finally, the silica was completely dissolved leaving behind only the organic axial filament, which was stained in blue. What is exciting is the fact that it is not only from the present-day spicules from *L. baicalensis* that the axial filaments can be released by this method (Fig. 12B) but also from fossil spicules. Using samples of an age of about 2 Ma from *L. baicalensis*-ancestor species, the organic axial filaments can be set free (Fig. 12A). This finding is a striking demonstration that biosilica of sponges is resistant in nature.

The successful approach in this century to exploit nature in a sustainable way is to apply the modern techniques of molecular biology and cell biology. Following this thinking, the silicatein cDNA was inserted into an expression system and obtained in a recombinant form (Krasko et al. 2002; Müller et al. 2003); both the sequence and the application in biomedicine are under patent protection (Müller et al. 2004a). The extent of biosilica formation by recombinant silicatein and using monomeric silica precursors, either organic or inorganic ortho-silicate, can be dramatically augmented by the presence of galectin (Schröder et al. 2006) (Fig. 13a). The extensive formation of silica can even be seen in an Eppendorf tube in 0.8-ml assays (Fig. 13a). During a 1-day reaction, no visible precipitate in the tube is found in the absence of silicatein (Fig. 13a: left). However, if silicatein was added aggregates/clumps were seen (Fig. 13a: middle) which even increased in size if silicatein was added together with galectin-2 (Fig. 13a: right).

After having established that substantial amounts of biosilica can be produced in vitro, it was necessary to discover by which mechanism(s) nature produces the amazing assortment of this material to the filigreed spicules. This problem was recently solved to some extent (Schröder et al. 2006). Electron microscopical analysis of broken spicules from *L. baicalensis* disclosed that the biosilica of the spicules is layered around the axial filament in a concentric lamellar manner (Fig. 13b). A subsequent analysis of cross-sections, applying the technique of electron immunogold labeling using polyclonal antibodies raised against the purified, recombinant silicatein (Müller et al. 2006a; Schröder et al. 2006), showed that silicatein is concentrically arranged around the surface of the growing spicule (Fig. 13c). At a higher magnification of the surface of a growing spicule of *L. baicalensis*, the fibrillar network (strings or nets) composed of silicatein and galectin is seen at the surface of the silica shell; Fig. 13d. A scheme is given which outlines the appositional growth of spicules from demosponges, organized by the concentrically arranged silicatein-galectin strings which deposit biosilica in two directions. This process results in the formation of a new lamella around the already existing spicule (Fig. 13e).

12 (Potential) Applications of *L. baicalensis* silicateins: Nanobiotechnology

Based on the outlined findings, it is now evident that the process of biomineralization during spicule formation is a biologically controlled extracellular process, which involves an enzyme (silicatein) depositing biosilica onto an organic matrix (galectin).

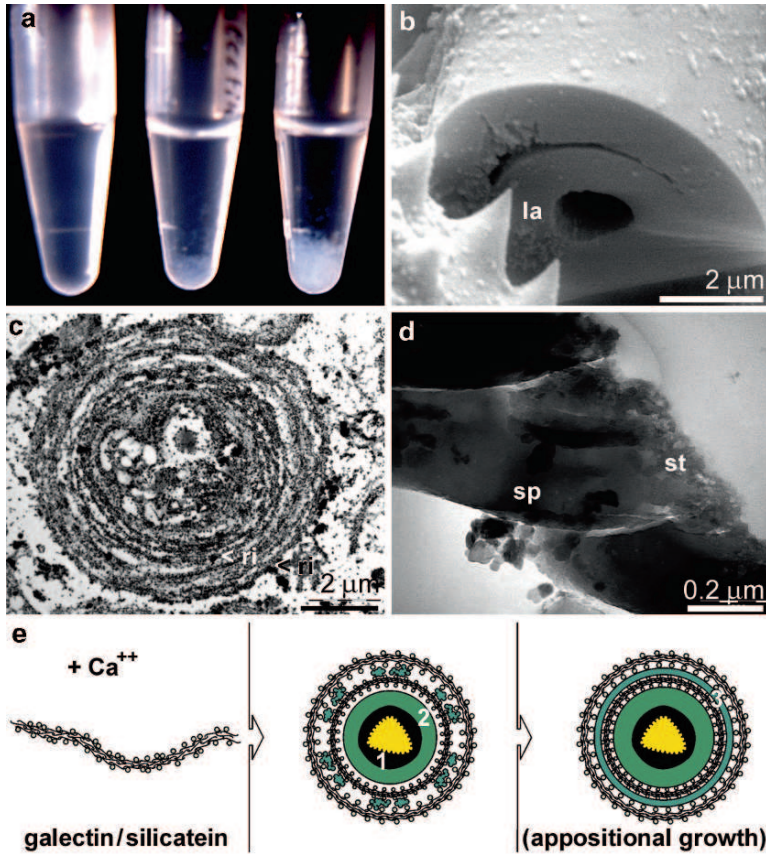


Fig. 13 Nature as a blueprint: formation of the filigreed spicules by an organized and concentric laminated apposition of concentric silica layers around the axial canal of a spicule. **(a)** Effect of galectin-2 on the size of silica aggregates, formed in vitro. Recombinant silicatein was incubated together with organic silica monomer TEOS for 120 min. *Left*, Reaction in the absence of any protein; *middle*, reaction in the presence silicatein without galectin-2; *right*, reaction in the presence of both silicatein and 100 $\mu\text{g/ml}$ galectin-2. The biosilica formed was stained with Rhodamine 123. **(b)** Cross fracture of a spicule from *Lubomirskia baicalensis*. The concentric lamellar (*la*) arrangement of the layers is seen. **(c)** Immunogold electron microscopy of cross sections through growing spicules in primmorphs; the immune complexes between the polyclonal anti-silicatein antibodies had been visualized with nanogold anti-rabbit IgG. The concentric rings (*ri*) are seen that surround the initially deposited silica layer(s). **(d)** At higher magnification the fibrillar network of a growing spicule (*sp*) of *L. baicalensis* is shown. These fibrillar, irregular strings(nets) (*st*) are composed of silicatein and lectin. **(e)** Schematic outline of the appositional growth of spicules from demosponges, inclusively *L. baicalensis*. In the mesohyl, galectin molecules associate in the presence of Ca^{2+} to strings(nets) that allow binding of silicatein molecules (*left*). The concentrically arranged silicatein-galectin strings deposit biosilica in two directions, originating both from the silicatein-galectin strings and from the surface of the spicules (centripetal and centrifugal) (*middle*). Finally a third silica lamella (*3*) is formed which is layered onto the previous two lamellae (*1* and *2*) (*right*)

It was now the challenge to see if this process can be used as a blueprint in order to fabricate, in biotechnological processes, materials applicable in biomedicine. A major breakthrough came through the work of W. Tremel's group who succeeded in showing that silicatein can be immobilized onto both, an inorganic matrix and an organic polymer layer through a linker molecule, comprising a nitrilotriacetic acid group which binds via nickel ions to the histidine-tagged silicatein. The other end of the linker comprises a thiol group which binds to the gold surface (Tahir et al. 2004) (Fig. 14). Such immobilized silicatein was able to synthesize biosilica. After this achievement, a further successful approach found that organic matrices can also be used as a platform to immobilize silicatein. In turn, gold surfaces were reacted with cysteamine to liberate amine groups to the surface. These groups interacted with the reactive polymer layer (poly[acetoxime methacrylate]), capable of reacting with primary amines. Subsequently, a similar linker (nitrilotriacetic acid – amine)

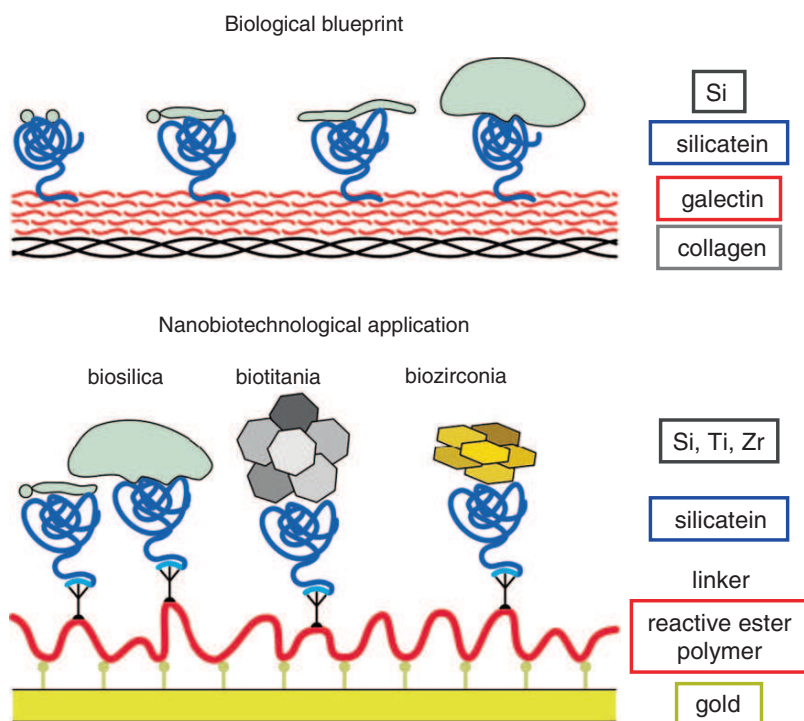


Fig. 14 Nature as model. (Top) Biosilica formation is mediated by silicatein and proceeds during the appositional deposition together with lectin strings. The complex between these two polymers is organized by collagen. (Below) For the biotechnological application, silicatein is attached to reactive ester polymers, bound onto the gold surface, via a linker. In turn silicatein can be applied for the synthesis of biosilica and also of biotitania/biozirconia. Biosilica will be useful for a series of biomedical application, while biotitania and/or biozirconia has its application in the semiconductor industry

was used to immobilize silicatein onto the reactive polymer (Tahir et al. 2005). This immobilized enzyme catalyzed not only the formation of polycondensed biosilica but also, importantly, structured titania and zirconia nanoparticles. This finding will surely have a major impact for the construction of three-dimensional semiconductors, if nanowires can be decorated with titania and/or zirconia nanoparticles.

13 (Potential) Applications of *L. baicalensis* Silicateins: Biomedicine

The stability of spicules' biosilica is highly impressive. As outlined above, the biosilica shell conserves the organic axial filament in fossil *L. baicalensis* spicules for hundreds of thousands of years. Besides the stability – especially for biomedical applications – it had to be investigated if biosilica has additionally two further properties: (1) biocompatibility and (2) biodegradation.

In a first approach, the biocompatibility of biosilica was studied (Schröder et al. 2005). In order to meet the demands for novel bioactive supports in surgery, orthopedics, and tissue engineering, the recombinant silicatein was applied to the synthesis of silica-containing bioactive surfaces under those ambient conditions that do not damage biomolecules such as proteins. We showed that growth of human osteosarcoma SaOS-2 cells on cluster plates pre-coated with collagen is not affected by additional coating of the plates with the recombinant silicatein and incubation with its enzymic substrate. However, the enzymatic modification of the plates by biosilica deposition on the protein-coated surface caused a marked increase in calcium phosphate formation of SaOS-2 cells as revealed by alizarin red-S staining to quantify calcium mineral content (Fig. 15e). The increased occurrence of calcium phosphate nodules on the modified surface could be visualized (Fig. 15a–d); the SaOS-2 cells grown onto collagen, which had been enzymatically modified by biosilica, form calcium phosphate nodules (Fig. 15b–d). The conclusion is that biosilica (silicatein)-modified surfaces are growth- and differentiation-promoting *in vitro*, and this suggests that a likewise reaction of calcium phosphate deposition might also be seen *in vivo*, via stimulation of the osteoblast mineralization function.

As always in nature, an anabolic reaction is counterbalanced by a catabolic one. This also holds for enzymic processes. Driven by this experience, our group screened for a biosilica degrading enzyme, which was discovered with the silicase (Schröder et al. 2003b) and subsequently protected (Müller et al. 2005b). Cloning of this enzyme revealed its high sequence similarity to carbonic anhydrase, an enzyme ubiquitously found in multicellular organisms. Both silicase and also – to a much lower extent – carbonic anhydrase allow the decomposition of biosilica, again under ambient conditions.

A further attractive, and commercially highly valuable, application of biosilica will be immuno-masking. A series of non-homologous molecules elicit allergic reactions in humans. Prominent examples are the proteins, proteolytic enzymes, in washing powder or on fleece/wool layers (Fig. 15f, g).

14 Conclusion: The Joint Laboratory for Molecular Biodiversity of Endemic Sponge

The lesson of history had been learnt and transformed to a sustainable collaboration between scientists of the two nations by the foundation of the “Joint Russian–German Laboratory for Biology of Sponges” in Irkutsk. Through the interlinking of the expertise of the two groups headed by S.I. Belikov and O.V. Kaluzhnaya (Irkutsk) and W.E.G. Müller and H.C. Schröder (Mainz) under the umbrella of academician M.A. Grachev, a tradition, started by German scientists, e.g., Gmelin, Pallas, and A v Humboldt, will contribute to a sustainable social and commercial progress in an under-populated area, which is so extremely rich in natural resources. Focusing on scientific biotechnological issues, biosilica will perhaps even dominate the present-day high economical trade factors, e.g., oil/gas or metals. However, the treasure of Lake Baikal is larger: it is a unique place at which (1) evolution in action can be studied; (2) a unique and conserved climate weather situation exists, which will provide us with early warning markers for the potential present-day global warming process; (3) huge amounts of solid methane, a powerful greenhouse gas that is also a valuable fuel for mechanical and electrical energy generation (Pecher 2002), have been detected as deposits deep below the Lake Baikal floor; and (4) more biotechnological innovations will emerge, e.g., those coming from other bio-silica forming organisms, e.g., diatoms (Popovskaya et al. 2002). Needless to say, the “Joint Laboratory” is open to the scientific community and will surely soon also attract commercially directed institutions. At present, the focus of the Laboratory centers around the topic of sponge biosilica. The “proof on concept” of biosilica for the application in nanobiotechnology applicable in biomedicine has been documented. The rich presence of silicatein genes in Lake Baikal endemic sponges, of which *L. baicalensis* is a model, has been recognized, their genes analyzed, and the product of this key molecule, silicatein, has been secured. Biosilica can be synthesized by recombinant technologies, and the material will have a pronounced impact in biomedicine, since it is biocompatible, biodegradable, and mechanically stable. In line with this, we are working at present on a new direction which seems at first sight an illusion, the application of biosilica wires for artificial nerve fibers.

Fig. 15 Biomimicry of nature. (a–d) Effect of biosilica-coated collagen on the synthesis of osteoblast mineralization (calcium phosphate); SEM images. The collagen coat was enzymatically modified with biosilica. (a) Culture of SaOS-2, grown in the absence of glycerophosphate, an additive required for the synthesis of calcium phosphate. (b–d) Addition of glycerophosphate (for 9 days) shows the precipitation of calcium phosphate nodules; one is marked (*arrowhead*). These mineralized nodules are shown in different magnifications. (e) Growth (cell density) of SaOS-2 cells on the enzymatically modified, osteoblast-stimulating, collagen surface. *Left*, Control culture grown on non-modified surface (after 9 days); *middle*, cultures grown onto Petri dishes, coated with silicatein alone; *right*, cultures grown on collagen which had been modified by biosilica. The cells were stained with alizarin red to assess the degree of calcium phosphate formation. (f, g) It is shown schematically how the silica shell (*yellow*) surrounds a protein molecule, represented by the barrels and extended links

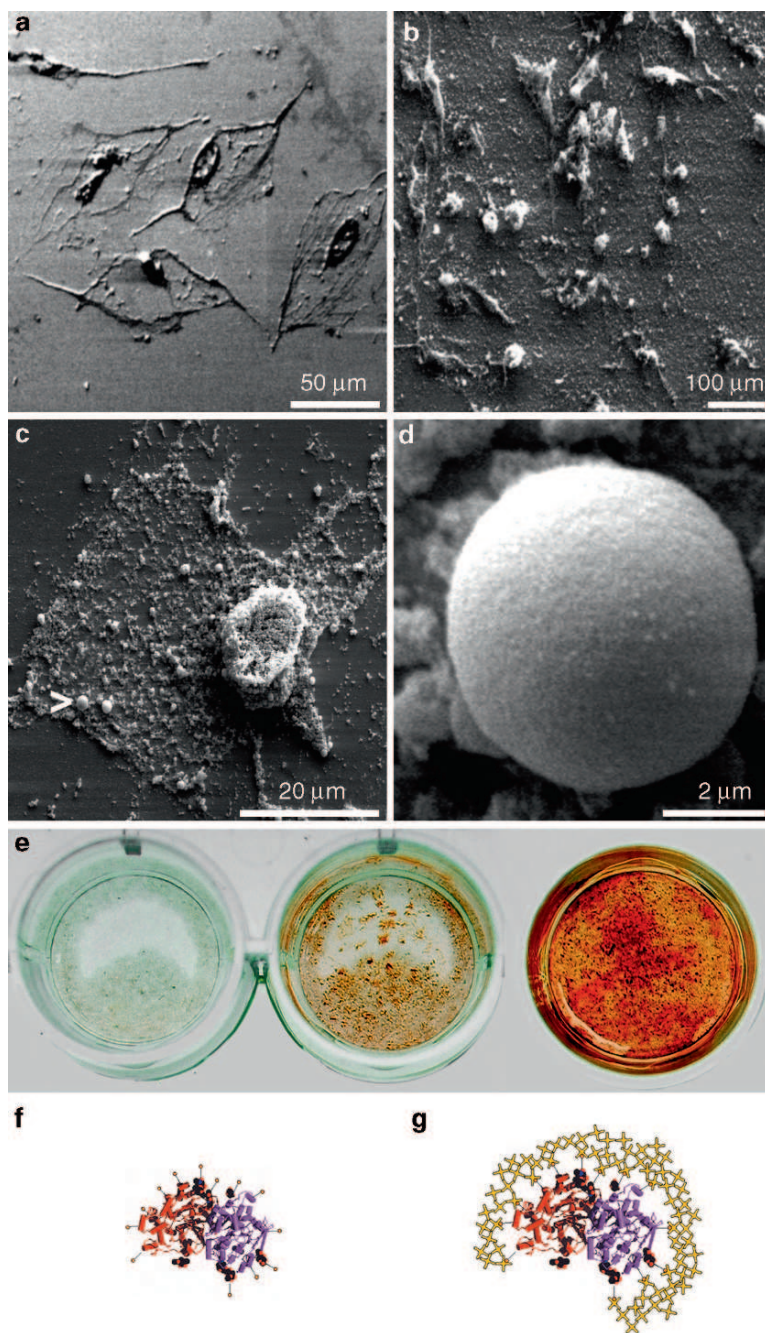


Fig. 15 (continued)

However, this dream might become a reality since the basic mechanistic, structural, and functional results are favorable. It can be demonstrated that biosilica structures (Müller et al. 2006d) act like optical glass fibers provided with unique properties, e.g., high efficiency for light transmission and acting as sharp high- and low-pass filters, suggesting that these fibers might be involved in a photoreception system. To close with Humboldt (1844); we must analyze the richness of Siberia with a global view and exploit it for technological development and hence for the prosperity of the population.

Acknowledgment This work was supported by grants from the Bundesministerium für Bildung und Forschung Germany (project: Center of Excellence *BIOTEC*marin), WTZ Germany – Russia (German–Russian cooperation through the BMBF [Founding of the “Joint Russian–German Laboratory for Biology of Sponges, Irkutsk”]), the European Commission, the Deutsche Forschungsgemeinschaft, and the International Human Frontier Science Program, as well as by a grant from the Presidium of the Russian Academy of Science (no. 25.5) and from RFBR (no. 03-04-4985).

References

- Adell T, Gamulin V, Perović-Ottstadt S, Wiens M, Korzhev M, Müller IM, Müller WEG (2004) Evolution of metazoan cell junction proteins: the scaffold protein MAGI and the transmembrane receptor tetraspanin in the demosponge *Suberites domuncula*. *J Mol Evol* 59:41–50
- Adell T, Grebenjuk VA, Wiens M, Müller WEG (2003a) Isolation and characterization of two T-box genes from sponges, the phylogenetically oldest metazoan taxon. *Dev Genes Evol* 213:421–434
- Adell T, Nefkens I, Müller WEG (2003b) Polarity factor “Frizzled” in the demosponge *Suberites domuncula*: identification, expression and localization of the receptor in the epithelium/pinacoderm. *FEBS Lett* 554:363–368
- Annandale N (1913) Notes on some sponges from Lake Baikal in the collection of the Imperial Academy of Science [St. Petersburg]. *Ann Mus Zool Acad Sci St. Petersburg* 18:18–101
- Annandale N (1914) Further notes on the sponges of Lake Baikal. *Rec Indian Mus* 10:137–148
- Brasier M, Green O, Shields G (1997) Ediacarian sponge spicule clusters from southwest Mongolia and the origins of the Cambrian fauna. *Geology* 25:303–306
- Burkharov AA, Fialkov VA (1996) Geological structure of Lake Baikal bottom. Observation from “Pisces.” Nauka, Novosibirsk
- Cha JN, Shimizu K, Zhou Y, Christianssen SC, Chmelka BF, Stucky GD, Morse DE (1999) Silicatein filaments and subunits from a marine sponge direct the polymerization of silica and silicones *in vitro*. *Proc Natl Acad Sci USA* 96:361–365
- Conway Morris S (1998) *The crucible of creation*. Oxford University Press, Oxford
- Dybowski W (1880) Studien über die Spongien des Russischen Reiches mit besonderer Berücksichtigung des Baikal-Sees. *Académie Impériale des Sciences, St. Petersburg*, pp. 1–71.
- Dybowski W (1884) Some remarks upon the variability of form in *Lubomirskia baicalensis*, and upon the distribution of the Baikal sponges in general. *Ann Mag Nat Hist/Zool* 7:29–34
- Eberhard JP (1751) *Abhandlung von dem Ursprung der Perle*. Rengerische Buchhandlung, Halle
- Efremova SM (2001) *Porifera. Index of Animal species inhabiting Lake Baikal and its catchment area*. Nauka, Novosibirsk, vol 1. Lake Baikal, Book 1, pp 182–192
- Galaziy GI (1988) *Baikal v voprosakh i otvetakh*. Publishing House “Mysl,” Moscow, 286 pp
- Georgi J (1797) *Geographisch-physikalische und Naturhistorische Beschreibung des Rußischen Reichs*. Five volumes. F. Nicolovius, Königsberg
- Gmelin JG (1751) *Reise durch Sibirien*. Abram Vandenhoecks, Göttingen

- Goldberg EL, Chebykin EP, Vorobyova SS, Grachev MA (2005) Uranium signals of paleoclimate humidity recorded in sediments of Lake Baikal. *Doklady Akademii Nauk* 400:72–77
- Greze VN, Greze II (1958) Ozero Chagytai. *Izvestija Vsesoyuznogo Geographiceskogo Obscestva* 90:279–284
- Hoffman PF, Kaufman AJ, Halverson GP, Schrag DP. (1998) A neoproterozoic snowball earth. *Science* 281:1342–1346
- Humboldt A v (1844) Central Asien. Untersuchungen über die Gebirgsketten und die vergleichende Klimatologie. 2 vols. CJ Klemann, Berlin
- Itskovich VB, Belikov SI, Efremova SM, Masuda Y (1999) Phylogenetic relationships between Lubomirskiidae, Spongillidae and some marine sponges according partial sequences of 18S rDNA. *Mem Queensland Mus* 44:275–280
- Johansen H (1925) Der Baikalsee. *Mitteilungen der Geographischen Gesellschaft München* 18:1–200
- Kaluzhnaya OV, Belikov SI, Schröder HC, Rothenberger M, Zapf S, Kaandorp JA, Borejko A, Müller IM, Müller WEG (2005a) Dynamics of skeletal formation in the Lake Baikal sponge *Lubomirskia baicalensis*. Part I: biological and biochemical studies. *Naturwissenschaften* 92:128–133
- Kaluzhnaya OV, Belikov SI, Schröder HC, Wiens M, Giovine M, Krasko A, Müller IM, Müller WEG (2005b) Dynamics of skeletal formation in the Lake Baikal sponge *Lubomirskia baicalensis*. Part II: Molecular biological studies. *Naturwissenschaften* 92:134–138
- Kozhov M (1963) Lake Baikal and its life. Junk, The Hague
- Krasko A, Batel R, Schröder HC, Müller IM, Müller WEG (2000) Expression of silicatein and collagen genes in the marine sponge *Suberites domuncula* is controlled by silicate and myotrophin. *Eur J Biochem* 267:4878–4887
- Krasko A, Schröder HC, Batel R, Grebenjuk VA, Steffen R, Müller IM, Müller WEG (2002) Iron induces proliferation and morphogenesis in primmorphs from the marine sponge *Suberites domuncula*. *DNA Cell Biol* 21:67–80
- Lesseps JBB de (1791) Reise von Kamtschatka nach Frankreich. Johannes F Hartknoch, Riga
- Loomis WF (1988) Four billion years. Sinauer, Sunderland, MA
- Manconi R, Pronzato R (2000) Suborder Spongillina subord. Nov.: freshwater sponges. In: Hooper JNA, Van Soest RWM (eds) *Systema Porifera: a guide to the classification of sponges*. Kluwer/Plenum, New York, pp 921–1019
- Martinson GG (1948) Fossil sponges from the Tunka-Depression in Prebaikal. [Iskopaemye gubki iz Tunkinskoi kotloviny v Pribaikalye]. *Doklady Akademii Nauk SSSR* 61:897–900 (in Russian)
- Masuda Y, Itskovich VB, Veinberg EV, Efremova SM (1997) Studies on the taxonomy and distribution of freshwater sponges in the Lake Baikal. In: Miyzaki N (ed) *Animal community, environment and phylogeny in Lake Baikal*. Otsuchi Marine Center/Ocean Research Institute, Tokyo, pp. 21–41
- Mats VD (1990) The original and evolution of the Baikal basin. In: Kvasov DD (ed) *History of lakes of the USSR: Ladozhskoye, Onezhskoye, Pskovsko, Chudskoye, Baikal, Khanka*. Nauka, Leningrad, pp 167–19
- Mats VD, Fujii S, Mashiko K, Osipov EY, Yefrimova IM, Klimansky AV (2000) Changes in Lake Baikal water levels and runoff direction in the Quaternary period. In: Minoura K (ed) *Lake Baikal*. Elsevier, Amsterdam, pp 15–34
- Mehl-Janussen D, Eckert C, Veinberg EV (2000) Investigations on the endemic freshwater Porifera of Lake Baikal (Lubomirskiidae): status and perspectives. *Terra Nostra* 9:49–59
- Morse DE (1999) Silicon biotechnology: harnessing biological silica production to construct new materials. *Trends Biotechnol* 17:230–232
- Müller GF (1732–1764) *Sammlungen russischer Geschichte*. St. Petersburg
- Müller GF (1779) *Sammlung Rußischer Geschichte des Herrn Geheimraths Müllers in Moscow*. Effenbach: U. Weiß; five volumes
- Müller WEG (1995) Molecular phylogeny of Metazoa (animals): monophyletic origin. *Naturwissenschaften* 82:321–329

- Müller WEG (ed) (1998a) Molecular evolution: evidence for monophyly of Metazoa. Progress in Molecular Subcellular Biology, vol 19. Springer Verlag, Berlin/Heidelberg/New York
- Müller WEG (1998b) Origin of Metazoa: sponges as living fossils. *Naturwissenschaften* 85:11–25
- Müller WEG (2001) How was metazoan threshold crossed: the hypothetical Urmetazoa. *Comparative Biochemistry and Physiology [A]* 129:433–460
- Müller WEG (2006) The stem cell concept in sponges (Porifera): metazoan traits. *Semin Cell Dev Biol* 17:481–491
- Müller WEG, Müller IM (2003) Origin of the metazoan immune system: identification of the molecules and their functions in sponges. *Integrative and Comparative Biology* 43:281–292
- Müller WEG, Wiens M, Batel R, Steffen R, Borojevic R, Custodio MR (1999) Establishment of a primary cell culture from a sponge: Primmorphs from *Suberites domuncula*. *Mar Ecol Prog Series* 178:205–219
- Müller WEG, Koziol C, Wiens M, Schröder HC (2000) Stress response in marine sponges: genes and molecules involved and their use as biomarkers. In: Storey KB, Storey J (eds) *Environmental stressors and gene responses*. Elsevier Science, Amsterdam, pp 193–208
- Müller WEG, Schröder HC, Skorokhod A, Bünz C, Müller IM, Grebenjuk VA (2001) Contribution of sponge genes to unravel the genome of the hypothetical ancestor of Metazoa (Urmetazoa). *Gene* 276:161–173
- Müller WEG, Krasko A, Le Pennec G, Steffen R, Ammar MSA, Wiens M, Müller IM, Schröder HC (2003) Molecular mechanism of spicule formation in the demosponge *Suberites domuncula*: silicatein – collagen – myotrophin. *Prog Mol Subcell Biol* 33:195–22
- Müller WEG, Schröder HC, Lorenz B, Krasko A (2004a) Silicatein-mediated synthesis of amorphous silicates and siloxanes and use thereof. European Patent No. 1320624
- Müller WEG, Wiens M, Adell T, Gamulin V, Schröder HC, Müller IM (2004b) The Bauplan of the Urmetazoa: The basis of the genetic complexity of Metazoa using the siliceous sponges [Porifera] as living fossils. *Int Rev Cytol* 235:53–92
- Müller WEG, Belikov SI, Schröder HC (2005a) Biosilica, the raw material of the coming millennium: sustainable production in Lake Baikal. *Science First Hand* 3:26–35 (in Russian)
- Müller WEG, Krasko A, Schröder HC (2005b) *In vitro* and *in vivo* degradation or synthesis of silicon dioxide and silicones, useful e.g., for treating silicosis or to prepare prosthetic materials, using a new silicase enzyme. Patent No. DE10246186.
- Müller WEG, Belikov SI, Tremel W, Perry CC, Gieskes WWC, Boreiko A, Schröder HC (2006a) Siliceous spicules in marine demosponges (example *Suberites domuncula*). *Micron* 37:107–120
- Müller WEG, Kaluzhnaya OV, Belikov SI, Rothenberger M, Schröder HC, Reiber A, Kaandorp JA, Manz B, Mietchen D, Volke F (2006b) Magnetic resonance imaging of the siliceous skeleton of the demosponge *Lubomirskia baicalensis*. *J Struct Biol* 153:31–41
- Müller WEG, Schröder HC, Wrede P, Kaluzhnaya OV, Belikov SI (2006c) Speciation of sponges in Baikal-Tuva region (an outline). *J Zool Syst Evol Res J* 44:105–117
- Müller WEG, Wendt K, Geppert C, Wiens M, Reiber A, Schröder HC (2006d) Novel photoreception system in sponges? Unique transmission properties of the stalk spicules from the hexactinellid *Hyalonema sieboldi*. *Biosens Bioelectron* 21:1149–1155
- Müller WEG, Boreiko A, Wang XH, Belikov SI, Wiens M, Grebenjuk VA, Schloßmacher U, Schröder HC (2007) Silicateins, the major biosilica forming enzymes present in demosponges: protein analysis and phylogenetic relationship. *Gene* 395:62–71
- William A (1814) Picturesque representations of the dress and manners of the Russians. John Murray, London
- Pallas PS (1771) Reise durch die verschiedenen Provinzen des russischen Reiches. Theil 3-Buch 2. Kayserliche Academie der Wissenschaften, St. Petersburg
- Pallas PS (1787) Charakteristik der Thierpflanzen. Raspische Buchhandlung, Nürnberg
- Pechenik JA (2000) Biology of the invertebrates. McGraw-Hill, Boston, MA
- Pecher IA (2002) Gas hydrates on the brink. *Nature* 420:622–623
- Pilcher H (2005) Back to our roots. *Nature* 435:1022–1023

- Popovskaya GI, Genkal SI, Likhoshway YV (2002) Diatoms of the plankton of Lake Baikal. Nauka, Novosibirsk
- Pronzato R, Manconi R. 2001. Atlas of European freshwater sponges. Ann Mus Civ St Nat Ferrara 4:3–64
- Reitner J, Wörheide G (2002) Non-lithistid Demospongiae – origins of their palaeobiodiversity and highlights in history of preservation. In: Hooper JNA, Van Soest RWM (eds) Systema Porifera: a guide to the classification of sponges. Kluwer/Plenum, New York, pp 52–70
- Rezvoj P (1927) Notes on sponges from the Lake Dzhigataj-kul in the Urjankhaj region. Doklady Akademii Nauk SSSR 3/8:296–300
- Rezvoj PD (1936) Süßwasserschwämme (Fam. Spongillidae et Lubomirskiidae). Faune De L'URSS vol. 2 (no. 2). Moskau Leningrad: Izdatelstvo Akademii Nauk SSSR 105–124 (in German)
- Röpstorff P, Reitner J (1994) Morphologie einiger Süßwasserporoifera (*Baikalospongia bacillifera*, *Lubomirskia baicalensis*, *Swartschweskia papyracea*) des Baikal-Sees (Sibirien, Rußland). Berliner Geowiss Abh E13:507–525
- Sankov VA, Parfeevets AV, Miroshnitchenko AI, Likhnev A, Arzhannikova AV (2003) Cenozoic dynamics of Baikal and Khubsugul basins. Berliner Paläontol Abh 4: 49–54
- Savarese M, Patterson MR, Chernykh VI, Fialkov VA (1997) Trophic effects of sponge feeding within Lake Baikal's littoral zone. 1. *In situ* pumping rate. Limnol Oceanogr 42:171–178
- Schäcke H, Müller IM, Müller WEG (1994) Tyrosine kinase from the marine sponge *Geodia cydonium*: the oldest member belonging to the receptor tyrosine kinase class II family. In: Müller WEG (ed) Use of aquatic invertebrates as tools for monitoring of environmental hazards. Gustav Fischer Verlag, Stuttgart/New York, pp 201–211
- Scherer AN (1820) Versuch einer systematischen Uebersicht der Heilquellen des Russischen Reichs. Akademie der Wissenschaften, St. Petersburg
- Schröder HC, Efremova SM, Itskovich VB, Belikov S, Masuda Y, Krasko A, Müller IM, Müller WEG (2003a) Molecular phylogeny of the freshwater sponges in Lake Baikal. J Zool Sys Evol Res 41:80–86
- Schröder HC, Krasko A, Le Pennec G, Adell T, Hassanein H, Müller IM, Müller WEG (2003b) Silicase, an enzyme which degrades biogenous amorphous silica: contribution to the metabolism of silica deposition in the demosponge *Suberites domuncula*. Prog Mol Subcell Biol 33:249–268
- Schröder HC, Perović-Ottstadt S, Rothenberger M, Wiens M, Schwertner H, Batel R, Korzhev M, Müller IM, Müller WEG (2004) Silica transport in the demosponge *Suberites domuncula*: fluorescence emission analysis using the PDMPO probe and cloning of a potential transporter. Biochem J 381 665–673
- Schröder HC, Boreiko A, Krasko A, Reiber A, Schwertner H, Müller WEG (2005) Mineralization of SaOS-2 cells on enzymatically (Silicatein) modified bioactive osteoblast-stimulating surfaces. J Biomed Mat Res Part B: Appl Biomat 75B: 387–392
- Schröder HC, Boreiko A, Korzhev M, Krasko A, Tahir MN, Tremel W, Eckert C, Ushijima H, Müller IM, Müller WEG (2006) Co-expression and functional interaction of silicatein with galectin: Matrix-guided formation of siliceous spicules in the marine demosponge *Suberites domuncula*. J Biol Chem 281:12001–12009
- Shimizu K, Cha J, Stucky GD, Morse DE (1998) Silicatein alpha: cathepsin L-like protein in sponge biosilica. Proc Natl Acad Sci USA 95: 6234–6238
- Simpson TL (1984) The cell biology of sponges. Springer-Verlag, New York
- Steiner M, Mehl D, Reitner J, Erdtmann BD (1993) Oldest entirely preserved sponges and other fossils from the Lowermost Cambrian and a new facies reconstruction of the Yangtze Platform (China). Berliner Geowiss Abh (E) 9:293–329
- Strahlenberg PJ (1730) Das Nord- und Ostliche Theil von Europa und Asia. Autoris, Stockholm
- Tahir MN, Théato P, Müller WEG, Schröder HC, Janshoff A, Zhang J, Huth J, Tremel W (2004) Monitoring the formation of biosilica catalysed by histidin-tagged silicatein. Chem Commun 24:2848–2849

- Tahir MN, Théato P, Müller WEG, Schröder HC, Borejko A, Faiß S, Janshoff A, Huth J, Tremel W (2005) Formation of layered titania and zirconia catalysed by surface-bound silicatein. *Chem Commun* 44:5533–5535
- Thompson JD, Higgins DG, Gibson TJ (1994) CLUSTAL W: improving the sensitivity of progressive multiple sequence alignment through sequence weighting, positions-specific gap penalties and weight matrix choice. *Nucleic Acids Res* 22:4673–4680
- Weissenfels N (1989) *Biologie und Mikroskopische Anatomie der Süßwasserschwämme (Spongillidae)*. Gustav Fischer Verlag, Stuttgart.
- Wiens M, Müller WEG (2006) Cell death in Porifera: molecular players in the game of apoptotic cell death in living fossils. *Can J Zool/Rev Can Zool* 84:307–321
- Wiens M, Belikov SI, Kaluzhnaya OV, Krasko A, Schröder HC, Perovic-Ottstadt S, Müller WEG (2006) Molecular control of serial module formation along the apical-basal axis in the sponge *Lubomirskia baicalensis*: silicateins, mannose-binding lectin and Mago Nashi. *Dev Genes Evol* 216:229–242
- Winter E, Uschmann G, Jarosch GDG (1968) Messerschmidt Forschungsreise durch Sibirien 1720–1727. Akademie-Verlag, Berlin
- Wöhler F (1828) Ueber künstliche Bildung des Harnstoffs. *Annalen der Physik und Chemie* 12: 253–256

Index

A

Academician Ridge, 188, 194, 197
Accretive growth, 240
Adhesive systems, 360, 361, 370–372
Akademichesky ridge, 33
Amphioxea, 85–89, 94, 95, 98, 99, 101
Amphistrongyla, 91–93, 96, 97, 99
Aquaporin, 145
Aquiferous system, 241
Archaeocytes, 67
Archean precursor, 9
Architecture, sponges, 239
Axinella polypoides, 239

B

Baicalia herderiana, 227
Baikal, 3
Baikal depression formation, 10
Baikal Drilling Project (BDP), 187
Baikalian sediments, 188, 194
Baikalian sponge, 186
Baikal-Muya terrane, 9
Baikalospongia
 B. bacillifera, 90–91, 95, 103, 109, 147, 225
 B. dzhegatajensis, 112, 115
 B. fungiformis, 92–93, 103, 109, 185
 B. intermedia, 94–96, 102, 103, 107, 108, 147, 187
 B. intermedia profundalis, 95–96, 109
 B. martinsoni, 91–92
 B. recta, 93–94, 103, 109
Baikal–Tuva region, 3
Baikalum-1, 210
Baikal Unit, 7, 10
Barguzin terrane, 10
Bending, 281

Bioinorganic biosilification, 182
Biomineralization, 295
Biomolecule, 341–343, 347–349, 351, 356
Biosilica, 280, 295
 benefit for human, 401
 coatings, 259
 sustainable production, 404
Biosilification, 174
Bonding, 346–347, 355
Bone
 regeneration scaffolds, 264
 replacement, 264
Brachyury, 71
Bragg mode, 327

C

Calcarea, 60
“Cambrian explosion,” 65
Capillarity, 351, 353
Cell-cell interaction, 61
Cell-substrate interaction, 61
Central-Asian orogenic belt, 5
Chara, 117
Chargytai, 3, 22
Chip sealing, 345–347
Citrate synthase, 158
Collencytes, 66
Compomers, 360, 362–364, 370–372
Composites, 277
 cements, 372
 resins, 362
 cements, 372–375
 flowables, 372
 synthetic, 292
Conformal contact, 344, 346–347
Core-shell materials, 262

“Crown” taxa, 65
 Cryoprotective proteins, 65
Cyclotella minuta, 123

D

Dental ceramics, 359
 crystals, 376
 lithium-disilicate, 376
 Dentistry, 359
 Deposition of skeleton, 242
 Derba-Kitoykin metamorphic terrane, 16
 Dinoflagellates, 145, 154
 Dzhida terrane, 16

E

East Sayan, 44
 Ediacaran-Cambrian boundary, 57
 Efremova, S.M., 185, 201
 Elastomeric materials, 345
 Encapsulation of bacteria, 265
 Endemic sponges, 139, 207
Ephydatia
 E. altaiensis, 115, 227
 E. fluviatilis, 105, 187
 E. gorjaevii, 105
 E. muelleri, 101–103, 107, 108
 E. olchonensis, 105
 E. tuva, 115, 116, 227
Eunapius, 99–101, 107
Euplectella aspergillum, 69, 277
 Eutrophic, 108
 Extinct species, 192, 193, 195, 199

F

Filler particles
 adhesives, 372
 classification, 369
 content, 362, 363, 365, 367–372, 374
 inorganic fillers, 366
 size, 369, 374
 Fluorescence spectroscopy
 decay kinetics, 337
 intensity, 337
 spectrum, 336, 338
 Food restriction/symbiosis, 65
 Fossil Baikalian sponge, 192
 Fossil sponge fauna, 185, 196, 197, 200
 Frizzled receptor, 71
 Fructose-1,6-bisphosphatase, 158
 Fused silica, 319, 320, 332, 335

G

Gemmoscleres, 82, 99, 101, 108
 Gemmule, 81, 82, 101, 102, 108
 Genomics, 349, 351
Geodia cydonium, 56, 70
 Glass-ionomer cements, 360–377
 Glycerol, 145
 Gmelin, 388
 Gureeva, M.A., 201
Gymnodinium sanguineum, 154

H

Haliclona oculata, 237
 Hexactinellida, 60
 Hexactinellid sponges, 277
 H filter, 353–354
 Holocene, 194
 Hovsgol, Lake, 27, 28, 36
 Hubei, 64
Hyalonema sieboldi, 70, 315
 Hydrated quartz, 316

I

Ikat terrane, 10
 Internal transcribed spacers, 112
 Iroquois, 68

K

Khamar-Daban, 44
 Khamar-Daban-Olkhon metamorphic terrane, 17
 Khubsugul, 3, 18
 Khubsugul Unit, 14, 20

L

Lab-on-chip, 351, 355
 Lake Baikal, 185, 224, 228
 discovery, 387
 paleo-outlets, 35
 Lake Chagytai, 115, 224, 227
 Lake Tore-Khol, 115, 224, 227
 Late Miocene, 185, 188, 200
 Late Pliocene, 185, 194, 195
 LIM class genes, 73
Lubomirskia
 L. abietina, 89–90, 103, 109
 L. baicalensis, 69, 85–88, 102, 103, 107,
 108, 145, 225, 383
 expressed sequence tag (EST), 396
 L. b. littoralis, 86

- L. fusifera*, 88–89, 102
- L. incrustans*, 87–88, 102, 185
- Lubomirskiidae, 81, 82, 85–98, 102, 103, 107, 108
- Lubomirskiidae family, 186, 187, 201

M

- Manzurka River, 36
- Martinson, G.G., 186, 201
- Mechanical behavior, loading rate, 290
- Megasclere, 82, 99, 101, 108
- Mesenchymal stem cell-like protein (MSCP), 66
- Mesoproterozoic, 5
- Mesozoa, 55
- Messerschmidt, 388
- Metazoa, 55
- Microarray(s), 342–343, 349–350
- Microcontact printing, 342–343, 345, 347
- Microfluidic lithography, 351
- Microfluidics, 341–343, 345–346, 351, 353–356
- Microhardness, 319–321
- Micromolding in capillaries, 343, 351
- Microsclere, 99, 101, 102, 108
- Micro-total analysis systems, 355
- Microtransfer molding, 343
- Mineral trioxide aggregate (MTA), 377
- Miocene, 200
- Mobile elements, 229
- “Molecular clock,” 56
- Molecular investigations, 202
- Molecular phylogeny of endemic freshwater sponges, 124
- Molecular systematics of lake Baikal/lake Tuva sponges, 111
- Monophyletic origin, 59
- Morphogen, 68
- Morphogenesis, 61
- Morphological features of spicules, 189, 192
- Myotrophin, 68

N

- Nanobiotechnology, 308, 341–343, 356, 383
- Nanolithography, 261
- Nanoparticles, 260
- Nanotechnology, 341–342, 344
- Nanowires, 261
- Natural photonic crystals, 322
- Neoproterozoic, 56, 59
- Northern Eurasia, 4

O

- Oligotrophy, 108
- Oocytes, 152
- Optical fibers, 267, 315, 316
 - cylindrical, 322
 - microstructured, 328, 331, 338
 - omniguide, 323
- Optical properties, 315
- Origin of Lubomirskiidae, 200

P

- Paired class* genes, 73
- Paleontological investigations, 187, 202
- Paleoproterozoic, 9
- Palindrome, 214
- Pallas, 388
- Parazoa, 55
- Patterning, 353
- Phanerozoic, 5
- Pheronema sp.*, 315
- Phosphoglucose isomerase, 159
- Photonic crystal, 322, 327, 335
- Pinacocytes, 67
- Pleistocene, 194
- Pliocene, late, 194
- Poly(dimethylsiloxane), 343
- Polyamins, 300
- Post-translational modification, 255
- Primmorphs, 148
- Primmorph system, 68
- Primorsk, 8
- Proteomics, 343, 349–351
- Proterozoic, late, 64
- Pyruvate dehydrogenase, 159

R

- Radiate accretive growth, 237
- Rapid evolution, 207
- Recent sponge fauna, 186, 197
- Receptor tyrosine kinase (RTK), 67
- Refractive index, 320, 323, 328, 335
 - nonlinear, 334
- Replica molding, 343
- Resin-modified glass-ionomer cements, 362
- Retrotransposon, 207
- Reynolds number, 353
- Rezinkovia*, 98–103
 - R. arbuscula*, 103, 105, 185
 - R. echinata*, 98–99, 107
- Rezvoi, P.D., 201
- Ribosomal DNA, 112

S

Sangilen metamorphic terrane, 20
 Sansha section, 63
 Sclerocytes, 66
 Self-assembly, 347
 Siberian craton, 5
 Silaffins, 300
 Silanization, 362, 365, 370, 375
 Silica

- composite spicules, 282
- condensation, 303
- melt-processed, 281
- structure, 296

 Silicase, 258
 Silicate-based compounds, 359
 Silicate glasses, 360, 362, 368, 371
 Silicatein, 69, 134, 251, 299, 404

- assembly, 255
- biomedicine, 409
- gene, 210

 Silication

- sand-blasting, 375
- silicate layer, 375

 Silicic acid homeostasis, 178
 Silicification, 173

- diatoms, 300
- plants, 301
- sponges, 298

 Silicon, 359–377
 Silicon in life, 173
 Skeletal architecture, 237
 Skeleton, 81, 85–100, 109
 Soft lithography, 341–343, 345–347, 355
Solactiniella plumata, 63
 Solvent-assisted micromolding, 343
 Spicules, 81, 86–99, 315

- basal, 317, 318, 322, 329, 336
- hierachical structure, 280
- mechanical behavior, 279
- optical properties, 320
- skeletal, 317, 318
- structure, 279

 Sponges

- fossil record, 63
- phylogeny, 60

 Sponge spicules, 185, 188

- fluorescence properties, 336
- structure, 317

Spongilla

- S. gutenbergiana*, 63
- S. lacustris*, 98–99, 103, 105, 107, 108
- S. microgemmata*, 105

Spongillidae, 81–82, 99–103, 107–109, 186, 187, 201
 Stem cells in sponges, 66
 Strontium, 38
 Sturtian glaciation, 56
Suberites domuncula, 56
 Supercontinuum generation, 331, 334, 335
Swartschewskaia, 96–98

- S. irregularis*, 103
- S. papyracea*, 96–97, 103, 185, 225

 Symbiotic relationship, 166

T

Tannuola terrane, 21
 Taxonomy of freshwater sponges, 81
 Tertrias, 187
 Tissue engineering, 341–343
 Titania, 260
 Toothpastes

- cleaning particles, 377
- radioactive dentine abrasion (RDA), 377

 Tore-Chol, 3, 22
 Torsion, 281
 Transcription factors, 61
 Transit species, 192, 193, 197
 Transmission spectrum, 320, 321, 334, 335

- anti-Stokes component, 332

 Tribochemical silication, 375
Trochospongilla sp., 82, 107
 T sensor, 353–354
 Tunka land basin, 200
 Tunka terrane, 17
 Tuva unit, 20

U

Ultra-short light pulses

- chromatic dispersion, 331, 333, 335
- Raman self-scattering, 332
- self-phase modulation, 331–333

 Upper Cretaceous, 186
 Upper Pleistocene, 185, 194

V

Varanger-Marinoan ice age, 56
 Volcanism, 40

- Hovsgol, 43
- lake Baikal Rift system, 42
- quaternary, 47

W

Waveguide

- Bragg, 323, 324, 326–328, 330
- cladding, 323, 325
- core, 322, 325
- leaky, 324, 326, 327

Y

- Young's modulus, 319, 321, 344, 346

Z

- Zirconia, 260
- Zoochlorellae, 85, 88, 89, 94, 95, 99